frontiers | Research Topics

Physiological ecology of trees under environmental stresses

Edited by
Song Heng Jin, Guolei Li, Geoff Wang and Tongli Wang

Published in
Frontiers in Plant Science

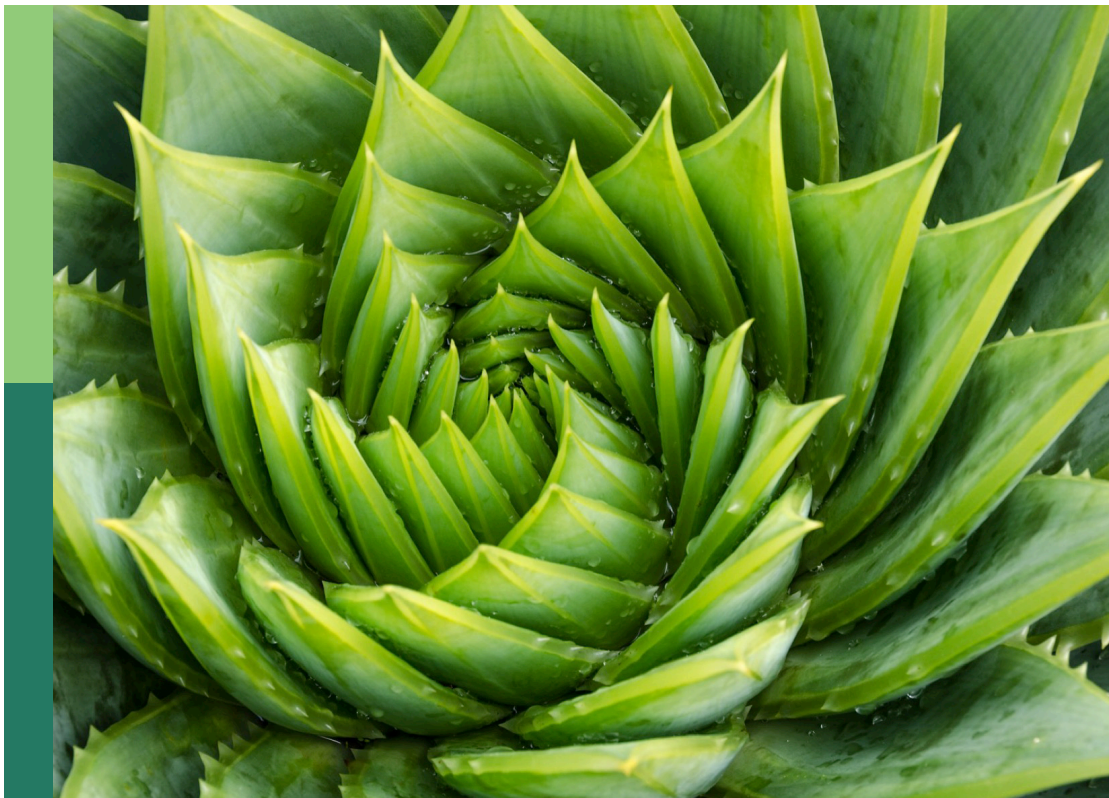

ISSN 1664-8714
ISBN 978-2-83251-803-8
DOI 10.3389/978-2-83251-803-8

About Frontiers

Frontiers is more than just an open access publisher of scholarly articles: it is a pioneering approach to the world of academia, radically improving the way scholarly research is managed. The grand vision of Frontiers is a world where all people have an equal opportunity to seek, share and generate knowledge. Frontiers provides immediate and permanent online open access to all its publications, but this alone is not enough to realize our grand goals.

Frontiers journal series

The Frontiers journal series is a multi-tier and interdisciplinary set of open-access, online journals, promising a paradigm shift from the current review, selection and dissemination processes in academic publishing. All Frontiers journals are driven by researchers for researchers; therefore, they constitute a service to the scholarly community. At the same time, the *Frontiers journal series* operates on a revolutionary invention, the tiered publishing system, initially addressing specific communities of scholars, and gradually climbing up to broader public understanding, thus serving the interests of the lay society, too.

Dedication to quality

Each Frontiers article is a landmark of the highest quality, thanks to genuinely collaborative interactions between authors and review editors, who include some of the world's best academicians. Research must be certified by peers before entering a stream of knowledge that may eventually reach the public - and shape society; therefore, Frontiers only applies the most rigorous and unbiased reviews. Frontiers revolutionizes research publishing by freely delivering the most outstanding research, evaluated with no bias from both the academic and social point of view. By applying the most advanced information technologies, Frontiers is catapulting scholarly publishing into a new generation.

What are Frontiers Research Topics?

Frontiers Research Topics are very popular trademarks of the *Frontiers journals series*: they are collections of at least ten articles, all centered on a particular subject. With their unique mix of varied contributions from Original Research to Review Articles, Frontiers Research Topics unify the most influential researchers, the latest key findings and historical advances in a hot research area.

Find out more on how to host your own Frontiers Research Topic or contribute to one as an author by contacting the Frontiers editorial office: frontiersin.org/about/contact

Physiological ecology of trees under environmental stresses

Topic editors

Song Heng Jin — Zhejiang Agriculture and Forestry University, China
Guolei Li — Beijing Forestry University, China
Geoff Wang — Clemson University, United States
Tongli Wang — University of British Columbia, Canada

Citation

Jin, S. H., Li, G., Wang, G., Wang, T., eds. (2023). *Physiological ecology of trees under environmental stresses*. Lausanne: Frontiers Media SA.
doi: 10.3389/978-2-83251-803-8

Table of contents

frontiers | Frontiers in Plant Science

TYPE Editorial
PUBLISHED 16 February 2023
DOI 10.3389/fpls.2023.1158821

OPEN ACCESS

EDITED AND REVIEWED BY
Yuanrun Zheng,
Institute of Botany (CAS), China

*CORRESPONDENCE
Yang Liu
yangliu8910@zafu.edu.cn
Songheng Jin
shjin@zafu.edu.cn

SPECIALTY SECTION
This article was submitted to Functional Plant Ecology, a section of the journal Frontiers in Plant Science

RECEIVED 04 February 2023
ACCEPTED 13 February 2023
PUBLISHED 16 February 2023

CITATION
Liu Y, Jin S and Li G (2023) Editorial: Physiological ecology of trees under environmental stresses.
Front. Plant Sci. 14:1158821.
doi: 10.3389/fpls.2023.1158821

Editorial: Physiological ecology of trees under environmental stresses

Yang Liu[1]*, Songheng Jin[1,2]* and Guolei Li[3]

[1]Jiyang College, Zhejiang A&F University, Zhuji, China, [2]School of Life Science and Health, Huzhou College, Huzhou, China, [3]College of Forestry, Beijing Forestry University, Beijing, China

KEYWORDS

nutrient acquisition, environmental stresses, nitric oxide, functional traits, forest research, microbial diversity, molecular adaptation mechanisms, trees

Editorial on the Research Topic
Physiological ecology of trees under environmental stresses

The impact of environmental changes not only affects the survival of trees but also is closely related to the interests of human beings. Woody plants are a key element of the ecosystem since they help mitigate the negative impacts of complex climate changes such as increased carbon dioxide, high temperature, drought, etc (FAO, 2018). When trees suffer from environmental stress, they have to respond physiologically and ecologically to all kinds of adversity to improve their survival ability. This includes changes from population to individual, and involves the knowledge of ecology, morphology, and also physiology (Rewald et al., 2020). To explore the physiological ecology of trees under environmental stresses is of great significance to improve forestry production and environmental protection. The goal of this Research Topic (RT) is to present an overview of the fundamental discoveries in the field of physiological ecology of trees under environmental stresses. Here we collected physiological, biochemical, and also genetic studies to improve our understanding of the response mechanisms of trees under abiotic stresses, especially climate changes such as global warming, drought, atmospheric nitrogen deposition, salinization, etc.

In recent years, the occurrence of high temperature events has caused more scholars to study the heat tolerance of trees (Fahad et al., 2018; Yu, 2019). Ji et al. studied the effects of high temperature on photosynthesis between two tree peony varieties with different high temperature tolerance. Their results indicate the variety with strong high temperature tolerance had higher connectivity with reaction center of light capture complex, less damage to oxygen-evolving complex activity, and better stability of PSII system. Hu et al. combined physiological analyses and RNA seq technology to provide a holistic view of the behavior of *Betula luminifera* populations facing heat stress. Several transcription factors (TFs) genes were identified by differentially expressed genes analysis. Additionally, the author carried out qRT-PCR experiment to investigate the regulatory of candidate TFs under heat stress, which will lay the foundation for the selection and breeding of *Betula luminifera* and facilitate wider diversity of resistant *Betula luminifera* varieties to fulfill current and future needs.

Nutrient acquisition and high quality seedlings are the basis of successful afforestation (Davis and Jacobs, 2005). Thus, fertilization is often used to improve tree growth, and promote resistance to biotic and abiotic stresses (Zhu et al., 2020). However, the effect of fertilization depends on site conditions and external environments (Gessler et al., 2017). Song et al. reported nutrient internal cycles of two aged *Metasequoia* plantations in responses to N addition gradients and P addition gradients using two relative independent experiments. The authors identified the response patterns of root-soil accumulation factor (RSAF) and leaf nutrient resorption efficiency (LNRE) varied with fertilization types and stand ages, and explored the trade-off mechanism between RSAF and LNRE driven by nutrient alteration. Yu et al. compared the transcription level change of *Torreya grandis* using simulated N deposition and strigolactone (GR24) treatment. The authors analyzed the effects of these two treatments on the soil bacteria of *Torreya grandis*. The research showed 4,008 DEGs were identified and Legionella, Lacunisphaera, Klebsiella, Bryobacter, and Janthinobacterium were significantly enriched in the soil in the N addition and GR24 treatment. Yang et al. detected how different drought durations and N fertilization as well as their interactions affect the physiological and growth responses of two coexisting species saplings and their resilience abilities after rewetting procedure. They found root carbon storage appears to be extremely important for tree growth and survival under prolonged drought. Wang et al. conducted a summer drought and fertilization experiment, and analyzed how drought and fertilization induced changes in non-structural carbohydrate (NSC) storage of oak saplings affect its spring leaf development. Their results indicate that drought did not significantly alter NSC reserves, but delayed the spring leaf expansion and reduced the leaf biomass, while fertilization enhanced NSC reserves and stimulated spring leaf expansion.

Climate change is one of the main causes of soil salinization, which in recent years has become a growing problem in agriculture and leads to a decrease in the cultivation area, harming plant growth, crop yield, and quality (Deinlein et al., 2014; Sun et al., 2016; Shang et al., 2022). High salinity is often coupled with ionic and osmotic stress in trees, which alters the biochemical and physiological processes in the plants (Stefanov et al., 2022). Yang et al. discussed the role of nitric oxide in ameliorating salinity stress in dioecious plants and established fact that nitric oxide does mitigate salt-mediated oxidative injuries in a vast variety of crops and plants. Grafting and salt stress have been regarded as the main abiotic stress types for Chinese hickory. Yang et al. explained the role and expression analysis of PIN family genes in Chinese Hickory under salt stress and grafting. The authors had analyzed the expression of the PIN gene family. Their results showed CcPIN1a might be involved in the regulation of the grafting process, while CcPIN1a and CcPIN8a were related to the regulation of salt stress in Chinese hickory.

Light is an important ecological factor that affects plant growth, survival and distribution (Tang et al., 2015). Zhou et al. studied the effects of different light intensities on growth, physiology, photosynthetic characteristics, endogenous hormones and antioxidant activity responses of *Carpinus betulus* seedlings. The results suggested that *Carpinus betulus* can make effective use of low light resources by adjusting its morphology, material distribution, photosynthetic rate and antioxidant enzyme system in suitable low-light environments. Yang et al. conducted relative benefit and scaling relationship analyses of leaves in three urban plants to reveal the response and adaptation to different light conditions, which is helpful to understand the ecological changes in urban trees. Their results showed the leaves of the three urban plants exhibited a shift in strategy during transfer from the canopy shaded to the sunny habitat for adapting to the lower light conditions. Wu et al. conducted proteome analyses in developing *Styrax tonkinensis* kernels to revel the starch and oil biosynthesis under fruit shading treatment with four biological replicates. They found that fruit shading is a negative treatment for lipid accumulation but not starch accumulation by restraining enzymic protein expression involved in fatty acids (FAs) and triacylglycerol (TAG) biosynthesis during *Styrax tonkinensis* kernel development.

The invasion of moso bamboo to natural evergreen broad-leafed forests or mixed forests is a crucial issue of forest ecosystem and may cause important effect on forest ecological functions (Ramula and Pihlaja, 2012; Wang et al., 2019). In recent decades, moso bamboo has been largely increasing in the subtropical area of China, raising ecological concerns about its invasion into other native forest ecosystems (Wang et al., 2017). While the ecological impacts of moso bamboo invasion into native forests have been widely studied, no study has considered its impact on forest productivity and on the relationship between species diversity and productivity. Chen et al. supplied reliable results on the impacts of bamboo invasion on species diversity and biomass. The authors found that bamboos exchange water *via* rhizomes and nighttime fluxes are highly important for the support of freshly sprouted culms.

In recent years, with the rapid development of industrialization and urbanization, the accumulation of heavy metals (HMs) in the environment has been increasing, especially in developed economic regions (Yang et al., 2020). As a developed economic region in China, the problem of HMs pollution in the Yangtze River Delta has become increasingly prominent. Li et al. illustrated a human health risk assessment of heavy metals in the bark and leaves of camphor trees located in Yangtze River Delta, China. The source and contribution rate of heavy metals in the study area were analyzed by Pb isotope ratio, and the human health risk assessment model was combined with Pb isotope ratio analysis to evaluate the health risk of heavy metal pollution sources in the study area. Their research results can provide scientific guidance for the prevention and control of heavy metal pollution of camphor trees and provide a reference for avoiding areas with high risk of heavy metal pollution.

Author contributions

YL and SJ provided the first draft of the MS. All co-authors jointly revised the manuscript and approved its publication.

Funding

We thank the National Key Research and Development Project (2019YFE0118900), the National Natural Science Foundation of China (No. 32001305, 31971641), "Pioneer" and"Leading Goose" R&D Program in Universities of Zhejiang (2022), Jiyang College of Zhejiang A&F University under Grant (No. RQ2020B14; JYKC2117).

Acknowledgments

We thank the authors and reviewers for their support in creating this RT. Explicit thanks go to our co-editors Geoff Wang, and Tongli Wang for help with the RT set-up and management.

Conflict of interest

The authors declare that the research was conducted in the absence of any commercial or financial relationships that could be construed as a potential conflict of interest.

Publisher's note

References

Davis, A. S., and Jacobs, D. F. (2005). Quantifying root system quality of nursery seedlings and relationship to afforestation performance. *New Forest.* 30, 295–311. doi: 10.1007/s11056-005-7480-y

Deinlein, U., Stephan, A. B., Horie, T., Luo, W., Xu, G., and Schroeder, J. I. (2014). Plant salt tolerance mechanisms. *Trends Plant Sci.* 19, 371–379. doi: 10.1016/j.tplants.2014.02.001

Fahad, S., Ihsan, M. Z., Khaliq, A., Daur, I., Saud, S., Alzamanan, S., et al. (2018). Consequences of high temperature under changing climate optima for rice pollen characteristics-concepts and perspectives. *Arch. Agron. Soil Sci.* 64 (11), 1473–1488. doi: 10.1093/aob/mci071

FAO (2018). *State of the world's forests 2018–forest pathways to ustainable developments* (Rome, Italy: Food and Agriculture Organization of the United Nations).

Gessler, A., Schaub, M., and McDowell, N. G. (2017). The role of nutrients in drought-induced tree mortality and recovery. *New Phytol.* 214 (2), 513–520. doi: 10.1111/nph.14340

Ramula, S., and Pihlaja, K. (2012). Plant communities and the reproductive success of native plants after the invasion of an ornamental herb. *Biol. Invasions* 14, 2079–2090. doi: 10.1007/s10530-012-0215-z

Rewald, B., Ammer, C., Hartmann, H., Malyshev, A. V., and Meier, I. C. (2020). Editorial: Woody plants and forest ecosystems in a complex world–ecological interactions and physiological functioning above and below ground. *Front. Plant Sci.* 11. doi: 10.3389/fpls.2020.00173

Shang, J. X., Li, X., Li, C., and Zhao, L. (2022). The role of nitric oxide in plant responses to salt stress. *Int. J. Mol. Sci.* 23, 6167. doi: 10.3390/IJMS23116167

Stefanov, M. A., Rashkov, G. D., and Apostolova, E. L. (2022). Assessment of the photosynthetic apparatus functions by chlorophyll fluorescence and P700 absorbance in C3 and C4 plants under physiological conditions and under salt stress. *Int. J. Mol. Sci.* 23, 3768. doi: 10.3390/ijms23073768

Sun, Z. W., Ren, L. K., Fan, J. W., Li, Q., Wang, K. J., Guo, M. M., et al. (2016). Salt response of photosynthetic electron transport system in wheat cultivars with contrasting tolerance. *Plant Soil Environ.* 62, 515–521. doi: 10.17221/529/2016-PSE

Tang, H., Hu, Y. Y., Yu, W. W., Song, L. L., and Wu, J. S. (2015). Growth, photosynthetic and physiological responses of *Torreya grandis* seedlings to varied light environments. *Trees-Struct. Funct.* 29 (4), 1011–1022. doi: 10.1007/s00468-015-1180-9

Wang, Y. J., Chen, D., Yan, R., Yu, F. H., and Van Kleunen, M. (2019). Invasive alien clonal plants are competitively superior over co-occurring native clonal plants. *Perspect. Plant Ecol.* 40, 125484. doi: 10.1016/j.ppees.2019.125484

Wang, Y. J., Müller-Schärer, H., Van Kleunen, M., Cai, A. M., Zhang, P., Yan, R., et al. (2017). Invasive alien plants benefit more from clonal integration in heterogeneous environments than natives. *New Phytol.* 216, 1072–1078. doi: 10.1111/nph.14820

Yang, S. H., Qu, Y. J., Ma, J., Liu, L. L., Wu, H. W., Liu, Q. Y., et al. (2020). Comparison of the concentrations, sources, and distributions of heavy metal (loid)s in agricultural soils of two provinces in the Yangtze river delta, China. *Environ. Pollut.* 264, 114688. doi: 10.1016/j.envpol.2020.114688

Yu, S. A. (2019). *The impact of climate change on crop production: an empirical study in zhejiang, China* (Zhejiang: Ph.D. Dissertation, Zhejiang University).

Zhu, Y., Li, S., Wang, C. Y., Dumroese, R. K., Li, G. L., and Li, Q. M. (2020). The effects of fall fertilization on the growth of Chinese pine and prince rupprecht's larch seedlings. *J. Forest. Res.* 31, 2163–2169. doi: 10.1007/s11676-019-01054-0

frontiers | Frontiers in Plant Science

ORIGINAL RESEARCH
published: 11 May 2022
doi: 10.3389/fpls.2022.905358

Effects of Long-Term Fertilization and Stand Age on Root Nutrient Acquisition and Leaf Nutrient Resorption of *Metasequoia glyptostroboides*

Rui Song[1,2], Ran Tong[2], Hui Zhang[3], G. Geoff Wang[4], Tonggui Wu[2] and Xiuqing Yang[1]**

[1] College of Forestry, Shanxi Agricultural University, Taigu, China, [2] East China Coastal Forest Ecosystem Long-term Research Station, Research Institute of Subtropical Forestry, Chinese Academy of Forestry, Hangzhou, China, [3] Forestry and Biotechnology College, Zhejiang A&F University, Hangzhou, China, [4] Department of Forestry and Environmental Conservation, Clemson University, Clemson, SC, United States

OPEN ACCESS

Edited by:
Runguo Zang,
Chinese Academy of Forestry, China

Reviewed by:
Fu-Sheng Chen,
Jiangxi Agricultural University, China
Liang Kou,
Institute of Geographic Sciences and Natural Resources Research (CAS), China

***Correspondence:**
Tonggui Wu
wutonggui@caf.ac.cn
Xiuqing Yang
xiuqingy2002@126.com

Specialty section:
This article was submitted to Functional Plant Ecology, a section of the journal Frontiers in Plant Science

Received: 27 March 2022
Accepted: 25 April 2022
Published: 11 May 2022

Citation:
Song R, Tong R, Zhang H, Wang GG, Wu T and Yang X (2022) Effects of Long-Term Fertilization and Stand Age on Root Nutrient Acquisition and Leaf Nutrient Resorption of Metasequoia glyptostroboides. Front. Plant Sci. 13:905358. doi: 10.3389/fpls.2022.905358

The plant nutrient acquisition strategies are diverse, such as root nutrient acquisition and leaf nutrient resorption, playing important roles in driving soil processes, vegetation performance as well as ecosystem nutrient cycling. However, it is still in a debate whether there is a synergy or tradeoff between above- and below-ground nutrient acquisition strategy under nitrogen (N) and phosphorus (P) addition, or with stand age. Herein, this study investigated the responses of root-soil accumulation factor (*RSAF*) and leaf nutrient resorption efficiency (*NuRE*) to long-term N and P fertilization, and further explored the trade-off between them in *Metasequoia glyptostroboides* plantations with different stand age. Results showed that under N fertilization in young plantations, leaf N resorption efficiency (*NRE*) increased, and root-soil accumulation factor for P (*RSAF-P*) decreased. For young forests under P fertilization, the *NRE* increased whereas *RSAF-P* decreased. For middle-aged forests under P fertilization, the *NRE* and leaf P resorption efficiency (*PRE*) increased and the *RSAF-P* decreased. Under P fertilization in young and middle-aged plantations, *PRE* had a significant positive correlation with *RSAF-P*. Under N fertilization in young plantations, *NRE* was significantly positive correlated with root-soil accumulation factor for N (*RSAF-N*). The covariance-based structural equation modeling (CB-SEM) analysis indicated that stand age had positive effects on *PRE* whether under N or P fertilization, as well as on *RSAF-P* under N fertilization, whereas had no effects on the *NRE* or *RSAF-N.* Overall, our results can shed light on the nutrient acquisition strategies of *M. glyptostroboides* plantations under future environmental changes and the results could be applied to the nutrient management practices.

Keywords: nutrient acquisition strategies, N and P fertilization, stand age, leaf, root

INTRODUCTION

The plant nutrient acquisition strategies cannot be underestimated in forest ecosystems, given that the plants usually do not have sufficient amounts of biologically available nutrients to support growth, survival, and reproduction, especially in nutrient-impoverished habitats (Abrahão et al., 2018; Wang et al., 2020). It has been always considered that roots are the major tissue for the plant to acquire nutrients, and root nutrient acquisition strategies play a decisive role in the maintenance of forest ecosystem health and vitality (Andersen et al., 2017; Ma et al., 2018; Li et al., 2019). In recent decades, some other plant nutrient acquisition strategies have also been proposed, such as leaf nutrient resorption proficiency and efficiency (Reed et al., 2012; He et al., 2020; Xu et al., 2020). Naturally, whether these plant nutrient acquisition strategies co-vary or exhibit coordinated responses to a changing environment has drawn great attention from ecologists.

Allocation of effort toward nutrient capture and resorption depends on both the environment nutrient availability and the cost involved in these processes (Wright and Westoby, 2003; Wang et al., 2014a). In barren soils, plants should bear traits that prioritize conservation over active absorption of resources, whereas the opposite was expected in nutrient-rich soils. Specifically, since nutrients derived from capture become less expensive than those from resorption as soil nutrient availability increases, the root capture strategy would be more favored than leaf resorption (Wright and Westoby, 2003; Kou et al., 2017). Inversely, species from nutrient-impoverished habitats also reduce nutrient losses by remobilizing a large fraction of the nutrients before senesced organ shedding (high remobilization efficiency), and shedding leaves with very low final nutrient concentrations (Killingbeck, 1996; Kobe et al., 2005; Hayes et al., 2014). Nevertheless, in cases of consistent environmental nutrient availability, the costs of the different plant nutrient acquisition strategies have not been effectively evaluated.

Increasing anthropogenic nitrogen (N) and phosphorus (P) deposition has enhanced N and P availability in many forest ecosystems, respectively, providing ideal venues for the studies of the trade-off relationships of plant nutrient acquisition strategies. It is well known that plants can maintain high nutrients level under nutrient enrichment through increasing above-ground nutrient conservation or improving below-ground nutrient uptake (Deng et al., 2016; Hofmann et al., 2016). Several studies showed the trade-off relationships between root nutrient acquisition and leaf nutrient resorption while only considering these two mechanisms (Deng et al., 2016; Kou et al., 2017). In contrast, other studies found the synergy relationship between these two mechanisms, and emphasized that only adopting above-ground nutrient conservation of below-ground nutrient uptake may not be applicative (Ushio et al., 2015; Hofmann et al., 2016).

The corresponding alterations in tree nutrient capture capacity during forest stand development had been widely demonstrated (Brant and Chen, 2015; Chen and Chen, 2022). For instance, the NRE rose and then dropped, and the PRE increased with stand age in *Medicago sativa*, which was closely related to the nutrient limitation of plant growth (Wang et al., 2014b). As trees had different root physiology and exudation patterns at different ages, their root nutrient capture capacity exhibited significant divergence (Liu et al., 2018). Yet, whether the patterns of the tree nutrient capture with different stand ages would alter under nutrient addition remained unclear.

As each mechanism demands distinct levels of resource investments, as well as its potential consequences for ecosystem functions, it is critical to understand how plants adjust above-ground conservation and below-ground uptake to alleviate N and P deficiency as stand development. Taken together, it is generally believed that a trade-off mechanism generally existed between the leaf nutrient resorption and the root acquisition strategies whether in the cases of sufficient or deficient nutrients supplies. In this study, we conducted N and P fertilization experiments to explore the effects of different gradient N and P fertilization on leaf nutrient resorption efficiency (*NuRE*) and root-soil accumulation factor (*RSAF*) in *M. glyptostroboides* plantations with different stand ages. Specifically, we aimed to: (1) describe the change trends of *NuRE* and *RSAF* with the increase of nutrient availability among nutrient fertilization types and along stand development; (2) explore the potential relationships between *NuRE* and *RSAF* under environmental changes.

MATERIALS AND METHODS

Study Site

The study was conducted in Dongtai Forest Farm (121° 45′E, 33° 42′N), a site located in the central coast of the Jiangsu Province, China. The climate of the study site is that of the monsoon subtropical moist marine climate zone. The altitude is 0–4 m, the annual average temperature, frost-free period, precipitation, and sunshine duration is 14.5°c, 220 days, 1055.7 mm, and 2130.5 h. The soil is alkaline sandy soil, which was more infertile than yellow-earth soil in the natural range of *M. glyptostroboides*. The study site was the pioneer area to plant the *M. glyptostroboides* in coastal China (**Figure 1**).

Experiment Design and Sample Collection

N and P experiment was initiated in 2014 of different ages (young forest: 6-year old; middle-age forests: 24-year old) with three 300 m × 100 m plots of *M. glyptostroboides* plantations in Dongtai forest farm, and ten 20 m × 30 m plots of each plot were selected for completely random block N and P addition experiments, of which 5 plots were used for N addition treatments and 5 plots for P addition treatments in each age class. Each plot was separated by a buffer zone. The basic information is shown in **Table 1**. N and P addition gradients setting: set the N addition treatments as CK, 0.8, 2.4, 4.0, and 6.0 mol·m^{-2}, respectively, and the fertilization was added in the form of urea [$CO(NH_2)_2$]; P fertilization treatment was set as CK, 0.05, 0.2, 0.6, and 1.0 mol·m^{-2}, respectively, and fertilization was added in the form of superphosphate [$Ca(H_2PO_4)_2$]. The fertilization gradients were based on a pretest and a previous seedling pot

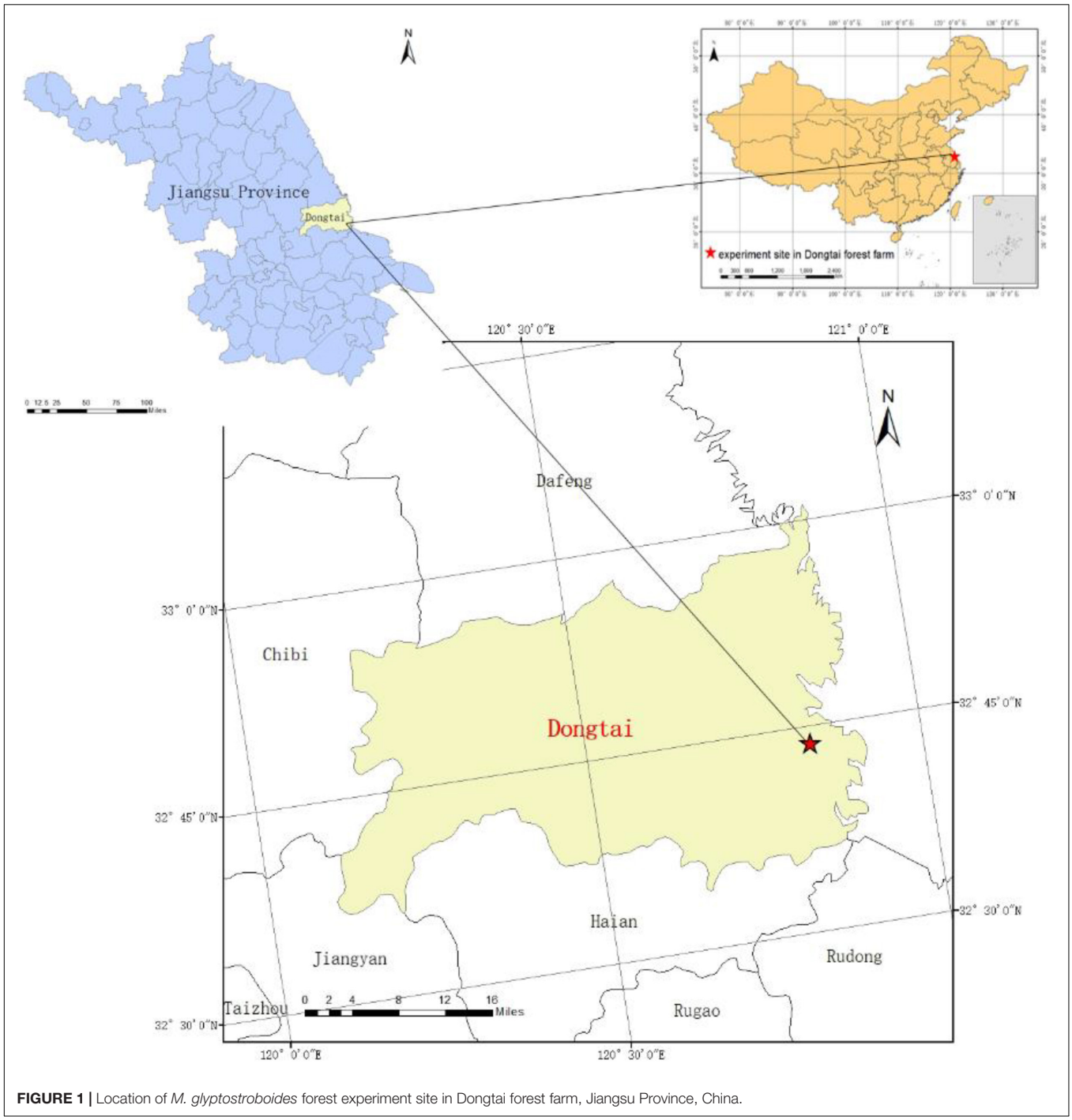

FIGURE 1 | Location of *M. glyptostroboides* forest experiment site in Dongtai forest farm, Jiangsu Province, China.

study (Wang et al., 2018). Fertilization dosage and time: the first addition time is from the end of March to the beginning of April, 60% of the total amount of fertilization added; the second addition time is in the middle of June, 40% of the total amount of fertilization added. In addition, N and P were applied to the field directly every year.

Three average trees in each plot were selected for collecting leaves, branches, and roots. Fully expanded leaves and branches from the upper and outer part of tree crowns were sampled. The fine roots (<2 mm) of each selected individual were sampled through the careful removal of the soil surrounding the roots. Five soil cores (2.5 cm in diameter) per plot were randomly collected from 0 to 10 cm depth following the removal of understory plants and surface litter, and thoroughly mixed to homogenize a sample. Leaves, branches, roots, and soils were sampled in August 2018 (the end of the growing season). Five litter traps (1.0 m^2, made of nylon mesh) per plot were fixed 1.0 m above the ground. Leaf litter was collected in late November 2018.

TABLE 1 | General characteristics of the young and middle-aged *M. glyptostroboides* stands.

Basic properties	Parameter	Young plantations	Middle-aged plantations
Stand structure	Average height (m)	10.33 ± 2.21	15.91 ± 2.20
	DBH (cm)	17.8 ± 0.86	27.75 ± 0.84
	DBH (growth)	4.8 ± 1.52	2.39 ± 0.69
	Density (tree/ hm^2)	417	417
	Crown width (m)	4.61 ± 0.65	5.01 ± 0.52
Soil physical properties	Water content (%)	0.22 ± 0.02	0.32 ± 0.03
	Total porosity (%)	44.09 ± 2.81	46.49 ± 2.39
	Capillary porosity (%)	42.46 ± 3.68	45.75 ± 2.37
Soil chemical properties	Organic C content (g kg^{-1})	8.19 ± 0.38	13.18 ± 4.09
	Total N content (g kg^{-1})	0.71 ± 0.01	0.94 ± 0.08
	Available N content (mg kg^{-1})	90.90 ± 4.27	132.67 ± 12.66
	Total P content (g kg^{-1})	0.85 ± 0.03	0.68 ± 0.10
	Available P content (mg kg^{-1})	14.27 ± 3.91	2.85 ± 0.15

The DBH (growth) is the DBH increasement during 2015–2019 year.

Chemical Measurements

All plant organs samples were dried in the oven at 105°C for 2 h, then dried at 75°C to constant weight, crushed with a mechanical grinder, and the samples were sieved to determine nutrient content. The C and N concentrations were determined for each sample using an autoanalyzer (Kjeltec 2300 Analyzer Unit, Foss, Sweden). P concentration was determined using the standard ammonium molybdate method (reference code GBW08513; General Administration of Quality Supervision, PRC).

Soil samples were air-dried after being sieved (2-mm mesh). Soil pH was determined by the potentiometric method, soil organic carbon (SOC) was determined with wet oxidation by sulfuric acid and potassium dichromate and back titration with ferrous sulfate. The total N concentration was determined by Kjeldahl method, Hydrolysable N concentration was determined by titration with a dilute solution of H_2SO_4 after extraction with a mixture of ferrous sulfate and sodium hydroxide. The total P and available P concentrations were determined with a molybdate blue colorimeter after extraction with 0.5 M sodium bicarbonate (Zhang et al., 2018).

Data Analysis

Nutrient resorption efficiency (NuRE) was defined as the proportional withdrawal of a nutrient during senescence and was calculated as follows:

$$NuRE = \left(1 - \frac{Nu_{senescenced}}{Nu_{green}} \times MLCF\right) \times 100\%$$

Where *NuRE* is N or P resorption efficiency, $Nu_{senescenced}$ and Nu_{green} represent N or P concentration (mass-based) in leaf and litter, respectively, and *MLCF* is mass loss correction factor with a value of 0.745 for deciduous coniferous species (Vergutz et al., 2012).

Root-soil accumulation factor (*RSAF*) for N and P were defined to describe the root N or P acquisition (Kou et al., 2017), as follows:

$$RSAF = \frac{Nu_{root}}{Nu_{soil}}$$

Where *RSAF* is root N or P accumulation factor, Nu_{root} and Nu_{soil} represent N or P concentration (mass-based) in absorptive fine root and soil, respectively.

Data analysis using the single factor variance (One-way ANOVA) analysis of the different fertilization gradients of plant organs stoichiometric characteristics, nutrient acquisition, nutrient recycling, and nutrient absorption efficiency under different stand ages, respectively, the influence of significance level set as $P = 0.05$, with minimal process significantly difference (LSD) determined the level of significance in SPSS 23.0 (SPSS Inc., Chicago, IL, United States). The covariance-based structural equation modeling (CB-SEM) analysis was conducted in SPSS Amos 26 (SPSS Inc., Chicago, IL, United States) to explore the effects of stand age on *NuRE* and *RSAF* under N and P fertilization. All data were tested to fulfill the assumptions of normality and homogeneity of variance, and transformations were carried out when necessary. Figures were plotted using Origin 2018 (Origin Lab Corporation, Northampton, MA, United States).

RESULTS

Effect of Nitrogen and Phosphorus Fertilization on Leaf Nutrient Resorption Efficiency and Root-Soil Accumulation Factor

Under N fertilization in young plantations, the *NRE* and *PRE* of CK treatment were 31.02 and 64.25%, respectively. The *NRE* remarkably increased while *PRE* kept relatively stable along N fertilization gradients (**Figure 2A**). The *RSAF-N* and *RSAF-P* of CK treatment were 131.75 and 198.49, respectively. The *RSAF-P* remarkably decreased while *RSAF-N* kept relatively stable along N fertilization gradients (**Figure 2B**).

Under P fertilization in young plantations, the *NRE* and *PRE* of CK treatment were 32.17 and 68.31%, respectively. The *NRE* remarkably increased, while PRE kept relatively stable along P fertilization gradients (**Figure 2C**). The *RSAF-N* and *RSAF-P* of CK treatment were 108.38 and 189.6, respectively. The *RSAF-N* and *RSAF-P* remarkably increased and decreased along P fertilization gradients (**Figure 2D**).

Under N fertilization in middle-aged plantations, the *NRE* and *PRE* of CK treatment were 45.02 and 54.24%, respectively. The *NRE* and *PRE* both kept relatively stable along N fertilization gradients (**Figure 3A**). The *RSAF-N* and *RSAF-P* of CK treatment were 82.59 and 126.71, respectively. The *RSAF-N* and *RSAF-P* both kept relatively stable along N fertilization gradients (**Figure 3B**).

Under P fertilization in middle-aged plantations, the *NRE* and *PRE* of CK treatment were 39.07 and 46.33%, respectively. The *NRE* and *PRE* both remarkably increased remarkably along P fertilization gradients (**Figure 3C**). The *RSAF-N* and *RSAF-P* of CK treatment were 83.64 and 121.24, respectively. The *RSAF-N* and *RSAF-P* both kept relatively stable along P fertilization gradients (**Figure 3D**).

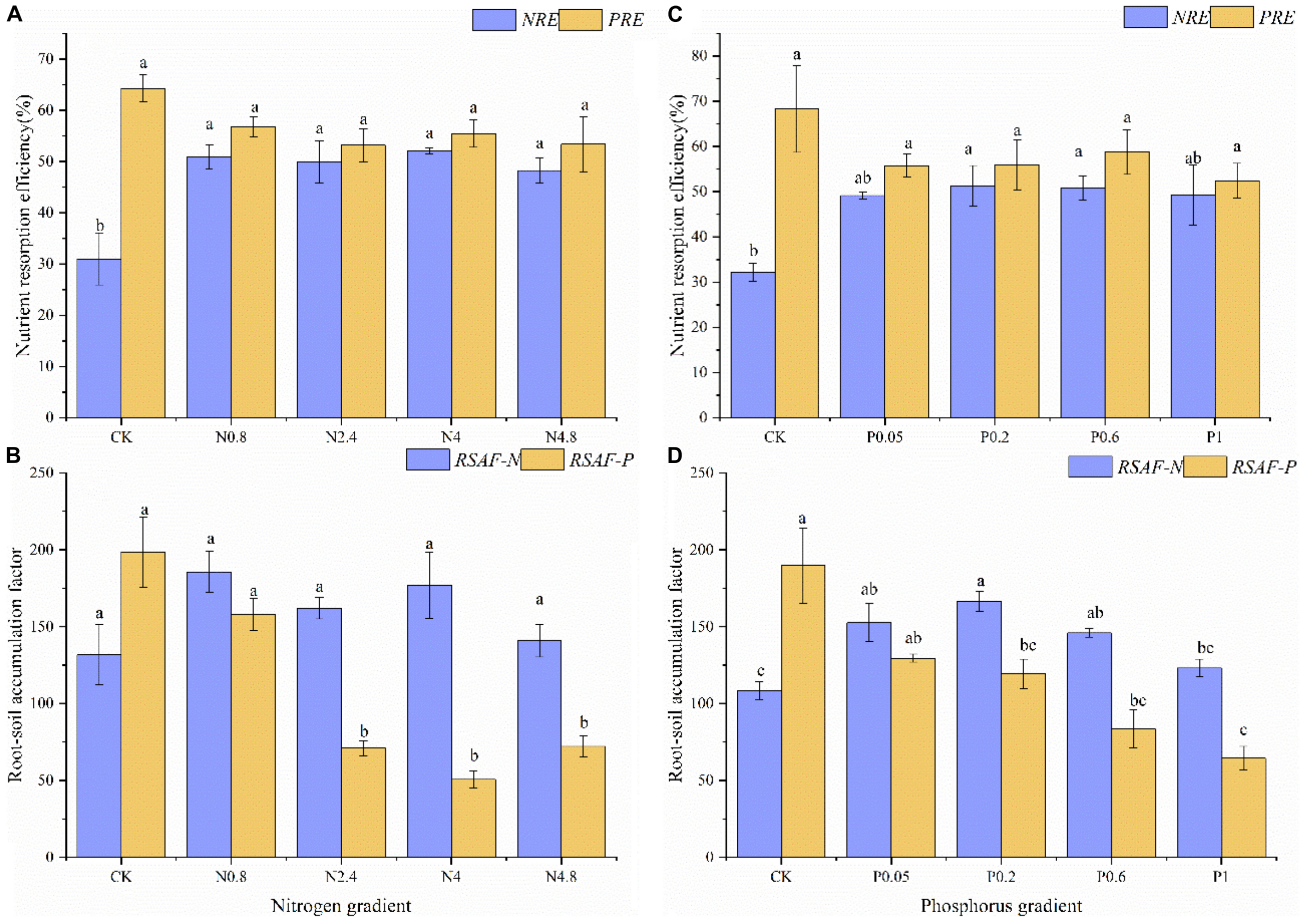

FIGURE 2 | Effects of N fertilization (CK: control, N0.8: 0.8 mol N, N2.4: 2.4 mol N, N4: 4 mol N, N4.8: 4.8 mol N) on *NuRE* **(A)** and *RSAF* **(B)** in *M. glyptostroboides* forests of young forests. Values are presented as mean ± S.E. (n = 3). Effects of P fertilization (CK: control, P0.05: 0.05 mol P, P0.2: 0.2 mol P, P0.6: 0.6 mol P, P1: 1 mol P) on *NuRE* **(C)** and *RSAF* **(D)** in *M. glyptostroboides* forests of young forests. Values are presented as mean ± S.E. (n = 3). Different lowercase letters in the bars and above the bars indicated significant difference ($P < 0.05$), respectively.

Effect of Nitrogen and Phosphorus Fertilization on Leaf N Resorption Efficiency/leaf P Resorption Efficiency and Root-Soil Accumulation Factor for N/Root-Soil Accumulation Factor for P

The *NRE/PRE* of CK treatment was 0.49 and 0.83 in young and middle-aged plantations under N fertilization, respectively. The *NRE/PRE* for young plantation increased significantly under N fertilization, while the *NRE/PRE* for middle-aged plantations kept relatively stable along N fertilization gradients (**Figure 4A**). The *RSAF-N/RSAF-P* of CK treatment were 0.69 and 0.68 in young and middle-aged plantations under N fertilization, respectively. The *RSAF-N/RSAF-P* for young plantation increased significantly under N fertilization, while the *RSAF-N/RSAF-P* in middle-aged plantations kept relatively stable along N fertilization gradients (**Figure 4B**).

The *NRE/PRE* of CK treatment was 0.50 and 0.88 in young and middle-aged plantations under P fertilization, respectively. The *NRE/PRE* in young and middle-aged plantations both kept relatively stable along P fertilization gradients (**Figure 4C**). The *RSAF-N/RSAF-P* of CK treatment were 0.59 and 0.70 in young and middle-aged plantations under P fertilization, respectively. The *RSAF-N/RSAF-P* remarkably increased under P fertilization, while the *RSAF-N/RSAF-P* in middle-aged plantations kept relatively stable along P fertilization gradients (**Figure 4D**).

The Relationships Between Leaf Nutrient Resorption Efficiency and Root-Soil Accumulation Factor Under Nitrogen and Phosphorus Fertilization

Under N fertilization, *NRE* showed no association with *RSAF-N*, while *PRE* was significantly positive correlated with *RSAF-P* in young and middle-aged plantations (**Figures 5A,C**). Under P fertilization, *NRE* was significantly positively correlated with *RSAF* for N in young plantation, whereas no significant relationships were found between *NRE* and *RSAF-N* in middle-aged plantation, as well as *PRE* and *RSAF-P* in both young and middle-aged plantations (**Figures 5B,D**).

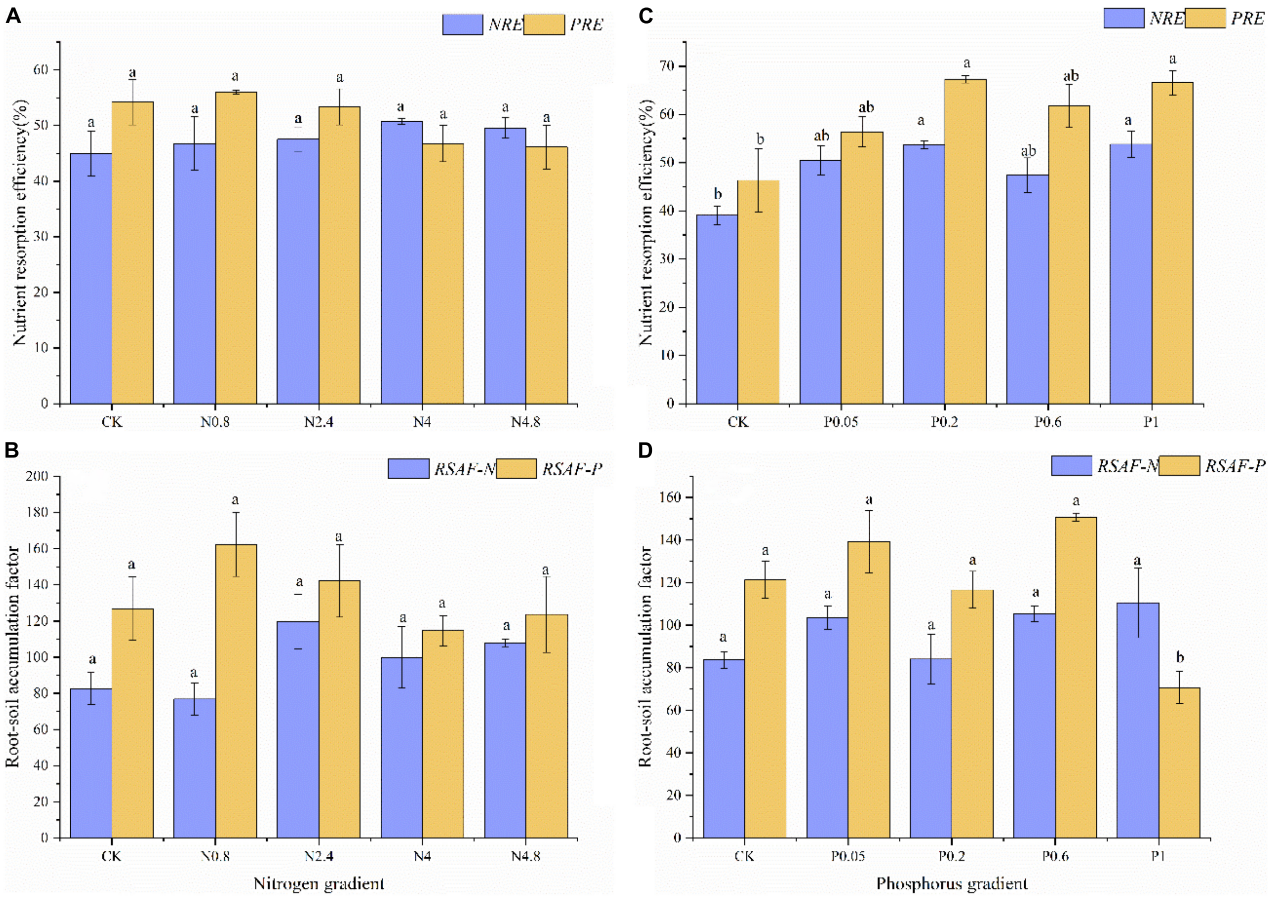

FIGURE 3 | Effects of N fertilization (CK: control, N0.8: 0.8 mol N, N2.4: 2.4 mol N, N4: 4 mol N, N4.8: 4.8 mol N) on *NuRE* **(A)** and *RSAF* **(B)** in *M. glyptostroboides* forests of middle-aged forests. Values are presented as mean ± S.E. (n = 3). Effects of P fertilization (CK: control, P0.05: 0.05 mol P, P0.2: 0.2 mol P, P0.6: 0.6 mol P, P1: 1 mol P) on *NuRE* **(C)** and *RSAF* **(D)** in *M. glyptostroboides* forests of middle-aged forests. Values are presented as mean ± S.E. (n = 3). Different lowercase letters in the bars and above the bars indicated significant difference ($P < 0.05$), respectively.

The Direct and Indirect Effect of Nutrient Fertilization and Stand Age on Leaf Nutrient Resorption Efficiency and Root-Soil Accumulation Factor

The covariance-based structural equation modeling (CB-SEM) analysis indicted that N fertilization and stand age together explained 84.3% of variations in *NRE* and 73.5% of variations in *PRE* (**Figure 6A**). N fertilization had a positive indirect effect on *NRE via* leaf N, and a negative indirect effect on *PRE* through leaf P and soil pH. Stand age had a positive direct effect on *PRE via* soil pH, and a negative indirect effect *via* soil total N and leaf P. N fertilization and stand age together explained 62.8% of variations in *RSAF-N* and 56.0% of variations in *RSAF-P* (**Figure 6B**). N fertilization and stand age had a negative and positive direct effect on *RSAF-P*, respectively. N fertilization had a positive indirect effect on *RSAF-N via* fine root N. Stand age had a negative indirect effect on *RSAF-N via* soil N:P.

P fertilization and stand age together explained 60.9% of variations in PRE (**Figure 6C**). Stand age had a positive direct effect on PRE, and P fertilization had a positive indirect effect on PRE *via* leaf P. P fertilization and stand age together explained 78.1% of variations in *RSAF-N*, and 44.4% of variations in *RSAF-P* (**Figure 6D**). P fertilization had a negative direct effect on *RSAF-P*, and stand age had a negative direct effect on *RSAF-N*. Stand age had a negative indirect effect on *RSAF-N via* fine root N and P.

DISCUSSION

Effects of Nitrogen Fertilization on Plant Nutrient Acquisition

Bioavailable N is increasing due to human activity, which greatly alters nutrient availability for plant growth and affects fundamental ecological processes (Wang et al., 2019a). Nutrient resorption from senescing leaves is one of the plants' essential nutrient conservation strategies, accounting for a large property of the nutrient demand for plants (Aerts, 1996). In this study, N fertilization increased leaf N concentration in young plantation, which was in line with the observations from the global-scale meta-analysis (Ostertag and DiManno, 2016;

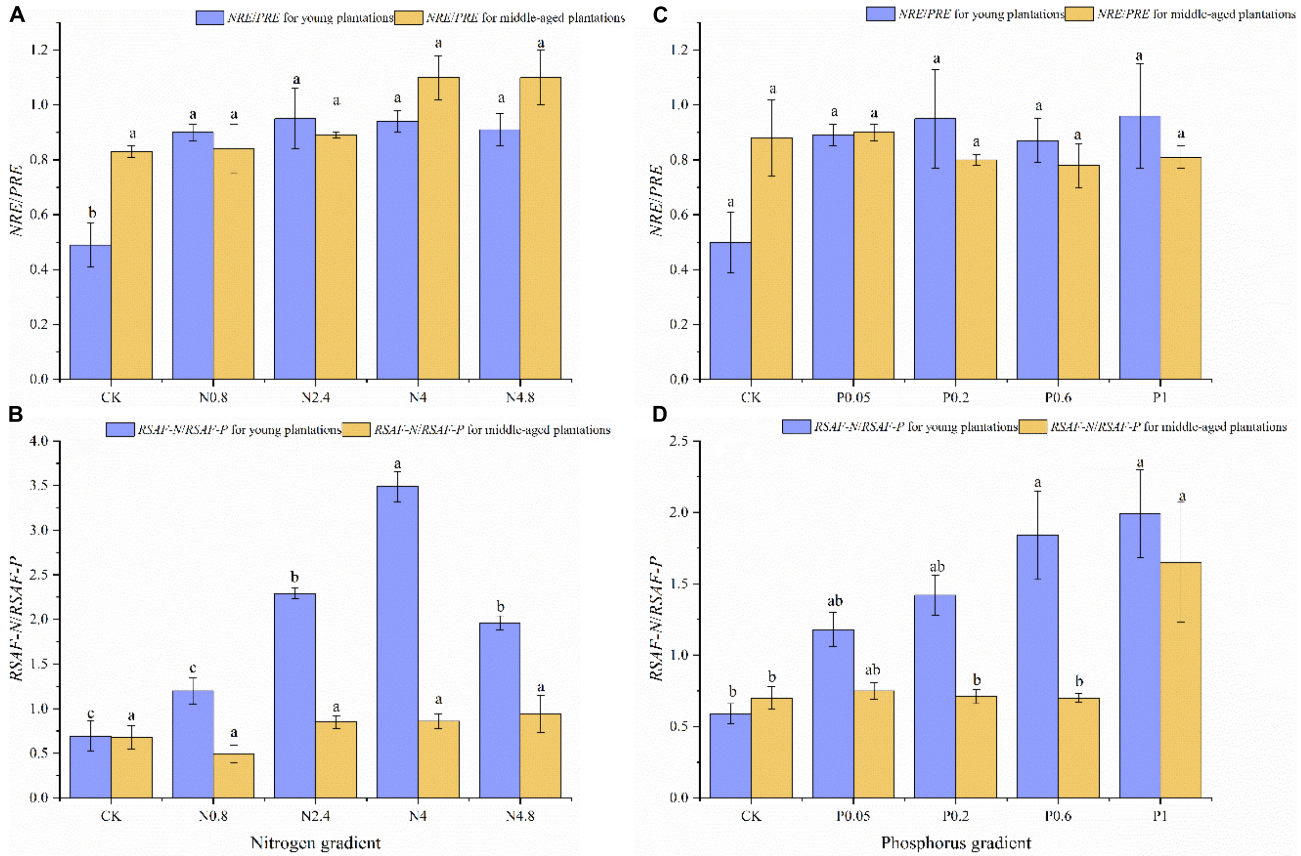

FIGURE 4 | Effects of N fertilization (CK: control, N0.8: 0.8 mol N, N2.4: 2.4 mol N, N4: 4 mol N, N4.8: 4.8 mol N) on *NRE/PRE* **(A)** and *RSAF-N/RSAF-P* **(B)** in *M. glyptostroboides* plantations of different stand ages. Values are presented as mean ± S.E. (n = 3). Effects of P fertilization (CK: control, P0.05: 0.05 mol P, P0.2: 0.2 mol P, P0.6: 0.6 mol P, P1: 1 mol P) on *NRE/PRE* **(C)** and *RSAF-N/RSAF/P* **(D)** in *M. glyptostroboides* plantations of different stand ages. Different lowercase letters in the bars and above the bars indicated significant difference ($P < 0.05$), respectively.

Sardans et al., 2017). However, in contrast to most previous studies, we found a significant increase in *NRE* for young plantation and no significant changes for middle-aged plantation under N fertilization (Yuan and Chen, 2015; Lu et al., 2019; Zhao et al., 2020). Our study also found that leaf litter N concentration kept relatively stable under N fertilization whether in young and middle-aged plantations (Wen et al., 2021). Thus, considering the violent strong natural and human-activities disturbances, we deemed that nutrient return of leaf litter to the soil, i.e., litter decomposition, might not be so essential, especially in the coastal man-made forests. Moreover, the *RSAF-P* decreased remarkably under N fertilization, which was not consistent with Kou et al. (2017), who reported that the *RSAF-P* kept relatively stable in *Pinus elliottii* plantations.

The *NRE*/*PRE* in leaf was recently developed to indicate the theoretical framework of N or P limitation for plant growth, which could be applied to quantitatively evaluate the spatial characteristics and key influencing factors of N and P limitation in the terrestrial ecosystems (Du et al., 2020). In this study, the *NRE/PRE* was always less than 1 under N fertilization, indicating that the plant growth was mostly limited by N. This result was consistent with one of our previous studies, which found N was the main limiting factor for *M. glyptostroboides* growth combining with the concept of stoichiometric homeostasis (Wang et al., 2019b). Moreover, the *NRE/PRE* of young plantation increased along the gradient of N fertilization, demonstrating that the N limitation got relieved to some extent (Li et al., 2016; Du et al., 2020).

It was always expected that plant tissues exhibited trade-offs relationships in water and nutrient acquisition, which is of great significance for plant stoichiometric homeostasis and the balance of matters and energy in the terrestrial ecosystems. While these trade-off relationships became unpredictable under the background of global change. In this study, we observed significant and positive associations between *PRE* and *RSAF-P* in both young and middle-aged plantations under N fertilization, which was not in line with Kou et al. (2017) for *Pinus elliottii* plantations. However, most of the trade-off relationships between leaf nutrient resorption and fine root nutrient acquisition had been lost under N fertilization. Therefore, we referred that the changes in environmental nutrient conditions might lead to the absence of trade-off relationships between under- and above-ground plant tissues.

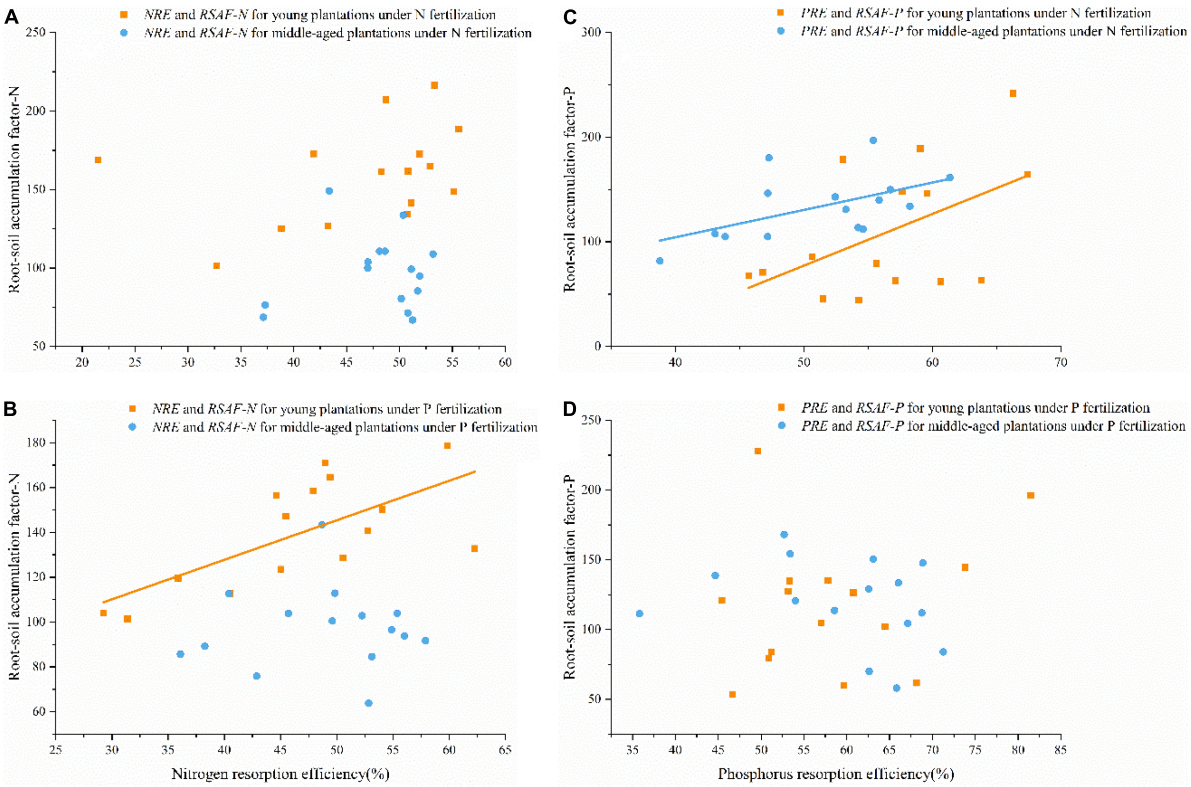

FIGURE 5 | (A) Relationships between *NRE* and *RSAF-N* under N fertilization in young and middle-aged plantations (no significance). **(B)** Relationships between *NRE* and *RSAF-N* under P fertilization in young (R^2 = 0.468, $P < 0.01$) and middle-aged (no significance) plantations. **(C)** Relationships between *PRE* and *RSAF-P* under N fertilization in young (R^2 = 0.266, $P < 0.05$) and middle-aged plantations (R^2 = 0.291, $P < 0.05$). **(D)** Relationships between *PRE* and *RSAF-P* under P fertilization in young and middle-aged plantations (no significance).

Effects of Phosphorus Fertilization on Plant Nutrient Acquisition

Atmospheric P deposition brought by agricultural activities, dust transport, and combustion source emissions had greatly altered the soil P availability that greatly influenced plant growth (Widdig et al., 2019; Pan et al., 2021). Generally, the availability of one nutrient would inevitably affect relative availability of other nutrients, particularly in the status of nutrient deficiency or imbalance (Kou et al., 2017). In the current study, the *NRE* of young and middle-aged plantation increased along the gradient of P fertilization, which was also reported in Yan et al. (2015). Furthermore, the *RSAF-N*/*RSAF-P* increased remarkably whether under P fertilization in young plantation, and kept relatively stable in middle-aged plantation. This finding was also in line with the above observations for above-ground plant tissues. Therefore, fine root nutrient acquisition might play an important role in indicating the nutrient limitation of plant growth. Meanwhile, we observed that the *RSAF-P* decreased significantly under P fertilization whether in young or middle-aged plantation, which might be attributed to the fact that the fine root nutrient acquisition existed some delayed effects. Meanwhile, some limitations appeared in this study such as considering the fine roots with a diameter less than 2 mm, ignoring the high morphological and functional heterogeneity in fine roots (Pregitzer et al., 2002; Kou et al., 2018), which might lead to an underestimate of the *RSAF*.

Notably, the *NRE* and *RSAF-N* in young plantation under P fertilization, were significantly correlated with each other, even exhibiting synergy relationships to some extent. These findings were also observed in previous research, which emphasized that only adopting aboveground N and P conservation or belowground N and P uptake might not be accurate (Ushio et al., 2015; Hofmann et al., 2016). Therefore, we concluded that the synergistic relationship for P acquisition might be explained by the two following reasons. Firstly, the relationships between fine root nutrient acquisition and leaf nutrient resorption were indeed positively related, whereas there might exist some other mechanisms which could balance these two nutrient conversation mechanisms. Secondly, there was no trade-off evolutionary mechanism between leaves and roots, which might leading to the consistent responses of leaf nutrient resorption and fine root nutrient acquisition to environment changes by chance.

Stand Age Mediates Fertilization Effects on Plant Nutrient Acquisition

Trees at different growth stages have great differences in physiological processes and nutrition requirements, resulting

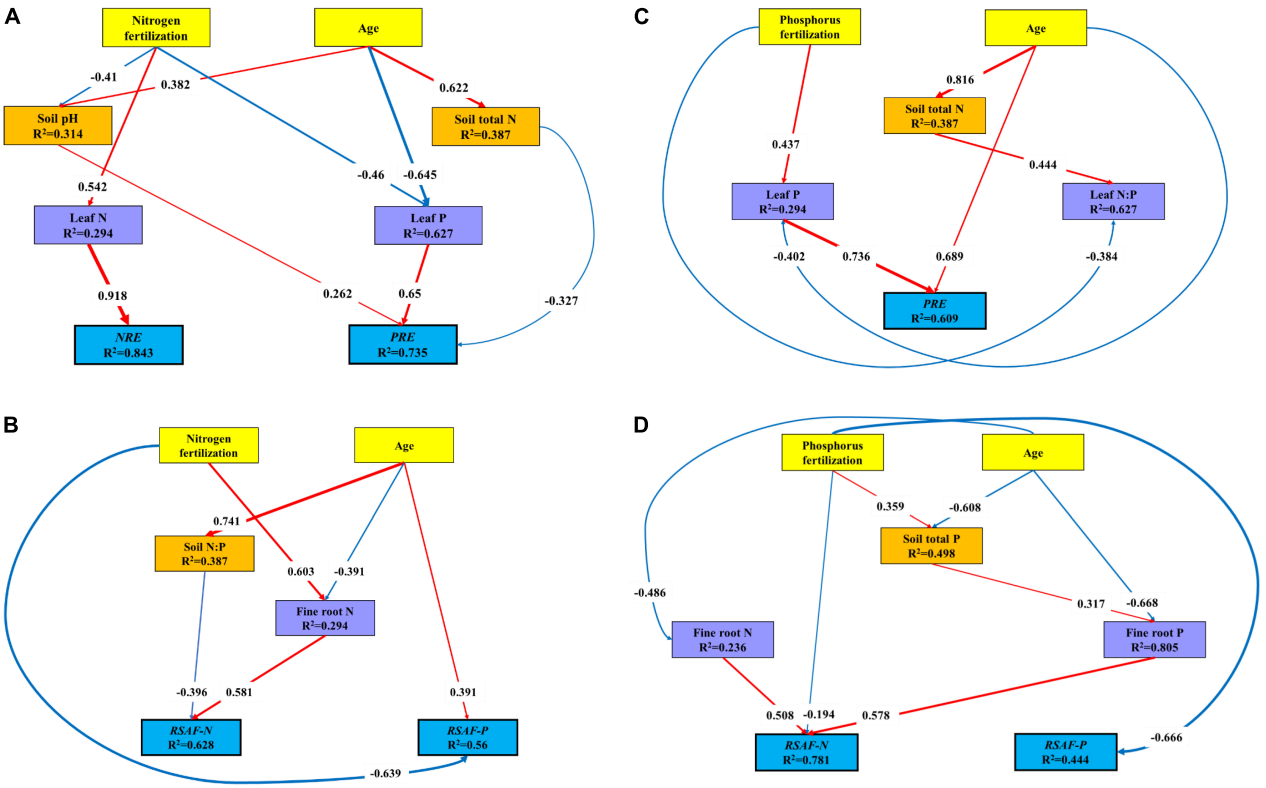

FIGURE 6 | Covariance-based structural equation modeling (CB-SEM) analysis of the direct and indirect effects among variables. All the paths in the model were significant, and the standardized coefficients were listed on them. The thickness of the solid arrows reflected the magnitude of the standardized SEM coefficients, the red solid line represented the positive effect while the blue solid line represented the negative effect. **(A)** Results of model fitting: X^2 = 13.51; Probability level = 0.563; df = 15; GFI = 0.9; RMSEA = 0.000; AIC = 55.51. **(B)** Results of model fitting: X^2 = 7.116; Probability level = 0.524; df = 8; GFI = 0.927; RMSEA = 0.000; AIC = 33.116. **(C)** Results of model fitting: X^2 = 5.915; Probability level = 0.55; df = 7; GFI = 0.938; RMSEA = 0.000; AIC = 33.915. **(D)** Results of model fitting: X^2 = 10.519; Probability level = 0.484; df = 11; GFI = 0.918; RMSEA = 0.000; AIC = 44.519.

in changes of nutrient acquisition strategies along an age sequence (Sun et al., 2016; Zhang et al., 2018). However, most previous studies considered the stand age effects on nutrient acquisition strategies in natural conditions, while little was known about its combination with environmental changes. In the current study, we used SEM analysis to explore the direct and indirect effects of stand age on *NuRE* and *RSAF* under N and P fertilization. Generally, stand age had positive effects on *PRE* whether under N or P fertilization, as well as on *RSAF-P* under N fertilization, which indicated that plant intended to resorb more P from senescing leaves and soil by fine root to deal with strengthening P-limitation during stand development (Zhang et al., 2018; Wang et al., 2019b). Thus, these findings confirmed that stand age mediated the fertilization effects on nutrient acquisition strategies.

CONCLUSION

This study evaluates how N and P fertilization affects nutrient acquisition strategies in *M. glyptostroboides* plantations with different stand ages of the coastal in China. We found that N fertilization increased *NRE*, while decreased *RSAF-P* in young plantations. P fertilization increased *NRE* and *PRE*, while decreased *RSAF-P* in middle-aged plantations. Little synergetic relationships were observed between *NuRE* and *RSAF* whether under N and P fertilization, as well as in young and middle-aged plantations. Stand age had positive effects on *PRE* and *RSAF-P*, whereas had no effects on the *NRE* or *RSAF-N*. These findings provided new insights into the predictions for the facts that how variations in nutrient availability induced by the global change will influence plant nutrient uptake and nutrient conservation strategies.

Please confirm that the Data Availability statement is accurate. Note that we have used the statement provided at Submission. If this is not the latest version, please let us know.Note that we have used the statement provided at Submission. If this is not the latest version, please let us know.

DATA AVAILABILITY STATEMENT

The original contributions presented in the study are included in the article/supplementary material,

further inquiries can be directed to the corresponding author/s.

AUTHOR CONTRIBUTIONS

TW and XY designed the project and participated in the manuscript. RS, RT, and GW wrote and revised the manuscript. RS and HZ analyzed the data and constructed the database. RS collected the samples. All authors revised and approved the manuscript.

FUNDING

This work was supported by the Fundamental Research Funds for National Natural Science Foundation of China (31770756).

REFERENCES

Abrahão, A., Ryan, M. H., Laliberté, E., Oliveira, R. S., and Lambers, H. (2018). Phosphorus- and nitrogen-acquisition strategies in two Bossiaea species (Fabaceae) along retrogressive soil chronosequences in south-western Australia. *Physiol. Plant.* 163, 323–343. doi: 10.1111/ppl.12704

Aerts, R. (1996). Nutrient resorption from senescing leaves of perennials: are there general patterns? *J. Ecol.* 84, 597–608. doi: 10.2307/2261481

Andersen, K. M., Mayor, J. R., and Turner, B. L. (2017). Plasticity in nitrogen uptake among plant species with contrasting nutrient acquisition strategies in a tropical forest. *Ecology* 98, 1388–1398. doi: 10.1002/ecy.1793

Brant, A. N., and Chen, H. Y. (2015). Patterns and mechanisms of nutrient resorption in plants. *Crit. Rev. Plant Sci.* 34, 471–486.

Chen, X., and Chen, H. Y. (2022). Foliar nutrient resorption dynamics of trembling aspen and white birch during secondary succession in the boreal forest of central Canada. *For. Ecol. Manag.* 505:119876.

Deng, M., Liu, L., Sun, Z., Piao, S., Ma, Y., Chen, Y., et al. (2016). Increased phosphate uptake but not resorption alleviates phosphorus deficiency induced by nitrogen deposition in temperate Larix principis-rupprechtii plantations. *New Phytol.* 212, 1019–1029. doi: 10.1111/nph.14083

Du, E., Terrer, C., Pellegrini, A. F., Ahlström, A., van Lissa, C. J., Zhao, X., et al. (2020). Global patterns of terrestrial nitrogen and phosphorus limitation. *Nat. Geosci.* 13, 221–226.

Hayes, P., Turner, B. L., Lambers, H., and Laliberté, E. (2014). Foliar nutrient concentrations and resorption efficiency in plants of contrasting nutrient-acquisition strategies along a 2-million-year dune chronosequence. *J. Ecol.* 102, 396–410. doi: 10.1111/1365-2745.12196

He, M., Yan, Z., Cui, X., Gong, Y., Li, K., and Han, W. (2020). Scaling the leaf nutrient resorption efficiency: nitrogen vs phosphorus in global plants. *Sci. Total Environ.* 729:138920. doi: 10.1016/j.scitotenv.2020.138920

Hofmann, K., Heuck, C., and Spohn, M. (2016). Phosphorus resorption by young beech trees and soil phosphatase activity as dependent on phosphorus availability. *Oecologia* 181, 369–379. doi: 10.1007/s00442-016-3581-x

Killingbeck, K. T. (1996). Nutrients in senesced leaves: keys to the search for potential resorption and resorption proficiency. *Ecology* 77, 1716–1727.

Kobe, R. K., Lepczyk, C. A., and Iyer, M. (2005). Resorption efficiency decreases with increasing green leaf nutrients in a global data set. *Ecology* 86, 2780–2792.

Kou, L., Jiang, L., Fu, X., Dai, X., Wang, H., and Li, S. (2018). Nitrogen deposition increases root production and turnover but slows root decomposition in *Pinus elliottii* plantations. *New Phytol.* 218, 1450–1461.

Kou, L., Wang, H., Gao, W., Chen, W., Yang, H., and Li, S. (2017). Nitrogen addition regulates tradeoff between root capture and foliar resorption of nitrogen and phosphorus in a subtropical pine plantation. *Trees* 31, 77–91. doi: 10.1007/s00468-016-1457-7

Li, L., Gao, X., Li, X., Lin, L., Zeng, F., Gui, D., et al. (2016). Nitrogen (N) and phosphorus (P) resorption of two dominant alpine perennial grass species in response to contrasting N and P availability. *Environ. Exp. Bot.* 127, 37–44. doi: 10.1016/j.envexpbot.2016.03.008

Li, L., McCormack, M. L., Chen, F., Wang, H., Ma, Z., and Guo, D. (2019). Different responses of absorptive roots and arbuscular mycorrhizal fungi to fertilization provide diverse nutrient acquisition strategies in Chinese fir. *For. Ecol. Manag.* 433, 64–72. doi: 10.1016/j.foreco.2018.10.055

Liu, M., Xu, F., Xu, X., Wanek, W., and Yang, X. (2018). Age alters uptake pattern of organic and inorganic nitrogen by rubber trees. *Tree Physiol.* 38, 1685–1693. doi: 10.1093/treephys/tpy031

Lu, J., Yang, M., Liu, M., Lu, Y., and Yang, H. (2019). Nitrogen and phosphorus fertilizations alter nitrogen, phosphorus and potassium resorption of alfalfa in the Loess Plateau of China. *J. Plant Nutr.* 42, 2234–2246. doi: 10.1080/01904167.2019.1648668

Ma, Z., Guo, D., Xu, X., Lu, M., Bardgett, R. D., Eissenstat, D. M., et al. (2018). Evolutionary history resolves global organization of root functional traits. *Nature* 555, 94–97.

Ostertag, R., and DiManno, N. M. (2016). Detecting terrestrial nutrient limitation: a global meta-analysis of foliar nutrient concentrations after fertilization. *Front. Earth Sci.* 4:23. doi: 10.3389/feart.2016.00023

Pan, Y., Liu, B., Cao, J., Liu, J., Tian, S., and Du, E. (2021). Enhanced atmospheric phosphorus deposition in Asia and Europe in the past two decades. *Atmos. Ocean. Sci. Lett.* 14:100051. doi: 10.1016/j.aosl.2021.100051

Pregitzer, K. S., DeForest, J. L., Burton, A. J., Allen, M. F., Ruess, R. W., and Hendrick, R. L. (2002). Fine root architecture of nine North American trees. *Ecol. Monogr.* 72, 293–309. doi: 10.2307/3100029

Reed, S. C., Townsend, A. R., Davidson, E. A., and Cleveland, C. C. (2012). Stoichiometric patterns in foliar nutrient resorption across multiple scales. *New Phytol.* 196, 173–180. doi: 10.1111/j.1469-8137.2012.04249.x

Sardans, J., Grau, O., Chen, H. Y., Janssens, I. A., Ciais, P., Piao, S., et al. (2017). Changes in nutrient concentrations of leaves and roots in response to global change factors. *Glob. Change Biol.* 23, 3849–3856. doi: 10.1111/gcb.13721

Sun, Z., Liu, L., Peng, S., Peñuelas, J., Zeng, H., and Piao, S. (2016). Age-related modulation of the nitrogen tesorption efficiency response to growth requirements and soil nitrogen availability in a temperate pine plantation. *Ecosystems* 19, 698–709. doi: 10.1007/s10021-016-9962-5

Ushio, M., Fujiki, Y., Hidaka, A., and Kitayama, K. (2015). Linkage of root physiology and morphology as an adaptation to soil phosphorus impoverishment in tropical montane forests. *Funct. Ecol.* 29, 1235–1245. doi: 10.1111/1365-2435.12424

Vergutz, L., Manzoni, S., Porporato, A., Novai, R. F., Jackson, R. B. (2012). Global resorption efficiencies and concentrations of carbon and nutrients in leaves of terrestrial plants. *Ecol. Monogr.* 82, 205–220. doi: 10.1890/11-0416.1

Wang, F., Fang, X., Wang, G. G., Mao, R., Lin, X., Wang, H., et al. (2019a). Effects of nutrient addition on foliar phosphorus fractions and their resorption in different-aged leaves of Chinese fir in subtropical China. *Plant Soil* 443, 41–54. doi: 10.1007/s11104-019-04221-8

Wang, J., Wang, J., Wang, L., Zhang, H., Guo, Z., Wang, G. G., et al. (2019b). Does stoichiometric homeostasis differ among tree organs and with tree age? *For. Ecol. Manag.* 453:117637. doi: 10.1016/j.foreco.2019.117637

Wang, J., Wang, J., Guo, W., Li, Y., Wang, G. G., and Wu, T. (2018). Stoichiometric homeostasis, physiology, and growth responses of three tree species to nitrogen and phosphorus addition. *Trees* 32, 1377–1386. doi: 10.1007/s00468-018-1719-7

Wang, L., Li, Y., Duan, Y., Lian, J., Luo, Y., Wang, X., et al. (2020). Effects of nitrogen addition and reproductive effort on nutrient resorption of a sand-fixing shrub. *Front. Plant Sci.* 11:588865. doi: 10.3389/fpls.2020.588865

Wang, M., Murphy, M. T., and Moore, T. R. (2014a). Nutrient resorption of two evergreen shrubs in response to long-term fertilization in a bog. *Oecologia* 174, 365–377. doi: 10.1007/s00442-013-2784-7

Wang, Z., Lu, J., Yang, H., Zhang, X., Luo, C., and Zhao, Y. (2014b). Resorption of nitrogen, phosphorus and potassium from leaves of lucerne stands of different ages. *Plant Soil* 383, 301–312. doi: 10.1007/s11104-014-2166-x

Wen, Y., Tong, R., Zhang, H., Feng, K., Song, R., Wang, G. G., et al. (2021). N addition decreased stand structure diversity in young but increased in middle-aged *Metasequoia glyptostroboides* plantations. *Glob. Ecol. Conserv.* 30:e01803. doi: 10.1016/j.gecco.2021.e01803

Widdig, M., Schleuss, P.-M., Weig, A. R., Guhr, A., Biederman, L. A., Borer, E. T., et al. (2019). Nitrogen and phosphorus additions alter the abundance of phosphorus-solubilizing bacteria and phosphatase activity in grassland soils. *Front. Environ. Sci.* 7:185. doi: 10.3389/fenvs.2019.00185

Wright, I. J., and Westoby, M. (2003). Nutrient concentration, resorption and lifespan: leaf traits of Australian sclerophyll species. *Funct. Ecol.* 17, 10–19. doi: 10.1046/j.1365-2435.2003.00694.x

Xu, M., Zhong, Z., Sun, Z., Han, X., Ren, C., and Yang, G. (2020). Soil available phosphorus and moisture drive nutrient resorption patterns in plantations on the Loess Plateau. *For. Ecol. Manag.* 461:117910. doi: 10.1016/j.foreco.2020.117910

Yan, Z., Kim, N., Han, W., Guo, Y., Han, T., Du, E., et al. (2015). Effects of nitrogen and phosphorus supply on growth rate, leaf stoichiometry, and nutrient resorption of *Arabidopsis* thaliana. *Plant Soil* 388, 147–155. doi: 10.1007/s11104-014-2316-1

Yuan, Z. Y., and Chen, H. Y. H. (2015). Negative effects of fertilization on plant nutrient resorption. *Ecolgy* 96, 373–380. doi: 10.1890/14-0140.1

Zhang, H., Wang, J., Wang, J., Guo, Z., Wang, G. G., Zeng, D., et al. (2018). Tree stoichiometry and nutrient resorption along a chronosequence of *Metasequoia glyptostroboides* forests in coastal China. *For. Ecol. Manag.* 430, 445–450. doi: 10.1016/j.foreco.2018.08.037

Zhao, N., Yu, G., Wang, Q., Wang, R., Zhang, J., Liu, C., et al. (2020). Conservative allocation strategy of multiple nutrients among major plant organs: from species to community. *J. Ecol.* 108, 267–278. doi: 10.1111/1365-2745.13256

Conflict of Interest: The authors declare that the research was conducted in the absence of any commercial or financial relationships that could be construed as a potential conflict of interest.

Publisher's Note: All claims expressed in this article are solely those of the authors and do not necessarily represent those of their affiliated organizations, or those of the publisher, the editors and the reviewers. Any product that may be evaluated in this article, or claim that may be made by its manufacturer, is not guaranteed or endorsed by the publisher.

frontiers | Frontiers in Plant Science

ORIGINAL RESEARCH
published: 12 May 2022
doi: 10.3389/fpls.2022.906071

Enhanced Salt Tolerance of *Torreya grandis* Genders Is Related to Nitric Oxide Level and Antioxidant Capacity

Yang Liu[1,2], Zhuoke Jiang[1], Yuting Ye[1], Donghui Wang[1] and Songheng Jin[1]**

[1]*Jiyang College, Zhejiang A&F University, Zhuji, China,* [2]*Zhejiang Provincial Key Laboratory of Resources Protection and Innovation of Traditional Chinese Medicine, Zhejiang A&F University, Hangzhou, China*

Nitric oxide (NO), a bioactive molecule, is often involved in the regulation of physiological and biochemical processes in stressed plants. However, the effects of NO donors on dioecious plants remain unclear. Using a pot experiment, female and male *Torreya grandis* were used to study the role of sex and NO in salt stress tolerance. In the present study, female and male *T. grandis* seedlings pretreated with an NO donor (sodium nitroprusside, SNP) were exposed to salt stress, and then leaf relative water content (RWC), photosynthetic pigments, chlorophyll fluorescence parameters, NO and glutathione levels, oxidative damage, and antioxidant enzyme activities were investigated. Female *T. grandis* plants had better tolerance to salinity, as they were characterized by significantly higher RWC, pigment content, and photochemical activities of photosystem II (PSII) and fewer negative effects associated with higher nitrate reductase (NR) activity and NO content. Pretreatment with an NO donor further increased the endogenous NO content and NR activity of both female and male *T. grandis* plants compared with salt treatment. Moreover, pretreatment with an NO donor alleviated salt-induced oxidative damage of *T. grandis*, especially in male plants, as indicated by reduced lipid peroxidation, through an enhanced antioxidant system, including proline and glutathione accumulation, and increased antioxidant enzyme activities. However, the ameliorating effect of the NO donor was not effective in the presence of the NO scavenger (Nω-nitro-L-arginine methyl ester, L-name). In conclusion, enhanced salt tolerance in *T. grandis* plants is related to nitric oxide levels and the supply of NO donors is an interesting strategy for alleviating the negative effect of salt on *T. grandis*. Our data provide new evidence to contribute to the current understanding of NO-induced salt stress tolerance.

Keywords: antioxidant capacity, *Torreya grandis*, nitric oxide, sexual difference, salt stress

OPEN ACCESS

Edited by:
Mirza Hasanuzzaman, Sher-e-Bangla Agricultural University, Bangladesh

Reviewed by:
Aditya Banerjee, St. Xavier's College, India
Shikha Singh, Allahabad University, India

****Correspondence:***
Yang Liu
yangliu8910@zafu.edu.cn; taoji.liuyang@qq.com
Songheng Jin
shjin@zafu.edu.cn

Specialty section:
This article was submitted to Functional Plant Ecology, a section of the journal Frontiers in Plant Science

Received: *28 March 2022*
Accepted: *20 April 2022*
Published: *12 May 2022*

Citation:
Liu Y, Jiang Z, Ye Y, Wang D and Jin S (2022) Enhanced Salt Tolerance of Torreya grandis Genders Is Related to Nitric Oxide Level and Antioxidant Capacity. Front. Plant Sci. 13:906071. doi: 10.3389/fpls.2022.906071

INTRODUCTION

It has been estimated that up to 70% of plant growth can be impacted by environmental stress, including drought, high salinity, heavy metal exposure, high or low temperatures, and light levels (Bhatnagar-Mathur et al., 2008; Mantri et al., 2012; Li et al., 2020). Salinity is a crucial factor affecting plant growth and metabolic responses throughout the world (Mostofa et al., 2015). In addition to direct ion damage, salt stress can produce secondary damage to

plants through the production of reactive oxygen species (ROS) and osmotic stress (Li et al., 2020). When salt content in the soil is significantly higher than the optimal concentration for plant survival, it causes a series of stress responses in plants, including maintenance of osmotic balance and activation of the antioxidant system (Wakeel et al., 2020). In recent years, a great deal of research has been done to explore potential ways to improve saline–alkali land, including the breeding of salt-tolerant varieties, the discovery of salt-tolerant genes, and the application of hormones and growth regulators (Wang et al., 2017; Fang and Xue, 2019).

Current studies have shown that nitric oxide (NO) in plants is mainly produced through two pathways, NO synthase (NOS) and nitrate reductase (NR) pathways (Corpas and Barroso, 2017; Astier et al., 2018), and is further involved in a series of physiological and biochemical reactions, including root morphogenesis (Corpas and Barroso, 2015), seed germination (Kopyra and Gwózdz, 2003), stomatal movement (Laxalt et al., 2016), and abiotic stress regulation (Begara-Morales et al., 2014). Nitric oxide is also involved in the salt tolerance of plant growth. For example, da Silva et al. (2017) reported that salinity-induced accumulation of endogenous NO is associated with modulation of the antioxidant and redox defense systems in *Nicotiana tabacum*. Ren et al. (2020) reported that pretreatment with NO alleviates salt stress in seed germination and seedling growth of *Brassica chinensis* by enhancing biochemical parameters and regulating osmolyte accumulation. However, most of the studies focused on vegetables and herbaceous plants (Ren et al., 2020; Valderrama et al., 2021; Wani et al., 2021), and there were few studies on woody plants (Chen et al., 2021).

Dioecious plants, as an important part of the terrestrial ecosystem, account for nearly 6% of angiosperms and play an indispensable role in the cycling stability of the ecosystem (Susanne-S and Ricklefs, 1995). In the process of natural differentiation and evolution, dioecious plants evolve sex specificity and show significant differences in growth, survival, reproductive pattern, spatial distribution, and resource allocation (Todd-E and Bliss, 1989). Many researchers have devoted themselves to studying differences in the growth, survival, spatial distribution, and resource allocation of dioecious plants (Retuerto et al., 2000; Rana and Liu, 2021). On a smaller scale, some scholars have found that male and female individuals of dioecious plants show different physiological, ecological, and biochemical traits under environmental stress (Chen et al., 2018; Wang et al., 2021). For example, drought stress reduces the water content of leaves and stress resistance in female *Populus yunnanensis* (Zhang et al., 2019). In addition, the mortality rate of female plants was higher than that of male plants, indicating that the drought resistance of male *Populus yunnanensis* was stronger than that of females (Zhang et al., 2019). However, researchers have found that in some dioecious plants, females are more resistant to stress than males. For example, He et al. (2016) found that female *Ginkgo biloba* showed superior growth performance and self-protection mechanisms compared with male *Ginkgo biloba* and also had a higher photosynthetic capacity under drought stress.

Torreya grandis is in a genus of deciduous conifer trees and is valued for its production of nuts and timber in China, but its distribution is limited by its cultivated area and prevailing weather conditions (Hu et al., 2022; Shen et al., 2022). Many studies have investigated bioactive substance synthesis and efficacy (Hu et al., 2022; Song et al., 2022) and the interactions of functional trait × environment interactions, such as the effect of salt stress on the photosynthetic activity of *T. grandis* (Li et al., 2014). However, comparatively little research has been done to elucidate sex differences in *T. grandis* under salt stress. Our previous study indicated that *T. grandis* seedlings showed significant gender differences under drought stress, and female plants had better performance in the process of photosynthesis (Wang et al., 2021). In this study, it was hypothesized that there are sexually different responses to salt, and we also hypothesized that: (1) this difference was related to endogenous NO levels and (2) exogenous NO would improve the salt tolerance of *T. grandis* through increased endogenous NO content and antioxidant enzyme activities. To test these hypotheses, an NO donor (SNP) and NaCl were added to both male and female *T. grandis* in this study. The aims of this study were: (1) to analyze the sexually different responses of *T. grandis* to salt and (2) to evaluate the role of NO in the salt stress tolerance of *T. grandis*. The photosynthetic pigment contents, chlorophyll fluorescence parameters, leaf relative water content, levels of endogenous NO and glutathione in the leaves, and antioxidant systems were evaluated.

MATERIALS AND METHODS

Plant Materials, Growth Conditions, and Treatments

Three-year-old *T. grandis* seedlings were obtained from the Zhuji Forestry Institute (29°43′N,120°16′E). A total of 72 seedlings with a similar mean ground diameter (10.0 mm) and seedling height (60 cm), split between males (n = 36) and females (n = 36), were used in the salt stress experiment. The trees were grown individually in plastic pots (20-cm diameter × 18-cm deep) in the greenhouse of Jiyang College of Zhejiang A&F University (Zhejiang Province, China; 29°45′N,120°15′E) in late May 2021. The greenhouse environment was controlled under a 16-h/8-h (day/night) photoperiod, with an average temperature of 30/18°C (day/night) and a relative humidity of 70 ± 5%. The plastic pots were placed in trays to prevent NaCl leaching.

Salt treatments were conducted in late June 2021. Both male and female plants were divided into four treatments: CK (control, distilled water), salt (100 mM NaCl), SNP (100 mM NaCl with 0.05 mM sodium nitroprusside [SNP]), and L-name (100 mM NaCl with 0.5 mM SNP and 0.2 mM Nω-nitro-L-arginine methyl ester [L-name]). There were three replications per treatment and three plants per replication. The NO donor (SNP) was sprayed over the surfaces of the *T. grandis* leaves three days before salt treatment (20 ml SNP per seedling). Dosage of NO was fixed according to previous studies of NO in other plants (Ren et al., 2020; Valderrama et al., 2021;

Wani et al., 2021). The NO scavenger used in our study was Nω-nitro-L-arginine methyl ester (L-name) (Suda et al., 2002). To avoid osmotic shock, NaCl solution was gradually added in eight steps to achieve a concentration of 0.2%, which was related to soil weight, according to Li et al. (2014). Irrigation was conducted every three days to maintain the field capacity at 70–75%, and all indexes were measured 60 days after treatment when obvious differences were observed.

Leaves from similar positions within the mid-portion of the main stem were collected from three replicates of each treatment after analyzing the chlorophyll fluorescence parameters. After that, the leaves of each sample were cleaned and immediately used for the analysis of photosynthetic pigments, NO content and enzymatic assays.

Determination of Photosynthetic Pigment Contents

First, finely cut leaves (collected from similar positions within the mid-portion of the main stem in each treatment) weighing 0.1 g were mixed and extracted with 8 ml 95% ethanol, according to Arnon (1949). The extraction of chlorophyll was then conducted at 4°C in the dark for 24 h and shaken about three times until the leaf samples were blanched. The absorbance of the samples was measured at 649, 665, and 470 nm using a spectrophotometer (Shimadzu UV-2550, Kyoto, Japan). The chlorophyll concentrations of *T. grandis* leaves were calculated following Arnon (1949).

Chlorophyll Fluorescence Apparatus

The PSII photochemical activity of *T. grandis* leaves was evaluated after dark adaption for 60 min (based on the previous experiment) using a multifunctional plant efficiency analyzer (Hansatech Instruments, Pentney, UK). The fluorescent parameters, including Fv/Fm (the maximum quantum yield of the primary PSII photochemistry), ABS/RC (the absorbed light energy by the PSII antenna photon flux per active reaction center), DIo/RC (total energy dissipated by the reaction center of PSII), and TRo/RC (total energy used to restore QA by the unit reaction center of PSII), were calculated from the OJIP test curves.

Assessment of Malondialdehyde Content and the Relative Electrolyte Leakage Rate

Lipid peroxidation was measured as the amount of malondialdehyde (MDA) determined by the thiobarbituric acid (TBA) reaction, using 0.3 g of the frozen leaf samples per replicate (n = 3) according to Deng et al. (2011). Meanwhile, 10 leaf discs (about 10 mm in diameter) from fully expanded leaves of *T. grandis* were used in each replicate (n = 3) to determine the relative electrolyte leakage conductivity (REC), according to Li et al. (2014).

Determination of Reactive Oxygen Species

The $O_2 \cdot^-$ production rates of *T. grandis* leaves under salt and NO treatments were assessed by monitoring the nitrite formed from hydroxylamine in the presence of $O_2 \cdot^-$ as described by Wang (1990). Frozen leaf material (1 g) was used for each replicate (n = 3). Similarly, a frozen leaf (1 g) was used in each replicate (n = 3) for the analysis of H_2O_2 content in *T. grandis* leaves, following Patterson et al. (1984).

Estimation of Leaf Relative Water Content

The relative water content (RWC) was measured according to the method of our previous study (Wang et al., 2021). The fresh leaves of each treatment were collected and weighed to obtain the fresh weight (FW). Leaves of *T. grandis* were then soaked in purified water at 25°C for 4 h to obtain the saturated fresh weight (SW). Subsequently, leaves were placed in a 70°C oven for 6 h to obtain the dry weight (DW). RWC was calculated as follows: $RWC = (FW - DW)/(SW - DW) \times 100\%$.

Determination of Proline Content

Proline (Pro) content was determined according to Bates et al. (1973). A total of 0.3 g of *T. grandis* leaves were homogenized in sulfosalicylic acid, and then, 2 ml of acid ninhydrin and 2 ml of glacial acetic acid were added. The samples were heated at 100°C and extracted with toluene, and the free toluene was then quantified at 528 nm using *L*-proline as a standard.

Evaluation of NO and Nitrate Reductase

Fresh leaves (0.3 g) were used in each replicate (n = 3) for the analysis of NO content, according to Cantrel et al. (2011). NO content was calculated using a standard curve of $NaNO_2$ (0–4 μg mL^{-1}) and expressed as μmol g^{-1} FW. The activity of nitrate reductase (NR; E.C. 1.6.6.1) was determined according to Jaworski (1971). Similarly, a fresh leaf (0.3 g) was used for each replicate (n = 3). The activity of NR was expressed as nmol NO_2^{-1} min^{-1} mg^{-1} protein.

Protein Extraction, GSH Content, and Antioxidant Enzymes

Antioxidant enzyme extracts from each treatment were obtained from 0.3 g frozen leaves, according to Yu et al. (2017). The leaves were homogenized at 4°C in 10 ml of 50 mM phosphate buffer solution (pH 7.8) containing 1% polyethylenepyrrole. The homogenate was then centrifuged at 10,000 × g at 4°C for 15 min. The supernatant was collected and used to measure GSH content and enzyme activity. Meanwhile, soluble proteins were determined according to Bradford (1976).

GSH content and glutathione reductase (GR) activity were assayed using kits from the Nanjing Jiancheng Bioengineering Institute (Nanjing, China), following the manufacturer's specifications. GR activity was expressed as nmol min^{-1} mg^{-1} protein. The GSH content was expressed as mg g^{-1} FW. SOD activity was analyzed following Beauchamp and Fridovich (1971) and was expressed as U g^{-1} protein. POD activity was estimated according to Ruan et al. (2002) and was expressed as U mg^{-1} protein. CAT activity was measured following Watanabe et al. (2003) and was expressed as μmol min^{-1} mg^{-1} protein. APX activity was measured using the method described by Nakano and Asada (1981) and was expressed as nmol min^{-1} mg^{-1} protein.

Statistical Analyses

Two-way analysis of variance (ANOVA), with sex and salt as the main factors and a sex × salt interaction term, was performed using SPSS 19.0 (SPSS Inc., Chicago, IL, USA) to evaluate the effects of sex and salt treatments and was followed by Duncan's test ($p < 0.05$). The data are presented as the mean ± standard deviation (SD).

RESULTS

Effects of Sex and Salt on Chlorophyll Contents and Chlorophyll Fluorescence

The chlorophyll contents and chlorophyll fluorescence parameters of *T. grandis* were found to be significantly different under salt treatments (**Table 1**). Moreover, a significant interaction of sex and salt was observed in the total chlorophyll content, Chl a content, Chl b content, and ratio of Chl a to Chl b of *T. grandis* (**Table 1**). Compared with the control, salt treatment significantly inhibited the growth of both T. *grandis* genders, which was evident from lower pigment contents and Fv/Fm values but higher ABS/RC, DIo/RC, and TRo/RC values (**Figures 1, 2**). Meanwhile, compared with male plants, female plants grown under salt were characterized by significantly higher Fv/Fm and pigment contents and a smaller Chl a/b ratio (**Figures 1, 2**). In comparison with salt-treated seedlings, SNP treatment caused an increase in pigment contents and PSII activity in both female and male *T. grandis* (**Figures 1, 2**). However, inclusion of NO scavenger (L-name) decreased this effect and again caused a reduction in Fv/Fm and pigment contents and also increased the values of ABS/RC, DIo/RC, and TRo/RC (**Figures 1, 2**).

Effects of Sex and Salt on the Level of Lipid Peroxidation

The effects of salt and NO donors on membrane damage of cells were analyzed by determining the MDA content and the relative electrolyte leakage rate, while oxidative stress was investigated in terms of the $O_2{\cdot}^-$ production rate and H_2O_2 content. Values of the MDA content, the relative electrolyte leakage rate, the $O_2{\cdot}^-$ production rate, and H_2O_2 content of *T. grandis* were all significantly affected by sex, salt, and their interaction (**Table 2**; $p < 0.05$). As shown in **Figure 3**, compared with the control, salt treatment significantly increased the MDA content, relative electrolyte leakage rate, $O_2{\cdot}^-$ production rate, and H_2O_2 content of *T. grandis* ($p < 0.05$). Meanwhile, compared with female plants, male plants grown under salt stress were characterized by significantly higher MDA content, relative electrolyte leakage rate, and $O_2{\cdot}^-$ production rate but reduced H_2O_2 content (**Figure 3**; $p < 0.05$). However, pretreatment with SNP resulted in significant decreases in these indexes compared with the salt-treated female and male plants ($p < 0.05$), but this was decreased by the NO scavenger under the L-name treatment.

Effects of Sex and Salt on RWC and Proline Content

The physiological water status and proline content of *T. grandis* plants are shown in **Figure 3**. Both the RWC and proline content of *T. grandis* were significantly affected by sex, salt, and their interaction (**Table 2**; $p < 0.05$). Compared with the control, the RWC in salt-treated *T. grandis* leaves decreased by 9.1% ($p < 0.05$) in female plants and 19.8% ($p < 0.05$) in male plants. The NO treatment reduced the effect of salt stress on the RWC decrease in the presence of 0.2% NaCl, and it was significant in the male plants (**Figure 4A**). In contrast, the inclusion of the NO scavenger (L-name) decreased the effect of SNP on the water status and caused a reduction in RWC; however, these changes were not significant ($p > 0.05$; **Figure 4A**). As shown in **Figure 4B**, the proline content of both female and male *T. grandis* significantly increased under both salt and SNP treatments compared with that of CK. However, this was significantly decreased by the NO scavenger under the L-name treatment.

Effects of Sex and Salt on NO Content and NR Activity

Two-way ANOVA showed that both the NR activity and NO content of *T. grandis* were significantly affected by sex, salt, and their interaction (**Table 2**; $p < 0.05$). Compared with male plants, female plants grown under salt were characterized by significantly higher NR activity and endogenous NO content (**Figure 5**; $p < 0.05$). As shown in **Figure 5**, compared with the control, salt treatment significantly increased the NR activity and endogenous NO content of *T. grandis* by 89.7 and 109.2%, respectively, in female plants and by 45.8 and

TABLE 1 | Summary of significance levels (two-way ANOVA) for the effects of gender, salt, and their interaction on the contents of photosynthetic pigments and fluorescence parameters.

Source		Total chlorophyll content (mg g^{-1} FW)	Chl a content (mg g^{-1} FW)	Chl b content (mg g^{-1} FW)	Chlorophyll a/b	Fv/Fm	ABS/RC	DIo/RC	TRo/RC
Gender (A)	MS	8,444.21	9,485.13	3,911.02	217.46	0.84	0.47	0.01	0.75
	P	0.0001	0.0001	0.0001	0.0001	0.3730	0.4958	0.9130	0.4002
Salt (B)	MS	17,773.85	23,560.85	5,420.36	199.65	10.53	4.63	8.62	3.43
	P	0.0001	0.0001	0.0001	0.0001	0.0005	0.0163	0.0012	0.0426
Interaction (A × B)	MS	1,016.62	1,057.87	596.68	218.37	1.90	1.81	1.87	1.86
	P	0.0001	0.0001	0.0001	0.0001	0.1699	0.1859	0.1743	0.1774

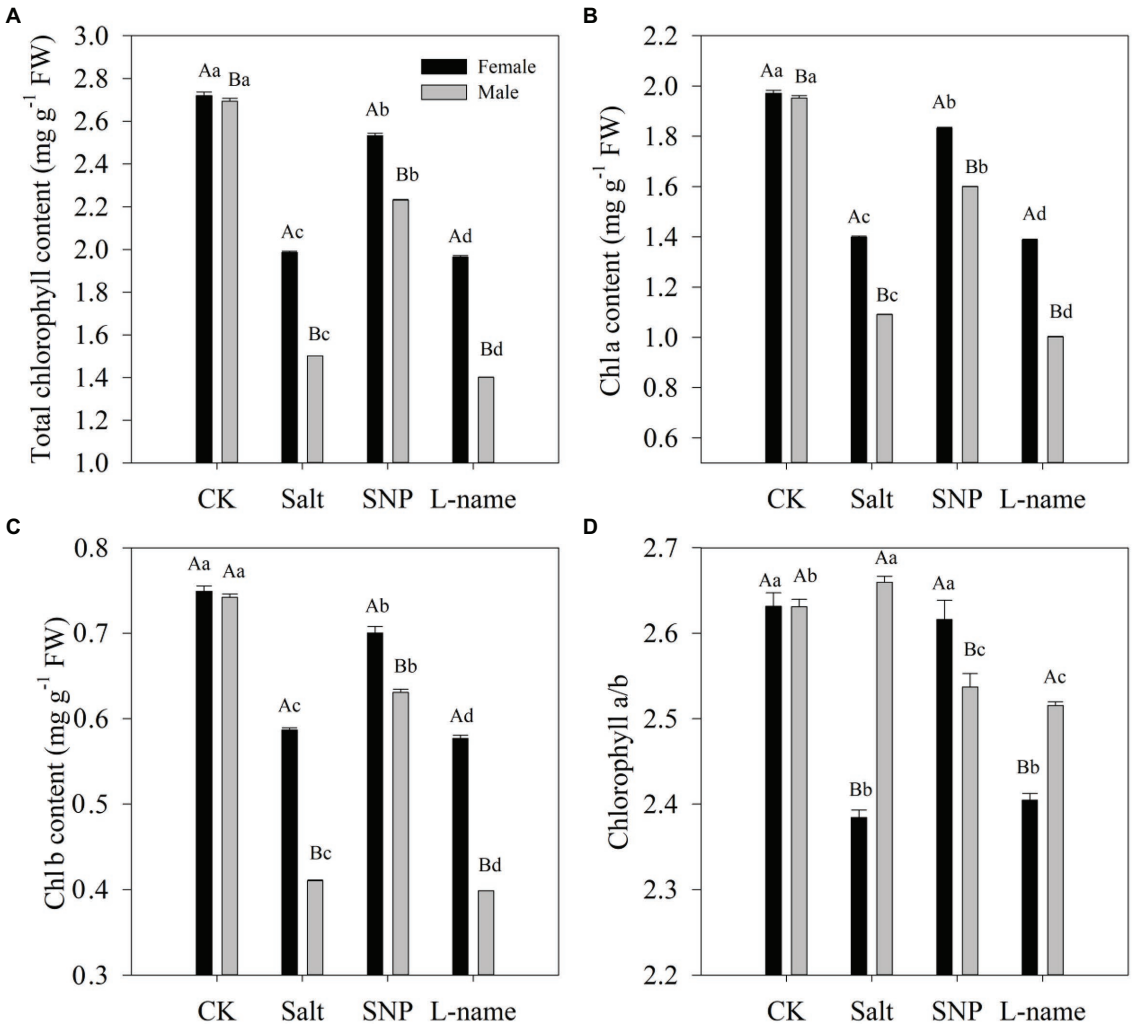

FIGURE 1 | Photosynthetic pigment contents [total chlorophyll content **(A)**, Chl a content **(B)**, Chl b content **(C)**, and ratio of Chl a to Chl b **(D)**] measured in *T. grandis* in response to different treatments. CK (control, distilled water), salt (100 mM NaCl), SNP (100 mM NaCl with 0.05 mM SNP), and L-name (100 mM NaCl with 0.5 mM SNP and L-name). Different uppercase letters indicate a significant difference between different genders at $p < 0.05$, and different lowercase letters indicate significant difference under salt treatment at $p < 0.05$, according to Duncan's test.

40.3%, respectively, in male plants. However, pretreatment with SNP before salt treatment resulted in a further increase in the NR activity (43.2 and 133.6% in female and male plants, respectively) and NO content (45.6 and 99.7% in female and male plants, respectively) in *T. grandis* leaves compared with the salt-treated plants ($p < 0.05$; **Figure 5**). However, the inclusion of the NO scavenger decreased the effect of SNP on NO synthesis, as it was evident that the L-name treatment reduced NR activity by 29.7 and 53.1% and NO content by 25.9 and 50.3% in female and male plants, respectively, compared to salt-stressed plants treated with SNP ($p < 0.05$; **Figure 5**).

Effects of Sex and Salt on Endogenous GSH Content and GR Activity

Figure 6 illustrates the endogenous GSH content and the activity of the key enzyme involved in GSH biosynthesis under different treatments. Two-way ANOVA showed that both GR activity and GSH content of *T. grandis* were significantly affected by sex, salt, and their interaction (**Table 2**; $p < 0.05$). Compared with female plants, male plants grown under salt stress were characterized by significantly higher GR activity and GSH content (**Figure 6**; $p < 0.05$). As shown, compared with the control, salt treatment increased the GR activity and GSH content of *T. grandis* by 22.5% ($p > 0.05$) and 40.3% ($p < 0.05$), respectively, in female plants and by 87.6% ($p < 0.05$) and 52.1% ($p < 0.05$), respectively, in male plants. However, pretreatment with an NO donor before salt treatment resulted in a further increase in GR activity (47.1 and 24.6% in females and males, respectively) and GSH content (63.3 and 97.7% in females and males, respectively) in *T. grandis* leaves relative to the salt-stressed plants ($p < 0.05$; **Figure 6**). However, the inclusion of L-name decreased the effect of NO on GSH synthesis.

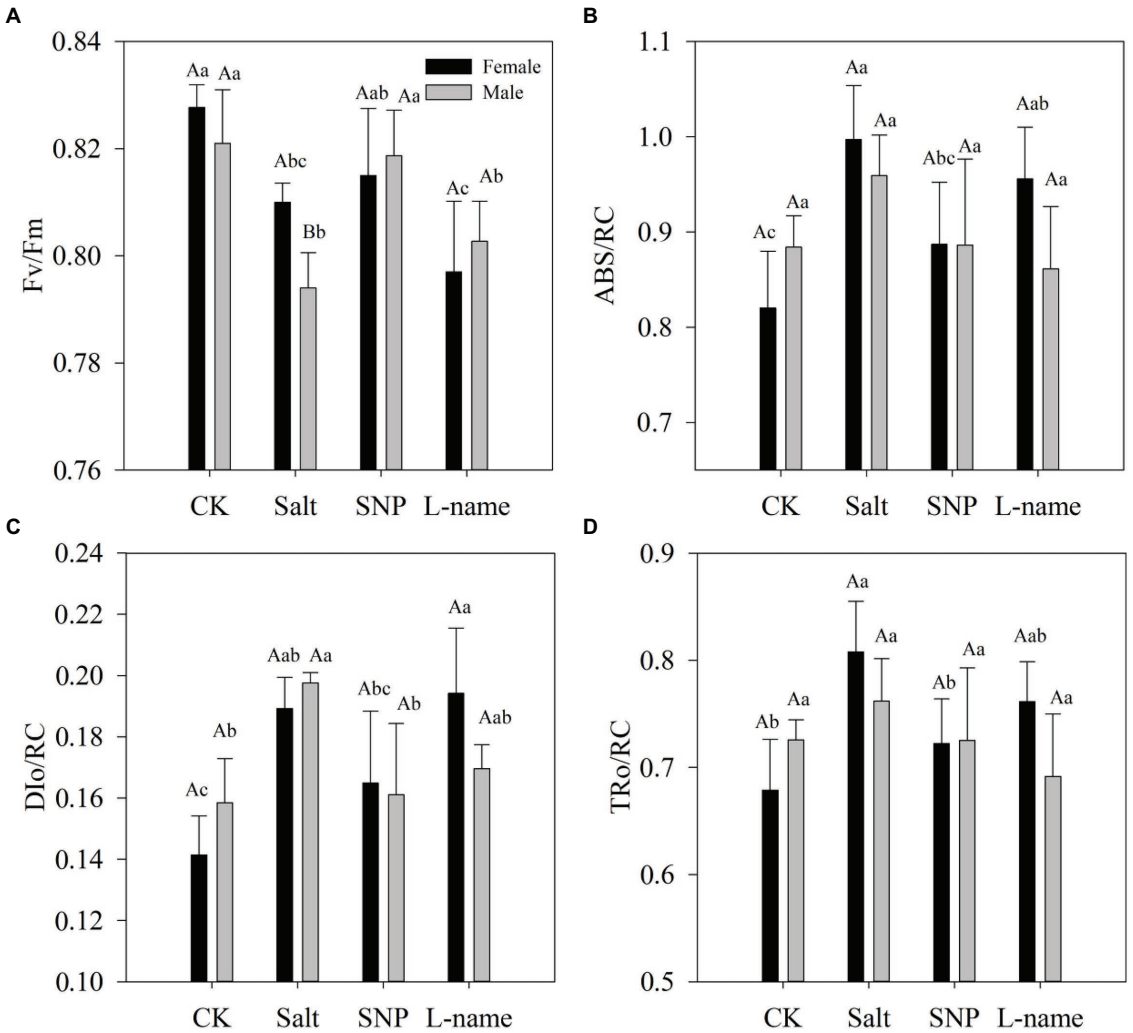

FIGURE 2 | Chlorophyll fluorescence parameters (Fv/Fm: **A**; ABS/RC: **B**, DIo/RC: **C**, TRo/RC: **D**) measured in *T. grandis* in response to different treatments. CK (control, distilled water), salt (100 mM NaCl), SNP (100 mM NaCl with 0.05 mM SNP), and L-name (100 mM NaCl with 0.5 mM SNP and L-name). Different uppercase letters indicate a significant difference between different genders at $p < 0.05$, and different lowercase letters indicate significant difference under salt treatment at $p < 0.05$, according to Duncan's test.

Effects of Sex and Salt on Antioxidant Enzyme Activity

Two-way ANOVA showed that the antioxidant enzyme activities of *T. grandis* were significantly affected by sex, salt, and their interaction (**Table 2**; $p < 0.05$). As shown in **Figures 7A–D**, the activities of the studied antioxidant enzymes significantly increased under salt treatment compared with the control plants. Compared with male plants, female plants grown under salt stress were characterized by significantly higher SOD and CAT activities but lower POD and APX activities (**Figure 7**; $p < 0.05$). Pretreatment with an NO donor before salt treatment further increased SOD (by 26.3% in males), POD (by 45.3 and 53.0% in females and males, respectively), CAT (by 94.8 and 312.8% in females and males, respectively), and APX (by 34.8 and 74.1% in females and males, respectively) activities compared with the salt treatment. However, the inclusion of L-name decreased the effect of NO on antioxidant enzyme activities (**Figure 7**). Thus, these results suggest that the modulation of antioxidant enzyme activities by an exogenous NO donor might alleviate the ROS-triggered oxidative damage caused by salt stress.

DISCUSSION

In recent years, studies have shown that NO is involved in plant morphological development, root growth, photosynthesis, and the regulation of antioxidant enzyme systems, especially when plants are subjected to environmental stress (Valderrama et al., 2021; Wani et al., 2021), but few studies have focused on the effects of NO donors on dioecious plants. This study confirmed our hypothesis that NO is involved in the salt-tolerant growth of both female and male *T. grandis*. Salt treatment inhibited the growth of female and male *T. grandis*

TABLE 2 | Summary of significance levels (two-way ANOVA) for the effects of gender, salt, and their interaction on RWC, proline content, the level of lipid peroxidation, NO content and NR activity, GSH content and GR activity, and antioxidant enzyme activities.

Source		RWC (%)	Proline content ($\mu g\,g^{-1}$ FW)	MDA content ($nmol\,g^{-1}$ FW)	REC (%)	$O_2^{\cdot-}$ production rate ($nmol\,g^{-1}\,min^{-1}$)	H_2O_2 content ($\mu mol\,g^{-1}$ FW)	NR activity ($nmol\,min^{-1}\,mg^{-1}$ protein)
Gender (A)	MS	4.51	1719.60	2049.20	28.90	36716.53	285.55	18.31
	P	0.0497	0.0001	0.0001	0.0001	0.0001	0.0001	0.0006
Salt (B)	MS	37.82	58628.69	921.47	379.65	52280.93	21405.36	281.25
	P	0.0001	0.0001	0.0001	0.0001	0.0001	0.0001	0.0001
Interaction (A × B)	MS	11.67	121.59	831.53	17.75	2766.38	530.26	31.92
	P	0.0003	0.0001	0.0001	0.0001	0.0001	0.0001	0.0001
Source		NO content ($\mu mol\,g^{-1}$ FW)	GR activity ($nmol\,min^{-1}\,mg^{-1}$ protein)	GSH content ($mg\,g^{-1}$ FW)	SOD activity ($U\,g^{-1}$ protein)	POD activity ($U\,mg^{-1}$ protein)	CAT activity ($\mu mol\,min^{-1}\,mg^{-1}$ protein)	APX activity ($nmol\,min^{-1}\,mg^{-1}$ protein)
Gender (A)	MS	35.62	112.59	1423.36	80.40	372.89	199.27	195.98
	P	0.0001	0.0001	0.0001	0.0001	0.0001	0.0001	0.0001
Salt (B)	MS	2476.18	111.60	23448.59	353.36	281.31	644.22	141.27
	P	0.0001	0.0001	0.0001	0.0001	0.0001	0.0001	0.0001
Interaction (A × B)	MS	163.24	19.83	425.80	93.39	28.85	81.52	25.87
	P	0.0001	0.0001	0.0001	0.0001	0.0001	0.0001	0.0001

seedlings, which was indicated by a lower photosynthetic pigment content and decreased Fv/Fm but significantly higher ABS/RC, DIo/RC, and TRo/RC (**Figures 1, 2**). Additionally, compared with male plants, female plants showed better tolerance to salinity, as they were characterized by significantly higher Fv/Fm and pigment contents and fewer negative effects (**Figures 1–3**). Our results are similar to those of previous drought tests on *T. grandis* (Wang et al., 2021), suggesting that female *T. grandis* are more tolerant of stress. However, a study by Li et al. (2013) on *Populus yunnanensis* reported that females were more sensitive and suffered from greater negative effects than males under salt stress. Therefore, these studies suggest that sex-linked differences in the growth of dioecious plants are not consistent among species, which can be interpreted as species-specific adaptation. Pretreatment with an NO donor (SNP) caused an increase in pigment contents and PSII activity of both female and male *T. grandis*; however, inclusion of the NO scavenger (L-name) decreased this effect (**Figures 1, 2**). Thus, these results suggest that pretreatment with NO donors is a simple and effective measure to reduce the effect of salt on the growth of *T. grandis*. These findings are consistent with previous reports on saffron (Babaei et al., 2021), *Arabidopisis thaliana* (Liu et al., 2015), and *Glycine max* (Vaishnav et al., 2016).

Chlorophyll is an important factor in photosynthesis in plants. In this study, salt and NO treatments significantly affected chlorophyll pigments and their ratios (**Figure 1**). Decreases in total chlorophyll content of both female and male *T. grandis* were observed under salt treatment, suggesting that salt stress caused damage to photosynthetic pigments. Similar results were also reported in *Mentha spicata* and *Oryza sativa* (Amri et al., 2011; Ounoki et al., 2021). However, compared with salt treatment, NO treatment in both female and male *T. grandis* resulted insignificantly higher leaf chlorophyll contents, which was inconsistent with that reported in mustard and cotton (Khan et al., 2012; Liu et al., 2013). Changes in the Chl a/b ratio often indicate a change in the ratio between the light-harvesting complexes (LHC) and the reaction center complexes of the photosystem (Venema et al., 2000). The significantly increased Chl a/b ratio in both female and male *T. grandis* under NO treatment showed that NO might participate in inducing these plants to change the ratio of chlorophyll pigments to maintain a good photoelectron transfer system. This was confirmed by the supply of the NO scavenger (L-name), which reversed the effect of SNP on pigment accumulation and caused a reduction in total chlorophyll, Chl a, and Chl b contents (**Figure 2**).

Chlorophyll fluorescence parameters are often used to reflect the photosystem changes of plants in the face of environmental stress, and the measurement is convenient, accurate, and sensitive (Pashkovskiy et al., 2018). Generally, plants grown under stress have lower Fv/Fm than non-stressed plants (Baker, 2008), which is consistent with the performance of *T. grandis* (**Figure 2**). The significantly higher values of Fv/Fm under treatment with an NO donor compared with those under salt treatment indicated that pretreatment with an NO donor can effectively maintain photochemical efficiency in *T. grandis* seedlings. The increase in ABS/RC in both female and male *T. grandis* under salt treatment can be explained by a decrease in the number of active reactive centers (RC) of PSII, which might serve as a defense mechanism to reduce the burden of its systems when salt stress occurs (Strasser et al., 2010). Another effective protective mechanism for plants under salt stress is the dissipation of the absorbed light energy into heat (Baena-Gonzalez and Aro, 2002), which was confirmed by the significantly higher values of non-photochemical quenching (NPQ) per reaction center of PSII (DIo/RC) in *T. grandis* seedlings under salt stress (**Figure 2C**). Furthermore, TRo/RC was significantly higher under salt, which indicated that *T. grandis* seedlings under salt stress had improved the efficiency of the remaining

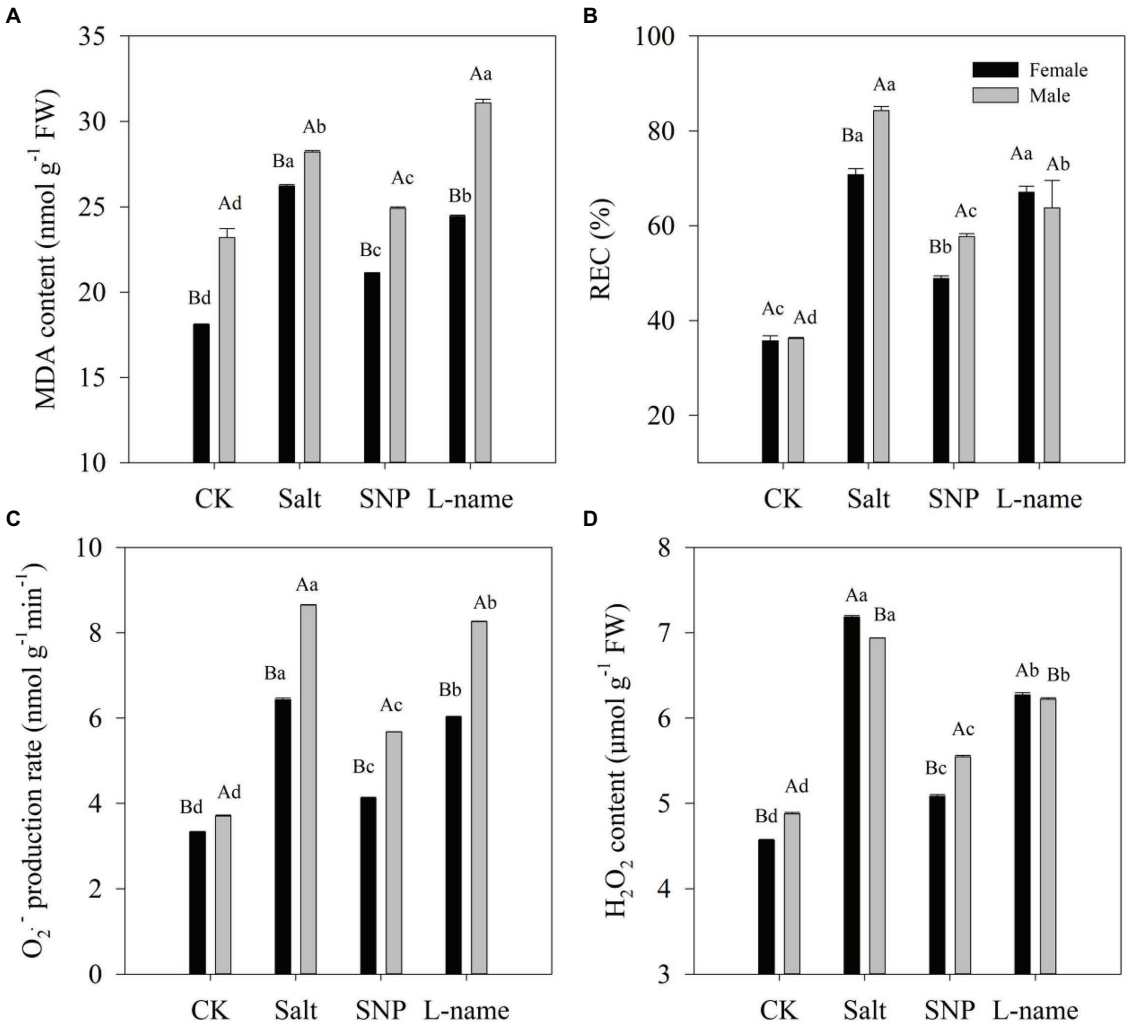

FIGURE 3 | Lipid peroxidation [MDA content **(A)**, REC **(B)**, O2·- production rate **(C)**, H2O2 content **(D)**] of *T. grandis* leaves in response to different treatments. CK (control, distilled water), salt (100 mM NaCl), SNP (100 mM NaCl with 0.05 mM SNP), and L-name (100 mM NaCl with 0.5 mM SNP and L-name). Different uppercase letters indicate a significant difference between different genders at $p < 0.05$, and different lowercase letters indicate significant difference under salt treatment at $p < 0.05$, according to Duncan's test.

active reaction centers. However, compared with salt-treated seedlings, NO treatment caused an increase in PSII activity in both female and male *T. grandis* (**Figure 2**), which is indicated by higher Fv/Fm and lower ABS/RC, DIo/RC, and TRo/RC. However, the inclusion of an NO scavenger (L-name) decreased this effect, caused a reduction in Fv/Fm, and increased the values of ABS/RC, DIo/RC, and TRo/RC (**Figure 2**). Together, these results confirm that the supply of an NO donor can maintain the photosynthetic capacity of *T. grandis* plants under salt stress.

When plants are stressed, the photosynthetic electron transport system produces a large number of reactive oxygen species (ROS), including $O_2 \cdot^-$ and H_2O_2 (You and Chan, 2015). This is consistent with the significantly increased values of $O_2 \cdot^-$ and H_2O_2 in the leaves of *T. grandis* under salt stress (**Figure 3**). Furthermore, the accumulation of ROS could lead to a break in the osmotic balance of plant cell membranes and eventually to membrane lipid peroxidation (Golldack et al., 2014). The increase in MDA content often indicates the occurrence of membrane lipid peroxidation, while the change in membrane permeability leads to an increase in relative conductivity (Li et al., 2014). Compared with female plants, male *T. grandis* seedlings grown under salt suffered from more negative effects, as they were characterized by a significantly higher MDA content, relative electrolyte leakage rate, and $O_2 \cdot^-$ production rate but decreased H_2O_2 content (**Figure 3**; $p < 0.05$). These results indicated that female *T. grandis* were more tolerant to environmental stress than male *T. grandis*, which is consistent with previous results using a drought test (Wang et al., 2021). Our results also showed that the addition of SNP could effectively maintain the balance of intracellular and intracellular permeable substances and the stability of the cell membrane in both male and female *T. grandis* (**Figure 3**). This was

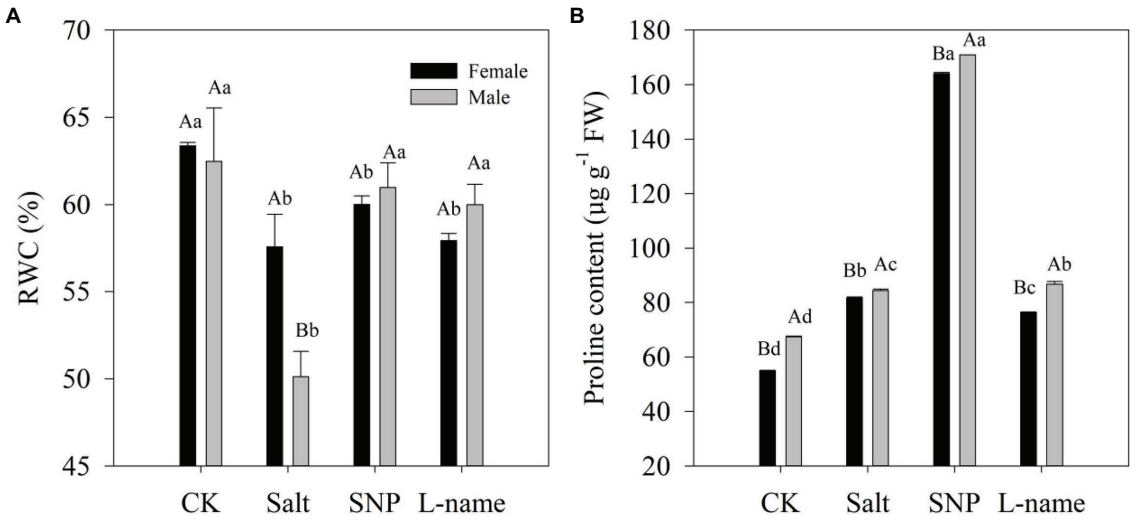

FIGURE 4 | Leaf relative water (RWC) content **(A)** and proline content **(B)** of *T. grandis* in response to different treatments. CK (control, distilled water), salt (100 mM NaCl), SNP (100 mM NaCl with 0.05 mM SNP), and L-name (100 mM NaCl with 0.5 mM SNP and L-name). Different uppercase letters indicate a significant difference between different genders at $p < 0.05$, and different lowercase letters indicate significant difference under salt treatment at $p < 0.05$, according to Duncan's test.

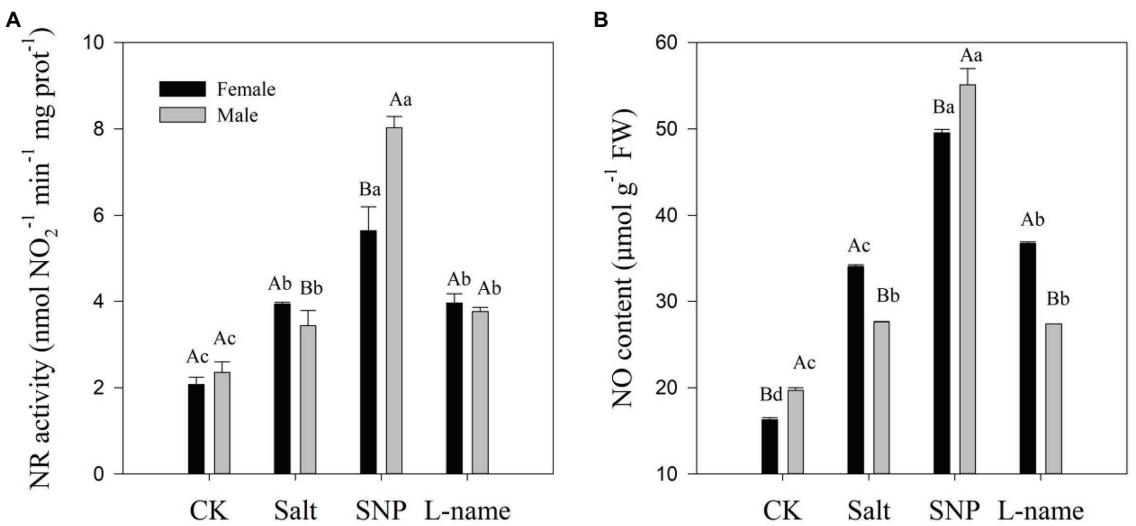

FIGURE 5 | Nitrate reductase (NR) activity **(A)** and NO content **(B)** of *T. grandis* in response to different treatments. CK (control, distilled water), salt (100 mM NaCl), SNP (100 mM NaCl with 0.05 mM SNP), and L-name (100 mM NaCl with 0.5 mM SNP and L-name). Different uppercase letters indicate a significant difference between different genders at $p < 0.05$, and different lowercase letters indicate significant difference under salt treatment at $p < 0.05$, according to Duncan's test.

also confirmed by the application of the NO scavenger (L-name), which again increased these parameters. These results were relatively consistent with the results in *Brassica oleracea* (Akram et al., 2020), broccoli (Ahmad et al., 2016), and cotton (Dong et al., 2014).

RWC commonly exhibits a decreasing trend under salt treatment (Li et al., 2014). In this study, we found that values of RWC declined under NaCl treatment, and sexual differences were significant, indicating that the leaf water situation of male and female *T. grandis* are quite different under salt stress. Compared with males, female *T. grandis seedlings* maintained significantly higher RWC under salt stress (**Figure 4A**), indicating that female *T. grandis* seedlings are more tolerant to salt stress than male plants. When plants suffer from salt stress, the accumulation of osmotic substances and proline content in leaf cells is often used as an effective means of alleviating stress. Both male and female *T. grandis* seedlings showed a higher accumulation of proline under salt stress, while SNP

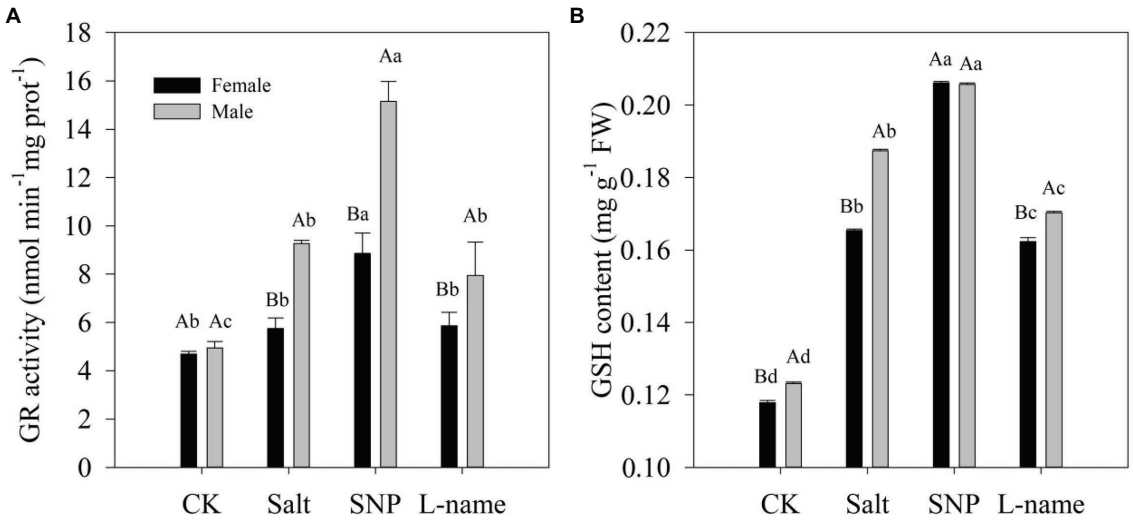

FIGURE 6 | Glutathione reductase (GR) activity **(A)** and GSH content **(B)** of *T. grandis* in response to different treatments. CK (control, distilled water), salt (100 mM NaCl), SNP (100 mM NaCl with 0.05 mM SNP), and L-name (100 mM NaCl with 0.5 mM SNP and L-name). Different uppercase letters indicate a significant difference between different genders at $p < 0.05$, and different lowercase letters indicate significant difference under salt treatment at $p < 0.05$, according to Duncan's test.

treatment further increased proline content and RWC (**Figure 4**). In contrast, the inclusion of the NO scavenger (L-name) decreased the effect of SNP on proline accumulation and caused a reduction in RWC, which confirmed that NO might be involved in maintaining the water content in *T. grandis*. A similar result was reported by Chen et al. (2021), who found that H_2S-induced NO alleviated the salt stress of Cyclocarya paliurus by improving proline accumulation.

The synthesis of NO increases when plants are subjected to stress, which has been reflected in this work and in previous research (Valderrama et al., 2021; Wani et al., 2021). Meanwhile, the results of this study showed that the activity of NR and NO content increased simultaneously, indicating that NR is an important enzyme in the synthesis of NO in *T. grandis* (Corpas and Barroso, 2017). NR-mediated NO production has been reported to be involved in plant physiological responses under stress (Mur et al., 2013). Studies on wheat seedlings have also indicated that the application of NO donors could significantly increase both NR activity and NO content (Khan et al., 2017). Compared with male *T. grandis*, female *T. grandis* induced significantly higher NR activity and NO content under salt stress, which to some extent explained the physiological and biochemical differences between male and female *T. grandis* under environmental stress. However, compared with females, male *T. grandis* treated with exogenous SNP synthesized more NO (**Figure 5B**), which may help male *T. grandis* alleviate the damage caused by salt stress, as they have a lower tolerance. The inclusion of the NO scavenger confirmed the effect of the external SNP supply on endogenous NO synthesis, which was consistent with the results of cotton (Dong et al., 2014) and *Zea mays* (Kharbech et al., 2020).

One of the mechanisms through which NO participates in plant stress resistance is the activation of the antioxidant system, including the non-enzymatic and enzymatic antioxidant systems (da-Silva, C. J., Modolo, L. V., 2017; Wani et al., 2021). A large number of studies have shown that the content of non-enzymatic substances, such as phenolics and soluble proteins, in salt-treated plants can be significantly increased with the participation of NO donors (Ahmad et al., 2016; da-Silva, C. J., Modolo, L. V., 2017; Chen et al., 2021). The results of this study showed that the GSH content and GR activity of *T. grandis* seedlings under salt stress were significantly increased after treatment with an NO donor (**Figure 6**). This result is consistent with previous studies on wheat (Hasanuzzaman et al., 2011), cotton (Liu et al., 2013), and chickpea (Ahmad et al., 2016). Our previous study also showed that NO induced by hydrogen sulfide was involved in the regulation of the salt tolerance of *T. grandis*, which was related to the massive synthesis of different phenolic antioxidants (Chen et al., 2021). In general, the accumulation of non-enzymatic substances is beneficial for plant cells to cope with osmotic damage caused by stress.

The production of antioxidant enzymes, such as SOD, POD, CAT, and APX, in plants often keeps ROS in a stable state, and these antioxidant systems are activated when ROS are greatly increased under stress (Wakeel et al., 2020). $O_2{\cdot}^-$ is dissimulated to H_2O_2 by SOD, which is then eliminated by CAT and APX, producing H_2O and O_2 (Lázaro et al., 2013). Female *T. grandis* under salt stress showed significantly higher SOD and CAT enzyme activities, while male T. *grandis* showed significantly higher POD and APX enzyme activities (**Figure 7**). This also explains the different responses of male and female *T. grandis* to salt stress. Compared with female *T. grandis*, salt-stressed male *T. grandis* had significantly higher SOD, POD, CAT, and APX enzyme activities after SNP treatment.

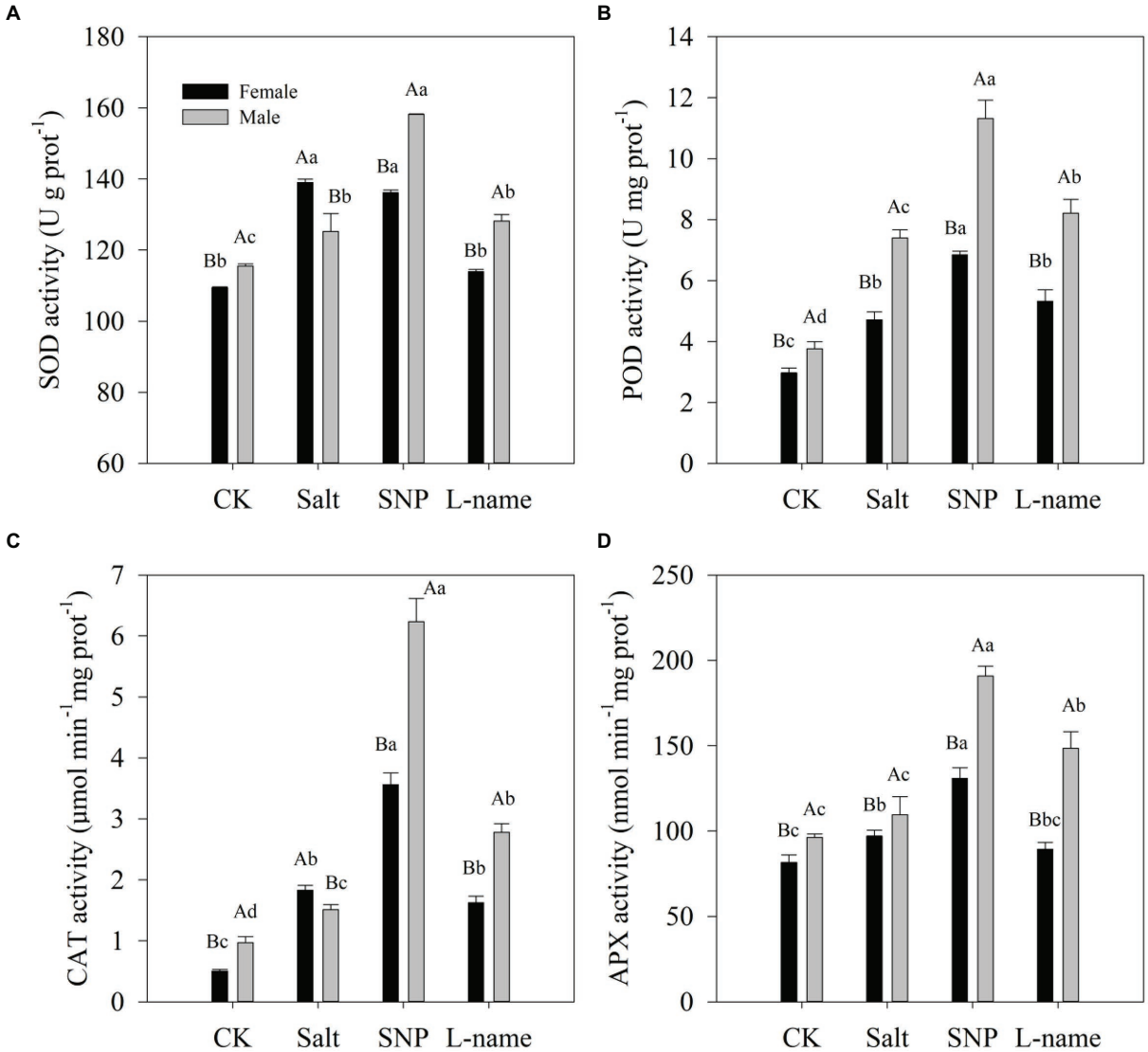

FIGURE 7 | Antioxidant enzyme activities of *T. grandis* in response to different treatments. CK (control, distilled water), salt (100 mM NaCl), SNP (100 mM NaCl with 0.05 mM SNP), and L-name (100 mM NaCl with 0.5 mM SNP and L-name). Different uppercase letters indicate a significant difference between different genders at $p < 0.05$, and different lowercase letters indicate significant difference under salt treatment at $p < 0.05$, according to Duncan's test.

This suggests that NO might be more effective in alleviating the salt stress of male *T. grandis* by improving the activities of antioxidant enzymes. These results also indicated that the increase in the activity of these antioxidant enzymes mediated by SNP might be due to post-translational modifications (PTM), such as persulfidation or S-nitrosation (Singh et al., 2017; Alamri et al., 2020).

Overall, our study showed that female *T. grandis* showed better tolerance to salinity, as they were characterized by significantly higher RWC, pigment contents, and Fv/Fm and fewer negative effects. This is associated with higher nitrate reductase (NR) activity and NO content. Pretreatment with an NO donor alleviated salt-induced oxidative damage of *T. grandis*, especially male *T. grandis*, as indicated by lowered lipid peroxidation through an enhanced antioxidant system, including proline and glutathione accumulation, and increased antioxidant enzyme activities. However, the ameliorating effect of the NO donor was not effective in the presence of an NO scavenger. The present study provides new evidence to contribute to the current understanding of NO-induced salt stress tolerance and the role of NO signaling in dioecious plants.

DATA AVAILABILITY STATEMENT

The raw data supporting the conclusions of this article will be made available by the authors, without undue reservation.

AUTHOR CONTRIBUTIONS

YL is responsible for the whole process of experimenting and writing the paper. SJ provide experimental guidance and amend the manuscript. JK, YT, and DW help to do the experiment. All authors contributed to the article and approved the submitted version.

FUNDING

This work was supported by the National Key Research and Development Project (2019YFE0118900), the National Natural Science Foundation of China (No. 32001305), Jiangsu Province Natural Science Foundation (No. BK20200771), "Pioneer" and "Leading Goose" R&D Program in Universities of Zhejiang (2022), and Jiyang College of Zhejiang A & F University under Grant (No. RQ2020B14; JYKC2117).

ACKNOWLEDGMENTS

We thank LetPub (www.letpub.com) for its linguistic assistance during the preparation of this manuscript.

REFERENCES

Ahmad, P., Abdel Latef, A. A., Hashem, A., Abd_Allah, E. F., Gucel, S., and Tran, L. S. P. (2016). Nitric oxide mitigates salt stress by regulating levels of osmolytes and antioxidant enzymes in chickpea. *Front. Plant Sci.* 7:347. doi: 10.3389/fpls.2016.00347

Akram, N. A., Hafeez, N., Farid-Ul-Haq, M., Ahmad, A., Sadiq, M., and Ashraf, M. (2020). Foliage application and seed priming with nitric oxide causes mitigation of salinity-induced metabolic adversaries in broccoli (*Brassica oleracea* L.) plants. *Acta Physiol. Plant.* 42:155. doi: 10.1007/s11738-020-03140-x

Alamri, S., Ali, H. M., Khan, M. I. R., Singh, V. P., and Siddiqui, M. H. (2020). Exogenous nitric oxide requires endogenous hydrogen sulfide to induce the resilience through sulfur assimilation in tomato seedlings under hexavalent chromium toxicity. *Plant Physiol. Biochem.* 155, 20–34. doi: 10.1016/j.plaphy.2020.07.003

Amri, E., Mirzaei, M., Moradi, M., and Zare, K. (2011). The effects of spermidine and putrescine polyamines on growth of pomegranate (*Punica granatum* L. cv 'Rabbab') in salinity circumstance. *Int. J. Plant Physiol. Biochem.* 3, 43–49. doi: 10.5897/IJPPB.9000044

Arnon, D. I. (1949). Copper enzymes in isolated chloroplasts. Polyphenoloxidase in *Beta vulgaris*. *Plant Physiol* 24, 1–15. doi: 10.1104/pp.24.1.1

Astier, J., Gross, I., and Durner, J. (2018). Nitric oxide production in plants: an update. *J. Exp. Bot.* 69, 3401–3411. doi: 10.1093/jxb/erx420

Babaei, S., Niknam, V., and Behmanesh, M. (2021). Comparative effects of nitric oxide and salicylic acid on salinity tolerance in saffron (*Crocus sativus*). *Plant Biosyst.* 155, 73–82. doi: 10.1080/11263504.2020.1727975

Baena-Gonzalez, E., and Aro, E. M. (2002). Biogenesis, assembly and turnover of photosystem II units. Philos. *Trans. R. Soc. Lond. B Biol. Sci.* 357, 1451–1460. doi: 10.1098/rstb.2002.1141

Baker, N. R. (2008). Chlorophyll fluorescence: a probe of photosynthesis in vivo. *Annu. Rev. Plant Biol.* 59, 89–113. doi: 10.1146/annurev.arplant.59.032607.092759

Bates, L. S., Waldren, R. P., and Teare, I. D. (1973). Rapid determination of free proline for water-stress studies. *Plant Soil* 39, 205–207. doi: 10.1007/BF00018060

Beauchamp, C., and Fridovich, I. (1971). Superoxide dismutase: improved assays and an assay applicable to acrylamidegels. *Anal. Biochem.* 44, 276–287. doi: 10.1016/0003-2697(71)90370-8

Begara-Morales, J. C., Sánchez-Calvo, B., Luque, F., Leyva-Pérez, M. O., Leterrier, M., Corpas, F. J., et al. (2014). Differential transcriptomic analysis by RNA-Seq of GSNO-responsive genes between *Arabidopsis* roots and leaves. *Plant Cell Physiol.* 55, 1080–1095. doi: 10.1093/pcp/pcu044

Bhatnagar-Mathur, P., Vadez, V., and Sharma, K. K. (2008). Transgenic approaches for abiotic stress tolerance in plants: retrospect and prospects. *Plant Cell Rep.* 27, 411–424. doi: 10.1007/s00299-007-0474-9

Bradford, M. M. (1976). A rapid and sensitive method for the quantitation of microgram quantities of protein utilizing the principle of protein-dye binding. *Anal. Biochem.* 72, 248–254. doi: 10.1016/0003-2697(76)90527-3

Cantrel, C., Vazquez, T., Puyaubert, J., Rezé, N., Lesch, M., Kaiser, W. M., et al. (2011). Nitric oxide participates in cold-responsive phosphosphingolipid formation and gene expression in Arabidopsis thaliana. *New Phytol.* 189, 415–427. doi: 10.1111/j.1469-8137.2010.03500.x

Chen, F., Shen, J., Min, D., Ke, L., Tian, X., Korpelainen, H., et al. (2018). Male *Populus cathayana* than female shows higher photosynthesis and less cellular injury through ABA-induced manganese transporting inhibition under high manganese condition. *Trees* 32, 255–263. doi: 10.1007/s00468-017-1628-1

Chen, P., Yang, W., Jin, S., and Liu, Y. (2021). Hydrogen sulfide alleviates salinity stress in *Cyclocarya paliurus* by maintaining chlorophyll fluorescence and regulating nitric oxide level and antioxidant capacity. *Plant Physiol. Biochem.* 167, 738–747. doi: 10.1016/j.plaphy.2021.09.004

Corpas, F. J., and Barroso, J. B. (2015). Functions of nitric oxide (NO) in roots during development and under adverse stress conditions. *Plan. Theory* 4, 240–252. doi: 10.3390/plants4020240

Corpas, F. J., and Barroso, J. B. (2017). Nitric oxide synthase-like activity in higher plants. *Nitric Oxide* 68, 5–6. doi: 10.1016/j.niox.2016.10.009

da Silva, C. J., Batista, F. E. P., and Modolo, L. V. (2017). Salinity-induced accumulation of endogenous H_2S and NO is associated with modulation of the antioxidant and redox defense systems in *Nicotiana tabacum* L. cv. *Havana*. *Plant Sci.* 256, 148–159. doi: 10.1016/j.plantsci.2016.12.011

da-Silva, C. J., and Modolo, L. V. (2017). Hydrogen sulfide: a new endogenous player in an old mechanism of plant tolerance to high salinity. *Act. Bot. Bras.* 32, 150–160. doi: 10.1590/0102-33062017abb0229

Deng, Y., and Shen, S., Chen, CF., Cheng, X., and Zhang, F. (2011). The embryo rescue derived intergeneric hybrid between chrysanthe-mum and *Ajania przewalskii* shows enhanced cold tolerance. *Plant Cell Rep.* 30, 2177–2186. doi:10.1007/s00299-011-1123-x

Dong, Y., Jinc, S., Liu, S., Xu, L., and Kong, J. (2014). Effects of exogenous nitric oxide on growth of cotton seedlings under NaCl stress. *J. Soil Sci. Plant Nutr.* 14, 1–13. doi: 10.4067/S0718-95162014005000001

Fang, Y. R., and Xue, L. (2019). Research advances in the effect of salt stress on plant chlorophyll fluorescence. *Eco. Sci.* 38, 225–234. (in Chinese)

Golldack, D., Li, C., Mohan, H., and Probst, N. (2014). Tolerance to drought and salt stress in plants: unraveling the signaling networks. *Front. Plant Sci.* 5:151. doi: 10.3389/fpls.2014.00151

Hasanuzzaman, M., Hossain, M. A., and Fujita, M. (2011). Nitric oxide modulates antioxidant defense and the methylglyoxal detoxification system and reduces salinity-induced damage of wheat seedlings. *Plant Biotechnol. Rep.* 5, 353–365. doi: 10.1007/s11816-011-0189-9

He, M., Shi, D., Wei, X., Hu, Y., Wang, T., and Xie, Y. (2016). Gender-related differences in adaptability to drought stress in the dioecious tree *Ginkgo biloba*. *Acta Physiol. Plant.* 38, 1–14. doi: 10.1007/s11738-016-2148-0

Hu, Y., Zhang, Z., Hua, B., Tao, L., Chen, W., Gao, Y., et al. (2022). The interaction of temperature and relative humidity affects the main aromatic components in postharvest *Torreya grandis* nuts. *Food Chem.* 368:130836. doi: 10.1016/j.foodchem.2021.130836

Jaworski, E. G. (1971). Nitrate reductase assay in intact plant tissues. *Biochem. Biophys. Res. Commun.* 43, 1274–1279. doi: 10.1016/S0006-291X(71)80010-4

Khan, M. N., Mobin, M., Abbas, Z. K., and Siddiqui, M. H. (2017). Nitric oxide-induced synthesis of hydrogen sulfide alleviates osmotic stress in wheat seedlings through sustaining antioxidant enzymes, osmolyte accumulation and cysteine homeostasis. *Nitric Oxide* 68, 91–102. doi: 10.1016/j.niox.2017.01.001

Khan, M. N., Siddiqui, M. H., Mohammad, F., and Naeem, M. (2012). Interactive role of nitric oxide and calcium chloride in enhancing tolerance to salt stress. *Nitric Oxide* 27, 210–218. doi: 10.1016/j.niox.2012.07.005

Kharbech, O., Sakouhi, L., Massoud, M. B., Mur, L. A. J., Corpas, F. J., Djebali, W., et al. (2020). Nitric oxide and hydrogen sulfide protect plasma membrane integrity and mitigate chromium-induced methylglyoxal toxicity in maize seedlings. *Plant Physiol. Biochem.* 157, 244–255. doi: 10.1016/j.plaphy.2020.10.017

Kopyra, M., and Gwózdz, E. A. (2003). Nitric oxide stimulates seed germination and counteracts the inhibitory effect of heavy metals and salinity on root growth of *Lupinus luteus*. *Plant Physiol. Biochem.* 41, 1011–1017. doi: 10.1016/j.plaphy.2003.09.003

Laxalt, A. M., García-Mata, C., and Lamattina, L. (2016). The dual role of nitric oxide in guard cells: promoting and attenuating the ABA and phospholipidderived signals leading to the stomatal closure. *Front. Plant Sci.* 7:476. doi: 10.3389/fpls.2016.00476

Lázaro, J. J., Jiménez, A., Camejo, D., Martí, M. C., Lázaro-Payo, A., Barranco-Medina, S., et al. (2013). Dissecting the integrative antioxidant and redox systems in plant mitochondria. Effect of stress and S-nitrosylation. *Front. Plant Sci.* 4:460. doi: 10.3389/fpls.2013.00460

Li, T., Hu, Y., Du, X., Tang, H., Shen, C., and Wu, J. (2014). Salicylic acid alleviates the adverse effects of salt stress in *Torreya grandis* cv. *Merrillii* seedlings by activating photosynthesis and enhancing antioxidant systems. *PLoS One* 9:e109492. doi: 10.1371/journal.pone.0109492

Li, H., Shi, J., Wang, Z., Zhang, W., and Yang, H. (2020). H_2S pretreatment mitigates the alkaline salt stress on *Malus hupehensis* roots by regulating Na^+/K^+ homeostasis and oxidative stress. *Plant Physiol. Biochem.* 156, 233–241. doi: 10.1016/j.plaphy.2020.09.009

Li, L., Zhang, Y., Luo, J., Korpelainen, H., and Li, C. (2013). Sex-specific responses of *Populus yunnanensis* exposed to elevated CO_2 and salinity. *Physiol. Plant.* 147, 477–488. doi: 10.1111/j.1399-3054.2012.01676.x

Liu, S., Dong, Y. J., Xu, L. L., Kong, J., and Bai, X. Y. (2013). Roles of exogenous nitric oxide in regulating ionic equilibrium and moderating oxidative stress in cotton seedlings during salt stress. *J. Soil Sci. Plant Nut.* 13, 929–941. doi: 10.4067/S0718-95162013005000073

Liu, W., Li, R. J., Han, T. T., Cai, W., Fu, Z. W., and Lu, Y. T. (2015). Salt stress reduces root meristem size by nitric oxide-mediated modulation of auxin accumulation and signaling in Arabidopsis. *Plant Physiol.* 168, 343–356. doi: 10.1104/pp.15.00030

Mantri, N., Patade, V., Penna, S., Ford, R., and Pang, E. (2012). "Abiotic stress responses in plants: present and future," in *Abiotic Stress Responses in Plants*. ed. H. Zhang (New York: Springer), 1–19.

Mostofa, M. G., Saegusa, D., Fujita, M., and Tran, L. S. P. (2015). Hydrogen sulfide regulates salt tolerance in rice by maintaining Na^+/K^+ balance, mineral homeostasis and oxidative metabolism under excessive salt stress. *Front. Plant Sci.* 6:1055. doi: 10.3389/fpls.2015.01055

Mur, L. A., Mandon, J., Persijn, S., Cristescu, S. M., Moshkov, I. E., Novikova, G. V., et al. (2013). Nitric oxide in plants: an assessment of the current state of knowledge. *AoB Plants* 5, 1–17. doi: 10.1093/aobpla/pls052

Nakano, Y., and Asada, K. (1981). Hydrogen peroxide is scavenged by ascorbate-specific peroxidase in spinach chloroplasts. *Plant Cell Physiol.* 22, 867–880. doi: 10.1093/oxfordjournals.pcp.a076232

Ounoki, R., Ágh, F., Hembrom, R., Ünnep, R., Szögi-Tatár, B., Böszörményi, A., et al. (2021). Salt stress affects plastid ultrastructure and photosynthetic activity but not the essential oil composition in spearmint (*Mentha spicata* L. var. *crispa* "Moroccan"). *Front. Plant Sci.* 12:739467. doi: 10.3389/fpls.2021.739467

Pashkovskiy, P. P., Soshinkova, T. N., Korolkova, D. V., Kartashov, A. V., Zlobin, I. E., and Lyubimov, V. Y. (2018). The effect of light quality on the pro−/antioxidant balance, activity of photosystem II, and expression of lightdependent genes in *Eutrema salsugineum* callus cells. *Photosynth. Res.* 136, 199–214. doi: 10.1007/s11120-017-0459-7

Patterson, B. D., MacRae, E. A., and Ferguson, I. B. (1984). Estimation of hydrogen peroxide in plant extracts using titanium (IV). *Anal. Biochem.* 139, 487–492. doi: 10.1016/0003-2697(84)90039-3

Rana, S., and Liu, Z. (2021). Study on the pattern of vegetative growth in young dioecious trees of *Idesia polycarpa* maxim. *Trees* 35, 69–80. doi: 10.1007/s00468-020-02013-7

Ren, Y., Wang, W., He, J., Zhang, L., Wei, Y., and Yang, M. (2020). Nitric oxide alleviates salt stress in seed germination and early seedling growth of pakchoi (*Brassica chinensis* L.) by enhancing physiological and biochemical parameters. *Ecotoxicol. Environ. Saf.* 187:109785. doi: 10.1016/j.ecoenv.2019.109785

Retuerto, R., Lema, B. F., Roiloa, S. R., and Obeso, J. R. (2000). Gender, light and water effects in carbon isotope discrimination, and growth rates in the dioecious tree *Ilex aquifolium*. *Funct. Ecol.* 14, 529–537. doi: 10.1046/j.1365-2435.2000.t01-1-00454.x

Ruan, H., Shen, W., Ye, M., and Xu, L. (2002). Protective effects of nitric oxide on salt stress-induced oxidative damage to wheat (*Triticum aestivum* L.) leaves. *Chi. Sci. Bull.* 47, 677–681. doi: 10.1360/02tb9154

Shen, J., Li, X., Zhu, X., Ding, Z., Huang, X., Chen, X., et al. (2022). Molecular and photosynthetic performance in the yellow leaf mutant of *Torreya grandis* according to transcriptome sequencing, chlorophyll a fluorescence, and modulated 820 nm reflection. *Cell* 11:431. doi: 10.3390/cells11030431

Singh, M., Kushwaha, B. K., Singh, S., Kumar, V., Singh, V. P., and Prasad, S. M. (2017). Sulphur alters chromium (VI) toxicity in *Solanum melongena* seedlings: role of Sulphur assimilation and Sulphur-containing antioxidants. *Plant Physiol. Biochem.* 112, 183–192. doi: 10.1016/j.plaphy.2016.12.024

Song, L., Meng, X., Yang, L., Ma, Z., Zhou, M., Yu, C., et al. (2022). Identification of key genes and enzymes contributing to nutrition conversion of Torreya grandis nuts during post-ripening process. *Food Chem.* 384:132454. doi: 10.1016/j.foodchem.2022.132454

Strasser, R. J., Tsimilli-Michael, M., Qiang, S., and Goltsev, V. (2010). Simultaneous in vivo recording of prompt and delayed fluorescence and 820-nm reflection changes during drying and after rehydration of the resurrection plant *Haberlea rhodopensis*. *Biochim. Biophys. Acta* 1797, 1313–1326. doi: 10.1016/j.bbabio.2010.03.008

Suda, O., Tsutsui, M., Morishita, T., Tanimoto, A., Horiuchi, M., Tasaki, H., et al. (2002). Long-term treatment with Nω-nitro-L-arginine methyl ester causes arteriosclerotic coronary lesions in endothelial nitric oxide synthase-deficient mice. *Circulation* 106, 1729–1735. doi: 10.1161/01.CIR.0000029749.16101.44

Susanne-S, R., and Ricklefs, R.-E. (1995). Dioecy and its correlates in the flowering plants. *Am. J. Bot.* 82, 596–606. doi: 10.1002/j.1537-2197.1995.tb11504.x

Todd-E, D., and Bliss, L.-C. (1989). Patterns of water use and the tissue water relations in the dioecious shrub, *Salix arctica*: the physiological basis for habitat partitioning between the sexes. *Oecologia* 79, 332–343. doi: 10.1007/BF00384312

Vaishnav, A., Kumari, S., Jain, S., Varma, A., Tuteja, N., and Choudhary, D. K. (2016). PGPR-mediated expression of salt tolerance gene in soybean through volatiles under sodium nitroprusside. *J. Basic Microbiol.* 56, 1274–1288. doi: 10.1002/jobm.201600188

Valderrama, R., Chaki, M., Begara-Morales, J. C., Petrivalský, M., and Barroso, J. B. (2021). Nitric oxide in plants. *Front. Plant Sci.* 12:705157. doi: 10.3389/fpls.2021.705157

Venema, J. H., Villerius, L., and van Hasselt, P. R. (2000). Effect of acclimation to suboptimal temperature on chilling-induced photodamage: comparison between a domestic and a high-altitude wild *Lycopersicon* species. *Plant Sci.* 152, 153–163. doi: 10.1016/S0168-9452(99)00228-9

Wakeel, A., Xu, M., and Gan, Y. (2020). Chromium-induced reactive oxygen species accumulation by altering the enzymatic antioxidant system and associated cytotoxic, genotoxic, ultrastructural, and photosynthetic changes in plants. *Int. J. Mol. Sci.* 21:728. doi: 10.3390/ijms21030728

Wang, A. G. (1990). Quantitative relation between the reaction of hydroxylamine and superoxi-de anion radicals in plants. *Plant Physiol. Commun.* 26, 55–57.

Wang, Q. Z., Liu, Q., Gao, Y. N., and Liu, X. (2017). Review on the mechanisms of the response to salinity-alkalinity stress in plants. *Acta Ecol. Sin.* 37, 5565–5577.

Wang, J., Liu, Y., Xu, Y., Chen, W., Han, Y., Wang, G. G., et al. (2021). Sexual differences in gas exchange and chlorophyll fluorescence of *Torreya grandis* under drought stress. *Trees* 36, 1–12. doi: 10.1007/s00468-021-02205-9

Wani, K. I., Naeem, M., Castroverde, C. D. M., Kalaji, H. M., Albaqami, M., and Aftab, T. (2021). Molecular mechanisms of nitric oxide (NO) signaling

and reactive oxygen species (ROS) homeostasis during abiotic stresses in plants. *Int. J. Mol. Sci.* 22:9656. doi: 10.3390/ijms22179656

Watanabe, N., Iwamoto, T., Bowen, K. D., Dickinson, D. A., Torres, M., and Forman, H. J. (2003). Bio-effectiveness of tat-catalase conjugate: a potential tool for the identification of H_2O_2-dependent cellular signal transduction pathways. *Biochem. Biophys. Res. Commun.* 303, 287–293. doi: 10.1016/S0006-291X(03)00335-8

You, J., and Chan, Z. (2015). ROS regulation during abiotic stress responses in crop plants. *Front. Plant Sci.* 6:1092. doi: 10.3389/fpls.2015.01092

Yu, W., Liu, Y., Song, L., Jacobs, D. F., Du, X., Ying, Y., et al. (2017). Effect of differential light quality on morphology, photosynthesis, and antioxidant enzyme activity in *Camptotheca acuminata* seedlings. *J. Plant Growth Regul.* 36, 148–160. doi: 10.1007/s00344-016-9625-y

Zhang, R., Liu, J., Liu, Q., He, H., Xu, X., and Dong, T. (2019). Sexual differences in growth and defence of *Populus yunnanensis* under drought stress. *Can. J. For. Res.* 49, 491–499. doi: 10.1139/cjfr-2018-0270

Conflict of Interest: The authors declare that the research was conducted in the absence of any commercial or financial relationships that could be construed as a potential conflict of interest.

Publisher's Note: All claims expressed in this article are solely those of the authors and do not necessarily represent those of their affiliated organizations, or those of the publisher, the editors and the reviewers. Any product that may be evaluated in this article, or claim that may be made by its manufacturer, is not guaranteed or endorsed by the publisher.

frontiers | Frontiers in Plant Science

ORIGINAL RESEARCH
published: 02 June 2022
doi: 10.3389/fpls.2022.905633

Effects of Fruit Shading on Gene and Protein Expression During Starch and Oil Accumulation in Developing *Styrax tonkinensis* Kernels

Qikui Wu[1,2,3], Hong Chen[1], Zihan Zhang[1,4], Chen Chen[1], Fangyuan Yu[1] and Robert D. Guy[3]**

[1]Collaborative Innovation Centre of Sustainable Forestry in Southern China, College of Forest Science, Nanjing Forestry University, Nanjing, China, [2]State Forestry and Grassland Administration Key Laboratory of Silviculture in Downstream Areas of the Yellow River, College of Forestry, Shandong Agricultural University, Tai'an, China, [3]Department of Forest and Conservation Sciences, Faculty of Forestry, University of British Columbia, Vancouver, BC, Canada, [4]State Key Laboratory of Tree Genetics and Breeding and Key Laboratory of Tree Breeding and Cultivation, State Forestry Administration, Research Institute of Forestry, Chinese Academy of Forestry, Beijing, China

OPEN ACCESS

Edited by:
Song Heng Jin, Zhejiang Agriculture and Forestry University, China

Reviewed by:
Yaqiong Wu, Jiangsu Province and Chinese Academy of Sciences, China
Shu Hui Du, Shanxi Agricultural University, China

***Correspondence:**
Fangyuan Yu
fyyu@njfu.edu.cn
Robert D. Guy
rob.guy@ubc.ca

Specialty section:
This article was submitted to Plant Proteomics and Protein Structural Biology, a section of the journal Frontiers in Plant Science

Received: *28 March 2022*
Accepted: *06 May 2022*
Published: *02 June 2022*

Citation:
Wu Q, Chen H, Zhang Z, Chen C, Yu F and Guy RD (2022) Effects of Fruit Shading on Gene and Protein Expression During Starch and Oil Accumulation in Developing Styrax tonkinensis Kernels. Front. Plant Sci. 13:905633. doi: 10.3389/fpls.2022.905633

Styrax tonkinensis has great potential as a biofuel feedstock source having industrial oilseeds with excellent fatty acids (FAs) composition and good fuel properties. Photosynthesis in the developing pericarp could affect the carbon distribution in kernel. During kernel development, more carbon sources are allocated to starch rather than lipid, when the pericarp photosynthesis is reduced by fruit shading treatment. After shading the fruits at 50 days after flowering (DAF), samples of shaded fruit (FSK) and controls (CK) were collected at 80 DAF and analyzed using the proteomic method. We identified 3,181 proteins, of which 277 were differentially expressed proteins, all downregulated in the FSK group. There were 56 proteins found involved in carbohydrate metabolism and lipid biosynthesis leading to oil accumulation with their iTRAQ ratios of FSK/CK ranging from 0.7123 to 1.1075. According to the qRT-PCR analyses, the key genes related to FA and triacylglycerol (TAG) biosynthesis were significantly downregulated between 60 and 90 DAF especially at 80 DAF, while the key genes involved in starch biosynthesis and FA desaturase had no significant difference between the two groups at 80 DAF. Fruit shading is a negative treatment for lipid accumulation but not starch accumulation by restraining enzymic protein expression involved in FA and TAG biosynthesis during *S. tonkinensis* kernel development.

Keywords: fruit shading, kernel development, carbon partitioning, oil biosynthesis, differentially expressed proteins

INTRODUCTION

Autotrophic plants acquire carbon through photosynthesis, which provides organic compounds for conversion into different metabolites (Ashraf and Harris, 2013). Photosynthate produced in chloroplast-containing "source" tissues is transported to different "sink" tissues or organs to be consumed in respiration or utilized in the synthesis of starch, oil, and proteins (Bennett

et al., 2011). The transport of photosynthates from source to sink is one of the most important factors affecting seed development (Li et al., 2011; Hua et al., 2012). Different light intensity caused by shading treatment resulted in significant differences in metabolites in blueberry leaves (Wu et al., 2022). Photosynthesis in the pericarp contributes a certain proportion of the source carbon deposited in kernels and affects seed quality and kernel nutrient accumulation (Xu et al., 2016). During fruit development, treatments used to manipulate the photosynthetic rate can affect the carbon distribution in kernels, especially between starch and lipid (Ma et al., 2014; Zhang et al., 2018).

Styrax tonkinensis (Pierre) Craib ex Hartwich, as a woody biodiesel species, has seed kernels with high oil content (more than 50%) during seed maturation (Wu et al., 2019a). Oleic acid (C18:1) and linoleic acid (C18:2) are the two major fatty acids (FAs) and account for more than 80% of the total FA content (Zhang et al., 2017). During kernel development, the biological metabolic processes of starch and FA biosynthesis are catalyzed by two series of enzymes; glucose-1-phosphate adenylyltransferase (AGP), starch synthase (glgA) and 1,4-alpha-glucan branching enzyme (glgB) play important roles in starch synthesis (Lin et al., 2006; Bourgis et al., 2011), while the pyruvate dehydrogenase complex (PDC), acetyl-CoA carboxylase complex (ACC), 3-oxoacyl-ACP reductase (KAR), enoyl-ACP reductase (EAR), acyl-CoA:DAG acyltransferase (DGAT), and phospholipid:diacylglyceryl transferase (PDAT) take on major responsibilities in FA and triacylglycerol (TAG) biosynthesis (Bates et al., 2013; Niu et al., 2015).

Mechanisms of oil accumulation have been analyzed at the molecular level using transcriptomic and proteomic methods in many oilseed plants, including *Elaeis guineensis* (Bourgis et al., 2011; Silva et al., 2014), *Vernicia fordii* (Zhang et al., 2014; Zhan et al., 2016), *Jatropha curcas* (Grover et al., 2014; Liu et al., 2015) and *S. tonkinensis* (Wu et al., 2020, 2021). In our previous studies, ACC and PDC were placed in the center of the regulatory network for oil accumulation during *S. tonkinensis* kernel development (Wu et al., 2020, 2021). However, at the protein level, the biological functioning of TAG-related enzymes, such as DGAT and PDAT, is unclear, as these endoplasmic reticulum-associated proteins appear at middle stages during kernel development (Wiese et al., 2007; Liu et al., 2018). According to the nutrient distribution in the continuum of the pericarp, seed coat, and kernel, the nutrient deposition center would be transferred into kernels from the maternal units (the pericarp and seed coat) which may function as a nutrient buffer storage area between the mother tree and the kernel (Bennett et al., 2011; Wu et al., 2019b).

In another previous study, we found that pericarp photosynthesis in *S. tonkinensis* was stimulated by treatment with the brassinosteroid hormone 24-epibrassinolide and attenuated by fruit shading (Zhang et al., 2018). Oil accumulation in developing *S. tonkinensis* kernels was markedly impaired at about 80 days after flowering (DAF) while the fruits grew in low light conditions under three layers of black, non-woven fabric bags (Shade#3 treatment). Meanwhile, a much larger proportion of carbon precursor was directed toward starch accumulation causing a high starch/oil ratio in the developing kernels under this treatment. A possible reason may be that the oil-related enzymes, such as ACC, DGAT, and PDAT, are more susceptible to carbon source shortage.

To further understand the effect of fruit shading on developing kernels at protein levels, we repeated the Shade#3 treatment on developing *S. tonkinensis* fruits to analyze changes in differentially expressed proteins (DEPs) involved in kernel development and nutrient distribution by the isobaric tags for relative and absolute quantification (iTRAQ) method. The aims of the present study were to: (i) assess proteomic profiles of samples of shaded fruit (FSK) and controls (CK) kernels; (ii) identify DEPs between the two groups; (iii) identify the proteins involved in starch and lipid biosynthesis; and (iv) illucidate the molecular mechanism of carbon partitioning under source shortage during *S. tonkinensis* kernel development.

MATERIALS AND METHODS

Plant Material

The study was performed on 20 eight-year-old *S. tonkinensis* trees (from Jishui, Jiangxi Province) at the Styracaceae Germplasm Repository (32°32′ N, 118°50′ E) situated in Nanjing, China, belonging to the north subtropical monsoon humid climate zone. The plants grew under natural conditions with moderate soil fertility. In accordance with our previous study (Zhang et al., 2018), we chose 20 infructescences from each tree for fruit shading using three layers of black, non-woven fabric bags (Shade#3) on 18 July 2018 (50 DAF). No leaves were included in the shading bags. Twenty untreated fruits from the same trees were labeled as a control group. For each group, fresh fruits were collected every 10 days from July 18 (50 DAF) to August 27 (90 DAF). At each sampling, shaded and unshaded fruits were randomly selected from each tree and pooled into four biological replicates (i.e., fruits from five trees per replicate). To adjust for their growth, the number of fruits collected per treatment per tree was reduced from five to three over the sampling period. Fruits were placed on dry ice for transport to the laboratory and, after removing the pericarps and seed coats, kernels were transferred to liquid nitrogen storage for iTRAQ and qRT-PCR analyses.

Protein Extraction and iTRAQ Analysis

Kernels collected from FSK and CK groups at 80 DAF were used for proteomic analysis, again with four biological replicates per treatment. Protein extraction and digestion were performed according to our previous study (Wu et al., 2021). The peptide mixture resulting from trypsin digestion was labeled using an 8-plex iTRAQ kit (AB Sciex, Framingham, United States) following the manufacturer's instructions and Ye et al. (2010). Peptides were labeled as follows: FSK samples with iTRAQ-113, 114, 115, and 116, CK samples with iTRAQ-117, 118, 119, and 121. The labeled peptides were pooled before lyophilization in a vacuum concentrator.

Reverse-phase high-performance liquid chromatography (HPLC) was used to separate labeled peptides following

procedures as described by Liu et al. (2017). The peptide mixture was re-dissolved in solvent A (20 mM ammonium formate adjusted to pH 10.0 with NH_4OH), and then fractionated by high pH separation using an Ultimate 3,000 liquid chromatography system (Thermo Fisher Scientific, Waltham, United States) connected to an XBridge C18 reverse-phase column (4.6 mm × 250 mm, 5 μm) equilibrated with solvent B (20:80 (v/v) ammonium formate buffer (pH 10.0):acetonitrile). After separation, 12 final fractions were collected and vacuum-dried for the next step. Re-dissolved peptides were analyzed by Nano-HPLC-MS/MS using an EASY nLC 1,000 system (Waters Corporation, Milford, United States) coupled to a Q-Exactive mass spectrometer (Thermo Fisher Scientific, Waltham, United States). The parameter settings were as described by our previous study (Wu et al., 2021).

After analyzing the tandem mass spectra with PEAKS Studio version 8.5 (Bioinformatics Solutions, Waterloo, Canada), customized protein sequence databases derived from transcriptome sequence analysis (Wu et al., 2020) were searched with PEAKS DB assuming trypsin as the digestion enzyme and with fragment ion mass and parent ion tolerances set at 0.05 Da and 7 ppm, respectively. The bioinformatics analyses were specified according to Lu et al. (2019). After protein identification, the DEPs between FSK and CK groups were recognized if their abundance ratios were over 1.5 or <0.667 with $p < 0.01$ (by ANOVA) and they contained at least two unique peptides. Identified proteins were classified using the public protein databases. Proteins involved in carbohydrate metabolism and lipid biosynthesis were subsequently tallied *via* the gene functional annotation.

Total RNA Extraction and qRT-PCR Analysis

Quantitative real-time PCR (qRT-PCR) of seven genes related to carbon flux from sucrose to fatty acids at five time points from 50 to 90 DAF was carried out. Total RNA extraction, first-strand cDNA synthesis, and amplification primer design (**Supplementary Table 1**) were performed as described in our previous study (Wu et al., 2020). All reactions were done on a StepOne Real-Time PCR System using SYBR Green Dye (Applied Biosystems, Foster City, United States; Takara, Dalian, China). Relative gene expression was evaluated using the $2^{-\Delta\Delta Ct}$ method with 18S ribosomal RNA as an internal control.

RESULTS

Mass Spectrometry Analysis and Protein Identification

Peptides and proteins of FSK and CK samples at 80 DAF were identified by the iTRAQ method. After searching the unique mass spectra and peptides against the *S. tonkinensis* transcription database, a total of 3,181 proteins were obtained (**Supplementary Table 2**). The proteomic data from all samples followed a normal distribution and showed high repeatability across biological replicates by principal component (PCA) and hierarchical cluster (HCA) analyses. For the PCA analysis (**Figure 1A**), all four replicates of the CK group were clustered together near the origin in the lower right quadrant, but well separated from the samples of the FSK group distributed across

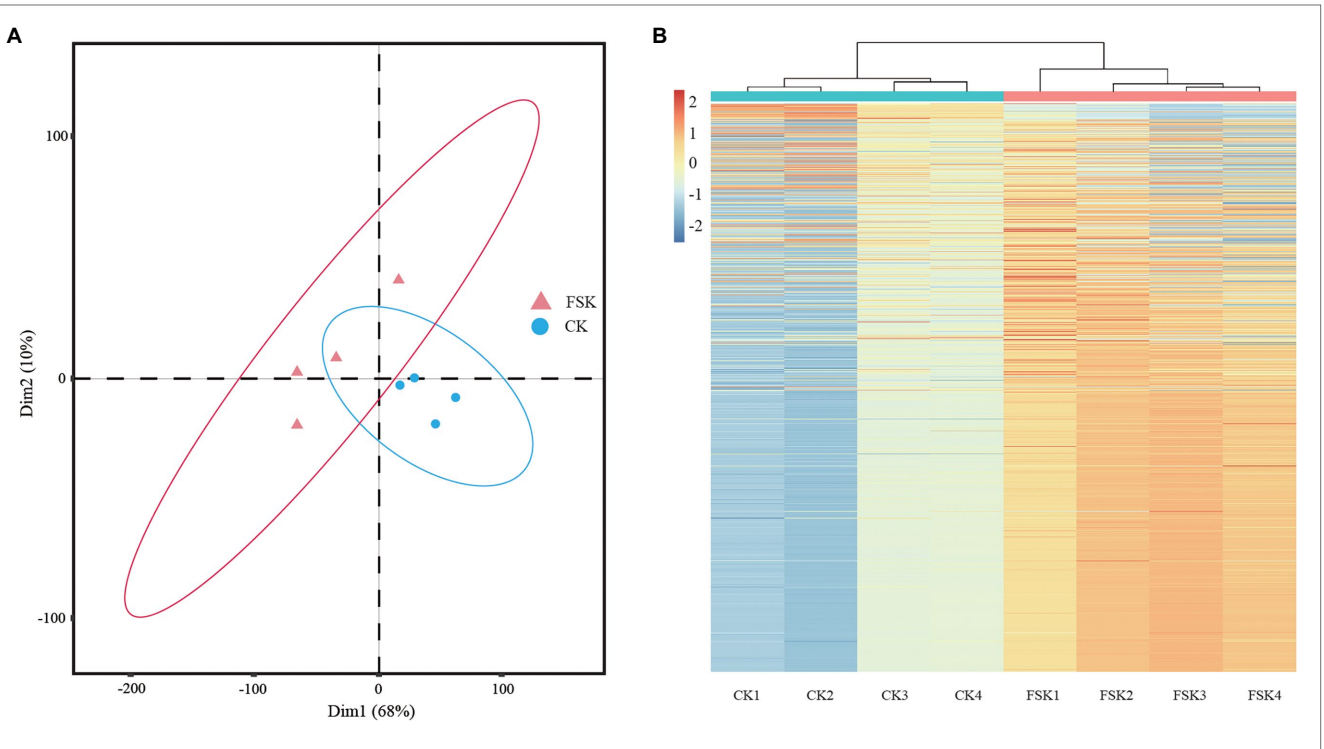

FIGURE 1 | Quality control of samples of different groups. **(A)** Principal component analysis of samples. **(B)** Hierarchical cluster analysis of samples.

the other three quadrants. For the HCA analysis (**Figure 1B**), replicates were clustered together depending on whether the fruit was shaded or not.

The 3,181 identified proteins were annotated against the Gene Ontology (GO) database and then categorized into three functional categories: biological process (BP), cellular component (CC), and molecular function (MF). The top 20 sub-categories of annotated proteins in each term were listed (**Supplementary Figure 1**). Under the BP term, the major sub-categories were "metabolic process" (1,491), "cellular process" (1,439), and "organic substance metabolic process" (1,314). Nested within the CC term, "cell part" (1,368) and "intracellular part" (1,317) were the major sub-categories. "Catalytic activity" (1,490) and "binding" (1,348) were the major MF groups.

Identification of Differentially Expressed Proteins

According to the relative expression levels, a total of 227 DEPs between the FSK and CK groups at 80 DAF were identified (**Supplementary Table 3**). All of the DEPs were downregulated in the FSK group relative to the CK group. To analysis their functions, all DEPs were annotated against GO, Clusters of Orthologous Groups (COG), and the Kyoto Encyclopedia of Genes and Genomes (KEGG) databases.

In the GO annotation analysis, the 227 DEPs were categorized into the same three functional categories (i.e., BP, CC, and MF). The sub-categories of annotated proteins arranged by value of *p* in each term are listed in **Figure 2**. The DEPs in the BP term were mainly distributed in "protein refolding," "'*de novo*' protein folding," "carbon utilization," and "gluconeogenesis." Under the CC term, the major sub-categories were "proton-transporting ATP synthase complex, catalytic core *F* (1)," "mitochondrion," "cytosol," and "cytoplasm." "NAD binding," "unfolded protein binding," "oxidoreductase activity," and "coenzyme binding" were the major MF sub-categories.

The COG annotation analysis classified the 227 DEPs into 20 categories (**Figure 3**) with the majority in "post-translational modification, protein turnover, chaperones" (79), followed by "energy production and conversion" (24), "carbohydrate transport and metabolism" (21), and "intracellular trafficking, secretion, and vesicular transport" (15). There were 10 proteins annotated into "lipid transport and metabolism."

In the KEGG annotation analysis, the 227 DEPs were assigned into four KEGG categories (metabolism, genetic information processing, cellular processes, and organismal systems), 16 sub-categories, and 79 KEGG pathways (**Figure 4**). Under the metabolism term, 51 DEPs were annotated into carbohydrate metabolism with the largest number within "glycolysis/gluconeogenesis" (11), followed by "starch and sucrose metabolism" (7), "amino sugar and nucleotide sugar metabolism" (6), "pyruvate metabolism" (6), and "glyoxylate and dicarboxylate metabolism" (5). Twenty-five, twenty, and thirteen DEPs were annotated into amino acid metabolism, energy metabolism,

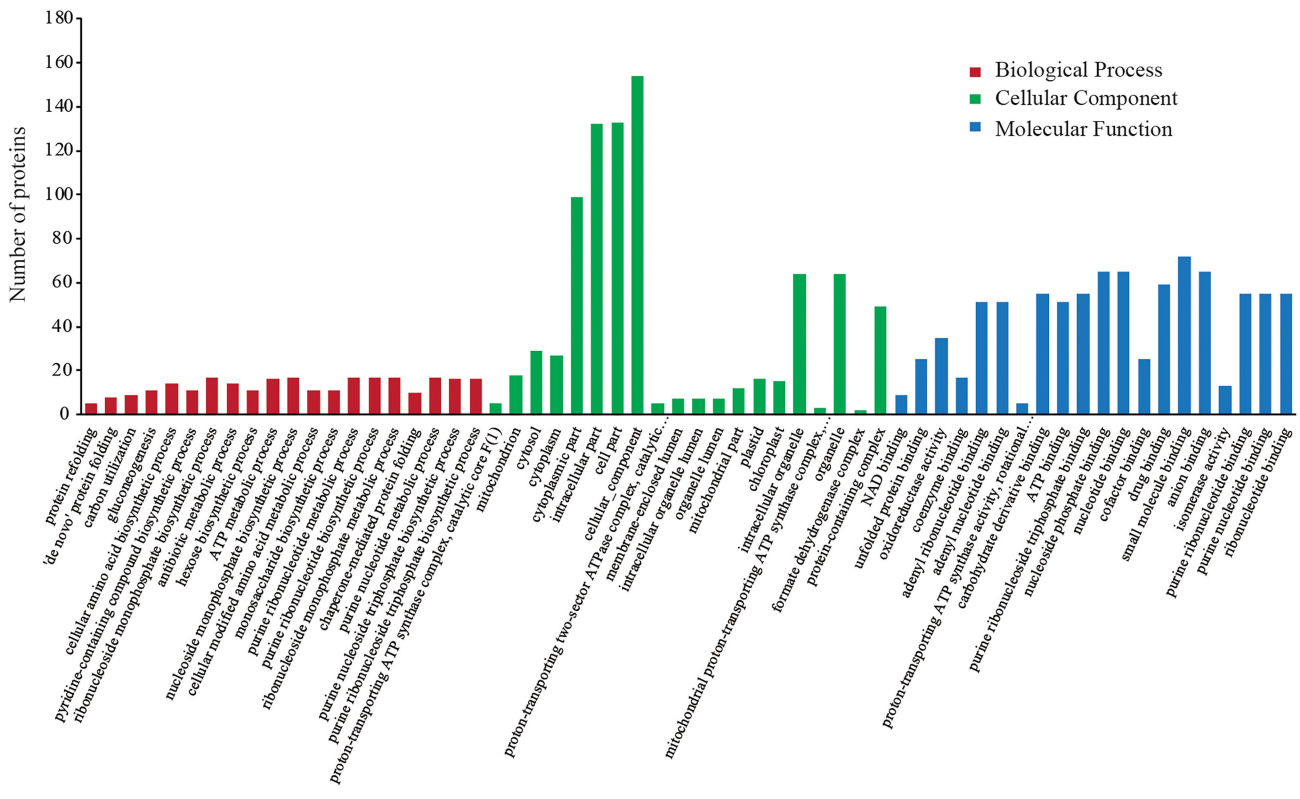

FIGURE 2 | GO annotation analysis of differentially expressed proteins (DEPs).

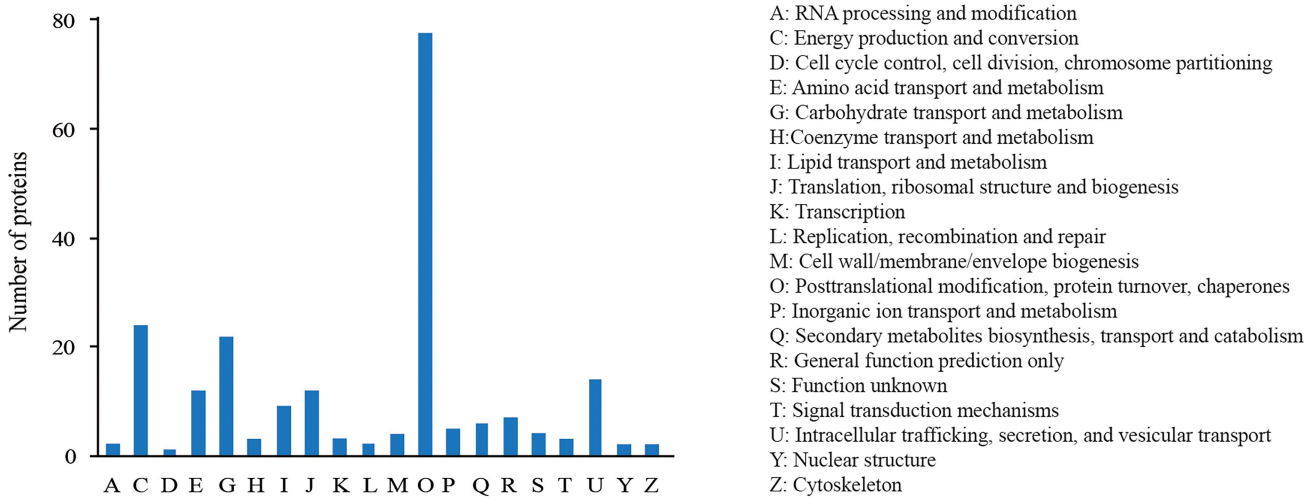

FIGURE 3 | COG annotation analysis of DEPs.

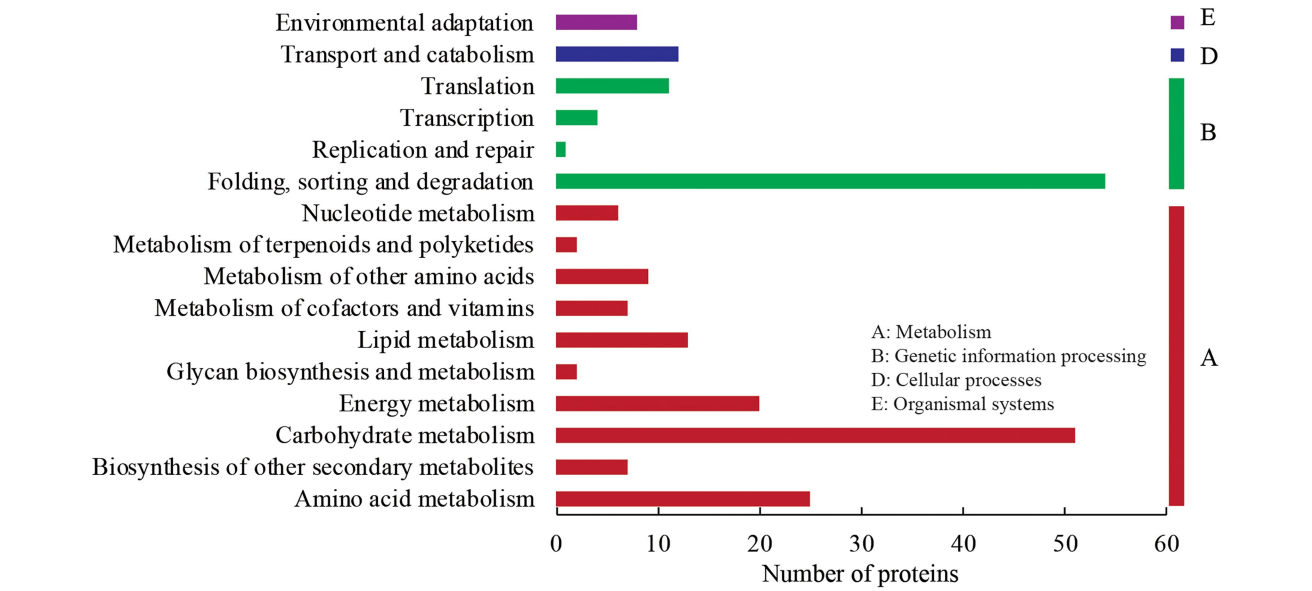

FIGURE 4 | KEGG annotation analysis of DEPs.

and lipid metabolism, respectively. Under the genetic information processing category, 54 DEPs were annotated into folding, sorting, and degradation with the majority in "protein processing in endoplasmic reticulum" (35). Additionally, there were 12 and 8 DEPs annotated into "transport and catabolism" (cellular processes) and "environmental adaptation" (organismal systems), respectively.

Identification of Protein Species Involved in Oil Accumulation

According to the annotation results, 56 of the 3,181 identified proteins are involved in carbohydrate metabolism and lipid biosynthesis leading to oil accumulation (**Supplementary Table 4**), including five proteins for starch and sucrose metabolism, 12 for glycolysis/gluconeogenesis, three for the pentose phosphate pathway, six for the TCA cycle, 13 for FA biosynthesis, seven for TAG biosynthesis, and three for FA metabolism. The iTRAQ ratios of all 56 proteins between the FSK and CK groups ranged from 0.7123 to 1.1075, with the majority being downregulated. According to the protein annotation, the identified transcription factors (TFs) were mainly concentrated in the PKL, C3H, MYB, and SBP families (**Supplementary Figure 2**). Most of the identified TFs showed downregulation trends in the Shade#3 treatment.

The ratios of sucrose synthase (SS) and sucrose phosphate synthase (SPS) between the FSK and CK groups were 0.9249 and 0.8741, respectively, with slight and non-significant

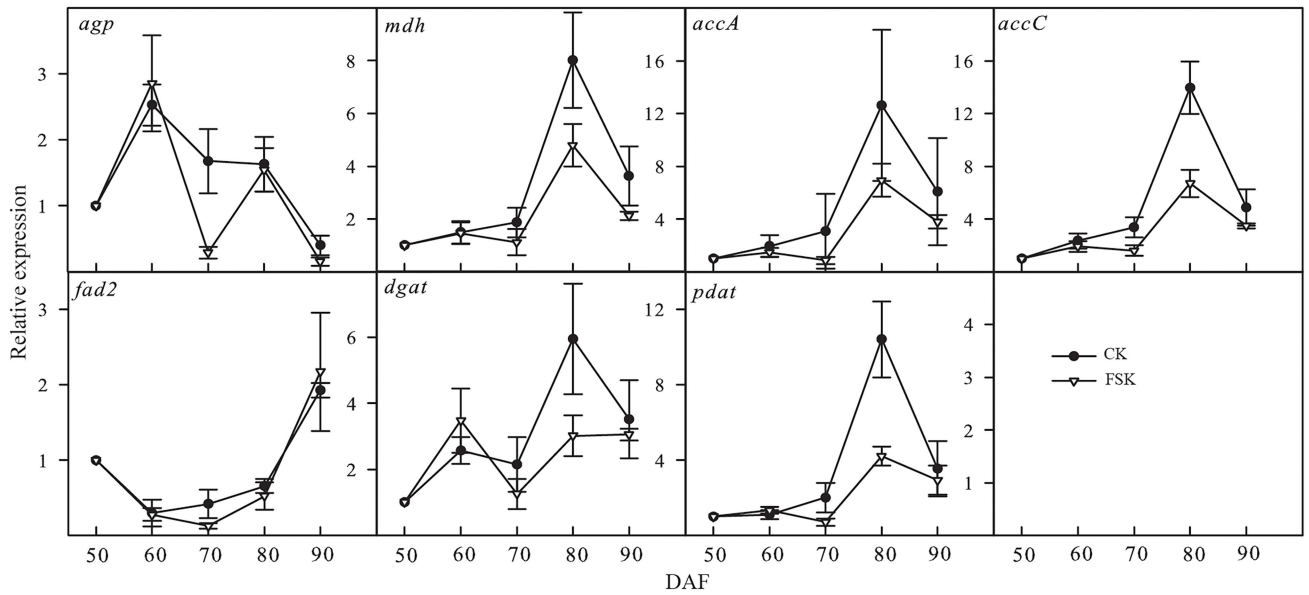

FIGURE 5 | Temporal expression patterns of genes involved in oil accumulation in the FSK and CK groups during *Styrax tonkinensis* kernel development from 50 to 90 DAF. Panels show relative expression levels determined by qRT-PCR of seven key genes (50 DAF as the control).

downregulation in FSK samples. The mean value of the ratios of enzymes involved in starch synthesis was 0.9813, including AGP (0.8381), glgA (0.9984), and glgB (1.1075). The mean values of the ratios of enzymes involved in glycolysis/gluconeogenesis, the pentose phosphate pathway, and TCA cycle were 0.8175, 0.8108, and 0.8237, respectively, most of which showed significant downregulation. The mean value of enzymes related to FA biosynthesis in plastid was 0.7964, with a lower ratio of KAR (0.7369) and EAR (0.7538). The mean value of enzymes involved in TAG biosynthesis in endoplasmic reticulum was 0.8157 with a lower ratio of DGAT (0.7534). The ratio of oil body membrane protein (i.e., OLE) was 0.8922 with slight and non-significant downregulation in FSK samples. The mean value of enzymes involved in oil metabolism was 0.8051 between FSK and CK groups.

qRT-PCR Analysis of Related Key Genes

Based on the results of our proteomic analysis, seven genes (*agp*, *mdh*, *accA*, *accC*, *fad2*, *dgat*, and *pdat*) known to be involved in oil accumulation were chosen for confirmation of mRNA expression levels by qRT-PCR (**Figure 5**). The dynamic expression of *agp* showed similar trends in the FSK and CK groups except at 70 DAF. The dynamic expression of fatty acid desaturase 2 (*fad2*) was very similar in both the FSK and CK during the whole observation period. The expression of the other key genes varied between 70 and 90 DAF, especially at 80 DAF where there was significantly lower expression in the FSK samples, relative to the CK group.

DISCUSSION

In higher plants, photosynthesis occurs in all green parts including leaves and other non-leaf organs, such as bracts, pedicels, and pericarps (Aschan and Pfanz, 2003; Kocurek et al., 2015). The change of photosynthesis rate effects the metabolite distribution (Wu et al., 2022). The supply of carbohydrate required by developing seed is affected significantly by treatments, such as fruit shading or pedicel ring cutting, which severely limits the delivery of photosynthate from the maternal plant (Hua et al., 2012). During soybean seed development, pod removal or leaf blade shading increased the protein percentage and decreased the oil content (Proulx and Naeve, 2009). In some plants, the seeds themselves can carry out photosynthesis that positively affects their growth (Andriotis et al., 2012; Galili et al., 2014). The percent oil content in green plant tissues increases with the increase of photosynthesis (Ohlrogge and Jaworski, 1997). In contrast, reduced inputs of source carbon decreases seed biomass accumulation and changes the nutrient composition of kernels by increasing the competitive accumulation of alternative storage compounds (Baud and Lepiniec, 2010).

Zhang et al. (2018) studied the effects of fruit spraying with 24-epibrassinolide and fruit shading treatments on kernel development in *S. tonkinensis*. They found significant changes in the allocation of carbon between starch and fatty acids at about 80 DAF when fruits were shaded by three layers of black, non-woven fabric bags (Shade#3). In our study, *S. tonkinensis* kernels were shaded with Shade#3 treatment from 50 DAF and then collected for iTRAQ-based proteomics analysis at 80 DAF and qRT-PCR analysis at 50, 60, 70, 80, and 90 DAF, respectively. There was high repeatability in the PCA and HCA analyses (Gerhardt et al., 2019). All the replicates from FSK and CK groups clustered together respectively, indicating that *S. tonkinensis* kernel biological processes at the protein level changed significantly with fruit shading. The number of proteins identified in this study (3,181) was more

than that (2,338) in the proteome analysis of *S. tonkinensis* kernel samples from different time points (Wu et al., 2021), which may be due to the gradual formation of proteins during kernel development, such as the proteins related to TAG formation in ER. All the 227 DEPs were downregulated in the FSK group, indicating that fruit shading inhibited *S. tonkinensis* kernel development by reducing photosynthesis in the pericarp and decreasing carbon source flow into kernels (Zhang et al., 2018; Wu et al., 2019b). The significant difference of protein expressions was shown at 80 DAF consistent with that the 70–80 DAF stage was identified to be an important time in the nutrient distribution in the continuum of the pericarp, seed coat, and kernel, while the deposition center for different nutrients moves to the kernel from either the pericarp or the seed coat (Wu et al., 2019b).

In developing kernels, the biological processes of oil biosynthesis are complex and involve carbohydrate decomposition, pyruvate, and acetyl-CoA formation, FA carbon chain extension, and TAG formation (Rawsthorne, 2002; Alonso et al., 2011; Lin et al., 2017). Meanwhile, oil accumulation is affected by starch synthesis, energy metabolism, amino acid metabolism (Ekman et al., 2008; Andriotis et al., 2012; Chaitanya et al., 2015). In our study, we identified 56 proteins related to 46 enzymes leading to oil accumulation and 10 of the proteins showed significant downregulation in the FSK group. According to the expression of related proteins in the FSK and CK groups, the expression ratio (FSK/CK) of proteins involved in FA biosynthesis was the lowest (0.7977), while those in starch biosynthesis was the highest (0.9813). In particular, the expression ratios of *glaA* and *glgB*, involved in starch biosynthesis, were 0.9984 and 1.1075 respectively, indicating that the fruit shading had no significant effect on the biological process of starch biosynthesis while simultaneously inhibiting oil accumulation in developing *S. tonkinensis* kernels (Wang et al., 1993; Zhang et al., 2018). For qRT-PCR analysis, *agp* involved in starch biosynthesis showed similar change trends in FSK and CK groups especially at 80 DAF, consistent with the change trend of related enzyme activities in the two groups (Zhang et al., 2018). Key genes involved in FA and TAG biosynthesis, such as *accA*, *accC*, *dgat*, and *pdat,* showed low expression in FSK groups, consistent with the change trends of related enzyme activity and oil content in the two groups. Moreover, the FA composition showed little change under fruit shading, consistent with little change in *fad2* expression at the transcript, protein, and enzyme activity levels (Zhang et al., 2018). The effect of fruit shading on kernel nutritional composition is to increase the relative starch content and decrease oil content by inhibiting the activity of related enzymes involved in oil accumulation.

CONCLUSION

In this study, 3,181 proteins and 227 DEPs were identified in samples of shaded fruit and controls kernels of *S. tonkinensis* at 80 DAF using the iTRAQ method. All the DEPs showed downregulated expression patterns in the FSK group. During *S. tonkinensis* kernel development, fruit shading treatment resulted in significant difference in oil content by constraining enzymic protein expression involved in FA and TAG biosynthesis and then leads to the decrease of seed oil content. Furthermore, the relative increase of starch content in shaded fruits is consistent with the observation that fruit shading had no effect on starch-related enzymic protein expression.

DATA AVAILABILITY STATEMENT

The raw data supporting the conclusions of this article will be made available by the authors, without undue reservation.

AUTHOR CONTRIBUTIONS

QW contributed to conceptualization, data curation, investigation, methodology, roles/writing—original draft, and writing—review and editing. HC contributed to data curation, methodology, and software. ZZ contributed to investigation and software. CC contributed to data curation and investigation. FY contributed to conceptualization, funding acquisition, project administration, supervision, and writing—review and editing. RG contributed to writing—original draft and writing—review and editing. All authors contributed to the article and approved the submitted version.

FUNDING

This work was supported by the Doctorate Fellowship Foundation of Nanjing Forestry University, Joint Research Project Based on Cooperative Program for Bachelor of Science in Forestry by Nanjing Forestry University and University of British Columbia, National Natural Science Foundation of China (3197140894), and A Project Funded by the Priority Academic Program Development of Jiangsu Higher Education Institutions (PAPD). The funders had no role in the design of the study and collection, analysis, and interpretation of data and in writing the manuscript.

ACKNOWLEDGMENTS

We thank Jihua Wang (Jiangsu Guoxing Co., Ltd) for providing *Styrax tonkinensis* seeds.

SUPPLEMENTARY MATERIAL

The Supplementary Material for this article can be found online at: https://www.frontiersin.org/articles/10.3389/fpls.2022.905633/full#supplementary-material

Supplementary Figure 1 | GO classification of proteins identified during *S. tonkinensis* kernel development.

Supplementary Figure 2 | The distribution of identified transcription factors during *S. tonkinensis* kernel development.

Supplementary Table 1 | Primer sequences used in the experiments.

Supplementary Table 2 | Proteins identified during *S. tonkinensis* kernel development.

Supplementary Table 3 | DEPs identified during *S. tonkinensis* kernel development.

Supplementary Table 4 | Identification of proteins involved in carbohydrate metabolism and oil accumulation during *S. tonkinensis* kernel development.

REFERENCES

Alonso, A. P., Val, D. L., and Shachar-Hill, Y. (2011). Central metabolic fluxes in the endosperm of developing maize seeds and their implications for metabolic engineering. *Metab. Eng.* 13, 96–107. doi: 10.1016/j.ymben.2010.10.002

Andriotis, V. M. E., Pike, M. J., Schwarz, S. L., Rawsthorne, S., Wang, T. L., and Smith, A. M. (2012). Altered starch turnover in the maternal plant has major effects on *Arabidopsis* fruit growth and seed composition. *Plant Physiol.* 160, 1175–1186. doi: 10.1104/pp.112.205062

Aschan, G., and Pfanz, H. (2003). Non-foliar photosynthesis–a strategy of additional carbon acquisition. *Flora* 198, 81–97. doi: 10.1078/0367-2530-00080

Ashraf, M., and Harris, P. J. C. (2013). Photosynthesis under stressful environments: an overview. *Photosynthetica* 51, 163–190. doi: 10.1007/s11099-013-0021-6

Bates, P. D., Stymne, S., and Ohlrogge, J. (2013). Biochemical pathways in seed oil synthesis. *Curr. Opin. Plant Biol.* 16, 358–364. doi: 10.1016/j.pbi.2013.02.015

Baud, S., and Lepiniec, L. (2010). Physiological and developmental regulation of seed oil production. *Prog. Lipid Res.* 49, 235–249. doi: 10.1016/j.plipres.2010.01.001

Bennett, E. J., Roberts, J. A., and Wagstaff, C. (2011). The role of the pod in seed development: strategies for manipulating yield. *New Phytol.* 190, 838–853. doi: 10.1111/j.1469-8137.2011.03714.x

Bourgis, F., Kilaru, A., Cao, X., Ngando-Ebongue, G. F., Drira, N., Ohlrogge, J. B., et al. (2011). Comparative transcriptome and metabolite analysis of oil palm and date palm mesocarp that differ dramatically in carbon partitioning. *Proc. Natl. Acad. Sci. U. S. A.* 108, 12527–12532. doi: 10.1073/pnas.1106502108

Chaitanya, B. S. K., Kumar, S., Anjaneyulu, E., Prasad, R. B. N., Sastry, P. S., and Reddy, A. R. (2015). Pivotal role of sugar fluxes between the inner integument and endosperm in lipid synthesis during seed ontogeny in *Jatropha curcas* L. *Ind. Crop Prod.* 76, 1106–1113. doi: 10.1016/j.indcrop.2015.08.035

Ekman, A., Hayden, D. M., Dehesh, K., Bulow, L., and Stymne, S. (2008). Carbon partitioning between oil and carbohydrates in developing oat (*Avena sativa* L.) seeds. *J. Exp. Bot.* 59, 4247–4257. doi: 10.1093/jxb/ern266

Galili, G., Avin-Wittenberg, T., Angelovici, R., and Fernie, A. R. (2014). The role of photosynthesis and amino acid metabolism in the energy status during seed development. *Front. Plant Sci.* 5:447. doi: 10.3389/fpls.2014.00447

Gerhardt, N., Schwolow, S., Rohn, S., Perez-Cacho, P. R., Galan-Soldevilla, H., Arce, L., et al. (2019). Quality assessment of olive oils based on temperature-ramped HS-GC-IMS and sensory evaluation: comparison of different processing approaches by LDA, kNN, and SVM. *Food Chem.* 278, 720–728. doi: 10.1016/j.foodchem.2018.11.095

Grover, A., Kumari, M., Singh, S., Rathode, S. S., Gupta, S. M., Pandey, P., et al. (2014). Analysis of *Jatropha curcas* transcriptome for oil enhancement and genic markers. *Physiol. Mol. Biol. Plants* 20, 139–142. doi: 10.1007/s12298-013-0204-4

Hua, W., Li, R. J., Zhan, G. M., Liu, J., Li, J., Wang, X. F., et al. (2012). Maternal control of seed oil content in *Brassica napus*: the role of silique wall photosynthesis. *Plant J.* 69, 432–444. doi: 10.1111/j.1365-313X.2011.04802.x

Kocurek, M., Kornas, A., Pilarski, J., Tokarz, K., Lüttge, U., and Miszalski, Z. (2015). Photosynthetic activity of stems in two *Clusia* species. *Trees Struct. Funct.* 29, 1029–1040. doi: 10.1007/s00468-015-1182-7

Li, F. P., Ma, C. Z., Wang, X., Gao, C. B., Zhang, J. F., Wang, Y. Y., et al. (2011). Characterization of sucrose transporter alleles and their association with seed yield-related traits in *Brassica napus* L. *BMC Plant Biol.* 11:168. doi: 10.1186/1471-2229-11-168

Lin, Z. X., An, J. Y., Wang, J., Niu, J., Ma, C., Wang, L. B., et al. (2017). Integrated analysis of 454 and Illumina transcriptomic sequencing characterizes carbon flux and energy source for fatty acid synthesis in developing *Lindera glauca* fruits for woody biodiesel. *Biotechnol. Biofuels* 10:134. doi: 10.1186/s13068-017-0820-2

Lin, Y., Ulanov, A. V., Lozovaya, V., Widholm, J., Zhang, G., Guo, J., et al. (2006). Genetic and transgenic perturbations of carbon reserve production in *Arabidopsis* seeds reveal metabolic interactions of biochemical pathways. *Planta* 225, 153–164. doi: 10.1007/s00425-006-0337-6

Liu, H., Li, H. F., Gu, J. Z., Deng, L., Ren, L., Hong, Y. B., et al. (2018). Identification of the candidate proteins related to oleic acid accumulation during peanut (*Arachis hypogaea* L.) seed development through comparative proteome analysis. *Int. J. Mol. Sci.* 19:1235. doi: 10.3390/ijms19041235

Liu, H., Wang, C. P., Chen, F., and Shen, S. H. (2015). Proteomic analysis of oil bodies in mature *Jatropha curcas* seeds with different lipid content. *J. Proteomics* 113, 403–414. doi: 10.1016/j.jprot.2014.10.013

Liu, J. H., Zhang, J., Miao, H. X., Jia, C. H., Wang, J. Y., Xu, B. Y., et al. (2017). Elucidating the mechanisms of the tomato mutation in regulating fruit quality using proteomics analysis. *J. Agric. Food Chem.* 65, 10048–10057. doi: 10.1021/acs.jafc.7b03656

Lu, D. B., Xia, Y., Chen, Z. W., Chen, A., Wu, Y., Jia, J. G., et al. (2019). Cardiac proteome profiling in ischemic and dilated cardiomyopathy mouse models. *Front. Physiol.* 10:750. doi: 10.3389/fphys.2019.00750

Ma, R. J., Zhang, B. B., Zhang, C. H., Cai, Z. X., and Yan, J. (2014). Effect of bagging on quality of Jinlinghuanglu peach. *Jiangsu J. Agric. Sci.* 30, 1127–1131. doi: 10.3969/j.issn.1000-4440.2014.05.031

Niu, J., An, J. Y., Wang, L. B., Fang, C. L., Ha, D. L., Fu, C. Y., et al. (2015). Transcriptomic analysis revealed the mechanism of oil dynamic accumulation during developing Siberian apricot (*Prunus sibirica* L.) seed kernels for the development of woody biodiesel. *Biotechnol. Biofuels* 8:29. doi: 10.1186/s13068-015-0213-3

Ohlrogge, J. B., and Jaworski, J. G. (1997). Regulation of fatty acid synthesis. *Annu. Rev. Plant. Physiol. Plant. Mol. Biol.* 48, 109–136. doi: 10.1146/annurev.arplant.48.1.109

Proulx, R. A., and Naeve, S. L. (2009). Pod removal, shade, and defoliation effects on soybean yield, protein, and oil. *Agron. J.* 101, 971–978. doi: 10.2134/agronj2008.0222x

Rawsthorne, S. (2002). Carbon flux and fatty acid synthesis in plants. *Prog. Lipid Res.* 41, 182–196. doi: 10.1016/S0163-7827(01)00023-6

Silva, R. D., Carmo, L. S. T., Luis, Z. G., Silva, L. P., Scherwinski-Pereira, J. E., and Mehta, A. (2014). Proteomic identification of differentially expressed proteins during the acquisition of somatic embryogenesis in oil palm (*Elaeis guineensis* Jacq.). *J. Proteomics* 104, 112–127. doi: 10.1016/j.jprot.2014.03.013

Wang, F., Sanz, A., Brenner, M. L., and Smith, A. (1993). Sucrose synthase, starch accumulation, and tomato fruit sink strength. *Plant Physiol.* 101, 321–327. doi: 10.1104/pp.101.1.321

Wiese, S., Reidegeld, K. A., Meyer, H. E., and Warscheid, B. (2007). Protein labeling by iTRAQ: A new tool for quantitative mass spectrometry in proteome research. *Proteomics* 7, 1004–1350. doi: 10.1002/pmic.200790019

Wu, Q. K., Cao, Y. Y., Chen, C., Gao, Z. Z., Yu, F. Y., and Guy, D. R. (2020). Transcriptome analysis of metabolic pathways associated with oil accumulation in developing seed kernels of *Styrax tonkinensis*, a woody biodiesel species. *BMC Plant Biol.* 20:121. doi: 10.1186/s12870-020-2327-4

Wu, Q. K., Chen, C., Wang, X. J., Zhang, Z. H., Yu, F. Y., and Guy, R. D. (2021). Proteomic analysis of metabolic mechanisms associated with fatty acid biosynthesis during *Styrax tonkinensis* kernel development. *J. Sci. Food Agric.* 101, 6053–6063. doi: 10.1002/jsfa.11262

Wu, Q. K., Fei, X. R., Gao, Y., Chen, C., Cao, Y. Y., and Yu, F. Y. (2019a). Comparative analysis of fuel properties of eight biodiesel plants species of Styrax spp. *China Oil Fat.* 44, 27–30. doi: 10.3969/j.issn.1003-7969.2019.01.007

Wu, Y. Q., Yang, H., Huang, Z. J., Zhang, C. H., Lyu, L., Li, W. L., et al. (2022). Metabolite profiling and classification of highbush blueberry leaves under different shade treatments. *Metabolism* 12:79. doi: 10.3390/metabo12010079

Wu, Q. K., Zhang, Z. H., Peng, H., Wu, Y. L., and Yu, F. Y. (2019b). The nutrient distribution in the continuum of the pericarp, seed coat, and kernel during *Styrax tonkinensis* fruit development. *PeerJ* 7:e7996. doi: 10.7717/peerj.7996

Xu, Q. Y., Wu, J. F., Cao, Y. R., Yang, X. Y., Wang, Z. J., Huang, J. Q., et al. (2016). Photosynthetic characteristics of leaves and fruits of Hickory (*Carya cathayensis* Sarg.) and pecan (Carya illinoensis K. Koch) during fruit development stages. *Trees Struct. Funct.* 30, 1523–1534. doi: 10.1007/s00468-016-1386-5

Ye, H., Sun, L., Huang, X., Zhang, P., and Zhao, X. (2010). A proteomics approach for plasma biomarker discovery with 8-plex iTRAQ labeling and SCX-LC-MA/MA. *Mol. Cell. Biochem.* 343, 91–99. doi: 10.1007/s11010-010-0502-x

Zhan, Z. Y., Chen, Y. C., Shockey, J., Han, X. J., and Wang, Y. D. (2016). Proteomic analysis of tung tree (*Vernicia fordii*) oilseeds during the developmental stages. *Molecules* 21:11. doi: 10.3390/molecules21111486

Zhang, L., Jia, B. G., Tan, X. F., Thammina, C. S., Long, H. X., Liu, M., et al. (2014). Fatty acid profile and unigene-derived simple sequence repeat markers in tung tree (*Vernicia fordii*). *PLoS One* 9:e105298. doi: 10.1371/journal.pone.0105298

Zhang, Z. H., Luo, Y., Wang, X. J., and Yu, F. Y. (2018). Fruit spray of 24-epibrassinolide and fruit shade alter pericarp photosynthesis activity and seed lipid accumulation in *Styrax tonkinensis*. *J. Plant Growth Regul.* 37, 1066–1084. doi: 10.1007/s00344-017-9769-4

Zhang, Z. H., Wang, X. J., Luo, Y., and Yu, F. Y. (2017). Carbon competition between fatty acids and starch during benzoin seeds maturation slows oil accumulation speed. *Trees Struct. Funct.* 31, 1025–1039. doi: 10.1007/s00468-017-1528-4

Conflict of Interest: The authors declare that the research was conducted in the absence of any commercial or financial relationships that could be construed as a potential conflict of interest.

Publisher's Note: All claims expressed in this article are solely those of the authors and do not necessarily represent those of their affiliated organizations, or those of the publisher, the editors and the reviewers. Any product that may be evaluated in this article, or claim that may be made by its manufacturer, is not guaranteed or endorsed by the publisher.

frontiers | Frontiers in Plant Science

ORIGINAL RESEARCH
published: 02 June 2022
doi: 10.3389/fpls.2022.908129

Effects of Strigolactone on *Torreya grandis* Gene Expression and Soil Microbial Community Structure Under Simulated Nitrogen Deposition

Chenliang Yu[1,2†], Qi Wang[1,2†], Shouke Zhang[1,2], Hao Zeng[1,2], Weijie Chen[1,2], Wenchao Chen[1,2], Heqiang Lou[1,2], Weiwu Yu[1,2,3] and Jiasheng Wu[1,2,3*]*

[1]State Key Laboratory of Subtropical Silviculture, Zhejiang A&F University, Hangzhou, China, [2]School of Forestry and Biotechnology, Zhejiang A&F University, Hangzhou, China, [3]NFGA Engineering Research Center for Torreya grandis 'Merrillii', Zhejiang A&F University, Hangzhou, China

OPEN ACCESS

Edited by:
Guolei Li,
Beijing Forestry University, China

Reviewed by:
Shuai Li,
Qingdao Agricultural University, China
Yong-Hua Liu,
Hainan University, China

***Correspondence:**
Weiwu Yu
yww888@zafu.edu.cn
Jiasheng Wu
wujs@zafu.edu.cn

[†]These authors have contributed equally to this work

Specialty section:
This article was submitted to Functional Plant Ecology, a section of the journal Frontiers in Plant Science

Received: 30 March 2022
Accepted: 02 May 2022
Published: 02 June 2022

Citation:
Yu C, Wang Q, Zhang S, Zeng H, Chen W, Chen W, Lou H, Yu W and Wu J (2022) Effects of Strigolactone on Torreya grandis Gene Expression and Soil Microbial Community Structure Under Simulated Nitrogen Deposition. Front. Plant Sci. 13:908129. doi: 10.3389/fpls.2022.908129

Nitrogen enters the terrestrial ecosystem through deposition. High nitrogen levels can affect physical and chemical properties of soil and inhibit normal growth and reproduction of forest plants. Nitrogen modulates the composition of soil microorganisms. Strigolactones inhibits plant branching, promotes root growth, nutrient absorption, and promotes arbuscular fungal mycelia branching. Plants are subjected to increasing atmospheric nitrogen deposition. Therefore, it is imperative to explore the relationship between strigolactone and nitrogen deposition of plants and abundance of soil microorganisms. In the present study, the effects of strigolactone on genetic responses and soil microorganisms of *Torreya grandis*, under simulated nitrogen deposition were explored using high-throughput sequencing techniques. *T. grandis* is a subtropical economic tree species in China. A total of 4,008 differentially expressed genes were identified in additional N deposition and GR24 treatment. These genes were associated with multiple GO terms and metabolic pathways. GO enrichment analysis showed that several DEGs were associated with enrichment of the transporter activity term. Both additional nitrogen deposition and GR24 treatment modulated the content of nutrient elements. The content of K reduced in leaves after additional N deposition treatment. The content of P increased in leaves after GR24 treatment. A total of 20 families and 29 DEGs associated with transporters were identified. These transporters may be regulated by transcription factors. A total of 1,402,819 clean reads and 1,778 amplicon sequence variants (ASVs) were generated through Bacterial 16S rRNA sequencing. Random forest classification revealed that Legionella, Lacunisphaera, Klebsiella, Bryobacter, and Janthinobacterium were significantly enriched in the soil in the additional N deposition group and the GR24 treatment group. Co-occurrence network analysis showed significant differences in composition of soil microbial community under different treatments. These results indicate a relationship between N deposition and strigolactones effect. The results provide new insights on the role of strigolactones in plants and composition of soil microorganisms under nitrogen deposition.

Keywords: microbial community, nitrogen deposition, RNA-seq, strigolactone, *Torreya grandis*

INTRODUCTION

Atmospheric nitrogen deposition has increased more than 10 times in the past 150 years and is expected to double by 2050, due to combustion of fossil fuels and wide use of agricultural fertilizers (Galloway and Cowling, 2002). Nitrogen deposition significantly affects the balance of various ecosystems under global environmental changes (Lin et al., 2020). In addition, nitrogen deposition plays an important role in global nitrogen cycle (Xu et al., 2019). China is among the top three highest nitrogen deposition regions in the world owing to rapid economic development in the country (Holland et al., 1999; Dentener et al., 2006; Wang et al., 2011; Lin et al., 2020). Nitrogen deposition rates was 30–70 kg/ (ha*yr) in China (Liu et al., 2013; Ti et al., 2021; Wu et al., 2021; ha*yr) Studies predict that these regions will exhibit the highest atmospheric nitrogen deposition in the world in future (Wang et al., 2011). A moderate amount of atmospheric nitrogen deposition promotes plant growth. However, when the ecosystem nitrogen reaches saturation, continuous increase in nitrogen deposition negatively affects plant growth (Lu et al., 2014). Excessive nitrogen levels as a results of nitrogen deposition causes phosphorus deficiency in soils, which in turn changes the physical and chemical properties of soil and reduces plant productivity (Lü and Tian, 2007). In addition, nitrogen deposition reduces soil pH, reduces plant diversity, and affects composition and activity of microbial communities (Clark and Tilman, 2008; Lu et al., 2014). Moreover, high levels of nitrogen affects decomposition of litter by microorganisms and mineralization of organic matter, ultimately changing the content of soil nutrient elements (Elser et al., 2007; Dima et al., 2015).

Soil microorganisms play a key role nutrient cycling in forest ecosystems (Dom et al., 2021). The research on soil microorganisms under the nitrogen deposition mainly focuses on the changes of microbial community structure in different forest types or different ecosystems (Wang et al., 2018a,b). Previous findings show that long-term nitrogen deposition has adverse effects on soil microorganisms (Díaz-Álvarez et al., 2018). Atmospheric nitrogen deposition can directly or indirectly affect growth, reproduction, and activity of forest soil microorganisms (Berg et al., 2011). Moreover, it can change the number, community structure, and function of soil microorganisms (Treseder, 2010). These changes ultimately affect material transformation and nutrient availability in soil (Treseder, 2010; Cusack et al., 2011). Previous studies report that excessive nitrogen deposition leads to decrease in fungal biomass in soil, changes fungal bacterial biomass ratio, affect diversity of ectomycorrhizal fungi species. Furthermore, high nitrogen deposition level is associated with decrease in soil enzyme activity and respiration rate, and change in microbial substrate utilization mode (Waldrop et al., 2004).

Strigolactones (SLs) are plant hormones produced in carotenoid biosynthesis pathway (Matusova et al., 2005). Studies report that SLs inhibit growth of plant lateral branches, induces seed germination, and stimulates hyphal branching of arbuscular mycorrhizal fungi (Kapulnik and Koltai, 2014; Al-Babili and Bouwmeester, 2015; Shindo et al., 2020). Secretion of strigolactones by roots plays an important role in fungus and host before mycorrhizal colonization (Müller et al., 2019). Arbuscular mycorrhizal fungi increase the absorption area of host plant roots, release organic acids and soil enzymes, activate soil phosphorus, and enhance the host phosphorus absorption capacity (Huang et al., 2018; Higo et al., 2020). Many studies have shown SLs has the potential ability to regulate plant roots and rhizosphere microorganisms interaction (van Zeijl et al., 2015; Carvalhais et al., 2019). There are clear evidence present that SLs promote biotic stress resistance against specific bacterial and fungal phytopathogens (Marzec, 2016). SLs are implicated in plant nutrient absorption. Nutrient deficiency induces SLs synthesis resulting in plant developmental plasticity (Pandey et al., 2016). Increase in level of SLs under a low-phosphorus environment is correlated with inhibition of aboveground branches and stimulation of lateral root growth (Brewer et al., 2013). Low nitrogen level promotes increase in the synthesis of SLs (Yoneyama et al., 2012; Shindo et al. 2020). Differences in biosynthesis or transport of SLs can affect development of shoots in response to supply of N elements (Cochetel et al., 2018). More than 25 natural strigolactones have been isolated from plant roots (Oancea et al., 2017). The synthetic strigolactone analog GR24 is widely used to explore the biological role of SLs (Umehara et al., 2008).

Torreya grandis "Merrillii" is a gymnosperm, and a member of the *Torreya* genus and Taxaceae family (Gao et al., 2021). It is a species of *Torreya grandis* Fort.ex Lind. that has undergone asexual reproduction (Li and Dai, 2007). *T. grandis* is a multi-purpose excellent economic tree used for production of fruit, oil, medicine, wood, greening, and ornamental purposes (Li and Dai, 2007; Chen et al., 2020). *T. grandis* mainly grows in Zhejiang Province in China. The purpose of this study was to explore whether SLs can improve stress response in *T. grandis* under additional N supply. In the present study, the effects of SLs on gene responses and soil microorganisms of associated with *T. grandis* subjected to simulated nitrogen deposition were evaluated using high-throughput sequencing techniques. The findings of the present study provide new insights and basis for further studies on the response of subtropical forest plants and soil microorganisms to nitrogen deposition.

MATERIALS AND METHODS

Plant Materials and Treatments

One year old *T. grandis* plants were used in this study. The plants were treated with ammonium nitrate (NH_4NO_3) to simulate additional N deposition. The concentration of nitrogen used was 160 kg N ha $^{-1}$ yr. $^{-1}$. The amount of spraying per year was converted into the amount for each month. Strigolactone treatments comprising spraying of 10 μM of GR24 solution to the shoots of *T. grandis* seedlings. Spray with a small pot, 1 ml for each seedling. A total of 20 seedlings were used for each treatment. Samples were obtained for transcriptome sequencing after 24 h and 72 h of treatment. We treated them once every 1 month. Further, samples were collected for element

content determination after 2 months of treatment. Soil samples were obtained for bacterial 16S sequencing after 2 months.

Determination of Nutritional Element Content

The samples were subjected to concentrated nitric acid perchloric acid digestion and analysis of nutritional elements was performed using inductively coupled plasma mass spectrometry (ICP-MS; Xseries 2 ICP-MS, Thermo, United States). A weight of 0.1 g of the sample was transferred to a 100 ml conical flask, and 10 ml of concentrated nitric acid added. The conical flask was then placed on a heating plate at 80°C for 30 min, and then gradually heated until the brown-red gas at the bottle mouth disappeared. Further, 2.5 ml of perchloric acid was added; then, the mixture was heated to 180°C, heating was continued until the liquid became transparent. The mixture was cooled then diluted to a 50 ml volumetric flask with distilled water. Subsequently, the mixture was filtered into a 50 ml conical flask. The content of each element was then determined by atomic absorption spectrophotometer.

Total RNA Extraction and Transcriptome Sequencing

TRNzol Universal Total RNA Extraction Reagent (DP424, TIANGEN Biotech, Beijing, China) was used to extract total RNA from the leaves of *T. grandis* subjected to different treatments. Nanodrop (Thermo, United States) was used to determine the purity (D260/D280) and concentration of RNA samples. Approximately 1 μg of RNA was obtained from each sample for library construction. mRNA with polyA tail was enriched by Oligo (dT) magnetic beads and randomly interrupted. One-stranded cDNA was synthesized with six-base random primers (random hexamers) by the M-MuLV reverse transcriptase system using mRNA as a template. Buffer, dNTPs, and DNA polymerase I were used to synthesize two-stranded cDNA. AMPure XP beads were used to purify the double-stranded cDNA. The purified double-stranded cDNA was then repaired, A-tailed, and connected to the sequencing adapter. Further, AMPure XP beads were used for fragment size selection. PCR amplification was conducted to obtain the final cDNA library. A total of 21 RNA-seq libraries were constructed. Sequencing was performed using the Illumina NovaSeq 6000 platform.

Transcriptome Data Quality Control and Analysis

Adapter sequence was removed from the obtained raw data then reads with low quality and high unknown base content were filtered out to obtain high-quality clean reads. The clean reads were compared with previously assembled transcript sequence using hisat2 software. Count data were acquired using feature Counts software (Han et al., 2020). Transcripts per million (TPM) method was used to estimate gene expression using the Trinity software (Haas et al., 2013). DESeq2 R package was used to identify differentially expressed genes (DEGs) at a false discovery rate (FDR) < 0.05. GeneOntology (GO) and Kyoto Encyclopedia of Genes and Genomes (KEGG) enrichment analysis of DEGs was performed using clusterprofiler (3.4.4) tool, with correction of the gene length deviation. GO terms or KEGG pathways with corrected value of p less than 0.05 were considered significantly enriched by the DEGs.

Weighted Gene Co-expressed Network Analysis

A total of 14,654 genes were obtained for further analysis based on the expression of more than 1 in 80% of the samples. Weighted gene co-expression network analysis (WGCNA) was conducted using WGCNA R package (Langfelder and Horvath, 2008). Hierarchical clustering on samples was performed using ward. D2 algorithm in hclust function. The soft threshold was calculated by picksoftthreshold function after ensuring that there was no outlier sample. The weighted adjacency matrix was constructed, and the related gene modules were identified based on the hierarchical clustering of the dissimilarity measure of the topological overlap matrix (TOM). A local network containing ion transport transporters related DEGs was established using the results of module division. A transcriptional regulation network was generated using Cytoscape software.

Soil DNA Extraction and Sequencing

Total DNA of soil samples was extracted using TIANamp Soil DNA Kit (Code:DP336, TianGen Biotech, Beijing, China). Concentration and purity of the soil were determined using 2000 spectrophotometer, and detection conducted using 1% agarose gel electrophoresis. Total microbial DNA of each soil sample was used as the template for PCR amplification with bacterial V3 ~ V4 region-specific primers 341F (5′-cctacggggcgwgcag-3′) and 806R (5′- ggactachvggtwtctaat-3′). The PCR product was recovered by agarose gel electrophoresis after detection of target fragments using AxyPrep PCR Clean-up Kit Recovery Kit. Truseq nano DNA LT library prep Kit (Illumina company) was used to construct a sequencing library based on the purified PCR product. DNA PCR-free sample preparation kit was used to quantify samples on qubit and qPCR fluorescence quantitative systems. Sequencing was performed using IlluminaMiSeq platform.

Cutadapt (V1.9.1) quality control software[1] was used to evaluate the sequencing quality of all 16S sequences, which were further grouped according to the different primers used for the samples. Usearch V10 software overlap was used to splice Clean Reads of each sample. Further, length filtering of the spliced data was performed according to the length range of different regions. Final valid data (non-Chimeric Reads) were obtained by denoising and removing chimeric sequences using dadA2 method in QIIME2 software (Bolyen et al., 2019). ASV sequences were compared with corresponding database sequences in QIIME2 software. NCBI database annotations were used to obtain the corresponding taxonomic information of each ASV. Specific species composition of each sample at each taxonomic level was obtained according to classification

[1]https://cutadapt.readthedocs.io/en/stable/

of ASVs and taxonomic status identification results. QIIME2 software was used to calculate Alpha diversity index and Beta diversity index for each sample.

Co-occurrence Network Analysis

A co-occurrence network was constructed with each treated sample. The main ecological clusters of strongly correlated ASVs were then determined. Paired Spearman correlations between ASVs were evaluated, and correlations with Spearman coefficient less than 0.60 and value of p greater than 0.01 were removed. The main modules in the network were visualized using Gephi tool.[2]

RESULTS

Transcriptome Sequencing Quality Analysis

Raw data was processed before analysis to ensure high quality during data analysis. The clean data were obtained by removing the adapter, and reads containing indeterminate base information and low-quality reads (**Supplementary Table S1**). A total of 20 million clean reads were obtained for each sample, with Q20 greater than 98% and Q30 greater than 94%. The sequencing error rate was 0.02–0.03%. These results indicate that the sequencing quality was good and the sequences can be used for subsequent bioinformatics analysis. Overall sample principal component analysis (PCA) was performed to explore the expression levels of genes in all samples. The results showed that the samples had good repeatability (**Supplementary Figure S1**). Details on identified unigenes are presented in **Supplementary Table S2**.

Analysis of DEGs Related to N Deposition and SLs Response

DESeq2 software was used to compare the expression levels of genes of *T. grandis* leaves under different treatments $p < 0.05$ was used as the screening criteria. DEGs for each comparison are shown in **Supplementary Figure S2**. Global DEGs profiles under additional N deposition or GR24 treatments were presented as a heatmap (**Figure 1A**). A total of 1,048 DEGs, including 556 upregulated and 492 downregulated genes, were identified under the additional N deposition treatment for 24 h. Further, 829 DEGs including 426 upregulated and 403 downregulated genes were identified for the 72 h treatment. A total of 468 DEGs, including 218 upregulated and 250 downregulated genes were identified after 24 h under GR24 treatment. A total of 527 DEGs, including 288 upregulated and 239 downregulated genes were identified after 72 h of GR24 treatment. A total of 931 and 335 DEGs were identified after 24 h and 72 h under additional N deposition+GR24 treatment (**Supplementary Figure S2**). A total of 4,008 non-redundant DEGs were obtained in all comparison groups (**Supplementary Table S3**). We also analyzed the expression trend of differentially expressed genes (**Figure 1B**). The results showed that there was significant difference in DEGs of cluster 0, 5, 8, 10, 18, and 19 ($p < 0.05$). Among them, the DEGs of cluster 19 increased in all treatments, while the expression of DEGs in cluster 0 decreased in all treatments. Notably, 281 and 240 DEGs were ascribed to treatment with additional N deposition for 24 h and 72 h, respectively (**Figure 1C**). In addition, 93 and 127 DEGs were attributed to GR24 treatment for 24 h and 72 h, respectively.

Go and KEGG Enrichment Analysis of Differentially Expressed Genes

GO analysis of the DEGs was conducted to determine the main biological functions of these genes (**Figure 2A**). A total of 25 GO terms were significantly enriched in the biological process (BP) category. The top three significantly enriched terms in the BP category were single-organism process, cellular process, and metabolic process. The findings showed that 19 GO terms were significantly enriched in the cellular component with cell, cell part, and membrane part as the top three terms. A total of 14 terms were identified for molecular function category, with binding, catalytic activity, and signal transducer activity being the most enriched terms.

The DEGs were associated with enrichment of different KEGG metabolic pathways (**Figure 2B**). The results showed that 32 pathways were significantly enriched ($p < 0.05$). Arachidonic acid metabolism and Brassinosteroid biosynthesis were significantly enriched in the additional N deposition treatment group after 24 h and GR24 treatment group after 72 h treatment. Vitamin B6 metabolism was significantly enriched in the additional N deposition treatment group after 24 h and the additional N deposition+GR24 treatment group after 24-h and 72-h treatment. Phenylalanine, tyrosine, and tryptophan biosynthesis were significantly enriched in the additional N deposition treatment group after 72 h, GR24 treatment group after 72-h treatment, and additional N deposition+GR24 treatment group after 72-h treatment. Starch and sucrose metabolism and Circadian rhythm—plant were significantly enriched after 72-h treatment in the additional N deposition group and the GR24 group after treatment for 24 h. These results indicate that there was a crosstalk between N deposition and strigolactone.

Nutritional Elements Analysis

Increase in nitrogen deposition leads to decrease in soil inorganic phosphorus content and significant increase in soil N/P ratio (Blanes et al., 2013). Nitrogen deposition affects absorption of nutrients by plants. GO enrichment analysis showed that several DEGs were associated with enrichment of the transporter activity terms. Therefore, further analysis of common nutritional elements was performed (**Figure 3**). The results showed that additional N deposition treatment reduced the content of Ca in leaves and stems and increased the level of Ca in roots. The content of K reduced in leaves after additional N deposition treatment. The content of P increased in leaves after GR24 treatment. GR24 treatment

[2]https://gephi.org/

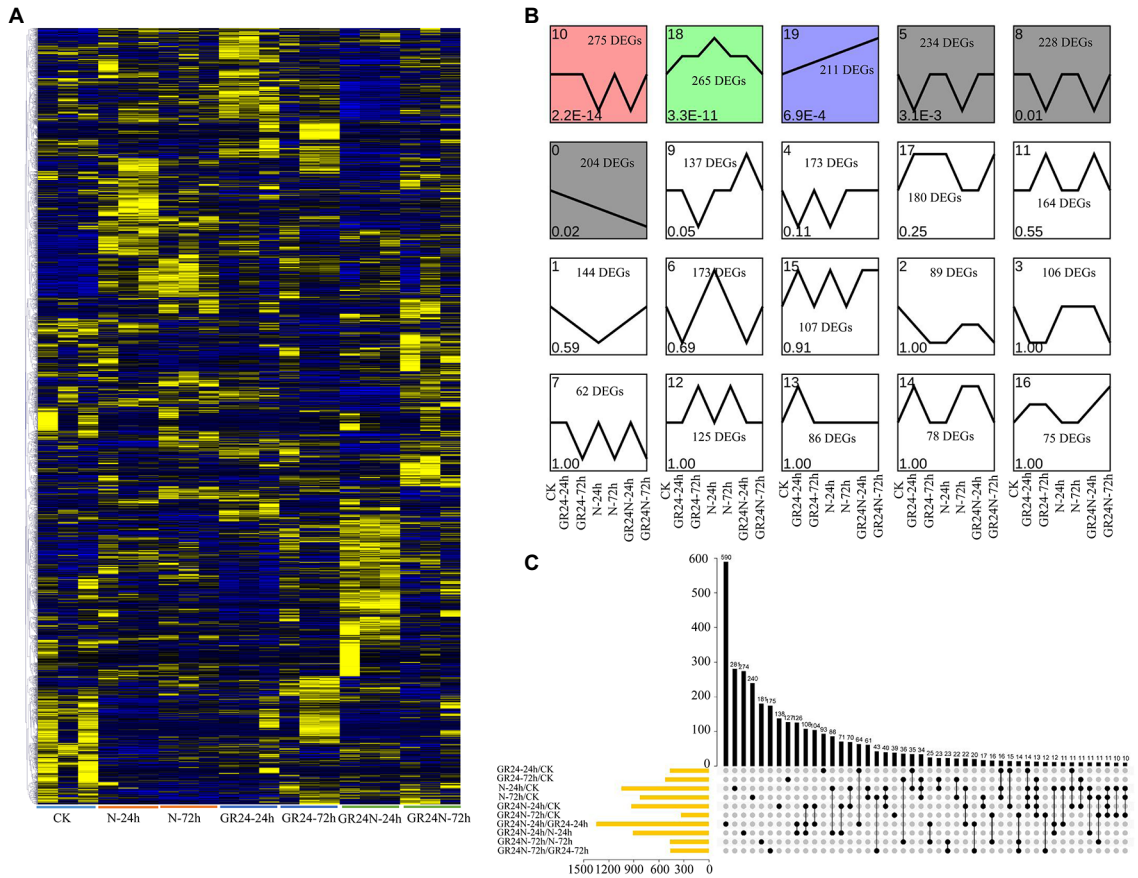

FIGURE 1 | Identification of the DEGs between additional N deposition and GR24 treatments in Torreya grandis. **(A)** Expression profiles of the DEGs under additional N deposition or GR24 treatments were shown by a heatmap. The original expression values were normalized by Z-score normalization. **(B)** DEGs module expression trends by the line chart. The expression trend line graph of each sub-module, the horizontal axis is the sample, and the vertical axis is the average expression level of all the genes in the sample. The trend of value of $p < 0.05$ is significant. **(C)** Upset plot of the DEGs in different comparisons.

reduced the content of Mg in stems. The three treatments reduced the content of S reduced in leaves. The content of Fe increased in leaves and reduced in roots after additional N or GR24 treatment. The content of Zn reduced in leaves after additional N treatment and increased in roots after GR24 treatment.

Analysis of DEGs Related to Element Transporter Genes and Transcription Factors

Further analysis was conducted to explore DEGs related transporters. A total of 20 families of transporters were identified (**Figure 4A**). The findings showed that 29 DEGs were transporters of nutritional elements (**Figure 4B**). The change of expression of these element transporters may be the main reason for the difference of nutrient absorption of *T. grandis* under different treatments. Transcription factors are the regulatory factors that mainly regulate transcription of some genes after cells respond to external stress. Further analysis was conducted on the transcription factors of different genes. The findings showed that the transcription factors may be involved in the signal transduction of N deposition and strigolactone and regulation of the nutrient transport vectors. A total of 26 families of transcription factors were identified (**Figure 4C**). SLs may regulate the expression of transporters by mediating the expression of these transcription factors. Further, WGCNA analysis shows that all unigenes were divided into 35 modules, which were defined by different color codes (**Figure 5**). Three unigene associated with the elements transporters were in the "blue" module including a Phosphate transporter 1; 4 (evm.TU.PTG005231L.4), a High affinity sulfate transporter 2(evm.TU.PTG000970L.10), and a zinc ABC transporter ATPase (evm.TU.PTG000400L.77). According to the weight value, we made the network interaction diagram of three genes.

Effects of Additional N Deposition and GR24 Treatment on Soil Microbial Community Structure

Previous studies report that nitrogen deposition affects growth, reproduction, and activity of soil microorganisms (Díaz-Álvarez et al., 2018). In addition, nitrogen deposition changes

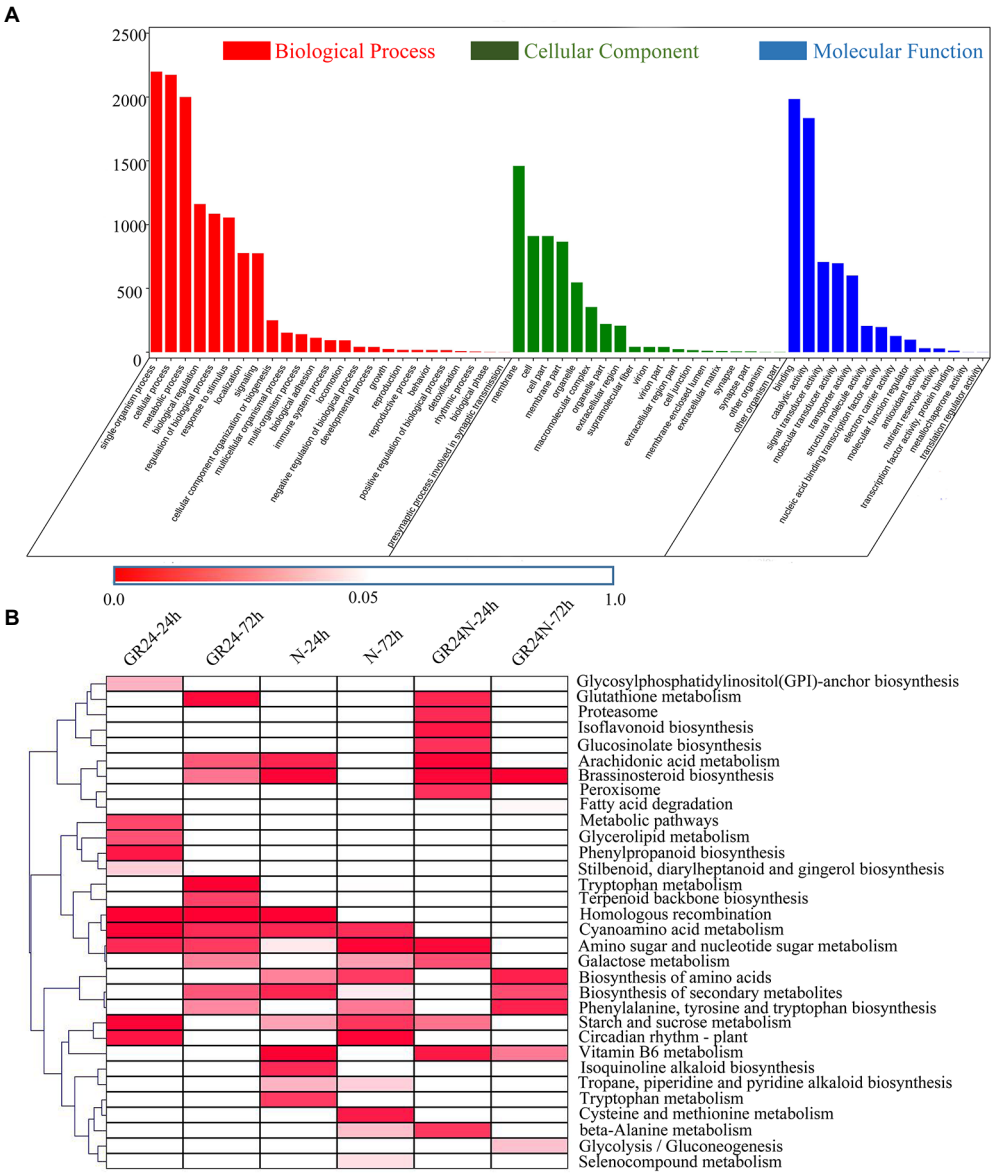

FIGURE 2 | Enrichment analysis of the DEGs in different comparisons. **(A)** GO enrichment analysis of all the DEGs based on three GO terms: biological process, cellular component, and molecular function. **(B)** KEGG enrichment analysis of the DEGs in the six comparisons. The significant values of *p* of each KEGG term under different treatments were shown by a heatmap.

the structure and function of soil microbial community. Therefore, 16S sequencing was conducted to explore the effect of nitrogen deposition on soil microorganisms associated with *T. grandis*. A total of 2,819,899 pairs of PE reads were obtained from 20 samples ($n = 5$; **Supplementary Table S4**). A total of 1,402,819 clean reads were generated after PE reads quality control and splicing. Each sample resulted in at least 35,711 clean reads, with an average of 70,141 clean reads. A total of 1778 amplicon sequence variants (ASVs) were obtained using the dada2 method in qiime2 software (**Figure 6A** and **Supplementary Table S5**). The findings showed that 868 ASVs were common to the four groups of samples (**Figure 6B**). Additional N deposition and GR24 treatment modulated the structure of soil bacteria at different classification levels (**Figure 6C**). Alpha diversity analysis of soil bacterial community structure under different treatments showed that the Chao1 and Shannon index were significantly higher in the additional N deposition+GR24 treatment group compared with the control group (**Figure 6D**). Shannon index and rank abundance curve in the tested soil samples gradually flattened, revealing a reasonable number of sequences (**Supplementary Figures S1C,D**). PERMANOVA (Adonis) analysis showed significant differences in microbial structure among the different treatments (**Supplementary Figure S3**).

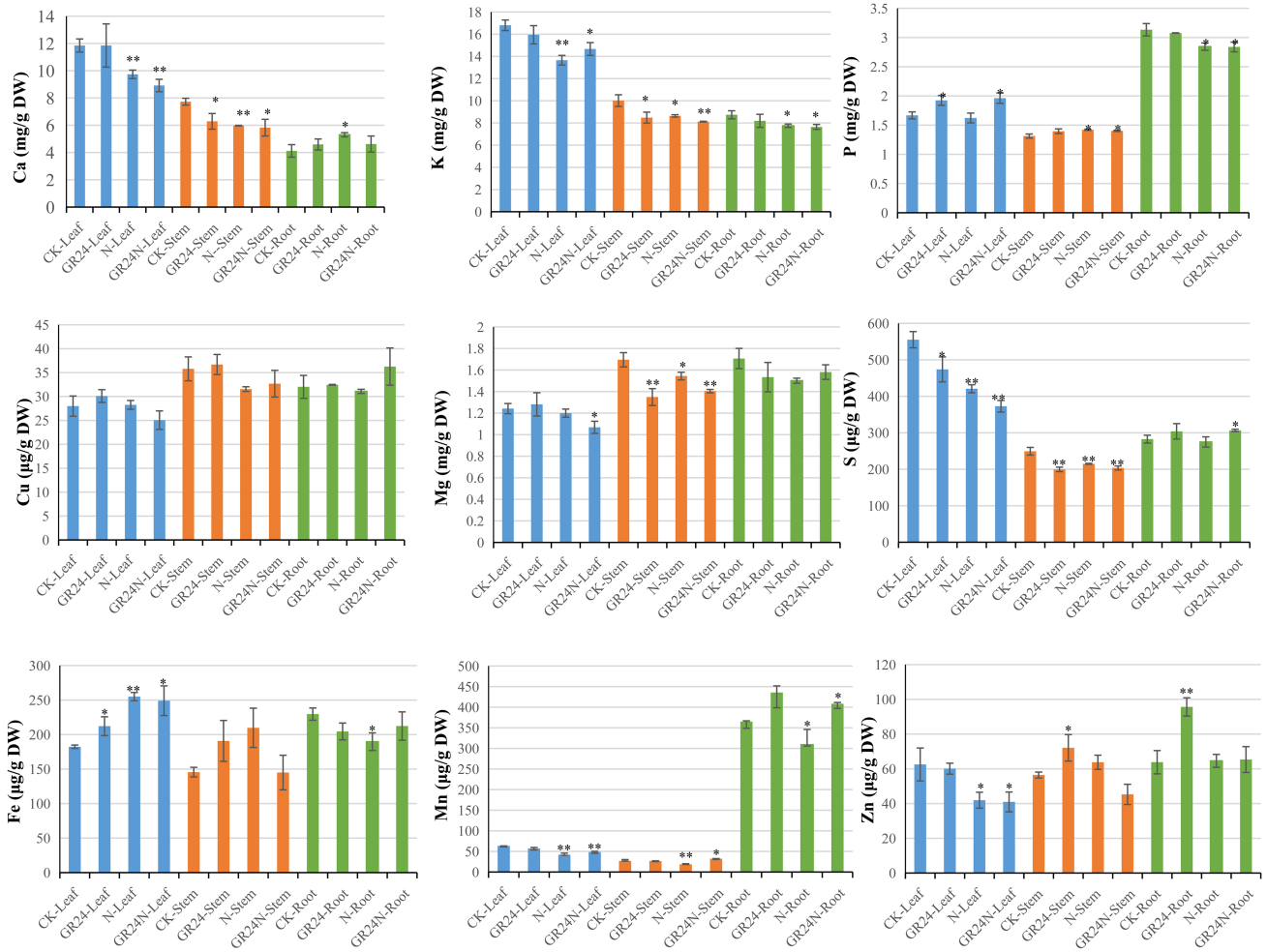

FIGURE 3 | The characteristics of nutrient elements contents in *Torreya grandis* after additional N deposition or GR24 treatments for two mouths. "*" represent $p \leq 0.05$, using unpaired student *t*-test; "**" represent $p \leq 0.01$, using unpaired student *t*-test.

Effect of Additional N Deposition and GR24 Treatment on Relative Abundance of Soil Bacteria

Random forest classification model was used to evaluate discriminatory taxa in soils under different treatments (**Figure 7**). The results revealed that Legionella, Lacunisphaera, Klebsiella, Bryobacter, and Janthinobacterium were significantly enriched in the additional N deposition or GR24 treatment soil microbiomes. A ternary diagram was generated which showed that some Proteobacteria were enriched in the additional N deposition-treated soil, whereas some acidobacteria were enriched in the control group soil. Co-occurrence network analysis showed that composition of soil microbial community at the classes level changed significantly under different treatments (**Figure 8**). The top five most abundant classes in the control group were Alphaproteobacteria, Acidobacteria, Gemmatimonadetes, Betaproteobacteria, and uncultured_bacterium_k_Bacteria. The top five abundant classes in GR24 treatment group were Alphaproteobacteria, Acidobacteria, Gemmatimonadetes, Nitrososphaeria, and Chitinophagia. The top five abundant classes in additional N deposition treatment group were Alphaproteobacteria, Acidobacteria, Gemmatimonadetes, Gammaproteobacteria and Chitinophagia. The top five most abundant classes in additional N deposition +GR24 treatment group were Alphaproteobacteria, Acidobacteria, uncultured_bacterium_k_Bacteria, Chitinophagia, and Gammaproteobacteria.

DISCUSSION

Nitrogen deposition affect the supply of soil nutrients in the ecosystem (Lü and Han, 2010). Change in soil nutrient content directly affects absorption and utilization of soil nutrients by plants and modulates the stoichiometric characteristics of plants (Tessier and Raynal, 2003). Plants respond to changes in the external environment by activating the signal cascade that modulates the expression pattern of downstream genes. In addition, they change their morphological structure and

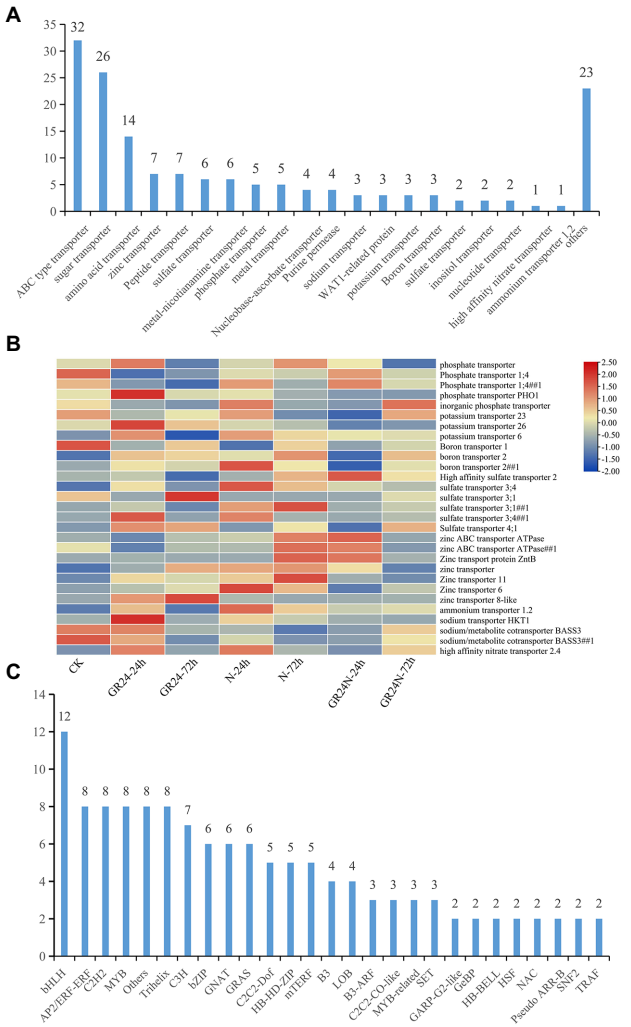

FIGURE 4 | Screening of differentially expressed genes related to transcription factors and substance transporters. **(A)** Identification of differential genes associated with transporters. **(B)** The heat map shows the expression levels of nutrient-related transporters in each treatment. **(C)** Identification of differentially expressed genes that are transcription factors. A total of 26 families of transcription factors were obtained.

physiological characteristics to adapt to the new environment (Jiang et al., 2021). Strigolactones, auxin, and cytokinin work synergistically to modulate lateral branch growth of plants and maintain the aboveground phenotypes of plants (Umehara et al., 2008). SLs affect root growth and root hair development, respond to external conditions of plant nitrogen and phosphorus deficiency, and regulate key hormone networks (Villaecija-Aguilar et al., 2019). Studies on different plant species report that nutrient levels, such as N/P in soil, are key regulators of SLs biosynthesis and secretion (Yoneyama et al., 2007; Kohlen et al., 2011). Notably, SLs also play important roles in the process of plant response to stress. SLs deficient mutants are more sensitive to drought and salt stress compared with the wild type (Torres-Vera et al., 2014; Li et al., 2020). The mutant phenotype can be restored by addition of exogenous GR24 (Ha et al., 2014). Wild-type plants treated with GR24 are more resistant to drought and salt stress compared with untreated plants (Ha et al., 2014). In the present study, transcriptome data from *T. grandis* shoots and Bacterial 16S rDNA sequencing data from the soil subjected to various treatments were used to evaluate the relationship between additional N deposition and SLs.

Differential gene analysis is an effective tool to explore gene expression changes over time (Zhan et al., 2018). In the current study, the number of DEGs after 72 h in the three treatment groups varied greatly. The findings showed that 205 and 130 DEGs were upregulated and downregulated, respectively, under the additional N deposition+GR24 treatment for 72 h. This finding shows a relationship between additional N deposition and SLs in *T. grandis* leaves. Nitrogen element and SL are implicated in regulation of plant metabolic pathways. Brassinosteroid biosynthesis pathway was significantly enriched under additional N deposition treatment for 24 h, GR24 treatment for 72 h and additional N deposition+ GR24 treatment for 24 h and 72 h. Brassinosteroids play an important role in plant growth and development and adaptation to the external environment (Ji et al., 2011; Gou et al., 2012). Additional N deposition or GR24 treatment affected synthesis of brassinosteroids. Amino sugar and nucleotide sugar metabolism and Cyanoamino acid metabolism were significantly enriched under additional N deposition treatment and GR24 treatment. These results show that SLs plays an important role in regulating the genes involved in these pathways.

Nitrogen plays a key role in modulating plant growth (Kiba et al., 2018). The content of nitrogen in plants or its effective utilization in soil directly modulates changes in various nutrient elements in plants and regulates the nutrient balance in plants (Li et al., 2012; Ravazzolo et al., 2020). Excessive nitrogen deposition reduces the growth of plants. This is because the excess nitrogen affects nutrient balance in plants (Bobbink and Roelofs, 1998). Nitrogen deposition changes the content of other elements including carbon, nitrogen, and phosphorus, which play important roles in plant physiological processes and may also affect some key processes in the ecosystem (Ruiqiang et al., 2016; Chen et al., 2017). Our results showed that short-term nitrogen deposition treatment induces a decrease in phosphorus content in the roots of *T. grandis*. GR24 treatment promotes increase in P content in leaves of *T. grandis*. The findings showed that the content of S, Fe, Mn, and Zn changed under additional N deposition treatment as well as GR24 treatment. Changes in the content of these elements may be attributed to dysregulation of the expression of the relevant transporters under N deposition or GR24 treatment. Environmental factors, such as soil nutrients, may directly or indirectly regulate the biosynthesis of SLs. Urea and nitrate may contribute to the synthesis and secretion of SLs in red clover root, while phosphorus and ammonium salts might hinder the synthesis (Yoneyama et al., 2001). SLs and its key signaling genes can affect the expression of transcription factors and thus affect plant root growth (Sun et al., 2021; Sylwia et al., 2021). celements are regulated by many transcription factors (Gong et al., 2020). Therefore, the effect of SLs on element content under the

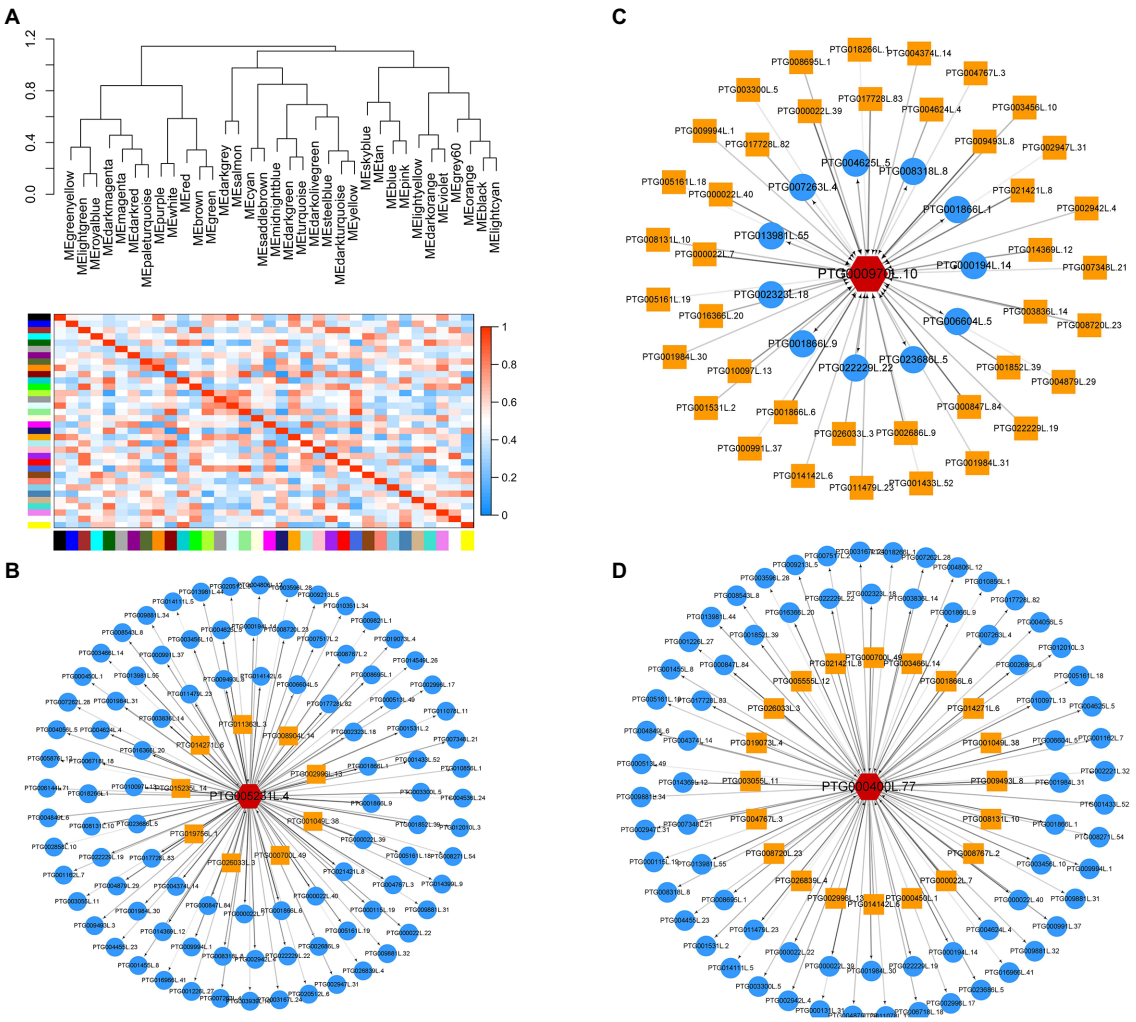

FIGURE 5 | Identification of WGCNA modules associated with nutrient-related transporters under additional N deposition and GR24 treatments. **(A)** Heat map of the correlation between modules. A total of 35 modules were identified. Cytoscape representation of three nutrient-related transporters including Phosphate transporter 1;4 (evm.TU.PTG005231L.4) **(B)**, High affinity sulfate transporter 2(evm.TU.PTG000970L.10) **(C)** zinc ABC transporter ATPase(evm.TU.PTG000400L.77) **(D)**. The yellow box represents the upstream of the target gene, and the blue circle represents the downstream.

background of nitrogen deposition may be realized by regulating the expression of transporter by transcription factors.

High levels of nitrogen deposition leads to soil acidification, imbalance in storage of soil nutrient elements, changes soil microbial community structure, and decreases microbial biomass (Waldrop et al., 2004; Lu et al., 2014). The specific functional microorganisms driving the nitrogen cycle have inconsistent responses to environmental changes, which can easily lead to the weakening of the coupling between nitrogen cycle links under the condition of increased nitrogen deposition, thus breaking the balance of nitrogen cycle (Levy-Booth et al., 2014). When growth is limited by phosphorus, plants will absorb excess N to synthesize phosphatase or induce microorganisms to secrete phosphatase, and the increase of phosphatase activity will release phosphorus absorbed in minerals and organic matter in large quantities, thus increasing the availability of soil P (Treseder and Vitousek, 2001). Phosphatase synthesis requires enough nitrogen (Treseder and Vitousek, 2001). The increase of soil P availability can promote the absorption and utilization of P by N-fixing bacteria and alleviate the restriction of P on nitrogen-fixing microorganisms in tropical and subtropical areas, which is an important factor to ensure the nitrogen fixation function of soil microorganisms under the background of high N deposition (Benjamin et al., 2008). The findings of the present study indicated that short-term nitrogen deposition and SLs treatment changed the composition and structure of soil bacteria, with significant changes observed in the group subjected to additional N deposition + GR24. The α diversity in additional N disposition + GR24 group was significantly different compared with that of the other treatment groups. Previous results indicated that nitrogen application had no significant effect on bacterial diversity, however, it significantly changed composition of microbial community (Fierer et al., 2012). The change in microbial diversity can be attributed to increase in nitrogen availability. In the

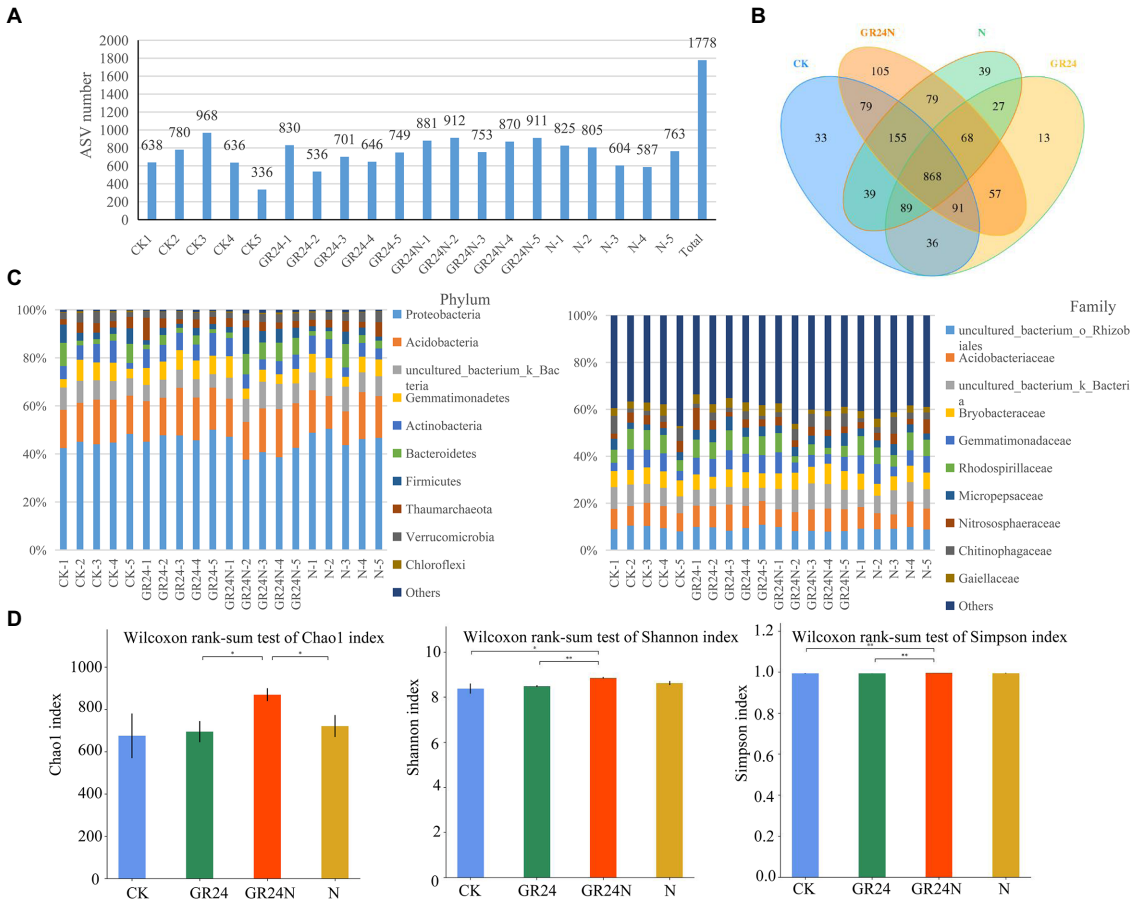

FIGURE 6 | Effects of additional N deposition and GR24 treatments on soil bacteria composition. **(A)** The number of ASVs obtained from each samples. ASVs were obtained by denoising the sequence using the dada2 method included in the QIIME2 software. **(B)** Venn diagram between treatments. **(C)** The histogram shows the species composition of soil bacteria in each sample (relative abundance at phylum and family levels). **(D)** Histogram of group differences in alpha diversity index. The significance of factors and the interaction between factors is marked at the top of the figure, where "*" represents $p < 0.05$ and "**" represents $p < 0.01$.

current study, nitrogen deposition treatment increased the relative abundance of gammaproteobacteria and chitinophagia, whereas GR24 treatment increased the relative abundance of nitrososphaeria and chitinophagia. Previous studies report that Proteobacteria comprises a variety of metabolic species and is widely involved in the biochemical cycle of carbon, nitrogen, and other elements in soil (Kersters et al., 2006; Fenliang et al., 2014). Conversion of ammonia to nitrite is a key step in the nitrogen cycle. Microorganisms involved in this process mainly include ammonia-oxidizing bacteria, which are members of betaproteobacteria and gamma Proteobacteria, and ammonia-oxidizing organisms which are members of archaea group (Hatzenpichler et al., 2008; Prosser and Nicol, 2008). Abundance of Gammaproteobacteria significantly increases with increase in contents of nitrogen and phosphorus (Simek et al., 2006). Nitrososphaeria is the most widely distributed Archaea on earth and is involved in ammonia oxidation (Sheridan et al., 2020). Chitinophagia class comprises endosporogenic microorganisms that degrade plant-derived carbohydrates in terrestrial ecosystems (Kishi et al., 2017). The results of this study showed that microorganisms implicated in nitrogen cycle were significantly enriched after GR24 treatment. Random forest classification analysis showed that Legionella was an important differentially expressed flora. The abundance of Legionella increased under nitrogen treatment and decreased under GR24 treatment. Legionella is a pathogenic bacteria (Atlas, 1999) widely distributed in various natural and artificial environments (van Heijnsbergen et al., 2016). The relative abundance of Bryobacter increased under GR24 treatment. Abundance of Bryobacter was positively correlated with soil health and directly correlated with available P concentration (Huang et al., 2020; Liang et al., 2020). These results indicate suggest that SLs promote increase in abundance of beneficial bacteria and reduction of harmful bacteria in soil.

CONCLUSION

In the present study, the effects of strigolactones on genetic responses and soil microorganisms associated with *T. grandis* were explored under simulated nitrogen deposition using high-throughput sequencing techniques. A total of 4,008 differentially expressed genes were identified in the study. These genes were

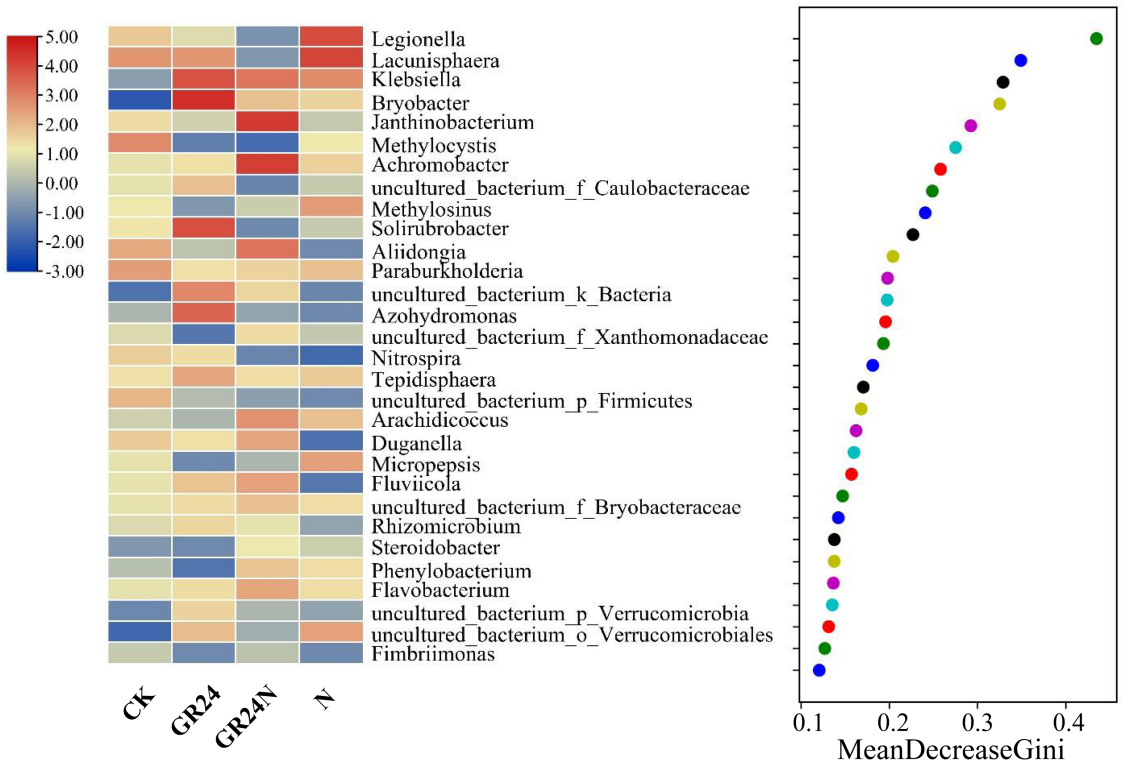

FIGURE 7 | Random forest classification analysis of dominant bacteria in additional N deposition and GR24 treatments.

associated with enrichment of multiple GO terms and metabolic pathways. Nitrogen deposition and GR24 treatment modulated the content of nutrient elements. A total of 1,778 ASVs were generated by 16S sequencing. Random forest classification model revealed that Legionella, Lacunisphaera, Klebsiella, Bryobacter, and Janthinobacterium were significantly enriched in the additional N deposition group or GR24 treatment group. Co-occurrence network analysis showed that species composition of soil microbial community was significantly different under the different treatments. These results indicate an association between N deposition and strigolactone activity.

DATA AVAILABILITY STATEMENT

The datasets presented in this study can be found in online repositories. The names of the repository/repositories and accession number(s) can be found at: https://www.ncbi.nlm.nih.gov/bioproject/PRJNA815869; https://www.ncbi.nlm.nih.gov/bioproject/PRJNA815930.

AUTHOR CONTRIBUTIONS

WY and JW designed the research. CY, QW, SZ, HZ, and WjC did running the experiments and data analysis and statistics. WcC and HL analyzed the data. CY, QW, WY, and JW did the manuscript writing and revising. All authors contributed to the article and approved the submitted manuscript.

FUNDING

This work was supported by the National Natural Science Foundation of China (Grant nos. 32171830 and 31800579); the breeding of new varieties of Torreya grandis Program (2021C02066-11); "Pioneer" and "Leading Goose" R&D Program of Zhejiang (2022C02061); and Scientific R&D Foundation for Talent Start-up Project of Zhejiang A&F University (2020FR073).

ACKNOWLEDGMENTS

We are grateful to the BENAGENE company and NOVOGENE company for technical support. 16S rRNA sequence analysis was performed using BMKCloud (www.biocloud.net).

SUPPLEMENTARY MATERIAL

The Supplementary Material for this article can be found online at: https://www.frontiersin.org/articles/10.3389/fpls.2022.908129/full#supplementary-material

Supplementary Figure S1 | Comparison of the reproducibility of transcriptome and 16S sequencing. Principle component analysis (PCA) for transcriptome(A) and bacterial community 16S rRNA gene sequences(B).

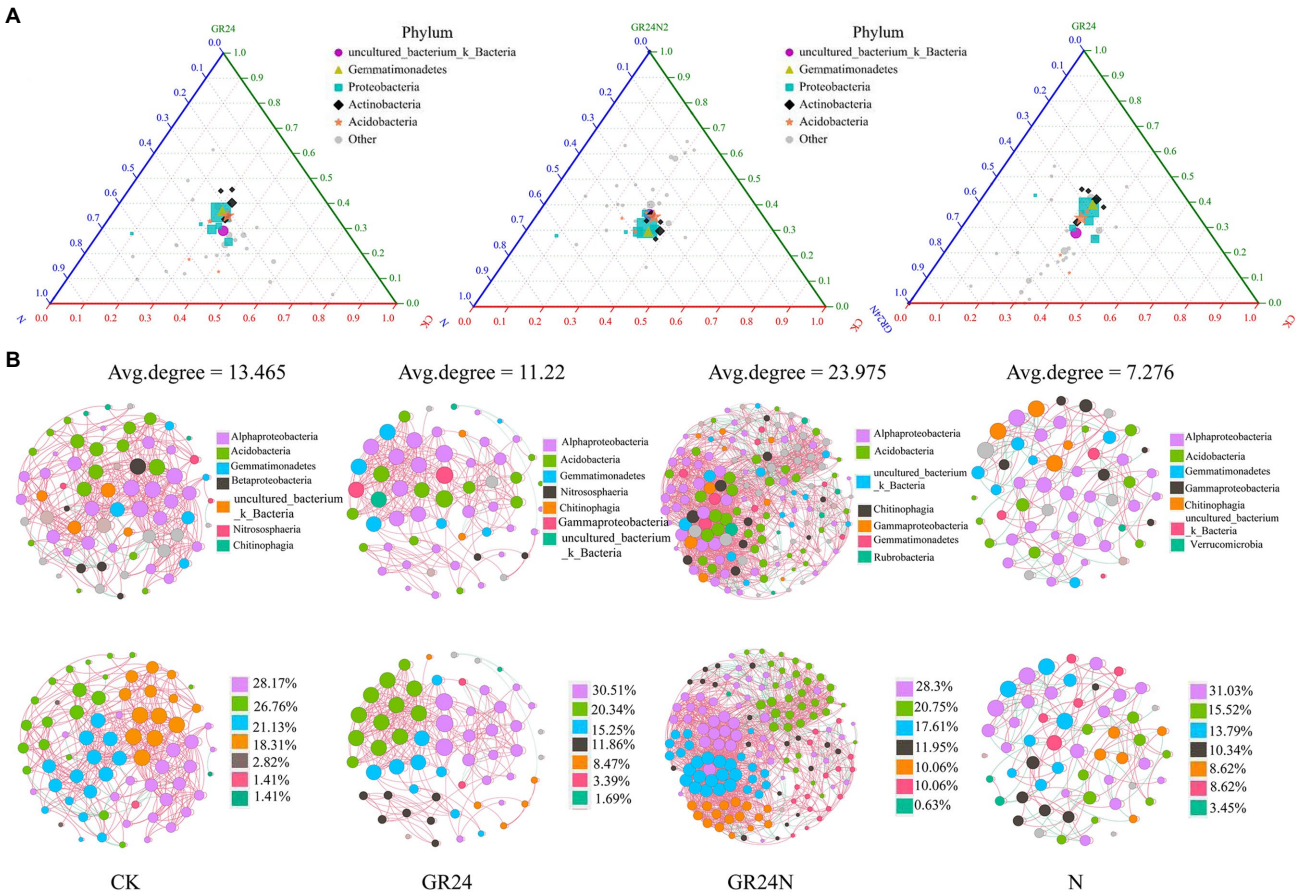

FIGURE 8 | Effects of additional N deposition and GR24 treatments on soil microbiome structures and diversities. **(A)** Ternary phase diagram of mock, additional N deposition and GR24 treatments soil microbiome. The species composition of the three groups of samples is compared and analyzed, and the proportion and relationship of different species in the samples can be visually displayed through the triangular graph. The circle in the triangle represents the species classification of all class levels contained under the phylum level, the size of the circle represents the average relative abundance of species, and the colored circle in the legend represents the species classification of the five phylum levels with the highest abundance. **(B)** Network of soil microbial populations additional N deposition and GR24 treatments at class level. Red lines indicate positive correlations and green lines for negative correlations. Node area is proportional to node degree calculated from each ASV abundance correlation. Correlation coefficients greater than 0.6 and P less than 0.05 were shown in the network.

Shannon index rarefaction curve(C) and Rank Abundance Curve (D) were used to assess the depth of coverage for each sample.

Supplementary Figure S2 | Analysis of the differentially expressed unigenes (DEGs) under N deposition or GR24.

Supplementary Figure S3 | Permanova analysis box diagram. Y-axis represents Beta distance; The box above 'All between 'represents the Beta distance data of samples between all groups, while the box above 'All within 'represents the Beta distance data of samples within all groups. The box below represents the Beta distance data of samples within different groups.

Supplementary Table S1 | Sequencing output statistics of 21 RNAseq samples.

Supplementary Table S2 | The expression profile of all identified genes.

Supplementary Table S3 | Detailed information of identified differentially expressed genes.

Supplementary Table S4 | Summary of 16S raw data processing.

Supplementary Table S5 | ASV abundance of all the 16S sequencing samples.

REFERENCES

Al-Babili, S., and Bouwmeester, H. J. (2015). Strigolactones, a novel carotenoid-derived plant hormone. *Annu. Rev. Plant Biol.* 66, 161–186. doi: 10.1146/annurev-arplant-043014-114759

Atlas, R. M. (1999). Legionella: from environmental habitats to disease pathology, detection and control. *Environ. Microbiol.* 1, 283–293. doi: 10.1046/j.1462-2920.1999.00046.x

Benjamin, H., Ying-Ping, W., Peter, V., and Christopher, F. (2008). A unifying framework for dinitrogen fixation in the terrestrial biosphere. *Nature* 454, 327–330. doi: 10.1038/nature07028

Berg, L., Vergeer, P., Rich, T., Smart, S. M., Dan, G., and Ashmore, M. R. (2011). Direct and indirect effects of nitrogen deposition on species composition change in calcareous grasslands. *Glob. Chang. Biol.* 17, 1871–1883. doi: 10.1111/j.1365-2486.2010.02345.x

Blanes, M. C., Vinegla, B., Salido, M. T., and Carreira, J. A. (2013). Coupled soil-availability and tree-limitation nutritional shifts induced by N deposition:

insights from N to P relationships in Abies pinsapo forests. *Plant Soil* 366, 67–81. doi: 10.1007/s11104-012-1397-y

Bobbink, R., and Roelofs, H. (1998). The effects of air-borne nitrogen pollutants on species diversity in natural and semi-natural European vegetation. *J. Ecol.* 86, 717–738. doi: 10.1046/j.1365-2745.1998.8650717.x

Bolyen, E., Rideout, J. R., Dillon, M. R., Bokulich, N. A., Abnet, C. C., Al-Ghalith, G. A., et al. (2019). Reproducible, interactive, scalable and extensible microbiome data science using QIIME 2. *Nat. Biotechnol.* 37, 852–857. doi: 10.1038/s41587-019-0209-9

Brewer, P. B., Koltai, H., and Beveridge, C. A. (2013). Diverse roles of strigolactones in plant development. *Mol. Plant* 6, 18–28. doi: 10.1093/mp/sss130

Carvalhais, L. C., Rincon-Florez, V. A., Brewer, P. B., Beveridge, C. A., Dennis, P. G., and Schenk, P. M. (2019). The ability of plants to produce strigolactones affects rhizosphere community composition of fungi but not bacteria. *Rhizosphere* 9, 18–26. doi: 10.1016/j.rhisph.2018.10.002

Chen, X., Brockway, D. G., and Guo, Q. (2020). Burstiness of Seed Production in Longleaf Pine and Chinese Torreya. *J. Sustain. For.* 1, 1–9. doi: 10.1080/10549811.2020.1746914

Chen, G. T., Tu, L. H., Peng, Y., Hu, H. L., Hu, T. X., Xu, Z. F., et al. (2017). Effect of nitrogen additions on root morphology and chemistry in a subtropical bamboo forest. *Plant Soil* 412, 441–451. doi: 10.1007/s11104-016-3074-z

Clark, C. M., and Tilman, D. (2008). Loss of plant species after chronic low-level nitrogen deposition to prairie grasslands. *Nature* 451, 712–715. doi: 10.1038/nature06503

Cochetel, N., Meteier, E., Merlin, I., Hevin, C., Pouvreau, J. B., Coutos-Thevenot, P., et al. (2018). Potential contribution of strigolactones in regulating scion growth and branching in grafted grapevine in response to nitrogen availability. *J. Exp. Bot.* 69, 4099–4112. doi: 10.1093/jxb/ery206

Cusack, D. F., Silver, W. L., Torn, M. S., Burton, S. D., and Firestone, M. K. (2011). Changes in microbial community characteristics and soil organic matter with nitrogen additions in two tropical forests. *Ecology* 92, 621–632. doi: 10.1890/10-0459.1

Dentener, F., Drevet, J., Lamarque, J.-F., Bey, I., Eickhout, B., Fiore, A. M., et al. (2006). Nitrogen and sulfur deposition on regional and global scales: A multimodel evaluation. *Glob. Biogeochem. Cycles* 20. doi: 10.1029/2005GB002672

Díaz-Álvarez, E. A., Lindig-Cisneros, R., and de la Barrera, E. (2018). Biomonitors of atmospheric nitrogen deposition: potential uses and limitations. *Conserv. Physiol.* 6:coy011. doi: 10.1093/conphys/coy011

Dima, C., Zhichun, L., Shuijin, H., and Yongfei, B. (2015). Effects of nitrogen enrichment on belowground communities in grassland: relative role of soil nitrogen availability vs. soil acidification - ScienceDirect. *Soil Biol. Biochem.* 89, 99–108. doi: 10.1016/j.soilbio.2015.06.028

Dom, S. P., Ikenaga, M., Lau, S. Y. L., Radu, S., Midot, F., Yap, M. L., et al. (2021). Linking prokaryotic community composition to carbon biogeochemical cycling across a tropical peat dome in Sarawak, Malaysia. *Sci. Rep.* 11:6416. doi: 10.1038/s41598-021-81865-6

Elser, J. J., Bracken, M. E. S., Cleland, E. E., Gruner, D. S., Harpole, W. S., Hillebrand, H., et al. (2007). Global analysis of nitrogen and phosphorus limitation of primary producers in freshwater, marine and terrestrial ecosystems. *Ecol. Lett.* 10, 1135–1142. doi: 10.1111/j.1461-0248.2007.01113.x

Fenliang, F., Chang, Y., Yongjun, T., Zhaojun, L., Alin, S., Steven, A. W., et al. (2014). Probing potential microbial coupling of carbon and nitrogen cycling during decomposition of maize residue by 13C-DNA-SIP. *Soil Biol. Biochem.* 70, 12–21. doi: 10.1016/j.soilbio.2013.12.002

Fierer, N., Lauber, C. L., Ramirez, K. S., Zaneveld, J., Bradford, M. A., and Knight, R. (2012). Comparative metagenomic, phylogenetic and physiological analyses of soil microbial communities across nitrogen gradients. *ISME J.* 6, 1007–1017. doi: 10.1038/ismej.2011.159

Galloway, J. N., and Cowling, E. B. (2002). Reactive nitrogen and the world: 200 years of change. *Ambio* 31, 64–71. doi: 10.1579/0044-7447-31.2.64

Gao, Y. D., Hu, Y. Y., Shen, J. Y., Meng, X. C., Suo, J. W., Zhang, Z. Y., et al. (2021). Acceleration of aril cracking by ethylene in Torreya grandis during nut maturation. *Front. Plant Sci.* 12:761139. doi: 10.3389/fpls.2021.761139

Gong, Z., Xiong, L., Shi, H., Yang, S., and Zhu, J. K. (2020). Plant abiotic stress response and nutrient use efficiency. *Sci. China Life Sci.* 63, 635–674. doi: 10.1007/s11427-020-1683-x

Gou, X., Yin, H., He, K., Du, J., Yi, J., Xu, S., et al. (2012). Genetic evidence for an indispensable role of somatic embryogenesis receptor kinases in brassinosteroid signaling. *PLoS Genet.* 8:e1002452. doi: 10.1371/journal.pgen.1002452

Ha, C. V., Leyva-González, M. A., Osakabe, Y., Tran, U. T., Nishiyama, R., Watanabe, Y., et al. (2014). Positive regulatory role of strigolactone in plant responses to drought and salt stress. *Proc. Natl. Acad. Sci. U. S. A.* 111, 851–856. doi: 10.1073/pnas.1322135111

Haas, B. J., Papanicolaou, A., Yassour, M., Grabherr, M., Blood, P. D., Bowden, J., et al. (2013). De novo transcript sequence reconstruction from RNA-seq using the trinity platform for reference generation and analysis. *Nat. Protoc.* 8, 1494–1512. doi: 10.1038/nprot.2013.084

Han, Z., Ahsan, M., Adil, M. F., Chen, X., and Zhang, G. (2020). Identification of the gene network modules highly associated with the synthesis of phenolics compounds in barley by transcriptome and metabolome analysis. *Food Chem.* 323:126862. doi: 10.1016/j.foodchem.2020.126862

Hatzenpichler, R., Lebedeva, E. V., Spieck, E., Stoecker, K., Richter, A., Daims, H., et al. (2008). A moderately thermophilic ammonia-oxidizing crenarchaeote from a hot spring. *Proc. Natl. Acad. Sci. U. S. A.* 105, 2134–2139. doi: 10.1073/pnas.0708857105

Higo, M., Azuma, M., Kamiyoshihara, Y., Kanda, A., Tatewaki, Y., and Isobe, K. (2020). Impact of phosphorus fertilization on tomato growth and Arbuscular Mycorrhizal fungal communities. *Microorganisms* 8:178. doi: 10.3390/microorganisms8020178

Holland, E. A., Dentener, F. J., Braswell, B. H., and Sulzman, J. M. (1999). Contemporary and pre-industrial global reactive nitrogen budgets. *Biogeochemistry* 46, 7–43. doi: 10.1023/a:1006148011944

Huang, K., Jiang, Q. P., Liu, L. H., Zhang, S. T., Liu, C. L., Chen, H. T., et al. (2020). Exploring the key microbial changes in the rhizosphere that affect the occurrence of tobacco root-knot nematodes. *AMB Express* 10:72. doi: 10.1186/s13568-020-01006-6

Huang, G. Q., Liang, W. Q., Sturrock, C. J., Pandey, B. K., Giri, J., Mairhofer, S., et al. (2018). Rice actin binding protein RMD controls crown root angle in response to external phosphate. *Nat. Commun.* 9:2346 PMID: 29892032

Ji, S., Han, Z., Kim, T. W., Wang, J., Cheng, W., Chang, J., et al. (2011). Structural insight into brassinosteroid perception by BRI1. *Nature* 474, 472–476.

Jiang, C. J., Li, X. L., Zou, J. X., Ren, J. Y., Jin, C. Y., Zhang, H., et al. (2021). Comparative transcriptome analysis of genes involved in the drought stress response of two peanut (*Arachis hypogaea* L.) varieties. *BMC Plant Biol.* 21:64

Kapulnik, Y., and Koltai, H. (2014). Strigolactone involvement in root development, response to abiotic stress, and interactions with the biotic soil environment. *Plant Physiol.* 166, 560–569. doi: 10.1104/pp.114.244939

Kersters, K., Vos, P.D., Gillis, M., Swings, J., and Stackebrandt, E. (2006). *Introduction to the Proteobacteria*. Springer New York.

Kiba, T., Inaba, J., Kudo, T., Ueda, N., Konishi, M., Mitsuda, N., et al. (2018). Repression of nitrogen starvation responses by members of the Arabidopsis GARP-type transcription factor NIGT1/HRS1 subfamily. *Plant Cell* 30, 925–945. doi: 10.1105/tpc.17.00810

Kishi, L. T., Lopes, E. M., Fernandes, C. C., Fernandes, G. C., Sacco, L. P., Carareto Alves, L. M., et al. (2017). Draft genome sequence of a Chitinophaga strain isolated from a lignocellulose biomass-degrading consortium. *Genome Announc.* 5:e01056-16. doi: 10.1128/genomeA.01056-16

Kohlen, W., Charnikhova, T., Liu, Q., Bours, R., Domagalska, M. A., Beguerie, S., et al. (2011). Strigolactones are transported through the xylem and play a key role in shoot architectural response to phosphate deficiency in Nonarbuscular Mycorrhizal host Arabidopsis. *Plant Physiol.* 155, 974–987. doi: 10.1104/pp.110.164640

Langfelder, P., and Horvath, S. (2008). WGCNA: an R package for weighted correlation network analysis. *BMC Bioinform.* 9:559. doi: 10.1186/1471-2105-9-559

Levy-Booth, D. J., Prescott, C. E., and Grayston, S. J. (2014). Microbial functional genes involved in nitrogen fixation, nitrification and denitrification in forest ecosystems. *Soil Biol. Biochem.* 75, 11–25. doi: 10.1016/j.soilbio.2014.03.021

Li, Z., and Dai, W. (2007). Chinese Torreya. Beijing: Science Press.

Li, H., Li, M. C., Luo, J., Cao, X., Qu, L., Gai, Y., et al. (2012). N-fertilization has different effects on the growth, carbon and nitrogen physiology, and wood properties of slow- and fast-growing Populus species. *J. Exp. Bot.* 63, 6173–6185. doi: 10.1093/jxb/ers271

Li, W., Nguyen, K. H., Chu, H. D., Watanabe, Y., Osakabe, Y., Sato, M., et al. (2020). Comparative functional analyses of DWARF14 and KARRIKIN INSENSITIVE 2 in drought adaptation of Arabidopsis thaliana. *Plant J.* 103, 111–127. doi: 10.1111/tpj.14712

Liang, X., Li, F., Wang, S., Hua, G., and Garrett, K. A. (2020). A rice variety with a high straw biomass retained nitrogen and phosphorus without affecting soil bacterial species. *Soil Ecol. Lett.* 2, 131–144. doi: 10.1007/s42832-020-0029-3

Lin, C., Wang, Y., Liu, M., Li, Q., Xiao, W., and Song, X. (2020). Effects of nitrogen deposition and phosphorus addition on arbuscular mycorrhizal fungi of Chinese fir (*Cunninghamia lanceolata*). *Sci. Rep.* 10:12260. doi: 10.1038/s41598-020-69213-6

Liu, X., Zhang, Y., Han, W., Tang, A., Shen, J., Cui, Z., et al. (2013). Enhanced nitrogen deposition over China. *Nature* 494, 459–462. doi: 10.1038/nature11917

Lü, X.-T., and Han, X. G. (2010). Nutrient resorption responses to water and nitrogen amendment in semi-arid grassland of Inner Mongolia, China. *Plant and Soil* 327, 481–491. doi: 10.1007/s11104-009-0078-y

Lu, X. K., Mao, Q. G., Gilliam, F. S., Luo, Y. Q., and Mo, J. M. (2014). Nitrogen deposition contributes to soil acidification in tropical ecosystems. *Glob. Chang. Biol.* 20, 3790–3801. doi: 10.1111/gcb.12665

Lü, C., and Tian, H. (2007). Spatial and temporal patterns of nitrogen deposition in China: Synthesis of 562 observational data - art. no. D22S05. *J. Geophys. Res.* 112:D22S05. doi: 10.1029/2006jd007990

Marzec, M. (2016). Strigolactones as part of the plant defence system. *Trends Plant Sci.* 21, 900–903. doi: 10.1016/j.tplants.2016.08.010

Matusova, R., Rani, K., Verstappen, F. W., Franssen, M. C., Beale, M. H., and Bouwmeester, H. J. (2005). The strigolactone germination stimulants of the plant-parasitic Striga and Orobanche spp. are derived from the carotenoid pathway. *Plant Physiol.* 139, 920–934. doi: 10.1104/pp.105.061382

Müller, L., Flokova, K., Schnabel, E., Sun, X., and Harrison, M. J. (2019). A CLE–SUNN module regulates strigolactone content and fungal colonization in arbuscular mycorrhiza. *Nat. Plants* 5, 933–939. doi: 10.1038/s41477-019-0501-1

Oancea, F., Georgescu, E., Matusova, R., Georgescu, F., Nicolescu, A., Raut, I., et al. (2017). New strigolactone mimics as exogenous signals for rhizosphere organisms. *Molecules* 22:961. doi: 10.3390/molecules22060961

Pandey, A., Sharma, M., and Pandey, G. K. (2016). Emerging roles of strigolactones in plant responses to stress and development. *Front. Plant Sci.* 7:434. doi: 10.3389/fpls.2016.00434

Prosser, J. I., and Nicol, G. W. (2008). Relative contributions of archaea and bacteria to aerobic ammonia oxidation in the environment. *Environ. Microbiol.* 10, 2931–2941. doi: 10.1111/j.1462-2920.2008.01775.x

Ravazzolo, L., Trevisan, S., Forestan, C., Varotto, S., Sut, S., Dall'Acqua, S., et al. (2020). Nitrate and ammonium affect the overall maize response to nitrogen availability by triggering specific and common transcriptional signatures in roots. *Int. J. Mol. Sci.* 21:686. doi: 10.3390/ijms21020686

Ruiqiang, L., Zhiqun, H., Luke, M., Xuhui, Z., Xiaohua, W., Zaipeng, Y., et al. (2016). Plasticity of fine-root functional traits in the litter layer in response to nitrogen addition in a subtropical forest plantation. *Plant Soil* 415, 317–330.

Sheridan, P. O., Raguideau, S., Quince, C., Holden, J., Zhang, L. H., Williams, T. A., et al. (2020). Gene duplication drives genome expansion in a major lineage of Thaumarchaeota. *Nat. Commun.* 11:5494.

Shindo, M., Yamamoto, S., Shimomura, K., and Umehara, M. (2020). Strigolactones decrease leaf angle in response to nutrient deficiencies in rice. *Front. Plant Sci.* 11:135. doi: 10.3389/fpls.2020.00135

Simek, K., Hornak, K., Jezbera, J., Nedoma, J., Vrba, J., Straskrabova, V., et al. (2006). Maximum growth rates and possible life strategies of different bacterioplankton groups in relation to phosphorus availability in a freshwater reservoir. *Environ. Microbiol.* 8, 1613–1624. doi: 10.1111/j.1462-2920.2006.01053.x

Sun, H., Guo, X., Qi, X., Feng, F., and Zhao, Q. (2021). SPL14/17 act downstream of strigolactone signalling to modulate rice root elongation in response to nitrate supply. *Plant J.* 106, 649–660. doi: 10.1111/tpj.15188

Sylwia, S., Lukas, B., Cedrick, M., Alan, W., Nick, V., Stan, V. P., et al. (2021). Transcriptional analysis in the Arabidopsis roots reveals new regulators that link rac -GR24 treatment with changes in Flavonol accumulation, root hair elongation and lateral root density. *Plant Cell Physiol.* 63, 104–119. doi: 10.1093/pcp/pcab149

Tessier, J. T., and Raynal, D. J. (2003). Use of nitrogen to phosphorus ratios in plant tissue as an indicator of nutrient limitation and nitrogen saturation. *J. Appl. Ecol.* 40, 523–534. doi: 10.1046/j.1365-2664.2003.00820.x

Ti, C., Ma, S., Peng, L., Tao, L., Wang, X., Dong, W., et al. (2021). Changes of δ15N values during the volatilization process after applying urea on soil. *Environ. Pollut.* 270:116204. doi: 10.1016/j.envpol.2020.116204

Torres-Vera, G., Pozo, J. M., Pozo, M. J., and Lopez-Raez, J. A. (2014). Do strigolactones contribute to plant defence? *Mol. Plant Pathol.* 15, 211–216. doi: 10.1111/mpp.12074

Treseder, K. K. (2010). Nitrogen additions and microbial biomass: a meta-analysis of ecosystem studies. *Ecol. Lett.* 11, 1111–1120. doi: 10.1111/j.1461-0248.2008.01230.x

Treseder, K. K., and Vitousek, P. M. (2001). Effects of soil nutrient availability on investment in acquisition of n and p in Hawaiian rain forests. *Ecology* 82, 946–954.

Umehara, M., Hanada, A., Yoshida, S., Akiyama, K., Arite, T., Takeda-Kamiya, N., et al. (2008). Inhibition of shoot branching by new terpenoid plant hormones. *Nature* 455, 195–200. doi: 10.1038/nature07272

van Heijnsbergen, E., van Deursen, A., Bouwknegt, M., Bruin, J. P., Husman, A. M. D., and Schalk, J. A. C. (2016). Presence and persistence of viable, clinically relevant legionella pneumophila bacteria in garden soil in the Netherlands. *Appl. Environ. Microbiol.* 82, 5125–5131. doi: 10.1128/Aem.00595-16

van Zeijl, A., Liu, W., Xiao, T. T., Kohlen, W., Yang, W. C., Bisseling, T., et al. (2015). The strigolactone biosynthesis gene DWARF27 is co-opted in rhizobium symbiosis. *BMC Plant Biol.* 15:260. doi: 10.1186/s12870-015-0651-x

Villaecija-Aguilar, J. A., Hamon-Josse, M., Carbonnel, S., Kretschmar, A., Schmidt, C., Dawid, C., et al. (2019). SMAX1/SMXL2 regulate root and root hair development downstream of KAI2-mediated signalling in Arabidopsis. *PLoS Genet.* 15:e1008327. doi: 10.1371/journal.pgen.1008327

Waldrop, M. P., Zak, D. R., and Sinsabaugh, R. L. (2004). Microbial community response to nitrogen deposition in northern forest ecosystems. *Soil Biol. Biochem.* 36, 1443–1451. doi: 10.1016/j.soilbio.2004.04.023

Wang, F. H., Chen, S. M., Wang, Y. Y., Zhang, Y. M., Hui, C. S., and Liu, B. B. (2018b). Long-term nitrogen fertilization elevates the activity and abundance of nitrifying and denitrifying microbial communities in an upland soil: implications for nitrogen loss From intensive agricultural systems. *Front. Microbiol.* 9:2424. doi: 10.3389/fmicb.2018.02424

Wang, C., Lu, X. K., Mori, T., Mao, Q. G., Zhou, K. J., Zhou, G. Y., et al. (2018a). Responses of soil microbial community to continuous experimental nitrogen additions for 13 years in a nitrogen-rich tropical forest. *Soil Biol. Biochem.* 121, 103–112. doi: 10.1016/j.soilbio.2018.03.009

Wang, S., Xing, J., Jang, C., Zhu, Y., Fu, J. S., and Hao, J. (2011). Impact assessment of ammonia emissions on inorganic aerosols in east china using response surface modeling technique. *Environ. Sci. Technol.* 45, 9293–9300. doi: 10.1021/es2022347

Wu, S. S., Huang, B., Wang, J. H., He, L. J., Wang, Z. Y., Yan, Z., et al. (2021). Spatiotemporal mapping and assessment of daily ground NO_2 concentrations in China using high-resolution TROPOMI retrievals. *Environ. Pollut.* 273:6456, 116456 PMID: 33477063

Xu, W., Zhang, L., and Liu, X. (2019). A database of atmospheric nitrogen concentration and deposition from the nationwide monitoring network in China. *Sci. Data* 6:51. doi: 10.1038/s41597-019-0061-2

Yoneyama, K., Takeuchi, Y., and Yokota, T. (2001). Production of clover broomrape seed germination stimulants by red clover root requires nitrate but is inhibited by phosphate and ammonium. *Physiol. Plant.* 112, 25–30. doi: 10.1034/j.1399-3054.2001.1120104.x

Yoneyama, K., Xie, X. N., Kim, H. I., Kisugi, T., Nomura, T., Sekimoto, H., et al. (2012). How do nitrogen and phosphorus deficiencies affect strigolactone production and exudation? *Planta* 235, 1197–1207. doi: 10.1007/s00425-011-1568-8

Yoneyama, K., Yoneyama, K., Takeuchi, Y., and Sekimoto, H. (2007). Phosphorus deficiency in red clover promotes exudation of orobanchol, the signal for mycorrhizal symbionts and germination stimulant for root parasites. *Planta* 225, 1031–1038. doi: 10.1007/s00425-006-0410-1

Zhan, Y., Qu, Y., Zhu, L., Shen, C., Feng, X., Yu, C., et al. (2018). Transcriptome analysis of tomato (*Solanum lycopersicum* L.) shoots reveals a crosstalk between auxin and strigolactone. *PLoS One* 13:e0201124. doi: 10.1371/journal.pone.0201124

Conflict of Interest: The authors declare that the research was conducted in the absence of any commercial or financial relationships that could be construed as a potential conflict of interest.

Publisher's Note: All claims expressed in this article are solely those of the authors and do not necessarily represent those of their affiliated organizations, or those of the publisher, the editors and the reviewers. Any product that may

be evaluated in this article, or claim that may be made by its manufacturer, is not guaranteed or endorsed by the publisher.

frontiers | Frontiers in Plant Science

ORIGINAL RESEARCH
published: 03 June 2022
doi: 10.3389/fpls.2022.929855

Root Carbon Resources Determine Survival and Growth of Young Trees Under Long Drought in Combination With Fertilization

*Yue Yang[1,2,3], Shengnan Ouyang[2,4], Arthur Gessler[2,5], Xiaoyu Wang[6], Risu Na[7], Hong S. He[3,8], Zhengfang Wu[3] and Mai-He Li[2,3]**

[1]College of Ecology and Environment, Hainan University, Haikou, China, [2]Swiss Federal Institute for Forest, Snow and Landscape Research WSL, Birmensdorf, Switzerland, [3]Key Laboratory of Geographical Processes and Ecological Security in Changbai Mountains, Ministry of Education, School of Geographical Sciences, Northeast Normal University, Changchun, China, [4]Institute for Forest Resources and Environment Research Center of Guizhou Province, Guizhou University, Guiyang, China, [5]Institute of Terrestrial Ecosystems, ETH Zurich, Zurich, Switzerland, [6]Jiyang College of Zhejiang A and F University, Zhuji, China, [7]School of Geographical Sciences, Inner Mongolia Normal University, Hohhot, China, [8]School of Natural Resources, University of Missouri, Columbia, MO, United States

OPEN ACCESS

Edited by:
Guolei Li,
Beijing Forestry University, China

Reviewed by:
Peng He,
Tianjin Normal University, China
Ninghua Zhu,
Central South University Forestry and Technology, China

***Correspondence:**
Mai-He Li
maihe.li@wsl.ch

Specialty section:
This article was submitted to Functional Plant Ecology, a section of the journal Frontiers in Plant Science

Received: 27 April 2022
Accepted: 13 May 2022
Published: 03 June 2022

Citation:
Yang Y, Ouyang S, Gessler A, Wang X, Na R, He HS, Wu Z and Li M-H (2022) Root Carbon Resources Determine Survival and Growth of Young Trees Under Long Drought in Combination With Fertilization. Front. Plant Sci. 13:929855. doi: 10.3389/fpls.2022.929855

Current increases in not only the intensity and frequency but also the duration of drought events could affect the growth, physiology, and mortality of trees. We experimentally studied the effects of drought duration in combination with fertilization on leaf water potential, gas exchange, growth, tissue levels of non-structural carbohydrates (NSCs), tissue NSC consumption over-winter, and recovery after drought release in oak (*Quercus petraea*) and beech (*Fagus sylvatica*) saplings. Long drought duration (>1 month) decreased leaf water potential, photosynthesis, and NSC concentrations in both oak and beech saplings. Nitrogen fertilization did not mitigate the negative drought effects on both species. The photosynthesis and relative height increment recovered in the following rewetting year. Height growth in the rewetting year was significantly positively correlated with both pre- and post-winter root NSC levels. Root carbon reserve is critical for tree growth and survival under long-lasting drought. Our results indicate that beech is more sensitive to drought and fertilization than oak. The present study, in a physiological perspective, experimentally confirmed the view that the European beech, compared to oak, may be more strongly affected by future environmental changes.

Keywords: non-structural carbohydrates, NSC, over-winter carbon consumption, photosynthesis, recovery, water deficit

INTRODUCTION

Global climate change has led to and is continuously resulting in increases not only in drought intensity but also in the frequency and duration of drought events globally (IPCC, 2013). Two main hypotheses have been proposed and are currently debated to explain the mechanisms for the widespread forest dieback caused by increased drought events (Hartmann et al., 2018; Spinoni et al., 2018): trees would die (1) due to hydraulic failure or (2) as a result of carbon

starvation (McDowell and Allen, 2015; Gessler et al., 2018). The hydraulic failure hypothesis proposes that the tree mortality results from the embolism of the xylem vessels under high evaporative demand and restricted soil water availability (Nardini et al., 2013), whereas the carbon starvation hypothesis suggests that tree mortality would be caused by a carbon supply limitation due to stomatal closure and thus reduced photosynthesis that cannot cover the carbon and energy demand for maintenance processes (McDowell et al., 2008; Rowland et al., 2015). Concerning carbon starvation, several studies have shown that the contents of starch, a compound that serves as carbon storage and is build up when assimilation exceeds plant's demand for carbon, were strongly reduced by severe soil water deficit (McDowell, 2011), implying carbon limitation (Reinhardt et al., 2015). Previous studies also suggested that hydraulic perturbation could prevent phloem transport (Sevanto, 2014) and consequently constrains carbon accessibility (Sala et al., 2012; Hartmann and Trumbore, 2016), even though the carbon availability in the tree crown area might not be restricted. Thus, hydraulic failure and carbon starvation are often seen to be associated with each other in the cascade of drought events leading to tree mortality (Adams et al., 2017).

Droughts, however, are very tougher to be defined, and thus a universally accepted drought definition considering both water-deficit intensity and duration is still lack (Buitink et al., 2021). Previous drought-related forest and agricultural studies, especially manipulation experiments, mainly focused on the effects of drought intensity (e.g., various levels of watering, such as very limited, limited, and optimum watering) on trees or plants (Allen et al., 2010; Yu et al., 2021), while less is known about the effects of drought duration on trees' physiology, growth, and mortality. Actually, seasonal drought with longer duration occurs often in subtropical regions around the world. In terms of seasonal drought, drought duration is somewhat comparable to drought intensity. A long-lasting drought event may cause irreversible changes in plant physiology which are different from those found in relatively short-term severe droughts. For example, recurrent or short-term lasting drought events may allow trees to recover and even acclimate to water restriction (Gessler et al., 2020), and thus, permit them to survive in the long-term. However, longer term lasting drought events may strongly affect the recovery ability of trees. Currently, unexpected whole-season drought occurs more frequently in many regions around the world. For instance, since the beginning of the 21st century Europe already experienced severe drought summer of 2003, 2010, 2013, 2015, and 2018 (Hanel et al., 2018; Brunner et al., 2019). Therefore, mechanistic understanding of tree and forest responses to various drought duration is particularly critical for sustainably forest management under future climate change.

Theoretically, trees' resilience and resistance to drought stress and the recovery and thus survival ability should be associated with the resource storage and availability. Non-structural carbohydrates (NSC = soluble sugars + starch) among other resources (e.g., nutrients, see Gessler et al., 2017) are known to contribute to tree resilience after stress (Li et al., 2002, 2008b). For many years, reserve storage was considered as a passive process resulting from an accumulation of resources when uptake and assimilation exceeded growth demand (Sala et al., 2012; Wiley and Helliker, 2012). An alternative hypothesis was proposed in which reserves storage would be rather an active process during the growing season and would act as a sink competing with other sinks (e.g., growth and reproduction) for available resources (Wiley and Helliker, 2012; Li et al., 2018a). Several studies investigated the NSC levels of trees during and at the end of the growing season following a growing season-long drought (Li et al., 2013; Schönbeck et al., 2018, 2020a,b). They found a drought-induced growth reduction but did not observe a drought-induced NSC decrease of trees, suggesting an active NSC storage under drought at the expense of growth (Wiley and Helliker, 2012; Li et al., 2018a). Recent evidence indicates that stress actively induces NSC transfer from aboveground tissues to roots stored (Kannenberg et al., 2018; Li et al., 2018a). In contrast, Li et al. (2018b) analyzed 27 case studies and found that drought decreased NSC concentration by 17.3% in roots, while it did not change NSC in aboveground tissues in the current season. To our knowledge, even less is known about the changes of NSC over-winter (post- vs. pre-winter) in trees previously stressed by drought.

Recently, it was proposed that nutrient addition (i.e., fertilization) will affect the fitness of trees under dry conditions, showing intensifying or mitigating effects on trees' tolerance to drought (Kreuzwieser and Gessler, 2010; Gessler et al., 2017; Schönbeck et al., 2020b). Nitrogen (N) deficiency can increase the sensitivity of stomata to low leaf water potential (Radin and Ackerson, 1981; Ghashghaie and Saugier, 1989), which further increases the risk of drought-induced carbon starvation (McDowell, 2011). N itself is a main growth-limiting nutrient in temperate terrestrial ecosystems and is also a major component of Rubisco and other photosynthetic enzymes and structures which regulate the photosynthetic activity and thus carbon gain and the NSC level of trees in response to environmental factors, such as drought (Bond et al., 1999; Meng et al., 2016). Schönbeck et al. (2020a) found that negative effects of moderate drought intensity (but not of severe drought) could be compensated by increased nutrient availability in Scot pine saplings. In contrast, Jacobs et al. (2004) reported that fertilization with blended fertilizer impaired the root system development and drought avoidance ability of drought-stressed Douglas-fir seedlings. Similarly, Dziedek et al. (2016) found that nitrogen addition increased the drought sensitivity of saplings of several deciduous tree species (Dziedek et al., 2016). Despite these studies, there is a strong knowledge gap about drought and nutrient interaction and especially about whether and to what extent nutrient addition affects winter NSC consumption and thus growth recovery in the season following drought.

The species, *Quercus petraea* (Matt.) Liebl. (*oak*) and *Fagus sylvatica* L. (beech), are two coexisting species in European forests. According to Ellenberg (2009), oak will become more competitive than beech at sites where as July temperatures increase to >18°C and precipitation decreases to <600 mm/year as a result of climate change. We proposed a conceptual model to describe the physiological, growth, survival, and

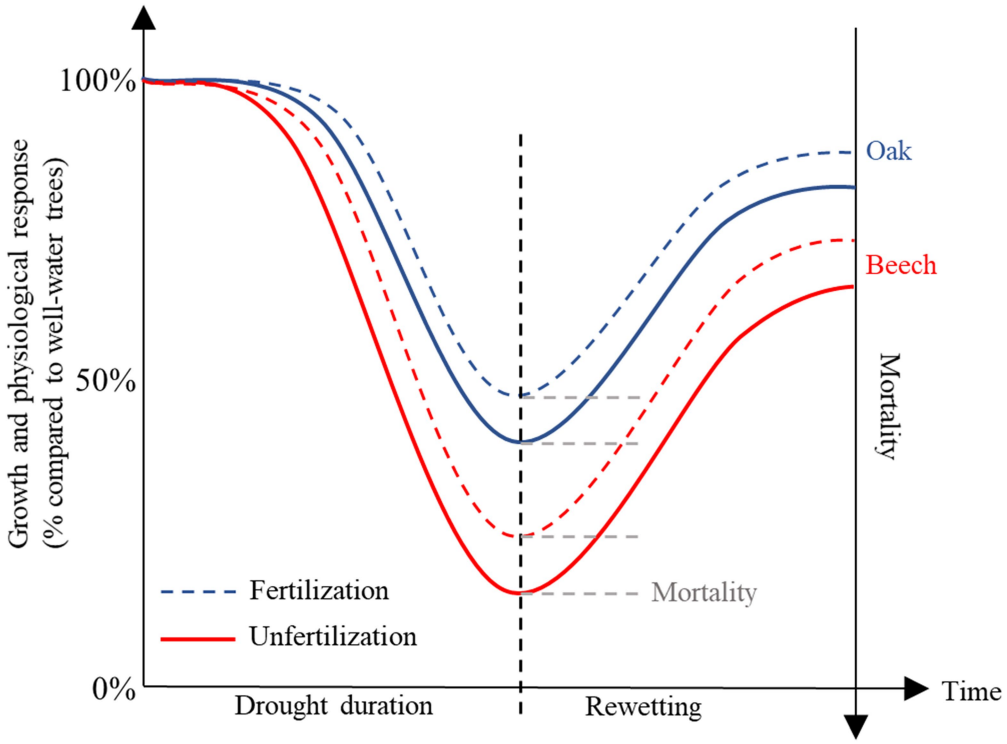

FIGURE 1 | A conceptual model proposed to describe the physiological, growth, mortality, and recovery responses of *Quercus petraea* (oak) and *Fagus sylvatica* (beech) to increasing drought duration in combination with fertilization and after drought release.

recovery responses of these two species to increasing drought duration and after drought release (**Figure 1**), and therefore carried out a greenhouse experiment with saplings of these two species treated with various drought duration in combination with light fertilization (defined as <2 g N kg^{-1} dry soil), followed by rewetting (**Figure 1**). We measured leaf water potential, gas exchange rate, tissue NSC under various drought durations in combination with fertilization, and the recovery potential (incl. gas exchange, growth rate, and mortality) after rewetting, to test following hypotheses: (1) the availability of tissue NSC decreases with increasing drought duration due to decreased leaf water potential and photosynthesis; (2) this decreased pre-winter and post-winter (at the early beginning of next growing season) NSC availability leads to lower recovery ability of trees after rewetting; (3) fertilization mitigates the negative drought effects on trees as proposed by Gessler et al. (2017); and (4) beech is more sensitive than oak to the treatments as proposed by Ellenberg (2009).

MATERIALS AND METHODS

Experimental Design and Treatments

The experiment was carried out in the greenhouse of the Swiss Federal Institute for Forest, Snow, and Landscape Research WSL (47°21′48″N, 8°27′23″E, 545 m a.s.l.), Birmensdorf, Switzerland. On February 27, 2018, 3-year-old sessile oak and European beech saplings (~30–40 cm in height) were planted into 10-liter plastic pots (26 cm in diameter). After transplanting into the pots, the plants were grown for 4 weeks under well-watered conditions (irrigation every 2–3 days) in the greenhouse to recover from the transplant shock. The cultivation soil consisted of semi-decomposed humus and commercial potting soil. The initial soil nitrogen and carbon contents were: 39 mg N kg^{-1} soil for NH_4^+-N, 573 mg N kg^{-1} soil for NO_3^--N, 22.42% for soil C, and 0.82% for total soil N. The greenhouse temperature and humidity during the period of drought duration treatment are shown in **Supplementary Figure A1**.

A split-plot experimental design with three blocks was employed in this study. Each block was divided into two main plots, one of which was randomly assigned for oak (48 individuals) and the other one for beech (48 individuals; **Supplementary Figure A2**). Each plot was then divided into two sub-plots, one of which was randomly assigned for fertilization (24 individuals) and the other one for the non-fertilization treatment (ambient, 24 individuals; **Supplementary Figure A2**). Each sub-plot was further divided in to four sub-sub-plots (rows) randomly assigned for one of the four drought duration treatments (six individuals each). Therefore, a total of 288 plant individuals (144 individuals for each species) was included (**Supplementary Figure A2**).

Fertilization treatment may be ineffective when the application occurs during drought. Therefore, the fertilization treatment was conducted on 10 June 2018 (just prior to the drought duration treatment) when the soils were still moisture

(**Supplementary Figure A2**). The fertilizer (Osmocote Exact 3-4M Standard, 7.0% NO_3^--N, 9.0% NH_4^+-N, 9% P_2O_5, ICL, Suffolk, United Kingdom), equal to 1.68 g N kg^{-1} dry soil (0.945 g N kg^{-1} dry soil NH_4^+-N, 0.735 g N kg^{-1} dry soil NO_3^--N) was added to each pot assigned for fertilization.

After the N-fertilization, plants were exposed to four drought duration treatments for 4 months in 2018 (**Supplementary Figure A3**). Plants in the well-watered treatment (D0) were watered thoroughly once a week. There were two moderate drought duration treatments, one of which was watered thoroughly biweekly (D1), and the other one was watered thoroughly once a month (D2; **Supplementary Figure A3**). The treatment of the longest drought duration in the present study was watered thoroughly once 2 months (D3; **Supplementary Figure A3**). We focused on the duration between two watering events and thus did not measure the soil water condition. After the harvest occurred on 1 October 2018, all remaining plants were treated (e.g., well-watering) in the same way until the end of the experiment (**Supplementary Figure A3**).

Leaf Water Potential, Gas Exchange, Height Measurement, and Mortality Record

To detect the effects of drought duration, all measurements and sampling were always carried out directly before the next watering (**Supplementary Figure A3**).

Three plants from both nutrient and all drought treatments were randomly selected from each sub-sub-plot and three mature leaves from each selected plant were used for water potential and gas exchange measurements during the drought treatment in 2018. The midday leaf water potential (ψ_{leaf}) was measured between 12:00 and 14:00 h on 5 August 2018 (**Supplementary Figure A3**), with a Scholander bomb (Model 600 pressure bomb; PMS Instrument Company, Albany, NY, United States). Net photosynthesis (A_{leaf}) was measured on 6 August and 28 September 2018 (**Supplementary Figure A3**), and after rewetting in the following year on 24 June 2019, with a LiCor 6400 system (LI-COR, Lincoln, United States). A_{leaf} was measured at 400 µmol mol^{-1} CO_2, 1,200 µmol m^2 s^{-1} photosynthetically active radiation, *ca.* 65% relative humidity, and 25°C air temperature.

Plant height of each individual was measured on 30 May 2018 (initial height), on 1 October 2018 (end of the treatment), and on 8 October 2019 (after one recovery season; **Supplementary Figure A3**), and height increments were calculated.

Harvest and Sampling

Destructive sampling (harvest) was conducted twice, one on 1 October 2018 as pre-winter samples, and the other one on 2 April 2019 as post-winter samples. One plant was randomly selected from each sub-sub-plot for each harvest time, and 48 individuals (24 individuals for each species; three for each nutrient and drought treatment) were harvested for each time (**Supplementary Figure A2**). The whole plant was harvested, the roots were carefully washed, and the plants were separated into leaves (Oct. 2018 only), shoots, and belowground tissue and separately sampled [leaves, shoots, mixed roots (i.e., fine and coarse roots)]. The samples were immediately put in an oven at 105°C for half an hour to stop the metabolic activity and then were dried at 65°C until stable weight. The dried samples were ground to fine powder, using a ball mill (MM 400; Retsch, Haan, Germany), for NSC analysis.

Mortality Record

At the beginning of the experiment on 31 May 2018, there were six individuals for each treatment in each sub-sub-plot (**Supplementary Figure A2**). During the experiment period, one plant out of the six individuals in each sub-sub-plot was destructively harvested on each sampling date of 1 October 2018 and 2 April 2019 (**Supplementary Figure A2**). Thus, each species had, theoretically, four individuals (=6–2) left in each sub-sub-plot (**Supplementary Figure A2**), and each species had 12 individuals (4 × 3 blocks = 12) for each treatment across the three blocks available at the end of the recovery season 2019. However, in some sub-sub-plots all the four plants died by the end of 2019. Therefore, it was not possible to statistically analyze the treatment effects on the mortality. Instead, we recorded the total dead individuals (A) that did not sprout new leaves or shoots from any part of a plant during the recovery season across the three blocks and calculated the total mortality rate with $(A/12) \times 100\%$.

Non-structural Carbohydrate Analysis

The NSC concentrations were measured according to the method by Wong (1990) modified by Hoch et al. (2002). NSC refers to the sum of mobile sugars (mainly glucose, fructose, and sucrose) and starch. First, 10–12 mg sample powder was boiled in 2 ml distilled water for half an hour. Then, 200 µl aliquot mixed with Invertase (Sigma-Aldrich, Buchs, Switzerland) were extracted to degrade sucrose to glucose and fructose. After centrifugation, glucose hexokinase and phosphogluconate isomerase (Sigma-Aldrich, Buchs, Switzerland) were added. The concentration of sugars was obtained as the total amount of glucose that was determined by 340 nm photometry (HR 7000, Hamilton, Rone, NE, United States) in a 96-well microplate photometer (Sigma-Aldrich, Buchs, Switzerland). 500 µl extract was taken from the sample aliquot and reacted with amyloglucosidase (Sigma-Aldrich, Buchs, Switzerland) for 15 h at 49°C, to break down starch to glucose, and to measure the total NSC concentration. The starch concentration was calculated as total NSC minus soluble sugars. NSC concentrations are expressed on a dry mass (d.m.) basis.

Calculation and Statistical Analysis

The relative height increment rate (RHI) was calculated based on height measured on 30 May 2018 (A), on 10 October 2018 (B), and on 8 October 2019 (C), using $[(B-A)/A] \times 100\%$ for the 2018 growth, and $[(C-B)/B] \times 100\%$ for the 2019 recovery growth. The NSC concentration was calculated as the sum of the concentration of soluble sugars plus that of starch for each sample.

All data were checked for normality with the Kolmogorov–Smirnov test and for homogeneity of variance with Levene's

test. The effects of species, drought duration, N-fertilization, and their interactions on the parameters measured on each date were analyzed using linear mixed effect models, with block and main plot as random effects. Within each species, the effects of drought duration, N-fertilization, and their interactions on the parameters measured on each date were also analyzed using linear mixed effect models, with block and main plot as random effects, followed, if significant, by Tukey's *post-hoc* test. Regression analysis was used to test the relationship between 2019 relative height increment rate and tissue NSC levels (both pre- and post-winter). All analyses are carried out by the package "LME" in R v.3.2.5 (R Core Team).

RESULTS

Leaf Water Potential and Photosynthesis During Drought Duration Treatment

Drought duration significantly decreased leaf water potential (**Table 1**; **Figures 2A,B**) in both species. A significant S×D interaction ($p<0.001$; **Table 1**) indicated that the leaf water potential of the two species responded to drought duration significantly differently, showing a ψ_{leaf} order of D0 = D1 > D2 = D3 for oak (**Figure 2A**), and of D0 > D1 > D2 = D3 for beech (**Figure 2B**). Neither N-fertilization nor any interaction of N with other factors affected leaf water potential (**Table 1**). In beech, N-fertilization significantly decreased ψ_{leaf} in D0 plants (**Figure 2B**).

Species, drought duration, N-fertilization, as well as their two-way and three-way interactions significantly affected the A_{leaf} of plants 2 months after the onset of the drought treatment on 6 August 2018 (except for non-effects of N and S×N interaction) and after 4 months on 28 September 2018 (**Table 1**). Oak's A_{leaf} significantly decreased with drought duration for the two measurement dates (**Figures 2C,E**), while in beech A_{leaf} significantly increased from D0 to D1, and then decreased in D2 and D3 (**Figures 2D,F**) on both dates. N-fertilization seemed to decrease A_{leaf} of oak under D1 and D2 (**Figures 2C,E**), whereas it significantly increased A_{leaf} of beech under D1 (**Figures 2D,F**). Photosynthesis almost ceased in D3 plants after 4 months of treatment (**Figures 2E,F**), especially in beech (**Figure 2F**).

During the drought duration treatment, the relative height increment (RHI) differed significantly only between species (**Table 1**), showing higher RHI in oak than in beech (**Figures 2G,H**). Neither N and D nor their interactions affected RHI (**Table 1**; **Figures 2G,H**).

Pre-winter NSC After Drought Duration Treatment

The pre-winter NSC levels in leaves differed significantly with species (**Table 2**). The shoot NSC levels, however, did not vary with species but were significantly affected by both drought treatment and N-fertilization (**Table 2**). The root NSC was significantly influenced by species and drought duration (**Table 2**). In addition, N-fertilization significantly interacted with species to affect the NSC levels in both shoots and roots (**Table 2**). Compared to the D0, D1, and D2 treatments, oaks in D3 had significantly higher leaf NSC levels

TABLE 1 | Results of linear mixed models with species (S), drought duration (D), nitrogen fertilization (N) as factors, for water potential (ψ_{leaf}), net photosynthetic rate during the drought duration treatment in 2018 and in the recovery growing season in 2019, relative height increment rate (RHI) in 2018 (drought) and 2019 (recovery).

	df	Leaf water potential		Photosynthesis (6 August 2018)		Photosynthesis (28 September 2018)		Photosynthesis (10 June 2019)		Relative height increment (2018)		Relative height increment (2019)	
		F	*p*	*F*	*p*	*F*	*p*	*F*	*p*	*F*	*p*	*F*	*p*
Species (S)	1	0.312	0.580	77.622	**<0.001**	132.315	**<0.001**	49.840	**<0.001**	17.219	<0.001	7.065	**<0.05**
D-duration (D)	3	13.826	**<0.001**	108.001	**<0.001**	233.175	**<0.001**	0.505	0.681	0.316	0.814	1.927	0.132
Nitrogen (N)	1	1.553	0.221	0.004	0.952	13.158	**<0.001**	0.310	0.580	2.332	0.138	0.381	0.539
S×D	3	6.982	**<0.001**	17.820	**<0.001**	9.902	**<0.001**	1.474	0.231	0.141	0.935	1.151	0.334
S×N	1	0.211	0.649	0.004	0.952	8.300	**<0.05**	0.972	0.328	0.569	0.457	0.112	0.739
D×N	3	0.781	0.513	9.317	**<0.001**	19.339	**<0.001**	0.381	0.767	0.561	0.645	1.759	0.162
S×D×N	3	0.047	0.986	11.456	**<0.001**	6.825	**<0.001**	1.006	0.397	0.290	0.833	0.720	0.543

Numbers of degrees of freedom (df), F- and p-values are given.
Bold text indicates a statistically significant difference with a p-value < 0.05.

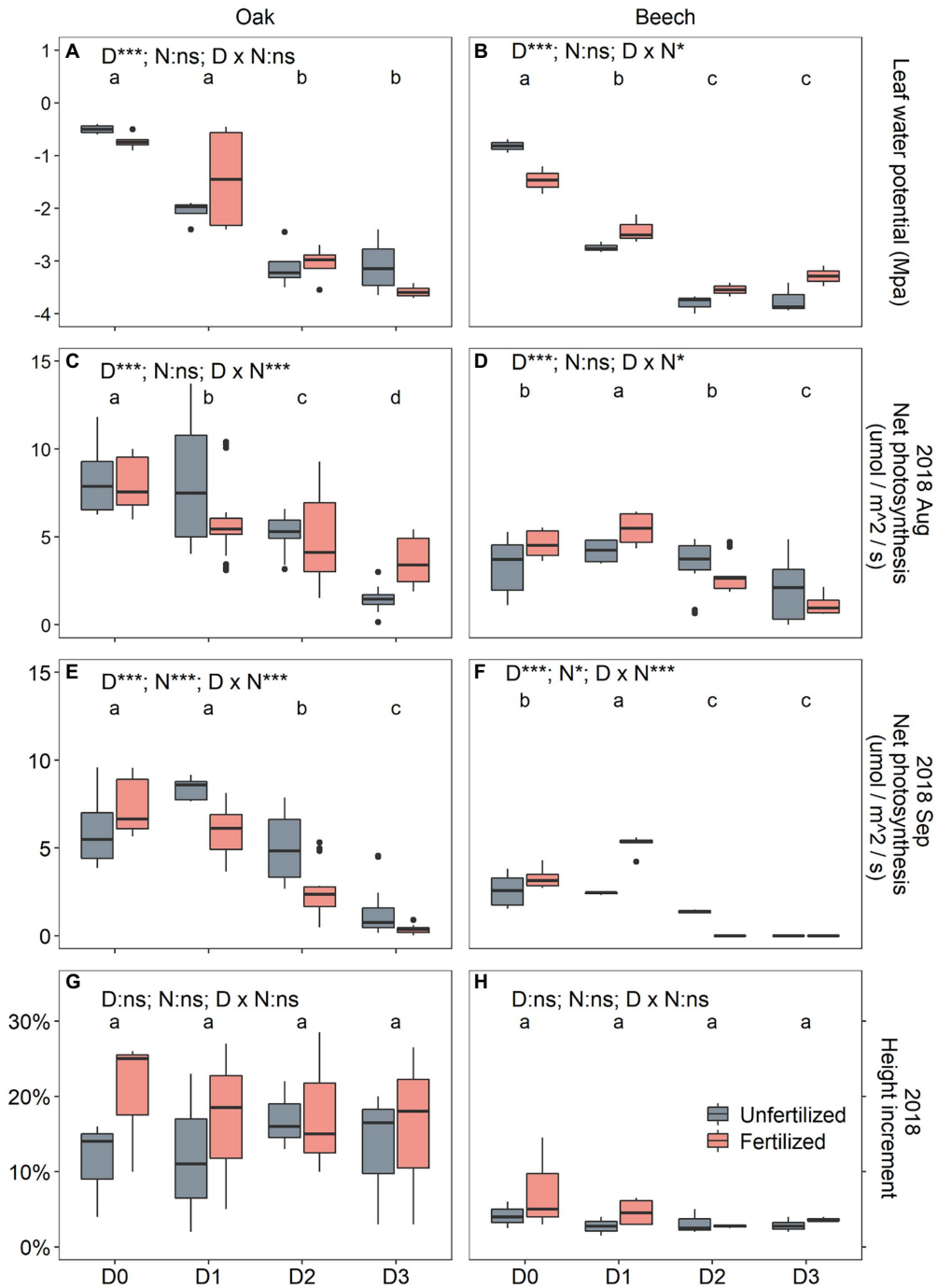

FIGURE 2 | Midday water potential (ψ_{leaf}) after 2 months of drought treatment on 5 August 2018 **(A,B)**, leaf net photosynthesis (A_{leaf}) after two (6 August 2018; **C,D**) and four (28 September 2018; **E,F**) months of drought duration treatment in 2018, and the relative height increment (RHI; **G,H**) between 30 May (initial) and 1 October 2018 (after 4 months of drought treatment) for oak (*Quercus petraea*) and beech (*Fagus sylvatica*) saplings. D0 (watering weekly), D1 (watering biweekly), D2 (watering monthly), and D3 (watering bimonthly) represent the drought duration. Different letter indicates significant difference in parameters among D0, D1, D2, and D3.

(**Figure 3A**), mainly caused by higher sugar concentration (**Supplementary Figure A4a**), but significantly lower shoot NSC (**Figure 3B**) mainly resulting from significantly lower starch levels (**Supplementary Figure A4e**). The root NSC of oak tended to decrease with increasing drought duration (**Figure 3C**), due to both decreasing sugar and starch levels (**Supplementary Figures A4c,f**). For beech, both leaf and root NSC levels did not change with drought (**Figures 3F,H**) but shoot NSC decreased with increasing

TABLE 2 | Results of linear mixed models with species (S), drought duration (D), nitrogen fertilization (N) as factors, for tissue NSC concentrations after the drought duration treatment in the growing season 2018 (pre-winter) and before the growing season 2019 (post-winter).

	df	Leaves		Shoots		Roots	
		F	***p***	***F***	***p***	***F***	***p***
October 2018 (Pre-winter)							
Species (S)	1	11.339	**<0.05**	0.003	0.958	6.207	**<0.05**
D-duration (D)	3	0.954	0.428	6.836	**<0.05**	2.768	**=0.05**
Nitrogen (N)	1	0.540	0.469	9.596	**<0.05**	0.276	0.603
S × D	3	1.864	0.158	0.228	0.876	1.100	0.365
S × N	1	1.932	0.175	16.091	**<0.001**	14.406	**<0.001**
D × N	3	0.156	0.925	0.303	0.823	2.002	0.136
S × D × N	3	0.869	0.468	0.076	0.973	0.495	0.689
April 2019 (Post-winter)							
Species (S)	1	(No leaves)		0.801	0.378	15.649	**<0.05**
D-duration (D)	3			12.511	**<0.001**	3.890	**<0.05**
Nitrogen (N)	1			0.627	0.435	0.227	0.637
S × D	3			1.122	0.356	2.451	0.083
S × N	1			5.977	**<0.05**	2.730	0.109
D × N	3			1.231	0.316	1.321	0.287
S × D × N	3			2.043	0.130	1.288	0.297

Numbers of degrees of freedom (df), F- and p-values are given.
Bold text indicates a statistically significant difference with a p-value < 0.05.

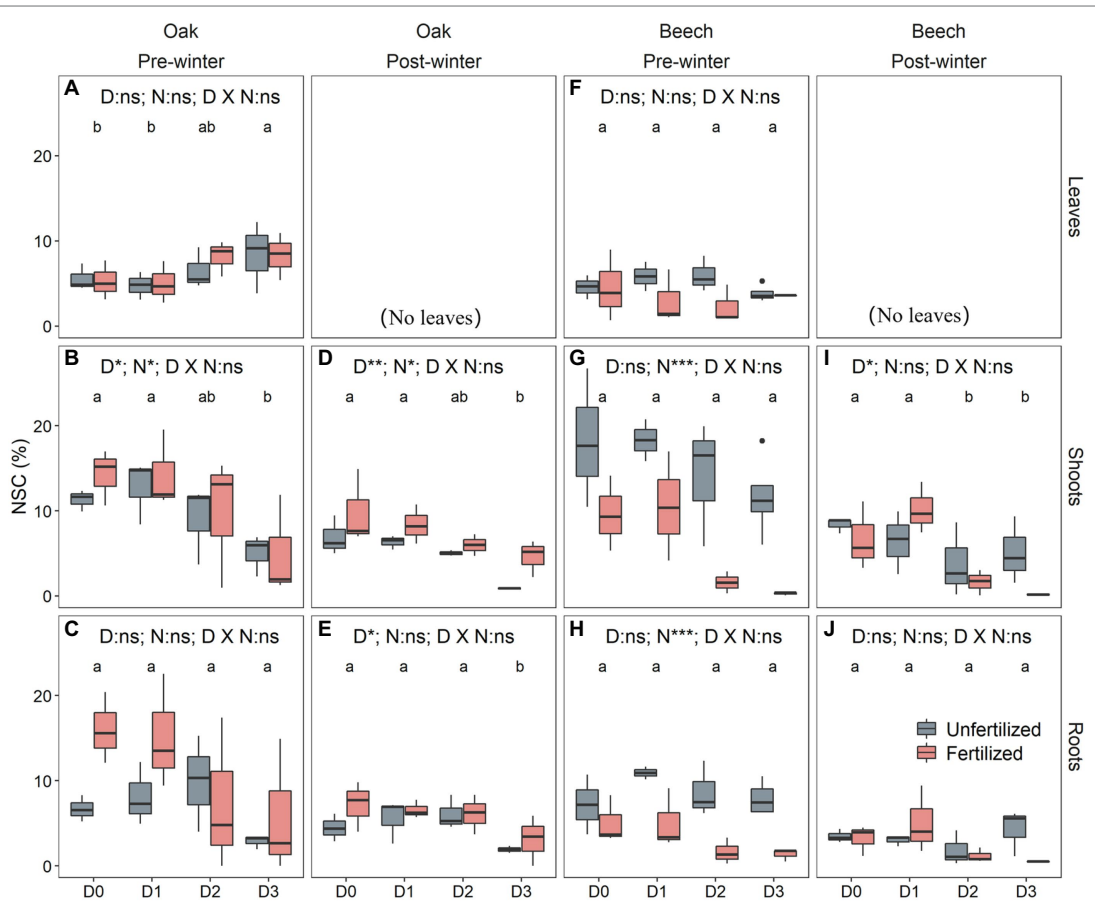

FIGURE 3 | Non-structural carbohydrate (NSC) concentrations in leaves **(A,F)**, shoots **(B,D,G,I)**, and roots **(C,E,H,J)** of oak (*Quercus petraea*) **(A–E)** and beech (*Fagus sylvatica*) **(F–J)** saplings after 4 months of drought duration treatment in 2018 (pre-winter) **(A–E,F–H)** and before the growing season 2019 (post-winter) **(D–E,I–J)**. D0 (watering weekly), D1 (watering biweekly), D2 (watering monthly), and D3 (watering bimonthly) represent the drought duration. Different letters indicate significant differences in parameters among D0, D1, D2, and D3.

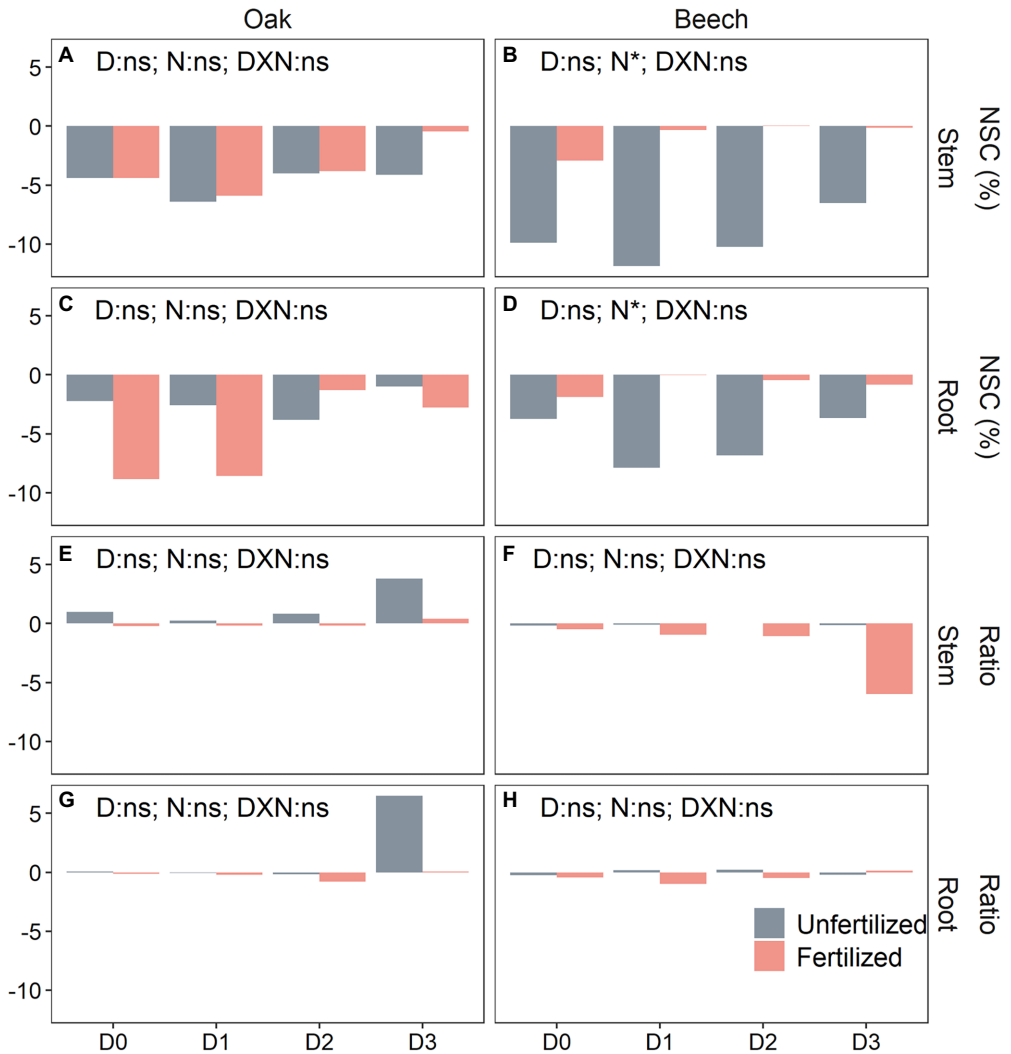

FIGURE 4 | Over-winter changes in non-structural carbohydrate (NSC) concentrations **(A–D)** (post-winter values minus pre-winter values) and the sugar/starch ratio **(E–H)** in stem **(A,B,E,F)** and root **(C,D,G,H)** of oak (*Quercus petraea*) and beech (*Fagus sylvatica*) saplings treated with four drought durations during the previous growing season. D0 (watering weekly), D1 (watering biweekly), D2 (watering monthly), and D3 (watering bimonthly) represent the drought duration.

drought duration (**Figure 3G**) caused by both decreased sugar (**Supplementary Figure A5b**) and starch (**Supplementary Figure A5l**). N-fertilization significantly increased the shoot NSC in oak (**Figure 3B**), whereas it significantly decreased NSC levels in shoots (**Figure 3G**) and roots (**Figure 3H**) of beech.

Post-winter NSC After Drought Duration Treatment Last Growing Season

The post-winter NSC levels in both shoots and roots were significantly affected by drought duration treatment in the previous growing season (**Table 2**). The post-winter root NSC was species-dependent ($p < 0.05$; **Table 2**), and species interacted with N-fertilization to influence the post-winter shoot NSC ($p < 0.05$; **Table 2**). There was no direct effect of N on NSC for both species (**Table 2**). Both shoots and roots of D3 oak had significantly lower post-winter NSC levels compared to the other drought treatments (**Figures 3D,E**), mainly caused by both lower sugar and starch levels for shoots (**Supplementary Figures A6a,c**) and by lower sugar levels for roots (**Supplementary Figure A6b**). In beech only shoots of D2 and D3, due to both lower sugar and starch levels (**Supplementary Figures A7a,c**), showed significantly lower post-winter NSC levels compared to the other drought treatments (**Figures 3I,J**). N-fertilization significantly increased shoot NSC in oak (**Figure 3D**) but it had no effects on shoot (**Figure 3I**) and root NSC (**Figure 3J**) in beech.

Changes in NSC Level Over-Winter

Only N-fertilization significantly affected the over-winter NSC consumption (post-winter level minus pre-winter level) in shoots but not in roots (**Supplementary Table A1**). Neither D nor N and their interactions changed the tissue NSC consumption in oak over-winter (**Figures 4A,C**), while N-fertilized beech

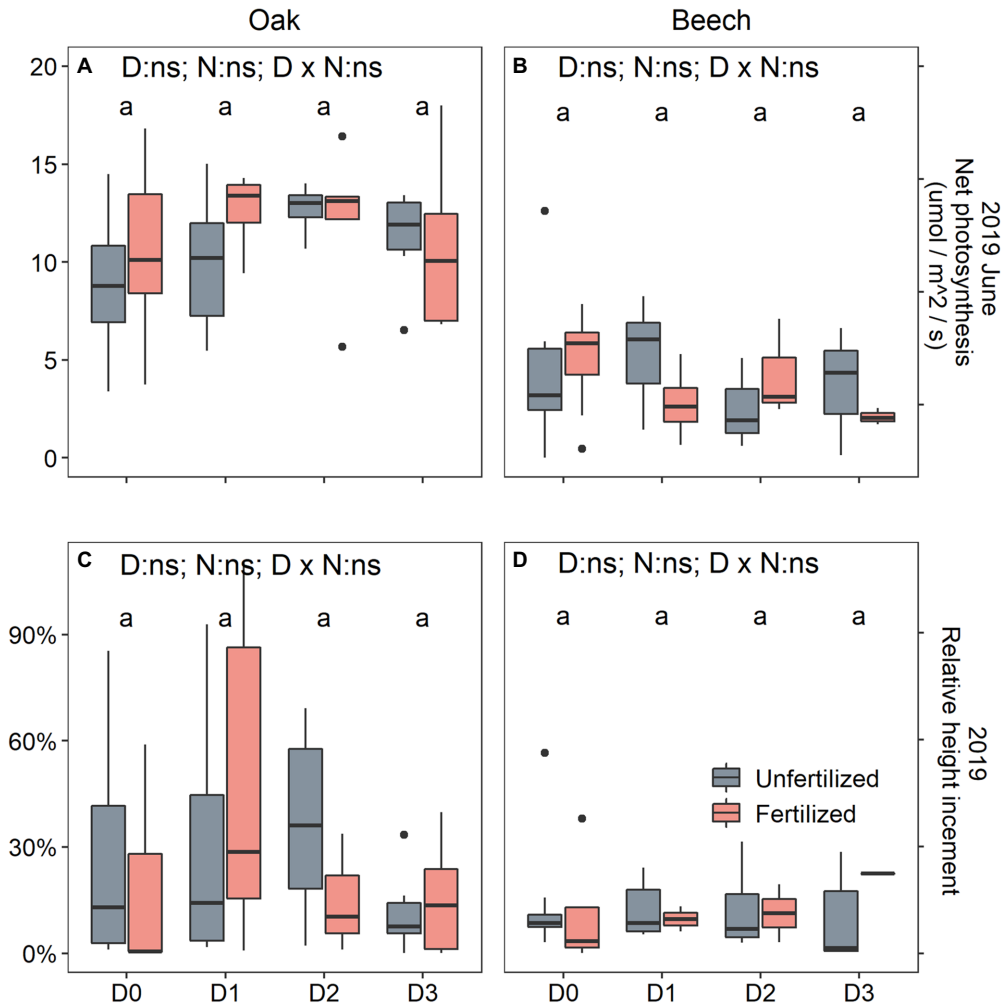

FIGURE 5 | Leaf net photosynthesis (A_{leaf}) **(A,B)** and relative height increment **(C,D)** of oak (*Quercus petraea*) **(A,C)** and beech (*Fagus sylvatica*) **(B,D)** saplings treated with four drought durations in 2018 and well-watered in 2019. D0 (watering weekly), D1 (watering biweekly), D2 (watering monthly), and D3 (watering bimonthly) represent the drought duration. Different letters indicate significant difference in parameters among D0, D1, D2, and D3.

significantly decreased the over-winter NSC consumption in both shoots and roots (**Figures 4B,D**). The changes in sugar/starch ratio were significantly influenced by both, species and N-fertilization (**Supplementary Table A1**). N-fertilization tended to decrease the sugar/starch ratio in beech, especially in shoots of D3 plants (**Figures 4F,H**), while the unfertilized oak saplings seemed to increase the tissue sugar/starch ratio over-winter, especially the D3 plants (**Figures 4E,G**).

Recovery Responses to Past Drought and Rewetting

After rewetting for one growing season, both the recovery photosynthesis measured on 10 June 2019 and recovery height growth measured on 8 October 2019 significantly responded to species only (**Table 1**), showing that both photosynthesis (**Figures 5A** vs. **4B**) and height growth (**Figures 5C** vs. **4D**) were greater in oak than in beech. Otherwise, previous season drought duration and N-fertilization treatment did not affect recovery responses of the two species (**Figure 5**).

After a recovery growing season that followed the drought duration treatment in combination with N-fertilization, the mortality of beech was higher than oak, and the mortality rate seemed to show a tendency to increase with drought duration for the two species (**Figure 6**). Especially, the N-fertilized beech saplings had much higher mortality rate within each drought duration treatment category (**Figure 6B**).

DISCUSSION

With increasing drought duration, tree mortality increased (**Figure 6**), leaf water potential and photosynthesis decreased for the two species (**Figure 2**), which is similar to those results found in drought intensity experiments with trees (Schönbeck et al., 2018; Lauder et al., 2019; Archambeau et al., 2020;

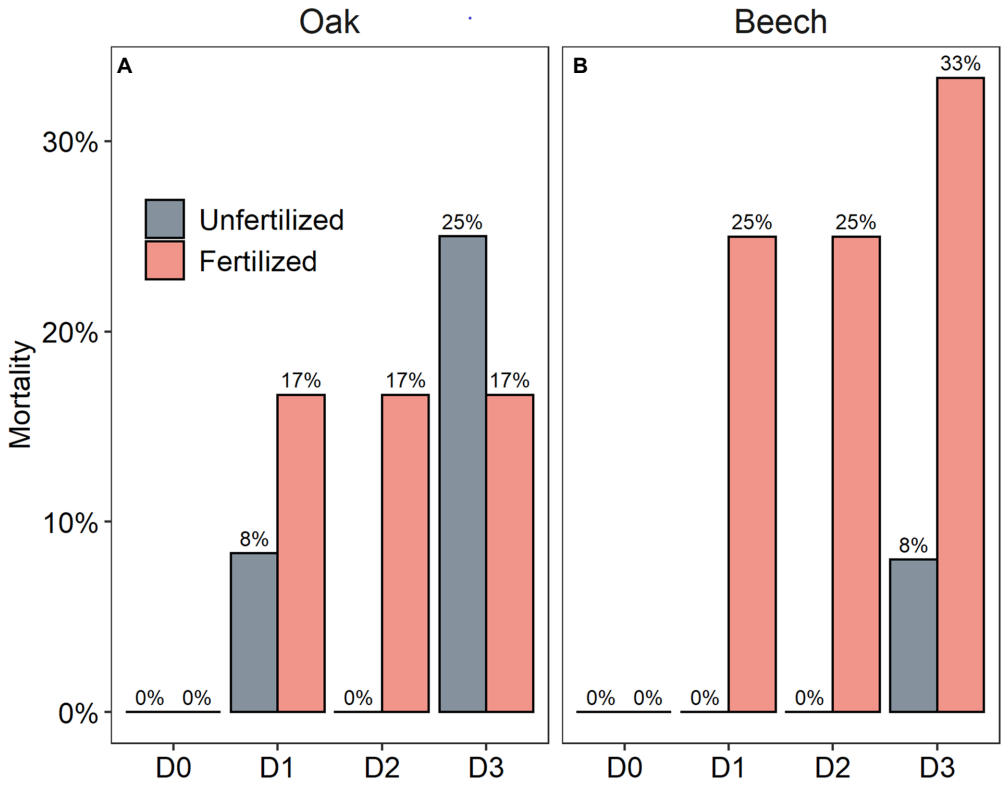

FIGURE 6 | Mortality rate of oak (*Quercus petraea*) **(A)** and beech (*Fagus sylvatica*) **(B)** saplings at the end of a recovery growing season following a growing season with four drought duration treatment (D0 = watering weekly, D1 = watering biweekly, D2 = watering monthly, and D3 = watering bimonthly) combined with N-fertilization (1.68 g N kg^{-1} dry soil fertilized vs. unfertilized).

Schönbeck et al., 2020a; Ouyang et al., 2021). For instance, extreme drought was found to significantly decrease predawn water potential and net photosynthetic rates and to increase the mortality for both *Pinus sylvestris* (Schönbeck et al., 2020a) and *Quercus pubescens* saplings (Ouyang et al., 2021). Drought, both severe drought intensity and long drought duration, decreases soil water availability and plant leaf water potential, and thus results in stomatal closure to prevent transpiration exceeding root water uptake capacity, which caused declined photosynthesis and CO_2 uptake (Li et al., 2020). Duan et al. (2019) found that severe drought intensity with short duration led to a stronger decrease in leaf water potential and photosynthesis of three tree species (*Syzygium rehderianum*, *Castanopsis chinensis*, and *Schima superba*) than moderate drought with longer duration. The water potential of *Robinia pseudoacacia* exhibited a linear decline with increasing drought duration, while *Quercus acutissima*'s water potential remained relatively stable during the first month of mild drought (Li et al., 2020), and thus, Li et al. (2020) concluded that the two tree species differ in their sensitivity to drought (Bhusal et al., 2021), which confirmed that *Quercus* species are anisohydric plants (Sade et al., 2012).

However, in spite of decreased photosynthesis (**Figures 2C–F**) and NSC levels (**Figures 3B,C,G,H**) with increasing drought duration, the relative tree height increment of the two species did not differ among the drought treatments in our study (**Figures 2G,H**). Li et al. (2013), Schönbeck et al. (2018, 2020a), and Ouyang et al. (2021) found that drought-stressed trees maintained relatively stable NSC levels at the expense of growth, implying an active process of NSC storage (Li et al., 2018a). For example, drought declined the growth but did not decrease tissue NSC level in *Quercus faginea* and *Pinus halepensis* (Sanz-Perez et al., 2009). The present study, however, seemed to support the view of Martinez-Vilalta et al. (2016) that NSC storage is mainly a passive process following the growth priority, because the growth did not vary with drought duration (**Figures 2G,H**) while the NSC levels in storage tissues, especially in shoots, decreased with increasing drought duration (**Figures 3B–E,G**). In this case, for example, the mortality (**Figure 6B**) of fertilized beech under D2 and D3 is thus mainly a result of carbon limitation that was confirmed by very low leaf photosynthetic rate (**Figures 2D,F**) and near-zero NSC level at the end season (**Figures 3G,H**). McDowell (2011) proposed that NSC concentrations can increase initially under drought due to the faster decline of growth than photosynthesis, but NSC concentrations may decline later on due to the prolonged suppression of photosynthesis and the utilization of stored C for meeting C demands especially under extreme drought.

Similar to results gained from most drought intensity experiments with trees (Li et al., 2013; Schönbeck et al., 2018,

2020a; Zhang et al., 2020; Ouyang et al., 2021), the present study found that the longer drought duration treatments (D2, D3) did not decrease the end-season leaf NSC (pre-winter) levels (**Figures 3A,F**), although the D2 and D3 treatment significantly decreased leaf photosynthesis of the two species (**Figures 2C–F**). This might be explained by the osmoregulation strategy of plants suffering from drought stress on the one hand (O'Brien et al., 2014; Dickman et al., 2015), and on the other hand, it may be a result of basipetal carbon translocation failure (Rowland et al., 2015), if the phloem function becomes impaired and carbon translocation gets limited or stopped by hydraulic failure caused by severe or long drought stress (Griffin-Nolan et al., 2021). In this case, lower NSC levels in the sink tissues of shoots, and especially roots, and thus carbon limitation may be expected. Recently, this expectation has been repeatedly confirmed in severe drought-stressed trees in controlled drought intensity experiment (e.g., Schönbeck et al., 2020a; Ouyang et al., 2021), and also in trees under longer drought duration (D2, D3) treatment in the present study (**Figures 3B,C,G,H**). Therefore, it may be speculated that a hydraulic failure induced carbon limitation seems to be the physiological mechanism underlying the high mortality of beech saplings, particularly the N-fertilized D2 and D3 beech (**Figure 6B**) which had very low end-season shoot and root NSC levels close to zero (**Figures 3G,H**). These results also seem to exclude that limited sink activity, for example, in root tissues as a result of drought is responsible for reduced sugar transport from the leaves to the sink tissues as in that case increased NSC concentrations are to be expected in both, roots and shoots (Hagedorn et al., 2016; Gessler and Grossiord, 2019).

We found that the responses of end-season NSC level to drought duration seemed to be both species- and tissue type-dependent (**Figures 3A,B,F–H**). For instance, leaf NSC increased (**Figure 3A**) but shoot NSC decreased (**Figure 3B**) in oak with increased drought duration, while they did not change in beech (**Figures 3F,G**). Similar to beech, root NSC reserve of aspen (*Populus tremuloides*) seedlings did not change over a 3-month period of severe drought (Galvez et al., 2011). However, moderate drought was found to increase NSC in stems and roots of *Q. pubescens* saplings (Ouyang et al., 2021). Experiments with more vs. less precipitation found that extreme drought (no irrigation for two consecutive years) reduced shoot and root NSC, whereas intermediate drought levels did not affect shoot and root NSC for *P. sylvestris* saplings (Schönbeck et al., 2020a).

Less is known about winter NSC consumption of trees previously exposed to drought of various intensities or duration. Trees, as exemplified by the deciduous species in the present study, consume NSC storage for maintenance respiration over-winter (Sperling et al., 2015). Therefore, we found that the post-winter NSC levels were lower than the pre-winter level in each tissue for both species (**Figures 3B** vs. **3D**; **Figures 3C** vs. **3E**; **Figures 3G** vs. **3I**; **Figures 3H** vs. **3J**). The winter temperature was beyond 5°C in the greenhouse of the present study (**Supplementary Figure A1**), but even near-freezing winter temperatures were found to significantly increase stem respiration by 10–170% in 13 out of 15 species studied in the western US, according to Sperling et al. (2015). Sperling et al. (2015) further calculated that "frost-induced respiration accelerated stem NSC consumption by 8.4 mg (glucose eq.) cm^{-3} $year^{-1}$ on average (cm^{-3} stem wood basis) in the western US, a level of depletion that may continue to significantly affect spring NSC availability." This is agreement with findings that in temperate deciduous trees, tissue NSC concentrations decline during winter dormancy. This decrease is more pronounced in stem than in roots as observed for aspen (*Populus grandidentata*) and oak (*Quercus rubra*; Gough et al., 2010). The present study, for the first time, indicated that the over-winter NSC consumption was not affected by drought duration for the two species but it was significantly decreased by N-fertilization for beech across the four drought treatments (**Supplementary Table A1**; **Figures 4A–D**). This result may indicate on the one hand a common response of winter NSC consumption of tree species that is independent on the previously imposed drought duration. On the other hand, our results suggest a species-specific sensitivity of winter NSC consumption to other environmental change, such as nutrient availability. We can only speculate why the NSC consumption was lower in fertilized beech but it is known that free amino acids and soluble proteins can increase stress resistance of beech (Stajner et al., 2013). Thus, an increased N availability might reduce stress-induced respiration in this species under winter temperature conditions (**Supplementary Figure A1**).

The over-winter changes (post-winter vs. pre-winter) in the sugar/starch ratio (**Figures 4E–H**) indicated that starch to sugar conversion occurred in oak saplings (**Figures 4E,G**; **Supplementary Figures A4, A6**), whereas a strong sugar consumption and depletion were the main reasons for decreased tissue sugar/starch ratio in beech saplings (**Figures 4F–H**; **Supplementary Figures A5, A7**). Similarly, starch concentrations were reduced and soluble sugars increased in *Prunus dulcis* during winter, and the NSC concentration were only slight reduced (Sperling et al., 2019). In winter, increased sugar concentrations in the xylem are important to avoid or reduce the number of freeze–thaw embolization cycles, because sugars increase the osmotic potential of xylem and thus lowering its freezing point (Sauter et al., 1973; Thierry et al., 2004; Li et al., 2018b).

Previous season drought duration treatment did not affect photosynthesis of the two species after rewetting in the next year (**Table 1**). The decreased photosynthesis determined in the longer duration drought treatments in 2018 (**Figures 2C–F**) recovered and all treatments showed the same level of photosynthesis in June 2019 (**Figures 5A,B**). This recovery indicates that there is no legacy of previous drought duration on photosynthetic carbon assimilation. Previous studies found that drought stress can result in incomplete and lagged growth recovery (Anderegg et al., 2013; Pederson et al., 2014; Huang et al., 2018). Extreme drought caused drought legacy response with reduced growth for deep−rooted forests for up to 4 years (Wu et al., 2018), and negative drought legacy was found to last about 1 year for different plant functional types in Tibetan Plateau (Li et al., 2020). However, fast recovery of carbon acquisition and allocation to different plant organs

after drought release was also observed in different tree species (Hagedorn et al., 2016; Joseph et al., 2020). In the present study, small saplings with large plasticity may be one reason for the quick recovery after rewetting, leading to a lack of legacy of past drought. Similar results have been observed in poplar (*Populus tremula*) saplings under water-deficit conditions (Lemaire et al., 2021). In addition, the longest drought duration (2 months) applied here may be still not long (or severe) enough to impair the physiological processes in the longer term. For example, an open top chamber experiment with 40 cm soil depth but without any watering for 2 years resulted only in a mortality rate of 60% for *P. sylvestris* (Schönbeck et al., 2020a) and 50% for *Q. pubescens* saplings (Ouyang et al., 2021). In line with the findings of Schönbeck et al. (2020a) for pine, we found a fertilization-induced higher mortality rate for beech but not for oak saplings (**Figure 6**). Ouyang et al. (2021) showed a lower mortality rate (32%) in fertilized compared to non-fertilized (50%) *Q. pubescens* saplings under extreme drought. In oak species, fertilization might thus not enhance drought effects but genus and species-specific mechanism still need to be elucidated.

The height growth of the two species was not correlated with shoot NSC storage but significantly positively correlated with both pre-winter ($p = 0.07$) and post-winter ($p = 0.01$) root storage (**Supplementary Figure A8**). The small values of R^2 (**Supplementary Figure A8**) suggest that root NSC is not the only or the most important factor determining the recovery growth. However, this result (**Supplementary Figure A8**) in conjunction with low photosynthetic rate (**Figures 2C–F**), low pre- and post-winter NSC levels in both shoots and roots of D2 and D3 saplings suggests a sink carbon limitation that determines the high mortality rate of D2 and D3 saplings for the two species, particularly for beech (**Figure 6**). This result supports a recent hypothesis that the climatic alpine treeline is determined by a winter root carbon limitation proposed by Li et al. (2018a). Our result is also supported by data for *P. sylvestris* (Schönbeck et al., 2020a) and *Q. pubescens* saplings (Ouyang et al., 2021) under extreme drought that also showed low root NSC. Indeed, root carbon shortage has been widely found in various tree and shrub species in stressed conditions recently (Shi et al., 2006; Li et al., 2008a,b; Genet et al., 2011; Zhu et al., 2012a,b; Ouyang et al., 2021; Wang et al., 2021).

Interactions between drought duration and N-fertilization were found only for gas exchange rate during the treatment period (**Table 1**), indicating that the effects of N-fertilization vary in direction (or magnitude) with drought duration only for photosynthesis but not on other parameters studied (**Table 2** and **Supplementary Table A1**). Schönbeck et al. (2020a) found that a mitigating effect of N-fertilization on the negative drought effects on *P. sylvestris* saplings occurred only when the drought stress was relatively mild. On the other hand, the effects of fertilization on drought may also be dependent upon the initial soil fertility, and a mitigating effect of fertilization on drought may not be expected in nutrient-rich soils (Kleczewski et al., 2010). For example, the soil used in the present study had a total soil N content of 0.82% with 39 mg N kg^{-1} soil for NH_4^+-N and 573 mg N kg^{-1}soil for NO_3^--N, which, probably, led to a non-significant effect of fertilization. In a summer drought experiment (no rainfall for two summer months during two consecutive years) it was found that the negative effects of drought on beech growth were amplified by N-fertilization (Dziedek et al., 2016), which is similar to our results that drought-induced mortality of beech was amplified by N-fertilization (**Figure 6B**). Theoretically, increases in N availability may promote the formation of xylem structures that transport water more efficiently in humid conditions (Borghetti et al., 2017) but may also easily lead to xylem embolism—due to larger cross section and bigger tracheids or vessels—in dry conditions, and therefore, further studies are needed to clarify the N-fertilization effects (e.g., addition rate and amount and frequency) in relation to drought intensity or duration not only on seedlings and saplings but also adult trees.

CONCLUSION

In line with our hypothesis 1, we found that longer drought duration decreased the physiological performance (e.g., leaf water potential, photosynthetic capacity, and NSC levels) but not the growth rate. This result suggest that growth is a higher priority than resource storage for the saplings of the two species stressed by long-lasting drought below a certain threshold, as recently proposed by Song et al. (2022). Previous growing season drought seems to not affect the tissue NSC consumption over-winter, and the post-winter root NSC level plays a more important role in determining the growth and survival for both species (see our hypothesis 2 in introduction), suggesting a root carbon limitation in severe drought-stressed saplings, particularly for beech. In line with recent findings (Schönbeck et al., 2018, 2020a; Ouyang et al., 2021), N-fertilization did not play a role to mitigating the negative drought effects on saplings of the two species (hypothesis 3). Compared to oak, beech had lower levels of physiological parameters and growth but showed higher winter NSC consumption and especially higher mortality rate with increasing drought duration in combination with fertilization, indicating that beech is more sensitive to drought and N deposition (hypothesis 4). The present study, in a physiological perspective, experimentally confirmed the view of Ellenberg (2009) that the European beech, compared to oak, may be more strongly affected by future environmental changes.

DATA AVAILABILITY STATEMENT

The raw data supporting the conclusions of this article will be made available by the authors, without undue reservation.

AUTHOR CONTRIBUTIONS

M-HL designed the experiment. SO conducted the experiment and collected the samples. RN and XW conducted the data

analysis. YY wrote the first draft of the manuscript. AG, HH, ZW, and M-HL put forward some constructive suggestions for the manuscript. All authors contributed to the article and approved the submitted version.

FUNDING

This study was supported by the Swiss National Fund (31003A_157126/1) and China Scholarship Council (CSC) (201906620095). Open access funding provided by WSL - Swiss Federal Institute for Forest, Snow and Landscape Research.

SUPPLEMENTARY MATERIAL

The Supplementary Material for this article can be found online at: https://www.frontiersin.org/articles/10.3389/fpls.2022.929855/full#supplementary-material

REFERENCES

Adams, H. D., Zeppel, M. J. B., Anderegg, W. R. L., Hartmann, H., Landhausser, S. M., Tissue, D. T., et al. (2017). A multi-species synthesis of physiological mechanisms in drought-induced tree mortality. *Nat. Ecol. Evol.* 1, 1285–1291. doi: 10.1038/s41559-017-0248-x

Allen, C. D., Macalady, A. K., Chenchouni, H., Bachelet, D., McDowell, N., Vennetier, M., et al. (2010). A global overview of drought and heat-induced tree mortality reveals emerging climate change risks for forests. *For. Ecol. Manag.* 259, 660–684. doi: 10.1016/j.foreco.2009.09.001

Anderegg, W. R. L., Plavcova, L., Anderegg, L. D. L., Hacke, U. G., Berry, J. A., and Field, C. B. (2013). Drought's legacy: multiyear hydraulic deterioration underlies widespread aspen forest die-off and portends increased future risk. *Glob. Chang. Biol.* 19, 1188–1196. doi: 10.1111/gcb.12100

Archambeau, J., Ruiz-Benito, P., Ratcliffe, S., Frejaville, T., Changenet, A., Castaneda, J. M. M., et al. (2020). Similar patterns of background mortality across Europe are mostly driven by drought in European beech and a combination of drought and competition in scots pine. *Agric. For. Meteorol.* 280:107772. doi: 10.1016/j.agrformet.2019.107772

Bhusal, N., Lee, M., Lee, H., Adhikari, A., Han, A. R., Han, A., et al. (2021). Evaluation of morphological, physiological, and biochemical traits for assessing drought resistance in eleven tree species. *Sci. Total Environ.* 779:146466. doi: 10.1016/j.scitotenv.2021.146466

Bond, B. J., Farnsworth, B. T., Coulombe, R. A., and Winner, W. E. (1999). Foliage physiology and biochemistry in response to light gradients in conifers with varying shade tolerance. *Oecologia* 120, 183–192. doi: 10.1007/s004420050847

Borghetti, M., Gentilesca, T., Leonardi, S., van Noije, T., Rita, A., and Mencuccini, M. (2017). Long-term temporal relationships between environmental conditions and xylem functional traits: a meta-analysis across a range of woody species along climatic and nitrogen deposition gradients. *Tree Physiol.* 37, 4–17. doi: 10.1093/treephys/tpw087

Brunner, M. I., Liechti, K., and Zappa, M. (2019). Extremeness of recent drought events in Switzerland: dependence on variable and return period choice. *Nat. Hazards Earth Syst. Sci.* 19, 2311–2323. doi: 10.5194/nhess-19-2311-2019

Buitink, J., van Hateren, T. C., and Teuling, A. J. (2021). Hydrological system complexity induces a drought frequency paradox. *Front. Water* 3:640976. doi: 10.3389/frwa.2021.640976

Dickman, L. T., McDowell, N. G., Sevanto, S., Pangle, R. E., and Pockman, W. T. (2015). Carbohydrate dynamics and mortality in a piñon-juniper woodland under three future precipitation scenarios. *Plant Cell Environ.* 38, 729–739. doi: 10.1111/pce.12441

Duan, H., Li, Y., Xu, Y., Zhou, S., Liu, J., Tissue, D. T., et al. (2019). Contrasting drought sensitivity and post-drought resilience among three co-occurring tree species in subtropical China. *Agric. For. Meteorol.* 272, 55–68.

Dziedek, C., Härdtle, W., von Oheimb, G., and Fichtner, A. (2016). Nitrogen addition enhances drought sensitivity of young deciduous tree species. *Front. Plant Sci.* 7:1100. doi: 10.3389/fpls.2016.01100

Ellenberg, H. H. (2009). *Vegetation Ecology of Central Europe. 4th Edn.* Cambridge University Press.

Galvez, D. A., Landhausser, S. M., and Tyree, M. T. (2011). Root carbon reserve dynamics in aspen seedlings: does simulated drought induce reserve limitation? *Tree Physiol.* 31, 250–257. doi: 10.1093/treephys/tpr012

Genet, M., Li, M., Luo, T., Fourcaud, T., Clément-Vidal, A., and Stokes, A. (2011). Linking carbon supply to root cell-wall chemistry and mechanics at high altitudes in *Abies georgei*. *Ann. Bot.* 107, 311–320. doi: 10.1093/aob/mcq237

Gessler, A., Bottero, A., Marshall, J., and Arend, M. (2020). The way back: recovery of trees from drought and its implication for acclimation. *New Phytol.* 228, 1704–1709. doi: 10.1111/nph.16703

Gessler, A., Cailleret, M., Joseph, J., Schönbeck, L., Schaub, M., Lehmann, M., et al. (2018). Drought induced tree mortality–a tree-ring isotope based conceptual model to assess mechanisms and predispositions. *New Phytol.* 219, 485–490. doi: 10.1111/nph.15154

Gessler, A., and Grossiord, C. (2019). Coordinating supply and demand: plant carbon allocation strategy ensuring survival in the long run. *New Phytol.* 222, 5–7. doi: 10.1111/nph.15583

Gessler, A., Schaub, M., and McDowell, N. G. (2017). The role of nutrients in drought-induced tree mortality and recovery. *New Phytol.* 214, 513–520. doi: 10.1111/nph.14340

Ghashghaie, J., and Saugier, B. (1989). Effects of nitrogen deficiency on leaf photosynthetic response of tall fescue to water deficit. *Plant Cell Environ.* 12, 261–271. doi: 10.1111/j.1365-3040.1989.tb01940.x

Gough, C. M., Flower, C. E., Vogel, C. S., and Curtis, P. S. (2010). Phenological and temperature controls on the temporal non-structural carbohydrate dynamics of *Populus grandidentata* and *Quercus rubra*. *Forests* 1, 65–81. doi: 10.3390/f1010065

Griffin-Nolan, R. J., Mohanbabu, N., Araldi-Brondolo, S., Ebert, A. R., LeVonne, J., Lumbsden-Pinto, J. I., et al. (2021). Friend or foe? The role of biotic agents in drought-induced plant mortality. *Plant Ecol.* 222, 537–548. doi: 10.1007/s11258-021-01126-4

Hagedorn, F., Joseph, J., Peter, M., Luster, J., Pritsch, K., Geppert, U., et al. (2016). Recovery of trees from drought depends on belowground sink control. *Nat. Plants* 2:16111. doi: 10.1038/nplants.2016.111

Hanel, M., Rakovec, O., Markonis, Y., Máca, P., Samaniego, L., Kyselý, J., et al. (2018). Revisiting the recent European droughts from a long-term perspective. *Sci. Rep.* 8:9499. doi: 10.1038/s41598-018-27464-4

Hartmann, H., Moura, C. F., Anderegg, W. R., Ruehr, N. K., Salmon, Y., Allen, C. D., et al. (2018). Research frontiers for improving our understanding of drought-induced tree and forest mortality. *New Phytol.* 218, 15–28. doi: 10.1111/nph.15048

Hartmann, H., and Trumbore, S. (2016). Understanding the roles of nonstructural carbohydrates in forest trees–from what we can measure to what we want to know. *New Phytol.* 211, 386–403. doi: 10.1111/nph.13955

Hoch, G., Popp, M., and Körner, C. (2002). Altitudinal increase of mobile carbon pools in *Pinus cembra* suggests sink limitation of growth at the Swiss treeline. *Oikos* 98, 361–374. doi: 10.1034/j.1600-0706.2002.980301.x

Huang, M. T., Wang, X. H., Keenan, T. F., and Piao, S. L. (2018). Drought timing influences the legacy of tree growth recovery. *Glob. Chang. Biol.* 24, 3546–3559. doi: 10.1111/gcb.14294

IPCC (2013). *Climate Change 2013: The Physical Science Basis. Contribution of Working Group I to the Fifth Assessment Report of the Intergovernmental Panel on Climate Change*. Cambridge, UK: Cambridge University Press.

Jacobs, D. F., Rose, R., Haase, D. L., and Alzugaray, P. O. (2004). Fertilization at planting impairs root system development and drought avoidance of Douglas-fir (*Pseudotsuga menziesii*) seedlings. *Ann. For. Sci.* 61, 643–651. doi: 10.1051/forest:2004065

Joseph, J., Gao, D. C., Backes, B., Bloch, C., Brunner, I., Gleixner, G., et al. (2020). Rhizosphere activity in an old-growth forest reacts rapidly to changes in soil moisture and shapes whole-tree carbon allocation. *Proc. Natl. Acad. Sci. U. S. A.* 117, 24885–24892. doi: 10.1073/pnas.2014084117

Kannenberg, S. A., Novick, K. A., and Phillips, R. P. (2018). Coarse roots prevent declines in whole-tree non-structural carbohydrate pools during drought in an isohydric and an anisohydric species. *Tree Physiol.* 38, 582–590. doi: 10.1093/treephys/tpx119

Kleczewski, N. M., Herms, D. A., and Bonello, P. (2010). Effects of soil type, fertilization and drought on carbon allocation to root growth and partitioning between secondary metabolism and ectomycorrhizae of *Betula papyrifera*. *Tree Physiol.* 30, 807–817. doi: 10.1093/treephys/tpq032

Kreuzwieser, J., and Gessler, A. (2010). Global climate change and tree nutrition: influence of water availability. *Tree Physiol.* 30, 1221–1234. doi: 10.1093/treephys/tpq055

Lauder, J. D., Moran, E. V., and Hart, S. C. (2019). Fight or flight? Potential tradeoffs between drought defense and reproduction in conifers. *Tree Physiol.* 39, 1071–1085. doi: 10.1093/treephys/tpz031

Lemaire, C., Blackman, C. J., Cochard, H., Menezes-Silva, P. E., Torres-Ruiz, J. M., and Herbette, S. (2021). Acclimation of hydraulic and morphological traits to water deficit delays hydraulic failure during simulated drought in poplar. *Tree Physiol.* 41, 2008–2021. doi: 10.1093/treephys/tpab086

Li, M.-H., Cherubini, P., Dobbertin, M., Arend, M., Xiao, W.-F., and Rigling, A. (2013). Responses of leaf nitrogen and mobile carbohydrates in different Quercus species/provenances to moderate climate changes. *Plant Biol.* 15, 177–184. doi: 10.1111/j.1438-8677.2012.00579.x

Li, W., Hartmann, H., Adams, H. D., Zhang, H., Jin, C., Zhao, C., et al. (2018b). The sweet side of global change–dynamic responses of non-structural carbohydrates to drought, elevated CO_2 and nitrogen fertilization in tree species. *Tree Physiol.* 38, 1706–1723. doi: 10.1093/treephys/tpy059

Li, M.-H., Hoch, G., and Körner, C. (2002). Source/sink removal affects mobile carbohydrates in *Pinus cembra* at the Swiss treeline. *Trees* 16, 331–337. doi: 10.1007/s00468-002-0172-8

Li, M.-H., Jiang, Y., Wang, A., Li, X., Zhu, W., Yan, C.-F., et al. (2018a). Active summer carbon storage for winter persistence in trees at the cold alpine treeline. *Tree Physiol.* 38, 1345–1355. doi: 10.1093/treephys/tpy020

Li, M.-H., Xiao, W.-F., Shi, P.-L., Wang, S.-G., Zhong, Y.-D., Liu, X.-L., et al. (2008a). Nitrogen and carbon source–sink relationships in trees at the Himalayan treelines compared with lower elevations. *Plant Cell Environ.* 31, 1377–1387. doi: 10.1111/j.1365-3040.2008.01848.x

Li, M.-H., Xiao, W.-F., Wang, S.-G., Cheng, G.-W., Cherubini, P., Cai, X.-H., et al. (2008b). Mobile carbohydrates in Himalayan treeline trees I. Evidence for carbon gain limitation but not for growth limitation. *Tree Physiol.* 28, 1287–1296. doi: 10.1093/treephys/28.8.1287

Li, P. L., Zhu, D., Wang, Y. L., and Liu, D. (2020). Elevation dependence of drought legacy effects on vegetation greenness over the Tibetan plateau. *Agric. For. Meteorol.* 295:108190. doi: 10.1016/j.agrformet.2020.108190

Martinez-Vilalta, J., Sala, A., Asensio, D., Galiano, L., Hoch, G., Palacio, S., et al. (2016). Dynamics of non-structural carbohydrates in terrestrial plants: a global synthesis. *Ecol. Monogr.* 86, 495–516.

McDowell, N. G. (2011). Mechanisms linking drought, hydraulics, carbon metabolism, and vegetation mortality. *Plant Physiol.* 155, 1051–1059. doi: 10.1104/pp.110.170704

McDowell, N. G., and Allen, C. D. (2015). Darcy's law predicts widespread forest mortality under climate warming. *Nat. Clim. Chang.* 5, 669–672. doi: 10.1038/nclimate2641

McDowell, N., Pockman, W. T., Allen, C. D., Breshears, D. D., Cobb, N., Kolb, T., et al. (2008). Mechanisms of plant survival and mortality during drought: why do some plants survive while others succumb to drought? *New Phytol.* 178, 719–739. doi: 10.1111/j.1469-8137.2008.02436.x

Meng, S., Zhang, C., Su, L., Li, Y., and Zhao, Z. (2016). Nitrogen uptake and metabolism of *Populus simonii* in response to PEG-induced drought stress. *Environ. Exp. Bot.* 123, 78–87. doi: 10.1016/j.envexpbot.2015.11.005

Nardini, A., Battistuzzo, M., and Savi, T. (2013). Shoot desiccation and hydraulic failure in temperate woody angiosperms during an extreme summer drought. *New Phytol.* 200, 322–329. doi: 10.1111/nph.12288

O'Brien, M. J., Leuzinger, S., Philipson, C. D., Tay, J., and Hector, A. (2014). Drought survival of tropical tree seedlings enhanced by non-structural carbohydrate levels. *Nat. Clim. Chang.* 4, 710–714. doi: 10.1038/nclimate2281

Ouyang, S.-N., Gessler, A., Saurer, M., Hagedorn, F., Gao, D.-C., Wang, X.-Y., et al. (2021). Root carbon and nutrient homeostasis determines downy oak sapling survival and recovery from drought. *Tree Physiol.* 41, 1400–1412. doi: 10.1093/treephys/tpab019

Pederson, N., Dyer, J. M., McEwan, R. W., Hessl, A. E., Mock, C. J., Orwig, D. A., et al. (2014). The legacy of episodic climatic events in shaping temperate, broadleaf forests. *Ecol. Monogr.* 84, 599–620. doi: 10.1890/13-1025.1

Radin, J. W., and Ackerson, R. C. (1981). Water relations of cotton plants under nitrogen deficiency: III. Stomatal conductance, photosynthesis, and abscisic acid accumulation during drought. *Plant Physiol.* 67, 115–119. doi: 10.1104/pp.67.1.115

Reinhardt, K., Germino, M. J., Kueppers, L. M., Domec, J.-C., and Mitton, J. (2015). Linking carbon and water relations to drought-induced mortality in *Pinus flexilis* seedlings. *Tree Physiol.* 35, 771–782. doi: 10.1093/treephys/tpv045

Rowland, L., da Costa, A. C. L., Galbraith, D. R., Oliveira, R., Binks, O. J., Oliveira, A., et al. (2015). Death from drought in tropical forests is triggered by hydraulics not carbon starvation. *Nature* 528, 119–122. doi: 10.1038/nature15539

Sade, N., Gebremedhin, A., and Moshelion, M. (2012). Risk-taking plants: anisohydric behavior as a stress-resistance trait. *Plant Signal. Behav.* 7, 767–770. doi: 10.4161/psb.20505

Sala, A., Woodruff, D. R., and Meinzer, F. C. (2012). Carbon dynamics in trees: feast or famine? *Tree Physiol.* 32, 764–775. doi: 10.1093/treephys/tpr143

Sanz-Perez, V., Castro-Diez, P., and Joffre, R. (2009). Seasonal carbon storage and growth in Mediterranean tree seedlings under different water conditions. *Tree Physiol.* 29, 1105–1116. doi: 10.1093/treephys/tpp045

Sauter, J. J., Iten, W., and Zimmermann, M. H. (1973). Studies on the release of sugar into the vessels of sugar maple (Acer saccharum). *Can. J. Bot.* 51, 1–8.

Schönbeck, L., Gessler, A., Hoch, G., McDowell, N. G., Rigling, A., Schaub, M., et al. (2018). Homeostatic levels of nonstructural carbohydrates after 13 yr of drought and irrigation in *Pinus sylvestris*. *New Phytol.* 219, 1314–1324. doi: 10.1111/nph.15224

Schönbeck, L., Gessler, A., Schaub, M., Rigling, A., Hoch, G., Kahmen, A., et al. (2020a). Soil nutrients and lowered source:sink ratio mitigate effects of mild but not of extreme drought in trees. *Environ. Exp. Bot.* 169:103905. doi: 10.1016/j.envexpbot.2019.103905

Schönbeck, L., Li, M.-H., Lehmann, M. M., Rigling, A., Schaub, M., Hoch, G., et al. (2020b). Soil nutrient availability alters tree carbon allocation dynamics during drought. *Tree Physiol.* 41, 697–707. doi: 10.1093/treephys/tpaa139

Sevanto, S. (2014). Phloem transport and drought. *J. Exp. Bot.* 65, 1751–1759. doi: 10.1093/jxb/ert467

Shi, P. L., Korner, C., and Hoch, G. (2006). End of season carbon supply status of woody species near the treeline in western China. *Basic Appl. Ecol.* 7, 370–377. doi: 10.1016/j.baae.2005.06.005

Song, L., Luo, W. T., Griffin-Nolan, R. J., Ma, W., Cai, J. P., Zuo, X. A., et al. (2022). Differential responses of grassland community nonstructural carbohydrate to experimental drought along a natural aridity gradient. *Sci. Total Environ.* 822:153589. doi: 10.1016/j.scitotenv.2022.153589

Sperling, O., Earles, J. M., Secchi, F., Godfrey, J., and Zwieniecki, M. A. (2015). Frost induces respiration and accelerates carbon depletion in trees. *PLoS One* 10:e0144124. doi: 10.1371/journal.pone.0144124

Sperling, O., Kamai, T., Tixier, A., Davidson, A., Jarvis-Shean, K., Raveh, E., et al. (2019). Predicting bloom dates by temperature mediated kinetics of carbohydrate metabolism in deciduous trees. *Agric. For. Meteorol.* 276–277:107643. doi: 10.1016/j.agrformet.2019.107643

Spinoni, J., Vogt, J. V., Naumann, G., Barbosa, P., and Dosio, A. (2018). Will drought events become more frequent and severe in Europe? *Int. J. Climatol.* 38, 1718–1736. doi: 10.1002/joc.5291

Stajner, D., Orlovic, S., Popovic, B. M., Kebert, M., Stojnic, S., and Klasnja, B. (2013). Chemical parameters of oxidative stress adaptability in beech. *J. Chem.* 2013, 1–8. doi: 10.1155/2013/592695

Thierry, A., Mélanie, D., Georges, A., Vincent, V., Soulaiman, S., Jean-Louis, J., et al. (2004). Temperature effects on xylem sap osmolarity in walnut trees: evidence for a vitalistic model of winter embolism repair. *Tree Physiol.* 24, 785–793.

Wang, X., Yu, F.-H., Jiang, Y., and Li, M.-H. (2021). Carbon and nutrient physiology in shrubs at the upper limits: a multispecies study. *J. Plant Ecol.* 14, 301–309. doi: 10.1093/jpe/rtaa097

Wiley, E., and Helliker, B. (2012). A re-evaluation of carbon storage in trees lends greater support for carbon limitation to growth. *New Phytol.* 195, 285–289. doi: 10.1111/j.1469-8137.2012.04180.x

Wong, S. C. (1990). Elevated atmospheric partial pressure of C02 and plant growth. *Photosynth. Res.* 23, 171–180. doi: 10.1007/BF00035008

Wu, X. C., Liu, H. Y., Li, X. Y., Ciais, P., Babst, F., Guo, W. C., et al. (2018). Differentiating drought legacy effects on vegetation growth over the temperate northern hemisphere. *Glob. Chang. Biol.* 24, 504–516. doi: 10.1111/gcb.13920

Yu, L. Y., Zhao, X. N., Gao, X. D., Jia, R. H., Yang, M. H., Yang, X. L., et al. (2021). Effect of natural factors and management practices on agricultural water use efficiency under drought: a meta-analysis of global drylands. *J. Hydrol.* 594:125977. doi: 10.1016/j.jhydrol.2021.125977

Zhang, P., Zhou, X., Fu, Y., Shao, J., Zhou, L., Li, S., et al. (2020). Differential effects of drought on nonstructural carbohydrate storage in seedlings and mature trees of four species in a subtropical forest. *For. Ecol. Manag.* 469:118159. doi: 10.1016/j.foreco.2020.118159

Zhu, W.-Z., Cao, M., Wang, S.-G., Xiao, W.-F., and Li, M.-H. (2012a). Seasonal dynamics of mobile carbon supply in *Quercus aquifolioides* at the upper elevational limit. *PLoS One* 7:e34213. doi: 10.1371/journal.pone.0034213

Zhu, W.-Z., Xiang, J.-S., Wang, S.-G., and Li, M.-H. (2012b). Resprouting ability and mobile carbohydrate reserves in an oak shrubland decline with increasing elevation on the eastern edge of the Qinghai–Tibet plateau. *For. Ecol. Manag.* 278, 118–126. doi: 10.1016/j.foreco.2012.04.032

Conflict of Interest: The authors declare that the research was conducted in the absence of any commercial or financial relationships that could be construed as a potential conflict of interest.

Publisher's Note: All claims expressed in this article are solely those of the authors and do not necessarily represent those of their affiliated organizations, or those of the publisher, the editors and the reviewers. Any product that may be evaluated in this article, or claim that may be made by its manufacturer, is not guaranteed or endorsed by the publisher.

frontiers | Frontiers in Plant Science

ORIGINAL RESEARCH
published: 11 July 2022
doi: 10.3389/fpls.2022.911447

Source Apportionment and Health Risk Assessment of Heavy Metals in Endemic Tree Species in Southern China: A Case Study of *Cinnamomum camphora* (L.) Presl

Ning Li[1], Yan Li[1,2], Shenglu Zhou[3], Huanchao Zhang[1] and Genmei Wang[1]*

[1] College of Forestry, Nanjing Forestry University, Nanjing, China, [2] Key Laboratory of Geographic Information Science of the Ministry of Education, School of Geographic Sciences, East China Normal University, Shanghai, China, [3] School of Geography and Ocean Science, Nanjing University, Nanjing, China

OPEN ACCESS

Edited by:
Song Heng Jin, Zhejiang Agriculture and Forestry University, China

Reviewed by:
Zhenyi Jia, Zhejiang Normal University, China
Qingbin Fan, Northwest Institute of Eco-Environment and Resources (CAS), China

***Correspondence:**
Yan Li
lyle@njfu.edu.cn

Specialty section:
This article was submitted to Functional Plant Ecology, a section of the journal Frontiers in Plant Science

Received: *02 April 2022*
Accepted: *15 June 2022*
Published: *11 July 2022*

Citation:
Li N, Li Y, Zhou S, Zhang H and Wang G (2022) Source Apportionment and Health Risk Assessment of Heavy Metals in Endemic Tree Species in Southern China: A Case Study of Cinnamomum camphora (L.) Presl. Front. Plant Sci. 13:911447. doi: 10.3389/fpls.2022.911447

As a developed economic region in China, the problem of heavy metals (HMs) pollution in the Yangtze River Delta has become increasingly prominent. As an important evergreen broad-leaved tree species in southern China, the camphor tree cannot only be used as a street tree but also its various tissues and organs can be used as raw materials for Chinese herbal medicine. In order to explore whether heavy metal contamination in the region threatens the safety of camphor trees as pharmaceutical raw materials, we collected the bark and leaves of the tree most commonly used for pharmaceuticals in Yixing City. Based on the determination of HMs content, the health risks after human intake are evaluated, the sources and contributions of HMs are analyzed, and then the health risks of pollution sources are spatially visualized. The results showed that under the influence of human activities, the camphor trees in the study area had obvious enrichment of HMs, and the over-standard rate of Pb in the bark was as high as 90%. The non-carcinogenic risks of bark and leaves are acceptable, but the carcinogenic risks are not acceptable. The bark had the highest average carcinogenic risk, approaching six times the threshold. The results of Pb isotope ratio analysis showed that the average contribution rate of industrial activities to HMs in camphor trees in the study area was the highest, reaching 49.70%, followed by fossil fuel burning (37.14%) and the contribution of natural sources was the smallest, only 13.16%. The locations of the high-risk areas caused by the three pollution sources in the study area are basically similar, mainly concentrated in the northwest, northeast, and southeast, which are consistent with the distribution of industries and resources in the study area. This study can provide a reference for the precise prevention of HMs pollution of camphor and the safe selection of its pharmaceutical materials.

Keywords: camphor tree, heavy metals, health risk, Pb isotope, source apportionment

INTRODUCTION

In recent years, with the rapid development of industrialization and urbanization, the accumulation of heavy metals (HMs) in the environment has been increasing, especially in developed economic regions (Yang S. H. et al., 2020). HMs are highly toxic, refractory, and persistent pollutants. They will enter the soil through various means such as atmospheric deposition, surface runoff, and sewage irrigation, then get absorbed by plants, and finally enter the human body through the food chain, thus threatening human health (Cui et al., 2022). At present, a large number of studies have paid attention to this problem, but most of these research objects are polluted soil, sediment, and atmospheric deposition (Men et al., 2020; Chen et al., 2021; Li et al., 2022). In addition, some researchers have conducted source analyses and health risk assessments of HMs in typical crops (Xiang et al., 2021; Zulkafflee et al., 2022). However, studies on HMs pollution of medicinal plants, especially medicinal higher woody plants, are relatively few.

The camphor tree is a subtropical evergreen species that has been cultivated in southern China for more than 1,500 years (Chen et al., 2020). The canopy of this tree stretches and its branches and leaves are luxuriant, making it an excellent tree for the streets and soundproof forest belts. Camphor trees also have important medicinal values. Its bark, roots, stems, leaves, and fruits are all rich in terpenoids, which have important pharmaceutical and industrial applications (Guo et al., 2016; Jiang et al., 2016). For example, D-borneol, a key ingredient in many traditional Chinese herbal formulas, is documented in multiple editions of the Chinese Pharmacopeia (Huang et al., 2016; Chai et al., 2019; Chen et al., 2019), can be used to treat cardiovascular diseases, including stroke, coronary heart disease, and angina pectoris (Yang Z. et al., 2020), and the market demand is very large. However, as HMs pollution in cities becomes more and more serious, are camphor trees also affected? A study compared the HMs accumulation capacity of six plants frequently seen on both the sides of the road and found that the camphor tree had the highest HMs accumulation index (Zhai et al., 2016), which intensified people's concerns about the safety of camphor tree bark or leaves as medicinal raw materials. Therefore, it is necessary to carry out a health risk assessment and pollution source apportionment of HMs in camphor trees.

Yixing City is located in the southwest of Jiangsu Province, west of Taihu Lake, and in the center of the Shanghai–Nanjing–Hangzhou triangle. There are many factories, convenient transportation, and a dense population in this area. Therefore, economic development is good, but the problem of environmental pollution is becoming more and more prominent. Dingshu Town on the west bank of Taihu Lake is the concentrated distribution area of pottery factories in Yixing City. These factories produce a lot of HMs pollution during the production process (Li et al., 2018). The cadmium content of "Cadmium Red" and "Cadmium Yellow," the raw materials for producing ceramics, is as high as 40 g/kg (Lin et al., 2015). Dingshu Town and Hufu Town are the concentrated distribution areas of camphor trees. HMs pollution in these areas may pose a threat to camphor trees and human health. Therefore, Dingshu Town and Hufu Town in Yixing City were selected as the study areas of this study.

The objectives of this study are: (1) to evaluate the health risks of HMs exposure in camphor tree bark and leaves to humans, (2) to analyze the source and contribution rate of HMs pollution, (3) to quantify source health risks by combining source apportionment with health risk assessment, and (4) to conduct a spatial analysis of source health risks. Our research results will help to effectively identify the high-risk areas caused by different HMs pollution sources to camphor trees and provide a reference for the priority treatment of different HMs pollution sources.

MATERIALS AND METHODS

Sample Collection and Determination

The study area is located in Dingshu Town and Hufu Town, Yixing City, in the Yangtze River Delta, China. We set up 10 sampling sites to cover all the land use types in the study area (**Figure 1**). A mixture of bark and leaf samples from three camphor trees and the corresponding six soil samples from the surrounding areas were collected at each sampling site. The samples were brought back to the laboratory in time for drying and grinding, and 100 mg was weighed for digestion. Guaranteed reagents such as HNO_3 and $HClO_4$ were used to digest HMs by graphene electric hot plate heating method. HMs content was determined using an inductively coupled plasma mass spectrometry (ICP-MS) (PerkinElmer SCIEX, Elan 9000). Blank samples and parallel samples were used for quality control.

The Pb concentration of the sample was diluted to approximately 30 ng/ml and the ratios of $^{208}Pb/^{206}Pb$ and $^{206}Pb/^{207}Pb$ were determined using ICP-MS. The equipment was calibrated using standard reference material SRM981 [National Institute of Standards and Technology (NIST), Gaithersburg, MD, United States]. To ensure the precision and accuracy of the measurements, the NIST SRM981 was used for every two samples.

Human Health Risk Assessment

When humans ingest Chinese herbal medicines made from camphor bark or leaves, the HMs in them may pose health risks to humans. This study uses the human health risk assessment model recommended by the United States Environmental Protection Agency (USEPA) to characterize the non-carcinogenic and carcinogenic risks (USEPA, 2011). The model calculation formula is as follows:

$$\mathrm{ADI} = \frac{C_i \times IR \times EF \times ED}{BW \times AT}$$

where, ADI is the average daily exposure dose (mg/kg/day) of directly ingested HMs; C_i is the concentration of HMs i in Chinese herbal medicines with bark or leaves as raw materials (mg/kg); IR is the maximum daily intake of the Chinese herbal medicines rate (kg/d), is 0.015 kg/d (Shandong Province Standard (SPS), 2012); EF is exposure frequency (d/a); ED is exposure duration (a); BW is average body weight (kg); and AT is the

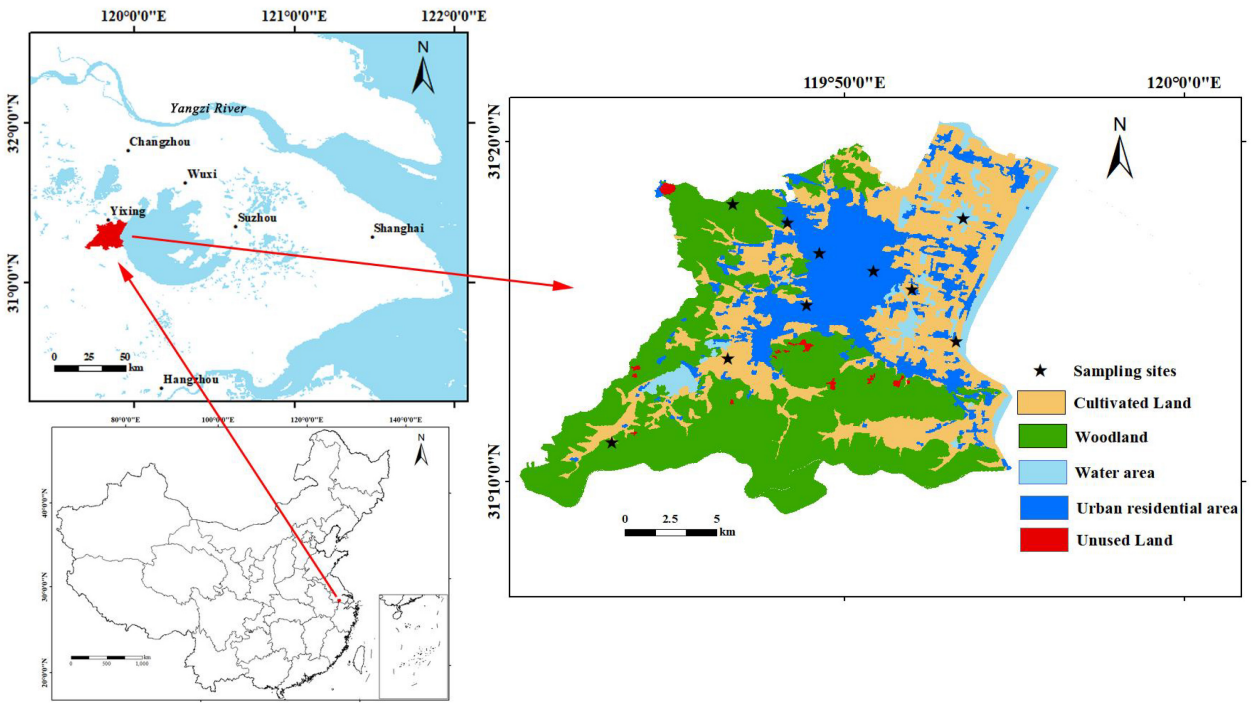

FIGURE 1 | Study area and sampling sites.

average exposure time (d); the values of the above parameters are shown in **Supplementary Table 1**.

$$THI = \sum HI_i = \sum \frac{ADI_i}{RfD_i}$$

$$TCR = \sum CR_i = \sum (ADI_i \times SF_i)$$

where, HI_i is the non-carcinogenic hazard index of heavy metal i, THI is the non-carcinogenic hazard index of all the HMs; RfD_i is the non-carcinogenic daily reference dose of heavy metal i; HI/THI < 1 indicates that the non-carcinogenic risk of HMs is acceptable, otherwise there is a non-carcinogenic risk, CR_i is the carcinogenic risk for heavy metal i, TCR is the total carcinogenic risk (TCR) for all the HMs, and SF is the carcinogenic slope factor. The RfD and SF values of different heavy metal elements are shown in **Supplementary Table 2**. The acceptable risk level of CR/TCR recommended by the USEPA is 10^{-6} to 10^{-4} and higher than 10^{-4} indicates a significant carcinogenic risk (USEPA, 2001).

Source Apportionment Based on the Pb Isotopes Ratio Analysis

Isosource is a stable isotope analysis software that is often used to calculate source contributions. Compared with binary or ternary mixed models, the advantage is that even when there is only one isotopic system and more than three types of pollution sources, the model can still obtain the most likely range of ratios contributed by different pollution sources (Chen et al., 2018b).

Input the Pb isotope ratio of potential pollution sources in the study area and the Pb isotope ratio of each sample into Isosource and the calculation formula is as follows:

$$R_m = \sum_{i=1}^{n} P_i R_i$$

$$I = \sum_{i}^{n} R_i$$

where, R_m is the isotopic ratio, P_i is the percentage contribution of source i, and R_i is the isotopic ratio of source i. There are two isotopic ratios and six possible sources in this study (**Supplementary Table 3**).

RESULTS

Characteristics of Heavy Metal Contents in Bark and Leaves of the Camphor Tree

The contents of different heavy metal elements in the bark and leaves of the camphor tree are shown in **Table 1**. The concentration of HMs in the bark is higher than that in leaves, which confirmed the findings of a study by Sawidis et al. (2011). The coefficient of variation (CV) of HMs in bark, except Cd, is higher than those of leaves; the CV of all the heavy metal elements in the bark is greater than 36%, which belongs to high variation; the CV of As, Cr, Ni, and Zn in leaves is between 16 and 36%, it belongs to moderate variation, while Cu, Cd, and Pb belong

TABLE 1 | Heavy metal content in bark and leaves of the camphor tree.

		As	Cr	Ni	Cu	Zn	Cd	Pb
Barks	Min (mg/kg)	0.68	1.38	1.38	5.66	28.60	0.18	2.62
	Max (mg/kg)	1.92	11.02	11.16	26.33	250.79	1.07	60.95
	Mean (mg/kg)	1.19	5.84	4.58	15.51	125.30	0.75	28.95
	SD	0.45	2.86	2.88	6.05	68.62	0.35	20.08
	CV (%)	37.80	49.00	62.97	39.00	54.76	47.44	69.37
	OSR (%)	0	/	/	/	/	0	90.00
Leaves	Min (mg/kg)	0.44	0.83	1.47	3.87	24.2	0.04	1.12
	Max (mg/kg)	1.02	2.12	3.18	12.82	48.39	0.24	4.7
	Mean (mg/kg)	0.78	1.59	2.09	6.72	33.34	0.10	2.33
	SD	0.19	0.37	0.52	2.56	8.13	0.06	1.03
	CV (%)	24.22	23.34	25.07	38.14	24.39	55.40	44.10
	OSR (%)	0	/	/	/	/	0	0
	ISO (mg/kg)	4.00	/	/	/	/	2.00	10.00

to high variation. A larger CV indicates a greater influence from human activities (coal burning, traffic burning, sewage irrigation, industrial activities, etc.) (Shi and Lu, 2018). According to the "Chinese Medicine—Limits of HMs in Chinese Herbal Medicine" published on the website of the International Organization for Standardization (ISO), the maximum reference values of Pb, As, and Cd in Chinese herbal medicine are 10.00, 4.00, and 2.00 mg/kg (International organization for standardization (ISO), 2015). It was determined that in all the samples, only the concentration of Pb in bark exceeded the limit value and the over-standard rate (OSR) was as high as 90.00%. Studies have shown that *Populus canescens* has a strong ability to accumulate Pb, which is an important reason for the high content of Pb in plants. However, high concentrations of Pb lead to a decrease in plant photosynthetic rate and biomass (Shi et al., 2021). As a potential carcinogen, Pb has been implicated in the etiology of many diseases, especially those related to the cardiovascular, renal, nervous system, and skeletal diseases (Järup, 2003). Some studies found that the average accumulation capacity of Black Locust, Poplar, and Ginkgo for HMs was Cd > Zn > Cu > Pb (Zhan et al., 2014) and the accumulation capacity of tea tree for Pb was also less than other HMs (She et al., 2020). Although the enrichment capacity of Pb is relatively small, in this study area, only the Pb in the bark has the largest variation coefficient (69.37%) and the highest OSR, which indicates that the camphor trees in the study area have been obviously polluted by Pb.

Human Health Risk Assessment of Heavy Metals in the Camphor Tree

The total non-carcinogenic risk (THI) of HMs in the bark and leaves of the camphor tree in the study area was acceptable (THI < 1.0), but the TCR was unacceptable (TCR > 1×10^{-4}) (**Figure 2**). For THI, Pb in bark contributed the most, reaching 56.00%, followed by As (26.86%); on the contrary, As in leaves contributed the most to THI, reaching 67.61%, followed by Pb (17.25%). Nonetheless, the THI of bark and leaves was still within the acceptable range, and it is worth noting that the THI of bark was already close to the threshold. For TCR, As in leaves still dominates, and the order of the contribution rate of HMs is As (44.82%) > Cr (30.35%) > Cd (24.07%) > Pb (0.76%); the contribution rate of HMs in bark was Cd (48.74%) > Cr (30.23%) > As (18.49%) > Pb (2.55%). Pb and Cd in the bark were the most likely to cause harm to humans, and similarly, As in leaves. Overall, the bark is more likely to be enriched with HMs than leaves, which poses a higher risk to human health and should be a major concern.

Source Apportionment of Heavy Metals

The results of Pearson correlation analysis showed that Pb in bark showed a very strong correlation with Cu, Zn, and Cd, respectively ($r > 0.8$), Pb-Cr was strongly correlated, Pb-As was moderately correlated, and only Pb-Ni was very weak or had no correlation (**Supplementary Figure 1**). The stronger the correlation, the more likely these HMs are from the same pathway (Wang et al., 2020). Therefore, the source of Pb in the bark can reflect the source of most HMs. The correlation between Pb in leaves and other HMs is not as strong as that in the bark; however, Pb-Cr also shows a strong correlation ($0.6 \leq r < 0.8$), Pb-As is moderately correlated ($0.4 \leq r < 0.6$), and Pb-Ni and Pb-Zn are weakly correlated ($0.2 \leq r < 0.4$). According to the analysis results in **Figure 2**, the HMs in the bark that has a larger impact on health risks are Pb, Cd, Cr, and As; similarly, As, Cr, Cd, and Pb in leaves have a larger impact on health risks.

A comparison of Pb isotopic composition in barks and leaves with potential sources is shown in **Figure 3**. A total of 18 of the 20 samples as well as the corresponding soils had Pb isotope ratios close to five anthropogenic sources (traffic emissions, coal burning, sewage, battery factories, and tanneries). A total of 5 of the 6 corresponding soil samples were close to the anthropogenic sources mentioned above. However, the Pb isotope ratio of the uncontaminated soil was far from the Pb isotope ratio of the samples. This suggests that uncontaminated soil has less impact on HMs in barks and leaves. Conversely, anthropogenic sources may be an important contributor to HMs pollution.

The calculation results showed that the influence patterns of different pollution sources on barks and leaves were different (**Figure 4**). Coal burning, battery factories, and traffic emissions contributed relatively high HMs in barks, all exceeding 20%

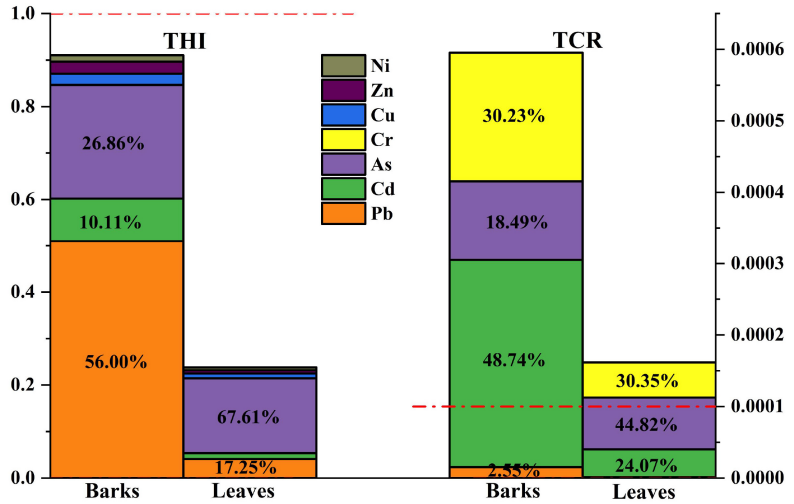

FIGURE 2 | Contribution of heavy metals (HMs) to human total non-carcinogenic risk (THI) and total carcinogenic risk (TCR).

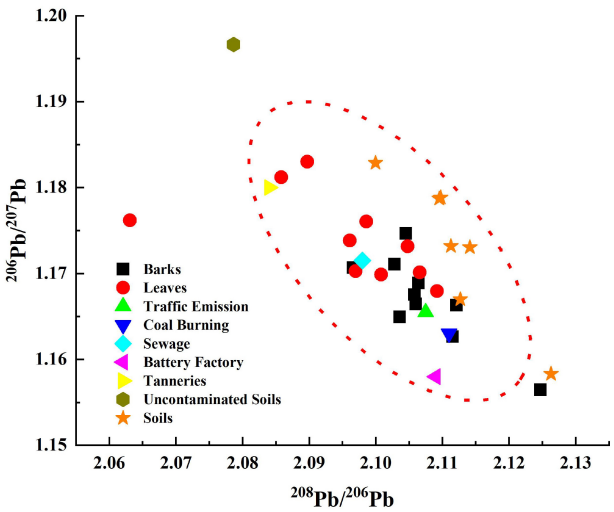

FIGURE 3 | Comparison of Pb isotope composition between samples and potential pollution sources.

(**Figure 4A**). However, the contribution rate of the three to leaves is not a lot different from that of other pollution sources, and they all remain between 15 and 18% (**Figure 4B**). In order to further improve the efficiency of the initial control of pollution sources, we classified the six pollution sources in the study area into three categories. Classify coal burning and traffic emission as fossil fuel burning; classify sewage, battery factories, and tanneries as industrial activities; and classify uncontaminated soil as a natural source. In general, the order of contribution of pollution sources in barks is industrial activities (48.20%), fossil fuel burning (42.08%), and natural sources (9.72%); the order of contribution of pollution sources in leaves is industrial activities (51.20%), fossil fuel burning (32.20%), and natural sources (16.60%) (**Figure 4C**).

Spatial Distribution of Health Risks From Heavy Metal Pollution Sources

The carcinogenic risk of camphor tree barks and leaves in the study area caused by different pollution sources is different, but except for **Figure 5F** (HMs from nature in leaves), the high-risk distribution areas corresponding to each source are basically the same (**Figure 5**). Among them, the high-risk areas of barks caused by industrial activities are distributed in the northwest, northeast, and southeast of the study area (**Figure 5A**); the high-risk areas of fossil fuel burning sources are basically the same as the former (**Figure 5C**); the difference is that it affects the northeast more than the former. This may be due to the fact that there is the G25 "Changchun–Shenzhen" expressway running from the northwest to southeast of the study area. Studies have shown that the combustion of gasoline and diesel can increase the concentrations of Zn, Cu, and Pb in the environment (Fan et al., 2022). Natural sources posed much less risk than the other two sources, with high-risk areas only reaching a threshold for carcinogenic risk (**Figure 5E**). The high-risk areas for leaves from industrial activities (**Figure 5B**) and natural sources (**Figure 5F**) also just exceeded the threshold, and it is worth noting that the high-risk areas for natural sources are distributed in the due north of the study area, which is an urban residential area. In terms of non-carcinogenic risk, the impact of the three heavy metal pollution sources on the entire study area was within an acceptable range, and their relatively high-risk distribution areas were consistent with those with high carcinogenic risk (**Supplementary Figure 2**).

DISCUSSION

The concentrations of Zn, Pb, Cd, and Cu in normal plants ranged from 10 to 150, 0.1 to 41.7, 0.2 to 0.8, and 3 to 30 mg/kg, respectively (Padmavathiamma and Li, 2007). The concentrations of Zn, Pb, Cd, and Cu in this study ranged

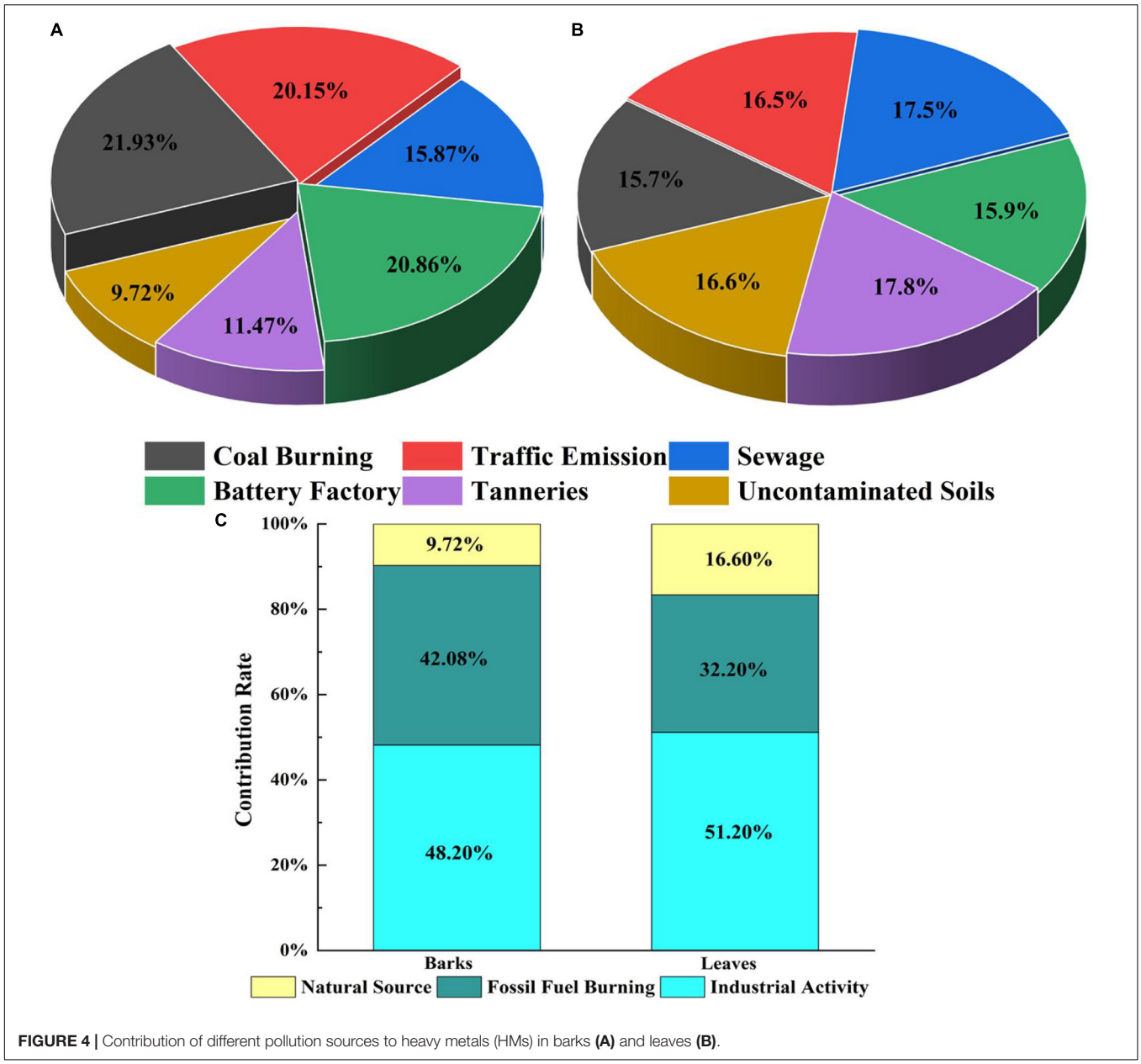

FIGURE 4 | Contribution of different pollution sources to heavy metals (HMs) in barks **(A)** and leaves **(B)**.

from 24.20 to 250.79, 1.12 to 60.95, 0.04 to 1.07, and 3.87 to 26.33 mg/kg, respectively. Except for Cu, the other three HMs all exceeded the normal range. Some researchers investigated the HMs content in the bark and leaves of camphor trees in Hefei, China. Through comparison, we found that the mean values of Pb and Cd in the bark and leaves of camphor trees in this study were generally consistent with the former (Fang et al., 2021). Typical concentrations of Cd in plants are less than 10 mg/kg (Tomašević et al., 2004) and the concentrations of Cd in this study ranged from 0.04 to 1.07 mg/kg. Overall, some camphor trees in the study area have been contaminated with HMs.

As a tall tree that easily accumulates HMs, the camphor tree can be used to remediate HMs-contaminated soils (Zhou et al., 2019). Therefore, when HMs-contaminated bark or leaves are brought into the market as medicinal raw materials, they may pose a risk to human health. The HMs in the camphor tree enter the human body through human ingestion, which will cause different degrees of non-carcinogenic and carcinogenic risks (Nag and Cummins, 2022). The results of the human health risk assessment showed that the average non-carcinogenic risk of camphor bark and leaves in the study area was within an acceptable range, but its carcinogenic risk was unacceptable, especially for the bark. The average carcinogenic risk of the bark is already close to six times the threshold and some high-risk areas may be higher.

The Pb isotope ratio analysis, as an efficient and accurate method for heavy metal tracer, has been applied to the

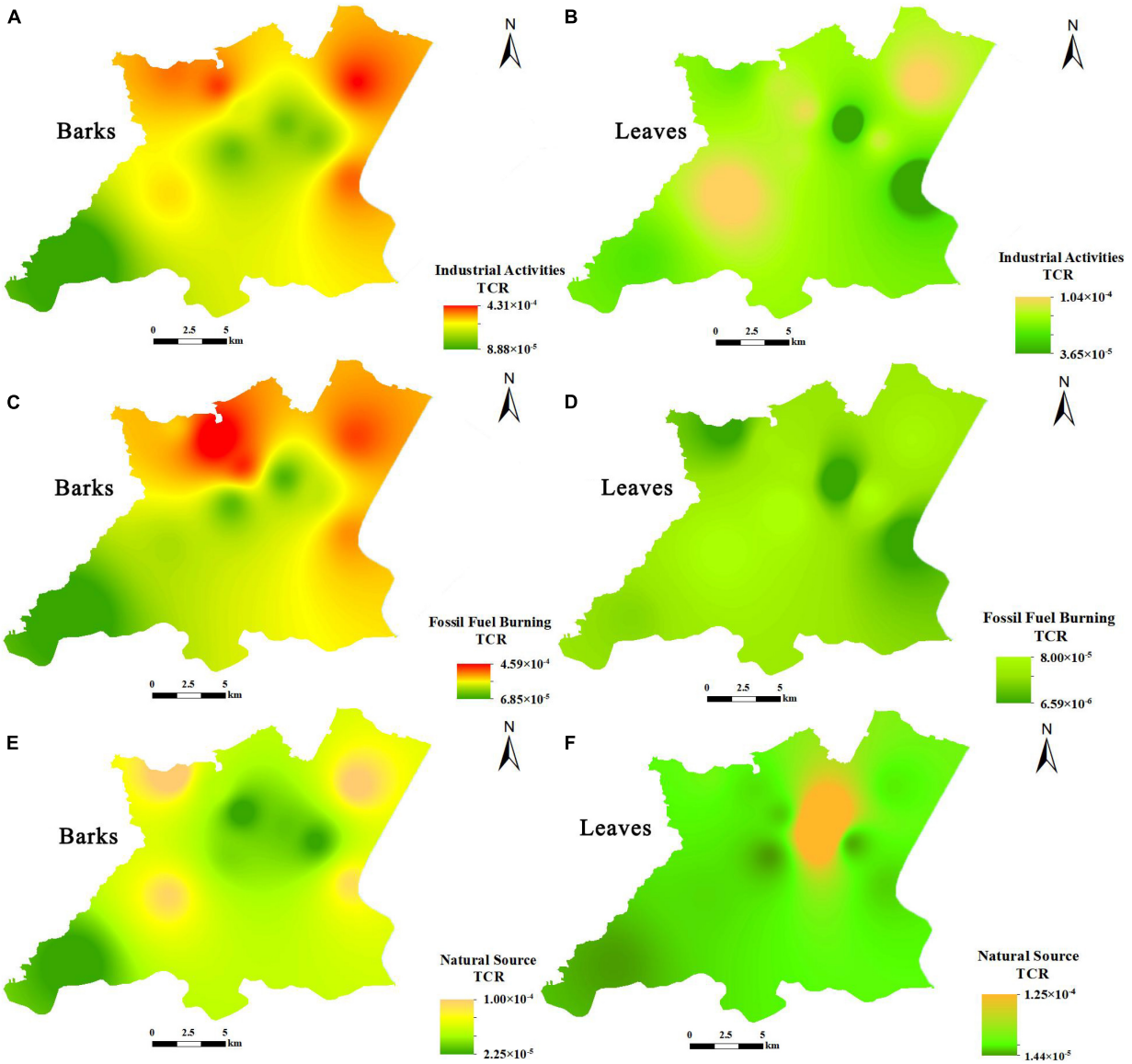

FIGURE 5 | Effects of pollution sources on the carcinogenic risk of camphor barks and leaves.

fields of ecology and environmental science in recent years (Beaumais et al., 2022; Dong et al., 2022). This study innovatively applied Pb isotopes to the source apportionment of HMs in the bark and leaves of the camphor tree and combined the source contribution with the human health risk assessment model to calculate the non-carcinogenic and carcinogenic risks of each pollution source to the camphor tree. The results showed that for bark, industrial activities mainly caused high risk to the northeast and southeast of the study area, while fossil fuel burning mainly caused high risk to the northwest of the study area. High-risk areas from natural sources are distributed around the edge of the study area, but their risk values are much lower than the former. Some studies have found that among different functional areas of the city, the HMs content of the camphor tree bark is the highest in industrial areas and the lowest in commercial areas, which was consistent with the results of this study. However, the average value of HMs in the bark in the commercial area is still much higher than that in this study (Zhang, 2019). The distribution of high risk areas caused by pollution sources to leaves is similar to that of bark, with the difference that the former has a lower risk value. The coastal areas of the West Taihu Lake and the northwestern part of the study area have high health risks, possibly due to the dense distribution of refractories, catalysts, and ceramic manufacturing plants in the area, which produce wastewater and exhaust gases containing large amounts of HMs (Chen et al., 2018a). The G25 Changchun–Shenzhen expressway in the study area is another important factor contributing to the high-risk area mentioned

above. Hu et al. (2014) observed that the average concentration of HMs on the main road increased with the increase in traffic flow; Cd and Cu would be generated from automobile engine and brake pad wear, Pb would be generated from automobile exhaust, and Zn would be generated from lubricating oil and tire wear (Yin et al., 2011). In general, the distribution area of camphor bark with high carcinogenic risk in the study area is consistent with the distribution of industry and resources in the area. Therefore, the prevention and control of HMs pollution should be focused on this region.

CONCLUSION

This study found that camphor trees in the study area have been contaminated by HMs, and high-risk areas should be avoided when using the barks or leaves of camphor trees in the study area to make Chinese herbal medicine. Pb and Cd are the major HMs that pose increased health risks. Although the THI of barks and leaves was within the acceptable range, the THI of barks was close to 1.0 and the contribution rate of Pb was as high as 56.00%. TCR should be given more attention. The TCR of the bark has been as high as 5.95×10^{-4} ($>1.0 \times 10^{-4}$), of which the contribution rate of Cd was 48.74%; the TCR of leaves was 1.62×10^{-4} ($>1.0 \times 10^{-4}$). The HMs pollution in the study area mainly came from industrial activities and fossil fuel burning and the average carcinogenic risk of the two barks reached an unacceptable level: 2.85×10^{-4} and 2.54×10^{-4}, respectively. The areas most affected by various pollution sources in the study area were basically the northwest, northeast, and southeast. This distribution pattern was related to the industry, population, and transportation resources in the study area. The conclusion of this study can provide a reference method for the source apportionment of HMs pollution in higher plants in developed economic areas and also provide a new perspective for environmental management departments to control and prevent HMs pollution of camphor trees.

DATA AVAILABILITY STATEMENT

The original contributions presented in this study are included in the article/**Supplementary Material**, further inquiries can be directed to the corresponding author.

AUTHOR CONTRIBUTIONS

NL wrote the first draft of the manuscript. All authors contributed to the study conception and design, performed material preparation, data collection, and analysis, commented on previous versions of the manuscript, read, and approved the final version of the manuscript.

FUNDING

This study was supported by the National Natural Science Foundation of China (No. 42101079), the China Postdoctoral Science Foundation (2021M701208), and the Postgraduate Research and Practice Innovation Program of Jiangsu Province (KYCX22_1122).

SUPPLEMENTARY MATERIAL

The Supplementary Material for this article can be found online at: https://www.frontiersin.org/articles/10.3389/fpls.2022.911447/full#supplementary-material

REFERENCES

Beaumais, A., Mangeret, A., Suhard, D., Blanchart, P., Neji, M., Cazala, C., et al. (2022). Combined U-Pb isotopic signatures of U mill tailings from France and Gabon: a new potential tracer to assess their fingerprint on the environment. *J. Hazard. Mater.* 430:128484. doi: 10.1016/j.jhazmat.2022.128484

Chai, Y., Yin, Z., Fan, Q., Zhang, Z., Ye, K., Xu, Y., et al. (2019). Protective effects of angong niuhuang pill on early atherosclerosis in apoe$^{-/-}$ mice by reducing the inflammatory response. *Evid-Based Compl. Alt.Med.* 2019:9747212. doi: 10.1155/2019/9747212

Chen, J., Tang, C., Zhang, R., Ye, S., Zhao, Z., Huang, Y., et al. (2020). Metabolomics analysis to evaluate the antibacterial activity of the essential oil from the leaves of *Cinnamomum camphora* (Linn.) Presl. *J. Ethnopharmacol.* 253:112652. doi: 10.1016/j.jep.2020.112652

Chen, L., Zhou, S. L., Shi, Y. X., Wang, C. H., Li, B. J., Li, Y., et al. (2018a). Heavymetals in food crops, soil, andwater in the lihe river watershed of the taihu region and their potential health risks when ingested. *Sci. Total Environ.* 615, 141–149. doi: 10.1016/j.scitotenv.2017.09.230

Chen, L., Zhou, S. L., Wu, S. H., Wang, C. H., Li, B. J., Li, Y., et al. (2018b). Combining emission inventory and isotope ratio analyses for quantitative source apportionment of heavy metals in agricultural soil. *Chemosphere* 204, 140–147. doi: 10.1016/j.chemosphere.2018.04.002

Chen, Q. M., Huang, F. M., and Cai, A. N. (2021). Spatiotemporal trends, sources and ecological risks of heavy metals in the surface sediments of weitou bay, China. *Int. J. Environ. Res. Public Health* 18:9562. doi: 10.3390/ijerph18189562

Chen, Z. X., Xu, Q.-q, Shan, C.-s, Shi, Y.-h, Wang, Y., Chang, R. C., et al. (2019). Borneol for regulating the permeability of the blood-brain barrier in experimental ischemic stroke: preclinical evidence and possible mechanism. *Oxid Med. Cell Longev.* 2019:2936737. doi: 10.1155/2019/2936737

Cui, L., Li, J., Gao, X. Y., Tian, B., Zhang, J. W., Wang, X. N., et al. (2022). Human health ambient water quality criteria for 13 heavy metals and health risk assessment in Taihu Lake. *Front. Environ. Sci. Eng.* 16:41. doi: 10.1007/s11783-021-1475-6

Dong, C., Liu, J., Harvey, P., and Yan, C. (2022). Characteristics and sources of Pb exposure via household dust from the urban area of Shanghai, China. *Sci. Total Environ.* 811:151984. doi: 10.1016/j.scitotenv.2021.151984

Fan, P., Lu, X. W., Yu, B., Fan, X. Y., Wang, L. Q., Lei, K., et al. (2022). Spatial distribution, risk estimation and source apportionment of potentially toxic metal(loid)s in resuspended megacity street dust. *Environ. Int.* 160:107073. doi: 10.1016/j.envint.2021.107073

Fang, T., Jiang, T., Yang, K., Li, J., Liang, Y., Zhao, X., et al. (2021). Biomonitoring of heavy metal contamination with roadside trees from metropolitan area of Hefei, China. *Environ. Monit. Assess.* 193:151. doi: 10.1007/s10661-021-08926-1

Guo, S., Geng, Z., Zhang, W., Liang, J., Wang, C., Deng, Z., et al. (2016). The chemical composition of essential oils from *Cinnamomum camphora* and their insecticidal activity against the stored product pests. *Int. J. Mol. Sci.* 17:1836. doi: 10.3390/ijms17111836

Hu, Y., Wang, D., Wei, L., Zhang, X., and Song, B. (2014). Bioaccumulation of heavy metals in plant leaves from yan' an city of the loess plateau, China. *Ecotoxicol. Environ. Saf.* 110, 82–88. doi: 10.1016/j.ecoenv.2014.08.021

Huang, J., Tang, X., Ye, F., He, J., and Kong, X. (2016). Clinical therapeutic effects of aspirin in combination with fufang danshen diwan, a traditional chinese medicine formula, on coronary heart disease: a systematic review and meta-analysis. *Cell Physiol. Biochem.* 39, 1955–1963. doi: 10.1159/000447892

International organization for standardization (ISO) (2015). Available online at: https://www.iso.org/standard/63150.html (accessed August, 2015).

Järup, L. (2003). Hazards of heavy metal contamination. *Brit. Med. Bull.* 68, 167–182. doi: 10.1093/bmb/ldg032

Jiang, H., Wang, J., Song, L., Cao, X., Yao, X., Tang, F., et al. (2016). GC×GC-TOFMS analysis of essential oils composition from leaves, twigs and seeds of *Cinnamomum camphora* L. Presl and their insecticidal and repellent activities. *Molecules*. 21, 423. doi: 10.3390/molecules21040423

Li, K., Wang, J., and Zhang, Y. (2022). Heavy metal pollution risk of cultivated land from industrial production in China: spatial pattern and its enlightenment. *Sci. Total Environ.* 828:154382. doi: 10.1016/j.scitotenv.2022.154382

Li, Y., Zhou, S. L., Zhu, Q., Li, B. J., Wang, J. X., Wang, C. H., et al. (2018). One-century sedimentary record of heavy metal pollution in western Taihu Lake, China. *Environ. Pollut.* 240, 709–716. doi: 10.1016/j.envpol.2018.05.006

Lin, L. Q., Cong, L., Yun, W. H., Yang, J., Ming, H., Wan, Z. B., et al. (2015). Association of soil cadmium contamination with ceramic industry: a case study in a Chinese town. *Sci. Total Environ.* 514, 26–32. doi: 10.1016/j.scitotenv.2015.01.084

Men, C., Liu, R. M., Xu, L. B., Wang, Q. R., Guo, L. J., Miao, Y. X., et al. (2020). Source-specific ecological risk analysis and critical source identification of heavy metals in road dust in Beijing, China. *J. Hazard. Mater.* 388:121763. doi: 10.1016/j.jhazmat.2019.121763

Nag, R., and Cummins, E. (2022). Human health risk assessment of lead (Pb) through the environmental-food pathway. *Sci. Total Environ.* 810:151168. doi: 10.1016/j.scitotenv.2021.151168

Padmavathiamma, P. K., and Li, L. Y. (2007). Phytoremediation Technology: Hyper-accumulation Metals in Plants. *Water Air. Soil. Poll.* 184, 105–126. doi: 10.1007/s11270-007-9401-5

Sawidis, T., Breuste, J., Mitrovic, M., Pavlovic, P., and Tsigaridas, K. (2011). Trees as bioindicator of heavy metal pollution in three European cities. *Environ. Pollut.* 159, 3560–3570. doi: 10.1016/j.envpol.2011.08.008

She, X. S., Gan, Z. T., Yao, T., Wang, S. Q., and Wang, Y. (2020). Bioconcentration and distribution of heavy metal elements in the soil-tea plant systems of An-tea producing areas. *J. Nanjing For. Univ. (Natural Sciences Edition)* 44, 102–110.

Shi, D. Q., and Lu, X. W. (2018). Accumulation degree and source apportionment of trace metals in smaller than 63 mu m road dust from the areas with different land uses: a case study of Xi'an, China. *Sci. Total Environ.* 636, 1211–1218. doi: 10.1016/j.scitotenv.2018.04.385

Shi, W. G., Li, J., Zhang, Y. H., Lei, J. P., and Luo, Z. B. (2021). A comparative study on lead tolerance and accumulation of seven poplar species. *J. Nanjing For. Univ. (Natural Sciences Edition)* 45, 61–70.

Shandong Province Standard (SPS) (2012). *Chinese Medicinal Materials*. 356.

Tomašević, M., Rajšić, S., Đorđević, D., Tasić, M., Krstić, J., and Novaković, V. (2004). Heavy metals accumulation in tree leaves from urban areas. *Environ. Chem. Lett.* 2, 151–154. doi: 10.1007/s10311-004-0081-8

USEPA (2001). *Risk Assessment Guidance for Superfund*, III. Washington DC: United States Environmental Protection Agency.

USEPA (2011). *Exposure Factors Handbook.Edition (Final)*. Washington, DC: US Environmental Protection Agency.

Wang, J., Niu, X., Sun, J., Zhang, Y., Zhang, T., Shen, Z., et al. (2020). Source profiles of PM2.5 emitted from four typical open burning sources and its cytotoxicity to vascular smooth muscle cells. *Sci. Total Environ.* 715:136949. doi: 10.1016/j.scitotenv.2020.136949

Xiang, M. T., Li, Y., Yang, J. Y., Lei, K. G., Li, Y., Li, F., et al. (2021). Heavy metal contamination risk assessment and correlation analysis of heavy metal contents in soil and crops. *Environ. Pollut.* 278:116911. doi: 10.1016/j.envpol.2021.116911

Yang, S. H., Qu, Y. J., Ma, J., Liu, L. L., Wu, H. W., Liu, Q. Y., et al. (2020). Comparison of the concentrations, sources, and distributions of heavy metal(loid)s in agricultural soils of two provinces in the Yangtze River Delta, China. *Environ. Pollut.* 264:114688. doi: 10.1016/j.envpol.2020.114688

Yang, Z., An, W., Liu, S., Huang, Y., Xie, C., Huang, S., et al. (2020). Mining of candidate genes involved in the biosynthesis of dextrorotatory borneol in *Cinnamomum burmannii* by transcriptomic analysis on three chemotypes. *Plant Biology. PeerJ.* 8:e9311. doi: 10.7717/peerj.9311

Yin, S., Shen, Z., Zhou, P., Zou, X., Che, S., and Wang, W. (2011). Quantifying air pollution attenuation within urban parks: an experimental approach in Shanghai, China. *Environ. Pollut.* 159, 2155–2163. doi: 10.1016/j.envpol.2011.03.009

Zhai, Y., Dai, Q., Jiang, K., Zhu, Y., Xu, B., Peng, C., et al. (2016). Traffic-related heavy metals uptake by wild plants grow along two main highways in Hunan Province, China: effects of soil factors, accumulation ability, and biological indication potential. *Environ. Sci. Pollut. Res.* 23, 13368–13377. doi: 10.1007/s11356-016-6507-6

Zhan, H., Jiang, Y., Yuan, J., Hu, X., Nartey, O. D., and Wang, B. (2014). Trace metal pollution in soil and wild plants from lead–zinc smelting areas in Huixian County, Northwest China. *J. Geochem. Explor.* 147, 182–188. doi: 10.1016/j.gexplo.2014.10.007

Zhang, Y. (2019). Heavy metal content in the bark of camphora tree in Xiangtan and its environmental significance. *Appl. Ecol. Environ. Res.* 17, 9827–9835.

Zhou, J., Cheng, K., Zheng, J., Liu, Z., Shen, W., Fan, H., et al. (2019). Physiological and Biochemical Characteristics of *Cinnamomum camphora* in Response to Cu- and Cd-Contaminated Soil. *Water Air. Soil. Poll.* 230:15. doi: 10.1007/s11270-018-4048-y

Zulkafflee, N. S., Redzuan, N. A. M., Nematbakhsh, S., Selamat, J., Ismail, M. R., Praveena, S. M., et al. (2022). Heavy metal contamination in *Oryza sativa* L. at the eastern region of malaysia and its risk assessment. *Int. J. Environ. Res. Public Health* 19:739. doi: 10.3390/ijerph19020739

Conflict of Interest: The authors declare that the research was conducted in the absence of any commercial or financial relationships that could be construed as a potential conflict of interest.

Publisher's Note: All claims expressed in this article are solely those of the authors and do not necessarily represent those of their affiliated organizations, or those of the publisher, the editors and the reviewers. Any product that may be evaluated in this article, or claim that may be made by its manufacturer, is not guaranteed or endorsed by the publisher.

frontiers | Frontiers in Plant Science

TYPE Original Research
PUBLISHED 23 September 2022
DOI 10.3389/fpls.2022.997818

OPEN ACCESS

EDITED BY
Song Heng Jin,
Zhejiang Agriculture and Forestry University, China

REVIEWED BY
Muthusamy Ramakrishnan,
Nanjing Forestry University, China
Mingyang Quan,
Beijing Forestry University, China

*CORRESPONDENCE
Huahong Huang
huanghh@zafu.edu.cn
Erpei Lin
zjulep@hotmail.com

†These authors have contributed equally to this work

SPECIALTY SECTION
This article was submitted to Functional Plant Ecology, a section of the journal Frontiers in Plant Science

RECEIVED 19 July 2022
ACCEPTED 29 August 2022
PUBLISHED 23 September 2022

CITATION
Hu X-G, Xu Y, Shen N, Liu M, Zhuang H, Borah P, Tong Z, Lin E and Huang H (2022) Comparative physiological analyses and the genetic basis reveal heat stress responses mechanism among different *Betula luminifera* populations. *Front. Plant Sci.* 13:997818. doi: 10.3389/fpls.2022.997818

Comparative physiological analyses and the genetic basis reveal heat stress responses mechanism among different *Betula luminifera* populations

Xian-Ge Hu†, Yilei Xu†, Ning Shen†, Mingtong Liu, Hebi Zhuang, Priyanka Borah, Zaikang Tong, Erpei Lin* and Huahong Huang*

The State Key Laboratory of Subtropical Silviculture, Institute of Biotechnology, College of Forestry and Biotechnology, Zhejiang A&F University, Hangzhou, China

Betula luminifera is a subtropical fast-growing timber species with high economic value. However, along with global warming, heat stress become one of the main environmental variables that limit the productivity of *B. luminifera*, and the response of diverse geographic populations to high temperatures is still unclear. In order to offer a comprehensive understanding of the behavior of *B. luminifera* under heat stress, the physiological responses of six *B. luminifera* populations (across the core distribution area) were described in this work in an integrated viewpoint. The results showed that a multi-level physiological regulatory network may exist in *B. luminifera*, the first response was the activity of resistant enzymes [e.g., peroxidase (POD)] at a preliminary stage of 2h heat stress, and then the proline (osmoregulation substance) content began to increase after 24h of continuous high-temperature treatment. In addition, photosynthesis was stronlgly affected by heat stress, and the net photosynthetic rate (P_n) showed a downward trend under heat treatment in all six *B. luminifera* populations. Interestingly, although the physiological change patterns of the six *B. luminifera* populations were relatively consistent for the same parameter, there were obvious differences among different populations. Comprehensive analysis revealed that the physiological response of Rongshui (RS) was the most stable, and this was the representative *B. luminifera* population. Illumina RNA-seq analysis was applied to reveal the specific biological process of *B. luminifera* under heat stress using the RS population, and a total of 116,484 unigenes were obtained. The differentially expressed genes (DEGs) between different time periods under heat stress were enriched in 34 KEGG pathways, and the limonene and pinene degradation pathway was commonly enriched in all pairwise comparisons. Moreover, transcription factors including bHLH (basic helix–loop–helix), MYB, WRKY, and NAC (NAM, ATAF1/2, and CUC2) were identified. In this study, the physiological response and tolerance mechanisms of *B. luminifera* under high temperature stress were revealed, which can conducive to the basis of *B. luminifera* selection and resistance assessment for cultivation and breeding.

KEYWORDS

***Betula luminifera*, populations, physiological, heat stress, transcription factor**

Introduction

Betula luminifera (H.) Winkl, belonging to the Betulaceae family, is a representative fast-growing timber plantation tree species (Chen, 2006; Zhang et al., 2010). *B. luminifera* is widely distributed in the subtropical regions and covers 14 provinces of China; the core distribution areas are mainly concentrated in Guizhou, Yunnan, Hunan, Guangxi, and Jiangxi provinces (Pan et al., 2017). This species is monoecious, mainly seed-propagated, and flowering is initiated after an average of 2 years (Cao and Fang, 2006). *B. luminifera* has an extremely high economic value among subtropical tree species because of its high-quality timber, short juvenile phase and fast growth (Li et al., 2018). In the subtropics, *B. luminifera* has become a recognizable landscape plant due to its high ornamental value in both garden and street landscaping. It's essential for the development of *B. luminifera* plantations to multiply elite germplasm on a large scale, with high yield and resilience to biotic and abiotic challenges. However, there are disappointingly few publications on the physiological responses and resistance evaluation of *B. luminifera* under biotic and abiotic challenges, particularly the variations in response to stress among different populations.

As an important economic plant in subtropical regions, the wood quality of *B. luminifera* will be influenced through various environmental variables. Statistical evidence already implied that as a result of climate change, extremely high temperatures will occur more frequently (Skendžić et al., 2021; Iyakaremye et al., 2022), so heat stress become a growing threat to plant. Heat stress can trigger alters on morphological and physiological in plants, significantly influencing plant production and development (Allakhverdiev et al., 2008). Plants are sessile organisms, making them more susceptible to temperature changes. To counteract abiotic stress, plants may be forced to change their cellular state. In fact, plants have a series of capabilities to adapt to irregular increases in temperature, including basal thermotolerance, to make sure plants survive when exposed directly to extremely high temperatures and acquire thermotolerance, in which plants enhance their resistance to fatal heat stress following a period of preexposure to a nonlethal high temperatures (Li et al., 2021).

Nevertheless, a number of harmful occurrences, such as excessive reactive oxygen species (ROS) generation and the deterioration of cellular structural elements (Li et al., 2018), still occur when plants encounter extremely high-temperature environments. After exposure to high temperatures, plant photosynthesis is typically hindered, and heat stress makes the photosynthetic machinery vulnerable to damage (Wang et al., 2018). Additionally, it has been found that heat stress can alter the integrity of thylakoid membranes and the ultrastructure of chloroplasts (Allakhverdiev et al., 2008; Yamamoto et al., 2008), which greatly reduced plant thermotolerance. Based on the determination of physiological parameters under stress treatment, the response mechanisms of transcriptomics and metabolomics were analyzed for *Populus tomentosa* under heat stress (Ren et al., 2019); 20 coconut populations' physiology response and resistance evaluation were obtained under low-temperature stress (Sun et al., 2021); and the physiological and transcriptomic response mechanism of *Santalum album* were revealed (Zhang et al., 2017). Therefore, the determination of physiological indexes is an effective means to assess plant responses to heat stress.

Populations with different adaptability are the foundation for breeding new varieties and creating new germplasm, and population selection and evaluation would advance the comprehension utilized of trees (Zhang et al., 2021). In this study, the physiological responses of six *B. luminifera* germplasm resources to heat stress were analyzed and assessed. The results showed that a multi-level physiological regulatory network may exist in *B. luminifera*, and the first response was the activity of resistant enzymes, and then the osmoregulation substance content began to increase after continuous high-temperature treatment. Furthermore, *B. luminifera* sequence transcriptomes under heat stress were obtained using second generation sequencing, and the differentially expressed genes (DEGs) and transcription factors (TFs) were identified and annotated. The analysis of heat resistance of *B. luminifera* populations will provide the basis for *B. luminifera* breeding, allowing for a greater diversity of resistant *B. luminifera* germplasms to fulfill current and future needs.

Materials and methods

Plant materials, growth conditions and treatments

This study was performed at Zhejiang Agriculture and Forestry University (30.23°N, 119.72°E) in China. The germplasm resources (seeds) of *B. luminifera* provenances were collected from six typical suitable habitats in different provinces: Guangxi [Rongshui (RS) population (109.26°E, 25.08°N), Yongfu (YF) population (110.01°E, 25.01°N)], Hunan [Shaoyang (SY) population (111.28°E, 26.99°N)], Guizhou (Yinjiang (YJ) population (108.41°E, 27.99°N), Xingren (XR) population (105.19°E, 25.44°N)] and Yunnan (Daguan (DG) population (103.89°E, 27.75°N)], and were grown in the State Key Laboratory of Subtropical Silviculture in Zhejiang Province, China (Figure 1A). The seeds were germinated in transparent petri dishes with two layers of filter paper and then transplanted to seedling clods (Jiffy-7® –Peat Pellets and Coco Pellets) with a diameter of 30 mm. After growing for 2 weeks, they were transplanted to the soil with regularly watering in normal environment for 3 months. For adaptation, healthy seedlings (height, ~25 cm) were cultured in growth chambers for 7 days (at 25°C on a 12 h day/night cycle; light intensity, 250 μmol m^{-2} s^{-1}) (Figures 1B,C). The relative value of humidity was kept at 65%.

Heat stress therapy consisted of raising the temperatures in growth chambers during the light/dark regime. We selected 12 individuals from each population for heat treatment. The treatment timeline was as follows: 25°C (room temperature); 25°C to 35°C, 0.5 h (warming); 35°C to 45°C, 0.5 h; and at 45°C during

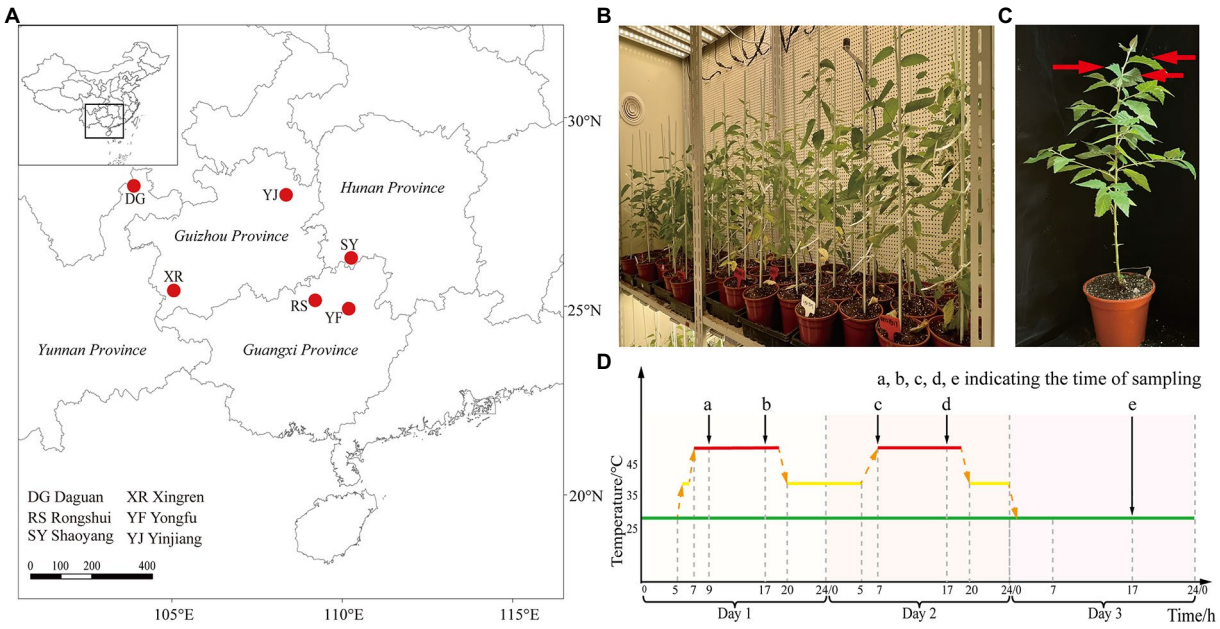

FIGURE 1
Plant material and experimental design. **(A)** The provenance locations of *B. luminifera* populations. **(B)** The growth chambers for the light/dark regime in heat stress treatment. **(C)** Sampling locations. Red arrows indicate sampling location. **(D)** Schematic diagram of the heat stress experimental design. The red line indicates the timeline of heat treatment, the green solid line indicates room temperature, and the black arrows (a, b, c, d, and e) indicate the time of sampling.

the day (Figure 1D). The sampling time for physiological index determination and RNA-seq analysis under heat treatment was 2, 10, 24, and 34 h, and recovery after 10 h (Figure 1D). The temperature setting in this study was inspired primarily by the previous heat treatment of *B. luminifera* (Pan et al., 2017) and seedling stage of other woody plants in response to heat stress (Chen et al., 2014; Ren et al., 2019). The third to fifth leaves from top to bottom were collected to measure photosynthesis-related parameters and physiological indexes (Figure 1C). Liquid nitrogen was used to freeze samples and stored at −80°C. To ensure repeatability of the results, the experiment was set up with three replicates, each consisting of four plants.

Estimation of the proline (pro) content

Proline (Pro) is a typical osmotic adjustment substance, which is commonly used to estimate plant resistance to diverse abiotic stimuli (Zhang et al., 2017; Ren et al., 2019; Sun et al., 2021). Pro helps to adjust and maintain the cell osmotic balance, participates in decreasing cell redox potential reactions and is an important indicator of the heat response in plants. In this study, the Pro contents were measured with the commercially available assay kits (Nanjing Jiancheng Bioengineering Institute, Nanjing, CHN). To determine the Pro content, 0.1 g of leaf tissues were pounded to a powder combined with a homogenization medium, and centrifuged at 3,500 rpm and 4°C for 10 min. In accordance with the manufacturer's instructions, the supernatant was then used for analysis. Pro content was calculated as g/g FW based on the mixture of 520 nm absorbance.

Estimation of the antioxidant enzymes activities

The microplate reader was used to determine the activities of enzymes [peroxidase (POD), catalase (CAT), and superoxide dismutase (SOD)] by using commercially available assay kits (Nanjing Jiancheng Bioengineering Institute, Nanjing, CHN). To determine the activities of antioxidant enzymes, 0.15 g of fresh leaves frozen in liquid nitrogen were homogenized in 1.35 ml of physiological saline solution. After centrifuging the homogenized samples for 10 min at 4°C and 3,500 rpm, the supernatants were used to analyze enzymes activity. The specific steps were implemented as per the manufacturer's instruction.

Utilizing xanthine and xanthine oxidase frameworks, the SOD activity was determined at 450 nm (Marklund and Marklund, 1974). One unit of SOD action was defined as the amount of enzyme needed to provide a 50% inhibition of the xanthine and xanthine oxidase system reaction during the extraction of 1 mg of protein per ml. The unit per milligram of protein used to describe SOD activity. The CAT activity was directed by detecting the decrease in absorbance at 405 nm caused by H_2O_2 breakdown (Luck, 1971). The assay principle was based on catalase's reaction to breakdown H_2O_2, which absorbs maximum at 405 nm. Spectrophotometrically, the POD activity was determined at

420 nm by activating oxidation in the presence of H_2O_2 (Reddy et al., 1985). Purpurogallin, which has a wavelength of 420 nm, is produced in the assay by the reaction of peroxidase and pyrogallol. The quantity of enzyme required to catalyze the reaction of 1 g of substrate by 1 mg of tissue protein once every minute at 37°C was referred to as one unit of POD activity.

Determination of photosynthetic parameters

Indexes of photosynthesis including the net photosynthetic rate (P_n), stomatal conductance (G_s), transpiration rate (T_r), and intercellular CO_2 concentration (C_i) of the third and fourth fully expanded leaves of 3-month-old *B. luminifera* seedlings exposed to heat stress were measured. The photosynthetic parameters of the *B. luminifera* populations were determined by using LI-6800 photosynthetic system with standardized parameters. The instrument settings were: 800 μ mol m^{-2} s^{-1} photosynthetic photon flux density (PPFD), 55% relative air humidity, and 400 μmol mol^{-1} ambient CO_2 concentration.

RNA isolation, library construction, and sequencing

Based on comprehensive analysis of above physiological indexes, one population was defined as a representative for *B. luminifera* heat resistance evaluation and was used for second generation sequencing analysis to reveal the genetic basis of *B. luminifera* under heat stress. TRIzol Reagent (pre-chilled) (Invitrogen, Carlsbad, CA, United States) was used to extract total RNA from heat-stressed *B. luminifera* (three biological replicates each). The RNA concentration, quality and integrity were determined using a NanDrop 2000 (Thermo Fisher Scientific Inc., Waltham, MA, United States) and Agilent 2,100 Bioanalyzer (Agilent Technologies, Inc., Santa Clara, CA, United States), respectively (Liu and Zhu, 2020). A total of 15 libraries were separately produced from heat-treated samples at 2, 10, 24, and 34 h, and recovery after 10 h (three biological replicates for each sampling time point) using the TruSeq RNA Sample Preparation Kit (Illumina, San Diego, CA, United States) following the manufacturer's instructions. Using poly-T oligo-attached magnetic beads, mRNA was extracted from total RNA. cDNA synthesis was implemented following our previous research (Hu et al., 2022). RNA sequencing was implemented by using Illumina NovaSeq 6,000 platform and 150 bp paired-end raw reads were generated.

RNA-seq data processing and analysis

Raw reads in FASTQ format from second generation sequencing data of heat-stress samples were first treated to eliminate reads containing adapter sequences, reads with more than 10% unknown bases, and low-quality reads (i.e., where more than 50% of the bases in a read had a quality value $Q \leq 20$). Using Trinity, a transcriptome *de novo* assembly was carried out (Grabherr et al., 2011) to obtain unigenes. Following assembly, BLASTx alignment between unigenes and the protein databases was carried out with a cut-off E-value of 10^{-5}, in the following priority order: NCBI non-redundant protein sequences (NR); Gene Ontology (GO); Kyoto Encyclopedia of Genes and Genome (KEGG); evolutionary genealogy of genes: Non-supervised Orthologous Groups (eggNOG); Protein family (Pfam); Swiss-Prot (a manually annotated and reviewed protein sequence database). The best alignment results were utilized to establish the unigenes' sequence direction.

Clean reads were mapped to the reference unigenes with Bowtie (Langmead et al., 2009), and RNA-Seq by Expectation Maximization (RSEM) was used to measure the levels of gene expression and obtain the number of read counts for each unigenes in each sample (Li and Dewey, 2011). The gene expression level was calculated using the fragments per kilobase million (FPKM) method (Mortazavi et al., 2008), and a bar graph was used to examine the number of transcripts among all heat stress samples after filtering. Based on the FPKM results, a correlation between samples was implemented by computing Pearson's correlation for pairs of samples. Using the R package (DESeq 1.10.1) (Love et al., 2014), differential expression analysis was carried out. Genes detected by DESeq that displayed an adjusted p-value ≤ 0.01 were designated as DEGs (Zhang et al., 2019). In addition, the heat-induced TFs were screened to identify highly expressed TF genes during heat stress.

Quantitative RT-PCR analysis

RNA was extracted from heat-treatment *B. luminifera* after 2, 10, 24, and 34 h of heat stress and 10 h of recovery. RNAs were processed with DNase I to eliminate genomic DNA contamination using the TurboDNA-free Kit (Ambion, Austin, TX, United States). Then total RNA from each sample was reverse transcribed by PrimeScript™ RT Reagent Kit (Perfect Real Time; Takara) and used as a templet. A large ribosomal subunit 39 gene (RPL39) was selected as an internal reference gene. The gene-specific primers were presented in Supplementary Table S1. Melting curve analysis was implemented for each primer pair prior to the next analyses. qRT-PCR was implemented with the TB Green Premix Ex Taq II (Tli RNaseH Plus; Takara) on CFX96 real-time PCR detection system (CFX96; Bio-Rad, United States). The expression pattern was assessed by our previous protocol (Hu et al., 2022). For each gene and sample, the qRT-PCR data were acquired from three biological and three technical repeats.

10.3389/fpls.2022.997818

Results

The difference of pro content among different populations under heat stress

The Pro accumulation in the six *B. luminifera* populations fluctuated slightly during the preliminary stage of heat stress (2 h), and increased sharply after 24 h of heat treatment (Figure 2). Interestingly, the maximum value of the Pro content for the six populations all appeared at 34 h of heat treatment. However, the fold change had a significant difference among the *B. luminifera* populations, e.g., the Pro content in the DG population was more than 1.9-fold higher than that in the other populations at 34 h of heat treatment. According to the change pattern of the Pro content in each population under heat treatment, the DG population was the fastest to respond to the heat treatment, followed by the XR, RS, SY, YJ, and YF populations, of which YF was the slowest and had a relatively mild response to the heat treatment. As the temperature returned to normal, the Pro content gradually decreased and returned to normal levels (Figure 2). Therefore, the increased Pro level at high temperature was beneficial for enhancing plants' endurance during the processing period, and the Pro content is an important indicator to evaluate *B. luminifera* heat resistance.

The difference in defense enzyme activities among different populations under heat stress

It was determined that the defense enzyme (SOD, CAT and POD) activity in the leaves of various populations of *B. luminifera* initially rose with temperature and time (Figure 3). In the first photoperiod under heat stress, the activities of almost all defense enzymes increased, and significant differences were found among the different *B. luminifera* populations. With the arrival of the dark cycle (temperature decreased to 35°C), the activities of these enzymes showed decreases (Figure 3). However, the enzyme activity continued to increase when the second stage of photoperiod began. In addition, irrespective of the light or dark regime, the activities of the defense enzymes (SOD, CAT, and POD) in the *B. luminifera* populations in response to heat treatment differed significantly. For example, although the SOD activity showed an increasing trend in the six populations in response to the heat treatment, the increase in the SY population was almost three-fold higher than that in the YJ population after 10 h of heat treatment. Overall, under heat treatment, except that the SOD activity of the SY population decreased continuously after reaching the maximum at 10 h of heat treatment, the change pattern of most of the *B. luminifera* populations increased with the extension of the heat treatment time but decreased appropriately during the dark cycle.

In our study, the change pattern of POD was almost consistent with that of SOD in the six *B. luminifera* populations, but the CAT activity of these populations decreased continuously after reaching the maximum at 10 h of heat treatment. In addition, even though the response of these defense enzyme activities in the *B. luminifera* populations to heat treatment were differed significantly, the change patterns of same enzyme activity among the six provenances were relatively consistent. The YJ and SY populations had the smallest and largest change ranges in SOD activity. The smallest and largest changes in POD activity occurred in the SY and DG populations respectively, and the YF and DG populations had the smallest and largest changes in CAT activity. In general, the changes in these three defense enzyme activities in the RS population were relatively stable.

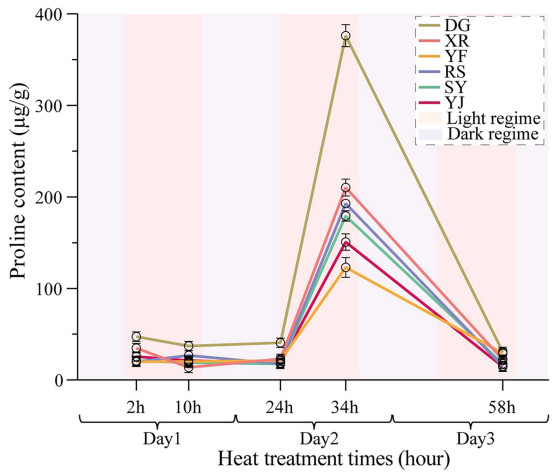

FIGURE 2
Effects of heat stress on *B. luminifera* populations' pro contents under different temperature treatments times.

Effects of heat stress on the photosynthetic parameters of the *Betula luminifera* populations

The net photosynthetic rate (P_n) of leaves can directly reflect the strength of photosynthesis. The P_n values of the six *B. luminifera* populations decreased under heat stress (Figure 4). The main differences in P_n among the *B. luminifera* populations were that the RS, SY and YF populations decreased significantly after 10 h of heat treatment (decreased by 65, 55, and 30% compared with the preliminary stage of 2 h of heat stress); the YJ and DG populations began to decrease after 24 h of heat treatment (decreased by 160 and 170%); and the XR population did not decrease until 34 h of heat treatment (decreased by 167%). Although the P_n of the RS and SY populations decreased significantly at the preliminary stage of heat stress, P_n increased again after the dark cycle (35°C). Therefore, based on the change trend of the net photosynthetic rate under heat stress, the photosynthetic parameters of the YF population were the most sensitive to temperature treatment, and P_n changed

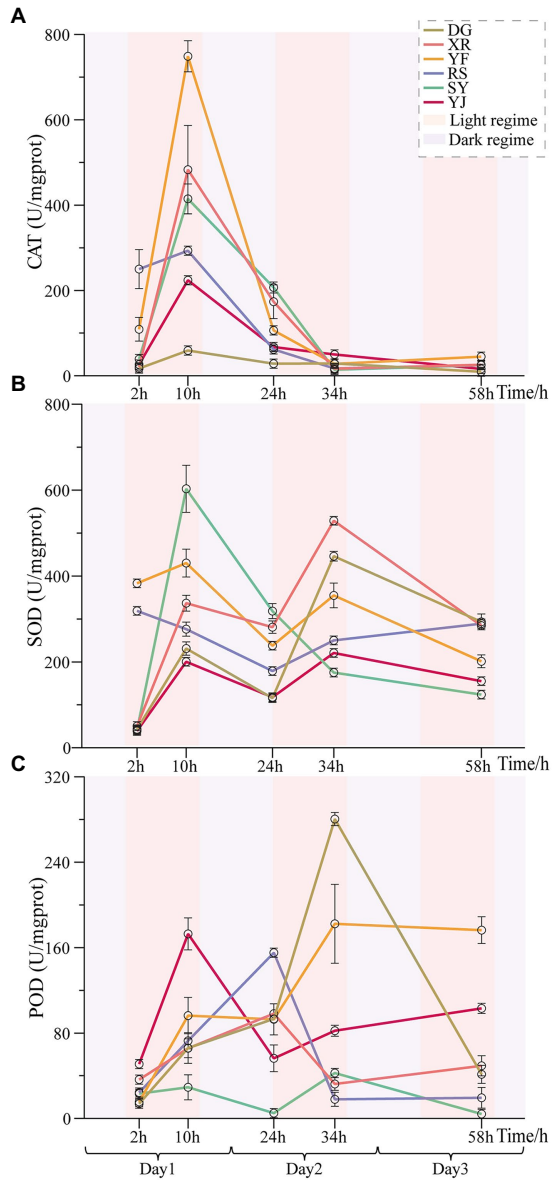

FIGURE 3
Effects of heat stress on POD, CAT, and SOD activities of *B. luminifera* populations under different temperature treatments times. **(A)** The change pattern of SOD activities. **(B)** The change pattern of POD activities. **(C)** The change pattern of CAT activities. Error bars indicating standard error (SE).

regularly with temperature increases and time. However, the P_n of the XR population was relatively stable and recovered rapidly when heat stress was suspended, indicating its strong heat resistance.

Leaf stomatal conductance (G_s) is the reciprocal of leaf stomatal resistance, which reflects the ability of plants to exchange CO_2 and water vapor, and is one of the important physiological indicators affecting P_n. Except for the XR population, the leaf G_s of the *B. luminifera* populations decreased at the preliminary stage of heat stress. In addition, except for the SY population, although the *B. luminifera* populations decreased during the heat stress, G_s was restored during the dark cycle (35°C). The transpiration rate (T_r) of leaves is also one of the important factors affecting P_n. In this study, the total dynamics of T_r in the *B. luminifera* populations under heat stress had a similar pattern as G_s (Figures 4B,C); one possible reason is that the opening or closing of stomata is the main factor affecting the transpiration rate. The intercellular CO_2 concentration (C_i) of the *B. luminifera* populations had a clear upward pattern with the increase of temperature and time, and decreased with the cessation of the heat stress. After 34 h of heat treatment, the greatest increases in the YF population were 33%, and the RS population had the smallest change, an increase of 26%.

Transcriptomic changes of *Betula luminifera* in response to heat stress

Significant distinctions existed between the physiological responses of the various *B. luminifera* populations to heat stress, while RS was the most stable and representative population based on comprehensive analysis of the above physiological parameters. Therefore, this representative population was selected to reveal the genetic basis of *B. luminifera* under heat stress. A total of 705,350,026 reads (Supplementary Table S2) were generated from the heat-stressed RS population by using the Illumina sequencing platform. After quality checks and data cleaning, 653,379,564 clean reads (Supplementary Table S2) were obtained. Based on the remaining high-quality clean reads, Trinity produced 364,563 transcripts with an average length of 1,198 bp, and 116,484 unigenes with an average length of 1,021 bp were obtained from these transcripts. The N50 and N90 sizes of the transcripts and unigenes were 1844 and 497 bp, 1,598 and 420 bp, respectively (Table 1). The total length of all unigenes was 118,960,472 bp (Table 1; see Supplementary Figure S1 for the length distribution of all unigenes). Additionally, comparisons with our previous transcriptome assemblies of *B. luminifera* (Cai et al., 2018) demonstrated that the properties of the *B. luminifera de novo* transcriptome assembly were of high quality.

Functional annotation of the *Betula luminifera* unigenes

We performed functional annotation using BLAST by comparing sequences against six databases (NR, GO, eggNOG, KEGG, Swiss-Prot, and Pfam) and received annotation results for 116,484 unigenes. In total, 58,650 unigenes were annotated in at least one database, with 7,370 annotated in all databases (Figure 5). The eggNOG database assigned a total of 50,872 unigenes to 26 functional clusters, with "signal transduction mechanisms" being the largest category (Figure 6A). According to three main categories (molecular function, cellular

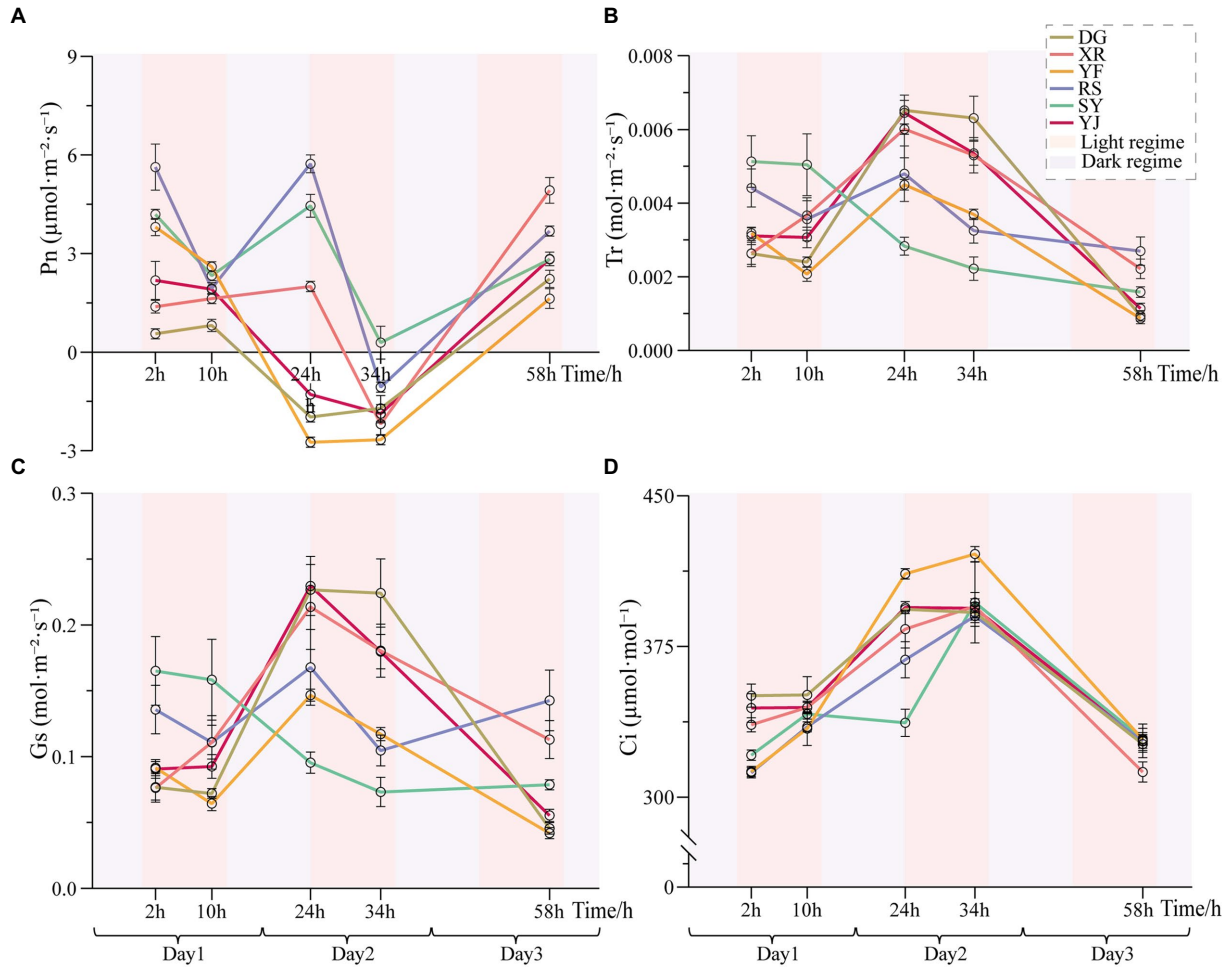

FIGURE 4
Photosynthetic parameters of *B. luminifera* populations under heat treatments. **(A)** Net photosynthetic rate (P_n). **(B)** Transpiration rate (T_r). **(C)** Stomatal conductance (G_s). **(D)** Intercellular CO_2 concentration (C_i). Error bars indicating standard error (SE).

TABLE 1 Summary data of the assembled transcripts and unigenes in *B. luminifera*.

	Transcripts	Unigene
N50 (bp)	1844	1,598
N90 (bp)	497	420
GC (%)	39.54	38.24
Sequence number	364,563	116,484
Maximum length (bp)	17,354	17,354
Mean length (bp)	1197.78	1021.26
Total length (bp)	436,667,824	118,960,472

component, and biological process), GO annotation classification was carried out to further categorize the *B. luminifera* transcripts (Figure 6B). For biological process classification, "reproduction" (26,703 unigenes), "cellular process" (23,959) and "sulfur utilization" (20,489) were the three major categories. The major cellular component categories were "protein-containing complex" (208), "cytoskeletal motor activity" (198) and "cellular anatomical entity" (190). Unigenes involved in "cytoskeletal motor activity" (156), "catalytic activity" (125) and "structural molecule activity" (69) were highly represented in molecular function subgroups (Figure 6B).

Based on blasting to other species in NR database, we also discovered that the sequences of *B. luminifera* and allied species shared similar functional information. *Carpinus fangiana* had the highest quantity of hits to *B. luminifera* (17,367), followed by *Carya illinoinensis* (4782) and *Juglans regia* (4761) (Figure 6C), indicating a high degree of homology between birch and walnut. The unigenes were discriminated through the KEGG database to explore the function of these genes involved in biological pathways. A number of 18,387 unigenes were sorted into five major KEGG functional catgaries (Figure 6D). A substantial majority of isoforms, including "Carbohydrate metabolism" (1517), "Energy metabolism" (919), and "Lipid metabolism,"(903) were dispersed in "Metabolism" category (6881) (Figure 6D).

Differential gene expression and functional enrichment analysis among different time periods

To explore the specific biological process of heat resistance in *B. luminifera*, the transcriptional level of all genes modulated by the temperature stress was measured based on Illumina platform. The expression patten of these DEGs between all 10 sample pairs was shown in Supplementary Figure S2. In total, 38,925 DEGs were identified in the heat treatment (Supplementary Table S3); gene clustering was utilized to classify DEGs with similar expression patterns for the subsequent analyses, and the FPKM values of various genes were utilized for hierarchical clustering analysis (Figure 7A); and the detailed information of up- and down-regulated genes among different time periods is shown in Figure 7B. For example, between 2 h and 10 h of heat treatment, a total of 11,647 DEGs, i.e., 5,539 up- and 6,108 down-regulated DEGs, were identified. In addition, compared to the preliminary stage of heat stress (2 h), the number of DEGs (both up- and down-regulated genes) increased with the extension of the treatment time (heat stress of 10, 24, and 34 h, and recovery 10 h). Furthermore, we compared five datasets using Venn diagrams (Figure 7C), and there were 24,547 DEGs common to the 10 comparative sampling time periods.

By analyzing the enriched KEGG terms, we had elucidated the biological functions of these DEGs. It was identified that 34 enriched KEGG pathways were identified for at least one duration of treatment (Figure 8A). When compared with the preliminary stage of 2 h heat stress, pathways (a), "Limonene and pinene degradation," "Photosynthesis-antenna proteins" and "Protein processing in endoplasmic reticulum" showed the highest enrichment. Compared to 10 h of heat stress (b), 12 enriched KEGG pathways were identified, the top 3 pathways were "Limonene and pinene degradation," "Pyruvate metabolism" and "Photosynthesis-antenna proteins." Compared to 24 h of heat stress (c), "Limonene and pinene degradation," "Phenylalanine metabolism" and "Glycine, serine and threonine metabolism" were the top 3 pathways. Compared to 34 h of heat stress (d), the top three enriched pathways were "Limonene and pinene degradation," "beta-Alanine metabolism" and "Pyruvate metabolism." Compared to the recovery samples (e), "Limonene and pinene degradation," "Phenylalanine metabolism" and "Protein processing in endoplasmic reticulum" showed the highest enrichment. Furthermore, "Limonene and pinene degradation" was markedky enriched in all time periods during the heat treatments. Figures 8B,C displayed the DEG expression profiles for the "Arginine and Proline Metabolism" and "Limonene and Pinene Degradation" pathways, respectively.

TFs have important functions in many facets for plant growing, as well as in the face of heat treatment. In this study, iTAK software (Zheng et al., 2016) was employed to forecast the TFs of *B. luminifera* under heat stress. A column diagram depicts the numbers of the top 20 largest TFs families annotated between 10 comparative sampling durations (Supplementary Figure S3). The top three transcription factor families among the 10 comparative sampling groups belong to

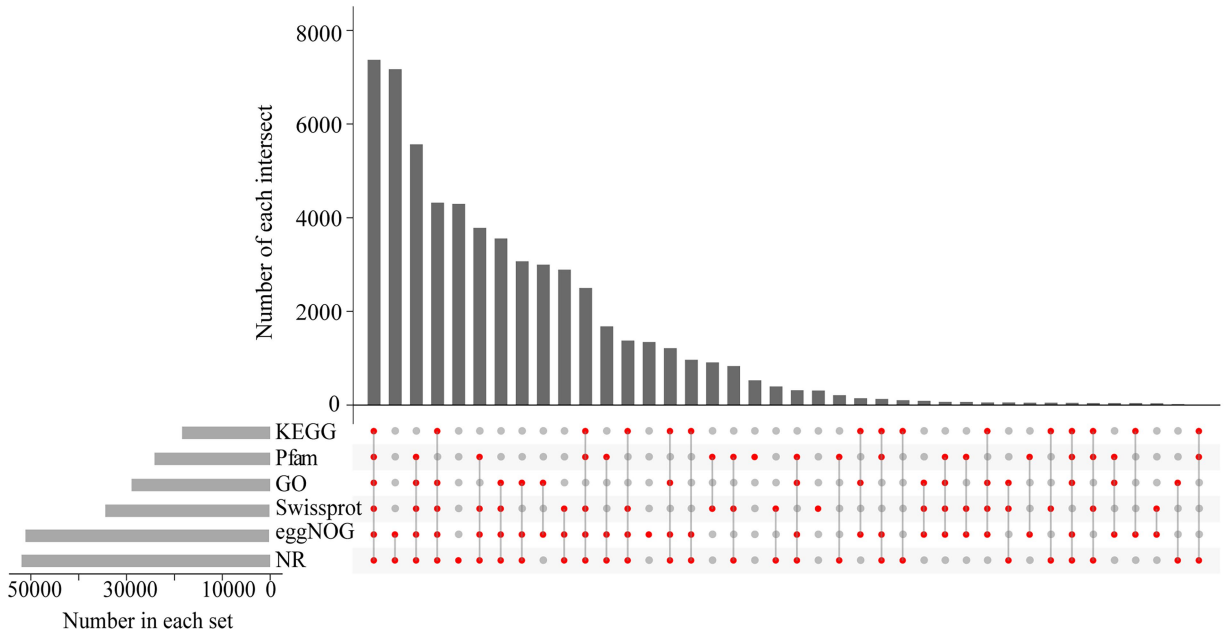

FIGURE 5
The unigenes homology searches against the protein databases.

10.3389/fpls.2022.997818

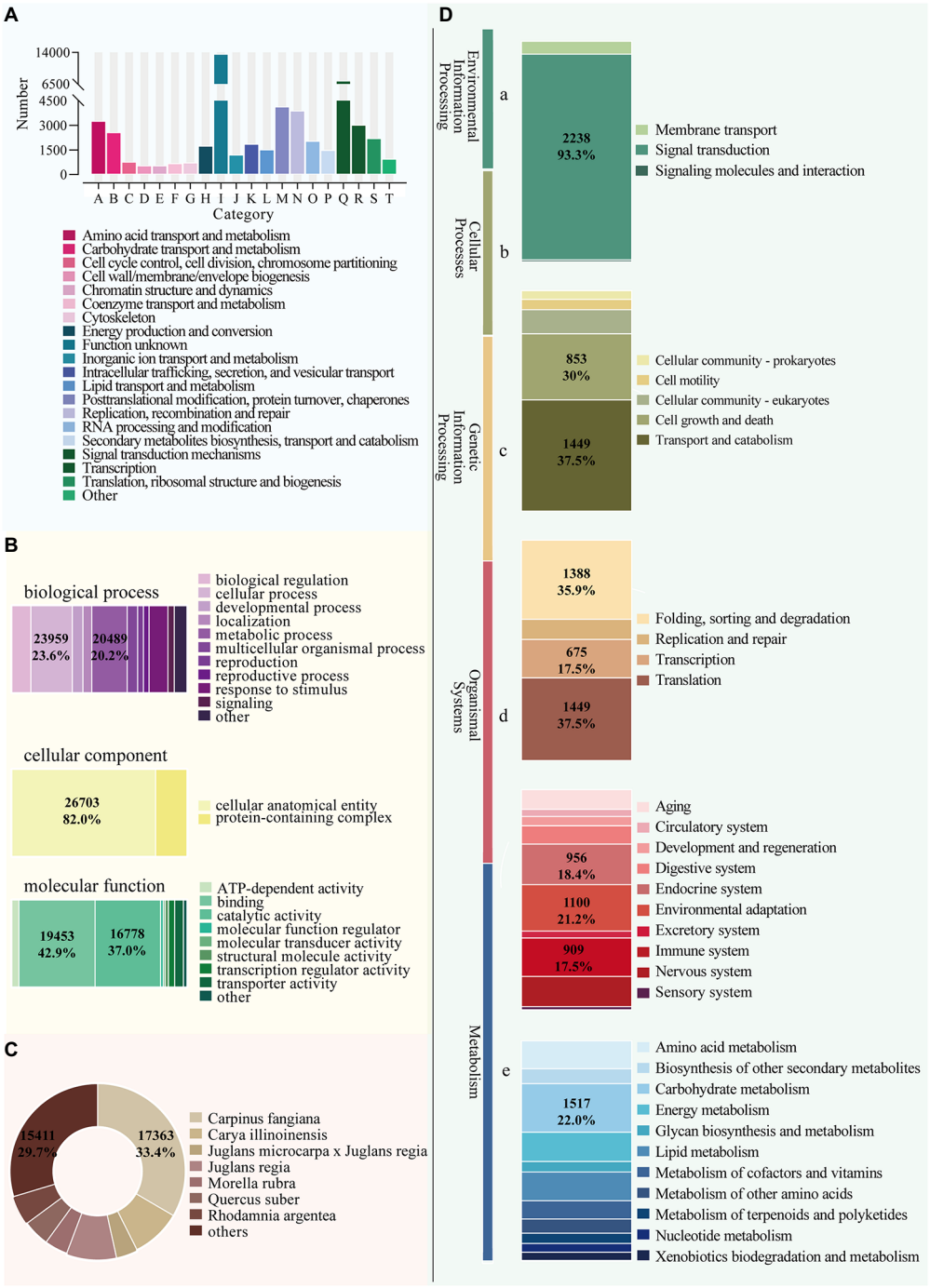

FIGURE 6
Functional annotation of *B. luminifera* unigenes generated by illumine sequencing. **(A)** Functional classification of unigenes by eggNOG analysis. **(B)** Functional classification of unigenes by GO analysis. **(C)** Functional annotation of unigenes by NR analysis. **(D)** A total of 21,184 unigenes were assigned to different KEGG terms. Different color blocks represent different terms, from top to down, "Environmental Information Processing" (a), "Cellular Processes" (b), "Genetic Information Processing" (c), "Organismal Systems" (d), and "Metabolism" (e).

the bHLH, ERF, MYB and NAC families. The expression profiles of these four TF families at different heat treatment times are presented in a heatmap (Figure 9A). Most of the genes in these families belong to three types of expression patterns. To further evaluate the second-generation sequencing data, eight transcription factor genes were chosen at random to perform qRT-PCR (Figure 9B). The gene expression profiles were comparable with the FPKM values based on second generation sequencing, confirming the reliability of the sequencing data.

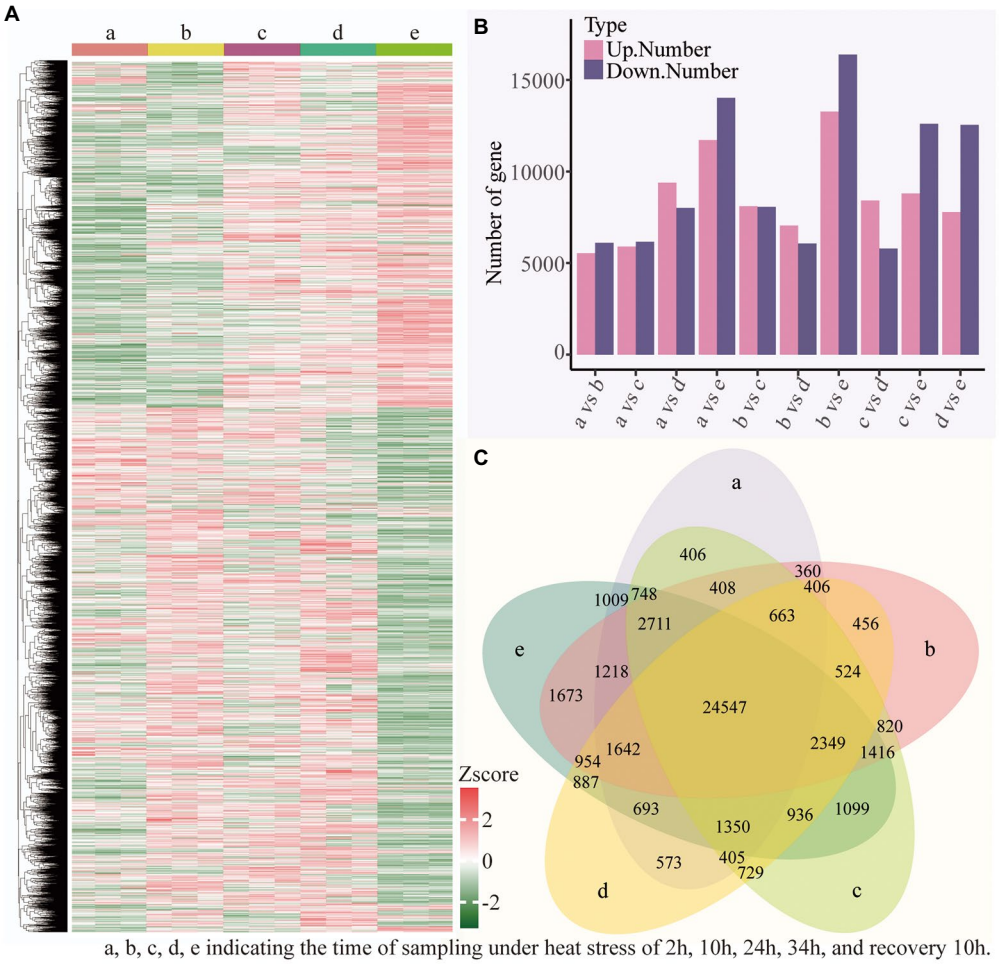

FIGURE 7
Transcriptional variations in *B. luminifera* under different treatments time period. **(A)** Hierarchical clustering analysis of the DEGs under different treatments time period. **(B)** The number of up- and down-regulated genes in different treatments time period. **(C)** Venn diagrams showed the proportions of the DEGs in different treatments time period.

Discussion

Content of osmotic adjustment substances in response to heat stress

In this study, the change in Pro differed significantly among the six *B. luminifera* populations; the DG and XR populations had higher contents under heat treatment, which may indicate those populations are more sensitive to heat stress. Pro is generally implemented in estimating plant tolerance to a variety abiotic stimulus since it contributes to control and preserve cell osmotic equilibrium and serves a key role in lessening cell redox potential responses (Misra and Saxena, 2009; Yan et al., 2015). Pro performs as a remarkably powerful non-enzymatic antioxidant implicated at plant cells' antioxidant defense (Gill and Tuteja, 2010). Additionally, heat-tolerant woody species like *P. tomentosa* and *Jatropha curcas* have also shown an increase in the Pro content of their tissues (Silva et al., 2010; Ren et al., 2019). In keeping with earlier reports, it was found that all six populations of *B. luminifera* had an increase in Pro content over the course of the heat stress's 24 h, indicating that *B. luminifera* can withstand short-term heat stress.

Pro production is a general physiological response to high-temperature treatment, representing heat stress play a negative function on plant growth, and the increased osmotic substances under high stress was advantageous to enhancing the resistance of plants with the processing time (Lv et al., 2011). The likely mechanism of Pro accumulation in *B. luminifera* leaves in the stimulus of heat stress treatment was that the generation rate of ROS gone up, membrane lipid peroxidation raised, and cell membrane lipids degraded, leading to leaves amassing considerable levels of Pro (Wang et al., 2017). In addition, the important Pro synthesis genes were identified in the arginine and Pro metabolism pathways (Figure 8B). Therefore, *B. luminifera* responds to heat stress most likely by regulating

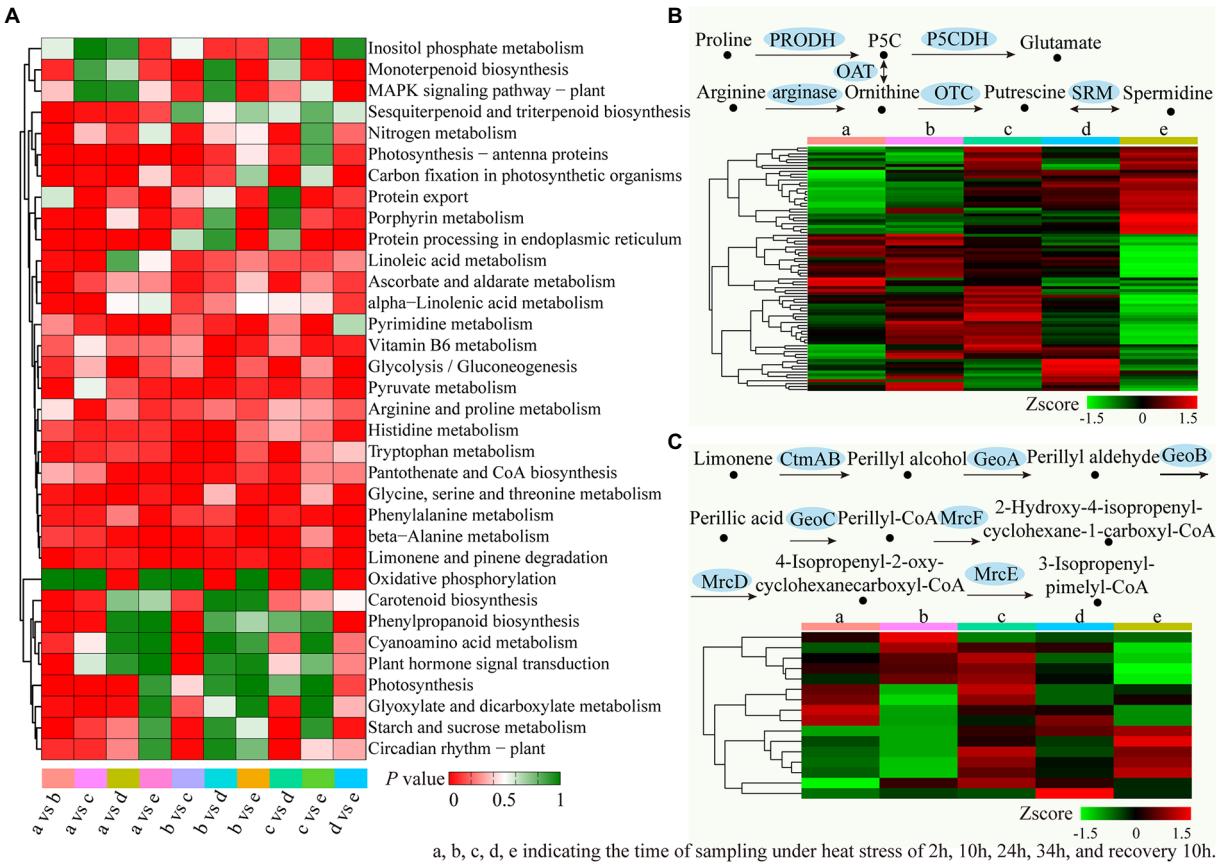

FIGURE 8
Enriched KEGG pathways analysis of the DEGs in different treatments time period. **(A)** The significant *p* values of each KEGG term in different treatments were shown by a heatmap. Red indicated significantly enriched KEGG terms. **(B)** Expression analysis of the unigenes related to the "arginine and proline metabolism" pathway. **(C)** Expression analysis of the unigenes related to the "Limonene and pinene degradation" pathway.

proline synthesis genes (e.g., P5CS) to increase Pro levels (Supplementary Table S3). The raised Pro content at high temperatures aided in enhancing *B. luminifera* resistance. Based on the change pattern of the Pro content in the six *B. luminifera* populations under heat stress, Pro can be viewed as a key indicator for assessing *B. luminifera* tolerance, and this result agrees well with previous heat treatment studies on woody plants (Chen et al., 2014; Ren et al., 2019).

Effects of heat stress on antioxidant activity

In this research, the increased antioxidant enzyme activities (SOD, POD, and CAT) suggested that cellular damage occurred when the *B. luminifera* populations were exposed to heat stress (45°C). Normally, oxidant–antioxidant balance exists in plants, which is critical for survival. However, heat stress causes ROS to be produced in greater abundance than normal (threshold value), which causes oxidative damage (Baxter et al., 2014). In response, plants can produce more antioxidant enzymes (e.g., POD and CAT) to deactivate or eliminate ROS (Ciou et al., 2011; Jin et al., 2011). Similar studies have been reported in other woody plants, e.g., *P. tomentosa* and *Jatropha curcas* (Silva et al., 2010; Ren et al., 2019). The same temperature treatment setting (45°C) were set to identify the heat-stress responsive miRNAs to disclose the miRNA-mediated regulatory network of *B. luminifera* under high temperatures (Pan et al., 2017).

Nevertheless, there were obvious differences in the responses of the different *B. luminifera* populations to heat treatment. Similar research results have also been reported for *Betula alnoides*, a related species of *B. luminifera*: the physiological indexes such as the leaf conductivity, net photosynthetic rate, transpiration and stomatal conductance were significantly different among populations under high-temperature treatment (45–50°C) (Chen et al., 2003). Overall, based on the change pattern of antioxidant enzyme (SOD, POD and CAT) activities under heat stress, the response of the RS population was in an intermediate fluctuating state among the six *B. luminifera* populations. Therefore, for the response of *B. luminifera* under heat treatment, the RS population was the

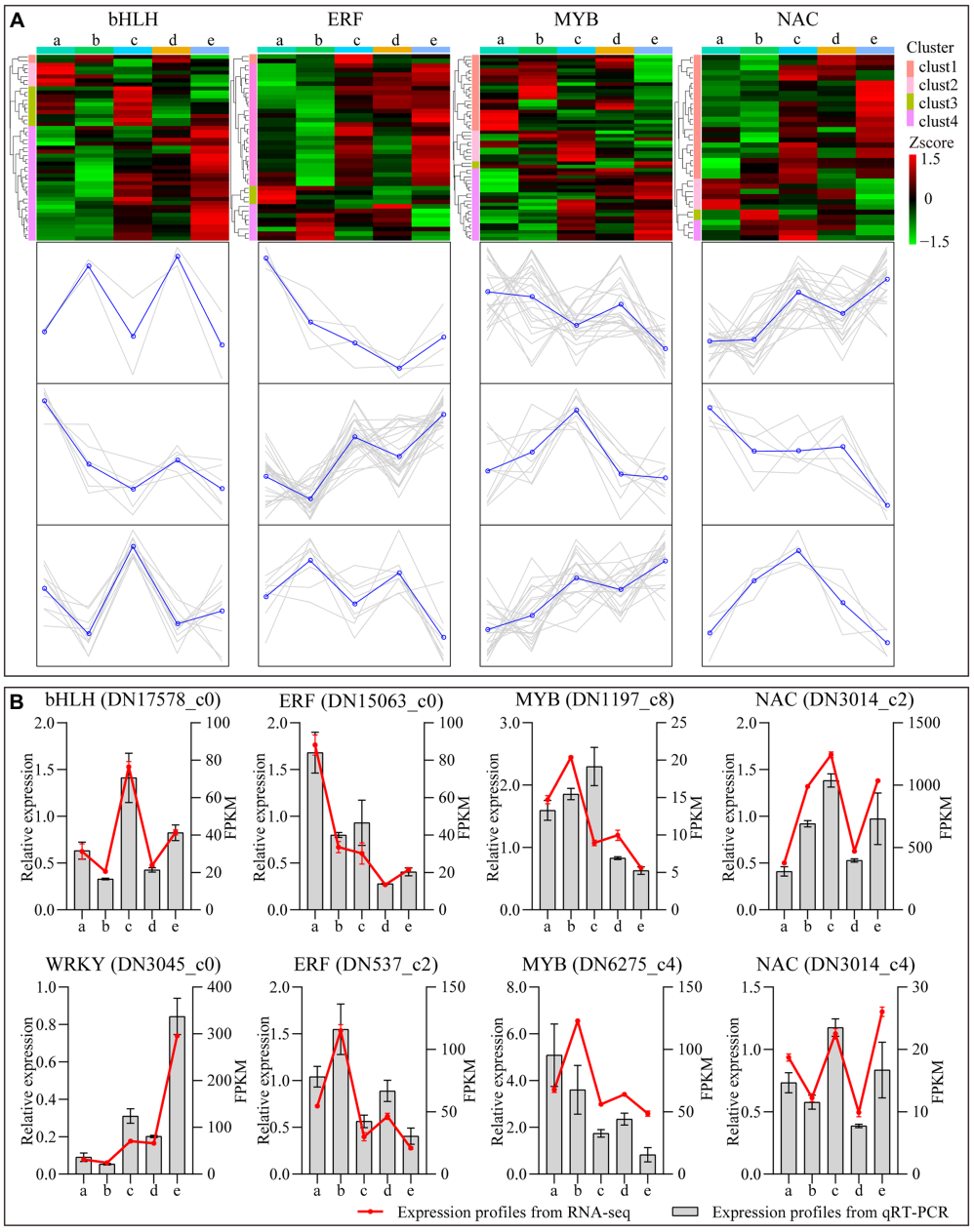

FIGURE 9
The differential expression pattern of the four TF families (MYB, NAC, and WRKY). **(A)** The differential expression pattern of the four TF families were depicted by a heatmap. **(B)** Validation of expression pattern of several TF genes by qRT-PCR.

representative of the six populations. In addition, physiological responses of different geographical populations to stress treatments that were significantly different have also been reported for other woody plants such as *Cocos nucifera* (Sun et al., 2021), *Azadirachta indica* (Zheng et al., 2008), and *Quercus variabilis* (Zhang et al., 2017). Therefore, analyzing the tolerance of *B. luminifera* seedlings from different populations under heat stress is of great help to select provenances with excellent resistance and to find artificial measures to improve the survival of seedlings.

Effects of heat stress on photosynthesis

In this study, heat stress had a significant impact on photosynthesis in all six *B. luminifera* populations. Particularly, the P_n was less than zero along with the extension of the heat treatment time. It is widely known that P_n value is equal to total photosynthetic rate subtracting respiration rate, thus P_n is the superimposed effect of photosynthesis and respiration. The P_n become negative in this study, probably because the photosynthetic rate of *B. luminifera* seedlings was less than the

respiration rate due to the damage of high temperature stress. This phenomenon also occurs in other plants under stress, the photosynthesis of plant leaves was reported to be inhibited beyond the optimal temperature range (Ashraf and Harris, 2013), other instances have included in *Anthurium* (Chen et al., 2021) and *Euphorbia pulcherrima* (Feng et al., 2009). Heat stress, in fact, will reduce plant photosynthetic capacity by causing damage to any component of the light-harvesting process, electron transport, and exploiting of assimilates in photosynthesis (Kurek et al., 2007; Sharkey and Zhang, 2010), especially for PS II, the photosynthetic system's most heat-sensitive component (Song et al., 2014). Several crucial subunits (e.g., Psb27/28) and cofactors (e.g., CP43) involved in photosynthetic electron transport are required for PS II repair throughout heat stress (Liu et al., 2011; Sakata et al., 2013), and light-harvesting-related proteins (LHCs) are also of essential for light harvesting and photoprotection (e.g., LHC sub-classes of Lhcb1-8) (Alboresi et al., 2008).

Our results also showed that there were notable variations in heat-stress responses among the different *B. luminifera* populations. Under heat stress, in the initial stage of heat treatment, the P_n values of the RS, SY, and YF *B. luminifera* populations decreased, whereas those of the DG, XR and YJ populations remained stable. In the second photoperiod, there was a significant decrease in P_n in all six populations relative to the initial stage of heat treatment. In addition, the SY and RS populations' photosynthesis recovered after a dark period, but the P_n also decreased in the new photoperiod. Interestingly, after the heat treatment stopped, P_n basically recovered, indicating that although the photosynthesis of *B. luminifera* was sensitive to heat treatment, it still had a certain degree of heat resistance. In addition, many related genes involved in the photosynthetic electron transport system in *B. luminifera* were enriched (Figure 8), indicating that the photosynthetic electron transport and photophosphorylation of *B. luminifera* were affected by heat stress. Overall, our results suggest that the photosynthesis of *B. luminifera* may be damaged under high temperature stress, caused to inhibition of the photosynthetic process in *B. luminifera*.

TFs involved in the response to high temperature treatment

In this study, we also performed transcriptome analysis on a representative population (RS) to reveal the genetic basis of *B. luminifera*'s self-regulation under heat stress. We established an approximately 98.0 GB-sized transcriptome data from *B. luminifera* heat-stressed leaves assembled into 116,484 unigenes, of which 44% were annotated against public databases. Our study will supply a substantial public data set and will assist functional gene researches of this important timber species. It is generally considered that when exposed in changing external temperatures, plants will increase their resistance through controlling gene induction and expression responded stress. According to the present study, 38,926 heat-inducible DEGs were identified. This dominance of gene expression under high temperatures shows a sustained adaptation during an extended time periods. In the public database, more than 93% of the DEGs from *B. luminifera* were annotated as homologs, suggesting that they are heat-stress responsive genes with previously reported homologs from other plants. Deeper study into these genes may reveal complete biological process underlying *B. luminifera* population responses to heat stress.

A series of TFs, e.g., bHLH, WRKY, NAC, and MYB, were identified and significantly differentially expressed with the extension of the high-temperature treatment time. In previous studies, TFs were shown to involved in stress-responsive gene transcriptional by recognizing DNA through sequence-specific pattern (Chen et al., 2014; Song et al., 2014; Ren et al., 2019). For instance, in *Manihot esculenta*, *WRKY*79 and heat shock TF 20 (*Hsf*20) enhanced melatonin biosynthesis through interacting with the promoter of N-acetylserotonin O-methyltransferase 2 (*ASMT*2) to increase disease resistance (Wei et al., 2017). In tomato, TF heat shock factor A1a (*HsfA1a*) promoted transcript accumulation of the melatonin biosynthesis gene *COMT1*, which strengthens plant resistance to cadmium (Cd) as a result (Cai et al., 2017). Therefore, the identification of TFs under stress is the key to understand the plant self-regulation network, and our research provides a genetic basis for revealing the adaptability of *B. luminifera* under heat stress.

Conclusion

In conclusion, our results demonstrated a large set of parallel changes in physiological responses (photosynthetic parameters, osmolytes and antioxidant enzymes) in *B. luminifera* populations to heat stress. The greatly differences in adaptability among different populations, meaning that there is great potential to breeding new varieties with high heat-resistance for *B. luminifera*. On the other hand, among different *B. luminifera* populations, the consistent physiological response was the activity of resistant enzymes change firstly, and then the osmoregulation substance content began to increase after continuous heat stress. In addition, the current study created an abundant transcriptome for the leaves of *B. luminifera* that respond to heat stress. And comprehensive physiological and transcriptomic analysis integrated with qRT-PCR were performed to provide fundamental knowledge about biological changes in *B. luminifera* populations under heat treatment. In general, our research provided a valuable insight into the heat resistance of *B.luminifera* populations, which can conducive to the foundation of *B. luminifera* selection and resistance evaluation for cultivation and breeding.

Data availability statement

The datasets presented in this study can be found in online repositories. The names of the repository/repositories and accession number(s) can be found at: GSA, CRA007596.

Author contributions

HH: conceptualization, supervision, and project administration. X-GH and YX: methodology. X-GH and HZ: software. X-GH, YX, and NS: validation. NS: formal analysis. PB: investigation. X-GH and PB: data curation. X-GH: writing-original draft preparation, visualization, and funding acquisition. X-GH, EL, and ZT: writing-review and editing. All authors contributed to the article and approved the submitted version.

Funding

This project was supported by Zhejiang Natural Science Foundation of China (LQ21C160002), National Science Foundation for Young Scientists of China (Grant No. 32001327), Zhejiang University Student's Science and Technology Plan and the New Talent Program (2021R412003), Key Scientific and Technological Grant of Zhejiang for Breeding New Agricultural Varieties (2021C02070-1), and Key research and development project of Zhejiang Province (2021C02037).

Conflict of interest

The authors declare that the research was conducted in the absence of any commercial or financial relationships that could be construed as a potential conflict of interest.

The handling editor declared a shared affiliation with the authors at the time of review.

Publisher's note

All claims expressed in this article are solely those of the authors and do not necessarily represent those of their affiliated organizations, or those of the publisher, the editors and the reviewers. Any product that may be evaluated in this article, or claim that may be made by its manufacturer, is not guaranteed or endorsed by the publisher.

Supplementary material

The Supplementary material for this article can be found online at: https://www.frontiersin.org/articles/10.3389/fpls.2022.997818/full#supplementary-material

References

Alboresi, A., Caffarri, S., Nogue, F., Bassi, R., and Morosinotto, T. (2008). In silico and biochemical analysis of physcomitrella patens photosynthetic antenna: identification of subunits which evolved upon land adaptation. *PLoS One* 3:e2033. doi: 10.1371/journal.pone.0002033

Allakhverdiev, S. I., Kreslavski, V. D., Klimov, V. V., Los, D. A., Carpentier, R., and Mohanty, P. (2008). Heat stress: an overview of molecular responses in photosynthesis. *Photosynth. Res.* 98, 541–550. doi: 10.1007/s11120-008-9331-0

Ashraf, M., and Harris, P. J. (2013). Photosynthesis under stressful environments: an overview. *Photosynthetica* 51, 163–190. doi: 10.1007/s11099-013-0021-6

Baxter, A., Mittler, R., and Suzuki, N. (2014). ROS as key players in plant stress signalling. *J. Exp. Bot.* 65, 1229–1240. doi: 10.1093/jxb/ert375

Cai, M., Huang, H., Ni, F., Tong, Z., Lin, E., and Zhu, M. J. P. (2018). RNA-Seq analysis of differential gene expression in *Betula luminifera* xylem during the early stages of tension wood formation. *PeerJ* 6:e5427. doi: 10.7717/peerj.5427

Cai, S. Y., Zhang, Y., Xu, Y. P., Qi, Z. Y., Li, M. Q., Ahammed, G. J., et al. (2017). HsfA1a upregulates melatonin biosynthesis to confer cadmium tolerance in tomato plants. *J. Pineal Res.* 62:e12387. doi: 10.1111/jpi.12387

Cao, J.-K., and Fang, L.-J. (2006). Studies on observation of growth rhythm of young *Betula luminifera*. *For. Res.* 19, 404–407.

Chen, W. (2006). Genetic diversity of the natural populations of *Betula luminifera*. *J. Beijing Forest. Univ.* 28, 28–34. doi: 10.13332/j.1000-1522.2006.06.005

Chen, L., Tarin, M. W. K., Huo, H., Zheng, Y., and Chen, J. (2021). Photosynthetic responses of Anthurium × 'red' under different light conditions. *Plan. Theory* 10:857. doi: 10.3390/plants10050857

Chen, Z.-G., Xie, Z.-Q., and Zheng, H.-S. (2003). The research of heat-tolerance of different provenances of *Betula alnoides* seedlings. *Acta Ecol. Sin.* 23, 2327–2332.

Chen, J., Yin, W., and Xia, X. (2014). Transcriptome profiles of *Populus* euphratica upon heat shock stress. *Curr. Genomics* 15, 326–340. doi: 10.2174/13892029150514110610183 5

Ciou, J.-Y., Lin, H.-H., Chiang, P.-Y., Wang, C.-C., and Charles, A. L. (2011). The role of polyphenol oxidase and peroxidase in the browning of water caltrop pericarp during heat treatment. *Food Chem.* 127, 523–527. doi: 10.1016/j.foodchem.2011.01.034

Feng, L., Yu, J., Tao, J., Su, J., and Zhang, C. (2009). Effects of high temperature stress on photosynthesis and chlorophyll fluorescence of *Euphorbia pulcherrima*. *J. Yangzhou Univ.* 30, 71–74.

Gill, S. S., and Tuteja, N. (2010). Reactive oxygen species and antioxidant machinery in abiotic stress tolerance in crop plants. *Plant Physiol. Biochem.* 48, 909–930. doi: 10.1016/j.plaphy.2010.08.016

Grabherr, M. G., Haas, B. J., Yassour, M., Levin, J. Z., Thompson, D. A., Amit, I., et al. (2011). Full-length transcriptome assembly from RNA-Seq data without a reference genome. *Nat. Biotechnol.* 29, 644–652. doi: 10.1038/nbt.1883

Hu, X.-G., Zhuang, H., Lin, E., Borah, P., Du, M., Gao, S., et al. (2022). Full-length transcriptome sequencing and comparative transcriptomic analyses provide comprehensive insight into molecular mechanisms of cellulose and lignin bosynthesis in *Cunninghamia lanceolata*. *Front. Plant Sci.* 13:883720. doi: 10.3389/fpls.2022.883720

Iyakaremye, V., Zeng, G., Ullah, I., Gahigi, A., Mumo, R., and Ayugi, B. (2022). Recent observed changes in extreme high-temperature events and associated meteorological conditions over Africa. *Int. J. Climatol.* 42, 4522–4537. doi: org/10.1002/joc.7485

Jin, B., Wang, L., Wang, J., Jiang, K.-Z., Wang, Y., Jiang, X.-X., et al. (2011). The effect of experimental warming on leaf functional traits, leaf structure and leaf biochemistry in *Arabidopsis thaliana*. *BMC Plant Biol.* 11, 1–10. doi: 10.1186/1471-2229-11-35

Kurek, I., Chang, T. K., Bertain, S. M., Madrigal, A., Liu, L., Lassner, M. W., et al. (2007). Enhanced thermostability of *Arabidopsis* rubisco activase improves photosynthesis and growth rates under moderate heat stress. *Plant Cell* 19, 3230–3241. doi: 10.1105/tpc.107.054171

Langmead, B., Trapnell, C., Pop, M., and Salzberg, S. L. (2009). Ultrafast and memory-efficient alignment of short DNA sequences to the human genome. *Genome Biol.* 10, R25–R10. doi: 10.1186/gb-2009-10-3-r25

Li, B., and Dewey, C. N. (2011). RSEM: accurate transcript quantification from RNA-Seq data with or without a reference genome. *BMC Bioinf.* 12, 1–16. doi: 10.1186/1471-2105-12-323

Li, B., Gao, K., Ren, H., and Tang, W. (2018). Molecular mechanisms governing plant responses to high temperatures. *J. Integr. Plant Biol.* 60, 757–779. doi: 10.1111/jipb.12701

Li, G., Hu, S., Zhao, X., Kumar, S., Li, Y., Yang, J., et al. (2021). Mechanisms of the morphological plasticity induced by phytohormones and the environment in plants. *Int. J. Mol. Sci.* 22:765. doi: 10.3390/ijms22020765

Liu, H., Huang, R. Y.-C., Chen, J., Gross, M. L., and Pakrasi, H. B. (2011). Psb27, a transiently associated protein, binds to the chlorophyll binding protein CP43 in photosystem II assembly intermediates. *Proc. Natl. Acad. Sci. U.S.A.* 108, 18536–18541. doi: 10.1073/pnas.1111597108

Liu, N., and Zhu, L. (2020). Metabolomic and transcriptomic investigation of metabolic perturbations in *Oryza sativa L.* triggered by three pesticides. *Environ. Sci. Technol.* 54, 6115–6124. doi: 10.1021/acs.est.0c00425

Love, M. I., Huber, W., and Anders, S. (2014). Moderated estimation of fold change and dispersion for RNA-seq data with DESeq2. *Genome Biol.* 15, 550–521. doi: 10.1186/s13059-014-0550-8

Luck, H. (1971). "Catalase" in *Methods of enzymatic analysis*. ed. H. W. Bergmeyer (New York, Section 3: Academic Press), 885–894.

Lv, W.-T., Lin, B., Zhang, M., and Hua, X.-J. (2011). Proline accumulation is inhibitory to *Arabidopsis* seedlings during heat stress. *Plant Physiol.* 156, 1921–1933. doi: 10.1104/pp.111.175810

Marklund, S., and Marklund, G. (1974). Involvement of the superoxide anion radical in the autoxidation of pyrogallol and a convenient assay for superoxide dismutase. *Eur. J. Biochem.* 47, 469–474. doi: 10.1111/j.1432-1033.1974.tb03714.x

Misra, N., and Saxena, P. (2009). Effect of salicylic acid on proline metabolism in lentil grown under salinity stress. *Plant Sci.* 177, 181–189. doi: 10.1016/j.plantsci.2009.05.007

Mortazavi, A., Williams, B. A., McCue, K., Schaeffer, L., and Wold, B. (2008). Mapping and quantifying mammalian transcriptomes by RNA-Seq. *Nat. Methods* 5, 621–628. doi: 10.1038/nmeth.1226

Pan, Y., Niu, M., Liang, J., Lin, E., Tong, Z., and Zhang, J. (2017). Identification of heat-responsive miRNAs to reveal the miRNA-mediated regulatory network of heat stress response in *Betula luminifera*. *Trees* 31, 1635–1652. doi: 10.1007/s00468-017-1575-x

Reddy, K. P., Subhani, S. M., Khan, P. A., and Kumar, K. B. (1985). Effect of light and benzyladenine on dark-treated growing rice (*Oryza sativa*) leaves II. Changes in peroxidase activity. *Plant Cell Physiol.* 26, 987–994. doi: 10.1111/j.1399-3054.1985.tb02822.x

Ren, S., Ma, K., Lu, Z., Chen, G., Cui, J., Tong, P., et al. (2019). Transcriptomic and metabolomic analysis of the heat-stress response of *Populus tomentosa* Carr. *Forests* 10:383. doi: 10.3390/f10050383

Sakata, S., Mizusawa, N., Kubota-Kawai, H., Sakurai, I., and Wada, H. (2013). Psb28 is involved in recovery of photosystem II at high temperature in Synechocystis sp. PCC 6803. *Biochim. Biophys. Acta Bioenerg.* 1827, 50–59. doi: 10.1016/j.bbabio.2012.10.004

Sharkey, T. D., and Zhang, R. (2010). High temperature effects on electron and proton circuits of photosynthesis. *J. Integr. Plant Biol.* 52, 712–722. doi: 10.1111/j.1744-7909.2010.00975.x

Silva, E. N., Ferreira-Silva, S. L., de Vasconcelos Fontenele, A., Ribeiro, R. V., Viégas, R. A., and Silveira, J. A. G. (2010). Photosynthetic changes and protective mechanisms against oxidative damage subjected to isolated and combined drought and heat stresses in *Jatropha curcas* plants. *J. Plant Physiol.* 167, 1157–1164. doi: 10.1016/j.jplph.2010.03.005

Skendžić, S., Zovko, M., Živković, I. P., Lešić, V., and Lemić, D. (2021). The impact of climate change on agricultural insect pests. *Insects* 12:440. doi: 10.3390/insects12050440

Song, Y., Chen, Q., Ci, D., Shao, X., and Zhang, D. (2014). Effects of high temperature on photosynthesis and related gene expression in *poplar*. *BMC Plant Biol.* 14, 1–20. doi: 10.1186/1471-2229-14-111

Sun, C., Zhang, R., Yuan, Z., Cao, H., and Martin, J. J. J. (2021). Physiology response and resistance evaluation of twenty coconut germplasm resources under low temperature stress. *Horticulturae* 7:234. doi: 10.3390/horticulturae7080234

Wang, Q.-L., Chen, J.-H., He, N.-Y., and Guo, F.-Q. (2018). Metabolic reprogramming in chloroplasts under heat stress in plants. *Int. J. Mol. Sci.* 19:849. doi: 10.3390/ijms19030849

Wang, D., Li, L., Xu, Y., Limwachiranon, J., Li, D., Ban, Z., et al. (2017). Effect of exogenous nitro oxide on chilling tolerance, polyamine, proline, and γ-aminobutyric acid in bamboo shoots (*Phyllostachys praecox f. prevernalis*). *J. Agr. Food. Chem.* 65, 5607–5613. doi: 10.1021/acs.jafc.7b02091

Wei, Y., Liu, G., Bai, Y., Xia, F., He, C., and Shi, H. (2017). Two transcriptional activators of N-acetylserotonin O-methyltransferase 2 and melatonin biosynthesis in cassava. *J. Exp. Bot.* 68, 4997–5006. doi: 10.1093/jxb/erx305

Yamamoto, Y., Aminaka, R., Yoshioka, M., Khatoon, M., Komayama, K., Takenaka, D., et al. (2008). Quality control of photosystem II: impact of light and heat stresses. *Photosynth. Res.* 98, 589–608. doi: 10.1007/s11120-008-9372-4

Yan, Z., Zhang, W., Chen, J., and Li, X. (2015). Methyl jasmonate alleviates cadmium toxicity in *Solanum nigrum* by regulating metal uptake and antioxidative capacity. *Biol. Plantarum* 59, 373–381. doi: 10.1007/s10535-015-0491-4

Zhang, J., Huang, H., Tong, Z., Cheng, L., Liang, Y., and Chen, Y. (2010). Genetic diversity in six natural populations of *Betula luminifera* from southern China. *Biodivers. Sci.* 18:233. doi: 10.3724/SP.J.1003.2010.233

Zhang, X., Teixeira da Silva, J. A., Niu, M., Li, M., He, C., Zhao, J., et al. (2017). Physiological and transcriptomic analyses reveal a response mechanism to cold stress in *Santalum album L.* leaves. *Sci. Rep.* 7, 1–18. doi: 10.1038/srep42165

Zhang, Q., Wei, Z., Yan, T., and Geng, X. (2021). Identification and evaluation of genetic diversity of agronomic traits in oat germplasm resources. *Acta Agrestia Sinica* 29, 309–316.

Zhang, C., Xu, B., Zhao, C.-R., Sun, J., Lai, Q., and Yu, C. (2019). Comparative *de novo* transcriptomics and untargeted metabolomic analyses elucidate complicated mechanisms regulating celery (*Apium graveolens L.*) responses to selenium stimuli. *PLoS One* 14:e0226752. doi: 10.1371/journal.pone.0226752

Zheng, Y., Jiao, C., Sun, H., Rosli, H. G., Pombo, M. A., Zhang, P., et al. (2016). iTAK: a program for genome-wide prediction and classification of plant transcription factors, transcriptional regulators, and protein kinases. *Mol. Plant* 9, 1667–1670. doi: 10.1016/j.molp.2016.09.014

Zheng, Y., Peng, X., and Zhang, Y. (2008). Photosynthetic ecophysiological responses of different *Azadirachta indica* provenances to change of temperature. *For. Res.* 21, 131–138.

frontiers | Frontiers in Plant Science

TYPE Original Research
PUBLISHED 29 September 2022
DOI 10.3389/fpls.2022.999990

OPEN ACCESS

EDITED BY
Tongli Wang,
University of British Columbia, Canada

REVIEWED BY
Behnam Asgari Lajayer,
University of Tabriz, Iran
Om Prakash Narayan,
Tufts University, United States

*CORRESPONDENCE
Huwei Yuan
hwyuan@zafu.edu.cn
Bingsong Zheng
bszheng@zafu.edu.cn

†These authors have contributed equally to this work

SPECIALTY SECTION
This article was submitted to Functional Plant Ecology, a section of the journal Frontiers in Plant Science

RECEIVED 21 July 2022
ACCEPTED 29 August 2022
PUBLISHED 29 September 2022

CITATION
Yang Y, Mei J, Chen J, Yang Y, Gu Y, Tang X, Lu H, Yang K, Sharma A, Wang X, Yan D, Wu R, Zheng B and Yuan H (2022) Expression analysis of *PIN* family genes in Chinese hickory reveals their potential roles during grafting and salt stress. *Front. Plant Sci.* 13:999990. doi: 10.3389/fpls.2022.999990

Expression analysis of *PIN* family genes in Chinese hickory reveals their potential roles during grafting and salt stress

Ying Yang[1,2†], Jiaqi Mei[1,2†], Juanjuan Chen[1,2,3†], Ying Yang[1,2], Yujie Gu[1,2], Xiaoyu Tang[1,2], Huijie Lu[1,2], Kangbiao Yang[1,2], Anket Sharma[1,2], Xiaofei Wang[1,2], Daoliang Yan[1,2], Rongling Wu[1,2], Bingsong Zheng[1,2*] and Huwei Yuan[1,2*]

[1]State Key Laboratory of Subtropical Silviculture, Zhejiang A&F University, Hangzhou, China, [2]Zhejiang Provincial Key Laboratory of Forest Aromatic Plants-based Healthcare Functions, Zhejiang A&F University, Hangzhou, China, [3]Research Institute of Subtropical Forestry, Chinese Academy of Forestry, Hangzhou, China

Grafting is an effective way to improve Chinese hickory while salt stress has caused great damage to the Chinese hickory industry. Grafting and salt stress have been regarded as the main abiotic stress types for Chinese hickory. However, how Chinese hickory responds to grafting and salt stress is less studied. Auxin has been proved to play an essential role in the stress response through its re-distribution regulation mediated by polar auxin transporters, including PIN-formed (PIN) proteins. In this study, the *PIN* gene family in Chinese hickory (*CcPINs*) was identified and structurally characterized for the first time. The expression profiles of the genes in response to grafting and salt stress were determined. A total of 11 *CcPINs* with the open reading frames (ORFs) of 1,026–1,983 bp were identified. Transient transformation in tobacco leaves demonstrated that CcPIN1a, CcPIN3, and CcPIN4 were localized in the plasma membrane. There were varying phylogenetic relationships between *CcPINs* and homologous genes in different species, but the closest relationships were with those in *Carya illinoinensis* and *Juglans regia*. Conserved N- and C-terminal transmembrane regions as well as sites controlling the functions of CcPINs were detected in CcPINs. Five types of *cis*-acting elements, including hormone- and stress-responsive elements, were detected on the promoters of *CcPINs*. *CcPINs* exhibited different expression profiles in different tissues, indicating their varied roles during growth and development. The 11 *CcPINs* responded differently to grafting and salt stress treatment. *CcPIN1a* might be involved in the regulation of the grafting process, while *CcPIN1a* and *CcPIN8a* were related to the regulation of salt stress in Chinese hickory. Our results will lay the foundation for understanding the potential regulatory functions of *CcPIN* genes during grafting and under salt stress treatment in Chinese hickory.

KEYWORDS

***Carya cathayensis*, *PIN*, transport, auxin, salt, grafting**

Introduction

Auxin is the first discovered phytohormone (Went, 1935) and plays an important role during different growth stages of plants (Yu et al., 2022), including gametogenesis, seed germination, root elongation, vascular patterning, and blossoming (Zhao, 2010). In addition, an important function of auxin is its regulation of the responses of plant species to different biotic and abiotic stresses (Kapazoglou et al., 2020; Dastborhan et al., 2021; Mearaji et al., 2021; Zhang et al., 2022). The functioning of auxin is closely related to its homeostatic regulation, which involves biosynthesis, conjugate formation, transport, and degradation (Zhang and Peer, 2017). Following biosynthesis, transport is the key step for auxin functioning (Gomes and Scortecci, 2021) because the site of action is usually different from that of synthesis.

Plants have evolved two methods for transporting auxin: the long-distance network (transporting auxin through phloem) and the cell-to-cell transport network (also named polar auxin transport) (Muday and DeLong, 2001; Robert and Friml, 2009). In plants, polar auxin transport is mainly mediated by AUXIN/LIKE AUXIN proteins (AUX/LAX, responsible for auxin influx), PIN-formed proteins (PIN, responsible for auxin efflux), PIN-LIKES (PILS, responsible for auxin transport between the cytosol and endoplasmic reticulum), and ATP-binding cassette subfamily B proteins (ABCB, responsible for auxin influx/efflux) (Swarup and Peret, 2012; Mohanta et al., 2018; Sauer and Kleine-Vehn, 2019). PIN proteins play major roles in auxin efflux because their polar localizations are always consistent with the directionality of auxin (Zhou and Luo, 2018).

PIN is a gene family composed of multiple genes with similar or different structures and functions. *AtPIN1* was the first discovered PIN protein in *Arabidopsis*. The mutant of *PIN1*, *pin1*, has no leaves or flowers in cauline inflorescence (Kuhlemeier and Reinhardt, 2001) and resembles pins, which is the reason why PIN1 and the subsequent proteins in this family were named PIN-formed proteins (PINs). PIN family proteins contain conserved N- and C-terminal transmembrane domains and intracellular central hydrophilic loops. There are two types of PIN proteins categorized according to the differences in structures of the central hydrophilic loop: canonical PIN proteins with a long central hydrophilic loop and non-canonical PIN proteins with a short hydrophilic loop. In *Arabidopsis*, canonical PIN proteins (AtPIN1, 2, 3, 4, and 7) are localized to the plasma membrane (PM) and mediate auxin efflux to the extracellular space (Bennett et al., 2014). Non-canonical PINs (AtPIN5 and 8) are localized to the endoplasmic reticulum (ER) and mediate intracellular auxin transport between the cytoplasm and ER (Mravec et al., 2009; Sauer and Kleine-Vehn, 2019). AtPIN6 possesses a long hydrophilic loop and is located on the PM and ER, and thus is classified as a non-canonical PIN (Bennett et al., 2014).

The functions of PIN proteins have been well studied in *Arabidopsis*. AtPIN1 regulates the shoot apical meristem, root elongation, and the development of xylem (Blilou et al., 2005; Alabdallah et al., 2017). AtPIN2 influences root gravitropism and responds to salt stress (Wang et al., 2019; Gibson et al., 2020). AtPIN3 is mainly expressed in root and vascular tissues. It regulates auxin distribution in roots, participates in lateral root growth, and responds to light and gravity (Blilou et al., 2005; Zhai et al., 2021; Li et al., 2022). Similar to AtPIN3, AtPIN4 is related to light and gravity responses. In addition, AtPIN4 participates in auxin flow to the quiescent center (Bureau et al., 2010). AtPIN5 mediates not only the transport of auxin from the cytoplasm to the ER, but also regulates auxin homeostasis and metabolism (Mravec et al., 2009). AtPIN6 regulates lateral root formation (Sauer and Kleine-Vehn, 2019). The functions of AtPIN7 are similar to those of AtPIN3 and AtPIN4, and it participates in the gravimetric response of roots (Lewis et al., 2011). The function of AtPIN8 is the opposite of that of AtPIN5, transporting auxin from the ER to the cytoplasm (Ding et al., 2012). In addition, there is functional redundancy for some PIN proteins (Blilou et al., 2005; Wang et al., 2021). For example, the mutant genes *pin1* and *pin2* exhibit functional redundancy regarding the regulation of root meristem and root length (Vieten et al., 2005).

In addition to developmental functions, *PIN* family genes also participate in the regulation of abiotic stress (Yu et al., 2017). For example, in pepper (*Capsicum annuum*) and *Sorghum bicolor*, the expression profiles of *PIN* genes were changed under high salt treatment (Shen et al., 2010; Zhang et al., 2018). The process of grafting creates wounding stress, which also influences the expression of *PIN* genes (Melnyk, 2017; Sharma and Zheng, 2019). The overexpression of *AtPINs-GUS* in *Arabidopsis* shows that *AtPINs* are expressed in the grafted union, indicating their involvement in grafting regulation (Wang et al., 2014). Transcriptome sequencing of *Arabidopsis* grafting also supports this conclusion (Melnyk et al., 2018).

Chinese hickory (*Carya cathayensis* Sarg.), belonging to the Juglandaceae family, is one of the most important trees economically in the Zhejiang and Anhui Provinces of China. Nuts from Chinese hickory trees are rich in nutritional compounds, including polyunsaturated fatty acids, phenolics, and flavonoids (Huang et al., 2022). However, a long juvenile phase and narrow distribution have restricted the development of the Chinese hickory industry. Grafting is an effective way to solve these problems. In addition, soil salinization has limited the development of the Chinese hickory industry.

To date, members of the *PIN* gene family have not been identified, and their potential roles during grafting and salt stress treatment in Chinese hickory are still unknown. In this study, *PIN* family genes in Chinese hickory were cloned and structurally analyzed, and their expression profiles in response to grafting and salt stress treatment were determined. Our

results will lay the foundation for revealing the molecular mechanism of *PIN* family genes in regulating grafting and salt stress in Chinese hickory.

Materials and methods

Identification of *PIN* family genes in Chinese hickory

Candidate gene sequences of PIN in Chinese hickory (*CcPINs*) were identified from the published genome (Huang et al., 2019). The process used to identify genes was the same as that used in a previous study (Yang et al., 2021). Hidden Markov model (HMM) profiles of the PIN domain (PF03547) were used for analysis. TBtools (Toolbox for Biologists, v1.098745) was used for the preliminary screening of *PIN* genes (Chen et al., 2020). The identified *CcPINs* were named according to their phylogenetic relationships with the homologs in *Arabidopsis* (**Supplementary Figure 1**).

Structural analysis of *CcPINs*

In addition to predicting the functions of *CcPINs* in Chinese hickory, the PIN proteins in Chinese hickory and 14 other species were chosen to undergo phylogenetic relationship analysis. The PIN proteins of 11 species were obtained from previous studies. PINs of the other three species (including *Juglans regia*, *Carya illinoinensis*, and *Nymphaea tetragona*) were analyzed based on the genome in Phytozome v13.[1] The identified method was the same as that used for Chinese hickory, as stated above. The PIN protein information for 15 species is shown in **Supplementary Table 1**.

The phylogenetic tree between PIN proteins in the 15 species was constructed by MEGAX using the neighbor-joining method and a bootstrap of 1,000 replicates. ClustalW was used for multiple sequence alignment analysis of CcPINs. The motif distribution of CcPIN proteins was predicted by MEME Suite.[2] The motif number was set to 8, and the maximum and minimum numbers of amino acids were set to 50 and 6, respectively. The online tool ExPASy was used to analyze biochemical information (length, molecular weight, isoelectric point, and size) of *CcPIN* genes. The transmembrane regions of CcPIN proteins were predicted by the TMHMM2 tool (TMHMM–2.0).[3] "Search for CARE" on the PlantCare website[4] was used to identify *cis*-acting regulatory elements on the promoters of *CcPIN* genes.

1 https://phytozome-next.jgi.doe.gov/
2 https://meme-suite.org/tools/meme
3 https://services.healthtech.dtu.dk/service.php?TMHMM-2.0
4 http://bioinformatics.psb.ugent.be/webtools/plantcare/html/

Plant material, treatment, and sampling

One-year-old Chinese hickory seedlings were used for tissue-specific expression analysis, while 2-year-old Chinese hickory seedlings were used as rootstocks for grafting and materials for salt stress treatment. Seedlings were planted in seedling pots with a diameter of 17 cm and height of 22 cm and cultivated in the greenhouse of Zhejiang A&F University. One seedling was planted in each pot with 5 L of soil. The soil formula included 50% peat, 13% pastoral soil, 15% organic fertilizer, 5% exocarp, 10% agricultural bran, 5% perlite, and 2% release fertilizer. The seedlings were grown under the following conditions: temperature of 25 ± 3°C, humidity of 60–70%, and photoperiod of 12-h light/12-h dark. The seedlings were watered every 5 days. Tobacco (*Nicotiana benthamiana*) was cultivated in the culture room at the temperature of 22°C, humidity of 60–70%, and photoperiod of 16-h light/8-h dark. For subcellular localization analysis, 45-day-old tobacco leaves were used.

For the grafting experiment, 2-year-old seedlings with similar phenotypes were used for rootstocks, and the grafting operation was conducted on April 20th, 2018. One-year-old branches (7–8 cm in length) with a new bud collection on the fruit-bearing trees were chosen as scions. For salt stress treatment, the 2-year-old seedlings were treated with 150 mm NaCl (Shanghai Hushi Laboratorial Equipment Co., Ltd., China) solution three times every 3 days, following the same method as a previous study (Chen et al., 2015). The equivalent water treatment was used for the control check (CK).

Graft unions were collected at 0, 3, 7, and 14 days after grafting, representing the initiation stage, isolation layer formation stage, callus formation and isolating layer disappearance stage, and vascular bridge formation and linkage stage during Chinese hickory grafting, respectively, as detected by cytological observation (Liu et al., 2009). In each treatment, three graft unions were mixed together and regarded as a single sample. For salt stress treatment, samples from different tissues, including roots, stems, and leaves, were collected after 0, 1, 3, and 10 days of treatment, representing the initial-, short-, medium- and long-term treatment stages as reported in similar studies of other woody plants (Chen et al., 2015; Zhao et al., 2015; Hang et al., 2020; Huang et al., 2020). The day on which the seedlings were treated with NaCl solution for the first time was regarded as day 0. For each tissue, collections from five different seedlings were mixed together and regarded as a single sample. For tissue-specific expression analysis, different tissues, including roots, stems, leaves, and shoots, of 1-year-old Chinese hickory seedlings were collected in early spring (on April 16, 2022), representing the fast-growing stage of the seedlings. For each tissue, collections from five different seedlings were mixed together and regarded as a single sample. All the samples were wrapped in aluminum foil, immediately immersed in liquid nitrogen, and stored in an ultra-low temperature refrigerator (−80°C) for future use.

RNA extraction, cDNA synthesis, and real-time quantitative PCR analysis

The total RNAs of Chinese hickory were extracted using a MiniBEST Universal RNA Extraction Kit [Code No. 9767, Takara Biomedical Technology (Beijing) Co., Ltd., China]. For the grafting experiment, the rootstocks and scions in a single sample were separated from each other, and the cells at the conjunction surfaces of the rootstocks and scions were scraped using blades, respectively. Total RNAs of the rootstocks and scions were extracted separately. For the salt stress experiment, the total RNAs of the roots, stems, and leaves collected at different time points were extracted separately. For the tissue-specific experiment, the total RNAs of the roots, stems, leaves, and shoots of 1-year-old seedlings were extracted separately. The cDNA used for cloning was synthesized using the PrimeScript^{TM} IV 1st strand cDNA Synthesis Mix [Code No. 6215A, Takara Biomedical Technology (Beijing) Co., Ltd., China]. PrimeSTAR Max DNA Polymerase [Code No. R045Q, Takara Biomedical Technology (Beijing) Co., Ltd., China] was used for PIN gene cloning. The cDNA used for Real-Time Quantitative PCR analysis (qRT-PCR) was obtained using the PrimeScript^{TM} RT Master Mix [Code No. RR036A, Takara Biomedical Technology (Beijing) Co., Ltd., China].

Real-Time Quantitative PCR analysis primers were designed on the National Center for Biotechnology Information (NCBI) primer prediction website.[5] The *CcActin* gene was used as the internal standard for normalization. The primers for qRT-PCR are listed in **Supplementary Table 2**. The methods used for qRT-PCR were followed according to a previously published study (Yuan et al., 2018). The qRT-PCR analysis was replicated at least three times.

Subcellular localization analysis

The coding sequence of *CcPINs* was cloned from the cDNA library of Chinese hickory and inserted into the modified pCAMBIA1300-GFP vector. Then, the obtained 35S:CcPINs-GFP was translated into *Escherichia coli* Trans1-T1 (TransGen Biotech Co., Ltd., China) and sequenced by Sangon Biotech (Shanghai) Co., Ltd., China. Plasmids from the identified strains were extracted and transformed into *Agrobacterium* strain GV3101 competent cells (AC1001, Shanghai Weidi Biotechnology Co., Ltd., China). Transient transformation of 45-day-old tobacco leaves was performed as previously described (Yamaji et al., 2009). The pm-rk (plasma membrane marker with red fluorescence, Nelson et al., 2007) was transiently co-transformed into tobacco leaves with *CcPINs*. After culturing for 48 h, the fluorescence signal in the transformed tobacco leaves was detected using a confocal microscope (LSM 880, Zeiss, Germany) with 488 and 594 nm argon lasers.

Statistical analysis and figure preparation

To calculate the relative expression levels of *CcPIN* genes, the $2^{-\Delta\Delta CT}$ method, introduced by Schmittgen and Livak (2008), was used. A one-way analysis of variance (ANOVA) and multiple comparisons [the least significant difference (LSD) method] were conducted using SPSS Statistics (version 17.0) to analyze the expression differences of *CcPIN* genes among different tissues and treatments.

The histogram and line figures were drawn using Microsoft Excel 2019. The phylogenetic tree was drawn using Mega X and embellished using Fig. Tree (v1.4.4). The figures illustrating motifs and gene structures were drawn using TBtools (Toolbox for Biologists, v1.098745). Finally, the figures were merged by Adobe Photoshop (version 2020).

Results

Identification of *PIN* family genes in Chinese hickory

Eleven *CcPIN* genes were identified, and the corresponding information is displayed in **Table 1**. The ORF length of the *CcPINs* ranged from 1,026 bp (CcPIN8a) to 1,983 bp (CcPIN3), encoding proteins with between 341 and 660 amino acids. The molecular weights of CcPINs ranged from 37,338.75 Da (CcPIN8a) to 72,046.05 Da (CcPIN3), and the predicted isoelectric points (pI) varied from 6.42 (CcPIN5) to 9.39 (CcPIN8a). The number of exons for *CcPIN* genes ranged from 5 to 7. To explore the potential locations where CcPINs perform their functions, several CcPINs were detected by subcellular localization. Transient transformation of *CcPINs* to tobacco leaves showed that CcPIN1a, CcPIN3, and CcPIN4 were expressed on the PM (**Figure 1**).

Phylogenetic relationships of *PIN* family proteins in Chinese hickory and other species

To predict the potential functions of *PIN* family genes in Chinese hickory, a phylogenetic tree was constructed to explore the phylogenetic relationships between the 11 PIN proteins in Chinese hickory and 121 PIN proteins from 14 other plant species. The 15 plant species used to construct

5 https://www.ncbi.nlm.nih.gov/tools/primer-blast/

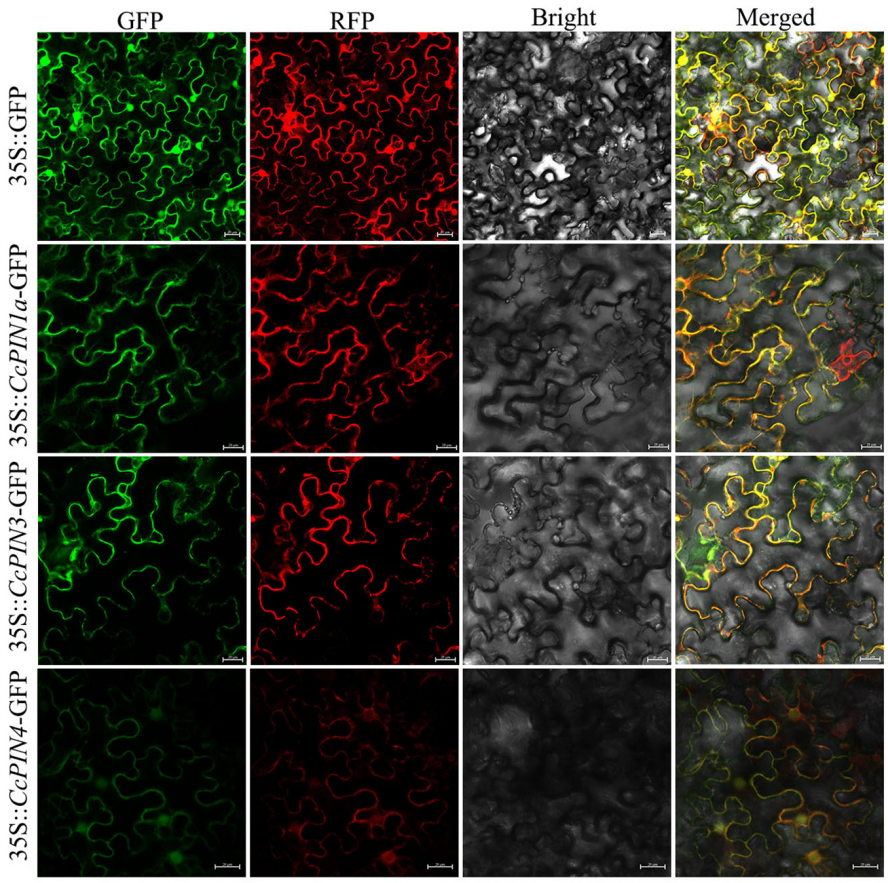

FIGURE 1
The subcellular localization of CcPIN1a, CcPIN3, and CcPIN4. The fluorescence images were captured in a dark field for green and red fluorescence, in a white field for the morphology of the cell, and in combination. GFP, green fluorescent protein fluorescence; RFP, red fluorescent protein fluorescence; Bright, bright field; Merged, GFP/RFP/bright field overlay. Bar = 20 μm.

the phylogenetic tree belonged to 5 types of charophytes, bryophytes, lycophytes, monilophytes, gymnosperms, and angiosperms according to the consensus phylogeny reported by Doyle (2018). Detailed information on the 132 PIN proteins is shown in **Supplementary Table 1**. A total of eight groups (I, II, III, IV, V, VI, VII, and VIII) were identified (**Figure 2A**). There was significant variation in the number of PIN proteins in the different groups. There was only one protein in Group I, three proteins in Group II, seven proteins in Group VI, and 11 proteins in Group VII. The number of proteins in Groups III, IV, and V was 22, 19, and 23, respectively, and the highest number of proteins was in Group VIII, with 46 (**Figure 2B**).

The number of PIN proteins varied in different species. There was only one PIN protein in *Klebsormidium flaccidium* and *Picea abies*, while the number of PIN proteins in the other 13 species changed from 4 to 15 (**Figure 2B**). In addition, there were more PINs (8–15) in angiosperm species than those in the other types (**Figure 2B**). Similar to *C. illinoinensis* and *J. regia*, the PINs in *C. cathayensis* were distributed in Groups III, IV, V, VII, and VIII, with the largest number of PINs in Group VIII. Most PINs in *Oryza sativa*, *Zea mays*, and *S. bicolor* were distributed in Groups III, IV, VI, VII, and VIII (**Figures 2A,B**).

Multiple sequence alignment, motif, and gene structure analysis of CcPINs

Multiple sequence alignment of CcPIN proteins is shown in **Figure 3**, which displays the high level of conservation in the N-terminal and C-terminal regions. There were short sequences in the middle region for CcPIN5, CcPIN8a, and CcPIN8b, with long sequences for the other CcPINs. In addition, "F165," the site controlling the distribution of PIN proteins on PM, the phosphorylation site "TPRXS," and the conserved "NPXXY" site were detected (**Figure 3**). Motif analysis of the eleven CcPIN proteins was performed using the MEME Suite, with the eight conversed motifs set. Motif 6 and Motif 8 were not detected in short CcPINs (CcPIN5 and CcPIN8) (**Figures 4A,B**). The conserved element "NPXXY" was found in motif 5 (**Figure 4D**), and the phosphorylated site "TPRXS" of MPK 4/6 kinases

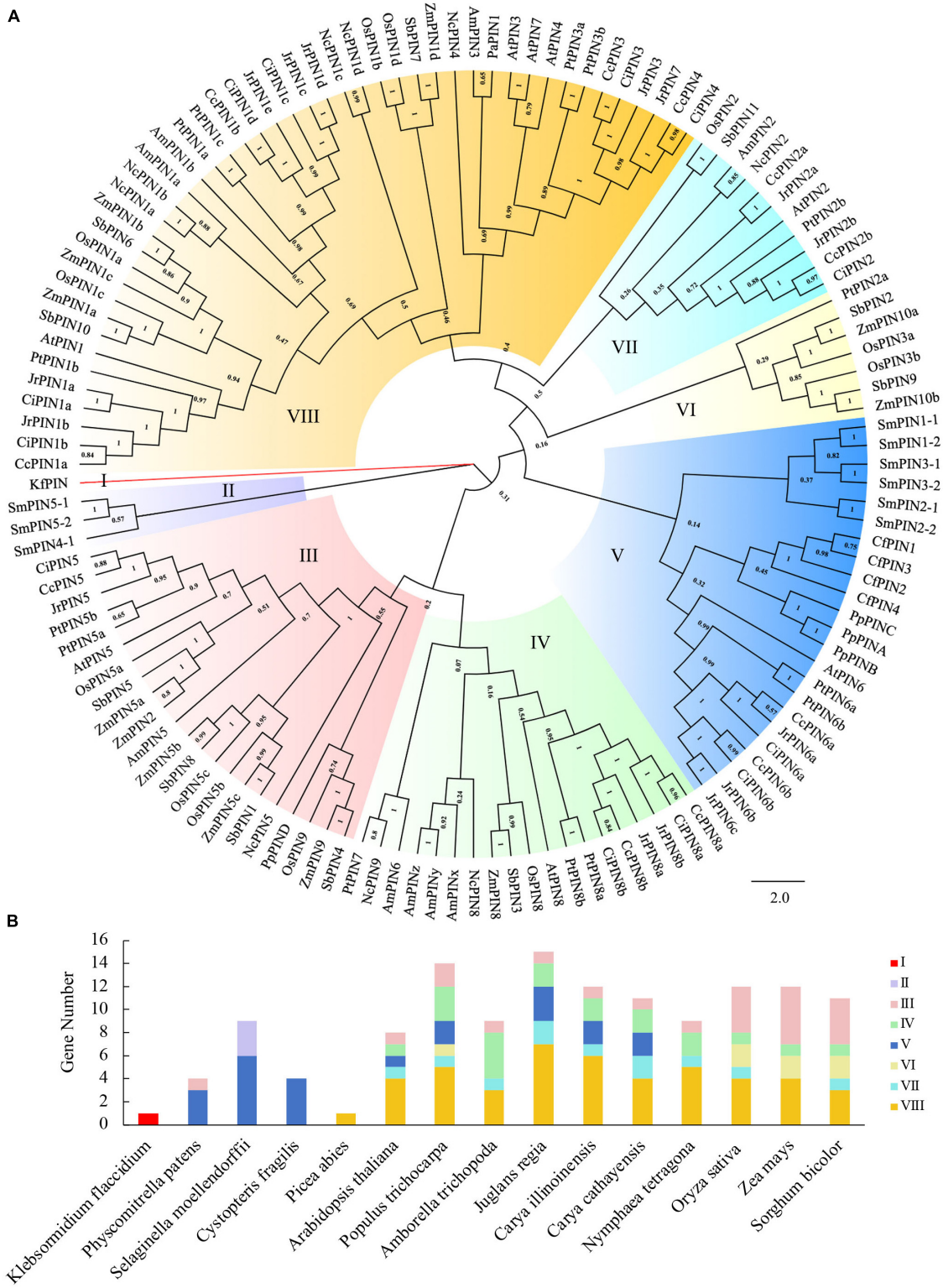

FIGURE 2
Phylogenetic analysis of PIN proteins from 15 species. **(A)** The phylogenetic tree. **(B)** The number and distribution of PINs in different species. Kf, *Klebsormidium flaccidium*; Pp, *Physcomitrella patens*; Sm, *Selaginella moellendorffii*; Cf, *Cystopteris fragilis*; Pa, *Picea abies*; At, *Arabidopsis thaliana*; Pt, *Populus trichocarpa*; Am, *Amborella trichopoda*; Jr, *Juglans regia*; Ci, *Carya illinoinensis*; Cc, *Carya cathayensis*; Nc, *Nymphaea tetragona*; Os, *Oryza sativa*; Zm, *Zea mays*; Sb, *Sorghum bicolor*.

10.3389/fpls.2022.999990

TABLE 1 Information on *CcPIN* genes and properties of their deduced proteins in Chinese hickory.

Gene name	Locus ID	Genomic location	Exon number	ORF (bp)	Length (aa)	pI	Mol wt (Da)	Ortholog with *Arabidopsis*
CcPIN1a	CCA123S0022	scaffold50249:506539-510501	6	1,809	602	8.81	65,648.89	AtPIN1
CcPIN1b	CCA070S0034	scaffold23721:408391-412462	6	1,779	592	8.95	63,882.92	AtPIN1
CcPIN2a	CCA088S0033	scaffold31775:857604-860474	6	1,524	507	8.76	55,524.96	AtPIN2
CcPIN2b	CCA067S0073	scaffold21864:981746-985490	6	1,926	641	9.22	69,513.49	AtPIN2
CcPIN3	CCA141OS0065	scaffold60275:585325-589367	6	1,983	660	7.69	72,046.05	AtPIN3
CcPIN4	CCA085TS0074	scaffold29914:809434-813085	6	1,932	643	8.45	70,068.83	AtPIN4
CcPIN5	CCA088S0013	scaffold31775:259812-263129	5	1,086	361	6.42	39,945.26	AtPIN5
CcPIN6a	CCA094S0041	scaffold35145:386749-392264	7	1,653	550	9.19	60,544.85	AtPIN6
CcPIN6b	CCA139IS0033	scaffold58974:378190-384204	7	1,629	542	9.26	59,537.80	AtPIN6
CcPIN8a	CCA077S0095	scaffold26004:732921-735316	6	1,026	341	9.39	37,338.75	AtPIN8
CcPIN8b	CCA109AS0128	scaffold43199:1045218-1047610	6	1,104	367	6.46	40,253.74	AtPIN8

pI denotes isoelectric point, and Mol wt denotes molecular weight.

was found in Motif 8 (Figure 4D). Transmembrane region prediction using TMHMM showed that there were N-terminal or C-terminal transmembrane regions for all CcPINs, with the total number ranging from 6 to 10 (Supplementary Figure 2). The coding sequences of *CcPINs* were compared with their corresponding DNA sequences on the genome. The numbers of exons in *CcPINs* ranged from five to eight (Figure 4C).

Protein–protein interaction network prediction of CcPINs

The PPI network was predicted between the homologs of CcPINs in *Arabidopsis* and other proteins in *Arabidopsis* by the String database, with the minimum required interaction score set to a high confidence score of 0.700, and the maximum number of interactors was limited to no more than 10. The PPI network consisted of 17 nodes and 39 edges (Figure 5A). Seven nodes were representative of PIN proteins. The corresponding information is shown in Supplementary Table 3. Different line colors represent protein-protein associations.

The nodes were annotated using Gene Ontology (GO) (Figure 5B and Supplementary Table 4). The results showed that most of the predicted proteins contributed to biological processes, such as "Cellular response to stimulus" (GO:0051716), "Auxin-activated signaling pathway" (GO:0009734), "Tissue development" (GO:0009888), and "Xylem and phloem pattern formation" (GO:0010051). The proteins also played a role in multiple cellular components including the "Plasma membrane" (GO:0005886), "Auxin polar transport" (GO:0009926), and "Cytoplasm" (GO:0005737). In addition, the molecular function of the proteins included "Auxin transmembrane transporter activity" (GO:0080161), "Auxin efflux transmembrane transporter activity" (GO:0010329), "Auxin influx transmembrane transporter activity" (GO:0010328), and "Auxin binding" (GO:0010011).

Cis-acting regulatory elements affecting the promoters of *CcPIN* family genes

Regulatory elements that are *cis*-acting on the promoters of genes were the sites for expression regulation of genes. To explore how the expression of *CcPINs* was regulated by the different transcriptional factors, the section 2,000 bp upstream of the start codon (ATG) of *CcPINs* was used to query for *cis*-acting element detection using PlantCare. Five types of *cis*-acting elements, including a binding site element, hormone responsiveness, light responsiveness, plant development, and stress responsiveness, were detected, with numbers of 9, 71, 147, 28, and 40, respectively (Figure 6).

10.3389/fpls.2022.999990

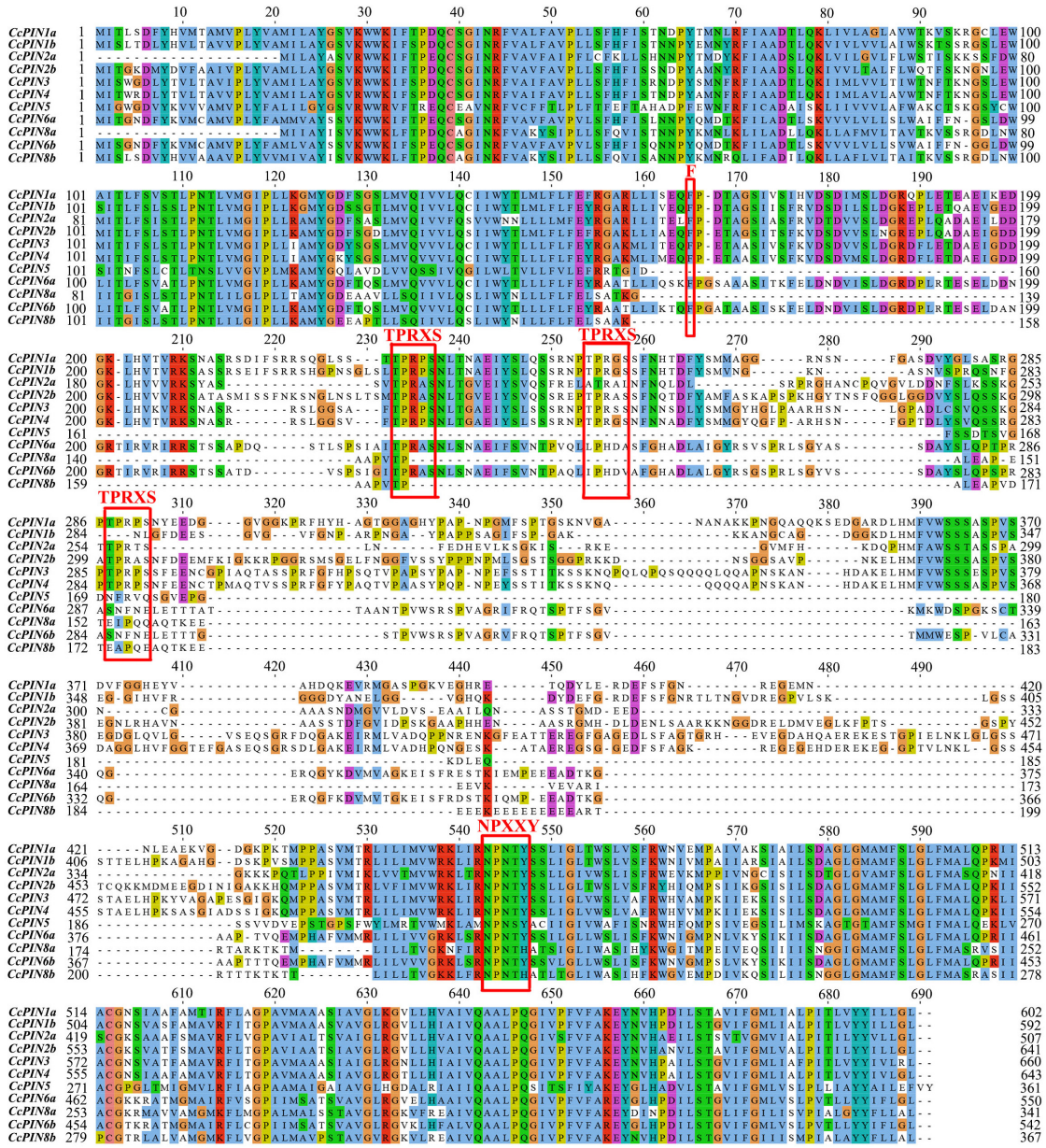

FIGURE 3
Multiple alignments of CcPINs by ClustalW. The possible functional sites are circled with red boxes.

Within each type, specific *cis*-acting elements were detected. For example, five types of hormone-responsive elements, including gibberellin-responsive elements (GARE-motif, P-box, TATC-box, and TGA-element), abscisic acid-responsive elements (ABRE), MeJA-responsive elements (CGTCA-motif, TGACG-motif), and salicylic acid-responsive elements (TCA-element), were detected. The number of *cis*-acting elements for a certain *CcPIN* gene ranged from 15 (CcPIN8a) to 36 (CcPIN4), where light-responsive elements were the most abundant. In addition, five types of stress-responsive elements were detected on the promoters of *CcPINs*.

Tissue-specific expression profiles of *CcPINs* in Chinese hickory

To explore the relative expression of *PIN* genes in different tissues, tissue-specific expression profiles of *CcPIN* genes in roots, stems, leaves, and shoots of Chinese hickory were obtained by qRT-PCR. The results showed that *CcPIN1a*, *CcPIN2a*, *CcPIN5*, and *CcPIN8a* were highly expressed in stems, *CcPIN4* and *CcPIN6a* showed the highest expression levels in shoots, and the highest expression of *CcPIN3* was in leaves (Figure 7). The tissue-specific expression patterns of *CcPIN*

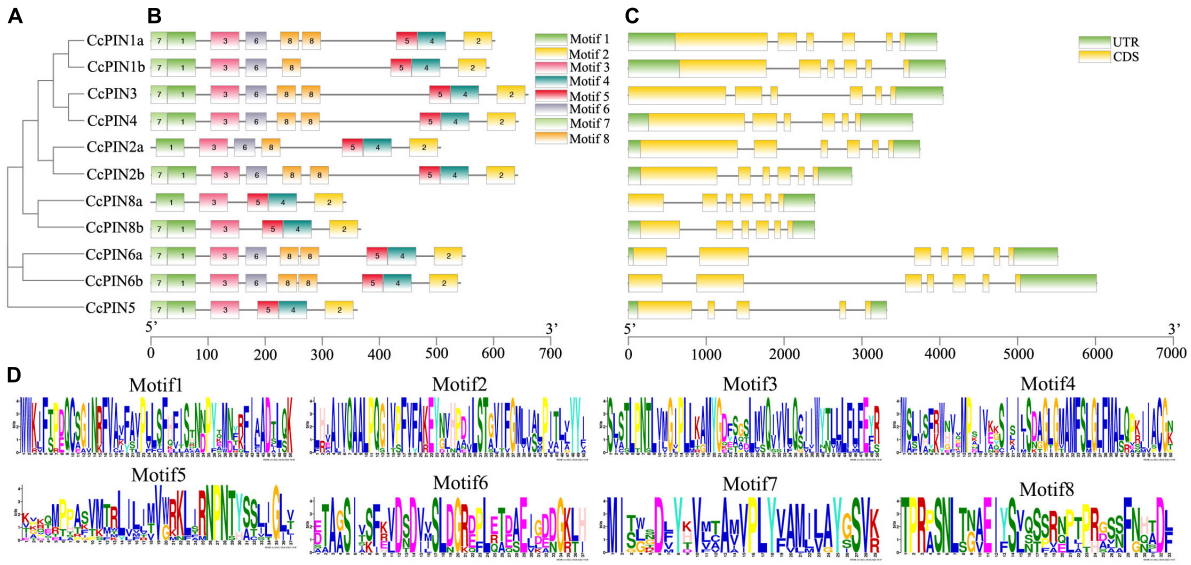

FIGURE 4
Motif and gene structure analysis of CcPINs. **(A)** Phylogenetic relationships. **(B)** Motif distribution. **(C)** Exon-intron structures. **(D)** Motif information.

genes showed that they might play different roles in different tissues in Chinese hickory.

Expression profiles of *CcPIN* genes during grafting and salt stress in Chinese hickory

To investigate whether *CcPINs* regulated grafting in Chinese hickory, the expression levels of *CcPINs* were measured at different stages of grafting (**Figure 8**). In scions, compared with 0 days after grafting, the expression level of *CcPIN1a* was significantly upregulated over sevenfold and eightfold at 3 and 7 days after grafting, respectively. However, at 14 days after grafting, the expression was decreased but still significantly higher than at 0 days after grafting. The expression of *CcPIN3* and *CcPIN6a* was downregulated in scions. The expression levels of *CcPIN4* and *CcPIN8a* significantly changed in rootstocks after grafting. The highest expression for *CcPIN4* was at 14 days after grafting in rootstocks, while *CcPIN2a* exhibited the highest expression at 3 days after grafting. *CcPIN5* showed stable expression during Chinese hickory grafting.

To investigate how *CcPINs* respond to salt stress, the expression of *CcPINs* in the roots, stems, and leaves of Chinese hickory was determined at different time points in the salt stress treatment. *CcPINs* showed different expression profiles in different tissues (**Figure 9**). In roots, *CcPIN1a* was significantly upregulated after the salt stress treatment; *CcPIN2a*, *CcPIN3*, and *CcPIN4* were downregulated at 3 days after the salt stress treatment; and *CcPIN8a* was downregulated at 1 day after the salt stress treatment. In stems, *CcPIN1a*, *CcPIN3*, and *CcPIN4* were upregulated at 1 day after the salt stress treatment, while *CcPIN3* and *CcPIN4* were downregulated at 3 days after the salt stress treatment. The expression levels of *CcPIN5*, *CcPIN6a*, and *CcPIN8a* were similar to those after the CK treatment. In the leaves, most of the *CcPIN* genes were downregulated at 3 days after the salt stress treatment, while the expression of *CcPIN8a* was upregulated. The different expression profiles of *CcPINs* indicated that some of them might take part in the regulation of salt stress in Chinese hickory.

Discussion

Chinese hickory is a native nut tree in China that is widely cultivated in Zhejiang and Anhui provinces. The nuts of Chinese hickory are not only rich in nutrition such as saturated and unsaturated fatty acids, proteins, essential amino acids for humans, and trace elements (Peng et al., 2013; Huang et al., 2022) but also have an important role in the medicinal field (Gao et al., 2020). High nutritional values have brought huge economic benefits for farmers. In 2021, the total output value of Chinese hickory in Lin'an distinct (Hangzhou, China) was 845 million RMB (~123.3 million dollars) (Gu, 2022). However, the slow vegetative growth and narrow growing range have limited the development of Chinese hickory. Grafting is a technique that is commonly used in horticulture and has been applied to Chinese hickory to solve the difficulties in the Chinese hickory industry. In addition, it has been predicted that the salt in soil will be increased with increasing global temperatures

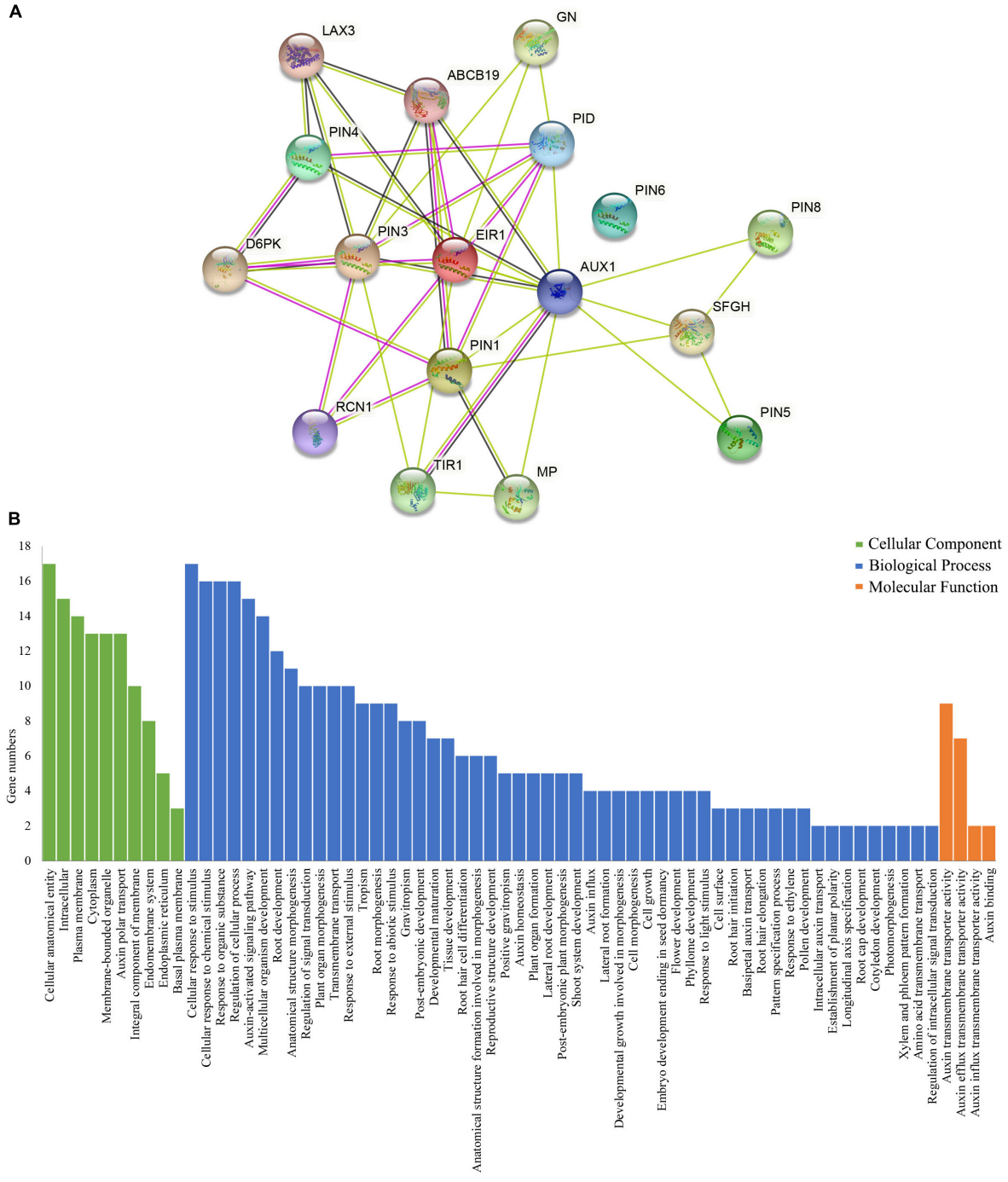

FIGURE 5
(A) QQProtein–protein interaction (PPI) network of PIN-formed (PINs) and **(B)** gene ontology (GO) annotation of proteins in the PPI.

(Dhankher and Foyer, 2018). Therefore, the study of grafting and salt stress in Chinese hickory is essential. PIN is an auxin efflux protein that participates in the regulation of plant grafting and salt stress (Wang et al., 2014; Chen et al., 2015). In the present study, we identified eleven PIN genes in Chinese hickory according to the published genome. The expression profiles in grafting and salt stress were determined to elucidate the function of *CcPINs*.

The number of identified *CcPIN* genes (11) was more than that in *Arabidopsis* (8). Phylogenetic analysis of 132 PIN proteins in 15 plant species was carried out to compare with *CcPINs*. On the phylogenetic tree, *CcPINs* were close to *CilPINs* in

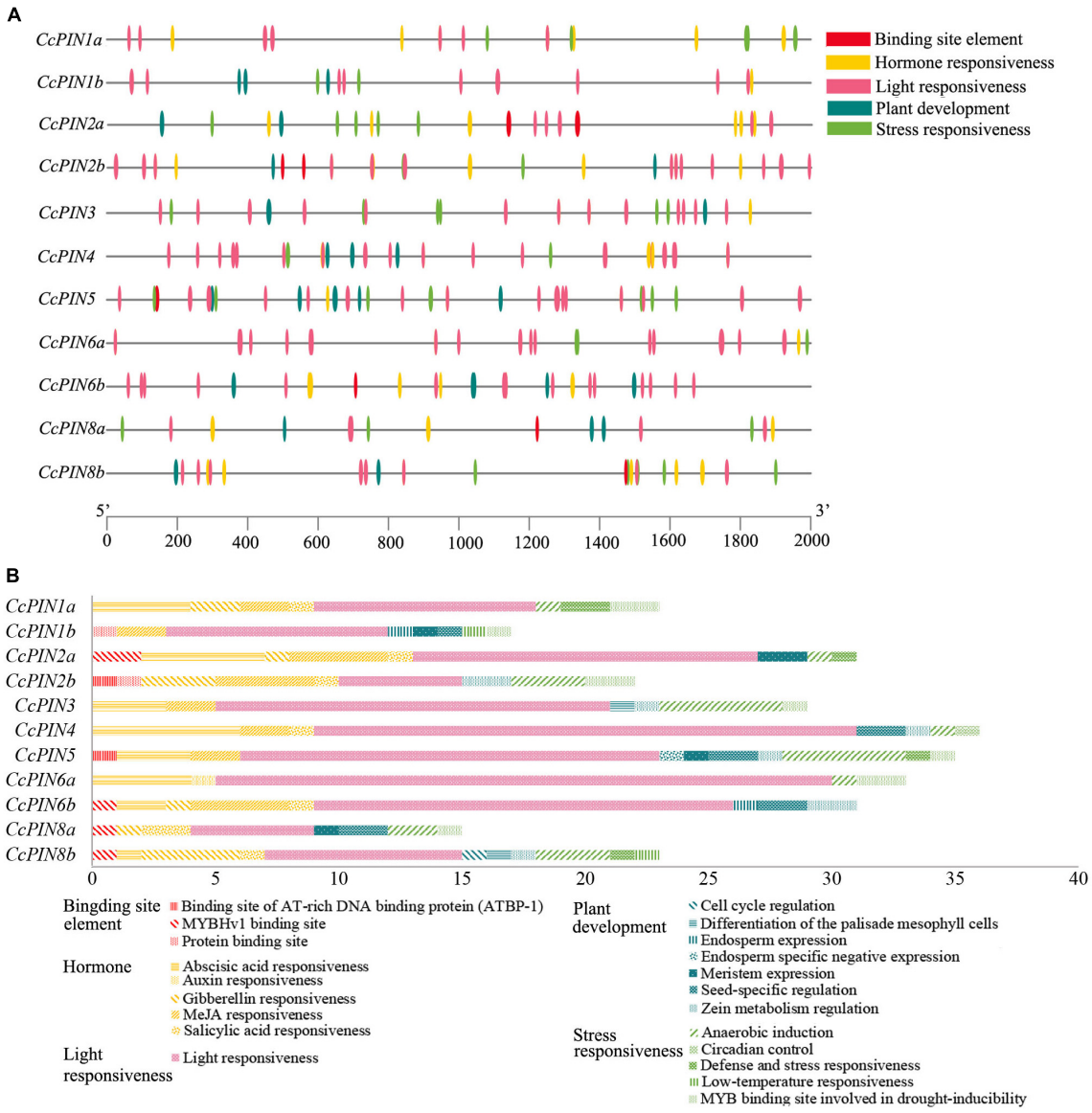

FIGURE 6
Cis-acting elements on the promoters of CcPIN family genes. **(A)** The distribution of *cis*-acting elements. **(B)** The number of *cis*-acting elements.

C. illinoinensis, which indicated that they might come from a common ancestor. To further study the similarity and diversity of *CcPIN* genes, an analysis of motif and intron/exon structure was executed. The exons of *CcPINs* were similar, and the various intron lengths were the main reason for different gene lengths, with similar results in other species (Wang et al., 2009; Hu et al., 2021).

PIN proteins play important roles in cellular auxin transport, and their function relies on corresponding sites in conserved regions (Zhou and Luo, 2018). In contrast, functional sites distributed in non-conserved regions might be unique in different species, and the phenomenon is related to sequence evolution (Zwiewka et al., 2019). In *Arabidopsis*, *PIN* genes consist of two conserved hydrophobic loops at the N- and C-terminus and a variable hydrophilic loop in the middle (Zhou and Luo, 2018). The analysis of multiple sequence alignments and motifs showed that there were similar motifs for *CcPINs*, and the motifs were distributed in a gene-conserved area. It was determined that F165 in AtPIN1 controls the polar distribution of the PIN protein (Sancho-Andrés et al., 2016). Functional F165 sites were also found in CcPIN proteins, indicating that they might perform the same function.

TPRXS, a phosphorylation site, appeared in motif 8 (**Figure 3**), and control of the polar distribution of PIN proteins was performed by phosphorylase kinase (Bassukas et al., 2022). The NPNXY site on the conserved domain is also related to

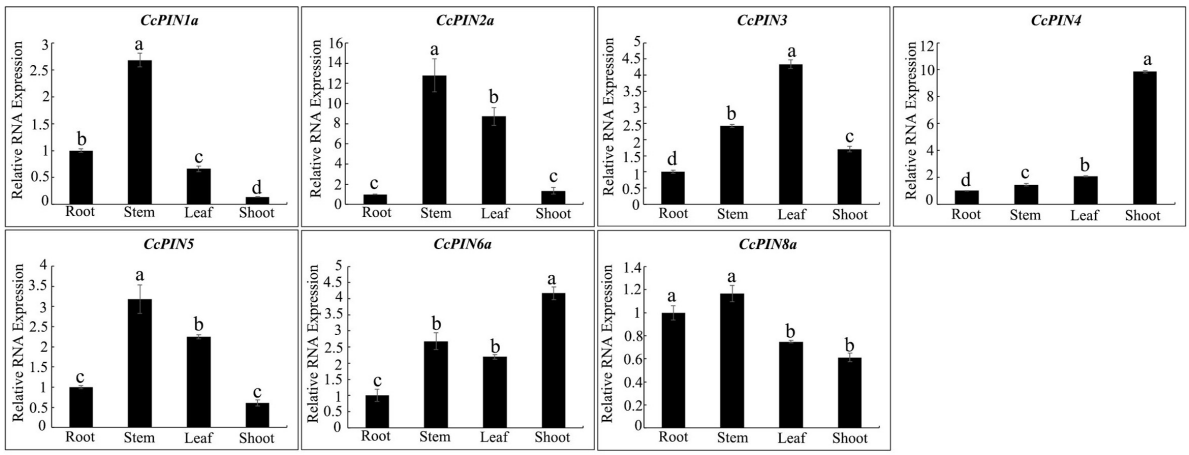

FIGURE 7
Tissue-specific expression profiles of *CcPIN* genes. Total RNA was extracted from roots, stems, leaves, and shoots of 1-year-old Chinese hickory. The relative expression levels of each *CcPIN* gene in roots were standardized as one. Different letters above the columns denote a significant difference in different tissues ($P < 0.05$).

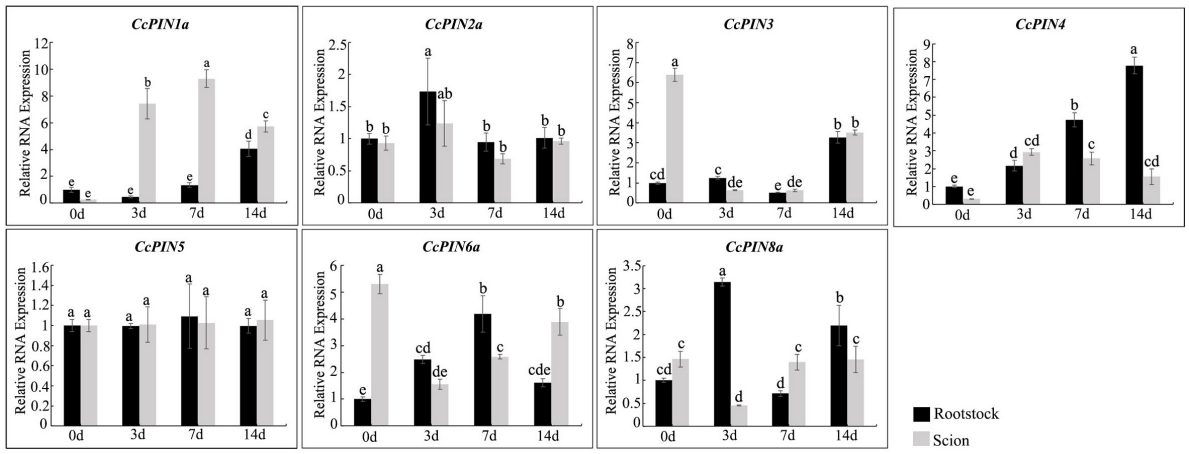

FIGURE 8
Relative RNA expression of *CcPIN* genes during the grafting of Chinese hickory. 0, 3, 7, and 14 d denote 0, 3, 7, and 14 days after grafting, respectively. The rootstocks collected at 0 day were regarded as the control sample. Different letters above the columns denote a significant difference in different treatments ($P < 0.05$).

PIN transport. Mutants of NPNXY in *AtPIN1* contributed to the accumulation of the PIN1 protein on the endoplasmic reticulum (Mravec et al., 2009). The multiple sequence alignment results show that all the CcPINs contained NPXXY in the conserved region, which suggests that the NPXXY motif performed the functional equivalent in Chinese hickory.

The plant hormone auxin regulates various developmental processes through its asymmetrical distribution on the PM (Vanneste and Friml, 2009). The different auxin distribution is executed by PINs (Wisniewska et al., 2006), and PIN-mediated auxin polar transport is crucial for auxin homeostasis. The PPI network predicted the multiple protein interactions with CcPINs through their homologous *AtPINs* genes. GO annotation showed that the predicted proteins were involved in many processes, and they participated in the regulation of auxin homeostasis together.

PINs are auxin efflux proteins that play important roles in plant life (Yu et al., 2022). To further explore the function of *CcPINs*, the expression levels from different tissues, including roots, stems, leaves, and shoots in Chinese hickory, were analyzed by qRT-PCR. The results showed that there was a high tissue-specific expression in the leaves, stems, and shoots of Chinese hickory, and the results were in accordance with those from previous studies. As previously reported, D6 PROTEIN KINASE and PINOID (PID)/WAG kinases activated auxin efflux transport PINs and influenced stem

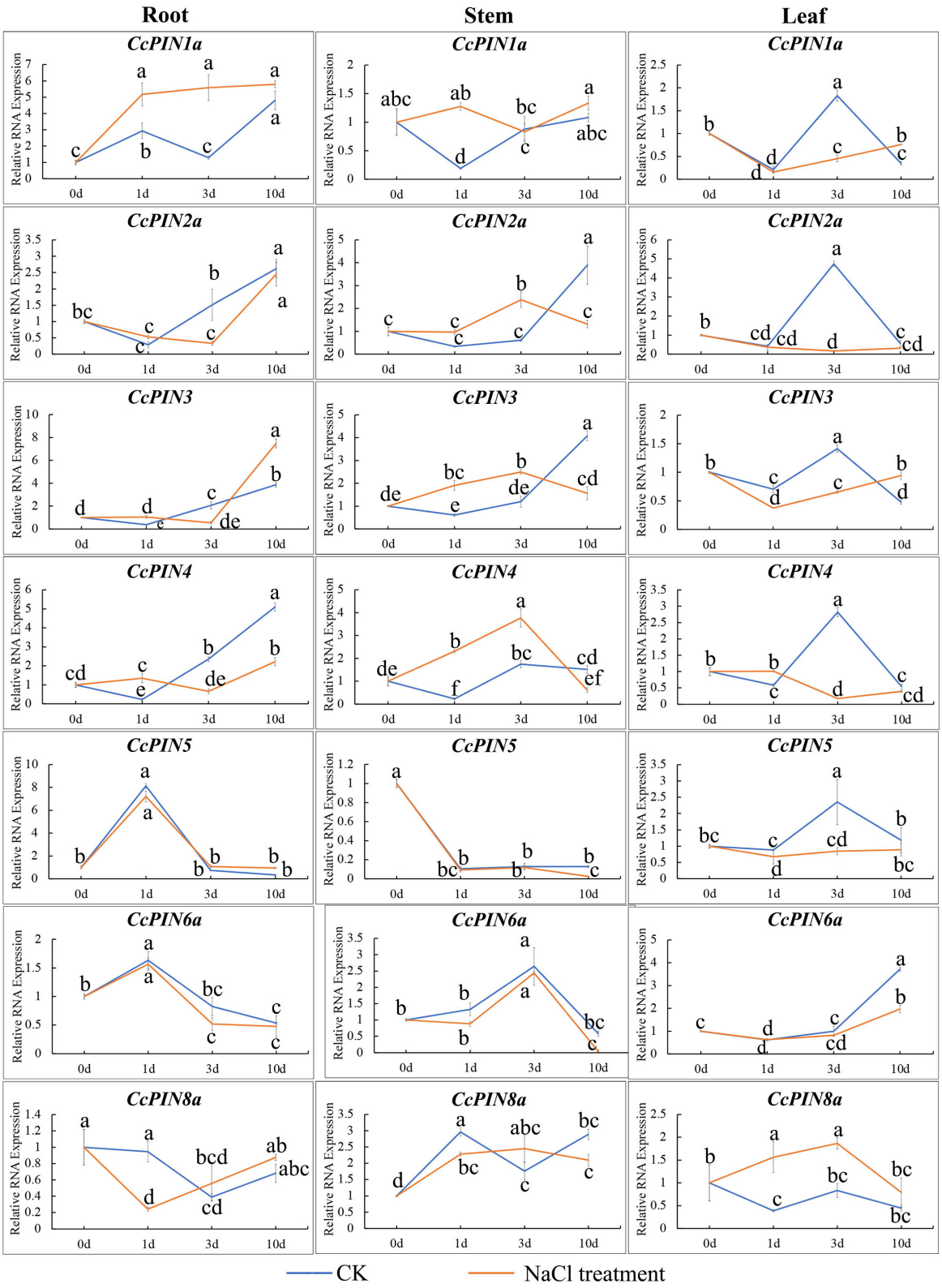

FIGURE 9
Relative RNA expression of *CcPIN* genes under CK (H_2O) and salt stress treatments. 0, 1, 3, and 10 d represent 0, 1, 3, and 10 days after treatment, respectively. The sample from the CK group collected 0 days after treatment was regarded as the control sample. Different letters near the points indicate a significant difference in different treatments ($P < 0.05$).

development (Wulf et al., 2019). In the woody plant Populus, *PtaPIN1* regulated stem growth, with high expression in the developing xylem (Carraro et al., 2012). *OsPIN5a* and *OSPIN5c* in rice were highly expressed in leaves. *PbPIN1*-3, *PbPIN2*-2, *PbPIN5*-1, and *PbPIN6* in pear trees were highly expressed in shoots (Qi et al., 2020). The tissue-specific transcriptional levels indicate that *CcPINs* participate in the regulation of hickory growth and development. Therefore, it is worthy of further research to clarify the detailed regulation process in Chinese hickory.

In the successful grafting of horticultural plants, the adhesion of different stems from rootstock and scion, namely the formation of the graft union, is necessary for grafting survival. During the process, callus formation and differentiation, and the reconnection of vascular tissues, are prominent (Melnyk et al., 2018; Sharma and Zheng, 2019). Auxin contributes to callus formation after a plant is wounded (Wulf et al., 2019). The imposed exogenous auxin also accelerates vascular reconnection (Wulf et al., 2019). In Chinese hickory grafting studies, morphological changes indicated that 3, 7, and 14 days after grafting were the crucial time points for isolation layer formation, callus formation, and vascular reconnection (Liu et al., 2009). Auxin-related genes, including *CcIAAs* and *CcGH3*, exhibited different expression levels at 0, 3, 7, and 14 days after grafting.

During *Arabidopsis* grafting, it has been proved that AtPIN1 participates in grafting with a high expression on the scion (Melnyk et al., 2018). To explore if auxin efflux proteins coding for *CcPIN* genes participated in the grafting process, the relative RNA expression of *CcPINs* was measured in rootstocks and scions at different time points by qRT-PCR. During the obtained results, the relative RNA expression level of *CcPIN1a* was upregulated 6–9 fold at the time points of 0, 3, 7, and 14 days after grafting. *CcPIN1a* is the ortholog of *AtPIN1*, indicating they might perform a similar function. Further study is necessary to elucidate the additional functions of *CcPIN1a* with respect to grafts. In addition to *CcPIN1a*, other *PIN* genes exhibited varied expression levels in grafting except for *CcPIN5*. The various expression profiles of *CcPIN* genes in different sections at the key stages of hickory grafting indicate their potential functions in grafting regulation.

When faced with salt stress, plants activate various mechanisms to resist the adverse environment. Auxin homeostasis and dynamic rearrangement are one of the regulatory pathways. A previous study showed that phospholipase D-derived phosphatidic acid combined with PID (PINOID/WAVY ROOT GROWTH) kinases enhanced the phosphorylation of PIN2, promoted auxin polar efflux ability, and contributed to the salt tolerance of *Arabidopsis* (Wang et al., 2019). *PIN1* and *PIN3* also participated in the process (Wang et al., 2019). During salt stress in watermelon, *ClPINs* performed functions of resisting salt with varying expressions (Yu et al., 2017). In the present study, samples of roots, stems, and leaves under salt stress were collected to explore the *CcPINs*' expression profiles of anti-salt ability in Chinese hickory. As shown in **Figure 9**, the expression of CcPIN2a in roots and leaves was significantly downregulated, with variations similar to those in the previous report (Wang et al., 2019).

Conclusion

To investigate the potential roles of auxin efflux transporters during stress treatments, eleven *CcPIN* genes with an ORF of 1,026–1,983 bp were identified in Chinese hickory for the first time, and their structural characteristics and expression responses to grafting and salt stress were detected by qRT-PCR. CcPINs were localized on the PM and had the closest relationships with homologous genes in *C. illinoinensis* and *J. regia*. Different hormone- and stress-responsive elements were detected on the promoter of *CcPINs*, indicating their expression regulation by stress treatments. *CcPINs* performed different functions during grafting and salt treatment. *CcPIN1a* has the potential to respond to grafting, while *CcPIN1a and CcPIN8a* might be involved in salt-stress regulation. In addition, *CcPINs* displayed different expression levels in different tissues, suggesting their varying roles during growth and development. Further investigations might be conducted on the mechanism of *CcPINs* for grafting and salt stress regulation.

Data availability statement

The original contributions presented in this study are included in the article/**Supplementary material**, further inquiries can be directed to the corresponding authors.

Author contributions

HY, BZ, XW, and DY conceived and designed the concept of the manuscript. YY (1st author), JM, JC, YY (4th author), and KY performed the experiments. YG, XT, HL, and HY analyzed the data. YY (1st author), JM, YG, and JC performed the formal analysis. YY (1st author), JM, and HY drafted the manuscript. AS, XW, DY, RW, BZ, and HY revised and finalized the manuscript. All authors endorsed the final version of the manuscript.

Funding

This study was supported by the National Natural Science Foundation of China (32071807, 31901346,

and 31971695); Key Project of Zhejiang Provincial Natural Science Foundation (LZ18C160001); National Key Research and Development Program of China (2018YFD1000604); Independent Research Project of State Key Laboratory of Subtropical Silviculture, Zhejiang A&F University (ZY20180208 and ZY20180308); Open Foundation of State Key Laboratory of Subtropical Silviculture, Zhejiang A&F University (KF201903, KF202007, and KF201708); The Talent Foundation of Zhejiang A&F University (2022LFR001); Overseas Expertise Introduction Project for Discipline Innovation (111 Project D18008); Key Research and Development Program of Zhejiang Province (2018C02004); National High Technology Research and Development Program of China (863 Program) (2013AA102605); Fruit Innovation Team Project of Zhejiang Province (2016C02052-12); Key Agricultural New Varieties Breeding Projects founded by the Zhejiang Province Science and Technology Department (2021C02066-12 and 2016C02052-13); Zhejiang Provincial Natural Science Foundation for Distinguished Young Scholar (LR13C160001); Open Foundation of First-Class Discipline of Forestry, Zhejiang Province (201703); and the First-Class General Financial Grant from the China Postdoctoral Science Foundation (2017M610377).

Conflict of interest

The authors declare that the research was conducted in the absence of any commercial or financial relationships that could be construed as a potential conflict of interest.

Publisher's note

Supplementary material

The Supplementary Material for this article can be found online at: https://www.frontiersin.org/articles/10.3389/fpls.2022.999990/full#supplementary-material

References

Alabdallah, O., Ahou, A., Mancuso, N., Pompili, V., Macone, A., Pashkoulov, D., et al. (2017). The *Arabidopsis* polyamine oxidase/dehydrogenase 5 interferes with cytokinin and auxin signaling pathways to control xylem differentiation. *J. Exp. Bot.* 68, 997–1012. doi: 10.1093/jxb/erw510

Bassukas, A. E. L., Xiao, Y., and Schwechheimer, C. (2022). Phosphorylation control of PIN auxin transporters. *Curr. Opin. Plant Biol.* 65:102146. doi: 10.1016/j.pbi.2021.102146

Bennett, T., Brockington, S., Rothfels, C., Graham, S., Stevenson, D., Kutchan, T., et al. (2014). Paralogous radiations of PIN proteins with multiple origins of noncanonical PIN structure. *Mol. Biol. Evol.* 31, 2042–2060. doi: 10.1093/molbev/msu147

Blilou, I., Xu, J., Wildwater, M., Willemsen, V., Paponov, I., Friml, J., et al. (2005). The PIN auxin efflux facilitator network controls growth and patterning in *Arabidopsis* roots. *Nature* 433, 39–44. doi: 10.1038/nature03184

Bureau, M., Rast, M., Illmer, J., and Simon, R. (2010). *JAGGED LATERAL ORGAN (JLO)* controls auxin dependent patterning during development of the *Arabidopsis* embryo and root. *Plant Mol. Biol.* 74, 479–491. doi: 10.1007/s11103-010-9688-2

Carraro, N., Tisdale-Orr, T. E., Clouse, R. M., Knoller, A. S., and Spicer, R. (2012). Diversification and expression of the PIN, AUX/LAX, and ABCB families of putative auxin transporters in Populus. *Front. Plant Sci.* 3:17. doi: 10.3389/fpls.2012.00017

Chen, C., Chen, H., Zhang, Y., Thomas, H. R., Frank, M. H., He, Y., et al. (2020). TBtools: An integrative toolkit developed for interactive analyses of big biological data. *Mol. Plant* 13, 1194–1202. doi: 10.1016/j.molp.2020.06.009

Chen, Y., Cai, J., Yang, F. X., Zhou, B., and Zhou, L. R. (2015). Ascorbate peroxidase from *Jatropha curcas* enhances salt tolerance in transgenic *Arabidopsis*. *Genet. Mol. Res.* 14, 4879–4889. doi: 10.4238/2015.May.11.20

Dastborhan, S., Kalisz, A., Kordi, S., Lajayer, B. A., and Pessarakli, M. (2021). "Physiological and biochemical responses of plants to drought and oxidative stresses," in *Handbook of plant and crop physiology*, ed. M. Pessarakli (Boca Raton, FL: CRC Press), 517–541.

Dhankher, O. P., and Foyer, C. H. (2018). Climate resilient crops for improving global food security and safety. *Plant Cell Environ.* 41, 877–884.

Ding, Z., Wang, B., Moreno, I., Dupláková, N., Simon, S., Carraro, N., et al. (2012). ER-localized auxin transporter PIN8 regulates auxin homeostasis and male gametophyte development in *Arabidopsis*. *Nat. Commun.* 3:941. doi: 10.1038/ncomms1941

Doyle, J. A. (2018). Phylogenetic analyses and morphological innovations in land plants. *Annu. Plant Rev.* 45, 1–50. doi: 10.1002/9781119312994.apr0486

Gao, F., Wu, J., Zhou, Y., Huang, J., Lu, J., and Qian, Y. (2020). An appropriate ratio of unsaturated fatty acids is the constituent of hickory nut extract for neurite outgrowth in human SH-SY5Y cells. *Food Sci. Nutr.* 8, 6346–6356. doi: 10.1002/fsn3.1623

Gibson, C. L., Isley, J. W., Falbel, T. G., Mattox, C. T., Lewis, D. R., Metcalf, K. E., et al. (2020). A conditional mutation in SCD1 reveals linkage between PIN protein trafficking, auxin transport, gravitropism, and lateral root initiation. *Front. Plant Sci.* 11:910. doi: 10.3389/fpls.2020.00910

Gomes, G. L. B., and Scortecci, K. C. (2021). Auxin and its role in plant development: Structure, signalling, regulation and response mechanisms. *Plant Biol.* 23, 894–904. doi: 10.1111/plb.13303

Gu, X. B. (2022). Small Chinese hickory nuts has brought economic benefits for industry development in Lin'an. *Zhejiang Forest.* 5, 10–11.

Hang, L. T., Mori, K., Tanaka, Y., Morikawa, M., and Toyama, T. (2020). Enhanced lipid productivity of *Chlamydomonas reinhardtii* with combination of NaCl and CaCl2 stresses. *Bioprocess Biosyst. Eng.* 43, 971–980. doi: 10.1007/s00449-020-02293-w

Hu, L., Wang, P., Long, X., Wu, W., Zhang, J., Pan, Y., et al. (2021). The PIN gene family in relic plant L. chinense: Genome-wide identification and gene expression profiling in different organizations and abiotic stress responses. *Plant Physiol. Biochem.* 162, 634–646. doi: 10.1016/j.plaphy.2021.03.030

Huang, C., Li, Y., Wang, K., Xi, J., Xu, Y., Si, X., et al. (2022). Analysis of lipidomics profile of *Carya cathayensis* nuts and lipid dynamic changes during embryonic development. *Food Chem.* 370, 130975. doi: 10.1016/j.foodchem.2021.130975

Huang, J., Wang, S., Wang, X., Fan, Y., and Han, Y. (2020). Structure and expression analysis of seven salt-related ERF genes of Populus. *PeerJ.* 20:e10206. doi: 10.7717/peerj.10206

Huang, Y., Xiao, L., Zhang, Z., Zhang, R., Wang, Z., Huang, C., et al. (2019). The genomes of pecan and Chinese hickory provide insights into *Carya* evolution and nut nutrition. *GigaScience* 8, giz036. doi: 10.1093/gigascience/giz036

Kapazoglou, A., Tani, E., Avramidou, E. V., Abraham, E. M., Gerakari, M., Megariti, S., et al. (2020). Epigenetic changes and transcriptional reprogramming upon woody plant grafting for crop sustainability in a changing environment. *Front. Plant Sci.* 11:613004. doi: 10.3389/fpls.2020.613004

Kuhlemeier, C., and Reinhardt, D. (2001). Auxin and phyllotaxis. *Trends Plant Sci.* 6, 187–189. doi: 10.1016/s1360-1385(01)01894-5

Lewis, D., Negi, S., Sukumar, P., and Muday, G. (2011). Ethylene inhibits lateral root development, increases IAA transport and expression of PIN3 and PIN7 auxin efflux carriers. *Development* 138, 3485–3495. doi: 10.1242/dev.065102

Li, R., Pan, Y., Hu, L., Yang, D., Yuan, M., Hao, Z., et al. (2022). PIN3 from liriodendron may function in inflorescence development and root elongation. *Forests* 13:568. doi: 10.3390/f13040568

Liu, C., Hong, J., Xia, G., and Huang, J. (2009). Cytological observation on healing responses in grafting of *Carya cathayensis*. *Sci. Silvae Sin.* 45, 34–38.

Mearaji, H. S., Ansari, A., Igdelou, N. K. M., Lajayer, B. A., and Pessarakli, M. (2021). "Phytohormones and abiotic stresses: Roles of phytohormones in plants under abiotic stresses," in *Handbook of plant and crop physiology*, ed. M. Pessarakli (Boca Raton, FL: CRC Press), 175–213.

Melnyk, C. W. (2017). Plant grafting: Insights into tissue regeneration. *Regeneration* 4, 3–14. doi: 10.1002/reg2.71

Melnyk, C. W., Gabel, A., Hardcastle, T. J., Robinson, S., Miyashima, S., Grosse, I., et al. (2018). Transcriptome dynamics at *Arabidopsis* graft junctions reveal an intertissue recognition mechanism that activates vascular regeneration. *Proc. Natl. Acad. Sci. U.S.A.* 115, E2447–E2456. doi: 10.1073/pnas.1718263115

Mohanta, T. K., Bashir, T., Hashem, A., Abd_Allah, E. F., Khan, A. L., and Al-Harrasi, A. S. (2018). Molecular players of auxin transport systems: Advances in genomic and molecular events. *J. Plant Interact.* 13, 483–495. doi: 10.1080/17429145.2018.1523476

Mravec, J., Skupa, P., Bailly, A., Hoyerova, K., Krecek, P., Bielach, A., et al. (2009). Subcellular homeostasis of phytohormone auxin is mediated by the ER-localized PIN5 transporter. *Nature* 459, 1136–1140. doi: 10.1038/nature08066

Muday, G., and DeLong, A. (2001). Polar auxin transport: Controlling where and how much. *Trends Plant Sci.* 6, 535–542. doi: 10.1016/s1360-1385(01)02101-x

Nelson, B. K., Cai, X., and Nebenührˌ A. (2007). A multicolor set of in vivo organelle markers for co-localization studies in *Arabidopsis* and other plants. *Plant J.* 51, 1126–1136. doi: 10.1111/j.1365-313X.2007.03212.x

Peng, Q., Bian, W., Wang, J. L., Wu, J., Ge, L. Y., Wang, F., et al. (2013). Effect of production techniques on nutrient content in Li'an pecans. *Sci. Technol. Food Ind.* 34, 173–175. doi: 10.13386/j.issn1002-0306.2013.20.056

Qi, L., Chen, L., Wang, C., Zhang, S., Yang, Y., Liu, J., et al. (2020). Characterization of the auxin efflux transporter PIN proteins in pear. *Plants (Basel)* 9:349. doi: 10.3390/plants9030349

Robert, H., and Friml, J. (2009). Auxin and other signals on the move in plants. *Nat. Chem. Biol.* 5, 325–332. doi: 10.1038/nchembio.170

Sancho-Andrés, G., Soriano-Ortega, E., Gao, C., Bernabé-Orts, J. M., Narasimhan, M., Müller, A. O., et al. (2016). Sorting motifs involved in the trafficking and localization of the PIN1 auxin efflux carrier. *Plant Physiol.* 171, 1965–1982. doi: 10.1104/pp.16.00373

Sauer, M., and Kleine-Vehn, J. (2019). PIN-FORMED and PIN-LIKES auxin transport facilitators. *Development* 146:dev168088. doi: 10.1242/dev.168088

Schmittgen, T. D., and Livak, K. J. (2008). Analyzing real-time PCR data by the comparative CT method. *Nat. Protoc.* 3, 1101–1108.

Sharma, A., and Zheng, B. (2019). Molecular responses during plant grafting and its regulation by auxins, cytokinins, and gibberellins. *Biomolecules* 9:397. doi: 10.3390/biom9090397

Shen, C., Bai, Y., Wang, S., Zhang, S., Wu, Y., Chen, M., et al. (2010). Expression profile of PIN, AUX/LAX and PGP auxin transporter gene families in *Sorghum bicolor* under phytohormone and abiotic stress. *FEBS J.* 277, 2954–2969. doi: 10.1111/j.1742-4658.2010.07706.x

Swarup, R., and Peret, B. (2012). AUX/LAX family of auxin influx carriers-an overview. *Front. Plant Sci.* 3:225. doi: 10.3389/fpls.2012.00225

Vanneste, S., and Friml, J. (2009). Auxin: A trigger for change in plant development. *Cell* 136, 1005–1016. doi: 10.1016/j.cell.2009.03.001

Vieten, A., Vanneste, S., Wisìniewska, J., Benkovaì, E., Benjamins, R., Beeckman, T., et al. (2005). Functional redundancy of PIN proteins is accompanied by auxin-dependent cross-regulation of PIN expression. *Development* 132, 4521–4531. doi: 10.1242/dev.02027

Wang, J., Guo, X., Xiao, Q., Zhu, J., Cheung, A. Y., Yuan, L., et al. (2021). Auxin efflux controls orderly nucellar degeneration and expansion of the female gametophyte in *Arabidopsis*. *New Phytol.* 230, 2261–2274. doi: 10.1111/nph.17152

Wang, J., Jin, Z., Yin, H., Yan, B., Ren, Z. Z., Xu, J., et al. (2014). Auxin redistribution and shifts in PIN gene expression during Arabidopsis grafting. *Russ. J. Plant Physiol.* 61, 688–696. doi: 10.1134/s102144371405015x

Wang, J.-R., Hu, H., Wang, G.-H., Li, J., Chen, J.-Y., and Wu, P. (2009). Expression of PIN genes in rice (*Oryza sativa* L.): Tissue specificity and regulation by hormones. *Mol. Plant.* 2, 823–831. doi: 10.1093/mp/ssp023

Wang, P., Shen, L., Guo, J., Jing, W., Qu, Y., Li, W., et al. (2019). Phosphatidic acid directly regulates PINOID-dependent phosphorylation and activation of the PIN-FORMED2 auxin efflux transporter in response to salt stress. *Plant Cell* 31, 250–271. doi: 10.1105/tpc.18.00528

Went, F. W. (1935). Auxin, the plant growth-hormone. *Bot. Rev.* 1, 162–182.

Wisniewska, J., Xu, J., Seifertová, D., Brewer, P. B., Ruzicka, K., Blilou, I., et al. (2006). Polar PIN localization directs auxin flow in plants. *Science* 312, 883–883. doi: 10.1126/science.1121356

Wulf, K. E., Reid, J. B., and Foo, E. (2019). Auxin transport and stem vascular reconnection–has our thinking become canalized? *Ann. Bot.* 123, 429–439. doi: 10.1093/aob/mcy180

Yamaji, N., Huang, C. F., Nagao, S., Yano, M., Sato, Y., Nagamura, Y., et al. (2009). A zinc finger transcription factor ART1 regulates multiple genes implicated in aluminum tolerance in rice. *Plant Cell* 21, 3339–3349. doi: 10.1105/tpc.109.070771

Yang, Y., Huang, Q., Wang, X., Mei, J., Sharma, A., Tripathi, D. K., et al. (2021). Genome-wide identification and expression profiles of ABCB gene family in Chinese hickory (*Carya cathayensis* Sarg.) during grafting. *Plant Physiol. Biochem.* 168, 477–487. doi: 10.1016/j.plaphy.2021.10.029

Yu, C., Dong, W., Zhan, Y., Huang, Z. A., Li, Z., Kim, I. S., et al. (2017). Genome-wide identification and expression analysis of ClLAX, ClPIN and ClABCB genes families in *Citrullus lanatus* under various abiotic stresses and grafting. *BMC Genet.* 18:33. doi: 10.1186/s12863-017-0500-z

Yu, Z., Zhang, F., and Ding, Z. (2022). Auxin signaling: Research advances over the past 30 years. *J. Integr. Plant Biol.* 2, 371–392. doi: 10.1111/jipb.13225

Yuan, H., Zhao, L., Chen, J., Yang, Y., Xu, D., Tao, S., et al. (2018). Identification and expression profiling of the Aux/IAA gene family in Chinese hickory (*Carya cathayensis* Sarg.) during the grafting process. *Plant Physiol. Biochem.* 127, 55–63. doi: 10.1016/j.plaphy.2018.03.010

Zhai, S., Cai, W., Xiang, Z. X., Chen, C., Lu, Y. T., and Yuan, T. T. (2021). PIN3-mediated auxin transport contributes to blue light-induced adventitious root formation in *Arabidopsis*. *Plant Sci.* 312:111044. doi: 10.1016/j.plantsci.2021.111044

Zhang, C., Dong, W., Huang, Z. A., Cho, M., Yu, Q., Wu, C., et al. (2018). Genome-wide identification and expression analysis of the CaLAX and CaPIN gene families in pepper (*Capsicum annuum* L.) under various abiotic stresses and hormone treatments. *Genome* 61, 121–130. doi: 10.1139/gen-2017-0163

Zhang, H., Zhu, J., Gong, Z., and Zhu, J.-K. (2022). Abiotic stress responses in plants. *Nat. Rev. Genet.* 23, 104–119. doi: 10.1038/s41576-021-00413-0

Zhang, J., and Peer, W. A. (2017). Auxin homeostasis: The DAO of catabolism. *J. Exp. Bot.* 68, 3145–3154. doi: 10.1093/jxb/erx221

Zhao, R., Sun, H., Zhao, N., Jing, X., Shen, X., and Chen, S. (2015). The *Arabidopsis* Ca^{2+}-dependent protein kinase CPK27 is required for plant response to salt-stress. *Gene* 563, 203–214. doi: 10.1016/j.gene.2015.03.024

Zhao, Y. (2010). Auxin biosynthesis and its role in plant development. *Annu. Rev. Plant Biol.* 61, 49–64. doi: 10.1146/annurev-arplant-042809-112308

Zhou, J. J., and Luo, J. (2018). The PIN-FORMED auxin efflux carriers in plants. *Int. J. Mol. Sci.* 19, 2759. doi: 10.3390/ijms19092759

Zwiewka, M., Bilanovièová, V., Seifu, Y. W., and Nodzyński, T. (2019). The nuts and bolts of PIN auxin efflux carriers. *Front. Plant Sci.* 10:985.

frontiers | Frontiers in Plant Science

TYPE Original Research
PUBLISHED 30 September 2022
DOI 10.3389/fpls.2022.1001785

OPEN ACCESS

EDITED BY
Guolei Li,
Beijing Forestry University, China

REVIEWED BY
Peijian Shi,
Nanjing Forestry University, China
Daxing Gu,
Guangxi Institute of Botany (CAS), China
Keitaro Fukushima,
Fukushima University, Japan
Fei-Hai Yu,
Taizhou University, China
Hiroyuki Shima,
University of Yamanashi, Japan

*CORRESPONDENCE
Dongming Fang
dmfang@zafu.edu.cn

SPECIALTY SECTION
This article was submitted to Functional Plant Ecology, a section of the journal Frontiers in Plant Science

RECEIVED 24 July 2022
ACCEPTED 31 August 2022
PUBLISHED 30 September 2022

CITATION
Chen X, Chen X, Huang S and Fang D (2022) Impacts of Moso bamboo (*Phyllostachys pubescens*) invasion on species diversity and aboveground biomass of secondary coniferous and broad-leaved mixed forest. *Front. Plant Sci.* 13:1001785. doi: 10.3389/fpls.2022.1001785

Impacts of Moso bamboo (*Phyllostachys pubescens*) invasion on species diversity and aboveground biomass of secondary coniferous and broad-leaved mixed forest

Xi Chen, Xin Chen, Shiqi Huang and Dongming Fang*

Jiyang College of Zhejiang A&F University, Zhuji, Zhejiang, China

In recent decades, Moso bamboo has been largely increasing in the subtropical area of China, raising ecological concerns about its invasion into other native forest ecosystems. One concern is whether the invasion of Moso bamboo significantly simplifies forest community composition and structure and declines biomass. This study adopted the space-for-time method to investigate a secondary coniferous and broad-leaved mixed forest (SF) being invaded by an adjacent Moso bamboo forest (MB) in the Wuxie forest reserve, Zhejiang Province. Three plots were established in each SF, MB, and transitional forest. The results showed that the species composition and species dominance of the arborous layer changed significantly ($P < 0.05$), which was indicated by the significantly decreased species richness (Margalef index, Shannon–Wiener index, and Simpson index) and evenness (Pielou evenness index). In contrast, the species richness of the shrub and herbaceous layers had two divergent indications (increasing or unchanged), and the evenness remained unchanged. The total and arborous-layer aboveground biomass of the forest community has had no noticeable change ($P < 0.05$). However, the biomass of the shrub and herbaceous layers showed an increasing trend (shrub significant but herbaceous not), but they only occupied a small proportion (~1%) of the total biomass. Finally, the aboveground biomass and the diversity index had no significant correlation in each layer and overall stands. We hope that the findings could provide a theoretical basis for the invasion mechanism and ecological consequences of the Moso bamboo invasion.

KEYWORDS

biomass, Moso bamboo invasion, *Phyllostachys pubescens*, secondary coniferous and broad-leaved mixed forest, species diversity

Introduction

The invasion of alien plant species into native plant communities has become a common phenomenon worldwide over the past several decades (Ramula and Pihlaja, 2012; Wang et al., 2017, 2019). Alien plant species become the dominant species of the new communities, for instance, due to their growth advantage or lack of enemies when they invade the new ecosystem (van Kleunen et al., 2010). Alien plant species inhibit the growth of other local plants, which eventually reduces biodiversity (Davies, 2011; Vilà et al., 2011) and affects the stability of community biomass (Bai et al., 2007). Similarly, native plants may become increasingly dominant in their original range, a phenomenon known as overabundance (Garrott et al., 1993), i.e., native plant invasion. The invasion of native plants into new ecosystems in the same region or country may also significantly impact biodiversity (Ouyang et al., 2016). Compared with the extensive studies that draw attention to the impact of alien plant invasion, relatively few studies consider the effects of native plant invasion (Nackley et al., 2017; Warren et al., 2017; Shi et al., 2018).

Generally, a forest with a closed canopy can resist the invasion of other species due to the weak light conditions under the canopy, which could weaken the growth of invading seedlings. Without human intervention, native species will not encroach on adjacent natural forests. However, when shade-tolerant tree species invade, the complete forest may only provide weak resistance (Martin et al., 2009). Moso bamboo (*Phyllostachys pubescens*) is widely distributed in southern China (Shi et al., 2020) and has competitive strengths *via* its strong rhizome-root system and leaf functional traits (Huang et al., 2019, 2020; Guo et al., 2021). Native Moso bamboo may invade the surrounding natural forest by itself (Bai et al., 2016) because the elongation of bamboo shoots may depend on the carbohydrate supply of bamboo rhizomes. The reserve stored in bamboo rhizomes can hold a large amount of energy and resources for shoot growth (Xue et al., 2021), largely independent of the light environment (Wang et al., 2016).

The invasion of Moso bamboo into subtropical evergreen forests has become a significant problem in many areas of southern China (Tian et al., 2020). In the past, Moso bamboo was the essential bamboo species for both shoot and timber production in China. Additionally, the Moso bamboo forest (MB) has a comparable net primary productivity (8.86 ± 3.46 Mg C ha^{-1} $year^{-1}$), which enables it to be a vast potential carbon pool (Lin et al., 2017). Therefore, managing pure Moso bamboo forests can bring considerable income to bamboo farmers. Thus, a large area of subtropical evergreen forest in southern China has been transformed into the MB by farmers (Chen et al., 2009). However, in recent years, due to the increase in Moso bamboo production capacity and the price decline, the management level of MB in many production areas has decreased. As a result, a large area of MB has been abandoned (Jiang et al., 2015), which has exacerbated the invasion of Moso bamboo. Previous studies have shown that Moso bamboo invasion may lead to a series of ecological and environmental problems, such as simplifying forest community composition and structure (Ouyang et al., 2016), declining species diversity (Okutomi et al., 1996; Nakai and Kisanuki, 2006; Yang et al., 2011; Akutsu et al., 2012; Bai et al., 2013; Zhang and Xue, 2018), and making the forest biomass change obviously (Yang et al., 2011; Fukushima et al., 2015; Lin et al., 2017; Song et al., 2017).

As the largest terrestrial ecosystem on earth, the forest has about half of the carbon reserves on land, which plays a vital role in maintaining the ecological balance of the whole world and human survival (Pan et al., 2011). The subtropical forest is the vegetation type mainly distributed in China, with a broad distribution area and rich biodiversity (Corlett, 2013). The relationship between species diversity and aboveground biomass of natural forest communities is still controversial (Lasky et al., 2014; Bracken et al., 2017; Silva Pedro et al., 2017). Studies have shown that species richness positively affects biomass or productivity of subtropical forests (Barrufol et al., 2013; Bruelheide et al., 2014; Cavanaugh et al., 2014) or has no effect (Wu et al., 2015). The different results may be due to the forest ecosystem's different restoration or succession times. It may also be due to the complexity of community structure and the resource effectiveness of habitat conditions (Ali and Yan, 2017; Mori et al., 2017; Ratcliffe et al., 2017; van der Sande et al., 2017). Plant invasion can significantly change the species diversity and biomass of biological communities. However, the relationship between biodiversity changes and biomass of forest communities during the Moso bamboo invasion remains largely unknown.

Therefore, we selected a typical site where Moso bamboo has been expanding into the coniferous and broad-leaved mixed forest to investigate the community characteristics. We applied the "Space for Time" method (Pickett, 1989), which assumes that spatial and temporal variation are equivalent, so the different temporal stages of the Moso bamboo invasion were simultaneously compared in the same area. The species diversity and aboveground biomass of three adjacent forest types were investigated, i.e., (1) the native secondary coniferous and broad-leaved mixed forest (SF), (2) transition tree-Moso-bamboo forest (TF), and (3) nearly pure MB. We attempted to verify three assumptions: (1) The invasion of Moso bamboo changed the species composition and reduced the diversity of the local ecosystem; (2) Moso bamboo invasion may reduce the aboveground biomass of the forest community; (3) The changes in species diversity of forest community may have correlations with the aboveground biomass during Moso bamboo invasion. We anticipated that the findings might provide theoretical and management references to local farmers and the government.

Materials and methods

Study site

The study was performed at Wuxie Nature Reserve (120·2′40″E; 294·4′15″N) in Zhuji, Zhejiang Province, China. The area has a subtropical monsoon climate with a mean annual temperature of 16.3°C and an annual precipitation of 1,573 mm. The area has many soil types, mainly hilly red soil, with good soil fertility. The zonal vegetation is SF and MB. Due to the strong expansion ability of the Moso bamboo rhizome, a mixed forest of coniferous and broad-leaved trees and bamboos is formed between the two types of forests.

Sampling design

In May 2020, we selected three transects spanning from a SF, *via* a transition zone, to a MB, representing three typical stages of the Moso bamboo invasion into subtropical forests. The altitude of the plot is 210–230 m, containing SF, representing the forest stage not invaded by Moso bamboos. The dominant species in the arborous layer of SF was *Schima superba*, with a forest age of 30–40 years. The associated species were *Liquidambar formosana* and *Pinus massoniana*. The average height of the arborous layer was 15.6 m, and the average diameter breast height (DBH) was 20.5 cm. The TF represented the forest stage moderately invaded by Moso bamboo, and the ratio of bamboo to wood is about 4:1. The average height and DBH of Moso bamboo were 16.3 m and 11.5 cm, respectively. Finally, the MB represented the forest stage heavily invaded by Moso bamboos, and the bamboos were the species with an absolute advantage in the arborous layers. The average height of Moso bamboo was 16.9 m, and the average DBH was 12.1 cm (**Table 1**).

Each transect had a width of 30 m and a length of 80 m. The utmost 5 m surrounding each horizontal transect was set as a buffer zone, and the middle area was used for setting up three 20 m × 20 m sampling plots with a 5-m spacing between them. In each sampling plot, biomass and diversity of the arborous layer were investigated. Furthermore, two 5 m × 5 m quadrats were set at the diagonal position of each sample plot and were used for shrub layer species investigation. Additionally, one 1 m × 1 m quadrats were placed in the center, and another four were established in the four corners of the sample plot, which were used for herbaceous layer species investigation. We measured the DBH of trees (>5 cm) from the arborous layer and recorded the species, DBH, height, and abundance. Woody plants with DBH less than 5 cm were measured in the shrub layer, including saplings and shrubs, and we recorded species names, ground diameter, height, abundance, and so on.

TABLE 1 The height and diameter breast height (DBH) class of Moso bamboo in secondary coniferous and broad-leaved mixed forest (SF), transitional forest, and Moso bamboo forest (MB) (mean ± SE).

Forest type	Height (m)	DBH (cm)
Transitional forest (TF)	16.30 ± 0.16**b**	11.50 ± 0.14**b**
Moso bamboo forest (MB)	16.87 ± 0.09**a**	12.13 ± 0.10**a**

Different lowercase letters indicate significant differences at $P < 0.05$.

Aboveground biomass

The tree height, DBH, and bamboo age were measured through quadrat investigation. Then the standing volume of trees in the sample plot was estimated according to the Chinese standing volume table (Zeng, 2018), and the aboveground biomass of the arborous layer per unit area was calculated through the volume biomass model (Wang et al., 2009; Shen and Tang, 2019). The formulas are as follows:

$$\text{Treevolume}: V = c_0 D^{c1} H^{c2} + \varepsilon \quad (1)$$

$$\text{Treebiomass}: B = \frac{v}{a + bv} \quad (2)$$

$$\text{Bamboobiomass}: W = 0.0520 D^{2.2052} A^{0.4457} \quad (3)$$

where V is the standing volume, D is the diameter at breast height (DBH), H is the tree height, c_i is the parameters (i = 0, 1, 2), ε is the error, B is the tree biomass, v is the volume per unit area, a and b are the constants of the corresponding forest type, W is the bamboo stem biomass, and A is the bamboo age.

The aboveground biomass of the shrub and herbaceous layers was obtained using the harvest method. We randomly selected a 5 m × 5 m investigation quadrat in each sample plot as the harvest quadrat of the shrub layer. Three vegetation survey quadrats with diagonal directions in the standard plot for the herbaceous layer were selected. The aboveground shrub and herbaceous layers were harvested in the set harvesting quadrat and brought back to the laboratory. The aboveground biomass of shrubs and herbs was measured after drying at 85°C to constant weight. We calculated the aboveground biomass of the shrub/herbaceous layer per unit area of each stand.

Species diversity

Margalef index, Shannon–Wiener index, Simpson index, and Pielou evenness index were used to estimate α diversity of community species. The formulas are as follows:

$$\text{Margalef index of species richness}: D_m = \frac{(S-1)}{\ln N} \quad (4)$$

$$\text{Simpson index}: D_s = \frac{\sum_{i=1}^{s} n_i(n_i-1)}{N(N-1)} \quad (5)$$

$$\text{Shannon} - \text{Wiener index}: H' = -\sum_{i=1}^{s} Pi \ln Pi \quad (6)$$

$$\text{Pielou evenness index}: E = \frac{H'}{\ln S} \quad (7)$$

where S is the total number of species, N is the sum of the number of individuals of all species, P_i is the proportion of the number of individuals of species i to the total number of individuals in the community, that is, $p_i = n_i/N$, n_i is the number of individuals of species i.

$$\text{Importance value IV} = (\text{relative abundance}, \text{relative frequency}, \text{relative significance})/3 \quad (8)$$

Statistical analyses

SAS 9.4 (SAS Institute Inc., Cary, NC, United States) and R Statistical Software (V4.2; R Core Team, 2022) were used to process, analyze, and graph the data.

First, the diversity indexes and biomass of the arborous layer in each sampling plot were calculated and measured. At the same time, the diversity indexes and biomass in each quadrat (5 m × 5 m for the shrub layer and 1 m × 1 m for the herbaceous layer) were calculated and measured. Then, the diversity indexes and biomass of these quadrats (two and five quadrats for the shrub and herbaceous layers, respectively) per sampling plot were averaged. In this case, we got three replicates of the diversity indexes and biomass in shrub and herbaceous layers, and they were further used for comparison between the three forest types.

Considering the limited three replicates per layer that may not meet the requirement of normal distribution by the analysis of variance (ANOVA), we selected a nonparametric test (Wilcoxon rank-sum test) to conduct the comparison in diversity indexes and biomass among SF, TF, and MB. The linear correlation between diversity index and biomass of arborous, shrub, and herb layers was separately analyzed.

Specifically, R package vegan (Dixon, 2003) was used to examine the species composition difference among the three forest types (MB, TF, and SF) with PerMANOVA (permutational multivariate ANOVA).

Results

Effects of Moso bamboo invasion on species composition and quantitative characteristics

The number of standing bamboo and trees in the three stands varied greatly. After the expansion of Moso bamboo, the number of standing bamboo and total standing trees in the MB increased significantly, increasing to 2,783 and 2,575 culms per hectare, respectively. The number of standing stems of other tree species decreased significantly; 208 plants/ha were reduced (Table 2). These results indicated that the number of standing bamboos increased during the expansion of Moso bamboo was significantly greater than the number of coniferous and broad-leaved mixed species decreased, resulting in a significant increase in the total number of standing individuals in the community.

Except in the herbaceous layer ($P > 0.05$), the species composition in the arborous, shrub, and whole layers was significantly different among the three communities ($P < 0.05$; Figure 1 and Table 3).

For the arborous layer, species richness decreased from 11 in SF and TF to 5 in MB. Only three species stayed in all three communities, i.e., *S. superba*, *P. massoniana*, and *Cyclobalanopsis glauca*, which corresponded to dominant, inferior, and minority roles in SF with important values of 27.6, 12.5, and 2.7, respectively (Table 3). The dominant species changed from *S. superba* and *L. formosana* in SF (important values of 27.6 and 27.1, respectively) to Moso bamboo in TF and MB (important values of 48.2 and 64.9, respectively). The top contributing species *S. superba* in SF descended to an inferior role in TF and MB (important values of 12.7 and 14.1, respectively), and *L. formosana* descended to an ignorable status in TF (important value of 2.4) and disappeared in MB. *P. massoniana* stayed relatively stable in all three communities, with important values of 12.5, 15.6, and 9.3 in SF, TF, and MB, respectively. *C. glauca* is always kept as a minority, although its important values increased over the invasion stages (2.7, 6.2, and 8.6 in SF, TF, and MB, respectively).

The shrub layer's species richness was relatively stable (5–6 species) over three communities, but none of them grew in all three communities (Table 3). In addition, the species composition differed significantly among the three forest types ($P < 0.05$; Figure 1 and Table 3). The dominant species were *Indocalamus tessellatus*, *Camellia japonica*, and *Symplocos stellaris* in SF, TF, and MB, respectively (important values of 31.6, 11.6, and 12.3, respectively). Compared with SF, the species composition was more even in both TF (important values ranging from 5.7 to 11.6) and MB (important values ranging from 5.7 to 12.3).

In the herbaceous layer of the three communities, the species richness was close to each other (five in SF and TF, and seven in MB), and the three communities had three of the same species (*Rubus buergeri*, *Nephrolepis auriculata*, and *Lepidomicrosorum buergerianum*). The statistical results indicated similar species composition among the communities ($P > 0.05$; Figure 1 and Table 3). Furthermore, the dominant species were the same, i.e., *R. buergeri*, but its important values dropped with the invasion progression (70.8, 57.5, and 45.3 in SF, TF, and MB, respectively).

TABLE 2 Effect of Moso bamboo invasion on stem number [ind./ha; (N = 3 in each group)].

Expansion phase	Forest type	Stems of Moso bamboo	Stems of other trees	Total stems
Early stage	SF	0.0 ± 0.0	483.3 ± 28.9	483.3 ± 28.9
Middle stage	TF	1,833.3 ± 624.7	441.7 ± 118.1	2,275.0 ± 633.9
Later stage	MB	2,783.3 ± 797.4	275.0 ± 75.0	3,058.3 ± 821.7
Changes between early and late stages		2,783.3 ± 797.4	−208.3 ± 101.0	2,575.0 ± 844.5

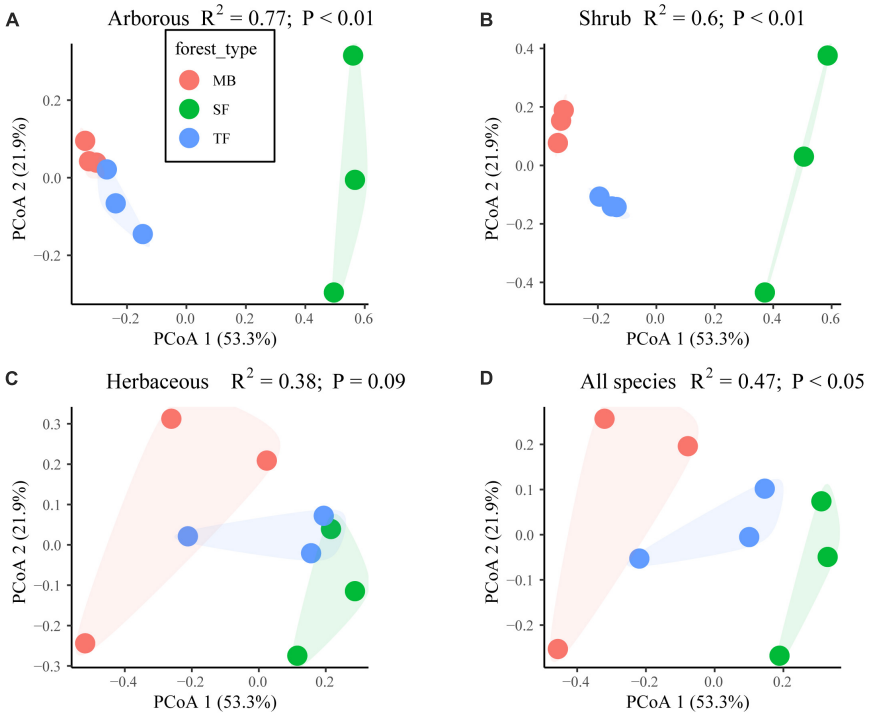

FIGURE 1
Effect of the Moso bamboo invasion on species composition difference of each layer among the three forest types [Moso bamboo forest (MB), transition tree-Moso-bamboo forest (TF), and secondary coniferous and broad-leaved mixed forest (SF)] in **(A)** arborous, **(B)** shrub, **(C)** herbaceous layers, and **(D)** the compound layers with all arborous, shrub, herbaceous species. Significant differences examined with PerMANOVA (permutational multivariate ANOVA) are indicated by $P < 0.05$ or 0.01. PCoA means principal co-ordinates analysis. PCoA1 and PCoA2 in the figures represented two components of PCoA with largest explaining power to the variation of the species composition difference.

Effects of the Moso bamboo invasion on species diversity

Changes in species diversity in the arborous layer

During the invasion of Moso bamboo into SF, species diversity in the arborous layer showed a significant decreasing trend, indicated by the significantly decreasing Shannon–Wiener index and increasing Simpson index over SF, TF, and MB ($P < 0.05$; Figure 2). Changes in the Margalef index seemed to support the same trend, but its values were not significantly different between the SF and TF ($P > 0.05$; Figure 2). Moreover, as the invasion progressed, the species' evenness got worse, as indicated by the reducing Pielou index ($P < 0.05$; Figure 2).

Changes in species diversity in the shrub layer

The Margalef index and Simpson index suggested no significant difference in the shrub layers among the three communities ($P > 0.05$; Figure 2), although the values seemed to point to increasing biodiversity over the invasion. In contrast, the Shannon–Wiener index indicated significantly higher species diversity in TF and MB than in SF ($P < 0.05$; Figure 2). The species evenness had no significant difference in the shrub layers among the three communities, as indicated by the Pielou index ($P > 0.05$; Figure 2).

Changes in species diversity in the herbaceous layer

The Margalef and Shannon–Wiener indexes suggested no difference in the herbaceous layers among the three

TABLE 3 Effects of Moso bamboo invasion on main species composition and importance value (mean ± SD).

Layer	Forest type	Species	Important value
Arborous	SF	*Schima superba*	27.6 ± 15.3
		Liquidambar formosana	27.1 ± 11.4
		Pinus massoniana	12.5 ± 5.7
		Castanopsis eyrei	6.2 ± 2.6
		Trachycarpus fortunei	6.1 ± 7.4
		Castanopsis sclerophylla	5.7 ± 3.6
		Ligustrum lucidum	3.4 ± 2.7
		Cunninghamia lanceolata	3.4 ± 2.7
		Cyclobalanopsis glauca	2.7 ± 1.5
		Liriodendron chinense	2.7 ± 1.5
		Michelia figo	2.6 ± 1.3
	TF	*Phyllostachys pubescens*	48.2 ± 7.8
		Pinus massoniana	15.6 ± 7.2
		Schima superba	12.7 ± 2.0
		Cyclobalanopsis glauca	6.2 ± 0.7
		Cunninghamia lanceolata	3.9 ± 0.7
		Castanopsis sclerophylla	3.6 ± 0.4
		Liquidambar formosana	2.4 ± 1.5
		Trachycarpus fortunei	1.9 ± 0.6
		Myrica rubra	1.8 ± 0.4
		Elaeocarpus decipiens	1.8 ± 0.4
		Ligustrum lucidum	1.7 ± 0.3
	MB	*Phyllostachys pubescens*	64.9 ± 2.9
		Schima superba	14.1 ± 0.1
		Pinus massoniana	9.3 ± 0.3
		Cyclobalanopsis glauca	8.6 ± 2.7
		Cunninghamia lanceolata	3.1 ± 0.6
Shrub	SF	*Indocalamus tessellatus*	31.6 ± 30.8
		Ligustrum lucidum	7.4 ± 3.9
		Quercus glauca	7.0 ± 4.3
		Lindera glauca	5.2 ± 4.4
		Symplocos stellaris	4.5 ± 2.4
	TF	*Camellia japonica*	11.6 ± 3.5
		Symplocos sumuntia	8.9 ± 2.7
		Cinnamomum japonicum	7.0 ± 4.8
		Symplocos stellaris	6.9 ± 6.3
		Ligustrum lucidum	5.8 ± 1.2
		Quercus glauca	5.7 ± 2.2
	MB	*Symplocos stellaris*	12.3 ± 3.9
		Camellia japonica	9.3 ± 4.3
		Symplocos sumuntia	9.2 ± 1.6
		Ilex chinensis	6.5 ± 5.4
		Lithocarpus glaber	5.7 ± 6.5
Herbaceous	SF	*Rubus buergeri*	70.8 ± 6.1
		Ophiopogon bodinieri	10.2 ± 9.4
		Nephrolepis auriculata	7.2 ± 4.3
		Lepidomicrosorum buergerianum	6.1 ± 2.3
		Anredera cordifolia	5.8 ± 1.7
	TF	*Rubus buergeri*	57.5 ± 11.6
		Lepidomicrosorum buergerianum	16.3 ± 0.7
		Nephrolepis auriculata	15.3 ± 12.0
		Ophiopogon bodinieri	6.6 ± 5.7
		Plantago depressa	4.3 ± 1.8
	MB	*Rubus buergeri*	45.3 ± 13.4
		Lepidomicrosorum buergerianum	15.1 ± 8.0
		Pyrrosia lingua	12.7 ± 6.9
		Nephrolepis auriculata	9.3 ± 10.8
		Tetrastigma formosanum	7.1 ± 7.1
		Gardneria multiflora	5.4 ± 4.1
		Anredera cordifolia	5.1 ± 3.6

In red, top-contributing species; in blue, species descending from the top-contributing nodes.

communities ($P > 0.05$), while the Simpson index indicated higher diversity in MB than in SF ($P < 0.05$; Figure 2). Finally, species evenness had no significant difference in the herbaceous layers among the three communities, as indicated by the Pielou index ($P > 0.05$; Figure 2).

Effects of Moso bamboo invasion on aboveground biomass

During the invasion of Moso bamboo into SF, the aboveground biomass showed no significant differences in arborous and herbaceous layers and the overall stand between the three forest types ($P > 0.05$; Table 4). In contrast, the aboveground biomass in the shrub layers was significantly higher in TF and MB than in SF ($P < 0.05$; Table 4). The proportions of aboveground biomass in each layer to the total biomass had no significant difference among the three forest types ($P > 0.05$; Table 4). The arborous layers occupied the largest proportion (~99%) of the aboveground biomass in all three forest types. With the invasion progress, the aboveground biomass of Moso bamboo in the community gradually increased to 3,538.63 ± 1,305.82 and 7,482.72 ± 2,532.43 g m^{-2} in the TF and MB, which correspondingly occupied 17.90 ± 6.41% and 41.56 ± 8.21% of the total aboveground biomass, respectively.

Relationship between diversity and aboveground biomass

The correlation between plant diversity and aboveground biomass was insignificant in the arborous, shrub, and herbaceous layers ($P > 0.05$; Table 5). It was also not significant

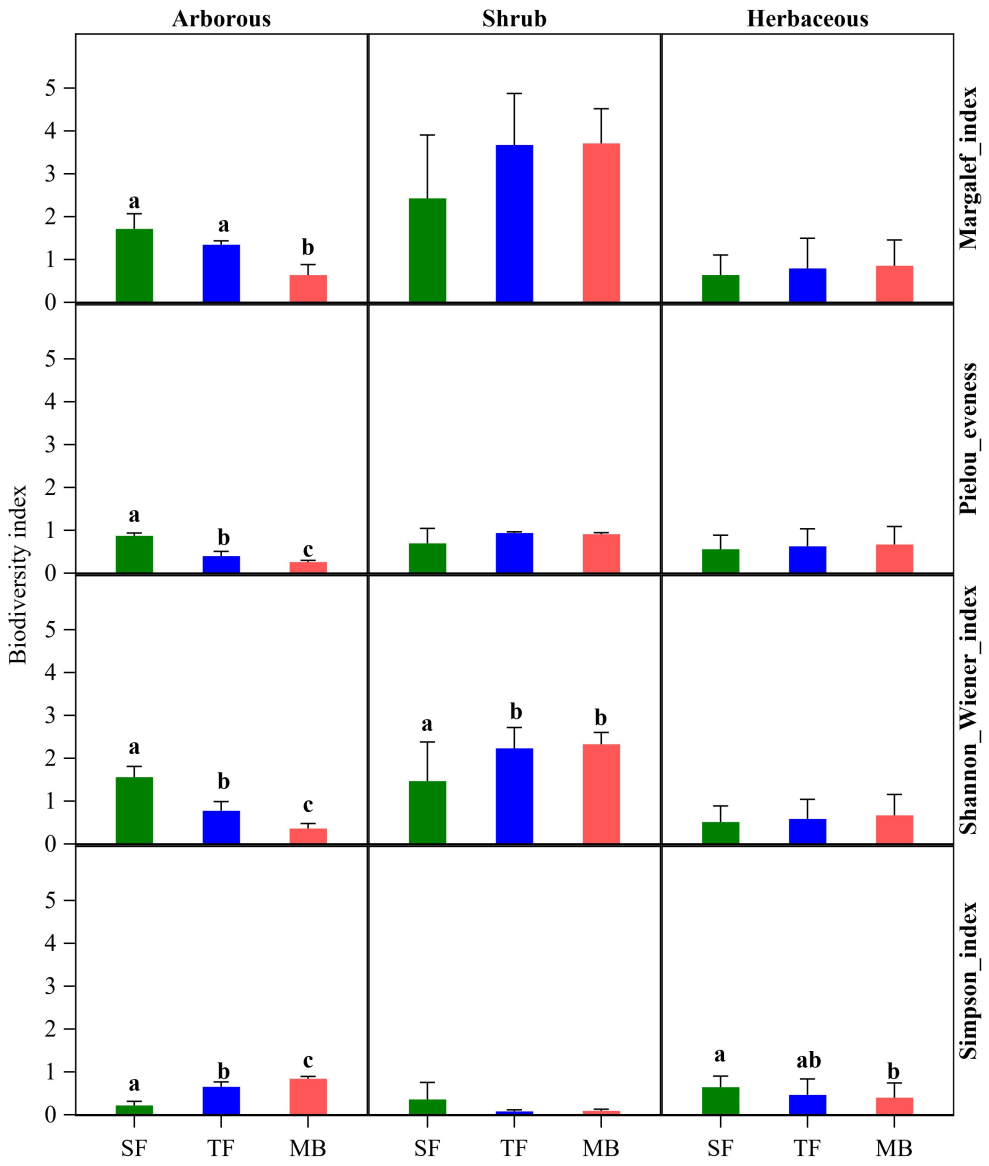

FIGURE 2
Effect of the Moso bamboo invasion on species diversity of each layer. Different letters in the same column indicate significant differences at $P < 0.05$.

TABLE 4 Effect of the Moso bamboo invasion on aboveground biomass (mean ± SD; $N = 3$ in each group) in each layer and their contribution to the total aboveground biomass.

	Forest type	Total aboveground biomass	Arborous (trees and Moso bamboo)	Shrub	Herbaceous	Moso bamboo
Biomass ($g\ m^{-2}$)	SF	19,529.92 ± 6,190.68	19,393.52 ± 6135.53	16.72 ± 1.52**a**	119.68 ± 57.48	–
	TF	19,679.57 ± 675.28	19,533.55 ± 683.46	22.37 ± 8.95**b**	123.64 ± 30.91	3,538.63 ± 1,305.82
	MB	17,749.90 ± 4158.71	17,557.27 ± 4,112.54	56.21 ± 27.78**b**	136.42 ± 24.22	7,482.72 ± 2,532.43
percent (%)	SF		99.31 ± 0.09%	0.09 ± 0.03%	0.59 ± 0.12%	–
	TF		99.26 ± 0.13%	0.11 ± 0.05%	0.63 ± 0.16%	17.90 ± 6.41%
	MB		98.91 ± 0.13%	0.31 ± 0.10%	0.78 ± 0.07%	41.56 ± 8.21%

Different letters in the shrub column indicate significant differences among the forest types in the same layer at $P < 0.05$.

TABLE 5 Effect of the Moso bamboo invasion on the relationships between aboveground biomass and biodiversity indexes in each layer and the whole stand comprised of three layers (N = 9 in each group).

Forest type	Biodiversity indexes	$Pr > F$	R^2
Arborous	Margalef_index	0.81	0.01
	Pielou_eveness	0.90	0.00
	Shannon_Wiener_index	0.97	0.00
	Simpson_index	0.97	0.00
Shrub	Margalef_index	0.30	0.15
	Pielou_eveness	0.59	0.04
	Shannon_Wiener_index	0.31	0.15
	Simpson_index	0.50	0.07
Herbaceous	Margalef_index	0.22	0.21
	Pielou_eveness	0.08	0.38
	Shannon_Wiener_index	0.20	0.22
	Simpson_index	0.22	0.21
All species	Margalef_index	0.34	0.13
	Pielou_evenness_index	0.09	0.36
	Shannon_Wiener_index	0.22	0.21
	Simpson_index	0.14	0.28

in the overall stand when all layers were considered ($P > 0.05$; **Table 5**).

Discussion

Effects of Moso bamboo invasion on species composition and diversity

Species composition is not only the basis of community structure and biodiversity but also the root of forest ecosystem processes (Tilman et al., 1997). Existing studies show that both alien and native plant invasions have a certain impact on the community's species composition (Garrott et al., 1993; Davies, 2011; Lima et al., 2012). This study found that the invasion of Moso bamboo significantly changed the species composition in the arborous and shrub layers but not in the herbaceous layer (**Figures 1A–C** and **Table 3**), which also changed the overall species composition significantly (**Figure 1D**). For example, the number of species had been reduced from 11 in SF to 5 in MB in the arborous layer. The important values of the main dominant arborous species *S. superba*, *L. formosana,* and *P. massoniana* decreased from 27.6, 27.1, and 12.5 before expansion to 14.1, 0, and 9.3, respectively (**Table 3**). On the contrary, Moso bamboo gradually dominated the arborous layers with important values of 48.2 and 64.9 in TF and MB, respectively. The interchanged dominance between trees and Moso bamboo in the arborous layer was consistent with several other research results (Bai et al., 2013; Yang et al., 2015; Ouyang et al., 2016). The findings supported our first hypothesis, i.e., that the invasion of Moso bamboo changed species composition, especially in the arborous and shrub layers. Although a few herbaceous species disappeared or newly appeared with the invasion, the species composition in the herbaceous layer was not significantly changed (**Figure 1D** and **Table 3**). Three herbaceous species (*R. buergeri*, *N. auriculata*, and *L. buergerianum*) have always been in the SF, TF, and MB, and *R. buergeri* has always been the most dominant species in the herbaceous layers of the three communities. The finding may indicate that the invasion of Moso bamboo did not alter the near-ground light or soil conditions suiting the local shade-tolerant herbaceous species.

Regarding species diversity of the three layers, the arborous layer was the most influenced by the invasion in this study. Compared with the pre-invaded SF, MB had significantly lower diversity, as indicated by all three diversity indexes (Margalef, Shannon–Wiener, and Simpson index; $P < 0.05$; **Figure 2**). At the same time, the species evenness was smaller in MB than in SF ($P < 0.05$; **Figure 2**). This result is consistent with several previous studies (Bai et al., 2013; Yang et al., 2015; Ouyang et al., 2016) and partly supports our first hypothesis that invasion decreases plant diversity. However, the first hypothesis was not fully supported by the results regarding the shrub and herbaceous layers. Among the three diversity indexes, only one of them (Shannon–Wiener and Simpson indexes for the shrub and herbaceous layers, respectively) indicated a significantly increased diversity. In contrast, the other two indexes inversely meant that the diversities of these two layers were unchanged (**Figure 2**). The finding was consistent with the results observed in the invasion progress of Moso bamboo into Chinese fir (Xu et al., 2019). In contrast, compared with the invaded coniferous and broad-leaved mixed forests (Bai et al., 2013; Yang et al., 2015; Ouyang et al., 2016) and the secondary evergreen broad-leaved forest (Ouyang et al., 2016), MB had lower diversity in both shrub and herbaceous layers. In another study on the invaded coniferous and broad-leaved mixed forests (Bai et al., 2013), species diversity was reduced in the shrub layers but improved in the herbaceous layer.

Species diversity varied in different studies, which may be related to the short observation time and the different invasion stages because understory species diversity is a dynamic process. The increase of species diversity in shrub and herb layers during the invasion of Moso bamboo into SF may result from increased light intensity under the forest (Liu et al., 2011) because better light conditions may reduce light competition to improve the species diversity of understory vegetation (Hautier et al., 2009). However, it should be noted that different plants have different adaptability to light, and the influence of light intensity on species diversity may be restricted by the light requirement of plants (Boothroyd-Roberts et al., 2013). Much higher or much lower light intensity is not conducive to increasing the species diversity of understory plants (Tao and Feng, 1998). On the contrary, Moso bamboo forests have low stem density

and soil-water content than other forest types (Shinohara and Otsuki, 2015), which may benefit understory diversity. In addition, Moso bamboo invasion increased soil bacterial diversity, soil pH, and soil organic carbon concentrations (Lin et al., 2014; Liu et al., 2021; Ouyang et al., 2022), which may also be beneficial to increasing the biodiversity under the forest. However, there is not enough direct evidence to support this argument. The mechanism of Moso bamboo invasion needs further study.

Effects of Moso bamboo invasion on aboveground biomass and its relationship with species diversity

Although the response relationship between the change of community species composition and forest ecosystem function is complex, many studies have shown that the loss of community species will lead to the decline of forest productivity and resistance and increase the instability of the system (Lavorel and Garnier, 2002; Barrufol et al., 2013; Bruelheide et al., 2014; Cavanaugh et al., 2014). In particular, the replacement of the dominant species in a community will affect the community environment on which other tree species depend, leading to the transformation of plant functional groups (Hooper et al., 2005), thus affecting the composition, structure, and function of the whole ecosystem (Lima et al., 2012). Contrary to our second hypothesis, the aboveground biomass in the entire stand and the arborous layer was not significantly reduced in TF and MB compared to the SF, which may be attributed to the increasing stem number of Moso bamboo (**Table 2**). This finding is consistent with the research results of Fukushima et al. (2015).

Previous studies have shown that Moso bamboo may obtain more nutrients and light resources by increasing the DBH and height to promote rapid growth and expansion during the invasion (Bai et al., 2012; Liu et al., 2016; Xu et al., 2019). However, in this study, the average DBH and height of Moso bamboo decreased during the invasion of Moso bamboo into SF (**Table 1**). This result may be due to the different invasion sites and forests (Liu et al., 2019). It may also be that the intraspecific competition of standing bamboo in the MB may be more intense, so it is necessary to obtain more light and nutrients by increasing height and DBH to get a competitive advantage. Its internal mechanism needs to be further studied.

The proportion of understory vegetation biomass in the total biomass of the forest ecosystem is small. Still, it plays a vital role in maintaining the succession and functional stability of the whole forest ecosystem (Sun et al., 2015). This study found that the aboveground biomass of the shrub and herbaceous layers and their proportion of the total aboveground biomass increased during the invasion of Moso bamboo to SF, but the increment in the herbaceous layer was not statistically significant (**Table 4**). Although the shrub and herb layers of the three stands contribute less to the biomass of the community, the understory often has more abundant species (**Table 3**). These species play an important role in the environment under plastic afforestation, affecting forest dynamics, soil carbon pool, and nutrient cycle (Nilsson and Wardle, 2005). Therefore, the change of species biomass in the understory should not be ignored when evaluating the ecological aftereffects of the Moso bamboo invasion.

The results showed no significant correlation between aboveground biomass and the diversity index of each layer and the whole stand during the Moso bamboo invasion ($P > 0.05$; **Table 5**), which indicated that the Moso bamboo invasion had no impact on the relationship. This result does not verify our third hypothesis that the positive correlation between species diversity and biomass is common across forest layers (Zhang et al., 2017). This insignificant relationship may be attributed to the intensity and direction of the correlation between biodiversity and ecosystem function changing under different environmental conditions (Cardinale et al., 2000). According to the stress gradient hypothesis, species are more competitive in the ideal environment but more mutual aid in an adverse environment. Therefore, it is more likely to find a positive correlation between species richness and aboveground biomass in adverse environmental conditions (Maestre et al., 2009). In this study, the arborous layer is rich in light resources. Therefore, Moso bamboo contributes a lot of biomass and excludes the survival of other species, which leads to no significant positive relationship between species richness and biomass.

Conclusion

Although the Moso bamboo invasion has drawn considerable attention to its impact, especially on biodiversity, few studies have reported the effects of the Moso bamboo invasion on forest biomass and the forest biodiversity–biomass relationship. By using the space-for-time method, we investigated the dynamics of species composition, diversity, and aboveground biomass of arborous, shrub, and herbaceous layers during Moso bamboo invasion into a SF. As the most significant part of the aboveground biomass (>99%), the arborous layer showed a decreasing trend in the aboveground biomass with the invasion progress. Still, the decrease was not statistically significant, which may be attributed to the increased five-fold stems. Moreover, the aboveground biomass in the arborous layer had no significant correlation with the significantly decreasing diversity. In the understory layers, shrubs had significantly increased aboveground biomass, while herbs did not. Similar to the arborous layer, both shrub and herbaceous layers did not significantly correlate their aboveground biomass and diversity indexes. However, these findings were concluded based on three plots per forest type and one transitional status, which may not

cover enough variation in both biodiversity and aboveground biomass. Additionally, belowground biomass is also an essential part of the forest, which should be considered. We hope the findings of this study contribute to some fundamentals for future research and understanding of Moso bamboo invasion.

Data availability statement

The original contributions presented in this study are included in the article/supplementary material, further inquiries can be directed to the corresponding author/s.

Author contributions

XiC: methodology, software, investigation, visualization, writing – original draft and review, and editing. XinC and SH: data curation and investigation. DF: methodology, writing – review and editing, conceptualization, and investigation. All authors contributed to the article and approved the submitted version.

Funding

This research was supported by the Talent Project of Jiyang College of Zhejiang A&F University (Grant numbers 05251700035 and 05251700038).

Conflict of interest

The authors declare that the research was conducted in the absence of any commercial or financial relationships that could be construed as a potential conflict of interest.

Publisher's note

All claims expressed in this article are solely those of the authors and do not necessarily represent those of their affiliated organizations, or those of the publisher, the editors and the reviewers. Any product that may be evaluated in this article, or claim that may be made by its manufacturer, is not guaranteed or endorsed by the publisher.

References

Akutsu, H., Aizawa, M., Matsue, K., and Ohkubo, T. (2012). Distribution and invasion of *Phyllostachys pubescens* stands into neighboring forests in Nasukarasuyama, Tochigi Prefecture. *Bull. Utsunomiya Univ. For.* 48, 139–152.

Ali, A., and Yan, E.-R. (2017). The forest strata-dependent relationship between biodiversity and aboveground biomass within a subtropical forest. *For. Ecol. Manag.* 401, 125–134. doi: 10.1016/j.foreco.2017.06.056

Bai, S., Wang, Y., Conant, R. T., Zhou, G., Xu, Y., Wang, N., et al. (2016). Can native clonal Moso bamboo encroach on adjacent natural forest without human intervention? *Sci. Rep.* 6:31504. doi: 10.1038/srep31504

Bai, S.-B., Zhou, G.-M., Wang, Y.-X., Liang, Q.-Q., Chen, J., Cheng, Y.-Y., et al. (2013). Plant species diversity and dynamics in forests invaded by Moso bamboo (*Phyllostachys edulis*) in Tianmu mountain nature reserve. *Biodiv. Sci.* 21, 288–295. doi: 10.3724/SP.J.1003.2013.08258

Bai, S.-B., Zhou, G.-M., Wang, Y.-X., Yu, S.-Q., Li, Y.-H., and Fang, F.-Y. (2012). Stand structure change of *Phyllostachys pubescens* forest expansion in tianmushan national nature reserve. *J. West China For. Sci.* 41, 77–82.

Bai, Y.-F., Wu, J.-G., Pan, Q.-M., Huang, J.-H., Wang, Q.-B., Li, F.-S., et al. (2007). Positive linear relationship between productivity and diversity: Evidence from the Eurasian Steppe. *J. Appl. Ecol.* 44, 1023–1034. doi: 10.1111/j.1365-2664.2007.01351.x

Barrufol, M., Schmid, B., Bruelheide, H., Chi, X., Hector, A., Ma, K., et al. (2013). Biodiversity promotes tree growth during succession in subtropical forest. *PLoS One* 8:e81246. doi: 10.1371/journal.pone.0081246

Boothroyd-Roberts, K., Gagnon, D., and Truax, B. (2013). Can hybrid poplar plantations accelerate the restoration of forest understory attributes on abandoned fields? *For. Ecol. Manag.* 287, 77–89. doi: 10.1016/j.foreco.2012.09.021

Bracken, M. E., Douglass, J. G., Perini, V., and Trussell, G. C. (2017). Spatial scale mediates the effects of biodiversity on marine primary producers. *Ecology* 98, 1434–1443. doi: 10.1002/ecy.1812

Bruelheide, H., Nadrowski, K., Assmann, T., Bauhus, J., Both, S., Buscot, F., et al. (2014). Designing forest biodiversity experiments: General considerations illustrated by a new large experiment in subtropical China. *Methods Ecol. Evol.* 5, 74–89. doi: 10.1111/2041-210X.12126

Cardinale, B. J., Nelson, K., and Palmer, M. A. (2000). Linking species diversity to the functioning of ecosystems: On the importance of environmental context. *OIKOS* 91, 175–183. doi: 10.1034/j.1600-0706.2000.910117.x

Cavanaugh, K. C., Gosnell, J. S., Davis, S. L., Ahumada, J., Boundja, P., Clark, D. B., et al. (2014). Carbon storage in tropical forests correlates with taxonomic diversity and functional dominance on a global scale. *Glob. Ecol. Biogeogr.* 23, 563–573. doi: 10.1111/geb.12143

Chen, Z.-Y., Yao, X.-M., and Tian, X.-M. (2009). The regression analysis between fertilization and the output, the economic benefit in *Phyllostachys pubescens* for culm-producing. *Chin. Agric. Sci. Bull.* 25, 166–169.

Corlett, R. T. (2013). Where are the Subtropics? *Biotropica* 45, 273–275. doi: 10.1111/btp.12028

Davies, K. W. (2011). Plant community diversity and native plant abundance decline with increasing abundance of an exotic annual grass. *Oecologia* 167, 481–491. doi: 10.1007/s00442-011-1992-2

Dixon, P. (2003). Vegan, a package of R functions for community ecology. *J. Veg. Sci.* 14, 927–930.

Fukushima, K., Usui, N., Ogawa, R., and Tokuchi, N. (2015). Impacts of Moso bamboo (*Phyllostachys pubescens*) invasion on dry matter and carbon and nitrogen stocks in a broad-leaved secondary forest located in Kyoto, western Japan. *Plant Species Biol.* 30, 81–95. doi: 10.1111/1442-1984.12066

Garrott, R. A., White, P., and White, C. A. V. (1993). Overabundance: An issue for conservation biologists? *Conserv. Biol.* 7, 946–949. doi: 10.1046/j.1523-1739.1993.740946.x

Guo, X.-C., Shi, P.-J., Niinemets, Ü., Hölscher, D., Wang, R., Liu, M.-D., et al. (2021). "Diminishing returns" for leaves of five age-groups of *Phyllostachys edulis* culms. *Am. J. Bot.* 108, 1662–1672. doi: 10.1002/ajb2.1738

Hautier, Y., Niklaus, P. A., and Hector, A. (2009). Competition for light causes plant biodiversity loss after eutrophication. *Science* 324, 636–638. doi: 10.1126/science.1169640

Hooper, D. U., Chapin Iii, F. S., Ewel, J. J., Hector, A., Inchausti, P., Lavorel, S., et al. (2005). Effects of biodiversity on ecosystem functioning: A consensus of current knowledge. *Ecol. Monogr.* 75, 3–35. doi: 10.1890/04-0922

Huang, W.-W., Reddy, G. V., Li, Y.-Y., Larsen, J. B., and Shi, P.-J. (2020). Increase in absolute leaf water content tends to keep pace with that of leaf dry mass—evidence from bamboo plants. *Symmetry* 12, 1345. doi: 10.3390/sym12081345

Huang, W.-W., Su, X.-F., Ratkowsky, D. A., Niklas, K. J., Gielis, J., and Shi, P.-J. (2019). The scaling relationships of leaf biomass vs. leaf surface area of 12 bamboo species. *Glob. Ecol. Conserv.* 20:e00793. doi: 10.1016/j.gecco.2019.e00793

Jiang, L.-H., Mao, C.-M., Wu, H.-Z., Duan, Q.-X., and Fang, Z.-X. (2015). Investigation and analysis of Moso forest management in songyang county, Zhejiang province. *World Bamboo Rattan* 13, 28–34.

Lasky, J. R., Uriarte, M., Boukili, V. K., Erickson, D. L., John Kress, W., and Chazdon, R. L. (2014). The relationship between tree biodiversity and biomass dynamics changes with tropical forest succession. *Ecol. Lett.* 17, 1158–1167. doi: 10.1111/ele.12322

Lavorel, S., and Garnier, É. (2002). Predicting changes in community composition and ecosystem functioning from plant traits: Revisiting the Holy Grail. *Funct. Ecol.* 16, 545–556. doi: 10.1046/j.1365-2435.2002.00664.x

Lima, R. A., Rother, D. C., Muler, A. E., Lepsch, I. F., and Rodrigues, R. R. (2012). Bamboo overabundance alters forest structure and dynamics in the Atlantic Forest hotspot. *Biol. Conserv.* 147, 32–39. doi: 10.1016/j.biocon.2012.01.015

Lin, M.-Y., Hsieh, I., Lin, P.-H., Laplace, S., Ohashi, M., Chen, T.-H., et al. (2017). Moso bamboo (*Phyllostachys pubescens*) forests as a significant carbon sink? A case study based on 4-year measurements in central Taiwan. *Ecol. Res.* 32, 845–857. doi: 10.1007/s11284-017-1497-5

Lin, Y.-T., Tang, S.-L., Pai, C.-W., Whitman, W. B., Coleman, D. C., and Chiu, C.-Y. (2014). Changes in the soil bacterial communities in a cedar plantation invaded by Moso bamboo. *Microb. Ecol.* 67, 421–429. doi: 10.1007/s00248-013-0291-3

Liu, C.-X., Zhou, Y., Qin, H., Liang, C.-F., Shao, S., Fuhrmann, J. J., et al. (2021). Moso bamboo invasion has contrasting effects on soil bacterial and fungal abundances, co-occurrence networks and their associations with enzyme activities in three broadleaved forests across subtropical China. *For. Ecol. Manag.* 498:119549. doi: 10.1016/j.foreco.2021.119549

Liu, S., Zhou, G.-M., and Bai, S.-B. (2011). Light intensity changes on *Cunninghamia lanceolata* in mixed stands with different concentrations of *Phyllostachys pubescens*. *J. Zhejiang A&F Univ.* 28, 550–554.

Liu, X., Siemann, E., Cui, C., Liu, Y., Guo, X., and Zhang, L. (2019). Moso bamboo (*Phyllostachys edulis*) invasion effects on litter, soil and microbial PLFA characteristics depend on sites and invaded forests. *Plant Soil* 438, 85–99. doi: 10.1007/s11104-019-04010-3

Liu, X.-Z., Fan, S.-H., Liu, G.-L., and Peng, C. (2016). Changing characteristics of main structural indexes of community during the expansion of Moso bamboo forests. *Chin. J. Ecol.* 35, 3165–3171.

Maestre, F. T., Callaway, R. M., Valladares, F., and Lortie, C. J. (2009). Refining the stress-gradient hypothesis for competition and facilitation in plant communities. *J. Ecol.* 97, 199–205. doi: 10.1111/j.1365-2745.2008.01476.x

Martin, P. H., Canham, C. D., and Marks, P. L. (2009). Why forests appear resistant to exotic plant invasions: Intentional introductions, stand dynamics, and the role of shade tolerance. *Front. Ecol. Environ.* 7:142–149. doi: 10.1890/070096

Mori, A. S., Osono, T., Cornelissen, J. H. C., Craine, J., and Uchida, M. (2017). Biodiversity–ecosystem function relationships change through primary succession. *OIKOS* 126, 1637–1649. doi: 10.1111/oik.04345

Nackley, L. L., West, A. G., Skowno, A. L., and Bond, W. J. (2017). The nebulous ecology of native invasions. *Trends Ecol. Evol.* 32, 814–824. doi: 10.1016/j.tree.2017.08.003

Nakai, A., and Kisanuki, H. (2006). Effect of the bamboo culm density on the tree species diversity and density of understory at a forest stand on a major bed along the Miya river downstream [Japan]. *Bull. Faculty Bioresour. Mie Univ.* (Japan) 21–28.

Nilsson, M.-C., and Wardle, D. A. (2005). Understory vegetation as a forest ecosystem driver: Evidence from the northern Swedish boreal forest. *Front. Ecol. Environ.* 3:421–428. doi: 10.1890/1540-9295(2005)003[0421:UVAAFE]2.0.CO;2

Okutomi, K., Shinoda, S., and Fukuda, H. (1996). Causal analysis of the invasion of broad-leaved forest by bamboo in Japan. *J. Veg. Sci.* 7, 723–728. doi: 10.2307/3236383

Ouyang, M., Tian, D., Pan, J.-M., Chen, G.-P., Su, H.-J., Yan, Z.-B., et al. (2022). Moso bamboo (*Phyllostachys edulis*) invasion increases forest soil pH in subtropical China. *CATENA* 215:106339. doi: 10.1016/j.catena.2022.106339

Ouyang, M., Yang, Q.-P., Chen, X., Yang, G.-Y., Shi, J.-M., and Fang, X.-M. (2016). Effects of the expansion of Phyllostachys edulis on species composition, structure and diversity of the secondary evergreen broad-leaved forests. *Biodiv. Sci.* 24, 649–657. doi: 10.17520/biods.2015290

Pan, Y.-D., Birdsey, R. A., Fang, J.-Y., Houghton, R., Kauppi, P. E., Kurz, W. A., et al. (2011). A large and persistent carbon sink in the world's forests. *Science* 333, 988–993. doi: 10.1126/science.1201609

Pickett, S. T. (1989). "Space-for-time substitution as an alternative to long-term studies," in *Long-term studies in ecology*, ed. G. E. Likens (New York, NY: Springer), 110–135. doi: 10.1007/978-1-4615-7358-6_5

R Core Team (2022). *R: A language and environment for statistical computing*. Vienna: R Foundation for Statistical Computing.

Ramula, S., and Pihlaja, K. (2012). Plant communities and the reproductive success of native plants after the invasion of an ornamental herb. *Biol. Invasions* 14, 2079–2090. doi: 10.1007/s10530-012-0215-z

Ratcliffe, S., Wirth, C., Jucker, T., Van Der Plas, F., Scherer-Lorenzen, M., Verheyen, K., et al. (2017). Biodiversity and ecosystem functioning relations in European forests depend on environmental context. *Ecol. Lett.* 20, 1414–1426. doi: 10.1111/ele.12849

Shen, Q.-Y., and Tang, M.-P. (2019). Stem biomass models of *Phyllostachysedulis* in Zhejiang province. *Sci. Silvae Sin.* 55, 181–188.

Shi, P.-J., Gao, J., Song, Z.-P., Liu, Y.-H., and Hui, C. (2018). Spatial segregation facilitates the coexistence of tree species in temperate forests. *Forests* 9:768. doi: 10.3390/f9120768

Shi, P.-J., Preisler, H. K., Quinn, B. K., Zhao, J., Huang, W.-W., Röll, A., et al. (2020). Precipitation is the most crucial factor determining the distribution of Moso bamboo in Mainland China. *Glob. Ecol. Conserv.* 22:e00924. doi: 10.1016/j.gecco.2020.e00924

Shinohara, Y., and Otsuki, K. (2015). Comparisons of soil-water content between a Moso bamboo (*Phyllostachys pubescens*) forest and an evergreen broadleaved forest in western Japan. *Plant Species Biol.* 30, 96–103. doi: 10.1111/1442-1984.12076

Silva Pedro, M., Rammer, W., and Seidl, R. (2017). Disentangling the effects of compositional and structural diversity on forest productivity. *J. Veg. Sci.* 28, 649–658. doi: 10.1111/jvs.12505

Song, Q.-N., Lu, H., Liu, J., Yang, J., Yang, G.-Y., and Yang, Q.-P. (2017). Accessing the impacts of bamboo expansion on NPP and N cycling in evergreen broadleaved forest in subtropical China. *Sci. Rep.* 7:40383. doi: 10.1038/srep40383

Sun, Y.-J., Ma, W., and Liu, Y.-H. (2015). Biomass of *Larix olgensis* plantations based on species diversity analyses in Heilongjiang, China. *Acta Ecol. Sin.* 35, 3329–3338. doi: 10.5846/stxb201306201752

Tao, F.-L., and Feng, Z.-W. (1998). Studies on plant species diversity under the canopy of *Larix kaempferi* community in west mountain area of Henan Province. *Chin. J. Ecol.* 17, 1–6.

Tian, X.-K., Wang, M.-Y., Meng, P., Zhang, J.-S., Zhou, B.-Z., Ge, X.-G., et al. (2020). Native bamboo invasions into subtropical forests alter microbial communities in litter and soil. *Forests* 11:314. doi: 10.3390/f11030314

Tilman, D., Knops, J., Wedin, D., Reich, P., Ritchie, M., and Siemann, E. (1997). The influence of functional diversity and composition on ecosystem processes. *Science* 277, 1300–1302. doi: 10.1126/science.277.5330.1300

van der Sande, M. T., Peña-Claros, M., Ascarrunz, N., Arets, E. J., Licona, J. C., Toledo, M., et al. (2017). Abiotic and biotic drivers of biomass change in a Neotropical forest. *J. Ecol.* 105, 1223–1234. doi: 10.1111/1365-2745.12756

van Kleunen, M., Weber, E., and Fischer, M. (2010). A meta-analysis of trait differences between invasive and non-invasive plant species. *Ecol. Lett.* 13, 235–245. doi: 10.1111/j.1461-0248.2009.01418.x

Vilà, M., Espinar, J. L., Hejda, M., Hulme, P. E., Jarošík, V., Maron, J. L., et al. (2011). Ecological impacts of invasive alien plants: A meta-analysis of their effects on species, communities and ecosystems. *Ecol. Lett.* 14, 702–708. doi: 10.1111/j.1461-0248.2011.01628.x

Wang, B., Liu, M., and Zhang, B. (2009). Dynamics of net production of chinese forest vegetation based on forest inventory data. *For. Resour. Manag.* 1, 35–43.

Wang, Y. J., Müller-Schärer, H., Van Kleunen, M., Cai, A. M., Zhang, P., Yan, R., et al. (2017). Invasive alien plants benefit more from clonal integration in heterogeneous environments than natives. *New Phytol.* 216, 1072–1078. doi: 10.1111/nph.14820

Wang, Y.-J., Chen, D., Yan, R., Yu, F.-H., and Van Kleunen, M. (2019). Invasive alien clonal plants are competitively superior over co-occurring native clonal plants. *Perspect. Plant Ecol. Evol. Syst.* 40:125484. doi: 10.1016/j.ppees.2019.125484

Wang, Y.-X., Bai, S.-B., Binkley, D., Zhou, G.-M., and Fang, F.-Y. (2016). The independence of clonal shoot's growth from light availability supports Moso bamboo invasion of closed-canopy forest. *For. Ecol. Manag.* 368, 105–110. doi: 10.1016/j.foreco.2016.02.037

Warren, R. J., King, J. R., Tarsa, C., Haas, B., and Henderson, J. (2017). A systematic review of context bias in invasion biology. *PLoS One* 12:e0182502. doi: 10.1371/journal.pone.0182502

Wu, X., Wang, X.-P., Tang, Z.-Y., Shen, Z.-H., Zheng, C.-Y., Xia, X.-L., et al. (2015). The relationship between species richness and biomass changes from boreal to subtropical forests in China. *Ecography* 38, 602–613.

Xu, D.-W., Liu, J.-F., He, Z.-S., and Zheng, S.-Q. (2019). Community species diversity after *Phyllostachys edulis* expansion to *Cunninghamia lanceolata* forest. *J. For. Environ.* 39, 37–41.

Xue, W., Shen, J. X., Guo, Z. W., Lei, J. P., Li, J. M., Yu, F. H., et al. (2021). Shoot removal interacts with soil temperature to affect survival, growth and physiology of young ramets of a bamboo. *For. Ecol. Manage.* 481:118735.

Yang, Q.-P., Wang, B., Guo, Q.-R., Zhao, G.-D., Fang, K., and Liu, Y.-Q. (2011). Effects of *Phyllostachys edulis* expansion on carbon storage of evergreen broad-leaved forest in Dagangshan Mountain, Jiangxi. *Acta Agric. Univ. Jiangxiensis* 33, 0529–0536.

Yang, Q.-P., Yang, G.-Y., Song, Q.-N., Shi, J.-M., Ouyang, M., Qi, H.-Y., et al. (2015). Ecological studies on bamboo expansion: Process, consequence and mechanism. *Chin. J. Plant Ecol.* 39, 110–124. doi: 10.17521/cjpe.2015.0012

Zeng, W. (2018). Validation of two-variable tree volume tables for main tree species in China. *For. Resour. Manage.* 5, 37–43.

Zhang, H.-N., and Xue, J.-H. (2018). Spatial pattern and competitive relationships of Moso bamboo in a native subtropical rainforest community. *Forests* 9:774. doi: 10.3390/f9120774

Zhang, Y., Chen, H. Y., and Taylor, A. R. (2017). Positive species diversity and aboveground biomass relationships are ubiquitous across forest strata despite interference from overstorey trees. *Funct. Ecol.* 31, 419–426. doi: 10.1111/1365-2435.12699

frontiers | Frontiers in Plant Science

TYPE Original Research
PUBLISHED 28 October 2022
DOI 10.3389/fpls.2022.969718

OPEN ACCESS

EDITED BY
Lucian Copolovici,
Aurel Vlaicu University of Arad,
Romania

REVIEWED BY
Chao Ma,
China Agricultural University, China
Kusum Khatri,
Ben-Gurion University of the Negev,
Israel

*CORRESPONDENCE
Xinzhang Song
xzsong@126.com
Songheng Jin
shjin@zafu.edu.cn
Xiangtao Zhu
zhuxt@zafu.edu.cn

†These authors have contributed equally to this work

SPECIALTY SECTION
This article was submitted to Functional Plant Ecology, a section of the journal Frontiers in Plant Science

RECEIVED 15 June 2022
ACCEPTED 12 September 2022
PUBLISHED 28 October 2022

CITATION
Ji W, Hong E, Chen X, Li Z, Lin B, Xia X, Li T, Song X, Jin S and Zhu X (2022) Photosynthetic and physiological responses of different peony cultivars to high temperature. *Front. Plant Sci.* 13:969718. doi: 10.3389/fpls.2022.969718

Photosynthetic and physiological responses of different peony cultivars to high temperature

Wen Ji[1†], Erman Hong[1†], Xia Chen[2†], Zhijun Li[2], Bangyu Lin[2], Xuanze Xia[2], Tianyao Li[2], Xinzhang Song[1*], Songheng Jin[2*] and Xiangtao Zhu[1,2*]

[1]State Key Laboratory of Subtropical Silviculture, Zhejiang A&F University, Hangzhou, China, [2]College of Jiyang, Zhejiang A&F University, Zhuji, China

In order to investigate the causes of the differences in heat tolerance ('Lu He Hong' and 'Zhi Hong'), we studied the physiological changes, photosynthetic properties and regulatory mechanism of the two peony cultivars at high temperature. The results showed that the physiological changed of different peony cultivars varied significantly under high temperature stress. With the extension of high temperature stress time, MDA content of 'Lu He Hong' increased,while 'Zhi Hong' rised first and then decreased, SOD activity of 'Lu He Hong' rised first and then decreased, that of 'Zhi Hong' kept rising, POD activity of 'Lu He Hong' kept decreasing, while 'Zhi Hong' rised. The photosynthetic instrument records the change of peony photosynthesis parameters at high temperature; the chlorophyll A (Chla) fluorescence transient is recorded using the plant efficiency analyzer (PEA), analyzed according to the JIP test (O-J-I-P fluorescence transient analysis), and several parameters were derived to explain the photosynthetic efficiency difference between different peony cultivars. The tested cultivars responded differently to the survey conditions, and the PCA analysis showed that the 'Zhi Hong' was more well tolerated and showed better thermal stability of the PSII. The reduced efficiency of the 'Lu He Hong' PSII antenna leads to higher heat dissipation values to increase the light energy absorbed by unit reaction center (ABS/RC), the energy captured by unit reaction center (TR_0/RC), and the energy dissipated by unit reaction center (DI_0/RC), which significantly leads to its lower total photosynthetic performance (PI_{total}). The light capture complex of the variety 'Zhi Hong' has high connectivity with its reaction center, less damage to OEC activity, and better stability of the PSII system. The results show that 'Zhi Hong' improves heat resistance by stabilizing the cell membrane, a strong antioxidant system, as well as a more stable photosynthetic system. The results of this study provide a theoretical basis for the screening of heat-resistant

peonies suitable for cultivation in Jiangnan area and for the selection and breeding of heat-resistant cultivars.

KEYWORDS

high temperature, peony, fluorescence transient, photosynthetic, JIP-test

Introduction

In recent years, with frequent occurrence of extreme weather, global climate change, mainly characterized by temperature rise, has become the focus of worldwide concern (Yu, 2019). High temperature is an important factor affecting crop productivity and plant growth in many regions of the world (Lesk et al., 2016). High temperature stress can adversely affect seed germination and seed viability, leading to thermal damage or death of seeds (Bita and Gerats, 2013). High temperature lead to various plant physiological changes such as scorched leaves and stems, leaf abscission and senescence, stem and root growth inhibition or reduced numbers, pollen tube growth and pollen sterility, and fruit damage leading to catastrophic loss of crop yield resulting in severe loss of productivity (Hemantaranjan et al., 2014). For example, high temperature can have a significant negative impact on the reproductive phenological stages of flowering, silk formation and seed filling in maize (Tiwari and Yadav, 2019), common bean plants are subjected to high temperature stress that restricts pollen tube growth and reduces pollen viability, resulting in low pod and fruit set rates (Gross and Kigel, 1994), rice tasseling and flowering above 35°C do not proceed normally and fertilization rates are significantly reduced (Morita et al., 2005). To counteract the damage caused by high temperature, plants have developed various defense mechanisms by regulating a variety of physiochemical mechanisms such as growth inhibition, leaf senescence, and basic physiological processes (Fahad et al., 2018), including a complex metabolic regulatory process called the heat shock response (Mittler et al., 2012).

Plants subjected to fairly common stresses, such as warmer summer conditions, respond by small but significant changes (Strasser and Tsimilli-Michael, 2001). Tests used to study changes induced by high temperature need to be very sensitive and informative. A very effective method is the measurement of Chla fluorescence, which can provide qualitative and quantitative information about the physiological state of photosynthetic organs, especially photosystem PSII. Numerous studies have shown that transient fluorescence kinetics is highly sensitive to various environmental changes (Kalaji et al., 2014a). Chlorophyll fluorescence kinetics is widely used in environmental science, agronomy, and plant science because of its fast, sensitive, and noninvasive properties (Strasser et al., 2004). Typical fast chlorophyll fluorescence induction kinetic curves have phases O, J, I, and P (Strasser and Govindjee, 1991), and in addition to these basic steps, some special stresses have been found under the L- (~150 μs) and K- (~300 μs) steps, as well as G- and H-steps between phases I-P (Strasser et al., 2004). The quantitative analysis of the fluorescence uptake kinetics O-J-I-P curve, called the JIP test based on the "biofilm energy flux theory" (Strasser and Strasser, 1995), translates the qualitative changes of the fluorescence uptake kinetics O-J-I-P curve into quantitative changes of selected phenomenological and biophysical-structural-functional parameters. proven to be a powerful and popular tool for quantifying PSII architecture and behavior (Tsimilli-Michael, 2019).

Peony (*Paeonia suffruticosa* Andr.) is one of the traditional flowers of China. It has a broad market prospect because of its tall, colorful and beautiful flowers. It can be used as potted flowers, cut flowers and horticultural materials to form a unique seasonal landscape (Li et al., 2011; Xue et al., 2018). Peony is suitable for cool climate and does not tolerate high temperature. In contrast, the summer in Jiangnan is hot and rainy, so peony growth and cultivation in Jiangnan is more influenced by climate (Zhang et al., 2015; Zhu et al., 2021). Summer is a critical period for rapid growth of peony leaves, nutrient accumulation and flower bud differentiation, but the high temperature in summer is the main reason that prevents peony from being widely cultivated in Jiangnan (Wang et al., 2012). Therefore, it is of great significance to study and master the growth and development rules of peony under high temperature stress to solve the problems of breeding of resistant peony cultivars, adjustment of variety structure and exploration of cultivation technology. However, recent studies have mainly focused on peony flower color (Gu et al., 2019; Guo et al., 2019) and seed oil extraction (Sun et al., 2017; Li et al., 2021). Effective protocols for micropropagation and the effects of different medium compositions and exogenous hormones on healing browning have also been investigated (Wen et al., 2016; Zhou et al., 2016). Few studies on heat tolerance of peony have been reported, mainly focusing on the photosynthetic characteristics and physiological and biochemical changes molecular mechanisms; the effect of exogenous hormone addition on high temperature tolerance of peony. It was found that high temperature stress inhibits the activity of superoxide dismutase, intensifies the

production of H_2O_2 and malondialdehyde, inhibits the activity of PSI and PSII and causes damage to the photosynthetic machinery (Luo et al., 2011; Liu et al., 2012; Liu, 2019); exogenous abscisic acid and epilactone can improve the high temperature tolerance of peony (Wu et al., 2018; Ren et al., 2018); and heat shock proteins and heat tolerance genes were identified and verified (Zhang et al., 2015; Liu et al., 2019). Studies on the mechanisms of photosynthesis inhibition by high temperature and on the differences in tolerance to high temperatures in different peony cultivars have been limited so far. The aim of this study was to investigate the daily responses of two peony cultivars at the photosynthetic level under high temperature conditions. We evaluated and analyzed the photochemical adaptations of the investigated peony cultivars using photosynthetic parameters and JIP tests. To explore the causes of heat tolerance differences among different peony varieties, it provides the selection of heat resistant peony for suitable cultivation in Jiangnan region and the theoretical basis for the breeding of heat resistant varieties.

Materials and methods

Plant materials and treatments

In November 2020, four-year-old peony plants ('Lu He Hong' and 'Zhi Hong') with consistent growth and healthy were selected and planted in plastic pots with an upper diameter of 28 cm, a lower diameter of 19 cm and a height of 23 cm. In June 2021, the experimental material was domesticated using an artificial climate chamber for 7 days, with a 25°C/20°C day and night cycle, air humidity set at 70%, light intensity set to 4000lx, and a daily light time to dark time ratio of 14h/10h. On day 8, the peony plants were divided into two groups: 'Lu He Hong' and 'Zhi Hong', and three plants in each group were treated at 40°C/35°C daily cycle at high temperature, with environmental conditions consistent with domestication. In addition, samples were sampled at 0,2,4, and 6 days after treatment. During sampling, photosynthetic and chlorophyll fluorescence parameters were measured first measured, then leaves were taken for stress physiological indicators and protective enzyme activity assays. In addition, all the leaves were fully expanded, and the upper growth and healthy functional leaves (the first pair of leaves under the top bud) were selected.

Determination items and methods

Stress physiological index and antioxidant enzyme activity measurement

The 0.1g leaves were first ground into fine powder in liquid nitrogen for subsequent indicator determination. The activities of malondialdehyde (MDA) content, superoxide dismutase (SOD, EC 1.15.1.1), and peroxidase (POD, EC1.11.1.7) were evaluated by the kit instructions (Suzhou Keming).

Determination of photosynthetic parameters

Photosynthetic parameters of peony leaves under high temperature treatment were measured in June 2021. The healthy functional leaves with similar growth in the middle and upper periphery of the plant (the first pair of leaves in the terminal bud) were selected, and LI-6400 portable photosynthesis instrument (LI-Cor6400XT PSC-4817, The net photosynthetic rate (Pn), stomatal conductance (Gs), intercellular CO_2 concentration (Ci) and transpiration rate (Tr) of peony leaves were measured every morning (9:00-11:00 on sunny days), with three leaves per plant were measured in different cultivars in triplicate. The first determination of the blades should be numbered and marked for the next determination.

Stomatal limitation value (Ls)=1-Ci/Ca, where Ci denotes the intercellular CO_2 concentration and Ca denotes the atmospheric CO_2 concentration (CO_{2a}). Water use efficiency (WUE) reflects the amount of CO_2 assimilated per unit of water content transpired by the plant and is expressed as the ratio of net photosynthetic rate to transpiration rate: WUE=Pn/Tr.

Chlorophyll fluorescence measurements

The rapid chlorophyll fluorescence induction kinetic curve (OJIP curve) and related parameters of peony leaves under high temperature treatment were measured using a Handy PEA plant efficiency analyzer (Hansatech, UK) from 9:00 to 11:00 am. The dark responses were measured by clamping the same leaves with dark-adapted clamps for 30 min before the measurement. Three leaves for different varieties were repeated three times. After the first test, the leaves should be labeled for continuous determination.

Statistical analysis

Principal component analysis (PCA) is an effective tool for analyzing parameters and sample clustering, and is used to study the distribution patterns of OJIP parameters and treatments. In SPSS 25 software, the default setting is PCA/exploratory factor analysis using the maximum variance method. The process is as follows: Analysis → Dimensionality Reduction → Factor Run this process for factors. The rotated component matrices of the selected "JIP-test parameters" and the "principal component factor score table" were preformed on the two-dimensional plane consisting of PC1 and PC2. The posterior parameter distributions were plotted using the component matrix table.

SPSS 25 software was used for one-way ANOVA, Excel and Origin2021 software were used for data processing and mapping. Fisher's least significant difference was used for mean comparison ($P<0.05$).

Results

Effects of high temperature stress on plant morphology of different peony cultivars

In this study, morphological changes of different peony cultivars were observed under high temperature treatment at 40°C (Figure 1). The results showed that the growth status of peony changed significantly under high temperature treatment. Among them, 'Lu He Hong' changed greatly, the leaves began to wilt after 2 days, and the leaves shrank and branches drooped on the 4th day. By the 6th day, the leaves are yellow and dry, the branches droop severely, and the plant was wilted seriously. The 'Zhi Hong' variety showed strong heat resistance, with the extension of high temperature treatment time, the leaves kept vitality, only showed a slight droop of branches and yellow leaf tip morphological changes, until 25 days of high temperature treatment, the plants still maintained good vitality.

Effects of high temperature stress on oxidative stress of different peony cultivars

High temperature stress can cause membrane lipid peroxidation damage in peony (Figure 2). At 40°C, the content of MDA in Lu He Hong increased significantly and reached the peak on the 6th day, which was 39.05% higher than that in the untreated condition. However, MDA content in Zhi Hong leaves increased first and then decreased, reached the maximum on the second day, and then returned to the untreated level.

Effects of high temperature stress on antioxidant enzymes of different peony cultivars

High temperature stress had a significant effect on the activities of POD and SOD. As shown in Figure 3A, the POD activity of Lu He Hong showed a downward trend, decreasing by 59.50, 62.49 and 73.03% on day 2, day 4 and day 6. The POD activity of leaves after high temperature stress was always higher than that of leaves without high temperature stress, which was 1.94 times higher than that of leaves without high temperature stress. The SOD activity of Lu He Hong leaves increased first and then decreased with the extension of high temperature stress time, while Zhi Hong showed a trend of decreasing first and then increasing (Figure 3B).

Effects of high temperature stress on photosynthetic parameters of different peony cultivars

High temperature effect the photosynthetic characteristics of leaves of different cultivars of peony (Figures 4, 5). Under high temperature, the net photosynthetic rate of the two cultivars of peony decreased to different degrees, among which, the net photosynthetic rate of 'Lu He Hong' decreased seriously, with a large decrease in 0-2 days, and slowly decreased two days later.

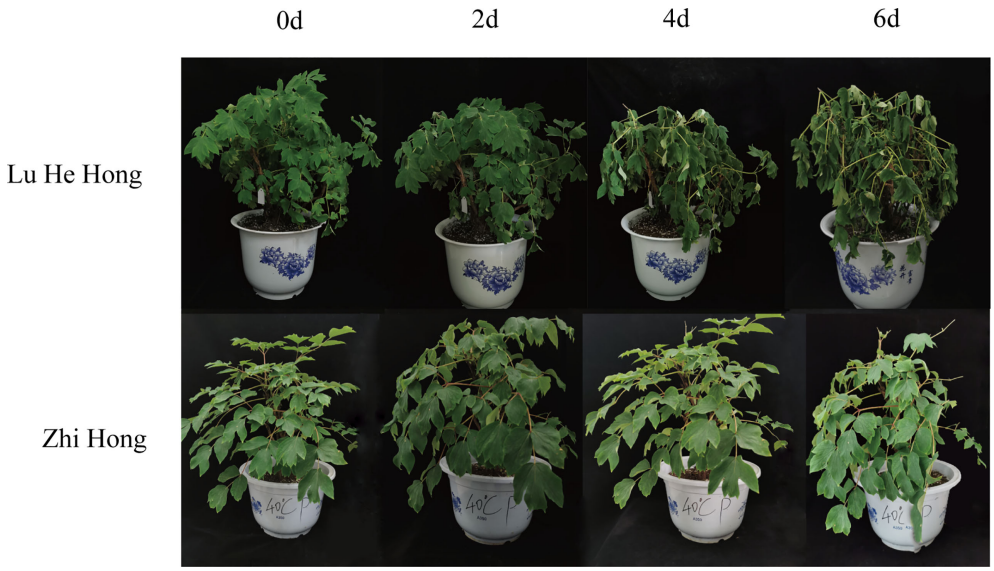

FIGURE 1
Effects of high temperature stress on morphology *P. suffruticosa* plantsof 'Lu He Hong' and 'Zhi Hong' cultivars.

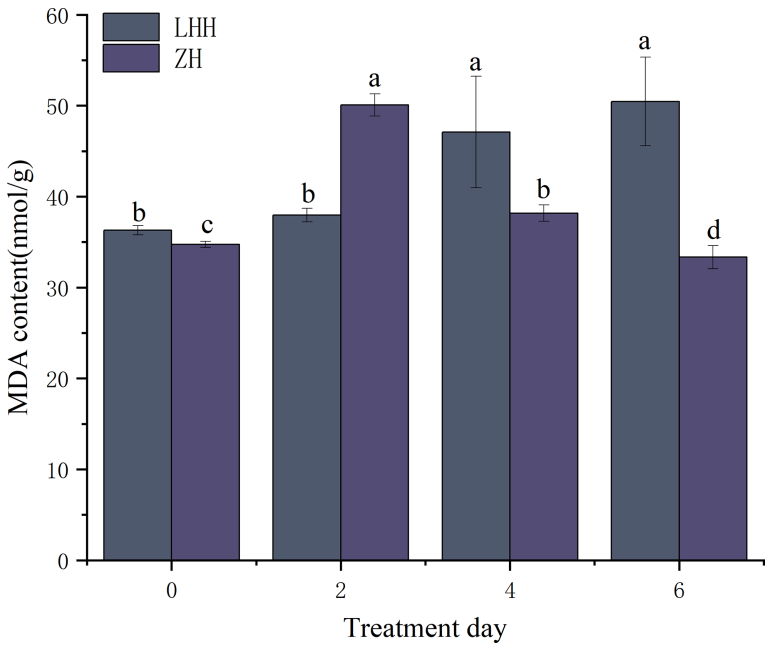

FIGURE 2
Effects of high temperature stress on oxidative stress in *P. suffruticosa* plants of 'Lu He Hong' (LHH) and 'Zhi Hong' (ZH) cultivars. Different letters in the same column indicate signifificant differences at the 0.05 level.

The 'Zhi Hong' began to rise after two days and returned to normal levels of net photosynthetic rate.

Under high temperature treatment, the intercellular CO_2 concentration (Ci) and stomatal limit (Ls) of leaves of different peony cultivars changed significantly (Figures 5A, B). 'Lu He Hong' showed an upward trend first, then a downward trend and finally an upward trend; 'Zhi Hong' showed a trend of first decline, then rise and finally decline. The stomatal limit value was opposite to Ci.

The 'Zhi Hong' first decreased and then increased, and the stomatal conductance began to increase after the second day. 'Lu He Hong' showed a trend of first decline, then rise and finally decline (Figure 5C).

Water use efficiency (WUE) is a key physiological indicator to judge whether plant growth is under stress. In this study, it was found that high temperature stress had an impact on water use efficiency of different peony cultivars (Figure 5D). The water use efficiency of leaves of 'Lu He Hong'

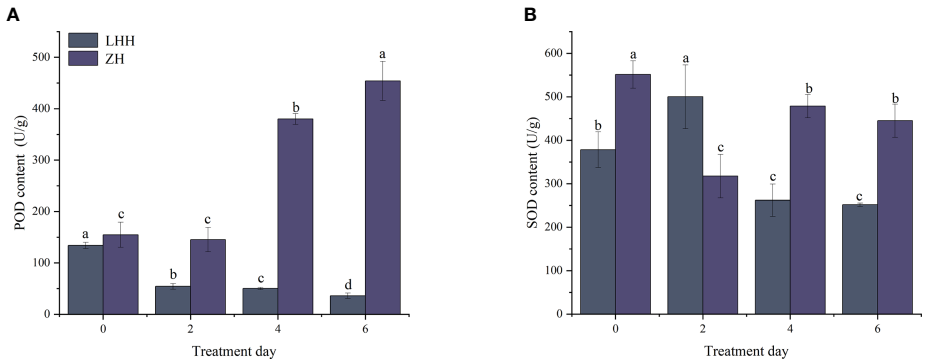

FIGURE 3
Effects of high temperature stress on oxidative stress in *P. suffruticosa* plants of 'Lu He Hong' (LHH) and 'Zhi Hong' (ZH) cultivars. **(A)** peroxidase (POD); **(B)** Superoxide dismutase(SOD). Different letters in the same column indicate significant differences at the 0.05 level.

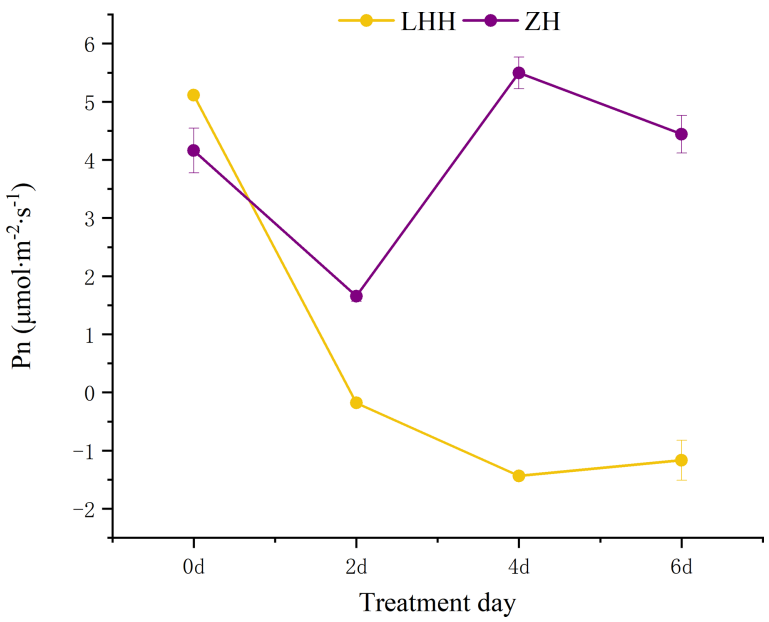

FIGURE 4
Effects of high temperature stress on Pn in *P. suffruticosa* plants of 'Lu He Hong' (LHH) and 'Zhi Hong' (ZH) cultivars. Different letters in the same column indicate signifificant differences at the 0.05 level.

decreased gradually with the extension of high temperature treatment time. Although the water use efficiency of 'Zhi Hong' fluctuated, it was always higher than that of 'Lu He Hong'.

Effects of high temperature stress on chlorophyll fluorescence of different peony cultivars

By constructing variable fluorescence curves, the changes of photosynthetic properties of different peony cultivars during leaf natural senescence were studied (Figure 6). The results showed that with the extension of high temperature treatment time, the fluorescence values of all cultivars of peony decreased in different degrees. The fluorescence value of 'Lu He Hong' decreased greatly (Figure 6A), while that of 'Zhi Hong' did not decrease significantly (Figure 6B).

In measurements, an additional step labeled K and L steps appeared at 300ms and 150ms of the fluorescence transient, respectively. The appearance of L and K bands at high temperature reflects the transient values of these grades, with significant differences among cultivars in L and K bands (Figure 7). L-peak can indicate aggregation between different components of PSII or energy transfer connectivity between antenna pigment and RCs, the active reaction center of PSII. The L-band of 'Lu He Hong' presented a negative transient value at 0-4 days of high temperature treatment, and a positive L-band at 6 days of high temperature treatment (Figure 7A). The L-band of 'Zhi Hong' showed a positive transient value when it was exposed to high temperature for 2 days, and a negative transient value when it was exposed to high temperature for 4-6 days (Figure 7C). The presence of K-band indicates the inactivation of OEC on the donor side of PSII. K-band is often observed in plants exposed to high temperatures and is an indicator of OEC damage. The K-band of 'Lu He Hong' showed a positive and rising trend (Figure 7B). After 2 days of high temperature treatment, the K-band of 'Zhi Hong' showed a positive value, and 4-6 days, the K-band showed a negative transient value (Figure 7D).

Another fluorescence normalized W_{IP} (normalized by I- and P-step) ascent kinetics, W_{IP}=0.5 can be used to reflect the reduction rate of the electron receptor at the end of the PSI receptor side (Figure 8). With the extension of high temperature time, the W_{IP} of the two peony cultivars changed significantly, and there were significant differences among the cultivars. The time of W_{IP} value of 0.5 was gradually decreased. The initial value of 'Lu He Hong' (Figure 8A) is smaller than that of 'Zhi Hong' (Figure 8B), but the variation range of 'Lu He Hong' is smaller than that of 'Zhi Hong'.

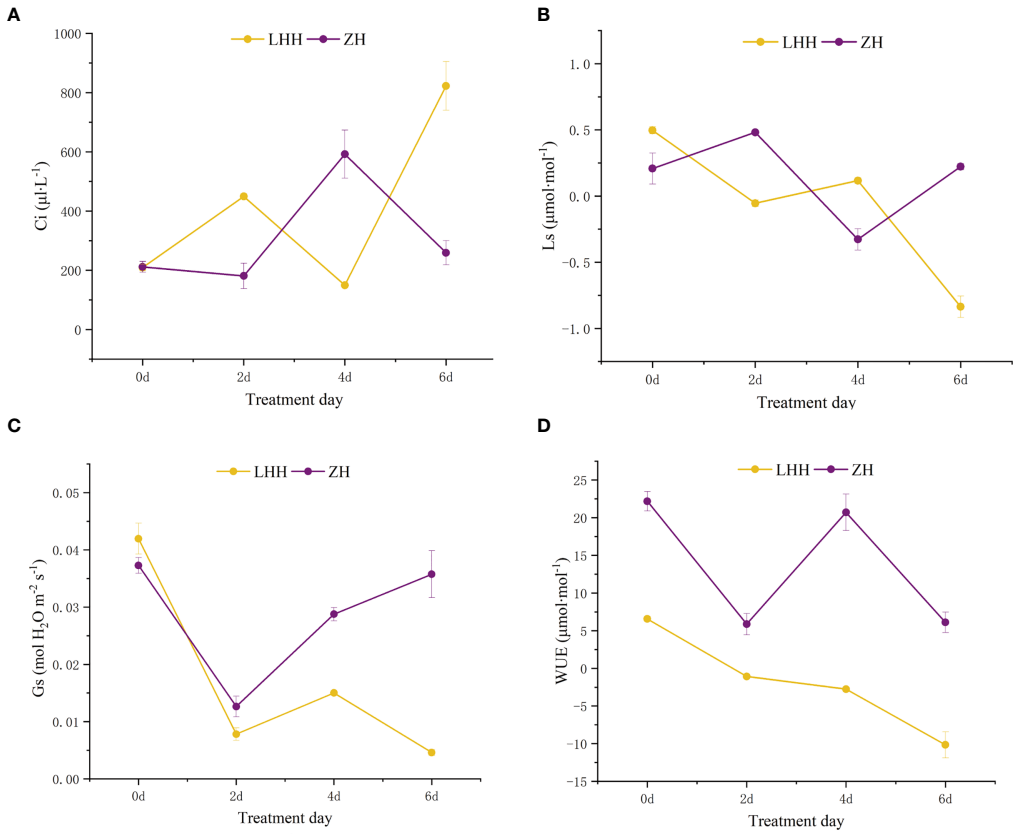

FIGURE 5
Effects of high temperature stress on gas exchange parameters in leaves in *P. suffruticosa* plants of 'Lu He Hong' (LHH) and 'Zhi Hong' (ZH) cultivars. Substomatal CO_2 concentration (Ci; **A**); stomatal limitation value (Ls; **B**) stomatal conductance (Gs; **C**) and water use efficiency(WUE; **D**) in leaves of *P. lactifora* under high temperature treatment (HT).

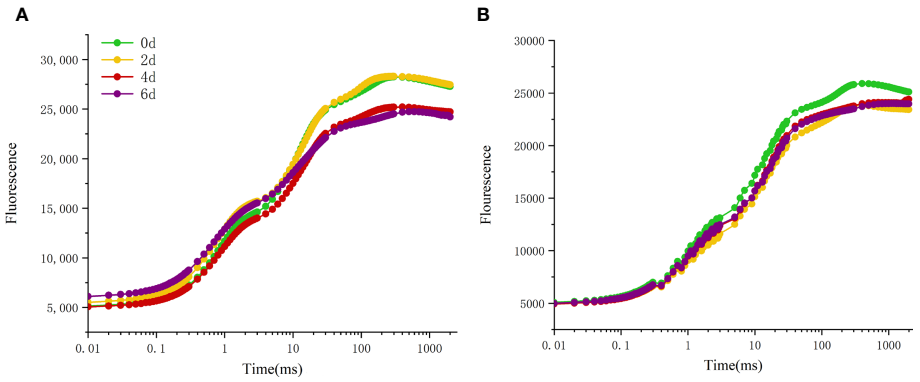

FIGURE 6
Effects of high temperature stress on OJIP curve in *P. suffruticosa* plants of 'Lu He Hong' (LHH) and 'Zhi Hong' (ZH) cultivars. **(A)** 'Lu He Hong'; **(B)** 'Zhi Hong'.

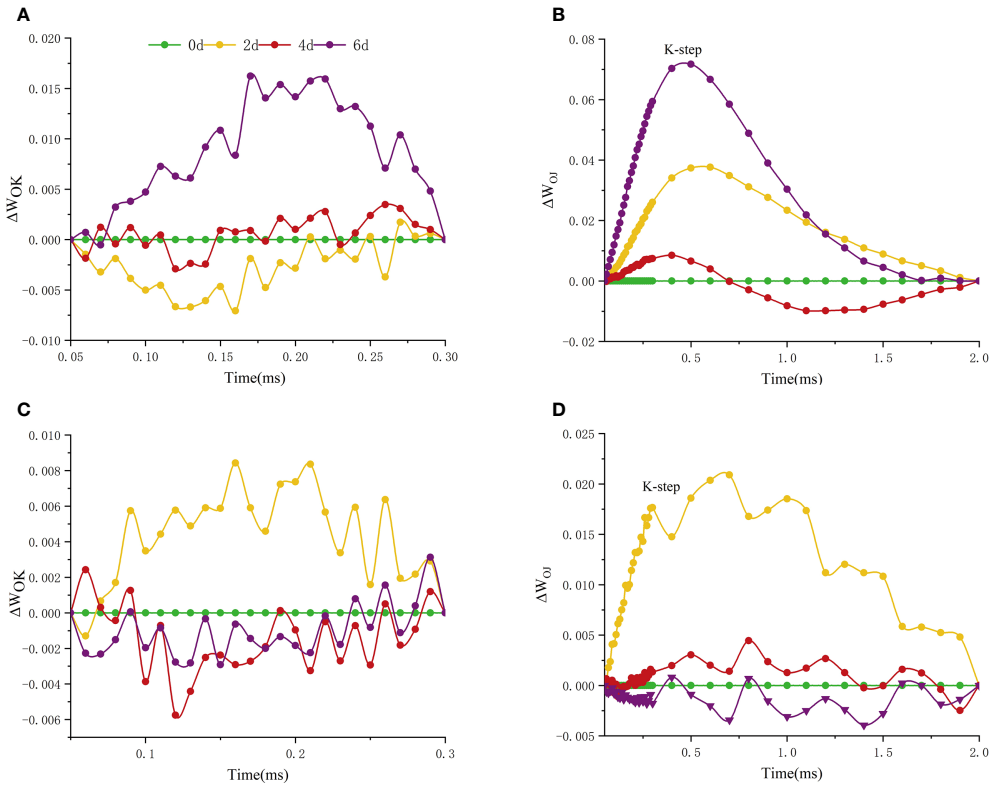

FIGURE 7
Effects of high temperature stress on the O-K and O-J phase kinetic curves in *P. suffruticosa* plants of 'Lu He Hong' (LHH) and 'Zhi Hong' (ZH) cultivars. **(A, C)** The O-K phase dynamics curve of 'Lu He Hong' and 'Zhi Hong' (double normalized by O-step (50 μs) and K-step (300 μs) to show L-band); **(B, D)** the O-J phase dynamics curve of 'Lu He Hong' and 'Zhi Hong' (double normalized by O-step (50 μs) and J-step (2 ms) to show K-band).

Significant differences were observed between most JIP test parameters (fluorescence index (F_o/F_m, F_v/F_m), relative variable fluorescence (V_J, V_I), quantum yield and efficiency (φ_{P0}, φ_{R0}, φ_{E0}, ψ_{E0}, and δ_{R0}), specific energy fluxes, and phenomenological fluxes (ABS/RC, TR_0/RC, ET_0/RC, DI_0/RC and RE_0/RC) and performance metrics (DF_{abs} and PI_{total}) were significantly different (Figure 9; Table S1). At two days of high temperature treatment, V_J, ABS/RC, TR_0/RC of 'Lu He Hong' leaves

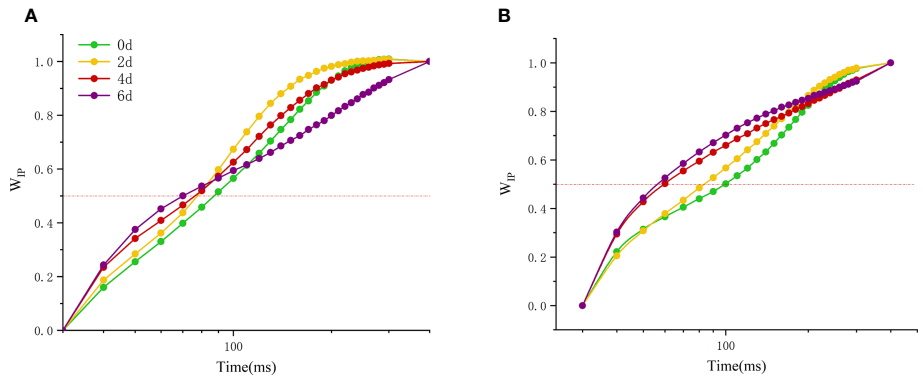

FIGURE 8
Effect of high temperature stress on the kinetic curve of I-P phase in *P. suffruticosa* plants of 'Lu He Hong' (LHH) and 'Zhi Hong' (ZH) cultivars. **(A)** 'Lu He Hong'; **(B)** 'Zhi Hong'.W_{IP}== $(F_t - F_I)/(F_P - F_I)$, I indicates the I-step at about 30 ms; P indicates the P-step at about 300 ms.

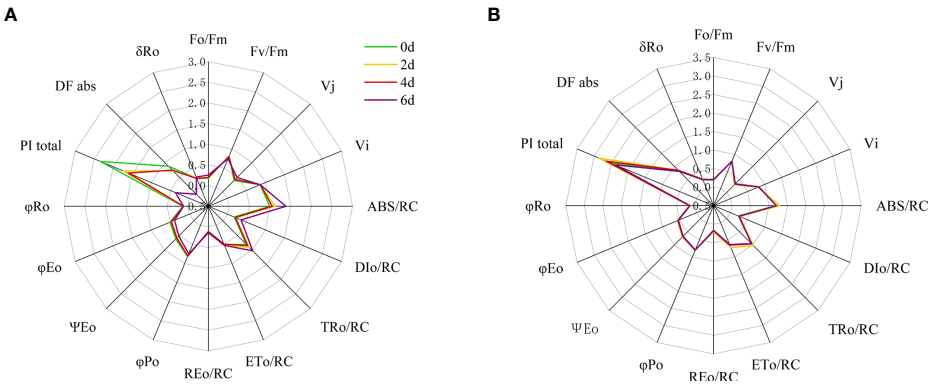

FIGURE 9
Radar plots of leaf structural and functional JIP test parameters of peony cultivars **(A)** 'Lu In this manusript, the comments are made. He Hong', **(B)** 'Zhi Hong'at 0, 2,4 and 6 days after heat treatment. Quantum ratio used for heat dissipation (φ_{Do}=1-φ_{Po}=(F_o/F_m)); the maximum quantum yield of the initial photochemical reaction (φ_{Po}=≡ TR_0/ABS = [1 − (F_o/F_m)] = F_v/F_m)); quantum yields of electron receptors at the end of the reduced PSI receptor side (φ_{Ro}== RE_0/ABS = φ_{Po} (1 − V_I)); quantum yield for electron transport (ET)(at t=0) (φ_{Eo}≡ET_0/ABS= [1–(F_o/F_m)]ψ_{Eo}); the efficiency of electron transfer other than Q_A driven by a single exciton captured by the active reaction center (at t=0) (Ψ_{Eo}= ET_0/TR_0 = [1 − (F_J/F_m)] = 1- V_J); Ratio of electrons from the reductive PSI receptor side terminal electron acceptor to electrons from the electron transport chain (δ_{R0}=RE_0/ET_0=(1-V_I)/(1-V_J)); absorption-based driving force expressed from the absorption of photons to the reduction of the electron transfer chain (DF_{abs}); Performance index (potential) for energy conservation from exciton to the reduction of PSI end acceptors (PI_{total}≡PI_{abs}[δ_{Ro}/(1 −δ_{Ro})]); absorption flux (of antenna Chls) per RC (ABS/RC=M_O (1/V_J)(1/φ_{Po})); trapped energy flux per RC(at t=0) (TR_0/RC=M_O (1/V_J)); electron transport flux (further than Q_A^-) per RC(at t=0) (ET_0/RC=M_O (1/V_J)ψ_{Eo}); dissipated energy flux per RC(at t=0) (DI_0/RC=(ABS/RC)-(TR_0/RC)); specific electron flux per unit PSII active reaction center for reduction of PSI terminal electron acceptor (at t=0) (RE_0/RC=(1-V_I)(M_O/V_J)).

increased significantly; ψE0, DF_{abs} and PI_{total} decreased significantly; Fo/Fm, Fv/Fm, V_I, DI_0/RC, ET_0/RC, RE_0/RC, φ_{P0}, φ_{R0}, φ_{E0}, δ_{R0} did not change significantly; on day 4, compared with day 2, DF_{abs} and PI_{total} increased significantly, while the remaining parameters did not change significantly; at 6th day, compared with day 4, V_J, ABS/RC, TR_0/RC, Fo/Fm, DI_0/RC, RE_0/RC, δ_{R0} showed a significant increase; ψ_{E0}, φ_{P0}, φ_{E0}, Fv/Fm, DF_{abs} and PI_{total} decreased significantly; V_I, ET_0/RC, and φ_{R0} did not change significantly (Figure 9A).

'Zhi Hong' showed no significant changes in φ_{E0}, φ_{R0}, δ_{R0}, DF_{abs} and PI_{total}, significant increases in Fo/Fm, ABS/RC, DI_0/RC, TR_0/RC, ET_0/RC, RE_0/RC, ψ_{E0}, and significant decreases in Fv/Fm, φ_{P0}, Vj, Vi decreased significantly; at day 4, compared with day 2, Fo/Fm, Fv/Fm, φ_{P0}, V_J, V_I, ψ_{E0}, φ_{E0}, φ_{R0}, δ_{R0}, DF_{abs}, and PI_{total} did not change significantly; ABS/RC, DI_0/RC, TR_0/RC, ET_0/RC, RE_0/RC occurred a significant decrease and returned to the non-high temperature treatment to the same level without high temperature treatment (Figure 9B).

To further evaluate the results, we conducted PCA analysis based on the collected JIP test parameters measured for each leaf during the high temperature treatment (Figure 10). The cumulative contribution values of PC1 and PC2 for all parameters analyzed in 'Lu He Hong' were 59.78% and

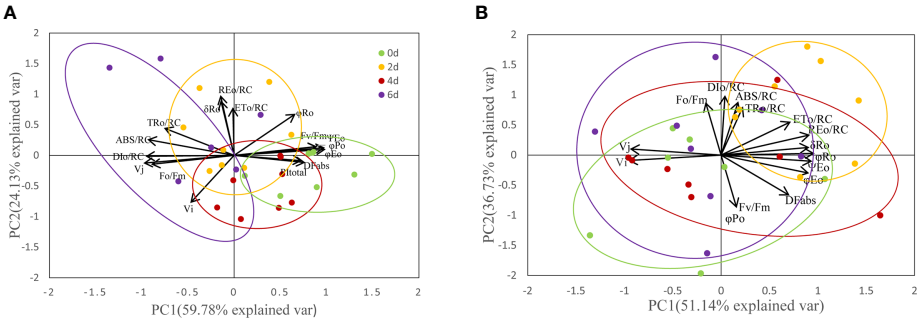

FIGURE 10
PCA of JIP parameters of Peony leaves treated at 40 °C for different time. **(A)** 'Lu He Hong'; **(B)** 'Zhi Hong'.

24.13%, with a joint cumulative contribution value of 83.91%; the cumulative contributions of PC1 and PC2 in 'Zhi Hong', the cumulative contribution values of PC1 and PC2 were 51.14% and 36.73%, respectively, and the joint cumulative contribution value was 87.86%. This indicates that the two-component factors obtained from the principal component analysis have a good separation description of the selected parameters. Through the principal component analysis, we found that the selected JIP test parameters formed three well-separated clusters. Among them, for 'Lu He Hong', the formation of PC1 was mainly due to the difference of PSII status parameters; the formation of PC2 was due to PSI parameters φ_{R0}, δ_{R0}, and PI_{total} (Figure 10A). While PC1 of 'Zhi Hong' corresponds to PSI activity, the higher value indicates higher PSI performance; PC2 corresponds to PSII activity, the higher PSII value, the higher PSII performance, representative parameters include Fv/Fm, DF_{abs}, φ_{Eo} and ABS/RC (Figure 10B). Cluster analysis of the experimental results showed that with the deepening of stress, the location of clustering also changed. PCA of all peony cultivars showed that the ellipsoid separation degree of 'Lu He Hong' was higher, indicating the severity of stress damage. The ellipsoid of 'Zhi Hong' has a good overlap area, indicating that the stress response is not obvious. Among them, the stress degree of 'Lu He Hong' was the most serious, showing high PSII performance at day 0. The PSII performance was damaged and PSI performance was improved after two days high temperature stress, while PSI performance was decreased after four days of high temperature treatment. On the sixth day, PSII performance was seriously damaged and PSI performance was improved. The stress response of 'Zhi Hong' was mild, and the properties of PSI and PSII did not change significantly.

Discussion

Reduction in plant photosynthesis and inhibition of photosynthesis are early indicators that plants are in a stressful environment (Olsovska and Brestic, 2001). In this study, we followed morphological changes as well as changes in photosynthetic parameters and OJIP chlorophyll fluorescence kinetics in two different peony cultivars under high temperature stress, and the study showed that high temperatures produced different degrees of damage to different cultivars of peony. In addition, the physiological and biochemical characteristics of peony were significantly affected by high temperature stress. Previous studies have shown that weather disasters will have a deeper impact on the photochemical performance of plants as future climate changes are more intense and longer duration of high temperatures (Kharshiing and Sinha, 2016).

Effect of high temperature stress on the physiological and biochemical indexes of different peony cultivars

As a form of high temperature stress, oxidative stress also has adverse effects on plant growth and development. In addition, excessive ROS accumulation caused peroxidation damage of membrane lipid in peony, and MDA content increased significantly with the development of high temperature stress, which may be due to the decrease of antioxidant enzyme activity. MDA is the final decomposition product of membrane lipid peroxidation. Under high temperature stress, the accumulation of MDA content will damage the structure and function of plant cell membrane. Antioxidant systems play an important role in protecting plants from the negative effects of ROS (Srivalli et al., 2003). The main antioxidant enzymes to eliminate ROS contain SOD, POD and so on. In this study, POD and SOD activities in peony leaves increased under high temperature stress, mainly because the plants initiated stress response and self-protection mechanism, adapted to the external environment by regulating antioxidant enzyme activities, and re-established the balance between production and removal of reactive oxygen species (Wang & Li, 2006). Regulation of ROS is the signal of the reactive oxygen species gene network in plant cells, which then regulates the activity of antioxidant enzymes. However, in the process of long-term high temperature stress, when the adaptation and self-protection capacity of plants is exceeded, the antioxidant enzyme activities are inhibited (Scalet et al, 1995). The POD activity of 'Lu He Hong' showed a decreasing trend, while the SOD activity increased first and then decreased. However, the activity of 'Zhi Hong' POD increased continuously, while SOD decreased first and then increased. It can be seen that the antioxidant system of 'Lu He Hong' is unstable, and the heat resistance of 'Zhi Hong' is strong.

Effect of high temperature stress on photosynthetic characteristics of different peony cultivars

Photosynthesis is the main factor affecting plant growth and development, and is the element most susceptible to high temperature stress (Lu et al., 2017; Du et al., 2022). When the ambient temperature is higher than the optimal temperature of the plant, the chloroplast structure will be damaged, and the photosynthetic performance will be reduced, and the relevant photosynthetic parameters will be changed (Chen et al., 2012). Net photosynthetic rate can directly represent the photosynthetic capacity of a single leaf (Jiang et al., 2004). Zhang et al. (2022) showed that under high temperature stress, the net photosynthetic rate of plants decreased continuously, but

there were significant differences among different cultivars. This study showed that the net photosynthetic rate of 'Lu He Hong' decreased with the deepening of stress degree, and that of 'Zhi Hong' decreased first and then increased to the normal level within six days under temperature stress, indicating that high temperature stress has a negative effect on the photosynthesis of peony plants, which is consistent with (Zhang et al., 2022). The research is consistent that 'Zhi Hong' has good heat resistance and can quickly adapt to heat stress. Stomatal restriction and non-stomatal restriction are one of the important factors leading to the decline of photosynthetic capacity of plants. Stomatal restriction and non-stomatal restriction factors causing the decrease of photosynthetic rate can be judged according to the change direction of Ci and Ls in leaves (Xu, 2013). In this study, the Pn decline of 'Lu He Hong' was firstly dominated by non-stomatal limiting factors, then by stomatal factors and finally by non-stomatal limiting factors, while the Pn decline of 'Zhi Hong' was firstly dominated by stomatal limiting factors, then by non-stomatal limiting factors and finally restored to stomatal limiting factors. When stomatal limitation factors are dominant, stomatal conductance of leaves decreases and CO_2 entering stomata decreases, which cannot meet the requirements of photosynthesis. However, the decrease of Pn not dominated by stomatal limitation is due to the increase of leaf temperature, the decrease of chloroplast activity and Rubisoo activity, and the decrease of RuBP carboxylase regeneration capacity, leading to the decrease of photosynthetic capacity of leaves (Gao et al., 2018). Therefore, the reason for the decrease in the net photosynthetic rate of 'Lu He Hong' in this study may be mainly due to the irreversible damage of the chloroplast structure, whereas the high tempeature resistant 'Zhi Hong' has a more stable chloroplast structure that can adapt to short-term high temperature stress. Stomata is a channel for gas exchange between plants and the environment. Stomatal conductance (Gs) represents the degree of stomatal opening and is a major factor in photosynthesis, respiration and transpiration rate of plants (Miner et al., 2017). In this study, Gs of 'Lu He Hong' decreased with the deepening of high temperature stress, indicating that high temperature stress had a negative impact on its stomatal conductance, which was consistent with the research results of Sarwar et al. (2019). 'Zhi Hong' results in stomatal closure during short-term heat treatment to prevent leaf dehydration, and with the deepening of high temperature stress, stomatal conductance increases and leaf temperature decreases to balance the ambient temperature. WUE reflects the amount of CO_2 assimilated by plants per unit water content of transpiration and is a comprehensive indicator to evaluate the adaptability of plants to the environment. The larger WUE value is, the less water consumed by fixed unit mass CO_2 (Zhang and Shan, 2002). Hao et al. (2017) found that water utilization rate of Peony decreased significantly under high temperature stress. In this study, 'Lu He Hong' decreased significantly with the prolongation of high temperature stress, which was consistent with previous studies. However, the WUE of 'Zhi Hong' is always higher than that of 'Lu He Hong', indicating that 'Zhi Hong' has full water utilization, can consume less water content and produce more nutrients, which is consistent with the research results, and 'Zhi Hong' has the characteristics of thermal stability.

Effect of high temperature stress on chlorophyll fluorescence of different peony cultivars

The rapid chlorophyll fluorescence induction kinetics curve refers to the fluorescence change process from O point to P point, which mainly reflects the initial photochemical reaction of PSII and the changes in the structure and state of photosynthetic apparatus (Krause and Weis, 1991). When plants are subjected to high temperature stress, K-band (300μs) will appear. This is because the donor side of PSII is damaged at high temperature. After a very short period of time, the chlorophyll fluorescence intensity increases rapidly, resulting in the transformation of OJIP curve into OKJIP curve (Chen et al., 2004), and the emergence of K-band indicates that OEC is damaged (Du et al., 2011). The positive K-band is caused by the decrease of the electron transfer rate at the donor side or the increase of the electron outflow rate at the acceptor side due to the inactivation of OEC. The balance between electron transfer and further electron transfer to Q_A is impaired, resulting in RC damage. The negative K-band is caused by an increase in the rate of electron transfer from the donor side or a decrease in the rate of electron outflow from the acceptor side (electron transfer delay) (Kalaji et al., 2014b). In this study, the parameter ΔW_{OJ} was introduced to analyze the changes of donor side and OEC of PSII of different peony cultivars, and there were significant differences among cultivars. The K-Band of 'Lu He Hong' increased with the extension of high temperature stress time, indicating that the stress caused damage to the oxygen release complex of the variety, and reduced the electron transfer rate of the PSII donor side. 'Zhi Hong' showed significant positive value of K-Band for two days under high temperature stress, indicating that the OEC was slightly damaged due to high temperature stress response during short-term high temperature treatment. K-band is negative after two days of high temperature treatment, and negative K-band has been widely used in recent literature as a marker of tolerance to various stresses(Mathur et al., 2011), which is consistent with 'Zhi Hong' showing good heat resistance. L-band can reflect the aggregation between different components of PSII or the energy transfer connectivity between antenna pigment and RCs, the active reaction center of PSII (Srivastava et al., 1997; Stirbet, 2013). A positive L-band indicates dissociation of the antenna

pigment complex with greater distance between PSII antennas and therefore less efficient energy exchange, while a negative L-band indicates greater grouping and more efficient energy exchange between neighboring PSII units (Tsimilli-Michael, 2019; Kalaji et al., 2018). L-band was negative within 4 days of high temperature treatment, indicating that it adapted to the damage caused by high temperature by increasing energy exchange under high temperature stress. Meanwhile, L-band showed a positive value by day 6, indicating that at this time, the energy exchange of 'Lu He Hong' decreased sharply, which may be irreversible damage caused by long periods of high temperature stress. In contrast, the L-band of 'Zhi Hong' only showed positive values at two days under high temperature, after which the L-band presented negative values, which indicated that 'Zhi Hong' had a better ability to adapt to heat stress and resist the damage caused by high temperature by increasing energy exchange. W_{IP} = 0.5 (half time of the rising curve) can be used to reflect the reduction rate of the electron acceptor pool at the end of the PSI (Guo et al., 2020) and also the half-life of the rising curve (Xu et al., 2021). It can be seen that both peony cultivars in this study were subjected to a significant increase in the reduction rate of the PSI terminal electron acceptor pool and a significant reduction in the half-life time under high temperature treatment.

Effect of high temperature stress on chlorophyll fluorescence parameters of different peony cultivars

Analysis using the JIP test parameters allowed us to assess the effect of different stresses on the efficiency and flux of electrons as well as the efficiency and flux of energy around PSI and PSII (Maxwell and Johanson, 2000). To quantify the changes in light absorption, utilization and chemical energy conversion and to analyze the fluorescence transients, the JIP test was performed in this study and the parameters shown on the radar plot provide a clearer picture of the changes under high temperature stress in different peony cultivars. The most significant change in JIP parameters was in the 'Lu He Hong', which is consistent with the change in its OJIP phase and the early appearance of L-band and K-band changes. 'Lu He Hong' on the second day of high temperature treatment only showed significant changes in Vj, PI_{total}, DF_{abs}, ABS/RC, TR_0/RC, and ψ_{E0} parameters changed significantly, although other indicators for significant changes, the appearance of L-band and K-band is an early indicator of impaired photochemical properties (Viljevac Vuletić and Španić, 2019). Fv/Fm (or φ_{P0}) is an indicator of PSII light energy conversion rate (Cai et al., 2017), and the decrease of Fv/Fm is an important indicator of photoinhibition (Strasser et al., 2004). In this study, Fv/Fm of the two cultivars significantly decreased under high temperature stress, indicating that high temperature would produce photoinhibition on peony and affect photosynthesis. J phase relatively variable fluorescence (V_J) represents the probability that a captured exciton moves an electron from the main acceptor (Q_A) into the electron transport chain. When Q_A reoxidation is restricted, the V_J value increases, resulting in the accumulation of Q_A reduction and the reduction of electron transport. The I step (V_I) decreases after high temperature and excessive light exposure, indicating that electron transport is lower than Q_A due to higher levels of Q_B- non-reduction centers (Mihaljević et al., 2020). Under high temperature stress, the V_J of 'Lu He Hong' showed an increasing trend, while φE0 decreased, indicating that the PQ pool had poor electron acceptance ability under high temperature stress, resulting in limited electron transfer ability of Q_A from acceptor to Q_B, thus the electron transfer from pheo to Q_A resulted in Q_A^-, This eventually leads to a large accumulation of Q_A^- (Kalaji et al., 2014b) and a decrease in the efficiency of PSII electron transfer (Öquist et al., 1992). V_J of 'Zhi Hong' decreased on the second day and electron transfer rate increased, and V_J returned to the original level after two days of stress, indicating that the variety has strong heat resistance and can better adapt to the environment under short-term high temperature stress. The relative fluorescence of I-phase did not change significantly in 'Lu He Hong', and 'Zhi Hong' decreased on the second day under high temperature stress but returned to normal level later. Blockage of electron transport leads to leakage of electrons in the electron transport chain, which attack intracellular O_2 and generate ROS, especially singlet reactive oxygen species, which play an important role in membrane lipid peroxidation (Chalanika et al., 2017). Therefore, the leaves of peony under high temperature stress will inevitably lead to the accumulation of ROS and damage to cell membrane structure, which is consistent with the significant increase of MDA in our results. Among them, the increase of MDA of 'Lu He Hong' is more significant than that of 'Zhi Hong', which is positively correlated with the electron transport efficiency.

DF_{abs} and PI_{total} can be found to be the parameters with significant changes in the pre-tolerant 'Lu He Hong'. The total performance index (PItotal) is the most prevalent and sensitive parameter in JIP testing, as it reflects changes in photosynthetic electron transport activity outside PSII, intersystem electron transport and PSI processes (Stefanov et al., 2011). A reduction in PI_{total} has been found in apple cultivars under high temperature stress (Mihaljević et al., 2020), indicating that high temperature stress negatively affects PSI in peony. In this experiment, with the deepening of high temperature stress, the DFabs and PItotal of 'Lu He Hong' decreased significantly, while 'Zhi Hong' did not change significantly, which means that the PSI of 'Lu He Hong' was unstable under high temperature stress. Performance indicators of the reduced overall energy flow from the excitons to the reduced PSI-terminal receptors coincide with the reduced electron acceptor state (R0) at the lateral end of the

PSI receptors. The fast chlorophyll fluorescence induction kinetic curve than activity parameters, including light energy absorbed per reaction center (ABS/RC), energy captured per reaction center for Q_A reduction (TR_0/RC), energy captured per reaction center for electron transfer (ET_0/RC), and energy dissipated per reaction center (DI_0/RC), can accurately reflect the plant photosynthetic organ absorption, conversion and dissipation of light energy by plant photosynthetic organs (Strasser et al., 2001; VanHeerden et al., 2004). In this study, the ABS/RC, TR_0/RC and DI_0/RC of 'Lu He Hong' and 'Zhi Hong' were significantly increased, but the specific activity parameters of 'Zhi Hong' returned to normal level after two days of high temperature treatment, which indicated that after the inactivation or cleavage of some reaction centers per unit area of the leaves triggered by high temperature stress, the efficiency of the remaining active reaction centers could be promoted to better dissipate the energy in the electron transport chain, which might be a self-protection mechanism of peony leaves.ABS/RC represents the effective antenna size of the active RC, which is influenced by the proportion of active and inactive reactive centers, and when the number of inactive centers increases, so does the proportion of ABS/RC (Mathur et al., 2011). This parameter value was higher in two peony cultivars, suggesting that PSII may have more efficiency of energy capture and a higher increase in inactive centers compared to 'Zhi Hong'. The increase in ABS/RC may be due to a reduced ratio of active RCs and an increase in absorbed light energy, which may be related to the deactivation of RCs or an increase in antenna size. Previous studies (Tao et al., 2022) showed that in general, RCs inactivation of plants is related to photoinhibition, that is, when the amount of light absorbed by plants exceeds the amount of light that can be utilized by their own photosystem, the photosynthetic function of plants decreases. Derks et al. (2015) found that when photoinhibition occurs in plants, the plants actively shut down some of the RCs and release the excess absorbed light energy through heat. The increase in this parameter was greater in 'Lu He Hong' than in 'Zhi Hong', suggesting that high temperature is more damaging to 'Lu He Hong' RCs. The increase in ABS/RC values is accompanied by an increase in the parameter TR0/RC, which represents the maximum speed at which RC can trap excitons (Stirbet and Strasser, 1996). TR_0/RC and DI_0/RC in the 'Lu He Hong' had a significant rise in RC, Fv/Fm significantly reduced, that all Q_A^- were reduced, can no longer oxidation. When Q_A^- reoxidation was suppressed, electron transfer to Q_A^- cannot effectively Q_B, because the active center can't capture a large number of photons, so the excess photon is known as the dissipation energy (Mathur et al., 2013). It was also observed that the efficiency of individual electrons from the interphotosystem electron transport chain to the terminal electron acceptor on the PSI acceptor side (δ_{R0}) of the more heat-tolerant 'Zhi Hong' did not change under high temperature treatment, whereas there was a significant increase in the less heat-tolerant 'Lu He Hong'. It may be due to the flow of electrons between the two photosystems, the flow of PSI terminal receptors are slightly accelerated and PSI activity is increased (Blankenship, 2014).

PCA was used to evaluate the PSI and PSII activities of peony leaves by multi-parameter analysis with more systematic and comprehensive effects. The results showed that several parameters related to PSI and PSII activities were influenced by temperature. In this study, we used a new method and idea to analyze the differences in photosynthetic and fluorescence-related parameters of leaves of two peony cultivars with different heat tolerance, and made a comprehensive evaluation of the photosynthetic performance of peony leaves to explore the reasons for the differences in heat tolerance among different peony cultivars. The results of this study provide a theoretical basis for the screening of heat-resistant peonies suitable for cultivation in Jiangnan area and for the selection and breeding of high temperature resistant varieties.

Conclusion

Peony has a long history of cultivation in China and has high ornamental value. However, due to the high temperature and rainy summer in southern China and global warming, it is difficult for peony to move southward. Different peony cultivars in order to understand the heat photosynthetic performance and physiological and biochemical changes, photosynthesis of two cultivars of peony and chlorophyll fluorescence, physiological and biochemical indexes were analyzed, and discussed the causes of differences in heat resistance between different cultivars of peony, for screening suitable for cultivation in the south of the Jiangnan the heat resistance of peony, as to provide theoretical basis for the breeding of heat resistant cultivars. Studies have shown that the more heat-resistant 'Zhi Hong' has a more stable cell membrane, which is not easy to be oxidized, and the antioxidant system is also more stable. In addition, 'Zhi Hong' with strong heat tolerance has stable green cell activity, has higher water utilization rate and can produce more nutrients, and can maintain high photosynthetic performance under high temperature stress, while 'Lu He Hong' photosynthetic capacity decreases continuously under high temperature stress, and the photosynthetic mechanism is unstable and vulnerable to damage. JIP-test analysis showed that OEC, PSI and PSII reaction centers and RCs of 'Zhi Hong' during high temperature stress are slightly damaged to adapt to the high temperature stress environment by increasing greater grouping and more efficient energy exchange between adjacent PSII units and maintaining the balance between electron transport, and 'Lu He Hong' performs poorly in these aspects, consistent with its poor heat resistance.

Data availability statement

The original contributions presented in the study are included in the article/Supplementary Material. Further inquiries can be directed to the corresponding authors.

Author contributions

XZ, XC, and WJ planned and designed the research. SJ, BL, ZL, XZ, and TL participated in photosynthesis and chlorophyll fluorescence measurement experiments. XC, WJ, and EH were responsible for the analysis of photosynthetic fluorescence data. XX and XS provided advice on photosynthetic fluorescence data analysis. WJ and EH were involved in manuscript editing. XC and XZ participated in the revision of the manuscript. All authors read and approved the final manuscript.

Funding

This research was funded by the National Key R&D Program of China, Grant Number 2019YFD1001500; the Basic Public Welfare Research Project in Zhejiang Province, Grant Number LGN22C160006; and the Talent Project of Jiyang College of Zhejiang A&F University, Grant Number RQ2020B04/RQ1911B05.

Conflict of interest

The authors declare that the research was conducted in the absence of any commercial or financial relationships that could be construed as a potential conflict of interest.

Publisher's note

All claims expressed in this article are solely those of the authors and do not necessarily represent those of their affiliated organizations, or those of the publisher, the editors and the reviewers. Any product that may be evaluated in this article, or claim that may be made by its manufacturer, is not guaranteed or endorsed by the publisher.

Supplementary material

The Supplementary Material for this article can be found online at: https://www.frontiersin.org/articles/10.3389/fpls.2022.969718/full#supplementary-material

References

Bita, C. E., and Gerats, T. (2013). Plant tolerance to high temperature in a changing environment: scientific fundamentals and production of heat stress-tolerant crops. *Front. Plant Sci.* 4. doi: 10.3389/fpls.2013.00273

Blankenship, R. E. (2014). "The basic principles of photosynthetic energy storage," in *Molecular mechanisms of photosynthesis*, *2nd Edition* (Chichester: John Wiley & Sons), 312.

Cai, J. G., Wei, M. Q., Zhang, Y., and We, Y. (2017). Effects of shading on photosynthetic characteristics and chlorophyll fluorescence parameters in leaves of hydrangea macrophylla. *Chin. J. Plant Ecology.* 5), 570–576. doi: 10.17521/cjpe.2016.0245

Chalanika, H., De Silva, C., and Asaeda, T. (2017). Effects of heat stress on growth, photosynthetic pigments, oxidative damage and competitive capacity of three submerged macrophytes. *J Plant Interact* 12, 228–236. doi: 10.1080/17429145.2017.1322153

Chen, H. X., Li, W. J., An, S. Z., and Gao, H. Y. (2004). Characterization of PSII photochemistry and thermostability in salt-treated *Rumex* leaves. *J. Plant Physiol.* 161, 257–264. doi: 10.1078/0176-1617-01231

Chen, W. R., Zheng, J. S., Li, Y. Q., and Guo, W. D. (2012). Effects of high temperature on photosynthesis, chlorophyll fuorescence, chloroplast ultrastructure, and antioxidant activities in fngered citron. *Russ J. Plant Physiol.* 59, 732–740. doi: 10.1134/s1021443712060040

Derks, A., Schaven, K., and Bruce, D. (2015). Diverse mechanisms for photoprotection in photosynthesis. dynamic regulation of photosystem II excitation in response to rapid environmental change. *Biochim. Biophys. Acta Bioenerg.* 1847 (4-5), 468–485. doi: 10.1016/j.bbabio.2015.02.008

Du, G. D., Lv, D. G., Zhao, L., Wang, S. S., and Cai, Q. (2011). Effects of high temperature on leaf photosynthetic characteristics and photosystemII photochemical activity of kernelused apricot. *Chin. J. Appl. Ecology.* 22 (3), 701–706.

Du, K., Wu, W. Q., Liao, T., Yang, J., and Kang, X. Y. (2022). Transcriptome analysis uncovering regulatory networks and hub genes of populus photosynthesis and chlorophyll content. *Genomics.* 114 (4), 110385. doi: 10.1016/j.ygeno.2022.110385

Fahad, S., Ihsan, M. Z., Khaliq, A., Daur, I., Saud, S., Alzamanan, S., et al. (2018). Consequences of high temperature under changing climate optima for rice pollen characteristics-concepts and perspectives. *Arch. Agron. Soil Sci.* 64 (11), 1473–1488. doi: 10.1093/aob/mci071

Gao, G. L., Feng, Q., Zhang, X. Y., Si, J. H., and Yu, T. F. (2018). An overview of stomatal and non-stomatal limitations to photosynthesis of plants. *Arid Zone Res.* 35 (4), 929–937.

Gross, Y., and Kigel, J. (1994). Differential sensitivity to high temperature of stages in the reproductive development of common bean (*Phaseolus vulgaris* l.). *Field Crops Res.* 36 (3), 201–212. doi: 10.1016/0378-4290(94)90112-0

Guo, Y., Lu, Y., Goltsev, V., Strasser, R. J., Kalaji, H. M., Wang, H., et al. (2020). Comparative effect of tenuazonic acid, diuron, bentazone, dibromothymoquinone and methyl viologen on the kinetics of chl a fluorescence rise OJIP and the MR820 signal. *Plant Physiol. Biochem* 156, 39–48. doi: 10.1016/j.plaphy.2020.08.044

Guo, L. P., Wang, Y. J., and Jaime, A. (2019). Teixeira da Silva, yongming fan, xiaonan yu. transcriptome and chemical analysis reveal putative genes involved in flower color change in *Paeonia* 'Coral sunset'. *Plant Physiol. Biochem.* 138, 130–139. doi: 10.1016/j.plaphy.2019.02.025

Gu, Z. Y., Zhu, J., Hao, Q., Yuan, Y. W., Duan, Y. W., Men, S. Q., et al. (2019). (2019). a novel R2R3-MYB transcription factor contributes to petal blotch formation by regulating organ-specific expression of PsCHS in tree peony (*Paeonia suffruticosa*). *Plant Cell Physiol.* 60 (3), 599–611. doi: 10.1093/pcp/pcy232

Hao, Z. J., Zhou, C. H., Liu, D., Wei, M. R., and Tao, J. (2017). Effects of high temperature stress on photosynthesi, chlorophyll fluorescence and ultrastructure of herbaceous Peony(*Paeonia lactiflora* pall.). *Mol. Plant Breed.* 6, 2359–2367.

Hemantaranjan, A., Bhanu, A. N., Singh, M. N., Yadav, D. K., Patel, P. K., Singh, R., et al. (2014). Heat stress responses and thermotolerance. *Adv. Plants Agri Res.* 3, 1–10. doi: 10.15406/apar.2014.01.00012

Jiang, D., Dai, T., Jing, Q., Cao, W., Zhou, Q., Zhao, H., et al. (2004). Effects of long-term fertilization on leaf photosynthetic characteristics and grain yield in winter wheat. *Photosynthetica* 42, 439–446. doi: 10.1023/b:phot.0000046164.77410

Kalaji, H. M., Bąba, W., Gediga, K., Goltsev, V., Samborska, I. A., Cetner, M. D., et al. (2018). Chlorophyll fluorescence as a tool for nutrient status identification in rapeseed plants. *Photosynth. Res.* 136, 329–343. doi: 10.1007/s11120-017-0467-7

Kalaji, H. M., Jajoo, A., Oukarroum, A., Brestic, M., Zivcak, M., Samborska, A. I., et al. (2014a). "The use of chlorophyll fluorescence kinetics analysis to study the performance of photosynthetic machinery in plants," in *Emerging technologies and management of crop stress tolerance*. Eds. P. Ahmad and S. Rasool (San Diego: Academic Press), 347–384.

Kalaji, H. M., Schansker, G., Ladle, R. J., Goltsev, V., Bosa, K., Allakhverdiev, I. S., et al. (2014b). Frequently asked questions about *in vivo* chlorophyll fluorescence: practical issues. *Photosynth. Res.* 122, 121–158. doi: 10.1007/s11120-014-0024-6

Kharshiing, E., and Sinha, S. P. (2016). Deficiency in phytochrome a alters photosynthetic activity, leaf starch metabolism and shoot biomass production in tomato. *J. Photoch Photobio B* 165, 157–162. doi: 10.1016/j.jphotobiol.2016.10.026

Krause, G. H., and Weis, E. (1991). Chlorophyll fluorescence and photosynthesis: the basics. *Annu. Rev. Plant Physiol. Plant Mol. Biol.* 42, 313–349. doi: 10.1146/annurev.pp.42.060191.001525

Lesk, C., Rowhani, P., and Ramankutty, N. (2016). Influence of extreme weather disasters on global crop production. *Nat.* 529 (7584), 84–87. doi: 10.1038/nature16467

Liu, J. J. (2019). Effect of high temperature and drought stress on PSII function and light distribution on peony leaves with different resistance. *Northern Horticulture* 11), 72–79.

Liu, C. Y., Chen, D. Y., Gai, S. P., Zhang, Y. X., and Zheng, G. S. (2012). Effects of high-and low temperature stress on the leaf PSII functions and physiological characteristics of tree peony (*Paeonia suffruticosa* cv. 'Roufurong'). *Chinese J. Appl. Ecol.* 23 (1), 133–139.

Liu, H. C., Zhu, K. Y., Tan, C., Zhang, J. Q., Zhou, J. H., Jin, L., et al. (2019). Identification and characterization of *PsDREB2* promoter involved in tissue specific expression and abiotic stress response from paeonia suffruticosa. *Peer J.* 7, e7052. doi: 10.7717/peerj.7052

Li, J., Zhang, X., and Zhao, X. (2011). *Tree peony in China* (Beijing, China: Encyclopedia of China Publishing House), 20–22.

Li, M., Zhao, G. H., Liu, J., Liang, X. P., Zhang, M., Zhou, G. C., et al. (2021). Optimization of ultrasound-assisted extraction of peony seed oil with response surface methodology and analysis of fatty acid. *Agric. Res.* 10 (4), 543–555. doi: 10.1007/s40003-021-00554-y

Lu, T., Meng, Z. J., Zhang, G. X., Qi, M. F., Sun, Z. P., Liu, Y. F., et al. (2017). Sub-High temperature and high light intensity induced irreversible inhibition on photosynthesis system of tomato plant (*Solanum lycopersicum* l.). *Front. Plant Sci.* 8, 365. doi: 10.3389/fpls.2017.00365

Luo, J., Han, J. R., Wang, Y., Ke, L., Yang, M., and Fei, Y. J. (2011). Response of heat stress on the physiological biochemistry of *Paeonia suffruticosa*. *J. Yangtze Univ. (Nat Sci. Edit).* 8 (2), 223–228.

Mathur, S., Jajoo, A., Mehta, P., and Bharti, S. (2011). Analysis of elevated temperature-induced inhibition of photosystem II using chlorophyll a fluorescence induction kinetics in wheat leaves (*Triticum aestivum*). *Plant Biol.* 13, 1–6. doi: 10.1111/j.1438-8677.2009.00319.x

Mathur, S., Mehta, P., and Anjana, J. (2013). Effects of dual stress (high salt and high temperature) on the photochemical efficiency of wheat leaves (Triticum aestivum). *Physiol. Mol. Biol. Plants* 19 (2), 179–188.

Maxwell, K., and Johanson, G. N. (2000). Chlorophyll fluorescence - a practical guide. *J. Exp. Bot.* 51, 659–668. doi: 10.1093/jxb/51.345.659

Mihaljević, I., Lepeduš, H., Šimić, D., Viljevac Vuletić, M., Tomaš, V., Vuković, D., et al. (2020). Photochemical efficiency of photosystem II in two apple cultivars affected by elevated temperature and excess light *in vivo*. *S. Afr. J. Bot.* 130, 316–326. doi: 10.1016/j.sajb.2020.01.017

Miner, G. L., Bauerle, W. L., and Baldocchi, D. D. (2017). Estimating the sensitivity of stomatal conductance to photosynthesis: A review. *Plant Cell Environ.* 40 (7), 1214–1218. doi: 10.1111/pce.12871

Mittler, R., Finka, A., and Goloubinoff, P. (2012). How do plants feel the heat? *Trends Biochem. Sci.* 37 (3), 118–125. doi: 10.1016/j.tibs.2011.11.007

Morita, S., Yonemaru, J., and Takanashi, J. (2005). Grain growth and endosperm cell size under high night temperatures in rice (*Oryza sativa* l.). *Ann. Bot.* 95 (4), 695–701. doi: 10.1093/aob/mci071

Olsovska, K., and Brestic, M. (2001). Function of hydraulic and chemical water stress signalization in evaluation of drought resistance of juvenile plants. *J. Cent. Eur. Agric.* 2 (34), 157–164.

Öquist, G., Chow, W. S., and Anderson, J. M. (1992). Photoinhibition of photosynthesis represents a mechanism for the long-term regulation of photosystem II. *Planta* 186, 450–460. doi: 10.1007/bf00195327

Pavlović, I., Mlinarić, S., Tarkowská, D., Oklestkova, J., Novák, O., Lepeduš, H., et al. (2019). Early brassica crops responses to salinity stress: A comparative analysis between Chinese cabbage, white cabbage, and kale. *Front. Plant Sci.* 10. doi: 10.3389/fpls.2019.00450

Ren, Z. B., Chen, F. Z., Shu, C. Q., Li, X. H., Liu, K. H., and Ji, X. M. (2018). Effects of exogenous 2, 4-epibrassinolide on heat resistance of peony. *J. Jianghan Univ.(Nat. Sci. Ed.).* 46 (5), 446–453.

Sarwar, M., Saleem, M. F., Ullah, N., Ali, S., Rizwan, M., Shahid, M. R., et al. (2019). Role of mineral nutrition in alleviation of heat stress in cotton plants grown in glasshouse and field conditions. *Sci. Rep.* 9 (1), 13022. doi: 10.1038/s41598-019-49404-6

Scalet, M., Federice, R., and Guido, M. C. (1995). *Peroxidase activity and polyamine changes in response to ozone and simulated acid rain in Aleppo pine needles*. *Environ. Exp. Bot.* 35 (3), 417–425. doi: 10.1016/0098-8472(95)00001-3

Srivalli, B., Vishanathan, C., and Renu, K. C. (2003). Antioxidant defense in response to abiotic stresses in plants. *Journal of Plant Biology* 30, 121–139.

Srivastava, A., Guiss´e, B., Greppin, H., and Strasser, R. J. (1997). Regulation of antenna structure and electron transport in photosystem II of pisum sativum under elevated temperature probed by the fast polyphasic chlorophyll a fluorescence transient: OKJIP. *Biochim. Biophys. Acta* 1320, 95–106. doi: 10.1016/s0005-2728(97)00017-0

Stefanov, D., Petkova, V., and Denev, I. D. (2011). Screening for heat tolerance in commonbean (Phaseolus vulgaris L) lines and cultivars using JIP test. *Sci. Hortic* 128, 1–6. doi: 10.1016/j.scienta.2010.12.003

Stirbet, A. D., and Strasser, R. J. (1996). Numerical simulation of the in vivo fluorescence in plants. *Math. Comput. Simul.* 42, 245–53. doi: 10.1016/0378-4754(95)00114-x

Stirbet, A. (2013). Excitonic connectivity between photosystem II units: What is it, and how to measure it? *Photosynth. Res.* 116, 189–214. doi: 10.1007/s11120-013-9863-9

Strasser, R. J., Appenroth, ,. K. J., StÖckel, J., and Srivastava, A. (2001). Multiple effect of chromate on the photosynthetic apparatus of spirorlela polyrhiza probed by OJIP chlorophyll a fluorescence measurements. *Environ. pollut.* 115 (1), 49–64. doi: 10.1016/s0269-7491(01)00091-4

Strasser, R. J., and Govindjee, (1991). "The fo and the O-J-I-P fluorescence rise in higher plants and algae," in *Regulation of chloroplast biogenesis*. Ed. J. H. Argyroudi-Akoyunoglou (New York: Plenum Press), 423–436.

Strasser, B. J., and Strasser, R. J. (1995). "Measuring fast fluorescence transients to address environmental questions: the JIP-test," in *Photosynthesis: from light to biosphere*. Ed. P. Mathis (Netherland: Kluwer Academic Publishers Press), 977–980.

Strasser, R. J., and Tsimilli-Michael, M. (2001). Stress in plants, from daily rhythm to global changes, detected and quantified by the JIP-test. *Chimie Nouvelle (SRC).* 75, 3321–3326.

Strasser, R. J., Tsimilli-Michael, M., and Srivastava, A. (2004). Analysis of the chlorophyll a fluorescence transient. *Chlorophyll Fluorescence* 321–362. doi: 10.1007/978-1-4020-3218-9_12

Sun, X. L., Li, W. G., Li, J., Zu, Y. G., and Zhao, X. H. (2017). Inclusion complex of peony (*Paeonia suffruticosa* andr.) seed oil with b-cyclodextrin: preparation, characterisation and bioavailability enhancement. *Int. J. Food Sci. Technol.* 52 (11), 2352–2361. doi: 10.1111/ijfs.13519

Tao, M. Z., Feng, X. P., He, Y., Zhang, J. N., Bai, X. L., Yang, G. F., et al. (2022). Monitoring of transgenic maize seedlings phenotyping exhibiting glyphosate tolerance. *Biorxiv. Org.* doi: 10.1101/2022.03.21.485126

Tiwari, Y. K., and Yadav, S. K. (2019). High temperature stress tolerance in maize (Zea mays l.): Physiological and molecular mechanisms. *J. Plant Biol.* 62 (2), 93–102. doi: 10.1007/s12374-018-0350-x

Tsimilli-Michael, M. (2019). Revisiting JIP-test: an educative review on concepts, assumptions, approximations, definitions and terminology. *Photosynthetica* 57 (SI), 90–107. doi: 10.32615/ps.2019.150

Van Heerden, P. D. R., Strasser, R. J., and Kruger, G. H. J. (2004). Reduction of dark chilling stress in N2-fixing soybean by nitrate as indicated by chlorophyll a fluorescence kinetics. *Physiol. Plant* 121 (2), 239–249. doi: 10.1111/j.0031-9317.2004.0312.x

Viljevac Vuletić, M., and Španić, V. (2019). Characterization of photosynthetic performance during natural leaf senescence in winter wheat: Multivariate analysis as a tool for phenotypic characterization. *Photosynthetica* 57 (SI), 116–128. doi: 10.32615/ps.2019.162

Wang, Y. Z., Jiang, H. F., Fu, L. M., and Zhang, X. J. (2012). Summer management points of greenhouse potted peony. *Rural Sci. Technol.* 10, 56.

Wang, L.-J., and Li, S.-H. (2006). Thermotolerance and related antioxidant enzyme activities induced by heat acclimation and salicylic acid in grape (*Vitis vinifera* L.) leaves. *Plant Growth Regulation* 48, 137–144.

Wen, S. S., Cheng, F. Y., Zhong, Y., Wang, X., Li, L. Z., Zhang, Y. X., et al. (2016). Efficient protocols for the micropropagation of tree peony (*Paeonia suffruticosa* 'Jin

pao hong', *P. suffruticosa* 'Wu long peng sheng' and p. × *lemoinei*'High noon') and application of arbuscular mycorrhizal fungi to improve plantlet establishment. *Sci. Hortic.* 201, 10–17. doi: 10.1016/j.scienta.2016.01.022

Wu, S., Jin, X. L., Jin, M. H., Sun, L. X., and Chen, R. (2018). Effects of exogenous abscisic acid on heat tolerance in tree peony seedlings under high temperature stress. advances in ornamental. *Horticulture China* 346–352.

Xu, D. Q. (2013). *Photosynthesis* (Beijing, China: Science Press).

Xue, J. Q., Li, T. T., Wang, S. L., Xue, Y. Q., Hu, F. R., and Zhang, X. X. (2018). Elucidation of the mechanism of reflowering in tree peony (*Paeonia suffruticosa*) 'Zi luo lan' by defoliation and gibberellic acid application. *Plant Physiol. Biochem.* 132, 571–578. doi: 10.1016/j.plaphy.2018.10.004

Xu, C., Wang, M. C., Yang, Z. Q., Han, W., and Zheng, S. H. (2021). Effects of high temperature on photosynthetic physiological characteristics of strawberry seedlings in greenhouse and construction of stress level. *Chinese J. Appl. Ecol.* 32 (1), 231–240

Yu, S. A. (2019). The impact of climate change on crop production: an empirical study in Zhejiang, China. Dissertation: China National Knowledge Infrastructure database. Zhejiang: Zhejiang University.

Zhang, L. X., Chang, Q. S., Hou, X. G., Wang, J. Z., Chen, S. D., Zhang, Q. M., et al. (2022). The effect of High−Temperature stress on the physiological indexes, chloroplast ultrastructure, and photosystems of two herbaceous peony cultivars. *J. Plant Growth Regul.* doi: 10.1007/s00344-022-10647-9

Zhang, Y. Z., Cheng, Y. W., Ya, H. Y., Han, J. M., and Zheng, L. (2015). Identification of heat shock proteins *via* transcriptome profiling of tree peony leaf exposed to high temperature. *Genet. Mol. Res.* 14 (3), 8431–8442. doi: 10.4238/2015.July.28.10

Zhang, S. Q., and Shan, L. (2002). Research progress on water use efficiency of plant. *Agric. Reseach In Arid Areas* 20 (4), 1–5.

Zhou, F. F., Wang, Z., Shi, L., Niu, J. J., Shang, W., He, D., et al. (2016). Effects of different medium composition and exogenous hormones on browning of tree peony (*Paeonia suffruticosa* andr.) callus in tissue culture. *Flower Res. J.* 24, 96–102. doi: 10.11623/frj.2016.24.2.03

Zhu, S. H., Ma, J., Hao, L. H., and Zhang, L. L. (2021). Identification and analysis of heat-resistant differential protein in leaves of *Paeonia suffruticosa*. *Mol. Plant Breed.* 19 (2), 419–431.

frontiers | Frontiers in Plant Science

TYPE Original Research
PUBLISHED 03 November 2022
DOI 10.3389/fpls.2022.1035191

OPEN ACCESS

EDITED BY
Geoff Wang,
Clemson University, United States

REVIEWED BY
Yang Cao,
Northwest A&F University Herbarium, China
Weibin Li,
Lanzhou University, China

*CORRESPONDENCE
Peng He
hepeng66@tjnu.edu.cn
Maihe Li
maihe.li@wsl.ch

SPECIALTY SECTION
This article was submitted to Functional Plant Ecology, a section of the journal Frontiers in Plant Science

RECEIVED 02 September 2022
ACCEPTED 20 October 2022
PUBLISHED 03 November 2022

CITATION
Wang X, Schönbeck L, Gessler A, Yang Y, Rigling A, Yu D, He P and Li M (2022) The effects of previous summer drought and fertilization on winter non-structural carbon reserves and spring leaf development of downy oak saplings.
Front. Plant Sci. 13:1035191.
doi: 10.3389/fpls.2022.1035191

The effects of previous summer drought and fertilization on winter non-structural carbon reserves and spring leaf development of downy oak saplings

Xiaoyu Wang[1,2], Leonie Schönbeck[3,4], Arthur Gessler[2,5], Yue Yang[2,6], Andreas Rigling[2,5], Dapao Yu[7], Peng He[2,8]* and Maihe Li[2,9,10]*

[1]Jiyang College, Zhejiang Provincial Key Laboratory of Germplasm Innovation and Utilization for Garden Plants, Zhejiang Agriculture and Forestry University, Hangzhou, China, [2]Forest Dynamics, Swiss Federal Institute for Forest, Snow and Landscape Research, Birmensdorf, Switzerland, [3]Department of Botany and Plant Sciences, University of California, Riverside, Riverside, United States, [4]Plant Ecology Research Laboratory, School of Architecture, Civil and Environmental Engineering, Swiss Federal Institute of Technology Lausanne, Lausanne, Geneva, Switzerland, [5]Institute of Terrestrial Ecosystems, Eidgenössische Technische Hochschule Zürich (ETH Zürich), Zurich, Switzerland, [6]College of Ecology and Environment, Hainan University, Haikou, Hainan, China, [7]Institute of Applied Ecology, Chinese Academy of Sciences (CAS), Shenyang, Liaoning, China, [8]Tianjin Key Laboratory of Animal and Plant Resistance, College of Life Sciences,Tianjin Normal University, Tianjin, China, [9]Key Laboratory of Geographical Processes and Ecological Security in Changbai Mountains, School of Geographical Sciences, Northeast Normal University, Changchun, Jilin, China, [10]School of Life Science, Hebei University, Baoding, Hebei, China

It is still unknown whether the previous summer season drought and fertilization will affect the winter non-structural carbohydrate (NSC) reserves, spring leaf development, and mortality of trees in the next year. We, therefore, conducted an experiment with *Quercus pubescens* (downy oaks) saplings grown under four drought levels from field capacity (well-watered; ~25% volumetric water content) to wilting point (extreme drought; ~6%), in combination with two fertilizer treatments (0 vs. 50 kg/ha/year blended) for one growing season to answer this question. We measured the pre- and post-winter NSC, and calculated the over-winter NSC consumption in storage tissues (i.e. shoots and roots) following drought and fertilization treatment, and recorded the spring leaf phenology, leaf biomass, and mortality next year. The results showed that, irrespective of drought intensity, carbon reserves were abundant in storage tissues, especially in roots. Extreme drought did not significantly alter NSC levels in tissues, but delayed the spring leaf expansion and reduced the leaf biomass. Previous season fertilization promoted shoot NSC use in extreme drought-stressed saplings over winter (showing reduced carbon reserves in shoots after winter), but it also showed positive effects on

survival next year. We conclude that: (1) drought-stressed downy oak saplings seem to be able to maintain sufficient mobile carbohydrates for survival, (2) fertilization can alleviate the negative effects of extreme drought on survival and recovery growth of tree saplings.

KEYWORDS

carbon consumption, carbon storage, leaf phenology, mobile carbohydrates, *Quercus pubescens*, overwinter, water deficit

Introduction

In the past decades, severe droughts and heatwaves have caused tree mortality and forest dieback across various biomes (Allen et al., 2010; Young et al., 2017), leading to profound changes in the structure and functioning of forest ecosystems on both global and local scale (Zhao and Running, 2010; Choat et al., 2018; Hartmann et al., 2018; Li et al., 2022). Natural drought events associated with increasing air temperature have been predicted to occur more frequently and to be of greater intensity in the future (IPCC, 2021), but it is still unclear whether and how trees tolerate and adapt to frequent droughts (Mcdowell et al., 2008; Allen et al., 2010; Mitchell et al., 2013; Adams et al., 2017; Choat et al., 2018).

Trees rely on stored non-structural carbohydrates (NSC, mainly composed of mobile sugars and starch) for growth and metabolisms (Hoch et al., 2003; Körner, 2003; Zhu et al., 2012a; Zhu et al., 2012b). Drought negatively affects photosynthesis and growth and can thus influence the levels of NSC in the growing season (Wiley, 2020). The NSC allocation patterns in response to drought have been extensively studied in trees during the growing season when both carbon supply and demand are directly affected (Li et al., 2008; Nardini et al., 2016; Li et al., 2018). However, to date, no consistent patterns in the NSC dynamics were found with some studies reporting decreased (Galiano et al., 2011; Woodruff et al., 2015) and others stable (Anderegg et al., 2012; Gruber et al., 2012; Schönbeck et al., 2018), or even higher (Piper, 2011; Piper and Fajardo, 2016; Kannenberg and Phillips, 2020) NSC concentrations in aboveground tissues during drought. The lack of unequivocal results might be attributed to varying tree size, species, and experiment time among different studies (Hoch, 2015). Contrary to aboveground parts, it is more commonly observed that root NSC decrease when trees are facing drought (Wiley, 2020). Li et al. (2018) analyzed 27 drought-related studies out of 57 NSC-related studies and reported that roots NSC decreased by 17.3%, but no NSC change was found in leaves and other aboveground woody tissues.

Drought may affect tissue NSC levels not only during the current growing season but also in the following winter and even next year (Lopez et al., 2007; Galvez et al., 2013). It was reported that previous growing-season drought can largely reduce the winter NSC reserves in roots of poplar seedlings (Galvez et al., 2013). In winter, NSC acts as an important substrate for sustaining respirational demands (Loescher et al., 1990), modifies cells membranes' cryoprotective ability and improves cold hardiness by using sugars and sugar-derived compounds as osmoprotectants (Morin et al., 2007; Tixier et al., 2019). Therefore, low availability of pre-winter NSC will affect trees' survival over winter, and low availability of post-winter NSC may strongly affect trees' re-growth in early spring (Zhu et al., 2012b), especially for deciduous species (Lebon et al., 2008; Keller et al., 2010; Klein et al., 2016; Tixier et al., 2017). But even in evergreen species such as Scots pine, the winter NSC storage in fine roots and stem wood were found to be positively correlated with their shoot growth in the following season (Schönbeck et al., 2018). A warm 2015 winter in California caused a decline in winter NSC storage in trees, which finally induced growth decline of three conifer species in 2016 (Earles et al., 2018).

Nutrient availability in the soil might affect the fitness of trees under dry conditions. Previous studies provided conflicting results, showing that increased nutrient availability can either intensify or mitigate the negative effects of drought on trees (Kreuzwieser and Gessler, 2010; Gessler et al., 2017). Jacobs et al. (2004) reported that fertilization (blended fertilizer) impaired the root system development and drought resistance of drought-stressed Douglas-fir seedlings. However, Schönbeck et al. (2020) found that the negative effects of moderate drought intensity (but not severe drought) on Scots pine saplings could be compensated by increased nutrient availability (blended fertilizer, NPK) during drought. Zhang et al. (2021) reported that nitrogen addition increased net photosynthetic rate and stomatal conductance, but did not significantly change foliar NSC levels of drought-stressed *Quercus mongolica* and *Fraxinus mandshurica* saplings. To our knowledge, the effects of previous summer drought and fertilization on plant NSC over winter and spring leaf development next year have rarely been studied.

Therefore, we conducted a split-plot experiment with saplings of *Quercus pubescens* (downy oaks), a species has outstanding significance in most Mediterranean forest ecosystems (Kuster et al., 2013), grown under drought (four

levels from well-watered to extreme drought with a volumetric water content of ~25%, 18%, 11% and 6%) and fertilizer (two levels: 0 vs. 50 kg/ha/year) treatments for one year (2016). We determined the NSC concentration in woody tissues in pre (Nov. 2016) and post-winter (March 2017), followed by an assessment of spring leaf development and leaf biomass of plants previously treated with drought and fertilization treatments. The study aimed to answer the questions of: (i) how the pre- and post-winter NSC reserves respond to drought events with different intensities (control, mild, strong, and extreme levels); (ii) whether the drought-stressed saplings can still mobilize and use the NSC storage in wood tissues during winter (by evaluating the over-winter NSC change); and (iii) whether and to what extent fertilization application affect winter NSC reserves, and how this change affects spring leaf development of previously drought-stressed oak saplings?

Material and methods

Experimental design and treatments

The experiment was conducted in the model ecosystem facility (MODOEK) of the Swiss Federal Institute for Forest, Snow and Landscape Research WSL (47°21′48″ N, 8°27′23″ E, 545 m a.s.l.), Birmensdorf, Switzerland (Figure 1; Figure S1). The MODOEK unit consists of 16 hexagonal glass-walled open top chambers, each with 3 m in height and 6.0 m^2 plantable area. Belowground, each chamber is divided into two lysimeters of 1.5 m depth and 3 m^2 area, which were filled at the bottom with a 1 m layer of gravel for fast drainage and on top a 40 cm layer of calcareous sandy loam soil, divided by a mesh that is impermeable for roots but not for water (Kuster et al., 2013; Schönbeck et al., 2020). Each lysimeter was separated down to the mesh layer, with plexiglass into two equally sized sections (each has 1.5 m^2 plantable area), two sections from different lysimeters were used for our experiment (Figure 1). Ten three-year-old *Quercus pubescens* Willd. (downy oak) saplings (20-25 cm in height, 0.3-0.5 cm in base diameter) were planted in each section in April, 2015, and they were grown with sufficient water supply in 2015.

The experiment was set up as split plot design considering both drought (4 levels) and fertilizer application (2 levels) treatments (Figure 1). From April 2016, each out of the 16 chambers was assigned one of the four water treatments (4 replicates for each water level): 100% (W100, corresponding to volumetric water content of ~25%), 50% (W50), 20% (W20), and 0% (W0, close to wilting point, volumetric water content of ~6%) of soil moisture at the field water capacity (Schönbeck et al., 2020). In April and July of 2016 and 2017, one section in each chamber was given 3 L water (F0: no fertilizer), the other one was fertilized with liquid fertilizer (F+: fertilizer treatment), close to 50 kg/ha/year (Wuxal, Universaldünger, NPK 4:4:3). The applied moisture was equal to 2 mm precipitation. The soil moisture and air temperature were automatically monitored at intervals of two hours (5 TM soil moisture and temperature

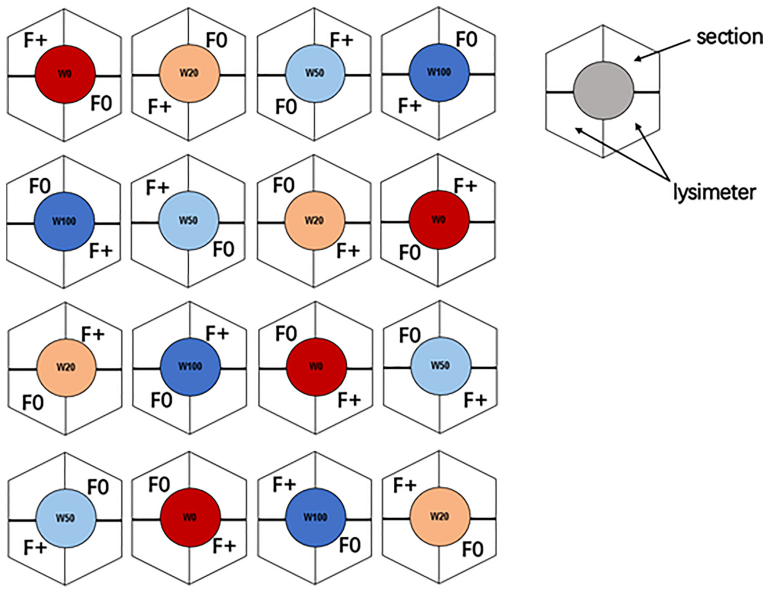

FIGURE 1
Experimental setup of the 16 open top chambers. Colors indicate the four different drought regimes: dark blue = W100 (close to field capacity), light blue = W50 (50% of field capacity), brown = W20 (20% of field capacity), and red = W0 (close to wilting point). Nutrient regime is represented with F0 (unfertilized) and F+ (fertilized) symbols.

logger, Metergroup, Munich, Germany) (data was shown in Figure S2).

Pre-winter and post-winter harvest

We defined the average weekly soil temperatures at 5-cm depth below 5°C as non-growing season (winter) (Figure S2), the pre- and post-winter sampling works were conducted in November 2016, and March 2017, respectively. In each sampling season, trees from each chamber (both F0 and F+ section) were randomly selected and fully harvested, thus, 64 individuals (4 drought levels × 2 fertilization levels × 4 replicates × 2 seasons) were harvested (dug out from the soil). All harvested oak saplings were alive at the time of harvest. The saplings were then separated into aboveground tissues (shoots) and mixed roots (i.e., coarse and fine roots). All samples were dried to constant mass at 65°C for approximately 72 h and weighted thereafter. A subsample of the oven-dried material was ground to fine powder and stored at 4°C for further chemical analysis.

Leaf phenology observation, mortality, and leaf biomass data collection

Spring leaf phenology was monitored in 2017, starting from April 3 (day 1) when bud swelling was first observed, to May 10 (day 37). Every two days within this period observations were carried out and three phenological stages were defined: (i) bud swelling, (ii) bud break, and (iii) leaf unfolding (Kuster et al., 2014). A stage was defined as reached for a given tree when > 50% of the buds showed the respective stage. For saplings that did not show any leaves (i.e. some saplings in the extreme dry W0 treatment) until May 10, 2017, a last observation was carried out in June 2017, to determine whether leaf phenology was delayed, or fully absent. If no leaves were present and the stem bark was brown and dry, the sapling was considered dead to calculate mortality. In July 2017 (mid-growing season), one sapling in each section was randomly selected for leaf biomass measurement.

Chemical analysis

The NSC concentrations of all plant tissues were determined following the method of Wong (1990), modified as described in Hoch et al. (2002). NSC are defined as low molecular sugars and starch. About 10-12 mg of the dried plant material was boiled in 2 ml distilled water for 30 min. For determination of the total amount of NSC, 500 µl of the extract (including dissolved sugars and starch) were incubated with a fungal amyloglucosidase from *Aspergillus niger* (Sigma-Aldrich, St. Louis, MO, USA) for 15 h at 49°C to digest starch into glucose. For determination of soluble sugars, an aliquot of 200 µl was taken from the extract after centrifugation and treated with Invertase and Isomerase (Sigma-Aldrich, St. Louis, MO, USA) to degrade sucrose and convert fructose into glucose. The total amount of glucose in each sample (total NSC and soluble sugars) was determined photometrically at 340 nm in a 96-well microplate photometer (HR 7000, Hamilton, Reno, NE, USA) after enzymatic conversion to gluconate-6- phosphate (hexokinase reaction, hexokinase from Sigma Diagnostics, St. Louis, MO, USA). The concentration of starch was calculated as total NSC minus free sugars. Pure starch and glucose-, fructose- and sucrose- solutions (1 mg/ml) were used as standards and standard plant powder (Orchard leaves, Leco, St. Joseph, MI, USA) was included to control reproducibility of the extraction. NSC concentrations are expressed on a percent dry matter basis. P and K content in the tissues were also measured, i.e., 5-6 mg of ground plant material was weighted into tin capsules that were combusted in an Element analyzer (ICP-OES, Optima 7300 von Perkin-Elmer) for chemical analysis.

Statistical analysis

The overwinter NSC changes were calculated as the difference between pre and post-winter NSC concentrations:

$$NSC\ \ change = PostNSC - PreNSC$$

Two-way ANOVA was then used to test how drought (W), fertilization (F), and their interaction (W × F) affect NSC concentrations in tissues at pre, post-winter, and the changes in NSC overwinter. Tukey HSD tests were carried out to examine pairwise differences when significant differences between drought or fertilization treatments were found, Bonferroni correction was used to adjust for multiple comparison.

For each oak individual (N = 252 in all chambers), the number of days required to reach the 3 different phenological states (Days) was calculated and a two-way ANOVA analysis (Days ~ Water * Fertilization) was used to test how drought and fertilization treatments affect the phenological development. To test the correlation between pre- and post-winter NSC (N = 32) on the one hand, and phenology (N=252) and biomass (N = 32) on the other, the number of days per phenological stage were averaged for each section. Linear regression models were established to study spring leaf development status and leaf biomass (July, 2017) in relation to NSC concentration in all tissues pre- and post-winter. Normality and homogeneity of standardized residuals were graphically checked on quantile-to-quantile and residual-vs-predicted plots. The significance level in this study was set at $p < 0.05$. All statistical tests and artworks were done with R software 4.1.2 (R Core Team, 2019, Vienna, Austria), under the RStudio environment.

Results

Pre-winter NSC concentrations

Extreme drought (W0) resulted in significantly increased sugar levels in both shoots and roots (Figures 2A, D), and decreased starch concentration in shoots, compared to other drought treatments (Figure 2B, left panel). Pre-winter total NSC concentrations in roots and shoots were unaffected by drought (Figures 2C, F). There was no fertilization treatment (F) effect on pre-winter NSC measurements in both shoots and roots, although starch concentrations in shoots tended to be lower in fertilized saplings compared to unfertilized saplings except for the W0 treatment (Figure 2B).

Post-winter NSC concentrations

Not drought but fertilization (F) treatments, and F interacting with drought significantly influenced shoots starch and the total NSC concentrations at post-winter (Figures 2B, C; right panel). The slight starch concentration differences between fertilization treatments observed pre-winter, were enlarged post-winter, mainly in W0 and W50. Here, fertilizer application led to a significant starch and total NSC (not significant for W50) reduction in the shoots (Figures 2B, C). Root NSC were unaffected by drought after winter, neither were shoot sugar concentrations (Figures 2A, F; Table S1).

Over-winter NSC concentration changes

Shoots and roots tissues in all treatments consumed NSC over winter. The dynamics were an order of magnitude larger in the roots than in the shoots, where NSC concentrations in general were very low (Figure 3). Extreme drought (W0) caused a net over-winter reduction in sugar concentrations in both shoots and roots, while sugar levels increased in all other water treatments (Figures 3A, D; Table S2). A D × F interaction affected the changes in starch and NSC concentrations in shoots (Figures 3B, C; Table S2). This was caused by the slight increase of starch in the W0/F0 treatment, compared to a reduction in all other treatments (Figure 3B). Shoots of fertilized saplings in W0 consumed significant more NSC over winter, and fertilized saplings in W0, W20 and W50 treatments tended to (not significant) consume more root NSC reserves (Figures 3C, E, F).

Spring phenology and leaf biomass

Extreme drought (W0) significantly delayed the spring leaf phenology (indicated by a higher number of days since April 3).

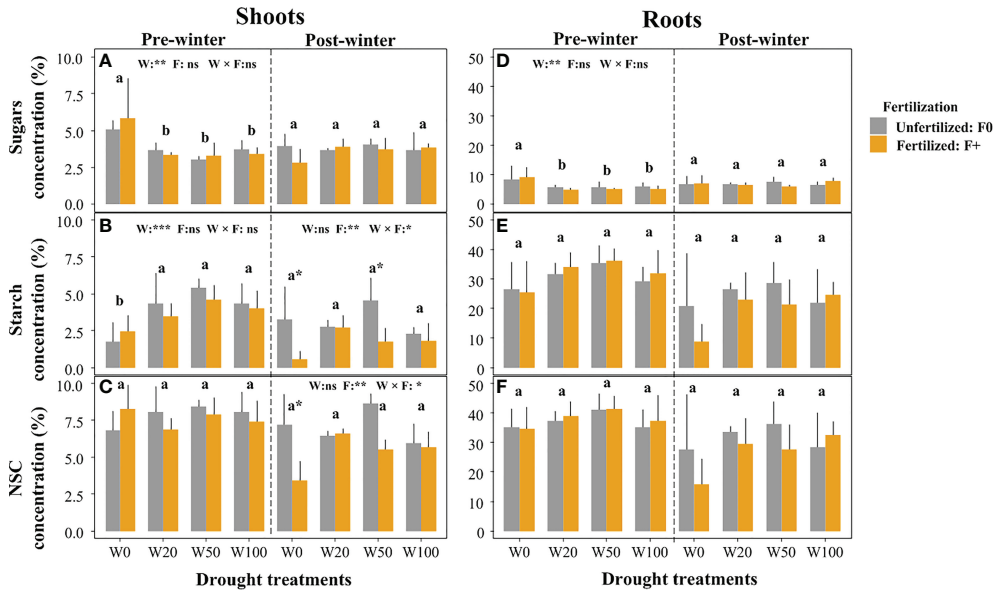

FIGURE 2
Effects of drought and fertilization on non-structural carbohydrates (NSC) in shoots and roots of downy oaks at pre winter (November, 2016) and post winter (March, 2017). **(A)** sugars in shoots, **(B)** starch in shoots, **(C)** the total NSC (sugars+starch) in shoots (left panel for pre-winter, and rightpanel for post-winter); **(D)** sugars in roots, **(E)** starch in roots, **(F)** the total NSC (sugars+starch) in roots. The drought treatments contain four levels: W100 (soil water capacity, ~25% VWC), W50, W20 and W0 (soil wilting point, ~6% VWC), W50 and W20 corresponding to approx. 50% and 20% field water capacity, respectively. Results of two-way ANOVA with drought (W) and fertilization (F) (their interaction effect was also considered) are given on the middle top of subfigures, using ns (non-significant), *p (< 0.05), ** (p < 0.01), or *** p(< 0.001) if significant effect was detected. Different lower-case letters represent significant differences in means among drought treatments tested with a Tukey *post-hoc* test, asterisks (on the bar) show significant differences between unfertilized (F0) and fertilized (F+) trees within the water treatment. Error bars indicate the SD of the mean values (n = 4). Note the y-axis scale change between shoots and roots.

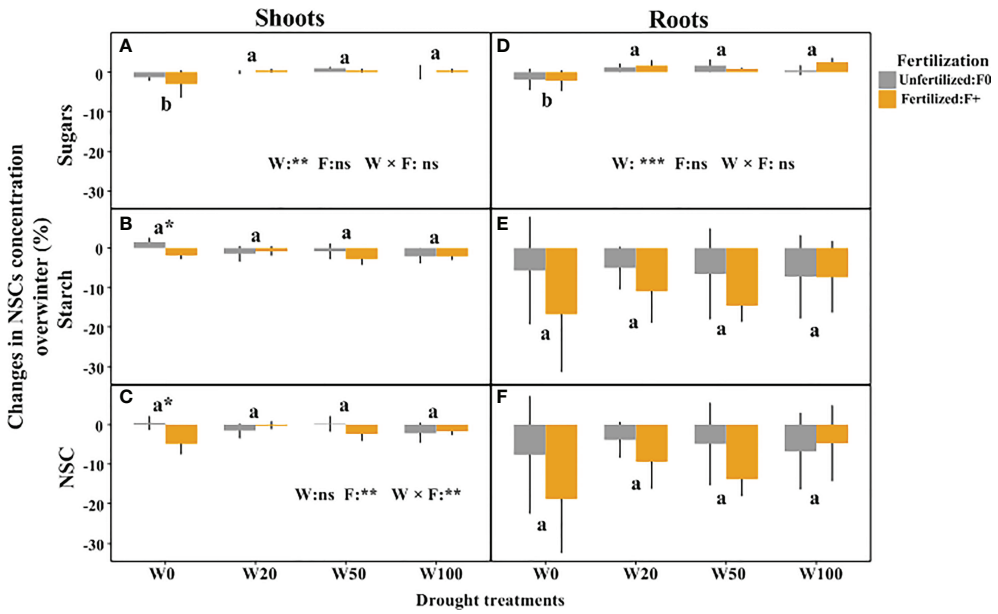

FIGURE 3
Changes in NSC concentrations overwinter in shoots and roots of downy oaks with different drought and fertilization treatments. **(A)** sugars changes in shoots, **(B)** starch changes in shoots, **(C)** the total NSC (sugars+starch) changes in shoots; **(D)** sugars changes in roots, **(E)** starch changes in roots, **(F)** thetotal NSC (sugars+starch) changes in roots. The drought treatments contain W100, W50, W20, and W0, represents 100%, 50%, 20%, and 0% of soil moisture at the field water capacity, respectively. Different lower cases letters represent significant differences in means among drought treatments tested by TukeyHSD, * signs show significant difference between unfertilized (F0) and fertilized (F+) trees within the water treatment. Error bars indicate the SD of the mean values (n = 4).

Fertilizer application did not affect leaf phenology timing (Figure 4; Table S3) but increased the number of saplings that successfully expanded leaves in the W0 treatment (Table 1). The leaf biomass in W50 saplings did not significantly differ from W100 saplings, but W20 and W0 droughts significantly decreased the biomass of new leaves (Figure 5). Within each drought treatment, fertilization did not affect the leaf biomass in 2017 (Figure 5).

Spring phenology and leaf growth in relation to pre- and post-winter NSC concentrations

The timing (days since April 3) of spring leaf phenology (bud swelling, bud break, leaf unfolding) and the leaf biomass in July were stronger correlated with pre-winter than with post-winter NSC concentrations (Table 2). Higher pre-winter starch concentrations

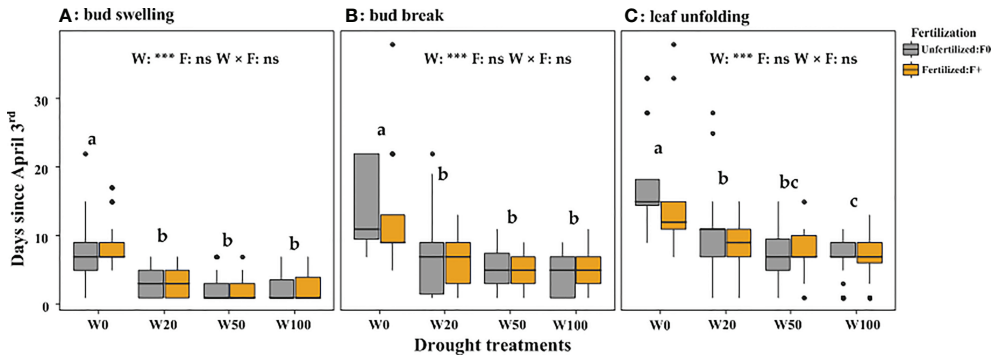

FIGURE 4
Number of days since April 3rd 2017 until bud swelling **(A)**, bud break **(B)** or leaf unfolding **(C)** for trees in the different drought and fertilization treatments. The drought treatments depicted as W100, W50, W20, and W0, represents 100%, 50%, 20%, and 0% of soil moisture at the field water capacity, respectively. Different lower cases letters indicate statistical differences (p < 0.05) among drought treatments.

TABLE 1 Number of oaks which failed to reach the phenology stages of bud swelling, bud break and leaf unfolding, under mild (W50), strong (W20) and extreme (W0) drought treatments.

Saplings number	W0/F0	W0/F+	W20/F0	W20/F+	W50/F0	W50/F+
Total number	31	32	32	32	32	32
Fail in bud swelling	6 (19.4%)	7 (21.9%)	1 (3.1%)	0 (0%)	1 (3.1%)	0 (0%)
Fail in bud break	18 (58.1%)	14 (43.8%)	1 (3.1%)	0 (0%)	1 (3.1%)	0 (0%)
Fail in leaf unfolding	19 (61.3%)	16 (50.0%)	1 (3.1%)	0 (0%)	1 (3.1%)	0 (0%)

Data in the brackets represent to ratio of failure individuals. Only treatments where phenology failure was observed are shown, thus well-watered W100 data was not shown.

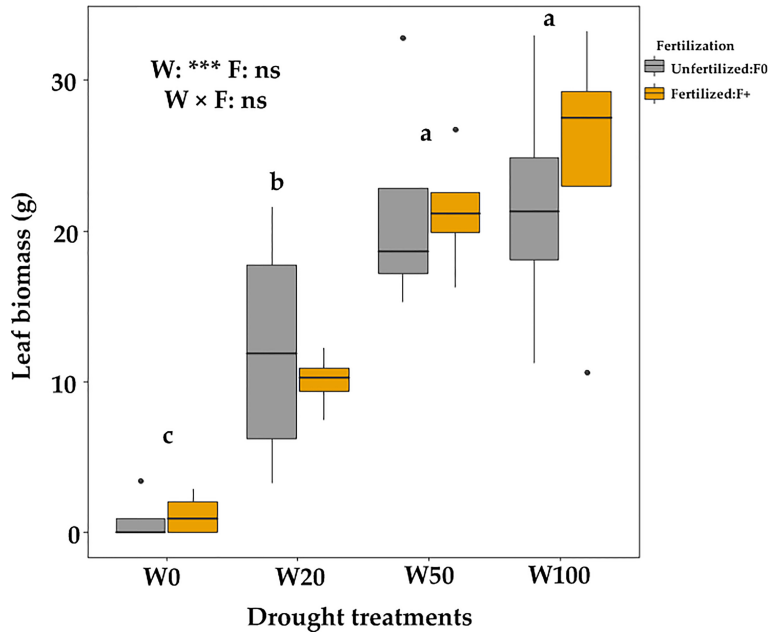

FIGURE 5
Leaf biomass of downy oaks (harvested in July, 2017) under different drought and fertilization treatments.

in shoots were correlated with earlier commencement, while higher sugar concentrations in shoots and roots were correlated with a delay of all the leaf phenology stages. Higher starch concentrations in the roots, both pre- and post-winter, were only correlated with earlier bud swelling. Leaf biomass was positively related to pre-winter starch concentration in shoots and negatively related to pre-winter sugar concentrations in both shoots and roots (Table 2).

Discussion

Impacts of previous drought and fertilization on pre-winter NSC

After one growing season, severely drought-stressed saplings did not show any signs of total NSC depletion, compared to the other drought and well-watered individuals (Figure 2). But they had strong reductions in leaf water content (Figure S3) and dry biomass in shoots and roots (Table S4, because of large variation in W100/F+ group, not statistically significant). Besides, it was observed that drought led to significantly decreased photosynthesis rate and leaf water potential in a comparable setting as well (Ouyang et al., 2021). Similar to our results, root NSC was not found to decrease during drought (Koppenaal et al., 1991; Zhang et al., 2015; Deng et al., 2019; Santos et al., 2021), while some others showed a drought-induced root NSC reduction (Li et al., 2018; Wiley, 2020). This suggests that downy oak can maintain stable NSC levels when exposing to strong drought (Wiley et al., 2013; Saffell et al., 2014), which is consistent with other studies on oak species (Nardini et al., 2016; Lavrič et al., 2017; Ouyang et al., 2021). Moreover, no fertilization effects on NSC were found across all drought treatments (Figure 2), which is inconsistent with results from a meta-analysis that nitrogen addition decreased NSC

10.3389/fpls.2022.1035191

TABLE 2 Correlation between the number of days until different leaf development stages and leaf biomass in relation to non-structural carbohydrate (NSC) concentrations in shoots and roots at pre- and post-winter.

NSC indices	Parameters	Bud swelling	Bud break	Leaf unfolding	Leaf biomass
Pre-winter					
Shoots sugar	*Pr(>|t|)*	**< 0.001**	**0.003**	**0.004**	**0.039**
	R^2	**0.482**	**0.266**	**0.254**	**0.134**
	slope	**-1.383**	**-1.569**	**-1.630**	**-2.951**
Shoots starch	*Pr(>|t|)*	**< 0.001**	**0.015**	**0.040**	**0.035**
	R^2	**0.343**	**0.188**	**0.138**	**0.139**
	slope	**0.986**	**0.128**	**1.027**	**2.540**
Roots sugar	*Pr(>|t|)*	**0.005**	**0.011**	**0.035**	**0.025**
	R^2	**0.233**	**0.205**	**0.144**	**0.157**
	slope	**-0.530**	**-0.748**	**-0.668**	**-1.761**
Roots starch	*Pr(>|t|)*	**0.013**	0.066	0.255	0.377
	R^2	**0.190**	0.112	0.044	0.026
	slope	**0.164**			
Post-winter					
Shoots sugar	*Pr(>|t|)*	0.055	0.206	**0.039**	0.480
	R^2	0.117	0.054	**0.139**	0.017
	slope			**2.209**	
Shoots starch	*Pr(>|t|)*	0.608	0.555	0.518	0.351
	R^2	0.009	0.012	0.015	0.029
	slope				
Roots sugar	*Pr(>|t|)*	0.486	0.592	0.939	0.305
	R^2	0.016	0.010	< 0.001	0.035
	slope				
Roots starch	*Pr(>|t|)*	**0.038**	0.289	0.223	0.665
	R^2	**0.136**	0.039	0.051	0.006
	slope	**0.097**			

-1 * DOY was used, thus positive and negative slope indicate a promotion or delay, respectively, of phenology with higher NSC. Slope of regression line is given if $Pr < 0.05$ (which is shown in bold).

concentrations in roots (-5.0%), but increased NSC in aboveground wood (+6.1%) (Li et al., 2019). This difference might be related to the fertilizer used (blended fertilizer in the present study and nitrogen addition in that meta-analysis), and may also be related to the amount of fertilizer added (e.g. large variations in the meta-analysis).

The extreme drought treatment (W0) decreased starch concentrations and increased sugar concentrations but did not change the total NSC in shoots (and to a lesser extent in the roots). This suggests that drought stressed oaks converted starch into sugars for osmotic adjustment and potentially to repair xylem embolisms (Silva et al., 2010; Secchi and Zwieniecki, 2011). Moreover, Wong et al. (2009) indicated that the drought stressed trees rely more on osmoregulation (chemical changes) rather than physiological changes of cell properties in cold tolerance development for protecting cytoplasm macromolecules and membranes, serving as osmoregulatory function, and lowering freezing point, thus higher sugars were observed in W0 trees.

Impacts of previous drought and fertilization on winter NSC consumption

In this study, drought treatments did not affect the overwinter consumption of the total NSC and starch in both shoots (Figures 3C, B) and roots (Figures 3F, E), but W0 significantly depleted sugars in both shoots and roots, whereas other drought treatments accumulated sugars in tissues (Figures 3A, D). Actually, a certain depletion level of NSC (especially starch) in winter is to be expected, because this is related to the maintenance of cellular respiration overwinter and to the starch-sugar conversion for frost protection (Bonhomme et al., 2005; Amico Roxas et al., 2021). In late winter, decline in sugar levels in wood tissues will support cellular respiration and metabolic activities to facilitate cellular changes with dehardening before budburst. For extreme drought stressed saplings, the conversion process of starch into sugars seemed to be impeded during winter (Figure 3A). This was also observed by Galvez et al. (2013), who showed that growing season drought hampered the conversion of starch into soluble sugars during winter for *Populus* saplings, and by Wong et al. (2009) who found that drought stressed sugar-maple trees declined sugar levels in branches, suggesting a lower degree of conversion of cellular components with hardening under drought stress.

Besides, a strong reduction in shoots' NSC concentrations overwinter was observed in fertilized W0 (W0/F+) saplings, leading to a significantly lower post-winter NSC compared to individuals from all the other treatments. Compared to unfertilized saplings, there was comparable, generally

decreased starch level in roots of fertilized trees in W0, W20 and W50 (also visible in W50 shoots). This result indicates that fertilization might promote starch use of drought stressed trees. Reduction of soil nutrient uptake due to drought will impair plant's nutritional status and general functioning especially for osmotic regulation and membrane stability (Kreuzwieser and Gessler, 2010). Fertilizer application may mitigate nutrient shortage and improve the former physiological functions to a certain extent. In the present study, fertilization did not lead to higher N accumulation in both leaves sampled in September 2016 (Table S5) and July 2017, and in other wood tissues (Nardini et al., 2016; Ouyang et al., 2021). But fertilization significantly promoted K accumulation in shoots at pre-winter within each water treatment level (Tables S6, S7). As inorganic solute, K^+ plays a central role in the water economy of plants, involves in osmotic regulation, maintenance of cell turgor and increases the stability of cell membranes (Saneoka et al., 2004; Ahanger et al., 2016). It also supports metabolic activity and frost hardiness by hydrolyzing starch into sugars (Elle and Sauter, 2000; Norozi et al., 2020). K has a favorable effect on water regulation and photosynthesis in plants (Snyder et al., 2005), but its effect on frost protection is unclear, as summarized by Charrier et al. (2015). In this study, the role and effects of K on key tree physiology functions including carbohydrate mobilization of drought stressed saplings were not specifically studied, which should be clarified in future studies.

The phenology and its relation to pre and post-winter NSC

Extreme drought significantly delayed spring leaf phenology of downy oaks, which is in line with findings on other oak species (Vander Mijnsbrugge et al., 2016; Čehulić et al., 2019). Under the extreme drought in the present study, fertilization did not change the timing of spring leaf phenology but increased the survival rate of plants (Table 3, Figure 4), despite of very low post-winter shoot NSC concentrations in W0/F+ (~3% in W0/F+ vs. ~7% in W0/F0, $P < 0.05$). Previous studies proposed that hydraulic failure and carbon starvation are two possible physiological mechanisms for drought-induced tree mortality or growth decline (Mcdowell et al., 2008; Li et al., 2022), decreased NSC accompanied by decreased mortality with fertilization in the present study suggest that drought-induced mortality was driven by hydraulic failure, rather than carbon starvation, especially under high nutrient availability. But high nutrient availability might have promoted the mobilization and utilization of carbohydrates during winter (Wong et al., 2009; Galvez et al., 2013; Schönbeck et al., 2020). This led to lower post-winter NSC concentrations but help to repair cavitation and build new xylem to compensate cavitation induced by frost and extreme drought (Barbaroux and Breda, 2002), or promote sugars reverted back into the xylem sap and apoplastic free space, resulting in lower mortality. Therefore, fertilization reduced the saplings' mortality rate of W0, recorded both in July 2017 (Table 3, 1.5 years drought, mortality rate: unfertilized 51.9% and fertilized 32.0%) and September 2018 (a follow up research with re-water treatment, mortality rate: unfertilized 78.6% and fertilized 51.2%) (Ouyang et al., 2021).

Pre-winter starch concentrations in shoots were positively correlated with the commencement of leaf phenology and with leaf biomass. Pre-winter sugars in shoots and roots were negatively correlated with the timings of all the stages and with leaf biomass (Table 2). Since pre-winter sugar and starch concentrations are highly related to the previous growing season water supply levels, we cannot confirm that pre-winter NSC affects leaf phenology and leaf growth directly or indirectly. A direct effect is supported by the results of Amico Roxas et al. (2021) who showed that through affecting bud endo- and ecto-dormancy periods (Fernandez et al., 2019; Tixier et al., 2019), fall NSC availability induces long-lasting effects on phenological timing of trees. However, we can also not exclude indirect effects: higher sugar levels (in shoots and roots) and lower starch (in the shoots) in the fall might indicate a still high demand for osmotic adjustment and potentially the need for cavitation refilling (Pérez-De-Lis et al., 2016; Savi et al., 2016),

TABLE 3 Mortality rate of downy oaks saplings with different drought and fertilizer application treatments (investigated after 1.5 years drought, in June 2017).

Treatments	Number of dead	Total number	Mortality rate (%)
W0/F0	14	27	51.9
W0/F+	8	25	32.0
W20/F0	1	28	3.6
W20/F+	0	27	0
W50/F0	3	28	10.7
W50/F+	0	27	0
W100/F0	0	29	0
W100/F+	0	28	0

especially in W0. Bud swelling depends on sugar input from sapwood vessels, and xylem sap osmolarity also plays an important role in the generation of the stem pressure needed to reverse winter embolisms in early spring (Ameglio et al., 2001). A reduced ability to repair embolism in trees with low xylem sap sugars concentration could thus negatively affects the supply of water to bud swelling (Ameglio et al., 2001). Thus, stronger cavitation might lead to lower water supply of buds and thus delayed bud swelling and growth in the following spring.

Roots contribute largely to the total starch pool in downy oak (Figure 2), and might thus play an important role in the phenology process. Higher NSC (starch) in the roots might help to maintain root activity during winter to enhance water absorption in early spring. Moreover, root starch reserves might be later released and transported to the branches to support bud break (Tixier et al., 2017) and leaf formation in spring (Klein et al., 2016). Lower root starch reserves might thus delay these processes. The result shows that higher sugar concentrations are correlated with earlier leaf unfolding in the spring might be because shoot sugars are a direct carbon source for new leaves and can also support embolism repair (Pérez-De-Lis et al., 2016; Savi et al., 2016; Pagliarani et al., 2019; Tomasella et al., 2019), and thus increase the supply of water to swelling buds, which was also confirmed by Park et al. (2009) and Pérez-De-Lis et al. (2016).

Conclusion

We examined previous summer drought and fertilization effects on carbon reserves over winter and spring leaf phenology of downy oak saplings next year. We found that, irrespective of drought intensity and the combined fertilization treatments, pre- and post-winter total NSC reserves were always abundant in storage tissues of previously treated saplings in expense of growth (Schönbeck et al., 2020; Ouyang et al., 2021). A mitigating effect of fertilization seemed to occur only when saplings grown under extreme drought, which is manifested in decreased mortality rate and increased recovery ability. This implies that increase in nutrient availability under extreme drought may alleviate phloem mobilization failure in some degree, and promote spring leaf development as a compensatory response. Based on this, we recommend to fertilize when plants subject to long-lasting extreme drought in temperate regions, to improve their drought resistance in the growing season, to increase the mobilization and utilization of sugar in winter, and to enhance the recovery ability next year.

Data availability statement

The original contributions presented in the study are included in the article/Supplementary Material. Further inquiries can be directed to the corresponding authors.

Author contributions

ML, LS, and AR designed, planned the experiment; XW, LS, and PH conducted the experiment and collected the data; XW, YY, DY and PH analyzed the data; ML led the manuscript writing; XW and ML wrote the first draft, XW, AG, LS, and ML revised the manuscript; ML finalized the article. All authors contributed to the article and approved the submitted version.

Funding

This work was financially supported by a Swiss National Fund grant (31003A_157126/1, to ML), a Natural Science Foundation of Zhejiang Province (LQ21C030001, to XW) and National Natural Science Foundation of China (32001147, to PH). XW's 12-month-research stay in Switzerland is financially supported by the China Scholarship Council, and PH's 18-month-research stay in Switzerland is financially supported by Sino-Swiss Science and Technology Cooperation (SSSTC) program (EG06-032016) and the China Scholarship Council. Open access funding provided by WSL - Swiss Federal Institute For Forest, Snow And Landscape Research

Acknowledgments

We sincerely appreciate suggestions for manuscript revisions from Deliang Lu, the editor and all the reviewers to improve quality of our paper.

Conflict of interest

The authors declare that the research was conducted in the absence of any commercial or financial relationships that could be construed as a potential conflict of interest.

Publisher's note

Supplementary material

The Supplementary Material for this article can be found online at: https://www.frontiersin.org/articles/10.3389/fpls.2022.1035191/full#supplementary-material

References

Adams, H. D., Zeppel, M. J. B., Anderegg, W. R. L., Hartmann, H., Landhäusser, S. M., Tissue, D. T., et al. (2017). A multi-species synthesis of physiological mechanisms in drought-induced tree mortality. *Nat. Ecol. Evol.* 1, 1285–1291. doi: 10.1038/s41559-017-0248-x

Ahanger, M. A., Morad-Talab, N., Abd-Allah, E. F., Ahmad, P., and Hajiboland, R. (2016). Plant growth under drought stress: Significance of mineral nutrients. *Water Stress Crop plants: Sustain. approach* 2, 649–668. doi: 10.1002/9781119054450.ch37

Allen, C. D., Macalady, A. K., Chenchouni, H., Bachelet, D., Mcdowell, N., Vennetier, M., et al. (2010). A global overview of drought and heat-induced tree mortality reveals emerging climate change risks for forests. *For. Ecol. Manage.* 259, 660–684. doi: 10.1016/j.foreco.2009.09.001

Ameglio, T., Ewers, F. W., Cochard, H., Martignac, M., Vandame, M., Bodet, C., et al. (2001). Winter stem xylem pressure in walnut trees: effects of carbohydrates, cooling and freezing. *Tree Physiol.* 21, 387–394. doi: 10.1093/treephys/21.6.387

Amico Roxas, A., Orozco, J., Guzmán-Delgado, P., and Zwieniecki, M. A. (2021). Spring phenology is affected by fall non-structural carbohydrate concentration and winter sugar redistribution in three Mediterranean nut tree species. *Tree Physiol* 41, 1425–1438. doi: 10.1093/treephys/tpab014

Anderegg, W. R. L., Berry, J. A., Smith, D. D., Sperry, J. S., Anderegg, L. D. L., and Field, C. B. (2012). The roles of hydraulic and carbon stress in a widespread climate-induced forest die-off. *Proc. Natl. Acad. Sci.* 109, 233–237. doi: 10.1073/pnas.1107891109

Barbaroux, C., and Breda, N. (2002). Contrasting distribution and seasonal dynamics of carbohydrate reserves in stem wood of adult ring-porous sessile oak and diffuse-porous beech trees. *Tree Physiol.* 22, 1201–1210. doi: 10.1093/treephys/22.17.1201

Bonhomme, M., Rageau, R., Lacointe, A., and Gendraud, M. (2005). Influences of cold deprivation during dormancy on carbohydrate contents of vegetative and floral primordia and nearby structures of peach buds (Prunus persica l. batch). *Scientia Hortic.* 105, 223–240. doi: 10.1016/j.scienta.2005.01.015

Čehulić, I., Sever, K., Katičić Bogdan, I., Jazbec, A., Škvorc, Ž., and Bogdan, S. (2019). Drought impact on leaf phenology and spring frost susceptibility in a quercus robur l. provenance trial. *Forests* 10, 50. doi: 10.3390/F10010050

Charrier, G., Ngao, J., Saudreau, M., and Améglio, T. (2015). Effects of environmental factors and management practices on microclimate, winter physiology, and frost resistance in trees. *Front. Plant Sci.* 6, 259. doi: 10.3389/fpls.2015.00259

Choat, B., Brodribb, T. J., Brodersen, C. R., Duursma, R. A., Lopez, R., and Medlyn, B. E. (2018). Triggers of tree mortality under drought. *Nature* 558, 531–539. doi: 10.1038/s41586-018-0240-x

Deng, X., Xiao, W., Shi, Z., Zeng, L., and Lei, L. (2019). Combined effects of drought and shading on growth and non-structural carbohydrates in pinus massoniana lamb. seedlings. *Forests* 11, 18. doi: 10.3390/f11010018

Earles, J. M., Stevens, J. T., Sperling, O., Orozco, J., North, M. P., and Zwieniecki, M. A. (2018). Extreme mid-winter drought weakens tree hydraulic–carbohydrate systems and slows growth. *New Phytol.* 219, 89–97. doi: 10.1111/nph.15136

Elle, D., and Sauter, J. J. (2000). Seasonal changes of activity of a starch granule bound endoamylase and of a starch phosphorylase in poplar wood (Populus× canadensis moench‹ robusta›) and their possible regulation by temperature and phytohormones. *J. Plant Physiol.* 156, 731–740. doi: 10.1016/S0176-1617(00)80239-4

Fernandez, E., Cuneo, I. F., Luedeling, E., Alvarado, L., Farias, D., and Saa, S. (2019). Starch and hexoses concentrations as physiological markers in dormancy progression of sweet cherry twigs. *Trees* 33, 1187–1201. doi: 10.1007/s00468-019-01855-0

Galiano, L., Martínez-Vilalta, J., and Lloret, F. (2011). Carbon reserves and canopy defoliation determine the recovery of scots pine 4 yr after a drought episode. *New Phytol.* 190, 750–759. doi: 10.1111/j.1469-8137.2010.03628.x

Galvez, D. A., Landhäusser, S. M., and Tyree, M. T. (2013). Low root reserve accumulation during drought may lead to winter mortality in poplar seedlings. *New Phytol.* 198, 139–148. doi: 10.1111/nph.12129

Gessler, A., Schaub, M., and Mcdowell, N. G. (2017). The role of nutrients in drought-induced tree mortality and recovery. *New Phytol.* 214, 513–520. doi: 10.1111/nph.14340

Gruber, A., Pirkebner, D., Florian, C., and Oberhuber, W. (2012). No evidence for depletion of carbohydrate pools in scots pine (Pinus sylvestris l.) under drought stress. *Plant Biol.* 14, 142–148. doi: 10.1111/j.1438-8677.2011.00467.x

Hartmann, H., Adams, H. D., Hammond, W. M., Hoch, G., Landhausser, S. M., Wiley, E., et al. (2018). Identifying differences in carbohydrate dynamics of seedlings and mature trees to improve carbon allocation in models for trees and forests. *Environ. Exp. Bot.* 152, 7–18. doi: 10.1016/j.envexpbot.2018.03.011

Hoch, G. (2015). "Carbon reserves as indicators for carbon limitation in trees," in *Progress in botany* (Cham: Springer), 321–346.

Hoch, G., Popp, M., and Körner, C. (2002). Altitudinal increase of mobile carbon pools in pinus cembra suggests sink limitation of growth at the Swiss treeline. *Oikos* 98, 361–374. doi: 10.1034/j.1600-0706.2002.980301.x

Hoch, G., Richter, A., and Körner, C. (2003). Non-structural carbon compounds in temperate forest trees. *Plant Cell Environ.* 26, 1067–1081. doi: 10.1046/j.0016-8025.2003.01032.x

IPCC (2021). "Climate change 2021: The physical science basis," in *Contribution of working group I to the sixth assessment report of the intergovernmental panel on climate change*. (United Kingdom and New York, NY, USA: Cambridge University Press, Cambridge). doi: 10.1017/9781009157896

Jacobs, D. F., Rose, R., Haase, D. L., and Alzugaray, P. O. (2004). Fertilization at planting impairs root system development and drought avoidance of Douglas-fir (Pseudotsuga menziesii) seedlings. *Ann. For. Sci.* 61, 643–651. doi: 10.1051/forest:2004065

Kannenberg, S. A., and Phillips, R. P. (2020). Non-structural carbohydrate pools not linked to hydraulic strategies or carbon supply in tree saplings during severe drought and subsequent recovery. *Tree Physiol.* 40, 259–271. doi: 10.1093/treephys/tpz132

Keller, M., Tarara, J. M., and Mills, L. J. (2010). Spring temperatures alter reproductive development in grapevines. *Aust. J. Grape Wine Res.* 16, 445–454. doi: 10.1111/j.1755-0238.2010.00105.x

Klein, T., Vitasse, Y., and Hoch, G. (2016). Coordination between growth, phenology and carbon storage in three coexisting deciduous tree species in a temperate forest. *Tree Physiol.* 36, 847–855. doi: 10.1093/treephys/tpw030

Koppenaal, R. S., Tschaplinski, T. J., and Colombo, S. J. (1991). Carbohydrate accumulation and turgor maintenance in seedling shoots and roots of two boreal conifers subjected to water stress. *Can. J. Bot.* 69, 2522–2528. doi: 10.1139/b91-314

Körner, C. (2003). Carbon limitation in trees. *J. Ecol.* 91, 4–17. doi: 10.1046/j.1365-2745.2003.00742.x

Kreuzwieser, J., and Gessler, A. (2010). Global climate change and tree nutrition: influence of water availability. *Tree Physiol.* 30, 1221–1234. doi: 10.1093/treephys/tpq055

Kuster, T. M., Arend, M., Gunthardt-Goerg, M. S., and Schulin, R. (2013). Root growth of different oak provenances in two soils under drought stress and air warming conditions. *Plant Soil* 369, 61–71. doi: 10.1007/s11104-012-1541-8

Kuster, T. M., Dobbertin, M., Günthardt-Goerg, M. S., Schaub, M., and Arend, M. (2014). A phenological timetable of oak growth under experimental drought and air warming. *PloS One* 9, e89724. doi: 10.1371/journal.pone.0089724

Lavrič, M., Eler, K., Ferlan, M., Vodnik, D., and Gričar, J. (2017). Chronological sequence of leaf phenology, xylem and phloem formation and sap flow of quercus pubescens from abandoned karst grasslands. *Front. Plant Sci.* 8, 314. doi: 10.3389/fpls.2017.00314

Lebon, G., Wojnarowiez, G., Holzapfel, B., Fontaine, F., Vaillant-Gaveau, N., and Clément, C. (2008). Sugars and flowering in the grapevine (Vitis vinifera l.). *J. Exp. Bot.* 59, 2565–2578. doi: 10.1093/jxb/ern135

Li, W., Hartmann, H., Adams, H. D., Zhang, H., Jin, C., Zhao, C., et al. (2018). The sweet side of global change–dynamic responses of non-structural carbohydrates to drought, elevated CO2 and nitrogen fertilization in tree species. *Tree Physiol.* 38, 1706–1723. doi: 10.1093/treephys/tpy059

Li, W., Mcdowell, N. G., Zhang, H., Wang, W., Mackay, D. S., Leff, R. T., et al. (2022). The influence of increasing atmospheric CO2 , temperature, and vapor pressure deficit on seawater-induced tree mortality. *New Phytol.* 235, 1767–1779. doi: 10.1111/nph.18275

Li, M.-H., Xiao, W.-F., Wang, S.-G., Cheng, G.-W., Cherubini, P., Cai, X.-H., et al. (2008). Mobile carbohydrates in Himalayan treeline trees i. evidence for carbon gain limitation but not for growth limitation. *Tree Physiol.* 28, 1287–1296. doi: 10.1093/treephys/28.8.1287

Li, W., Zhang, H., Huang, G., Liu, R. X., Wu, H., Zhao, C., et al. (2019). Effects of nitrogen enrichment on tree carbon allocation: A global synthesis. *Glob. Ecol. Biogeogr.* 29, 573–589. doi: 10.1111/geb.13042

Loescher, W. H., Mccamant, T., and Keller, J. D. (1990). Carbohydrate reserves, translocation, and storage in woody plant roots. *HortScience* 25, 274–281. doi: 10.21273/HORTSCI.25.3.274

Lopez, G., Girona, J., and Marsal, J. (2007). Response of winter root starch concentration to severe water stress and fruit load and its subsequent effects on

early peach fruit development. *Tree Physiol.* 27, 1619–1626. doi: 10.1093/treephys/27.11.1619

Mcdowell, N. G., Pockman, W. T., Allen, C. D., Breshears, D. D., Cobb, N. S., Kolb, T. E., et al. (2008). Mechanisms of plant survival and mortality during drought: why do some plants survive while others succumb to drought? *New Phytol.* 178, 4, 719–739. doi: 10.1111/j.1469-8137.2008.02436.x

Mitchell, P. J., O'grady, A. P., Tissue, D. T., White, D. A., Ottenschlaeger, M. L., and Pinkard, E. A. (2013). Drought response strategies define the relative contributions of hydraulic dysfunction and carbohydrate depletion during tree mortality. *New Phytol.* 197, 862–872. doi: 10.1111/nph.12064

Morin, X., Améglio, T., Ahas, R., Kurz-Besson, C., Lanta, V., Lebourgeois, F., et al. (2007). Variation in cold hardiness and carbohydrate concentration from dormancy induction to bud burst among provenances of three European oak species. *Tree Physiol.* 27, 817–825. doi: 10.1093/treephys/27.6.817

Nardini, A., Casolo, V., Dal Borgo, A., Savi, T., Stenni, B., Bertoncin, P., et al. (2016). Rooting depth, water relations and non-structural carbohydrate dynamics in three woody angiosperms differentially affected by an extreme summer drought. *Plant Cell Environ.* 39, 618–627. doi: 10.1111/pce.12646

Norozi, M., Valizadehkaji, B., Karimi, R., and Solgi, M. (2020). Potassium and zinc-induced frost tolerance in pistachio flowers is associated with physiological and biochemical changes. *Trees* 34, 1021–1032. doi: 10.1007/s00468-020-01978-9

Ouyang, S.-N., Gessler, A., Saurer, M., Hagedorn, F., Gao, D.-C., Wang, X.-Y., et al. (2021). Root carbon and nutrient homeostasis determines downy oak sapling survival and recovery from drought. *Tree Physiol* 41, 1400–1412. doi: 10.1093/treephys/tpab019

Pagliarani, C., Casolo, V., Ashofteh Beiragi, M., Cavalletto, S., Siciliano, I., Schubert, A., et al. (2019). Priming xylem for stress recovery depends on coordinated activity of sugar metabolic pathways and changes in xylem sap pH. *Plant Cell Environ.* 42, 1775–1787. doi: 10.1111/pce.13533

Park, J.-Y., Canam, T., Kang, K.-Y., Unda, F., and Mansfield, S. D. (2009). Sucrose phosphate synthase expression influences poplar phenology. *Tree Physiol.* 29, 937–946. doi: 10.1093/treephys/tpp028

Pérez-De-Lis, G., García-González, I., Rozas, V., and Olano, J. M. (2016). Feedbacks between earlywood anatomy and non-structural carbohydrates affect spring phenology and wood production in ring-porous oaks. *Biogeosciences* 13, 5499–5510. doi: 10.5194/bg-13-5499-2016

Piper, F. I. (2011). Drought induces opposite changes in the concentration of non-structural carbohydrates of two evergreen nothofagus species of differential drought resistance. *Ann. For. Sci.* 68, 415–424. doi: 10.1007/s13595-011-0030-1

Piper, F. I., and Fajardo, A. (2016). Carbon dynamics of acer pseudoplatanus seedlings under drought and complete darkness. *Tree Physiol.* 36, 1400–1408. doi: 10.1093/treephys/tpw063

Saffell, B. J., Meinzer, F. C., Woodruff, D. R., Shaw, D. C., Voelker, S. L., Lachenbruch, B., et al. (2014). Seasonal carbohydrate dynamics and growth in Douglas-fir trees experiencing chronic, fungal-mediated reduction in functional leaf area. *Tree Physiol.* 34, 218–228. doi: 10.1093/treephys/tpu002

Saneoka, H., Moghaieb, R. E. A., Premachandra, G. S., and Fujita, K. (2004). Nitrogen nutrition and water stress effects on cell membrane stability and leaf water relations in agrostis palustris huds. *Environ. Exp. Bot.* 52, 131–138. doi: 10.1016/j.envexpbot.2004.01.011

Santos, M., Barros, V., Lima, L., Frosi, G., and Santos, M. G. (2021). Whole plant water status and non-structural carbohydrates under progressive drought in a caatinga deciduous woody species. *Trees* 35, 1257–1266. doi: 10.1007/s00468-021-02113-y

Savi, T., Casolo, V., Luglio, J., Bertuzzi, S., Gullo, M. A. L., and Nardini, A. (2016). Species-specific reversal of stem xylem embolism after a prolonged drought correlates to endpoint concentration of soluble sugars. *Plant Physiol. Biochem.* 106, 198–207. doi: 10.1016/j.plaphy.2016.04.051

Schönbeck, L., Gessler, A., Hoch, G., Mcdowell, N. G., Rigling, A., Schaub, M., et al. (2018). Homeostatic levels of nonstructural carbohydrates after 13 yr of drought and irrigation in pinus sylvestris. *New Phytol.* 219, 1314–1324. doi: 10.1111/nph.15224

Schönbeck, L., Gessler, A., Schaub, M., Rigling, A., Hoch, G., Kahmen, A., et al. (2020). Soil nutrients and lowered source: sink ratio mitigate effects of mild but not of extreme drought in trees. *Environ. Exp. Bot.* 169, 103905. doi: 10.1016/j.envexpbot.2019.103905

Secchi, F., and Zwieniecki, M. A. (2011). Sensing embolism in xylem vessels: the role of sucrose as a trigger for refilling. *Plant Cell Environ.* 34, 514–524. doi: 10.1111/j.1365-3040.2010.02259.x

Silva, E. N., Ferreira-Silva, S. L., Viégas, R. A., and Silveira, J. A. G. (2010). The role of organic and inorganic solutes in the osmotic adjustment of drought-stressed jatropha curcas plants. *Environ. Exp. Bot.* 69, 279–285. doi: 10.1016/j.envexpbot.2010.05.001

Snyder, R. L., Abreu, J. P. D. M., and Matulich, S. (2005). *Frost protection: fundamentals, practice, and economics*. (Cambridge University Press, Rome: FAO).

Tixier, A., Gambetta, G. A., Godfrey, J. M., Orozco, J., and Zwieniecki, M. A. (2019). Non-structural carbohydrates in dormant perennials; the tale of winter survival and spring arrival. *Front. Forests Global Change* 2, 18. doi: 10.3389/ffgc.2019.00018

Tixier, A., Sperling, O., Orozco, J., Lampinen, B., Roxas, A. A., Saa, S., et al. (2017). Spring bud growth depends on sugar delivery by xylem and water recirculation by phloem münch flow in juglans regia. *Planta* 246, 495–508. doi: 10.1007/s00425-017-2707-7

Tomasella, M., Petrussa, E., Petruzzellis, F., Nardini, A., and Casolo, V. (2019). The possible role of non-structural carbohydrates in the regulation of tree hydraulics. *Int. J. Mol. Sci.* 21, 144. doi: 10.3390/ijms21010144

Vander Mijnsbrugge, K., Turcsán, A., Maes, J., Duchêne, N., Meeus, S., Steppe, K., et al. (2016). Repeated summer drought and re-watering during the first growing year of oak (Quercus petraea) delay autumn senescence and bud burst in the following spring. *Front. Plant Sci.* 7, 419. doi: 10.3389/fpls.2016.00419

Wiley, E. (2020). Do carbon reserves increase tree survival during stress and following disturbance? *Curr. Forestry Rep.* 6, 14–25. doi: 10.1007/ s40725-019-00106-2

Wiley, E., Huepenbecker, S., Casper, B. B., and Helliker, B. R. (2013). The effects of defoliation on carbon allocation: can carbon limitation reduce growth in favour of storage? *Tree Physiol.* 33, 1216–1228. doi: 10.1093/treephys/tpt093

Wong, S. C. (1990). Elevated atmospheric partial pressure of CO2 and plant growth II. non-structural carbohydrate content in cotton plants and its effect on growth parameters. *Photosynthesis Res.* 23, 171–180. doi: 10.1007/BF00035008

Wong, B. L., Baggett, K. L., and Rye, A. H. (2009). Cold-season patterns of reserve and soluble carbohydrates in sugar maple and ice-damaged trees of two age classes following drought. *Botany* 87, 293–305. doi: 10.1139/B08-123

Woodruff, D. R., Meinzer, F. C., Marias, D. E., Sevanto, S., Jenkins, M. W., and Mcdowell, N. G. (2015). Linking nonstructural carbohydrate dynamics to gas exchange and leaf hydraulic behavior in pinus edulis and juniperus monosperma. *New Phytol.* 206, 411–421. doi: 10.1111/nph.13170

Young, D. J. N., Stevens, J. T., Earles, J. M., Moore, J., Ellis, A., Jirka, A. L., et al. (2017). Long-term climate and competition explain forest mortality patterns under extreme drought. *Ecol. Lett.* 20, 78–86. doi: 10.1111/ele.12711

Zhang, T., Cao, Y., Chen, Y., and Liu, G. (2015). Non-structural carbohydrate dynamics in robinia pseudoacacia saplings under three levels of continuous drought stress. *Trees* 29, 1837–1849. doi: 10.1007/s00468-015-1265-5

Zhang, H., Li, X. R., Guan, D., Wang, A.-Z., Yuan, F., Wu, J. J. A., et al. (2021). Nitrogen nutrition addition mitigated drought stress by improving carbon exchange and reserves among two temperate trees. *Agric For Meteorol.* 311, 108693 doi: 10.1016/j.agrformet.2021.108693

Zhao, M., and Running, S. W. (2010). Drought-induced reduction in global terrestrial net primary production from 2000 through 2009. *science* 329, 940–943. doi: 10.1126/science.1192666

Zhu, W.-Z., Cao, M., Wang, S.-G., Xiao, W.-F., and Li, M.-H. (2012a). Seasonal dynamics of mobile carbon supply in quercus aquifolioides at the upper elevational limit. *PloS One* 7, e34213. doi: 10.1371/journal.pone.0034213

Zhu, W.-Z., Xiang, J.-S., Wang, S.-G., and Li, M.-H. (2012b). Resprouting ability and mobile carbohydrate reserves in an oak shrubland decline with increasing elevation on the eastern edge of the qinghai–Tibet plateau. *For. Ecol. Manage.* 278, 118–126. doi: 10.1016/j.foreco.2012.04.032

frontiers | Frontiers in Plant Science

TYPE Original Research
PUBLISHED 01 December 2022
DOI 10.3389/fpls.2022.1055984

OPEN ACCESS

EDITED BY
Song Heng Jin,
Zhejiang Agriculture and Forestry University, China

REVIEWED BY
Zihan Zhang,
Chinese Academy of Forestry, China
Yang Xiulian,
Nanjing Forestry University, China
Taikui Zhang,
The Pennsylvania State University (PSU), United States

*CORRESPONDENCE
Zunling Zhu
zhuzunling@aliyun.com

SPECIALTY SECTION
This article was submitted to Functional Plant Ecology, a section of the journal Frontiers in Plant Science

RECEIVED 28 September 2022
ACCEPTED 15 November 2022
PUBLISHED 01 December 2022

CITATION
Zhou Q, Zhao F, Zhang H and Zhu Z (2022) Responses of the growth, photosynthetic characteristics, endogenous hormones and antioxidant activity of *Carpinus betulus* L. seedlings to different light intensities.
Front. Plant Sci. 13:1055984.
doi: 10.3389/fpls.2022.1055984

Responses of the growth, photosynthetic characteristics, endogenous hormones and antioxidant activity of *Carpinus betulus* L. seedlings to different light intensities

Qi Zhou[1,2], Feng Zhao[3], Huihui Zhang[2,4] and Zunling Zhu[2,4]*

[1]School of Environment and Ecology, Jiangsu Open University, Nanjing, China, [2]Co-Innovation Center for Sustainable Forestry in Southern China, Nanjing Forestry University, Nanjing, China, [3]School of Engineering and Architecture, Jiangsu Open University, Nanjing, China, [4]College of Landscape Architecture, Nanjing Forestry University, Nanjing, China

Light is an important ecological factor that affects plant growth, survival and distribution. *Carpinus betulus* L. is native to central Europe and is used as an ornamental plant with strong adaptability. It is an important tree species for landscaping and timber use. What's more, the antioxidant- and anticancer-related properties of *C. betulus* leaf extracts are remarkable, that make it a possible raw material for medicine. Light intensity is an important environmental factor affecting the growth and physicochemical changes of *C. betulus*, but the mechanism of its effect on this species still remains unknown. In this study, the growth, photosynthetic characteristics, endogenous hormones and antioxidant activity responses of *C. betulus* seedlings to four light intensity gradients (T0: normal light; T1: 75%; T2: 50%; T3: 25% of normal light) were studied after 60 days of shading treatments. The results showed a significant effect of low light intensity on the values of the growth and physiological parameters of *C. betulus*. The low light intensity caused the inhibition of plant biomass accumulation and the degradation of photosynthetic capacity and stomatal behavior and aggravated the cell membrane lipid peroxidation. However, the plant height growth, leaf area, specific leaf area, photosynthetic pigment content, and contents of GA_3 and ABA of *C. betulus* increased with decreasing light intensity. We found that *C. betulus* can tolerate mild (T1) and moderate (T2) shading stress by developing photoprotective mechanisms and maintaining relatively high concentrations of organic osmolytes and high antioxidant enzyme activities (superoxide dismutase, peroxidase, catalase and ascorbate peroxidase), but the ability of *C. betulus* to synthesize osmotic substances and enzymatic antioxidants was impaired under severe shading conditions (T3). Our results suggest that *C. betulus* can make effective use of low light resources by adjusting its morphology, material distribution, photosynthetic rate and antioxidant enzyme system in suitable low-light environments (50%~75% of normal

light); however, light intensity levels that are too low (25% of normal light) will have adverse effects on plant growth. The results of this study provide not only new insights into the response mechanisms of *C. betulus* to light intensity but also a scientific basis for the cultivation and application of *C. betulus* in China.

KEYWORDS

***Carpinus betulus*, light intensity, morphological indexes, physiology, photosynthetic responses, endogenous hormones, antioxidant activity**

Introduction

Light is the material basis with which all plants in nature carry out various life-sustaining activities (Kami et al., 2010). Light is a primary determinant of the geographical distribution and growth of plants through light intensity, light quality, photoperiod and other factors (Jason et al., 2018). As one of these important factors, light intensity has an important impact on plant growth, morphology, physiological metabolism, signal transduction and photosynthetic physiology (Fan et al., 2013; Lu et al., 2018). The relationship between plants and the light environment has always been a hot topic in ecology.

When the light intensity in the environment changes, the growth state of plants will inevitably change to a certain extent, and this change is mainly caused by the influence of the active light capture ability of the plant and the ability to synthesize photosynthates (Chen et al., 2014). Studies have found that in a weak light environment, the leaf area, total biomass, specific leaf area, and leaf area ratio of plants will increase, thus making leaves larger and thinner, increasing the area of light interception, improving the utilization efficiency of limited light resources, increasing stomatal conductance, and maintaining a high photosynthetic rate to ensure normal plant functions in low-light environments (Guo et al., 2019; Pan et al., 2020). Moreover, the absorption and utilization of light energy can be enhanced in plants growing in low-light conditions through increases in chlorophyll content, apparent quantum efficiency, actual photochemical quantum yield of PSII (Φ_{PSII}) and electron transfer rate (ETR) (Guenni et al., 2018; Shi et al., 2018) and reductions in energy waste by reducing the light compensation point, dark respiration rate, photorespiration rate and heat dissipation ratio (Cai et al., 2017; Ghorbanzadeh et al., 2020). However, in a strong light environment, plants can reduce the capture of excess light and the damage caused to plants by increasing leaf thickness, reducing leaf area, reducing chlorophyll content, and reducing the transpiration of leaf water by closing stomata (Mokany et al., 2006).

Through the long evolutionary process, plants have formed a series of protective mechanisms that enable them to adapt to the complex and dynamic light environment. Studies have found that when plants grow in an unsuitable light environment, osmotic regulatory substances such as soluble sugar (SS), soluble protein (SP) and proline (Pro) can maintain the balance of cell osmotic potential and reduce the damage to the cell membrane caused by osmotic stress through changes in content (Yin and Shen, 2016). Antioxidant systems also play an important role in plants coping with unfavorable light conditions, resulting in the accumulation of intracellular reactive oxygen species (ROS) when plants are exposed to environmental stress; thus, the activities of protective enzymes such as superoxide dismutase (SOD), catalase (POD) and peroxygenase (CAT) and the content of nonenzymatic antioxidants increase (Liu Y. et al., 2018; Zushi et al., 2020), and the contents of active oxygen species such as O^{-2}, H_2O_2, OH^- and malondialdehyde (MDA) decrease. These changes can reduce peroxidation damage to the cell membrane and improve the adaptability of plants to unfavorable light environments (Ellouzi et al., 2011). Plants tolerate shade stress in a variety of ways (Israeli et al., 1995; Koike, 2010; Modrzyński et al., 2015). Some studies have found that moderate shade can benefit plants not only by preventing them from being burned by light but also by allowing them to meet their light requirements for growth (Petritan et al., 2007). Therefore, it is important to study how plants tolerate shade stress to more effectively establish stable, diverse and stratified planting structures when constructing landscape gardens.

Carpinus betulus L. is a deciduous tree belonging to the Betulaceae family with beautiful foliage and golden leaves in autumn. It plays an important role in forest communities in temperate regions of Europe and Asia Minor (Sikkema et al., 2016) and has been introduced and cultivated in many places in China with good ecological adaptability (Shi et al., 2017). In landscapes, *C. betulus* is often planted in the form of street trees or hedgerows and is well-known in private and public green

areas for its autumn leaves. It is a suitable species for both ornamental and urban habitats and has been used for biological monitoring of particulate matter (Prinz and Finkeldey, 2015). Additional studies have shown that the antioxidant- and anticancer-related properties of *C. betulus* leaf extracts are exceptional (Cieckiewicz et al., 2012; Hofmann et al., 2016) and that compared to other common coniferous and deciduous trees, these extracts contain very high amounts of total phenols and phenolic acids (Kuiters and Sarink, 1986). All these results indicate that *C. betulus* leaves are a promising renewable resource for the biorefinery and utilization of its antioxidant extractives in the future for healthcare and medical products. The high ornamental and economic value of *C. betulus* makes it extremely popular globally. In recent years, *C. betulus* has been widely used in China, and its adaptability is good. Recent studies on *C. betulus* have mostly concentrated on breeding (Chalupa, 1990), seed biology (Zhu et al., 2013), heat resistance (Shi and Zhu, 2015), drought and salt tolerance (Stojnić et al., 2016; Zhou et al., 2018). At present, with the rapid development of urban construction in China, the urban shade space is becoming larger, air pollution and smog get more severe in big cities (Xue et al., 2022). It is of great significance to select the plant resources with high ornamental value and shade tolerance to carry out scientific and effective greening of the shade space and give play to the best ecological environmental benefits of green space. Light has a great influence on the growth of *C. betulus*. However, information on the response of *C. betulus* to different light intensities is scarce.

Therefore, the main objective of this study is to comprehensively assess the influence of shade stress on *C. betulus* and to determine the mechanisms of adaptation employed by this plant to tolerate low-light stress. We hypothesized that the growth, biomass accumulation and leaf gas exchange rate of *C. betulus* seedlings would decrease under the effects of light stress. We examined the growth and physicochemical changes in seedlings grown under different degrees of shading created through artificial shading treatment, explored the adaptability of *C. betulus* seedlings to different light conditions, and sought to determine the most suitable light conditions to promote the growth and development of *C. betulus* seedlings. The aim of this study was to provide scientific data and findings related to the light management of *C. betulus* and to make better use of *Carpinus* species in landscaping and industrial production.

Materials and methods

Plant materials and light treatments

The tests were carried out in the Landscape Experimental Teaching Center of Nanjing Forestry University in May, Nanjing (33° 04' N, 118° 47' E), Jiangsu Province. The area is characterized by a warm and humid subtropical monsoon climate with an annual rainfall of 1200 mm. The average annual temperature is 15.7°C, the maximum temperature is 40.7°C, and the minimum temperature is -14°C. Two-year-old *C. betulus* seedlings were obtained from Nanjing Forestry University. On April 2016, we selected well-grown seedlings with a similar mean ground diameter (0.7-0.8 cm) and seedling height (50-60 cm) and transplanted them into pots (20 cm diameter × 22 cm height). The potting soil was a soil:peat:vermiculite:pearlite (1:1:1:1, v:v:v:v, pH 6.50) mixture. The substrate was imported with an organic matter content of 75.5 g/kg, total P content of 2.80 g/kg, total N content of 73.5 g/kg, and total K content of 9.0 g/kg. The content of soil nutrients was determined by a TFW-VI soil nutrient and moisture tester (TFW-VI, Wuhan, China). The pots were then placed in a glasshouse at a temperature of 25 ± 2.0°C and relative humidity of 70 ± 5%, with standardized fertilizer and water management.

Light treatments were conducted in June 2016 outside of the greenhouse. Four types of light treatments were administered as follows: no shading net (T0, CK, 100% normal light), 25% shading net (T1, 75% normal light), 50% shading net (T2, 50% normal light) and 75% shading net (T3, 25% normal light). These four types of shading net are common in the market; the shading net was 1.8 m away from the ground to simulate natural shading, and a TES-1334A was used to determine the light intensity. Each treatment had 3 replicates with 15 plants in each replicate and one seedling per basin (i.e., 45 seedlings per treatment). All the seedlings were watered to field capacity twice a week during the summer months. Weeding was carried out when needed. After 60 days of growth, measurements were carried out, and samples were collected for various physiological analyses, with three replicates for the measured parameters. When sampling, we chose mature new leaves pointing in the same direction from the upper part of *C. betulus*. Fresh leaves were collected from plants, immediately frozen in liquid nitrogen and stored at -80°C. The leaves were used for the determination of physiological and biochemical indexes.

Plant growth measurement

Before the shading stress treatment, seedling height (H_0) and diameter (D_0) were determined from three seedlings in each group. After 60 days of treatment, the height (H_1) and diameter (D_1) were determined again. Plant height increment was calculated as $H_1 - H_0$, and ground diameter increment was calculated as $D_1 - D_0$. Fully expanded fresh leaves (the third or fourth leaf from the top of the shoots) were measured before biomass harvest using a portable leaf area meter (LI-3000C, LI-COR, Lincoln, Nebraska, USA). Then, the plants were harvested, the samples were separated into roots, stems and leaves, and the taproot length (roots were washed with distilled water, blotted dry on filter paper, measured the taproot length with a ruler) was calculated. The samples were dried at 80°C in an oven for 48 h,

and the dry weights of the samples were recorded. The specific leaf area (SLA) was calculated: SLA (cm^2/g) = leaf area (cm^2)/leaf dry weight (g). Portions of these samples were frozen in liquid nitrogen and stored at −80°C.

Scanning electron microscopy of leaf stomatal and section characteristics

The third or fourth fresh leaf from the top of *C. Betulus* seedlings was collected on the final day of the shading treatment from the three seedlings in each group. The cleaned leaves were cut into small pieces (approximately 5 × 5 mm) with a sharp blade and then placed in formalin acetic acid (FAA). After dehydration in a graded ethanol series, penetration with isoamyl acetate aldehyde, and drying in a critical point drying apparatus (K850, Emitech, London, UK), the samples were mounted on stubs and coated with gold using an ion sputtering apparatus (E1010, Hitachi, Tokyo, Japan). Then, a scanning electron microscope (SEM, Quanta 200, FEI, Hillsborough, Oregon, USA) was used to observe the blade surface and cross-section of the leaves, and images were taken using the same instrument. The stomatal density (number/mm^2) and stomatal size (length and width) were evaluated following the method reported by Camposeo et al. (2011). The number of open stomata, leaf thickness (μm) and palisade tissue thickness (μm) for each sample were measured under a photomicroscope system with a computer attachment. Stomatal aperture (μm) was measured by the following method: three complete and clear stomata in each field were randomly selected, and stomatal opening (the maximum value of pores formed between guard cells) was measured.

Leaf gas exchanges and chlorophyll fluorescence parameters

Photosynthetic parameters were determined in the third to fourth fully expanded fresh leaves of each plant from 8:00~11:00 a.m on the final day of the different light treatments using a portable photosynthetic system (Ciras-2, Shanghai, China). The parameters recorded included the net photosynthetic rate (Pn), transpiration rate (Tr), stomatal conductance (Gs), and intercellular CO_2 concentration (Ci). Chlorophyll fluorescence parameters were determined by the fluorescence leaf chamber of the Ciras-2 photosynthetic system on the same day. The potential activity of PSII (Fv/Fo), maximum photochemical efficiency of photosystem II (Fv/Fm), photochemical quantum efficiency (Φ_{PSII}), photochemical quenching parameter (qP), nonphotochemical quenching parameter (NPQ), and electron transfer rate (ETR) were measured on fully dark-adapted leaves. Three seedlings were randomly selected for each treatment, and the parameter measurements were performed on three leaves per plant.

Determination of photosynthetic pigment contents

The chlorophyll a (Chl a), chlorophyll b (Chl b), and total carotenoid (Car) contents of the fresh leaves in the different light treatments were measured with the spectrophotometric method (Porra et al., 1989). Chlorophyll from 4~5 pieces of fresh leaves was extracted with a mixture of acetone and 95% ethanol (1:1, v:v), and the absorbance of the samples was measured at wavelengths of 645 nm and 663 nm by ultraviolet-visible spectrophotometry (Lambda25, PerkinElmer, Waltham, Massachusetts, USA). Then, the photosynthetic pigment contents (mg/g) were calculated with three replicates.

Determination of lipid peroxidation

Lipid peroxidation of fresh leaves under the different light conditions was assessed by malondialdehyde (MDA) content and relative electrolytic conductivity (REC) with three replicates. The MDA content was measured following the method of Hodges et al. (1999). The relative electrolytic conductivity (REC) was determined according to the method of Dionisio-Sese and Tobita (1998).

Organic osmolytes

Three main types of organic osmolytes, including soluble sugars, soluble proteins, and proline, were analyzed. The soluble sugar content of leaves under the different light conditions was measured by the anthrone colorimetric method according to the method reported by Magné et al. (2006). The content of soluble protein was measured by Coomassie brilliant blue G-250 staining (Bradford, 1976). Proline was extracted from the leaves of *C. betulus* and determined by the method described by Abrahám et al. (2015).

Endogenous hormones

The contents of auxin (IAA), abscisic acid (ABA) and gibberellin (GA_3) in leaves of *C. betulus* under different light treatments were detected by HPLC-MS/MS by the method reported by Ma et al. (2008). The mobile phase contained 0.1% formic acid and was eluted by gradient reversed-phase HPLC. The pH was adjusted to 3.2 with methanol-modified triethylamine (TEA), and the solute was detected at a wavelength of 265 nm.

Antioxidant enzymes

0.3 g frozen leaves were ground at 4°C in a mortar in 6 mL of a pH 7.8 phosphate buffer solution. The homogenate was

centrifuged at 10,000 rpm at 4°C for 20 min. The supernatant was collected as a leaf crude enzyme extract for enzyme measurements and stored at 4°C. The activities of superoxide dismutase (SOD), peroxidase (POD), catalase (CAT) and ascorbate peroxidase (APX) were determined in the leaf enzyme extracts of *C. betulus*. SOD activity was analyzed following Beyer and Fridovich (1987). POD activity was estimated according to the method reported by Civello et al. (1995). CAT activity was measured following Díaz-Vivancos et al. (2008). APX activity was measured using the method described by Nakano and Asada (1981).

Statistical analysis

Data were analyzed by calculating the means and standard deviation (SD) using one-way ANOVA, and the means were separated with Duncan's multiple range test at the 5% probability level using SPSS statistical package version 22.0 (IBM Corp, Amonk, New York, USA). All tables and graphs were made using MS Excel 2019.

Results

Effects of light intensity on plant growth

Plant growth exhibits a certain adaptability to changes in light intensity. The *C. betulus* seedlings could maintain basically normal growth, and the survival rate was 100% throughout the study. However, there were significant differences in plant growth under different shading treatments (T1~T3), the leaf color of *C. betulus* seedlings gradually darkens compared with the CK as the degree of shading increased (Figure 1). As shown in Table 1, the plant height growth, leaf area, and SLA of *C. betulus* increased with decreasing light intensity, and those indicators were significantly higher ($P < 0.05$) in the plants grown under the shaded conditions (T1~T3) than in the control plants (T0). However, the ground diameter increment, taproot length, root biomass, stem biomass, leaf biomass, root:shoot ratio, and total biomass were inhibited by shade stress. The taproot length and total biomass of the treatment group were significantly lower than those of the control group.

Effects of light intensity on leaf stomatal and section characteristics

The effects of light intensity on leaf stomatal and section characteristics are shown in Table 2 and Figure 2. The stomatal density and opened stomata of the *C. betulus* leaves from plants grown under the T1 treatment were not significantly different from those grown under the T0 treatment. However, with increased shading (T2~T3), except for the palisade:spongy ratio and palisade tissue thickness:leaf thickness ratio, all the other morphological indicators of leaves (Table 2) decreased significantly compared with those of the control group ($P < 0.05$). In the T3 treatment, the stomatal density was 73.27% of that of the control, and the stomata length, stomata width, stomatal aperture and leaf thickness were reduced to nearly half of those of the control. Moreover, only 35.58% of the open stomata was observed in the T3 group. Although the palisade tissue thickness and spongy tissue thickness of the leaves of treated plants were reduced with decreased light intensity, their ratio increased gradually. The palisade tissue thickness:leaf thickness ratio in T1 was lower than the control, but it was significant higher than the control in T2 and T3 treatments.

The stomatal size, the palisade and parenchyma tissues in the leaves of *C. betulus* seedlings had different degrees of change under various levels of light intensity. The stomatal density and degree of stomatal opening decreased with decreasing light intensity, and the stomata were nearly closed in the T3 treatment (Figures 2A, B). Figure 3C shows a typical scanning electron micrograph of the cross-section of *C. betulus* leaves under the different shading treatments, including the upper and lower epidermis and palisade and spongy tissues. The palisade tissue of *C. betulus* was elongated and arranged in an orderly manner in the control (Figure 3C, T0). However, in the T1~T3 treatments, the leaf thickness decreased, the

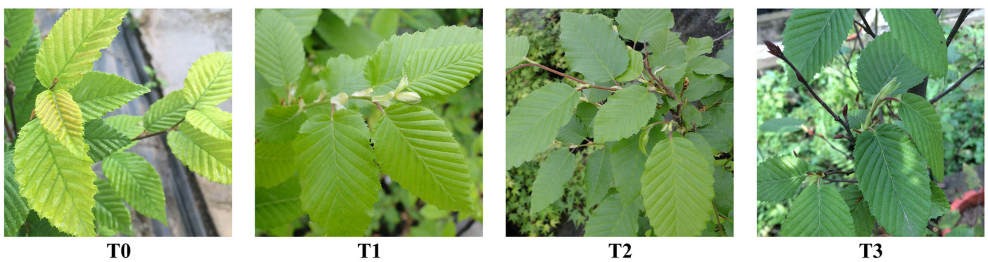

FIGURE 1
The growth of the leaves of *C. betulus* seedlings under different light intensity (T0~T3) after 60 days.

TABLE 1 Effects of various light intensities on plant height increment (cm), ground diameter increment (cm), taproot length (cm), leaf area (cm^2), specific leaf area (SLA, cm^2/g), roots, stems and leaf biomass (g), root:shoot ratio (R:S) and total biomass (g) after 60 days of treatment.

Treatment	Plant height increment (cm)	Ground diameter increment (cm)	Taproot length (cm)	Leaf area (cm^2)	Specific leaf area (SLA, cm^2/g)
T0	5.26 ± 0.32d	0.16 ± 0.011a	20.86 ± 1.82a	12.58 ± 1.67c	299.52 ± 8.16d
T1	6.52 ± 0.58c	0.12 ± 0.019ab	18.15 ± 1.25b	13.98 ± 1.26b	367.89 ± 12.08c
T2	7.82 ± 1.48b	0.10 ± 0.012b	16.91 ± 0.83c	14.22 ± 1.58ab	406.28 ± 15.15b
T3	8.54 ± 1.76a	0.08 ± 0.008c	14.45 ± 1.06d	14.98 ± 1.42a	447.27 ± 16.32a
Treatment	**Root biomass (g)**	**Stem biomass (g)**	**Leaf biomass (g)**	**Root:shoot ratio (R:S)**	**Total biomass (g)**
T0	4.25 ± 0.24a	3.38 ± 0.18a	3.46 ± 0.17a	0.62 ± 0.021a	11.09 ± 0.32a
T1	3.73 ± 0.32ab	3.06 ± 0.21ab	3.15 ± 0.21ab	0.60 ± 0.015ab	9.94 ± 0.45b
T2	3.32 ± 0.19bc	2.89 ± 0.15b	2.87 ± 0.25b	0.58 ± 0.018b	9.08 ± 0.22bc
T3	2.92 ± 0.12c	2.58 ± 0.13c	2.63 ± 0.16c	0.56 ± 0.017b	8.13 ± 0.13c

Data in the table are the means ± SDs (n = 3); different lowercase letters in each column indicate significant differences among treatments ($P < 0.05$).

palisade and spongy parenchyma tissues gradually became loosely arranged, and the spaces between these tissues became larger.

Effects of light intensity on photosynthetic parameters and chlorophyll fluorescence parameters

As shown in Figures 3A–D, Pn first increased and then decreased with increasing shading. There was no significant difference between T1 and CK of Pn, while under the T2 and T3 treatments, Pn decreased significantly ($P < 0.05$). The changes in Gs and Tr were consistent and decreased with increasing shading degree. In the treatment with minimal shading (T1), there was no significant difference between the two groups, but under the T3 treatment, Gs and Tr decreased by 44.08% and 49.12%, respectively, compared with the control. However, Ci increased with increasing shading degree, and the Ci of the T3 treatment group was significantly higher than that of the control group ($P < 0.05$). In conclusion, the treatment with minimal shading (T1) had little effect on the photosynthetic capacity of *C. betulus* seedlings, but under the moderate and severe shading treatments (T2 and T3), the photosynthetic capacity of *C. betulus* seedlings was adversely affected.

Light intensity had different degrees of influence on the chlorophyll fluorescence parameters of *C. betulus* leaves (Figures 4A–F). The potential activity of PSII (Fv/Fo) and the maximum photochemical quantum yield of PSII (Fv/Fm) showed similar trends, decreasing with increasing shading degree, and were significantly different from the control under the severe shading treatment (T3). However, the changes in the actual photochemical quantum yield of PSII (Φ_{PSII}), photochemical quenching coefficient (qP), nonphotochemical quenching coefficient (NPQ) and electron

TABLE 2 The main effects of light intensity on leaf stomata and leaf section characteristics of *C. betulus*.

Treatment	Stomatal density (number/mm^2)	Stomatal length (μm)	Stomatal width (μm)	Stomatal aperture (μm)	Open stomata (%)
T0	245.69 ± 23.46a	16.28 ± 2.24a	10.82 ± 1.33a	2.28 ± 0.31a	98.25 ± 6.08a
T1	238.58 ± 21.12ab	12.53 ± 1.48b	9.02 ± 1.58b	1.92 ± 0.27b	90.36 ± 4.64ab
T2	215.46 ± 18.28b	10.65 ± 1.82bc	7.35 ± 1.66c	1.70 ± 0.23bc	75.85 ± 5.86b
T3	180.01 ± 16.53c	8.07 ± 1.56c	4.56 ± 1.02d	1.31 ± 0.12c	35.58 ± 3.62c
Treatment	**Leaf thickness (μm)**	**Palisade tissue thickness (μm)**	**Spongy tissue thickness (μm)**	**Palisade/spongy (%)**	**Palisade tissue thickness/leaf thickness (%)**
T0	86.21 ± 4.88a	20.69 ± 2.32a	27.58 ± 3.06a	75.02 ± 3.06c	24.00 ± 3.68c
T1	77.58 ± 7.54b	17.24 ± 2.54b	20.69 ± 2.68b	83.33 ± 2.82b	22.22 ± 2.84d
T2	60.34 ± 5.72c	15.51 ± 1.68c	17.35 ± 1.50c	89.39 ± 3.52b	25.70 ± 2.55b
T3	44.83 ± 6.68d	14.10 ± 1.22c	14.82 ± 1.69d	95.14 ± 4.03a	31.45 ± 3.26a

The data in the table are the means ± SDs (n=3); different lowercase letters in each column indicate significant differences between treatments ($P < 0.05$). The parameters measured included stomatal density (number/mm^2), stomatal length (μm), stomatal width (μm), stomatal aperture (μm), open stomata (%), leaf thickness (μm), palisade tissue thickness (μm), spongy tissue thickness (μm), palisade tissue thickness/spongy tissue thickness (%) and palisade tissue thickness/leaf thickness (%).

10.3389/fpls.2022.1055984

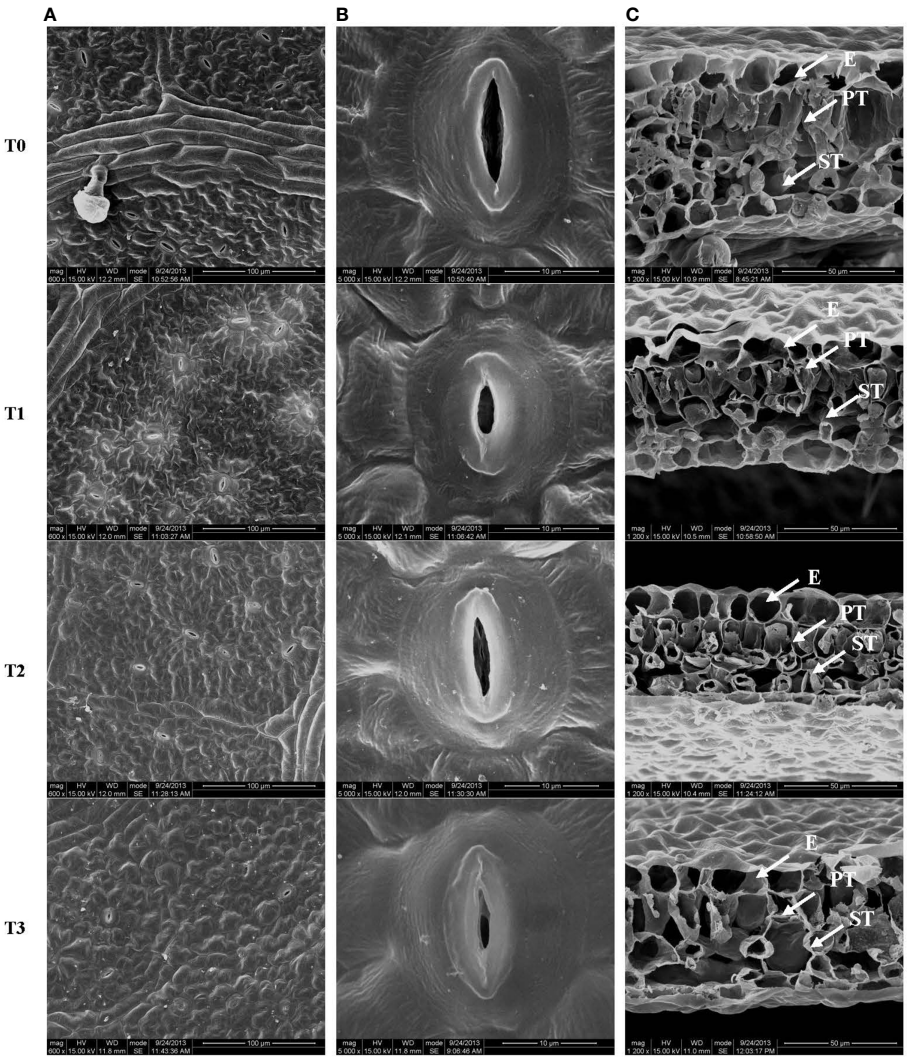

FIGURE 2
Stomatal structure on the leaf surface **(A, B)** and leaf cross-section **(C)** from *C. betulus* leaves under different light intensity treatments (T0~T3). E, epidermis; PT, palisade tissue; ST, spongy tissue. Scale: 100 μm **(A)**, 10 μm **(B)**, 50 μm **(C)**.

transport rate (ETR) were different from those of other indexes, which first increased and then decreased with increasing shading degree. Among these parameters, Φ_{PSII}, qP and ETR were significantly higher in the T2 treatment than in the control, and NPQ was significantly higher in the T1 treatment than in the control ($P < 0.05$). In the T3 treatment, qP and NPQ were 17.59% and 52.94% lower, respectively, than in the control.

Effects of light intensity on photosynthetic pigment contents

As shown in Table 3, shading had a significant impact on the contents of photosynthetic pigments in the leaves of *C. betulus*. The contents of chlorophyll a, b and total chlorophyll increased significantly compared with the CK ($P < 0.05$), as the degree of shading increased. The total chlorophyll content in the T1, T2 and T3 treatments was 1.22, 1.41 and 1.91 times that in the control (T0), respectively. These results indicated that the light capture ability of *C. betulus* seedlings under low light could be improved by increasing the chlorophyll content, thus improving the utilization efficiency of light energy. In contrast, the chlorophyll a/b value decreased with increasing shading degree, and the difference between each shade treatment and the control reached a significant level ($P < 0.05$), indicating that the increase in chlorophyll b content was greater than that in chlorophyll a content. The carotenoid content also increased as the degree of shading increased, and the difference with T0 was significant ($P < 0.05$).

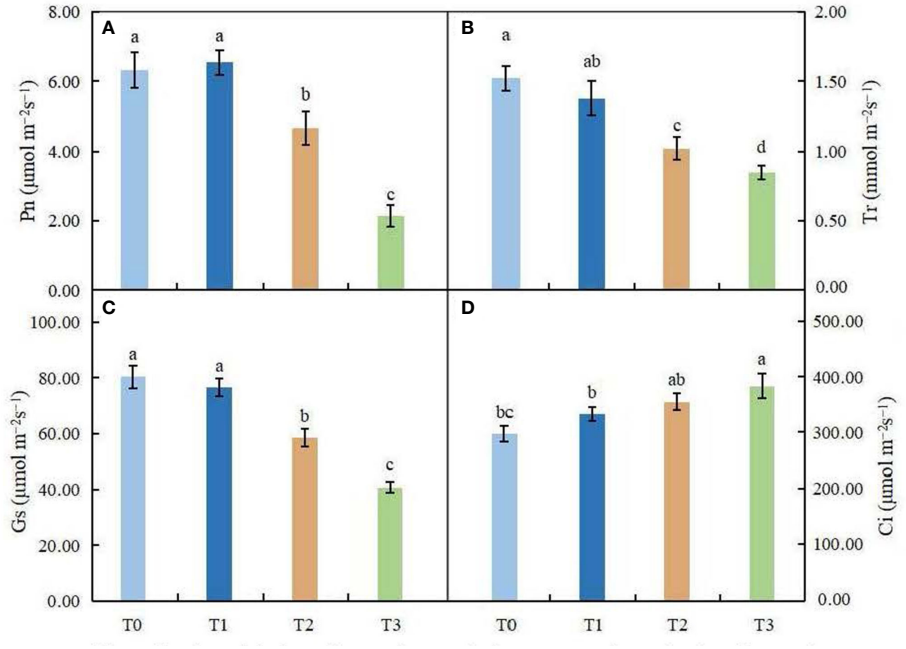

FIGURE 3
Effects of various light intensities on photosynthesis parameters in *C. betulus* after 60 days. *Pn*, net photosynthetic rate **(A)**; *Tr*, transpiration rate **(B)**; *Gs*, stomatal conductance **(C)**; *Ci*, intercellular CO_2 concentration **(D)**. Different lowercase letters indicate significant differences between treatments ($P < 0.05$), n = 3.

Effects of light intensity on lipid peroxidation

The changes in MDA content and relative electrical conductivity (REC) in leaves of *C. betulus* are shown in Figures 5A, B. With the decrease in light intensity, MDA content and REC showed a gradually increasing trend. ANOVA showed that MDA content in leaves was significantly different among different treatments ($P < 0.05$), indicating that shading affected MDA accumulation in leaves of *C. betulus*. The REC under the T1 treatment was not significantly different from that under the control, but in the T2 and T3 treatments, it was significantly higher than that of the control ($P < 0.05$).

Effects of light intensity on organic osmolytes

The soluble sugar content did not change significantly in leaves under the T1 and T2 treatments, but in the high shading treatment (T3), it was significantly lower than that in the control (Figure 6A). Compared with the control, the soluble protein content was significantly affected by different shading treatments ($P < 0.05$). In the T1 treatment, the content of soluble proteins was higher than that in the control, and a great reduction in protein content was found in the T2 and T3 treatments (Figure 6B). We observed that the proline content increased obviously in leaves under the T1~T2 treatments; however, the proline content was significantly lower in the high shading treatment (T3) than in the control group (Figure 6C).

Effects of light intensity on endogenous hormones

The contents of endogenous hormones in leaves of *C. betulus* under different light treatments were significantly different from those in the control ($P < 0.05$, Figures 6D–F). The content of IAA decreased with decreasing light intensity and reached the minimum value (50.52 $ng \cdot g^{-1}$) in the T3 treatment, with a value that was 41.16% lower than that in the control. However, the contents of GA_3 and ABA increased gradually with decreasing light intensity under different light conditions and reached their maximum values in the T3 treatment.

Effects of light intensity on antioxidant enzyme activities

The effect of light intensity on antioxidant enzyme activities in leaves of *C. betulus* is shown in Figures 7A-D. ANOVA results indicated that the antioxidant enzyme activities were

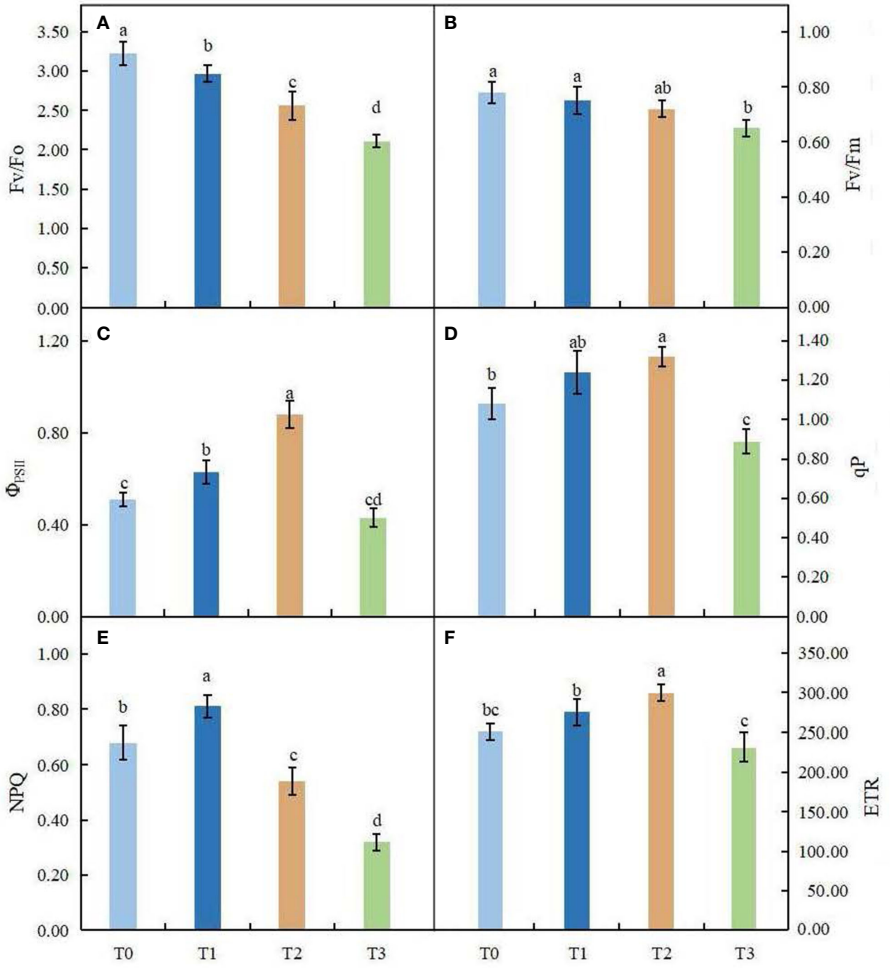

FIGURE 4
Effects of various light intensity on chlorophyll fluorescence parameters in *C. betulus* after 60 days. Fv/Fo, potential activity of PSII **(A)**; *Fv/Fm*, maximum quantum yield of photosystem II **(B)**; Φ_{PSII}, photochemical quantum efficiency **(C)**; qP, photochemical quenching parameter **(D)**; NPQ, nonphotochemical quenching parameter **(E)**; ETR, electron transfer rate **(F)**. Different lowercase letters indicate significant differences between treatments ($P < 0.05$), n = 3.

significantly different between the different treatments and the control ($P < 0.05$). The SOD, POD and CAT activities of *C. betulus* leaves increased in the T1 and T2 treatments, reached a maximum value in the T2 treatment, and then decreased in the T3 treatment. The shading treatments caused a significant increase in the activity of APX after 60 days, and the maximum value (388.58 $U \cdot g^{-1}$ min^{-1}) was found in the T1 treatment. Although the activity of APX decreased under the T2 and T3 treatments, it was still significantly higher than that in the control, by 29.37% and 14.41%, respectively.

TABLE 3 The main effects of light intensity on chlorophyll a content, chlorophyll b content, total chlorophyll content, chlorophyll a/b and carotenoid content of *C. betulus*.

Treatment	Chl a content (mg/g)	Chl b content (mg/g)	Total chlorophyll content (mg/g)	Chlorophyll a/b	Car content (mg/g)
T0	2.52 ± 0.18c	0.61 ± 0.04c	3.13 ± 0.32d	4.13 ± 0.68a	0.65 ± 0.06c
T1	3.04 ± 0.11b	0.78 ± 0.03b	3.82 ± 0.25c	3.89 ± 0.56b	0.98 ± 0.08b
T2	3.38 ± 0.22b	1.02 ± 0.05ab	4.40 ± 0.84b	3.31 ± 0.72c	1.25 ± 0.15ab
T3	4.54 ± 0.34a	1.25 ± 0.12a	5.99 ± 0.96a	3.13 ± 0.34c	1.48 ± 0.12a

The data in the table are the means ± SDs (n = 3); different lowercase letters in each column indicate significant differences between treatments (P < 0.05).

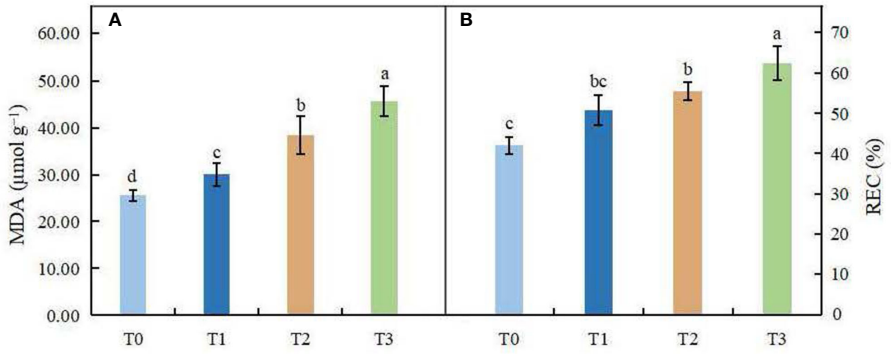

FIGURE 5
Effects of various light intensity levels on MDA content **(A)** and relative electrolytic conductivity (REC, **B**) in *C. betulus* after 60 days. Different lowercase letters indicate significant differences between treatments ($P < 0.05$), n = 3.

Discussion

Light intensity is an important environmental factor that is closely related to plant growth and development. When the external light environment changes, the growth, biomass and material distribution of plants will be affected to a certain extent. Under normal circumstances, the biomass and relative growth rate of plants will become lower in low-light environments (Pik et al., 2020). To adapt to shaded environments, plants usually undergo growth and morphological adjustments, a process called morphological plasticity, to adapt to the complex light environment. Some studies have shown that when plants are exposed to shade stress, they tend to have a decreasing base diameter and increasing plant height; that is, they show the characteristics of being 'slender'. This may be because to obtain the maximum amount of light, the plant reduces the carbon used for basal diameter growth and allocates more assimilated carbon to vertical plant growth to capture more light energy (Liu C. et al., 2018). It was found in this study that with the decrease in light intensity, the plant height growth increased, but the ground diameter increment, taproot length, root, stem, leaf and total biomass decreased continuously. These results indicated that shading had a great effect on the growth of *C. betulus*, and the lower the light intensity was, the more restricted the growth. Biomass allocation patterns and their changes in aboveground and belowground parts are important representations of tree adaptation strategies to the environment (Guenni et al., 2018). Usually, when restricted by light conditions, trees allocate more resources to aboveground plant parts (Xue et al., 2022). By reducing the allocation of resources to root biomass and increasing the allocation of resources to leaf and stem biomass, trees will obtain more light resources, which is conducive to improving their ability to compete for light and therefore survive (Ma et al., 2014). The study of Toledo-Aceves and Swaine (2007) showed that with the weakening of light intensity, the allocation ratio of the root biomass of pioneer tree species in tropical rainforests decreased, while the allocation ratio of aboveground biomass increased. In this study, we found that the root:shoot ratio of *C. betulus* decreased with decreasing light intensity, which supported the above view. This finding indicated that the biomass allocation of the underground plant parts gradually became lower than that of the aboveground parts with the weakening of light to improve the ability of the plant to capture light and maintain plant growth.

Since leaves are the largest organ by which plants interact with the external environment, their morphological structure is very sensitive to changes in the ecological environment; therefore, changes in morphological and physiological characteristics can best reflect the influence of the light environment on plants and the ability of plants to adapt to the light environment (Fan et al., 2013; Yao et al., 2017). Studies have shown that most plants in a weak light environment can change blade shape, such as by increasing leaf length, leaf width, leaf area, leaf number and plant height to adapt to an environment with insufficient light intensity; in bright light, plants will adapt by increasing blade thickness, secreting a waxy layer and increasing leaf area to cope with strong light inhibition (Mokany et al., 2006; Klavins and Klavins, 2020). This study found that the leaf area and SLA of *C. betulus* increased with decreasing light intensity. This result showed that when the outside light intensity weakened, in order to capture more limited energy, plant height increased and the leaf area enlarged, thus reducing the consumption of plant nutrient substances by increasing the SLA, reducing the leaf thickness within a limited scope, and expanding the leaf area. These changes allowed the plant to more efficiently capture light energy and lower the compensation to the decline in the photosynthetic rate of the photon flux density phenomenon, thus enabling survival in the weak light environment, which is consistent with the view of Moreira et al. (2009). Leaves are the

10.3389/fpls.2022.1055984

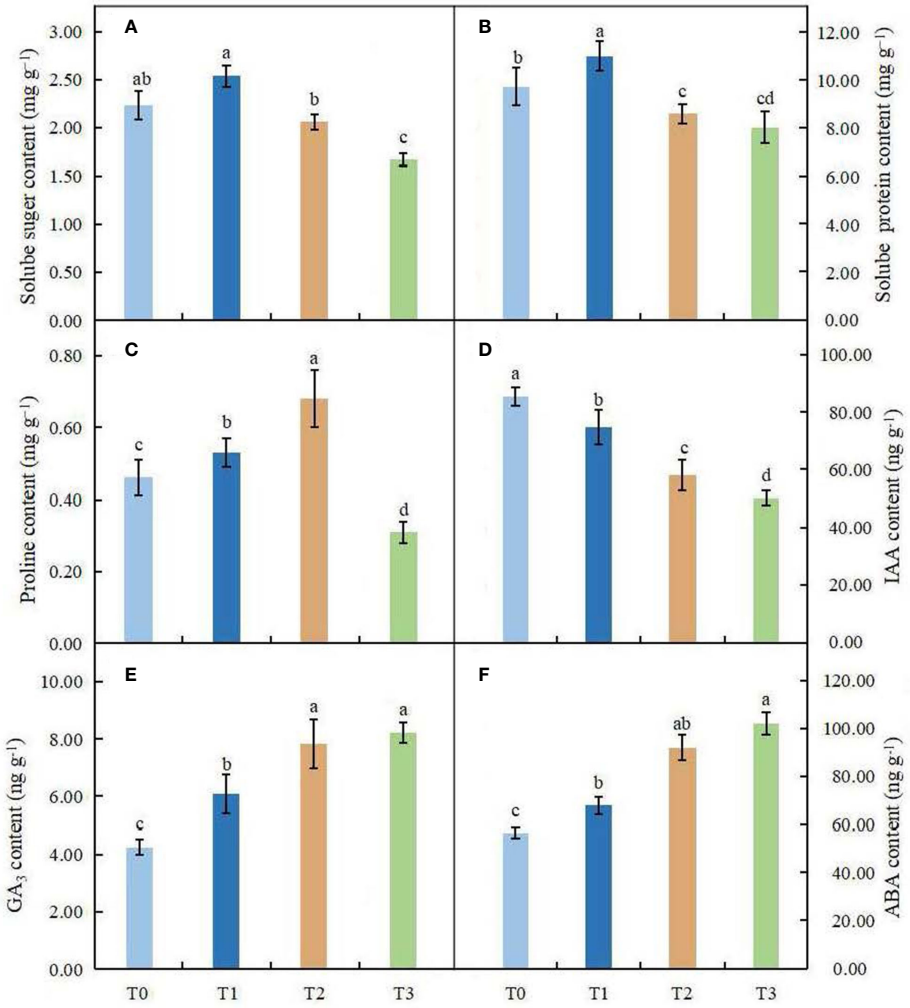

FIGURE 6
Effects of various light intensities on the soluble sugar content **(A)**, soluble protein content **(B)**, proline content **(C)**, IAA content **(D)**, GA_3 content **(E)** and ABA content **(F)** in leaves of *C. betulus* after 60 days. Different lowercase letters indicate significant differences between treatments ($P < 0.05$), n = 3.

main site of photosynthesis, and changes in the anatomical characteristics of leaves will inevitably affect the photosynthetic efficiency of plants (Jumrani and Bhatia, 2020; Knauer et al., 2020). It was found that the thinness of the upper and lower epidermis and palisade tissues, the presence of palisade tissue cells with a low aspect:axis ratio, and the loose arrangement of the spongy tissue cells could improve light transmission and chloroplast light capture ability (Barbosa et al., 2021). This conclusion was further confirmed by the anatomical observation of leaves of *C. betulus* under different light intensities; that is, with the decrease in light intensity, the leaf thickness and presence of palisade tissue and spongy tissue of *C. betulus* decreased significantly, and the arrangement of cells in the spongy tissue gradually loosened, gradually increasing the gap between cells. This finding suggested that plants can adapt to different light environments by adjusting their leaf structures. The plasticity of plant leaf anatomical characteristics in response to changes in the light environment has been widely studied and has been confirmed in *Corylus avellana* (Catoni et al., 2015), *Sesleria nitida* (Puglielli et al., 2015) and other plants, and the patterns are basically consistent across species.

Photosynthesis by plants is a physiological process that is sensitive to environmental factors, and light intensity is one of the main factors affecting photosynthesis. Chlorophyll content, chlorophyll fluorescence parameters and photosynthetic parameters are important indexes for measuring the strength of plant photosynthesis (Dai et al., 2009; Zhang et al., 2017). Although different plants have different characteristics in response to changes in the light environment, under adversity and stress, plants will develop in the direction that is conducive to photosynthesis

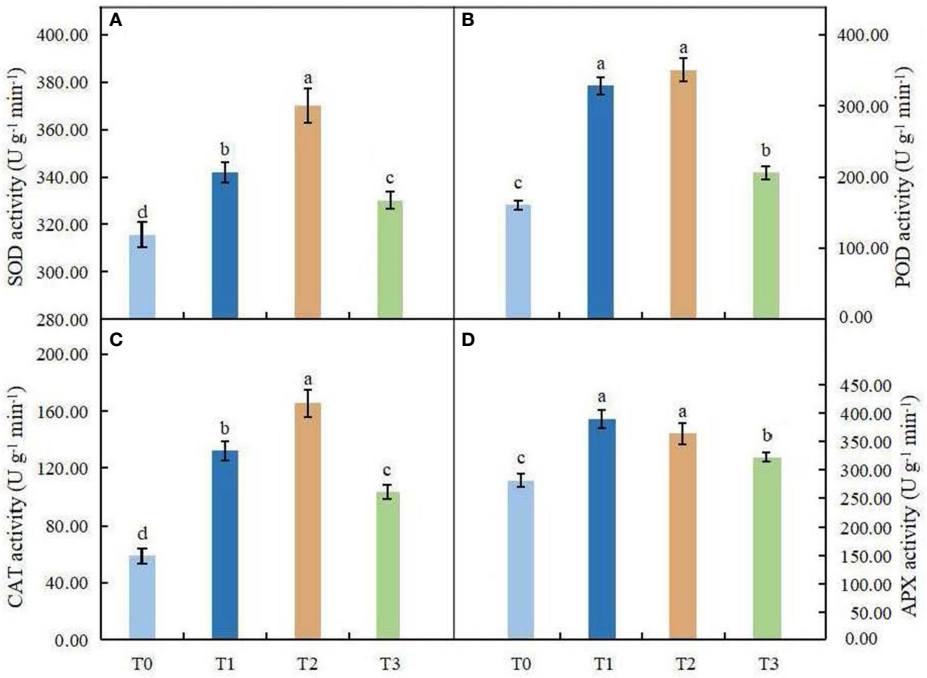

FIGURE 7
Effects of various light intensities on SOD activity **(A)**, POD activity **(B)**, CAT activity **(C)**, and APX activity **(D)** in leaves of *C. betulus* after 60 days. Different lowercase letters indicate significant differences between treatments ($P < 0.05$), n = 3.

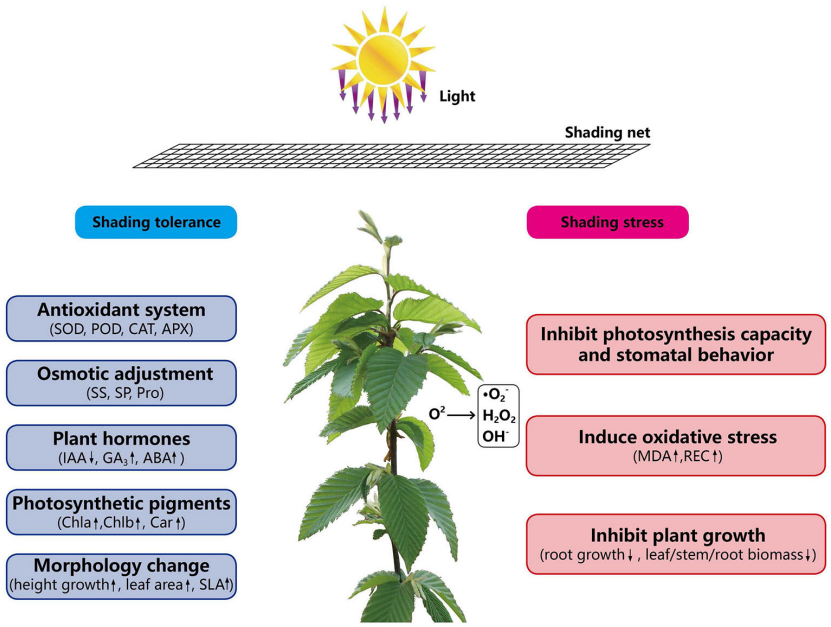

FIGURE 8
The mechanism of shading response of *C. betulus* seedlings.

(Jutamanee and Rungwattana, 2017). In general, the decrease in the photosynthetic rate among plants under stress is mainly caused by stomatal limitation and nonstomatal limitation (Rezai et al., 2018). Stomatal limitation is due to the decrease in stomatal conductance, and CO_2 from the external environment is restricted from entering the plant through the leaf stomata, which leads to a decrease in the photosynthetic rate. However, the reduction in the photosynthetic rate caused by nonstomatal limitation is mainly caused by the reduction in photosynthesis-related enzyme activities and the damage to photosynthetic organs caused by stress, and intercellular carbon dioxide may still be maintained at a high level at this time. Ci is an important basis for judging whether stomatal factors cause changes in the photosynthetic rate (Takeda and Maruta, 2008). Ci is positively correlated with Pn, Tr and Gs, indicating that the decline in photosynthesis is caused by stomatal factors hindering CO_2 utilization; otherwise, it is caused by nonstomatal factors. The results of this study showed that with the decrease in shading, the trend of Pn in *C. betulus* was basically consistent with that of Gs and Tr, which showed overall decreasing trends, and the lowest value was reached at 25% light intensity. However, the content of Ci was negatively correlated with the Pn, Tr and Gs, which indicated that photosynthesis in *C. betulus* was affected by nonstomatal factors, and the decrease in the leaf photosynthetic rate was caused by the restriction of Rubp carboxylation and photochemistry. A similar phenomenon has been observed in *Asarum forbesii* (Lu et al., 2022) and *Emmenopterys henryi* (Li et al., 2020). This further indicated that when the light intensity was too low, the plants had a light deficit and could not obtain the necessary light energy for life-sustaining activities, resulting in the lowest photosynthetic rate.

Chlorophyll fluorescence, part of the photosynthetic process, mainly reflects the efficiency of light absorption, transmission and utilization by plants and is commonly used to characterize the level of photosynthetic efficiency of plants (Genty et al., 1989; Pashkovskiy et al., 2018). Fv/Fm is an indicator of the photoconversion efficiency of PSII, while Fv/Fo indicates the potential activity of the PSII photoreaction center. The higher the Fv/Fm and Fv/Fo are, the higher the photoconversion efficiency of PSII (Zhang, 1999). Baker (2013) found that the Fv/Fm of plants is generally 0.75~0.85 under normal conditions. In this experiment, the Fv/Fm and Fv/Fo in the treatment groups were lower than those in the control group with the increase of shading degree ($P < 0.05$), indicating that the open proportion of the PSII reaction center in *C. betulus* under the shading treatment decreased and the light energy utilization efficiency was reduced. NPQ reflects nonphotochemically dissipated energy, which is one of the photoprotective mechanisms of plants (Heraud and Beardall, 2000). In this experiment, Φ_{PSII}, qP, ETR and NPQ of *C. betulus* leaves increased first and then decreased with increasing shading degree, and under the severe shading treatment (T3), Φ_{PSII}, qP, ETR and NPQ were significantly lower than those under the other shading treatment groups, indicating that the photosynthetic apparatus of *C. betulus* leaves may be partially inactivated or damaged under severe shading conditions. The primary photochemical activity of PSII decreased, the photosynthetic electron transport rate was inhibited, the proportion of heat energy dissipation in the absorbed light energy increased, and the utilization efficiency of absorbed light energy of PSII decreased, resulting in a decrease in the photosynthetic rate. These results indicated that *C. betulus* had a certain adaptability to low light, but this ability was limited. Light intensity that is too low reduces the photosynthetic efficiency of plants and affects the normal growth of plants.

Chlorophyll has the function of absorbing and transferring light photons and is an important component in the maintenance of normal photosynthesis of plants. Its content is closely related to the site conditions of plant growth and the characteristics of plants (Agathokleous et al., 2020). Chl a and Chl b are the main photosynthetic pigments, and carotenoids can absorb light energy and transfer it to chlorophyll to assist plants in photosynthesis (Liu et al., 2014). The content and proportion of these pigments are important indicators for plants to cope with environmental stress (Chai et al., 2018). In this study, the contents of Chl a, Chl b, Chl (a +b) and carotenoids in *C. betulus* increased gradually compared with the CK with decreasing light intensity, which indicated that low light intensity may beneficial to the synthesis of chlorophyll and carotenoid, and made the treatment groups show greener leaf color than the control (Figure 1). *C. betulus* seedlings could improve the efficiency with which it captured light radiation by increasing the chlorophyll content in low-light environments, thus adapting to different low-light environments. The chlorophyll a/b value is one of the important indexes to measure the shade tolerance of plants, and plants can adapt to shading by reducing chlorophyll a/b (Dai et al., 2009). Some studies have suggested that the chlorophyll a/b value of shade plants is below 3.0 (Lichtenthaler et al., 1981; Hoflacher and Bauer, 1982). The Chl a/b of *C. betulus* was positively correlated with light intensity, decreasing with the decrease in light intensity, and the Chl a/b values were all higher than 3.0, indicating that *C. betulus* is a typical plant with high requirements for light intensity in the growing environment.

Osmotic regulatory substances play an important role in plant resistance to abiotic stress. When reactive oxygen species are produced rather than antioxidants, the cytoplasmic membrane can perform substantial membrane lipid peroxidation; at this time, the permeability of the plant cell membrane will increase, leading to cytoplasmic extravasation and physiological and metabolic plant disorders (Ramanjulu and Bartels, 2002). Then, the plants will reduce the cell water loss caused by stress by adjusting the contents of osmotic regulatory substances such as SS, SP and Pro to maintain the balance of cell osmotic pressure and thus reduce the degree of damage caused by stress (Hamouda et al., 2015). SS and SP are not only important nutrients but also participate in the osmoregulation process of plant cells, and SS can also remove ROS in vacuoles and chloroplasts and indirectly activate the antioxidant enzyme system (Van and Valluru, 2009). Pro has been shown to be an

effective free radical scavenger that plays an important role in stabilizing protoplasmic colloids and cell metabolic processes and maintaining osmoregulatory balance (Mutava et al., 2015). This study found that the contents of SS and SP in *C. betulus* leaves first increased and then decreased with decreasing light intensity, suggesting that under mild shade stress, *C. betulus* can remove ROS from vacuoles and chloroplasts by increasing SS and SP contents and maintain turgor pressure by osmotic regulation through the synergistic effect of carbon and nitrogen metabolism pathways. However, under moderate and severe shading stress, the SS and SP contents gradually decreased to their lowest levels in the T3 treatment, which may be due to the lack of light. The rate of photosynthesis in the leaves decreased sharply, and the synthesis of SS and SP was blocked; these effects will lead to a shortage of nutrients in plants, causing adverse effects on growth. The Pro content in *C. betulus* increased under mild and moderate levels of shade (i.e., the T1 and T2 treatments) but decreased significantly under heavy shade conditions (the T3 treatment), suggesting that the Pro content of *C. betulus* can still be maintained at a relatively high content under appropriate shading conditions, scavenging free radicals in plant cells and counteracting the effect of light intensity factors on cell osmoregulation, while its synthesis is blocked in extremely low light, thus limiting the effect of osmoregulation.

ROS are one-electron reduction products of a class of oxygen, which are important signal transduction substances in plants (Kaushik and Aryadeep, 2014). A study found that when plants suffer adversity stress, on the one hand, ROS material will stimulate plants to produce a series of physiological and biochemical reactions and resistance to environmental stresses of the outside world; on the other hand, when the generation and removal of ROS in plant cells are in an unbalanced state, membrane lipid peroxidation will occur in the cell membrane, and protein oxidation will cause damage to the cell membrane, resulting in the imbalance of normal physiological metabolism of plants and even leading to the death of plants (Pareek et al., 2017). MDA is the final product of membrane lipid peroxidation and one of the important signs of membrane system damage (Sofo et al., 2004). This study found that the MDA content and relative conductivity of *C. betulus* leaves increased with decreasing light intensity, which was the lowest under natural light intensity and the highest under the T3 condition. These results indicated that shading caused low-light stress in *C. betulus*, which led to damage to membrane function or membrane structure, an increase in membrane permeability, and serious membrane lipid peroxidation, and the same phenomenon was also found in *Quercus wutaishanica* (Zhang et al., 2021). SOD, POD and CAT are important antioxidant enzymes (Zhao et al., 2019). When plants are under environmental stress, ROS can induce their activity to increase and remove the accumulated $O^{\cdot-2}$ and H_2O_2 in the cells, thus playing a protective role for plant cells (Koca et al., 2006). SOD first converts $O^{\cdot-2}$ into H_2O_2 and O_2 and then dissociates the generated H_2O_2 and endogenous H_2O_2 to stimulate POD and CAT activities, and the three synergistic processes eliminate excessive reactive oxygen species in plants (Neto et al., 2006). Studies have found that shading, drought, salinity and other stresses can induce the activities of SOD, POD, CAT and other antioxidant enzymes and increase the ability of plants to remove reactive oxygen species, but this process is species-specific and varies with different stress types (Favaretto et al., 2011; Bharuth et al., 2020; Liu et al., 2022). This study found that the activities of SOD, POD, CAT and APX in leaves of *C. betulus* first increased and then decreased with increasing shading intensity, but the activities of protective enzymes were higher than those of the control under different shading conditions. This indicated that under a low-light environment, *C. betulus* can regulate the activity of protective enzymes in the body to remove the $O^{\cdot-2}$ and H_2O_2 produced by shading stress. However, under severe shading conditions, the metabolic balance in plants was disrupted, and the enzyme activity and free radical scavenging function were irreversibly decreased, resulting in severe membrane lipid peroxidation in *C. betulus*. With the decrease in light intensity, the protective enzyme activities of *C. betulus* showed the same trend, indicating that there was an obvious synergistic effect of antioxidant enzymes *in vivo*.

Auxin (IAA), gibberellin (GA_3) and abscisic acid (ABA) are important endogenous hormones in plants. Studies have shown that light is not only an important environmental factor for plant photosynthesis but can also regulate plant growth and development through endogenous hormones by using genes related to photoreceptor signaling (Jiang et al., 2021). Cui et al. (2014) found that shading decreased the contents of IAA and GA_3 and increased the contents of ABA in the leaves of summer maize. In this study, the content of IAA decreased with decreasing light intensity, but the contents of GA_3 and ABA showed the opposite trend, which differed from the above research results. ABA mainly inhibits cell division and elongation and inhibits the growth of roots, stems, leaves and other organs (Khorshidi and Nojavan, 2006). The ABA content in leaves of *C. betulus* increased under shaded conditions, which strengthened the inhibitory effect of shading on leaf growth. GA_3 can promote leaf growth and maintain leaf function, and an increase in GA_3 content can promote the growth of leaves (Ulger et al., 2004). GA_3 would also promote the seedling height, the increase of plant height increment in low light conditions may be due to the increase of GA_3 content. What's more, studies have also shown that GA_3 in leaves can inhibit chlorophyll decomposition, and the two have a synergistic effect (Li et al., 2010), that may be the reason of why chlorophyll content in *C. betulus* increased as the degree of shading increased. Therefore, on the one hand, low light intensity increased GA_3 and maintained leaf development. On the other hand, reducing the IAA content and increasing the ABA content resulted in leaf thinning and reduced dry matter accumulation. Therefore, the

synergistic effect of different endogenous hormones promoted the elongation and broadening of leaves and increased the leaf area of *C. betulus* under low light conditions.

Shade tolerance is determined by genetic characteristics of plants and many biological and abiotic factors. In this study, the morphological, physiological and ecological response of *C. betulus* seedlings under different light intensities were studied (Figure 8). In the future, further studies can be conducted from the perspective of proteins and molecules levels to comprehensively analyze the mechanism of shade tolerance in plants.

Conclusions

This study presents new information on the growth and ecophysiological responses of *C. betulus* seedlings to different light intensities. *C. betulus* was affected by shading stress through the inhibition of plant biomass accumulation, photosynthetic capacity and stomatal behavior, and increas ing MDA content and relative electrolytic conductivity, suggesting a limited degree of shade tolerance. Our results found that *C. betulus* seedlings can activate relevant mechanisms to adapt to low light stress, such as adjusting growth and leaf morphology, accumulating relatively high concentrations of organic solutes to maintain cellular osmotic balance and improving the activity of antioxidant enzymes as a defense against shading stress. A reduction in the growth of *C. betulus* seedlings was observed under severe shading conditions (T3). *C. betulus* seedlings can adapt to sunlight, grow best in natural light, and can tolerate certain degrees of shading, which is capable of growing under shading with 75% or 50% light transmittance. However, under heavy shading (25% light transmittance), *C. betulus* develops insufficient resistance to low-light environments and has a difficult time growing. Our study provides a better understanding of the responses of *C. betulus* to low-light stress at the physiological and biochemical levels. This ornamental tree species has the potential to be cultivated in the middle and upper layers of landscape gardens in China.

Data availability statement

The original contributions presented in the study are included in the article/supplementary material. Further inquiries can be directed to the corresponding author.

Author contributions

QZ and ZZ conceived and designed the experiments; QZ, FZ, and HZ performed the experiments and analyzed the data; and QZ wrote the paper. All authors read and approved the final paper.

Funding

This research was funded by the National Natural Science Foundation of China (31770752), the Jiangsu Science and Technology Support Program (BY2015006–01), the 333 Projects of Jiangsu Province (BRA2018065), and the Natural Science Foundation for Universities of Jiangsu Province (20KJB220006) and is a project of the 13th Five-Year Plan of Jiangsu Open University (2020-D-01).

Acknowledgments

We would like to thank Jing Yang, a laboratory specialist at the Advanced Analysis Testing Center (AATC), Nanjing Forestry University, China, for assistance with the observations of the microstructures of the plants. We express our gratitude to Feibing Wang, a research assistant at the College of Landscape Architecture, Nanjing Forestry University, China, for her help cultivating the seedlings.

Conflict of interest

The authors declare that the research was conducted in the absence of any commercial or financial relationships that could be construed as a potential conflict of interest.

The reviewer YX declared a shared affiliation with the author HZ, ZZ to the handling editor at the time of review.

Publisher's note

References

Abrahám, E., Hourton-Cabassa, C., Erdei, L., and Szabados, L. (2015). Methods for determination of proline in plants. *Methods Mol. Biol.* 639, 317–331. doi: 10.1007/978-1-60761-702-0_20

Agathokleous, E., Feng, Z., and Penuelas, J. (2020). Chlorophyll hormesis: are chlorophylls major components of stress biology in higher plants? *Sci. Total Environ.* 726, 138637. doi: 10.1016/j.scitotenv.2020.138637

Baker, N. R. (2013). Chlorophyll fluorescence:A probe of photosynthesis *in vivo*. *Annu. Rev. Plant Biol.* 59, 89–113. doi: 10.1146/annurev.arplant.59.032607.092759

Barbosa, S. M., Abreu, N., Oliveira, M., Cruz, J. N., and Gurgel, E. (2021). Effects of light intensity on the anatomical structure, secretory structures, histochemistry and essential oil composition of *Aeollanthus suaveolens* mart. ex spreng. (Lamiaceae). *Biochem. Syst. Ecol.* 95, 104224. doi: 10.1016/j.bse.2021.104224

Beyer, W. F., and Fridovich, I. (1987). Assaying for superoxide dismutase activity: Some large consequences of minor changes in conditions. *Anal. Biochem.* 161, 559–566. doi: 10.1016/0003-2697(87)90489-1

Bharuth, V., Naidoo, C., Pammenter, N. W., Lamb, J. M., and Moodley, T. (2020). Responses to chilling of recalcitrant seeds of *Ekebergia capensis* from different provenances. *S. Afr. J. Bota.* 130 (2), 8–24. doi: 10.1016/j.sajb.2019.12.001

Bradford, M. M. (1976). A rapid and sensitive method for the quantitation of microgram quantities of protein utilizing the principle of protein-dye binding. *Anal. Biochem.* 72, 248–254. doi: 10.1006/abio.1976.9999

Cai, J. G., Wei, M. Q., Zhang, Y., and Wei, Y. L. (2017). Effects of shading on photosynthetic characteristics and chlorophyll fluorescence parameters in leaves of *Hydrangea macrophylla*. *Chin. J. Plant Ecol.* 41 (5), 570–576. doi: 10.17521/cjpe.2016.0245

Camposeo, S., Palasciano, M., Vivaldi, G. A., and Godini, A. (2011). Effect of increasing climatic water deficit on some leaf and stomatal parameters of wild and cultivated almonds under Mediterranean conditions. *Sci. Hortic.* 127, 234–241. doi: 10.1016/j.scienta.2010.09.022

Catoni, R., Granata, M. U., Sartori, F., Varone, L., and Gratani, L. (2015). *Corylus avellana* responsiveness to light variations: Morphological, anatomical, and physiological leaf trait plasticity. *Photosynthetica.* 53 (1), 1–12. doi: 10.1007/s11099-015-0078-5

Chai, S., Tang, J., Mallik, A., Shi, Y., Zou, R., Li, J., et al. (2018). Eco-physiological basis of shade adaptation of *Camellia nitidissima*, a rare and endangered forest understory plant of southeast Asia. *BMC Ecol.* 18 (1), 5. doi: 10.1186/s12898-018-0159-y

Chalupa, V. (1990). Micropropagation of hornbeam (*Carpinus betulus* l.) and ash (*Fraxinus excelsior* l.). *Biol. Plant* 32, 332–338. doi: 10.1007/bf02898493

Chen, D., Fu, Y., Liu, G., and Hong, L. (2014). Low light intensity effects on the growth, photosynthetic characteristics, antioxidant capacity, yield and quality of wheat (*Triticum aestivum* l.) at different growth stages in BLSS. *Adv. Space Res.* 53 (11), 1557–1566. doi: 10.1016/j.asr.2014.02.004

Cieckiewicz, E., Angenot, L., Gras, T., Kiss, R., and Frédérich, M. (2012). Potential anticancer activity of young *Carpinus betulus* leaves. *Phytomedicine.* 19 (3-4), 278–283. doi: 10.1016/j.phymed.2011.09.072

Civello, P. M., Martinez, G. A., Chaves, A. R., and Anon, M. C. (1995). Peroxidase from strawberry fruit (*Fragaria ananassa* duch.): Partial purification and determination of some properties. *J. Agric. Food Chem.* 43, 2596–2601. doi: 10.1021/jf00058a008

Cui, H. Y., Jin, L. B., Li, B., Dong, S. T., Liu, P., Zhao, B., et al. (2014). Effects of shading on endogenous hormones regulation in kernel development of summer maize in the field. *J. Appl. Ecol.* 25 (5), 1373. doi: 10.13287/j.1001-9332.20140313.0021

Dai, Y., Shen, Z., Liu, Y., Wang, L., Hannaway, D., and Lu, H. (2009). Effects of shade treatments on the photosynthetic capacity, chlorophyll fluorescence, and chlorophyll content of *Tetrastigma hemsleyanum* diels et gilg. *Environ. Exp. Bot.* 65 (2-3), 177–182. doi: 10.1016/j.envexpbot.2008.12.008

Díaz-Vivancos, P., Clemente-Moreno, M. J., Rubio, M., Olmos, E., García, J. A., and Martínez-Gómez, P. (2008). Alteration in the chloroplastic metabolism leads to ROS accumulation in pea plants in response to plum pox virus. *J. Exp. Bot.* 59, 2147–2160. doi: 10.1093/jxb/ern082

Dionisio-Sese, M. L., and Tobita, S. (1998). Antioxidant responses of rice seedlings to salinity stress. *Plant Sci.* 135, 1–9. doi: 10.1016/s0168-9452(98)00025-9

Ellouzi, H., Ben, H. K., Cela, J., Munné-Bosch, S., and Abdelly, C. (2011). Early effects of salt stress on the physiological and oxidative status of *Cakile maritima* (halophyte) and *Arabidopsis thaliana* (glycophyte). *Physiol. Plant* 142, 12–143. doi: 10.1111/j.1399-3054.2011.01450.x

Fan, X. X., Xu, Z. G., Liu, X. Y., Tang, C. M., Wang, L. W., and Han, X. L. (2013). Effects of light intensity on the growth and leaf development of young tomato plants grown under a combination of red and blue light. *Sci. Hortic.* 153, 50–55. doi: 10.1016/j.scienta.2013.01.017

Favaretto, V. F., Martinez, C. A., Soriani, H. H., and Furriel, R. (2011). Differential responses of antioxidant enzymes in pioneer and late-successional tropical tree species grown under sun and shade conditions. *Environ. Exp. Botany.* 70 (1), 20–28. doi: 10.1016/j.envexpbot.2010.06.003

Genty, B., Briantais, J. M., and Baker, N. R. (1989). The relationship between the quantum yield of photosynthetic electron transport and quenching of chlorophyll fluorescence. *BBA-Gen. Subjects.* 990 (1), 87–92. doi: 10.1080/09670260500502521

Ghorbanzadeh, P., Aliniaeifard, S., Esmaeili, M., Mashal, M., Azadegan, B., and Seif, M. (2020). Dependency of growth, water use efficiency, chlorophyll fluorescence, and stomatal characteristics of lettuce plants to light intensity. *J. Plant Growth Regul.* 40, 2191–2207. doi: 10.1007/s00344-020-10269-z

Guenni, O., Romero, E., Guédez, Y., Lelys, B. D. G., and Pittermann, J. (2018). Influence of low light intensity on growth and biomass allocation, leaf photosynthesis and canopy radiation interception and use in two forage species of centrosema (DC.) benth. *Grass Forage Sci.* 73 (4), 967–978. doi: 10.1111/gfs.12368

Guo, Q. Q., Li, H. E., Gao, C., and Yang, R. (2019). Leaf traits and photosynthetic characteristics of endangered *Sinopodophyllum hexandrum* (Royle) ying under different light regimesin southeastern Tibet plateau. *Photosynthetica.* 57 (2), 548–555. doi: 10.32615/ps.2019.080

Hamouda, I., Badri, M., Mejri, M., Cruz, C., Siddique, K. H. M., and Hessini, K. (2015). Salt tolerance of *Beta macrocarpa* is associated with efficient osmotic adjustment and increased apoplastic water content. *Plant Biol.* 18, 123–134. doi: 10.1111/plb.12419

Heraud, P., and Beardall, J. (2000). Changes in chlorophyll fluorescence during exposure of dunaliella tertiolecta to UV radiation indicate a dynamic interaction between damage and repair processes. *Photosynth. Res.* 63 (2), 123–134. doi: 10.1023/A:1006319802047

Hodges, D. M., Delong, J. M., Forney, C. F., and Prange, P. K. (1999). Improving the thiobarbituric acid-reactive-substances assay for estimating lipid peroxidation in plant tissues containing anthocyanin and other interfering compounds. *Planta.* 207, 604–611. doi: 10.1007/s004250050524

Hoflacher, H., and Bauer, H. (1982). Light acclimation in leaves of the juvenile and adult life phases of ivy (*Hedera helix*). *Physiol. Plantarum.* 56, 177–182. doi: 10.1111/j.1399-3054.1982.tb00321.x

Hofmann, T., Nebehaj, E., and Albert, L. (2016). Antioxidant properties and detailed polyphenol profiling of European hornbeam (*Carpinus betulus* l.) leaves by multiple antioxidant capacity assays and high-performance liquid chromatography/multistage electrospray mass spectrometry. *Ind. Crops Prod.* 87, 340–349. doi: 10.1016/j.indcrop.2016.04.037

Israeli, Y., Plaut, Z., and Schwartz, A. (1995). Effect of shade on banana morphology, growth and production. *Sci. Hortic.* 62 (1-2), 45–56. doi: 10.1016/0304-4238(95)00763-J

Jason, L., Leonardos, E. D., and Bernard, G. (2018). Effects of light quality and intensity on diurnal patterns and rates of photo-assimilate translocation and transpiration in tomato leaves. *Front. Plant Sci.* 9. doi: 10.3389/fpls.2018.00756

Jiang, Y., Ding, X., Wang, Y., Zou, J., and Nie, W. F. (2021). Decreased low-light regulate plant morphogenesis through the manipulation of hormone biosynthesis in *Solanum lycopersicum*. *Environ.Exp. Bot.* 185 (1669-1676), 104409. doi: 10.1016/j.envexpbot.2021.104409

Jumrani, K., and Bhatia, V. S. (2020). Influence of different light intensities on specific leaf weight, stomatal density photosynthesis and seed yield in soybean. *Plant Physiol. Rep.* 25 (2), 277–283. doi: 10.1007/s40502-020-00508-6

Jutamanee, K., and Rungwattana, K. (2017). Photosynthesis and chlorophyll fluorescence of calathea 'Medallion' exposed to different light intensity. *Acta Hortic.* 1167), 345–348. doi: 10.17660/ActaHortic.2017.1167.49

Kami, C., Lorrain, S., Hornitschek, P., and Fankhauser, C. (2010). Light-regulated plant growth and development. *Curr. Top. Dev. Biol.* 91, 29. doi: 10.1016/S0070-2153(10)91002-8

Kaushik, D., and Aryadeep, R. (2014). Reactive oxygen species (ROS) and response of antioxidants as ROS-scavengers during environmental stress in plants. *Front. Environ. Sci.* 2. doi: 10.3389/fenvs.2014.00053

Khorshidi, M., and Nojavan, A. M. (2006). The effects of abscisic acid and $CaCl_2$ on the activities of antioxidant enzymes under cold stress in maize seedlings in the dark. *Pak. J. Biol. Sci.* 9 (1), 385–407. doi: 10.3109/02841867909128225

Klavins, L., and Klavins, M. (2020). Cuticular wax composition of wild and cultivated northern berries. *Foods.* 9 (5), 587. doi: 10.3390/foods9050587

Knauer, J., Zaehle, S., Kauwe, M. G. D., Haverd, V., Reichstein, M., and Sun, Y. (2020). Mesophyll conductance in land surface models: Effects on photosynthesis and transpiration. *Plant J.* 101 (4), 858–873. doi: 10.1111/tpj.14587

Koca, H., Ozdemir, F., and Turkan, I. (2006). Effect of salt stress on lipid peroxidation and superoxide dismutase and peroxidase activities of *Lycopersicon*

esculentum and *L. pennellii*. *Biol. Plantarum.* 50 (4), 745–748. doi: 10.1007/s10535-006-0121-2

Koike, T. (2010). Photosynthetic responses to light intensity of deciduous broad-leaved tree seedlings raised under various artificial shade. *Environ. Control Biol.* 24 (2), 51–58. doi: 10.2525/ecb1963.24.51

Kuiters, A. T., and Sarink, H. M. (1986). Leaching of phenolic compounds from leaf and needle litter of several deciduous and coniferous trees. *Soil Biol. Biochem.* 18 (5), 475–480. doi: 10.1016/0038-0717(86)90003-9

Lichtenthaler, H. K., Buschmann, C., Doll, M., Fietz, H. J., Bach, T., Kozel, U., et al. (1981). Photosynthetic activity, chloroplast ultrastructure, and leaf characteristics of high-light and low-light plants and of sun and shade leaves. *Photosynth. Res.* 2 (2), 115–141. doi: 10.1007/BF00028752

Li, D. L., Jin, Y. Q., Cui, M. F., Huang, L. X., and Pei, W. H. (2020). Effects of shading on physiological characteristics and ultrastructure of mesophyll cell of *Emmenopterys henryi* leaves. *Bull. Bot. Res.* 40 (1), 29–40. doi: 10.7525/j.issn.1673-5102.2020.01.006

Liu, Y., Jiang, Z., Ye, Y., Wang, D., and Jin, S. (2022). Enhanced salt tolerance of *Torreya grandis* genders is related to nitric oxide level and antioxidant capacity. *Front. Plant Sci.* 13. doi: 10.3389/fpls.2022.906071

Liu, C., Tian, T., Li, S., Wang, F., and Liang, Y. (2018). Growth response of chinese woody plant seedlings to different light intensities. *Acta Ecol. Sin.* 38 (2), 518–527. doi: 10.5846/stxb201611012221

Liu, Y., Wang, T., Fang, S., Zhou, M., and Qin, J. (2018). Responses of morphology, gas exchange, photochemical activity of photosystem ii, and antioxidant balance in *Cyclocarya paliurus* to light spectra. *Front. Plant Sci.* 13. doi: 10.3389/fpls.2018.01704

Liu, W., Yang, Q., Qiu, Z., and Zhao, J. (2014). Effects of light intensity and nutrient addition on growth, photosynthetic pigments and nutritional quality of pea seedlings. *Acta Hortic.* 1037), 391–396. doi: 10.17660/ActaHortic.2014.1037.48

Li, J. R., Yu, K., Wei, J. R., Ma, Q., Wang, B. Q., and Yu, D. (2010). Gibberellin retards chlorophyll degradation during senescence of *Paris polyphylla*. *Biol. plantarum.* 54, 395–399. doi: 10.1007/s10535-010-0072-5

Lu, L. X., Shi, H. Z., Guo, Q. S., Zhao, K., Chang, H. Y., Zou, J., et al. (2022). Effects of shading on photosynthetic physiology and energy metabolism of *Asarum forbesii*. *China J. Chin. Materia Med.* 47 (15), 4048–4054. doi: 10.19540/j.cnki.cjcmm.20220416.104

Lu, D., Wang, G. G., Yan, Q., Tian, G., and Zhu, J. (2018). Effects of gap size and within-gap position on seedling growth and biomass allocation: is the gap partitioning hypothesis applicable to the temperate secondary forest ecosystems in northeast China? *For. Ecol. Manage.* 429, 351–362. doi: 10.1016/j.foreco.2018.07.031

Magné, C., Saladin, G., and Clément, C. (2006). Transient effect of the herbicide flazasulfuron on carbohydrate physiology in *Vitis vinifera* l. *Chemosphere.* 62, 650–657. doi: 10.1016/j.chemosphere.2005.04.119

Ma, Z., Ge, L. Y., Lee, A. S. Y., Yong, J. W. H., Tan, S. N., and Ong, E. S. (2008). Simultaneous analysis of different classes of phytohormones in coconut (Cocos nucifera l.) water using high-performance liquid chromatography and liquid chromatography-tandem mass spectrometry after solid-phase extraction. *Anal. Chim. Acta* 610(2), 274–281. doi: 10.1016/j.aca.2008.01.045

Ma, Z. L., Yang, W. Q., Wu, F. Z., and Gao, S. (2014). Effects of shading on the aboveground biomass and stiochiometry characteristics of *Medicago sativa*. *Chin. J. Appl. Ecol.* 25 (11), 3139–3144. doi: 10.13287/j.1001-9332.20140829.010

Modrzyński, J., Chmura, D. J., Tjoelker, M. G., and Thomas, S. (2015). Seedling growth and biomass allocation in relation to leaf habit and shade tolerance among 10 temperate tree species. *Tree Physiol.* 8), 8. doi: 10.1093/treephys/tpv053

Mokany, K., Raison, R. J., and Prokushkin, A. S. (2006). Critical analysis of root : shoot ratios in terrestrial biomes. *Global Change Biol.* 12 (1), 84–96. doi: 10.1111/j.1365-2486.2005.001043.x

Moreira, A. S. F. P., Filho, J. P. D. L., Zotz, G., and Isaias, R. M. D. S. (2009). Anatomy and photosynthetic parameters of roots and leaves of two shade-adapted orchids, *Dichaea cogniauxiana* shltr. and *Epidendrum secundum* jacq. *Flora Jena.* 204 (8), 604–611. doi: 10.1016/j.flora.2008.08.003

Mutava, R. N., Prince, S., Syed, N. H., Song, L., Valliyodan, B., Chen, W., et al. (2015). Understanding abiotic stress tolerance mechanisms in soybean: A comparative evaluation of soybean response to drought and flooding stress. *Plant Physiol. Bioch.* 86, 109–120. doi: 10.1016/j.plaphy.2014.11.010

Nakano, Y., and Asada, K. (1981). Hydrogen peroxide is scavenged by ascorbate specific peroxidase in spinach chloroplasts. *Plant Cell Physiol.* 22, 867–880. doi: 10.1093/oxfordjournals.pcp.a076232

Neto, A., Prisco, J. T., Enéas-Filho, J., Abreu, C., and Gomes-Filho, E. (2006). Effect of salt stress on antioxidative enzymes and lipid peroxidation in leaves and roots of salt-tolerant and salt-sensitive maize genotypes. *Environ. Exp. Bot.* 56 (1), 87–94. doi: 10.1016/j.envexpbot.2005.01.008

Pan, T., Wang, Y., Wang, L., Ding, J., and Zou, Z. (2020). Increased CO_2 and light intensity regulate growth and leaf gas exchange in tomato. *Physiol. Plantarum.* 168 (3), 694–708. doi: 10.1111/ppl.13015

Pareek, A., Khurana, A., Sharma, A. K., and Kumar, R. (2017). An overview of signaling regulons during cold stress tolerance in plants. *Curr. Genomics* 18 (6), 498–511. doi: 10.2174/1389202918666170228141345

Pashkovskiy, P. P., Soshinkova, T. N., Korolkova, D. V., Kartashov, A. V., Zlobin, I. E., and Lyubimov, V. Y. (2018). The effect of light quality on the pro–/antioxidant balance, activity of photosystem II, and expression of lightdependent genes in *Eutrema salsugineum* callus cells. *Photosynth. Res.* 136, 199–214. doi: 10.1007/s11120-017-0459-7

Petritan, A. M., Lüpke, B. V., and Petritan, I. C. (2007). Effects of shade on growth and mortality of maple (*Acer pseudoplatanus*), ash (*Fraxinus excelsior*) and beech (*Fagus sylvatica*) saplings. *Forestr.* 80 (4), 397–412. doi: 10.1093/forestry/cpm030

Pik, D., Lucero, J. E., Lortie, C. J., and Braun, J. (2020). Light intensity and seed density differentially affect the establishment, survival, and biomass of an exotic invader and three species of native competitors. *Community Ecol.* 21 (3), 259–272. doi: 10.1007/s42974-020-00027-2

Porra, R. J., Thompson, W. A., and Kriedemann, P. E. (1989). Determination of accurate extinction coefficients and simultaneous equations for assaying chlorophylls a and b extracted with four different solvents: Verification of the concentration of chlorophyll standards by atomic absorption spectroscopy. *Biochim. Biophys. Acta* 975, 384–394. doi: 10.1016/s0005-2728(89)80347-0

Prinz, K., and Finkeldey, R. (2015). Characterization and transferability of microsatellite markers developed for *Carpinus betulus* (Betulaceae). *Appl. Plant Sci.* 3, 1500053. doi: 10.3732/apps.1500053

Puglielli, G., Crescente, M. F., Frattaroli, A. R., and Gratani, L. (2015). Morphological, anatomical and physiological leaf trait plasticity of *Sesleria nitida (Poaceae)* in open vs shaded conditions. *Pol. J. Ecol.* 63 (1), 10–22. doi: 10.3161/15052249PJE2015.63.1.002

Ramanjulu, S., and Bartels, D. (2002). Drought and desiccation induced modulation of gene expression in plants. *Plant Cell Environ.* 25 (2), 141–151. doi: 10.1046/j.0016-8025.2001.00764.x

Rezai, S., Etemadi, N., Yousefi, M., and Majidi, M. M. (2018). Effect of light intensity on leaf morphology, photosynthetic capacity, and chlorophyll content in sage (*Salvia officinalis* l.). *Hortic. Sci. Technol.* 36 (1), 46–57. doi: 10.12972/kjhst.20180006

Shi, K., Ze, L. I., Zhang, W., Xiao, H. E., Zeng, Y., and Tan, X. (2018). Influence of different light intensity on the growth, diurnal change of photosynthesis and chlorophyll fluorescence of tung tree seedling. *J. Cent. South Univ. Forest. T.* 38 (8), 35–42,50. doi: 10.14067/j.cnki.1673-923x.2018.08.006

Shi, M., Zhou, Q., and Zhu, Z. L. (2017). Nutrition physiology of *Carpinus betulus* in different regions. *J. Northwest Forestry Univ.* 32, 41–45. doi: 10.3969/j.issn.1001-7461.2017.03.08

Shi, M., and Zhu, Z. L. (2015). Heat resistance evaluation of different cultivars of *Carpinus betulus* over summering. *J. Northwest For. Univ.* 30, 59–64. doi: 10.3969/j.issn.1001-7461.2015.06.10

Sikkema, R., Caudullo, G., and Rigo, D. D. (2016). "Carpinus betulus in Europe: Distribution, habitat, usage and threats," in *In European atlas of forest tree species* (Luxembourg: Publications Office of the European Union), 73–75.

Sofo, A., Dichio, B., Xiloyannis, C., and Masia, A. (2004). Effects of different irradiance levels on some antioxidant enzymes and on malondialdehyde content during rewatering in olive tree. *Plant Sci.* 166 (2), 293–302. doi: 10.1016/j.plantsci.2003.09.018

Stojnić, S., Pekeč, S., Kebert, M., Pilipović, A., Stojanović, D., Stojanović, M., et al. (2016). Drought effects on physiology and biochemistry of pedunculate oak (*Quercus robur* l.) and hornbeam (*Carpinus betulus* l.) saplings grown in urban area of novi sad, Serbia. *Southeast Eur. For.* 7, 57–63. doi: 10.15177/seefor.16-03

Takeda, T., and Maruta, H. (2008). Studies on CO_2 exchange in crop plants : VI. the effect of light intensity and spacing on the photosynthetic rate of rice plant in community conditions. *Jpn. J. Crop Sci.* 24 (4), 331–338. doi: 10.1626/jcs.24.331

Toledo-Aceves, T., and Swaine, M. D. (2007). Biomass allocation and photosynthetic responses of lianas and pioneer tree seedlings to light. *Acta Oecol.* 34 (1), 38–49. doi: 10.1016/j.actao.2008.03.003

Ulger, S., Sonmez, S., Karkacier, M., Ertoy, N., Akdesir, O., and Aksu, M. (2004). Determination of endogenous hormones, sugars and mineral nutrition levels during the induction, initiation and differentiation stage and their effects on flower formation in olive. *Plant Growth Regul.* 42 (1), 89–95. doi: 10.1023/B:GROW.0000014897.22172.7d

Van, D. E. W., and Valluru, R. (2009). Sucrose, sucrosyl oligosaccharides, and oxidative stress: scavenging and salvaging? *J. Exp. Bot.* 60 (1), 9–18. doi: 10.1093/jxb/ern297

Xue, Q., Chen, B., Yang, X. M., Yang, Y. J., Li, Z. W., Bao, S., et al. (2022). Biomass allocation, water use characteristics, and photosynthetic light response of four commelinaceae plants under different light intensities. *Acta Prataculturae Sinica.* 31 (1), 69–80. doi: 10.11686/cyxb2021250

Yao, X. Y., Liu, X. Y., Xu, Z. G., and Jiao, X. L. (2017). Effects of light intensity on leaf microstructure and growth of rape seedlings cultivated under a combination of red and blue LEDs. *J. Integr. Agric.* 16 (001), 97–105. doi: 10.1016/S2095-3119(16)61393-X

Yin, D. S., and Shen, H. L. (2016). Shade tolerance and the adaptability of forest plants in morphology and physiology: a review. *Chin. J. Appl. Ecol.* 27 (8), 2687–2698. doi: 10.13287/j.1001-9332.201608.018

Zhang, S. R. (1999). A discussion on chlorophyll fluorescence kinetics parameters and their significance. *Chin. Bull. Botany*. 16 (4), 444–448. doi: 10.3969/j.issn.1674-3466.1999.04.021

Zhang, L., Wang, J., Zhang, J. F., Deng, X. J., Luo, Y. H., and Yan, X. F. (2021). Responses of growth and physiological characteristics of *Quercus wutaishanica* seedlings to the light intensity. *J. cent. south univ. For. Technol.* 41 (11), 73–81. doi: 10.14067/j.cnki.1673-923x.2021.11.009

Zhang, M. Y., Yang, Z. Q., and Hou, M. Y. (2017). Simulation of light response of photosynthesis of *Cucumis sativus* l. leaves under water stress. *Chin. J. Agrometeorol.* 38 (10), 644–654. doi: 10.3969/j.issn.1000-6362.2017.10.003

Zhao, H., Liang, H., Chu, Y., Sun, C., and Zheng, C. (2019). Effects of salt stress on chlorophyll fluorescence and the antioxidant system in *Ginkgo biloba* l. seedlings. *Hortic. Sci.* 54 (12), 2125–2133. doi: 10.21273/HORTSCI14432-19

Zhou, Q., Zhu, Z. L., Shi, M., and Cheng, L. X. (2018). Growth and physicochemical changes of *Carpinus betulus* l. influenced by salinity treatments [J]. *Forests.* 9 (6), 354. doi: 10.3390/f9060354

Zhu, Z. L., Xu, Y. Y., and Wang, S. (2013). Structure changes of *Carpinus betulus* seed under fluctuating temperature stratification. *J. Northeast For. Univ.* 41, 1–5. doi: 10.13759/j.cnki.dlxb.2013.07.026

Zushi, K., Suehara, C., and Shirai, M. (2020). Effect of light intensity and wavelengths on ascorbic acid content and the antioxidant system in tomato fruit grown *in vitro*. *Sci. Hortic.* 274, 109673. doi: 10.1016/j.scienta.2020.109673

frontiers | Frontiers in Plant Science

TYPE Original Research
PUBLISHED 25 January 2023
DOI 10.3389/fpls.2023.1000647

OPEN ACCESS

EDITED BY
Song Heng Jin,
Zhejiang Agriculture and Forestry University, China

REVIEWED BY
Benoit Pallas,
INRAE Occitanie Montpellier, France
Qikui Wu,
Shandong Agricultural University, China

*CORRESPONDENCE
Guopeng Chen
chgp1986@gmail.com

SPECIALTY SECTION
This article was submitted to Functional Plant Ecology, a section of the journal Frontiers in Plant Science

RECEIVED 22 July 2022
ACCEPTED 09 January 2023
PUBLISHED 25 January 2023

CITATION
Yang K, Chen G, Xian J and Chang H (2023) Divergent adaptations of leaf functional traits to light intensity across common urban plant species in Lanzhou, northwestern China.
Front. Plant Sci. 14:1000647.
doi: 10.3389/fpls.2023.1000647

Divergent adaptations of leaf functional traits to light intensity across common urban plant species in Lanzhou, northwestern China

Ketong Yang[1], Guopeng Chen[1]*, Junren Xian[2] and Hailong Chang[3]

[1]College of Forestry, Gansu Agricultural University, Lanzhou, China, [2]College of Environmental Sciences, Sichuan Agricultural University, Chendu, China, [3]College of Land Resources and Environment, Jiangxi Agricultural University, Nanchang, China

Leaves are the most important photosynthetic organs in plants. Understanding the growth strategy of leaves in different habitats is crucial for elucidating the mechanisms underlying plant response and adaptation to the environment change. This study investigated the scaling relationships of the laminar area (LA), leaf fresh mass (LFM), leaf dry mass (LDM), and explored leaf nitrogen (N) and phosphorus (P) content in leaves, and the relative benefits of these pairwise traits in three common urban plants (*Yulania denudata*, *Parthenocissus quinquefolia*, and *Wisteria sinensis*) under different light conditions, including (full-sun and canopy-shade). The results showed that: the scaling exponent of LDM vs LA (> 1, $p < 0.05$) meant that the LDM increased faster than LA, and supported the hypothesis of diminishing returns. The LFM and LDM had isometric relationships in all the three species, suggesting that the leaf water content of the leaves was nearly unaltered during laminar growth. *Y. denudata* and *W. sinensis* had higher relative benefit in full-sun habitats, while the reverse was observed in *P. quinquefolia*. The N and P content and the N:P ratio in full-sun leaves were generally higher than those of canopy-shade leaves. The leaves of the three urban plants exhibited a shift in strategy during transfer from the canopy shaded to the sunny habitat for adapting to the lower light conditions. The response of plant leaves to the environment shapes the rich variations at the leaf level, and quantification of the relative benefits of plants in different habitats provides novel insights into the response and adaptation strategies of plants.

KEYWORDS

light environment, relative benefit, scaling relationship, phenotypic plasticity, stoichiometry, urban plants

1 Introduction

Leaves represent the primary light harvesting organs in vascular plants, and are the main components responsible for energy transfer between plants and the external environment (Milla and Reich, 2007; Sun et al., 2017). It is therefore important to understand how plants adapt to environmental variations by adjustment and complementation for ensuring survival and seeking maximum benefits. Despite differences, leaf sizes, laminar area (LA), and mass of lamina are closely related to each other (Wright et al., 2004; Li et al., 2008; Shi et al., 2020). Therefore, analyses of the relationship between LA and mass of lamina can aid in effective evaluation of the photosynthetic capacity, terrestrial biomass, and even ecosystem functions (Zhang and Feng, 2004; Niklas et al., 2007).

In scaling relationships, any two traits can be expressed by the scaling equation $y = \beta x^{\alpha}$, where x and y are pairwise traits, β is the scaling (normalization) constant, and α is the scaling exponent (Niklas et al., 2007; Sun et al., 2017). In practical applications, this power function is often transformed to a logarithmic function, in which case the scaling equation takes the form $\log y = \log \beta + \alpha \log x$ (Milla and Reich, 2007; Cheng et al., 2009). In this context, the hypothesis of diminishing returns predicts that the relationship between LA and laminar mass is greater than unity (that is, $\alpha > 1$), indicating that despite incremental gains in laminar mass, the LA does not increase proportionally (Huang et al., 2019; Shi et al., 2020). If this hypothesis is true, the specific leaf area (SLA), which is a crucial index of photosynthetic efficiency and determined using the equation SLA = LA/leaf dry mass (LDM), would decrease with increasing LA.

In previous studies, researchers have often considered LA and LDM as benefits and costs, respectively, and they can calculate SLA (Milla and Reich, 2007; Li et al., 2008; Dinesh et al., 2019). Numerous empirical studies have demonstrated that specific areas of leaves are positively correlated with the net photosynthetic rate (Niklas et al., 2007), and the underlying message here is that LA and LDM are closely related to photosynthesis (Huang et al., 2019; Shi et al., 2020). As aforementioned, the formula can be used for theoretically determining the fresh and dry mass of laminae, and the relationship between the dry mass and fresh mass reflects the dynamic characteristics of the water content of leaves. Therefore, elucidating the complex relationship among laminar fresh mass, dry mass, and area by analyzing their scaling relationship is important for understanding the structural relationship of leaves.

When exposed to habitat stress, plants frequently employ phenotypic plasticity for adapting to the environment (Lusk, 2004; Kelsey and Jason, 2018; Esperón et al., 2020). When the levels of stress are extremely high, plants may induce a shift in ecological strategy, as described in the leaf economics spectrum (LES) (Wright et al., 2004). Apart from leaf morphology, alterations are also observed in leaf inclusions (water content or enzyme activity, for instance), including the LA, nitrogen (N) and phosphorus (P) content, and other parameters, in heterogeneous habitats (Liu et al., 2007; Dinesh et al., 2019). Light is an abiotic factor that is necessary for the survival of plants, and alterations in the intensity of light affect the normal growth and photosynthetic rate of plants, especially for understory species (Aleric and Kirkman, 2005; Selaya et al., 2008; Valladares and Niinemets, 2008; Liu et al., 2016). A previous study demonstrated that the presence of shade significantly decreases leaf size and laminar mass per unit area (reciprocal of SLA) in rainforest plants (Meng et al., 2014). Some other studies have confirmed that nitrogen concentration per unit leaf area was greater in current-year foliage from high-light environments than in current-year foliage from low-light environments (Zhang and Feng, 2004; Katahata et al., 2007). Unfortunately, quantitative comparisons are not effective in clarifying whether there has been a shift in plant adaptation strategies. It is therefore necessary to determine whether plants gain more relative benefits in shaded or unshaded habitats, and whether the alterations in different functional traits result from phenotypic plasticity or a shift in ecological strategy.

To this end, we selected three urban plants, namely, *Yulania denudata*, *Parthenocissus quinquefolia*, and *Wisteria sinensis*, and determined seven major functional traits of the leaves under different light intensities (full sun and canopy shade). We subsequently calculated the relative benefits in the different habitats, and proposed the following hypotheses: (1) the scaling relationship between the LA and laminar mass supports the hypothesis of diminishing returns; and (2) the adaptation strategy of leaves shifted under different conditions of light.

2 Materials and methods

2.1 Study site

The study was conducted in and around the campus of Gansu Agricultural University, Lanzhou, China. Lanzhou city is located in the north-west of the Loess plateau, and has a dominant subtropical continental monsoon climate with four distinct seasons. Summer is hot and rainy, with rainfall accounting for more than 60% of the year, while winter is cold and dry. The lowest and highest temperatures are -10°C (in February) and 36°C (in July), respectively. The annual mean temperature is 10.3°C and the annual mean precipitation is 357 mm. The soil types are primarily calcareous, chestnut, and cinnamon, and are nutrient barren with scarce natural vegetation.

2.2 Plant material

Urban plants are the main vegetation cover in cities, which are watered on a regular basis every month. In this study, we selected three common plants, namely, *Y. denudata*, *P. quinquefolia*, and *W. sinensis*. *Y. denudata* is a deciduous tree, *P. quinquefolia* and *W. sinensis* are deciduous lianas. Some of them were growing under the canopy of large trees or on the north side of tall buildings, while some were completely exposed to the sun. Based on the differences in light exposure, the habitats were classified as shaded and unshaded, or low light and high light habitats (Table 1).

The sampling was conducted in the month of July in 2021. A total of 20 individuals (10 individuals each under low and high light) were selected for each of the three species, and at least 80~150 leaves were collected from different habitats. The leaves were collected at the height of 1.8 m and the light intensity at the corresponding position was simultaneously measured with a handheld illuminometer (TES-1334A, Taiwan, China). All the collected leaves were subsequently placed in plastic self-sealing bags in a portable incubator with ice bags

TABLE 1 Light intensity of urban plants in different habitats.

Plant species	Light intensity	Mean ± SD (Lux)
Y. denudata	Low	4088.80 ± 968.40[a]
	High	100319.07 ± 3585.41[b]
P. quinquefolia	Low	3012.80 ± 215.20[a]
	High	102865.60 ± 6670.33[b]
W. sinensis	Low	2080.27 ± 1150.53[a]
	High	106990.27 ± 4926.55[b]

The different lowercase letters indicate significant differences at the 0.05 level.

for preventing the leaf blades from deforming and losing water. The leaf samples were then transferred to the laboratory for subsequent measurements.

2.3 Leaf traits measurement

The collected leaf samples were individually scanned using a scanner (EPSON V39, Indonesia), and the images were saved in bitmap format at a resolution of 300 dpi. The ImageJ software (version 1.48, National Institutes of Mental Health, Maryland, America) was used to generate the leaf profiles as black and white images. The length, width, and area (LA, cm^2) of the leaf blades were measured using the ImageJ software. The leaf fresh mass (LFM, g) was determined, following which the leaves were dried in a ventilated oven (Taisite, WHL45B, Tianjin, China) at 105°C for 20 min, and the temperature was reduced to 75°C until a constant dry mass was reached, which represented the leaf dry mass (LDM, g) (Pérez et al., 2013; Huang et al., 2019). The LFM and LDM were measured using an electronic balance (0.0001 g, Zhuojing Experimental Equipment Co. Ltd., BMS, Shanghai, China). Specific leaf area (SLA, cm^2/g) was calculated by LA/LDM. The dried leaves were finally crushed and passed through a fine 800 mesh sieve for analyzing the total N and P content. The total N content was determined by the H_2SO_4-H_2O_2 method, and the total P was determined using the molybdenum antimony scandium colorimetric method. Finally, the phenotypic plasticity index (*PPI*) was calculated according to Valladares et al. (2006) method, i.e. PPI = [(max - min)/max], and it was a dimensionless parameter, the greater value indicated stronger phenotypic plasticity.

2.4 Scaling relationship analysis

The relationships among LA, LFM, and LDM (namely, LDM vs. LFM, LFM vs. LA, and LDM vs. LA) can be described by a mathematical equation of the type $y = \beta x^{\alpha}$, which can be linearized as $\log(y) = \log(\beta) + \alpha \log(x)$, where x and y determine whether the relationship is isometric ($\alpha = 1$) or allometric ($\alpha > 1$ or $\alpha < 1$). The β term represents the y-intercept of the relationship, and its value does not determine the nature of the relationship. If two lines with the same slope are compared, the difference between their respective β values indicates the difference between the indices. The 95% confidence intervals (95% CI) of α and β were calculated by Standardized Major Axis (SMA) regression (i.e. Model type II) using the Standardized Major Axis Tests and Routines (SMATR) software, version 2.0 (Falster et al., 2006). In order to make the data more closely to the normal distribution, the leaf trait values were analyzed by scaling after lg10 conversion. Additionally, the significant difference between the slope and unity was calculated for all the parameters for assessing the relationship between the allometric growth index and unity by Wald significance test (Warton et al., 2006). If the difference between the slope and unity was not significant, the relationship between the two indices was considered to be isometric; however, if the slope was greater than or less than unity, the relationship between the two indices was considered to be allometric.

2.5 Relative benefit analysis

The trade-offs between pairwise traits (A vs B) were calculated as described hereafter. The benefit for a single object (A or B) is defined as the relative deviation from the mean for a given observation. Given the observations for an individual object A, the magnitude of benefit for object A (B_A, A/B) is calculated as: $B_A = (A_{OBS}-A_{min})/(A_{max}-A_{min})$ (Bradford and D'Amato, 2012), where A_{OBS} represents the observed value of A/B, while A_{max} and A_{min} are calculated from all the observed values of A/B (Sun and Wang, 2016). The trade-offs range from 0 to 1, and can be conceptualized as the proportion of possible benefits in object A (A/B). In cases where certain objects are considered to be more valuable or important than others, individual objects (A/B) can be weighted for incorporating these differences during the calculation of overall benefits and trade-offs. A simple strategy for quantifying the magnitude of the trade-offs between A and B involves calculating the root mean square error (RMSE) of the individual benefits of A or B (Lu et al., 2014; Sun and Wang, 2016). The RMSE approximates the average deviation from the mean benefit, and is calculated in two dimensions by determining the distance between the coordinates of the paired traits and the "1:1 line" where the trade-off is zero (Bradford and D'Amato, 2012). This method represents an effective strategy for quantifying the relationship between A and B. A preliminary definition of relative benefit has been provided by Bradford and D'Amato (2012), and studies by Lu et al. (2014) and Sun and Wang (2016) have provided detailed descriptions.

2.6 Statistical analysis

The differences in the N and P contents and the N:P ratio across the different habitats were determined by one-way analyses of variance (ANOVA). Light habitats and species difference and their interaction were conducted by two-ways ANOVA analysis. Principal component analysis (PCA) was performed for investigating the shifts in adaptation strategy across different conditions of light. Data analyses were performed using SPSS 20.0 (Chicago, IBM Corp, USA), and the graphs were prepared using Origin 2019 (https://www.originlab.com). The measurements obtained for the different parameters are presented as the mean ± standard deviation (SD).

3 Results

3.1 Variations in leaf traits and *PPI* under different light habitats

The intensity of light significantly altered all the leaf traits with the exception of the LFM of *P. quinquefolia* and the LA of *W. sinensis*. The LFM, LDM, and LA of *Y. denudata* were 1.48 ± 0.47 g, 0.33 ± 0.11 g, and 76.67 ± 20.05 cm^2, respectively, under conditions of low light (Table 2); which significantly decreased to 0.91 ± 0.24 g, 0.26 ± 0.07 g, and 41.45 ± 10.01 cm^2, respectively, as the intensity of light increased. The LDM and LA of *P. quinquefolia* were 0.19 ± 0.07 g and 59.75 ± 19.70 cm^2, respectively, under conditions of low light; which changed to 0.23 ± 0.10 g and 47.58 ± 16.27 cm^2, respectively, when the intensity of light increased, while the LFM remained unaltered. The LFM and LDM of *W. sinensis* increased significantly from 0.31 ± 0.18 g and 0.08 ± 0.05 g, respectively, to 0.45 ± 0.16 g and 0.17 ± 0.06 g, respectively, as the intensity of light increased, while the LA remained unaltered. For the three urban plants, the SLA in low light habitat was significantly larger than that in high light habitat (p<0.05). Interestingly, we observed that the *PPI* of *Y. denudata* and *P. quinquefolia* for the leaf traits were 0.52–0.77 and 0.54–0.84, respectively, under conditions of low light; and were 0.41–0.77 and 0.70–0.91, respectively, under conditions of high light. However, the *PPI* of *W. sinensis* was higher under low light condition (0.49–0.93) and lower (0.54–0.80) under high light condition. We found that the *PPI* of SLA was always the smallest for all kinds of plants and light habitats.

3.2 Scaling relationship between leaf traits and their relative benefits

For *Y. denudata*, the slopes between leaf traits were significantly higher than 1 (p<0.05) (Figure 1; Table 3), except that the slope of LDM vs LFM was not significant in the high light habitat (p=0.319). Similarly, the slope of LDM vs LFM for *P. quinquefolia* did not show markedly significant differences from unity under conditions of both low and high light habitats, while the slopes of the other pairwise traits, namely, LFM vs LA and LDM vs LA, were significantly different from unity (p<0.001). For *W. sinensis*, the slopes of only LDM vs LFM under both conditions of light, and LFM vs LA under conditions of low light were not statistically different from unity, while the slopes of the other pairwise traits were significantly different from unity (p<0.001). By summarizing the relative benefits for the three species, we observed that *Y. denudata* had higher relative benefits under low light habitat for all the pairwise traits (Figure 2), while the reverse was observed for *P. quinquefolia* and *W. sinensis*.

3.3 N and P content of leaves under different light habitats

The plants that grew under high light intensity had higher N, P content and N:P ratios compared to low light intensity (Figure 3). The

TABLE 2 The difference and phenotypic plasticity index (*PPI*) of urban plant leaf traits in different light habitats.

Plant species	Traits	Low light		High light	
		Mean ± SD	*PPI*	Mean ± SD	*PPI*
Y. denudata	LFM (g)	1.48 ± 0.47	0.73	0.91 ± 0.24 *	0.77
	LDM (g)	0.33 ± 0.11	0.77	0.26 ± 0.07 *	0.77
	LA (cm^2)	76.67 ± 20.05	0.64	41.45 ± 10.01 *	0.71
	SLA (cm^2/g)	236.47 ± 36.37	0.52	160.54 ± 16.37 *	0.41
P. quinquefolia	LFM (g)	0.89 ± 0.34	0.83	0.89 ± 0.39 ^{ns}	0.90
	LDM (g)	0.19 ± 0.07	0.84	0.23 ± 0.10 *	0.91
	LA (cm^2)	59.75 ± 19.70	0.77	47.58 ± 16.27 *	0.83
	SLA (cm^2/g)	325.58 ± 47.73	0.54	219.35 ± 34.49 *	0.70
W. sinensis	LFM (g)	0.31 ± 0.18	0.92	0.45 ± 0.16 *	0.79
	LDM (g)	0.08 ± 0.05	0.93	0.17 ± 0.06 *	0.80
	LA (cm^2)	30.88 ± 16.47	0.90	28.63 ± 9.23 ^{ns}	0.78
	SLA (cm^2/g)	399.81 ± 46.82	0.49	171.51 ± 21.39 *	0.54

ns indicated no significant difference in leaf trait values under different light habitats, * indicated significant difference at the 0.05 level.

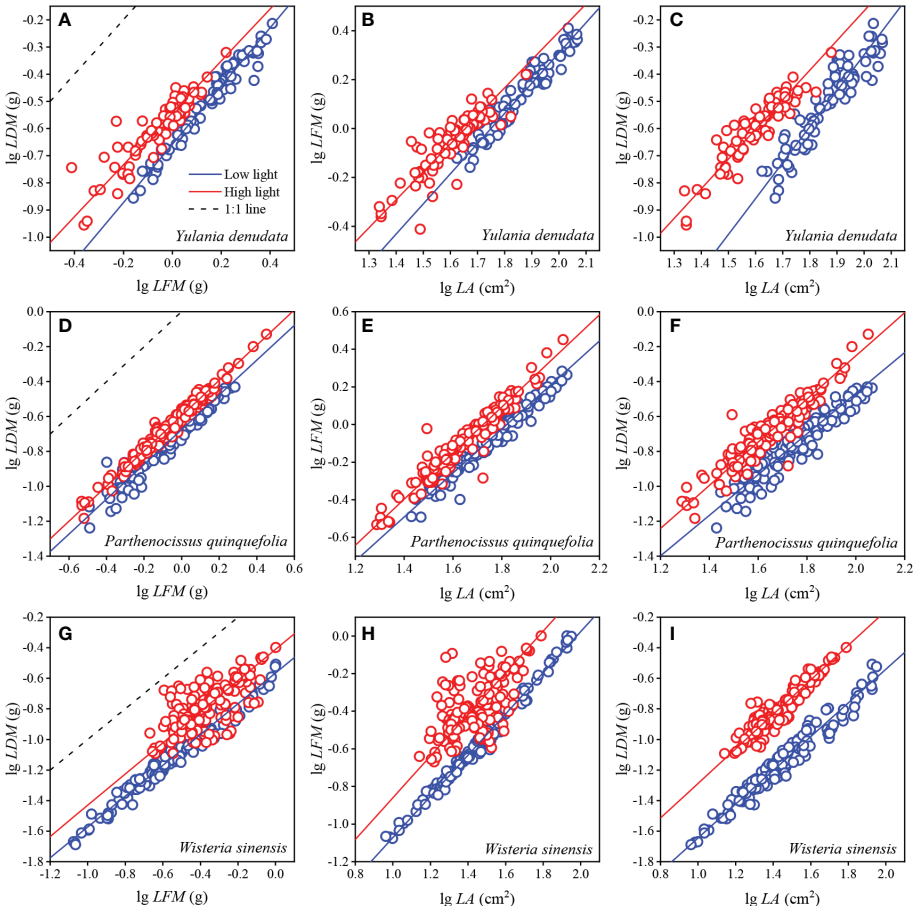

FIGURE 1
Scaling relationships between leaf traits in different urban plants. **(A–C)** represent the fitting relationship between *LDM* with *LFM*, *LFM* with *LA*, and *LDM* with *LA* of *Y. denudata* leaves, respectively. **(D–F)** represent the fitting relationship between *LDM* with *LFM*, *LFM* with *LA*, and *LDM* with *LA* of *P. quinquefolia* leaves, respectively. **(G–I)** represent the fitting relationship between *LDM* with *LFM*, *LFM* with *LA*, and *LDM* with *LA* of *W. sinensis* leaves, respectively. Circles represent the observed values; the blue and red solid lines represent SMA fitting lines between leaf traits under low and high light habitats, respectively; and dotted lines represent 1:1 line. Some 1:1 lines are not shown due to the proportional value of the axes.

TABLE 3 Scaling relationships of leaf traits in urban plants under different light habitats.

Plant species	Traits	Habitats	R^2	p	Slope	Intercept	Isometric
					α	β	p
Y. denudata	LDM vs LFM	LL	0.96	< 0.01	1.07	-0.66	< 0.050
		HL	0.83	< 0.01	0.95	-0.54	0.319
	LFM vs LA	LL	0.92	< 0.01	1.24	-2.16	< 0.001
		HL	0.75	< 0.01	1.14	-1.89	< 0.050
	LDM vs LA	LL	0.86	< 0.01	1.32	-2.97	< 0.001
		HL	0.86	< 0.01	1.09	-2.35	< 0.050
P. quinquefolia	LDM vs LFM	LL	0.93	< 0.01	1.00	-0.68	0.850
		HL	0.97	< 0.01	1.01	-0.60	0.514
	LFM vs LA	LL	0.96	< 0.01	1.17	-2.13	< 0.001
		HL	0.92	< 0.01	1.23	-2.11	< 0.001
	LDM vs LA	LL	0.87	< 0.01	1.17	-2.80	< 0.001
		HL	0.89	< 0.01	1.24	-2.73	< 0.001

(Continued)

TABLE 3 Continued

Plant species	Traits	Habitats	R^2	p	Slope	Intercept	Isometric
					α	β	p
W. sinensis	LDM vs LFM	LL	0.96	< 0.01	1.01	-0.56	0.608
		HL	0.49	< 0.01	1.02	-0.41	0.722
	LFM vs LA	LL	0.99	< 0.01	1.10	-2.17	< 0.001
		HL	0.41	< 0.01	1.11	-1.97	0.111
	LDM vs LA	LL	0.95	< 0.01	1.11	-2.75	< 0.001
		HL	0.88	< 0.01	1.13	-2.42	< 0.001

LFM and LDM are represented in g; LA is represented in cm^2. LL, low light; HL, high light. α is the slope or the scaling exponent; β is the intercept or scaling constant; the first p indicates linear correlation; the isometric p indicates whether the slope is significantly different from 1, and $p < 0.05$ indicates that the slope is significantly different from 1.

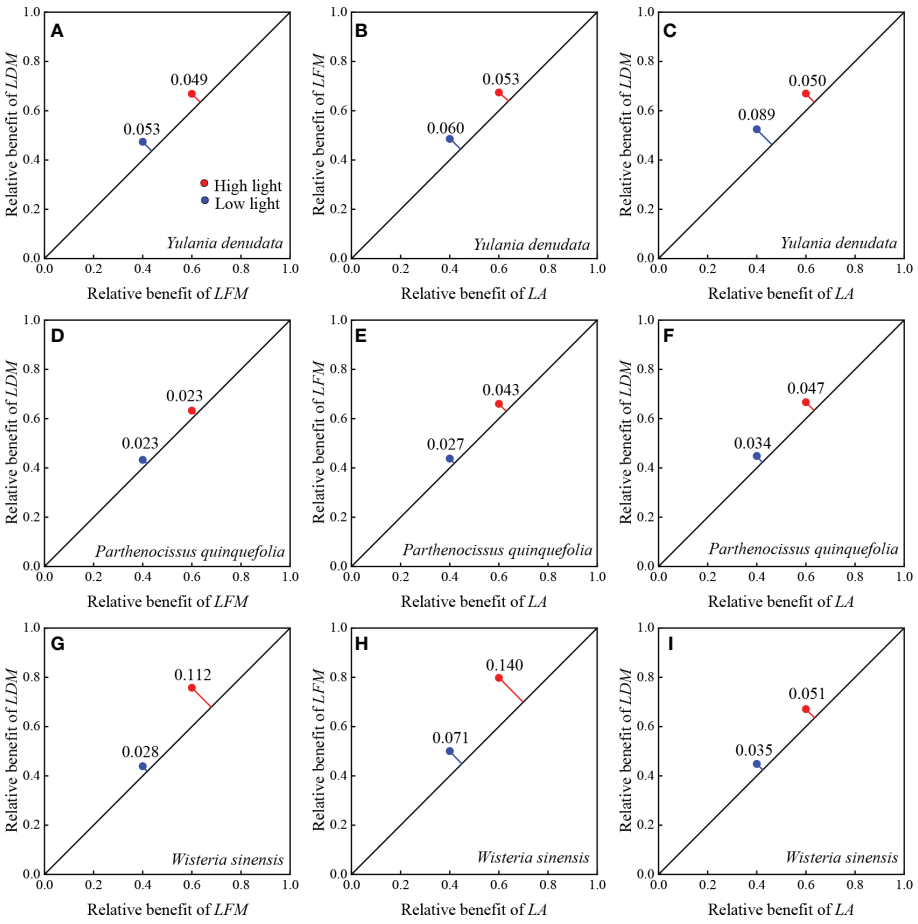

FIGURE 2
Relative benefits between paired leaf traits of different urban plant. **(A–C)** represent the relative benefit between *LDM* with *LFM*, *LFM* with *LA*, and *LDM* with *LA* of *Y. denudata* leaves, respectively. **(D–F)** represent the relative benefit between *LDM* with *LFM*, *LFM* with *LA*, and *LDM* with *LA* of *P. quinquefolia* leaves, respectively. **(G–I)** represent the relative benefit between *LDM* with *LFM*, *LFM* with *LA*, and *LDM* with *LA* of *W. sinensis* leaves, respectively. The blue and red points indicate low light and high light habitats, respectively. The relative benefit is represented by the RMSE of paired traits. The RMSE represents the distance from the coordinate of the paired traits to the diagonal 1:1 line where the trade-off is zero. The farther the distance, the larger the relative benefit.

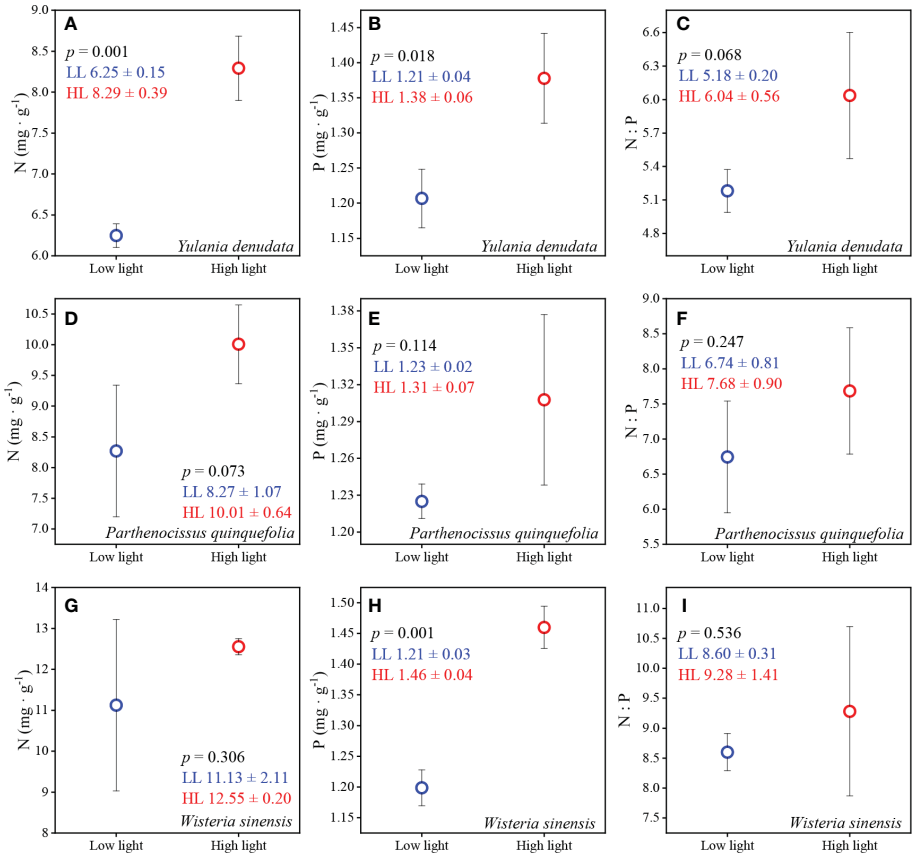

FIGURE 3
The N and P contents and N:P ratios under conditions of different light habitats. **(A–C)** represent the N, P content and N:P of *Y. denudata* leaves under different light habitats, respectively. **(D–F)** represent the N, P content and N:P of *P. quinquefolia* leaves under different light habitats, respectively. **(G–I)** represent the N, P content and N:P of *W. sinensis* leaves under different light habitats, respectively. The blue and red circles represent low light and high light, respectively. The numerical values in the figures represent the mean ± SD. $p < 0.05$ indicates a significant difference between the two light environments.

N and P contents of *Y. denudata* were 6.25 ± 0.15 mg·g^{-1} and 1.21 ± 0.04 mg·g^{-1}, respectively, under low light conditions, and were significantly lower than those under high light intensity, which were 8.29 ± 0.39 mg·g^{-1} and 1.38 ± 0.06 mg·g^{-1}, respectively. The N:P ratio under low and high light intensities were 5.18 ± 0.20 and 6.04 ± 0.56 (p=0.068), respectively. The N, P, and N:P ratio were 8.27 ± 1.07 mg·g^{-1}, 1.23 ± 0.02 mg·g^{-1}, and 6.74 ± 0.81, respectively, for *P. quinquefolia* under low light condition, and 10.01 ± 0.64 mg·g^{-1}, 1.31 ± 0.07mg·g^{-1}, and 7.68 ± 0.90, respectively, under high light intensity. *W. sinensis* had different N content and N:P ratios under different light intensities, which were 11.13 ± 2.11mg·g^{-1} and 8.60 ± 0.31, respectively, under high light intensity, and 12.55 ± 0.20 mg·g^{-1} and 9.28 ± 1.41, respectively, under low light intensity. The P content in the leaves of *W. sinensis* was high, being 1.46 ± 0.04mg·g^{-1}, which was significantly higher than that under conditions of low light, which was 1.21 ± 0.03mg·g^{-1}.

3.4 Combined effects of light and species on leaf traits

Two-ways ANOVA analysis showed that light habitats had significant effect on all traits except N:P (F=0.772, $p > 0.05$) (Table 4). Species differences had significant effects on all traits except LDM (F=2.799, $p > 0.05$). In addition, the interaction of the light habitats and species difference had significant impact on LFM, LDM, LA, SLA, and P content ($p < 0.05$). These results further supplemented and explained the results of one-way ANOVA analysis for element content.

3.5 Shift in the adaptation strategies of leaves under different light habitats

PCA of the six leaf traits demonstrated that the explanatory rates of the first and second principal components were 77.7% and 19.2%, respectively (Figure 4). The absolute value of LFM, LDM, LA, N content, and N:P ratio were greater than 0.3 on the PC1 axis, while the absolute value of the LDM and P content were greater than 0.3 on PC2 axis, which indicated that these six traits can effectively explain the variation in leaf traits under different light habitats in different dimensions. Lastly, the results of PCA revealed an obvious shift in the adaptation strategy from a larger LA and lower N and P contents under low light habitat to a smaller LA and higher N and P contents under high light habitat in the three plants.

TABLE 4 Results of two-ways ANOVA for the effects of light conditions, species and their interactions on functional traits of urban plants.

Morphological trait	Factor	*df*	LFM	LDM	LA	SLA
			F	*F*	*F*	*F*
	Light	1	37.854 ***	9.959 **	189.92 ***	2394.029 ***
	Species	2	438.488 ***	271.936 ***	248.150 ***	304.924 ***
	Light×Species	2	75.412 ***	59.954 ***	56.778 ***	300.128 ***
Chemical trait	Factor	*df*	N	P	N:P	
			F	*F*	*F*	
	Light	1	13.256 **	61.765 ***	0.772 ns	
	Species	2	30.919 ***	2.799 ns	20.714 **	
	Light×Species	2	0.141 ns	5.552 *	1.549 ns	

* $p < 0.05$; ** $p < 0.01$; *** $p < 0.001$; ns, no significant.

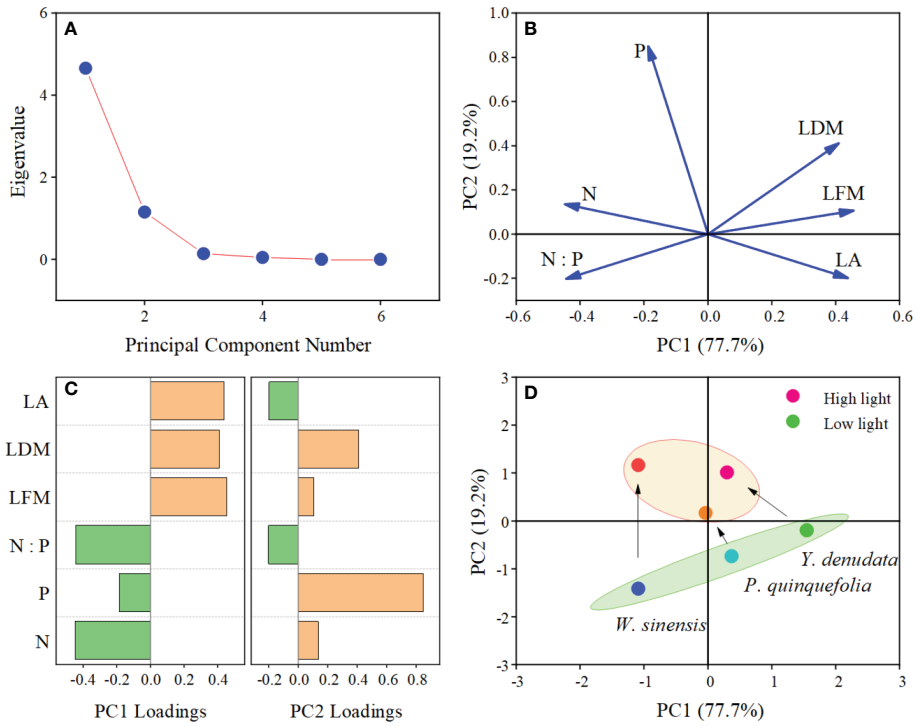

FIGURE 4
PCA analysis of leaf traits of urban plants in different light habitats. **(A)** Scree plot; **(B)** Loading plot; **(C)** Loadings of plant traits on the first and second axes; **(D)** Score plot and strategy shifts of the different plants under different light habitats.

4 Discussion

Plants show different traits in different light habitats. Consistent with our hypothesis, light significantly changed leaf morphological traits and element content. The relationship between LDM and LA of all plants in different light habitats showed diminishing returns, that is, with the increase of leaf dry mass, the increase of leaf area gradually decreased. Except for *Y. denudata*, most LDM and LFM showed isomeric relationship, that is, leaf water content gradually increased with leaf mass. From low light to high light, the leaves tended to have higher P content. In conclusion, the plants growth strategies changed under different light habitats.

4.1 Scaling relationships between leaf traits and relative benefits

The scaling relationships of leaf traits has been confirmed by a number of empirical studies, which demonstrated that the habitat, developmental factors, and phylogeny affect the relationships between leaf traits (Niklas et al., 2007; Shi et al., 2020). A previous study by Sun et al. (2017) on five species of bamboos demonstrated a scaling relationship between LDM and LA under different conditions of light. Similarly, our results indicated that there was a scaling relationship between LDM and LA under different light condition, which supported the law of diminishing returns. Briefly, as the LA increased, the LDM increased more rapidly, which consequently decreased the SLA. Interestingly, the scaling exponent (α) of the LDM and LA of *Y. denudata* under low light (α = 1.32) was larger than that of high light intensity (α = 1.09), whereas the scaling exponents of *P. quinquefolia* (α = 1.17 and 1.24, respectively, under low and high light) and *W. sinensis* (α = 1.11 and 1.13, respectively, under low and high light) showed a reverse trend. We speculated that this could be attributed to the differences in plant life forms and leaf forms (for instance simple and compound leaves). *Y. denudata* is a small tree, while the other two plants are woody lianas. There are significant differences in the hydraulic structures of these plants, which may lead to differences in laminar and petiolar investment (Maréchaux et al., 2017). A considerable portion of the biomass of *Y. denudata* is contributed to strengthening the support system and petiolar transportation. In terms of leaf forms, both *P. quinquefolia* and *W. sinensis* have compound leaves, implying that apart from petioles, the laminar biomass of these plants is also invested in rachides (Xu et al., 2009). If a scaling relationship exists between petioles (rachides) and laminar biomass, plants with different leaf forms may have significant differences in the investment of laminar biomass (Yang et al., 2009).

In general, regions with high light intensity have lower water content in soils than regions with low light intensity; therefore, trade-offs between laminar water content and LDM during plant growth are more likely under high light intensity than under low light (Meng et al., 2014; Umaña and Swenson, 2019; Li et al., 2020). The relationship between LDM and LFM may reflect the variations in laminar water content, which is the basis of photosynthesis (Santiago et al, 2018; Dinesh et al., 2019). Our study also demonstrated the LDM and LFM increased at an equal rate (nearly 1:1) under almost all conditions, indicating that when the LFM increased, the LDM also increased gradually, while the water content of the leaves remained constant. These findings are inconsistent with the results of the study by Shi et al. (2020) on *Fallopia multiflora*. These variations are attributed to differences in the environment between these studies. Natural rainfall is the only source of water for wild plants; however, water is not a limiting factor for urban plants. Therefore, urban plants do not have a very strong demand for water storage during growth (Song et al., 2021).

Plant SLA in low light habitat was significantly larger than that in high light habitat, which was consistent with most other studies (Baird et al., 2017; Power et al., 2019). Plants in high light environments need to invest more in defense against heat and damage than shaded plants. Plants under shade may increase their LA to gain more light, which is consistent with the significant difference in LA between different light habitats. We also observed that the *PPI* of SLA was the smallest compared with other traits, which also indicated that SLA was stable and could be used to refer to the photosynthetic capacity of plants (Liu et al., 2016; Dinesh et al., 2019).

The trade-offs between pairwise traits in different habitats can more clearly illustrate the adaptation of plants to the environment. Only rarely studies have quantified plant habitat preferences using relative benefits (Cheng et al., 2021; Wang et al., 2021). In general, *P. quinquefolia* and *W. sinensis* have greater relative benefits under high light habitat, while *Y. denudata* have greater relative benefits under low light conditions. This indicates that *P. quinquefolia* and *W. sinensis* can maximize the advantages of functional traits under high light conditions, while the reverse is observed in *Y. denudata*. This may also be the underlying reason why *Y. denudata* has a higher slope in low light. In contrast, the slope of the *P. quinquefolia* and *W. sinensis* varied little in different light conditions.

4.2 Stoichiometric characteristics and strategy shift in leaves

The adaptation of plants to different habitats not only manifests in leaf morphology but is also observed in the alterations in leaf inclusions. The results of this study confirmed that the leaves of plants growing under conditions of low light had lower N and P contents and N:P ratios. However, this finding was not consistent with the results of the study by Niinemets et al. (2006), which reported that plants with larger SLA, corresponding to plants under conditions of low light in this study, have higher N and P content. Nevertheless, some studies have suggested that the N and P content of leaves are expected to increase with increasing light (Katahata et al., 2007; Puglielli et al., 2020). Compared to conditions of low light, high light conditions enhance photosynthesis to a certain extent, and also promote plant growth and development, thereby gradually increasing the N and P content in leaves. The N:P ratio of the three plants studied herein was less than 14 or 20 under different light conditions, indicating that the growth of these plants was restricted by N availability (Koerselman and Meuleman, 1996; Güsewell, 2004; Yan et al., 2017). The plants growing under conditions of low light were more severely restricted by N deficiency, compared to those growing under conditions of high light. We hypothesized that the lower light intensity restricted photosynthesis and leaf growth, and that the canopy intercepted most of the atmospheric N deposition in the soil. Low N deposition in the soil in which plants are growing can be an important factor limiting N uptake, especially for urban plants.

The relationships between leaf traits enhance plant adaptability to the heterogeneous environment. As predicted by the LES (Wright et al., 2004), the dimensions of LFM, LDM, and LA are different from the N, P contents and N:P ratios, and their coordination may ensure the normal growth of plants under different conditions of light (Baird et al., 2017; Puglielli et al., 2020). It is worth mentioning that the three urban plants studied herein employed adaptive strategy shifting in environments with different conditions of light. The relative displacement of *P. quinquefolia* was found to be minimal, suggesting that it has a higher tolerance to conditions of low light than *W. sinensis* and *Y. denudta*. While certain plants are naturally

capable of tolerating shade, most plants require sufficient light for carbon gains. Among the six traits, P content appeared to be independent of the others, and the contribution of P to the PC2 axis was high. This is consistent with the result of significant difference of P content in leaves under different light habitats, and also suggests that future research should pay attention to the change of P content.

5 Conclusion

Adaptive strategy shifting is an important mechanism ensuring the survival of plants in heterogeneous environments. This study evaluated plant tendencies under different conditions of light by incorporating the relative benefits of pairwise leaf traits, and the results demonstrated that plants perform adaptative strategy shifting in environments under different conditions of light. In general, the relationship between LA and LDM under different conditions of light supported the law of diminishing returns without exception, and there were significant differences in the stoichiometric characteristics of leaves under different conditions of light. In future studies, the coupling relationship between leaf traits and elements should be clarified, and the adaptation of plants to habitat changes should be more fully understood in combination with plant biomass and root or other traits.

Data availability statement

The data analyzed in this study is subject to the following licenses/restrictions. To obtain data, contact the corresponding author. Requests to access these datasets should be directed to KY, yangkt1996@126.com.

Author contributions

KY and HC: methodology, formal analysis, visualization, writing-original draft. GC and JX: conceptualization, project administration. All authors contributed to the article and approved the submitted version.

Funding

This work was supported by the National Natural Science Foundation of China (31800352), Youth Talents Supporting Program of Gansu Province (GXH20210611-11), Science and Technology Innovation Fund of Gansu Agricultural University (GSAU-RCZX201708), Star of Innovation Project for Outstanding Graduate Students of Gansu Education Department (2021CXZX-398), National College Students' Innovative Entrepreneurial Training Plan Program (201710733029).

Conflict of interest

The authors declare that the research was conducted in the absence of any commercial or financial relationships that could be construed as a potential conflict of interest.

Publisher's note

References

Aleric, K., and Kirkman, L. (2005). Growth and photosynthetic responses of the federally endangered shrub, lindera melissifolia (Lauraceae), to varied light environments. *Am. J. Bot. 92* 4, 682–689. doi: 10.3732/ajb.92.4.682

Baird, A. S., Anderegg, L. D. L., Lacey, M. E., Janneke, H. R., and Van Volkenburgh, E. (2017). Comparative leaf growth strategies in response to low-water and low-light availability: Variation in leaf physiology underlies variation in leaf mass per area in populus tremuloides. *Tree Physiol.* 37, 1140–1150. doi: 10.1093/treephys/tpx035

Bradford, J. B., and D'Amato, A. W. (2012). Recognizing trade-offs in multi-objective land management. *Front. Ecol. Environ.* 10 (4), 210–216. doi: 10.1890/110031

Cheng, Z., Cui, Z., Shi, J. J., Liu, Y., Pierre, K. J. L., and Wu, G. L. (2021). Plant functional types drive differential responses of grassland ecosystem functions along a precipitation gradient. *Ecol. Indic.* 133, 108433. doi: 10.1016/j.ecolind.2021.108433

Cheng, D. L., Wang, G. X., and Zhong, Q. L. (2009). Age-related relationship between annual productivity and body size of trees: Testing the metabolic theory. *Pol. J. Ecol.* 57, 441–449. doi: 10.1176/appi.ajp.160.2.341

Dinesh, T., Nikita, R., and Amit, C. (2019). Increase in light interception cost and metabolic mass component of leaves are coupled for efficient resource use in the high altitude vegetation. *Oikos.* 128, 254–263. doi: 10.1111/oik.05538

Esperón, R. M., Rymer, P., Power, S., Challis, A., Marchin, R., and Tjoelker, M. (2020). Functional adaptations and trait plasticity of urban trees along a climatic gradient. *Urban For. Urban Greening.* 54, 126771. doi: 10.1016/j.ufug.2020.126771

Falster, D., Warton, D., and Wright, I. (2006) *User's guide to SMATR: Standardized major axis tests and routines version 2.0.* Available at: http://www.bio.mq.edu.au/ecology/SMATR/ (Accessed May 3, 2013).

Güsewell, S. (2004). N:P ratios in terrestrial plants: Variation and functional significance. *New Phytol.* 164, 243–266. doi: 10.1111/j.1469-8137.2004.01192.x

Huang, W. W., Ratkowsky, D. A., Hui, C., Wang, P., Su, J. L., and Shi, P. J. (2019). Leaf fresh weight versus dry weight: Which is better for describing the scaling relationship between leaf biomass and leaf area for broad-leaved plants. *Forest.* 10, 256. doi: 10.3390/f10030256

Katahata, S. I., Naramoto, M., Kakubari, Y., and Mukai, Y. (2007). Photosynthetic capacity and nitrogen partitioning in foliage of the evergreen shrub daphniphyllum humile along a natural light gradient. *Tree Physiol.* 27, 199–208. doi: 10.1093/treephys/27.2.199

Kelsey, A. M., and Jason, D. F. (2018). Acclimation of leaf traits in seasonal light environments: Are non-native species more plastic? *J. Ecol.* 106, 2019–2030. doi: 10.1111/1365-2745.12952

Koerselman, W., and Meuleman, A. F. M. (1996). The vegetation N:P ratio: a new tool to detect the nature of nutrient limitation. *J. Appl. Ecol.* 33, 1441–1450. doi: 10.2307/2404783

Liu, Y. J., Dawson, W., Prati, D., Haeuser, E., Feng, Y. H., and Kleuuen, M. (2016). Does greater specific leaf area plasticity help plants to maintain a high performance when shaded? *Ann. Bot.* 118, 1329–1336. doi: 10.1093/aob/mcw180

Liu, Y. Q., Sun, X. Y., Wang, Y., and Liu, Y. (2007). Effects of shades on the photosynthetic characteristics and chlorophyll fluorescence parameters of urtica dioica. *Acta Ecol. Sin.* 27 (8), 3457–3464. doi: 10.1016/S1872-2032(07)60072-9

Li, D. L., Wu, S. Y., Liang, Z., and Li, S. C. (2020). The impacts of urbanization and climate change on urban vegetation dynamics in China. *Urban For. Urban Greening.* 54, 126764. doi: 10.1016/j.ufug.2020.126764

Li, G. Y., Yang, D. M., and Sun, S. C. (2008). Allometric relationships between lamina area, lamina mass and petiole mass of 93 temperate woody species vary with leaf habit, leaf form and altitude. *Funct. Ecol.* 22, 557–564. doi: 10.1111/j.1365-2435.2008.01407.x

Lu, N., Fu, B. J., Jin, T. T., and Chang, R. Y. (2014). Trade-off analyses of multiple ecosystem services by plantations along a precipitation gradient across loess plateau landscapes. *Landscape Ecol.* 29 (10), 1697–1708. doi: 10.1007/s10980-014-0101-4

Lusk, C. H. (2004). Leaf area and growth of juvenile temperate evergreens in low light: Species of contrasting shade tolerance change rank during ontogeny. *Funct. Ecol.* 18, 820–828. doi: 10.1111/j.0269-8463.2004.00897.x

Maréchaux, I., Bartlett, M., Iribar, A., Sack, L., and Chave, J. (2017). Stronger seasonal adjustment in leaf turgor loss point in lianas than trees in an Amazonian forest. *Biol. Lett.* 13, 20160819. doi: 10.1098/rsbl.2016.0819

Meng, F. Q., Cao, R., Yang, D. M., Niklas, K. J., and Sun, S. C. (2014). Trade-offs between light interception and leaf water shedding: A comparison of shade- and sun-adapted species in a subtropical rainforest. *Oecologia.* 174, 13–22. doi: 10.1007/s00442-013-2746-0

Milla, R., and Reich, P. B. (2007). The scaling of leaf area and mass: The cost of light interception increases with leaf size. *Proc. R. Soc Biol. Sci.* 274, 2109–2114. doi: 10.1098/rspb.2007.0417

Niinemets, Ü., Cescatti, A., Rodeghiero, M., and Tosens, T. (2006). Complex adjustments of photosynthetic potentials and internal diffusion conductance to current and previous light availabilities and leaf age in Mediterranean evergreen species quercus ilex. *Plant Cell Environ.* 29 (6), 1159–1178. doi: 10.1111/j.1365-3040.2006.01499.x

Niklas, K. J., Cobb, E. D., Niinemets, Ü., Reich, P. B., Sellin, A., Shipley, B., et al. (2007). Diminishing returns in the scaling of functional leaf traits across and within species groups. *Proc. Natl. Acad. Sci.* 104, 8891–8896. doi: 10.1073/pnas.0701135104

Pérez, H. N., Diaz, S., Garnier, E., Lavorel, S., Poorter, H., Jaureguiberry, P., et al. (2013). New handbook for standardised measurement of plant functional traits worldwide. *Aust. J. Bot.* 61, 167–234. doi: 10.1071/BT12225

Power, S. C., Verboom, G. A., Bond, W. J., and Cramer, M. D. (2019). Does a tradeoff between trait plasticity and resource conservatism contribute to the maintenance of alternative stable states? *New Phytol.* 223, 1809–1819. doi: 10.1111/nph.15981

Puglielli, G., Laanisto, L., Poorter, H., and Niinemets, Ü. (2020). Global patterns of biomass allocation in woody species with different tolerances of shade and drought: Evidence for multiple strategies. *New Phytol.* 229, 308–322. doi: 10.1111/nph.16879

Santiago, L. S., De Guzman, M. E., Baraloto, C., Vogenberg, J. E., Brodie, M., Hérault, B., et al. (2018). Coordination and trade-offs among hydraulic safety, efficiency and drought avoidance traits in Amazonian rainforest canopy tree species. *New Phytol.* 218, 1015–1024. doi: 10.1111/nph.15058

Selaya, N. G., Oomen, R., Netten, J., Werger, M., and Anten, N. (2008). Biomass allocation and leaf life span in relation to light interception by tropical forest plants during the first years of secondary succession. *J. Ecol.* 96, 1211–1221. doi: 10.1111/j.1365-2745.2008.01441.x

Shi, P. J., Li, Y. R., Hui, C., Ratkowsky, D. A., Yu, X. J., and Niinemets, Ü. (2020). Does the law of diminishing returns in leaf scaling apply to vines? - evidence from 12 species of climbing plants. *Global Ecol. Conserv.* 21, e00830. doi: 10.1016/j.gecco.2019.e00830

Song, S. S., Leng, H. B., Feng, S. C., Meng, C., Luo, B. Y., Zhao, L. Y., et al. (2021). Biomass allocation pattern of urban shrubs in the Yangtze river delta region, China-a field observation of 13 shrub species. *Urban For. Urban Greening.* 63, 127228. doi: 10.1016/j.ufug.2021.127228

Sun, J., Fan, R. R., Niklas, K. J., Zhong, Q. L., Yang, F. C., Li, M., et al. (2017). "Diminishing returns" in the scaling of leaf area vs. dry mass in wuyi mountain bamboos, southeast China. *Am. J. Bot.* 104 (7), 993–998. doi: 10.3732/ajb.1700068

Sun, J., and Wang, H. M. (2016). Soil nitrogen and carbon determine the trade-off of the above- and below-ground biomass across alpine grasslands, Tibetan plateau. *Ecol. Indic.* 60, 1070–1076. doi: 10.1016/j.ecolind.2015.08.038

Umaña, M. N., and Swenson, N. G. (2019). Intraspecific variation in traits and tree growth along an elevational gradient in a subtropical forest. *Oecologia.* 191, 153–164. doi: 10.1007/s00442-019-04453-6

Valladares, F., and Niinemets, Ü. (2008). Shade tolerance, a key plant feature of complex nature and consequences. *Annu. Rev. Ecol. Evol. Syst.* 39, 237–257. doi: 10.1146/annurev.ecolsys.39.110707.173506

Valladares, F., Sanchez-Gomez, D., and Zavala, M. A. (2006). Quantitative estimation of phenotypic plasticity: Bridging the gap between the evolutionary concept and its ecological applications. *J. Ecol.* 94, 1103–1116. doi: 10.1111/j.1365-2745.2006.01176.x

Wang, L., Wang, X., Chen, L., Song, N. P., and Yang, X. G. (2021). Trade-off between soil moisture and species diversity in semi-arid steppes in the loess plateau of China. *Sci. Total Environ.* 750, 141646. doi: 10.1016/j.scitotenv.2020.141646

Warton, D. I., Wright, I. J., Falster, D. S., and Westoby, M. (2006). Bivariate line-fitting methods for allometry. *Biol. Rev.* 81, 259–291. doi: 10.1017/S1464793106007007

Wright, I., Reich, P., Westoby, M., Ackerly, D., Baruch, Z., Bongers, F., et al. (2004). The worldwide leaf economics spectrum. *Nature.* 428, 821–827. doi: 10.1038/nature02403

Xu, F., Guo, W. H., Xu, W. H., Wei, Y. H., and Wang, R. Q. (2009). Leaf morphology correlates with water and light availability: What consequences for simple and compound leaves? *Prog. Nat. Sci.* 19 (12), 1789–1798. doi: 10.1016/j.pnsc.2009.10.001

Yang, D. M., Li, G. Y., and Sun, S. C. (2009). The effects of leaf size, leaf habit, and leaf form on leaf/stem relationships in plant twigs of temperate woody species. *J. Veg. Sci.* 20, 359–366. doi: 10.1111/j.1654-1103.2009.05573.x

Yan, Z. B., Tian, D., Han, W. X., Tang, Z. Y., and Fang, J. Y. (2017). An assessment on the uncertainty of the nitrogen to phosphorus ratio as a threshold for nutrient limitation in plants. *Ann. Bot.* 120, 937–942. doi: 10.1093/aob/mcx106

Zhang, Y. J., and Feng, Y. L. (2004). The relationships between photosynthetic capacity and lamina mass per unit area, nitrogen content and partitioning in seedlings of two ficus species grown under different irradiance. *Chin. J. Plant Physiol. Mol. Biol.* 30 (3), 269–276.

Frontiers in Plant Science

Cultivates the science of plant biology and its applications

The most cited plant science journal, which advances our understanding of plant biology for sustainable food security, functional ecosystems and human health.

Discover the latest Research Topics

See more →

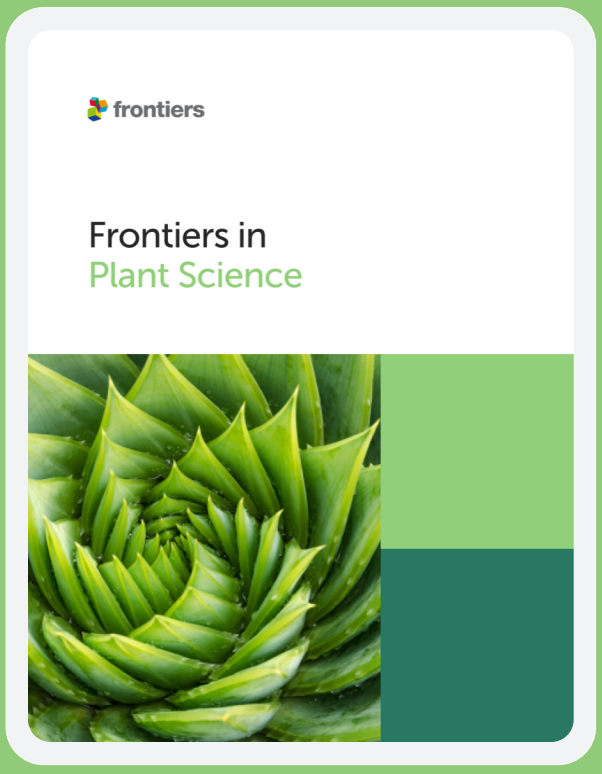

Frontiers

Avenue du Tribunal-Fédéral 34
1005 Lausanne, Switzerland
frontiersin.org

Contact us

+41 (0)21 510 17 00
frontiersin.org/about/contact